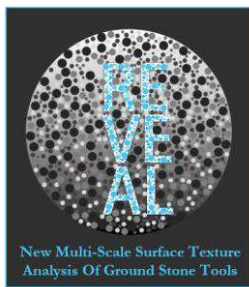Università degli Studi di Torino

Department of Physics

PhD Programme in "Technology Driven Sciences: Technologies for Cultural Heritage" (TECH4CULTURE)

XXXV Cycle

Retrieve a novel: new multi-scale surface texture analysis of Ground Stone Tools

By Giusi Sorrentino

Supervisor:

Prof. Alessandro Lo Giudice

Co-supervisors:

Prof.ssa Laura Longo, Prof. Ing. Marco Paggi,

Prof. Alessandro Re, Prof. Alessandro Borghi

2023

Table of Contents

Acknowledgements

Abstract

[In heartfelt appreciation for the support of my family members, numerous friends and colleagues from Moldova and Italy throughout this journey, the abstract has also been translated into these languages.]

Throughout the course of human evolution stones have served as essential implements for the mechanical processing of various resources. However, categorising these stones as unequivocal "tools" presents a nuanced challenge. The rise of lithic technologies, particularly flaked methods across the Pleistocene, reduced the attention towards macrolithic tools in Middle and Upper Palaeolithic studies. Indeed, putative ground stone tools (GSTs) were rarely recovered in archaeological excavations until recent years, remaining conspicuously underrepresented. This neglect resulted also from methodological constraints, such as heuristics, equipment, and time constraints, all limitations that reflect the theoretical framework.

The recent increased focus on Late Pleistocene plant transformation technology, renewed the interest towards the non-flaked component of the lithic assemblage and regard pebble stones as putative tools used for pounding and grinding different plant resources.

A noteworthy exception can be traced in the meticulous attention and care devoted to these artefacts paid by Chetraru and Borziac during the excavations conducted at the site of Brînzeni I, a cave located in the Edinet district in NW Moldova. The excavation of the site, carried out during the 1960s, demonstrated the key role played by Brînzeni I cave, strategically located in a favourable catchment for the procurement of raw materials, access to water and food resources. It thus served as an ideal refuge for *Homo sapiens* during the colonisation of Europe during the Marine Isotopic Stage 3 (MIS 3, 60-25 kyr).

Within the site's oldest cultural layer, attributed to the Upper Palaeolithic, a total of 114 potential GSTs were meticulously recovered, each of them documented and mapped on the excavation plan. Following their retrieval, these tools underwent thorough cleaning and were prudently stored in the storage room of the National Museum of History of Moldova, remaining undisturbed until the present study. The choice of having this site as a case study was driven by the distinct emphasis on their retrieval, their state of conservation, and the substantial quantity of GSTs, unprecedented in any other Upper Palaeolithic contexts.

The study's objective is to establish a systematic investigative protocol for the recognition and identification of these tools, primarily through the analysis and quantification of intentional surface modifications associated with their use. The mechanical processing of raw materials results in surface alterations, including flattened areas, striations, pits, crystal chipping, and other changes that can affect the stone's texture and its overall geometry. Investigating these aspects supports the final functional interpretation of the stone tools. Additionally, the aim of the research was to create a reference collection to facilitate comparative analysis and to address three main questions:

- Is it possible to differentiate among trace patterns left by the processing of different plant organs?
- What is the impact of the petrographic and morphological characteristics of the lithic resources employed?
- Does the duration of use have an impact on use-wear traces appearance, morphology, development and types?

Recent advancements in imaging technology have empowered the traceology community to adopt objective and quantitative approaches for analysing use-wear. The approach presented here employs a multimodal strategy involving both morphological and quantitative analyses. Techniques ranging from macro to submicron scales are utilised to measure the geometry and surface texture of GSTs. These techniques encompass:

- Photogrammetry for capturing GST geometry and creating 3D digital replica for various preliminary morphometrical evaluation;
- The use of microscopes with varying resolutions and magnifications, such as Dino-Lite, stereomicroscope, optical microscopy (OM), 3D digital microscope, and scanning electron microscope (SEM), to obtain images and perform qualitative observations and evaluation of the surface features;
- Profilometry for obtaining 3D data from selected areas to assess the microtopography of GST surfaces.

The pipeline was tested on selected slabs and pebbles collected along the Racovăţ River, which flows just at the foot of the cliff where Brînzeni I cave opens, and employed to process various plant organs. In order to verify the tribological mechanisms occurring during the transformative tasks and the related wear patterns, the replicative collection also includes cross-reference experiments conducted on compatible cobbles collected from the Fiora River (Manciano, Italy). These stones were selected based on their morphometric and

petrographic similarity to the Moldovan archaeological and experimental GSTs. The approach combines both magnification and resolution in 2D and 3D to identify key features within use-wear traces, enabling discrimination between the processing of different resources. The 3D techniques also facilitate precise measurement and quantitative interpretation while highlighting potential biases in existing literature regarding methods for data acquisition and analysis.

This integrated methodology, initially applied to experimental tools, was subsequently extended to a selection of the archaeological GSTs from Brînzeni I. The results were then compared with data from the experimental collection to glean insights into their functional use.

The analysis demonstrates that most of the selected items were used as multifunctional tools, in concomitant or sequential secondary uses involving plants processing but also different non-vegetal resources as ochre. Furthermore, the analysis of use-wear at various stages of development on experimental tools reveals distinct patterns associated with the transformation of specific plant organs, which exhibit variations depending on the stage of tool use.

[Cu apreciere profundă pentru sprijinul acordat de membrii familiei mele, numeroşi prieteni şi colegi din Moldova şi Italia pe parcursul acestei călătorii, rezumatul a fost, de asemenea, tradus în aceste limbi.]

De-a lungul evoluţiei umane, pietrele au servit ca unelte esenţiale pentru prelucrarea mecanică a diferitelor resurse. Cu toate acestea, clasificarea acestor pietre ca „unelte" fără echivoc prezintă o provocare nuanţată. Apariţia tehnologiilor litice, în special a metodelor cu aşchii în Pleistocen, a redus atenţia acordată uneltelor macrolitice în studiile din Paleoliticul mediu şi superior. Într-adevăr, presupusele unelte din piatră cioplită (denumite în continuare GST, abrevierea provine de la termenul în limba engleză "ground stone tool") au fost rareori recuperate în săpăturile arheologice până în ultimii ani, rămânând slab reprezentate. Această neglijare a rezultat şi din constrângeri metodologice, cum ar fi euristica, echipamentul şi constrângerile de timp, toate limitări care reflectă cadrul teoretic.

Recenta atenţie sporită acordată tehnologiei de transformare a plantelor din Pleistocenul târziu, a reînnoit interesul faţă de componenta non-laminată a asamblajului litic

şi consideră pietrele cioplite ca fiind unelte presupuse utilizate pentru zdrobire şi măcinare a diferitor resurse vegetale.

O excepţie notabilă poate fi urmărită în atenţia şi grija meticuloasă acordată acestor artefacte de către Chetraru şi Borziac în timpul săpăturilor efectuate în situl de la Brînzeni I, peşteră situată în raionul Edineţ din nord-vestul Moldovei. Săpăturile efectuate pe parcursul anilor 1960 au demonstrat rolul cheie jucat de peştera Brînzeni I, situată strategic într-un bazin hidrografic favorabil pentru procurarea materiilor prime, accesul la apă şi la resursele alimentare. Ea a servit astfel drept un refugiu ideal pentru *Homo sapiens* în timpul colonizării Europei pe parcursul etapei izotopice marine 3 (MIS 3, 60-25 kyr).

În cadrul celui mai vechi strat cultural al sitului, atribuit Paleoliticului superior, au fost recuperate cu meticulozitate un total de 114 GST potenţiale, fiecare dintre acestea fiind documentat şi cartografiat pe planul de săpătură. În urma recuperării lor, aceste unelte au fost supuse unei curăţări minuţioase şi au fost depozitate cu prudenţă în depozitul Muzeului Naţional de Istorie a Moldovei, rămânând neatinse până la realizarea prezentului studiu. Alegerea de a avea acest sit ca studiu de caz a fost determinată de accentul distinct pus pe recuperarea lor, starea lor de conservare şi cantitatea substanţială de GST, fără precedent în alte contexte din Paleoliticul superior.

Obiectivul studiului este de a stabili un protocol de investigaţie sistematică pentru recunoaşterea şi identificarea acestor unelte, în primul rând prin analiza şi cuantificarea modificărilor intenţionate ale suprafeţei asociate cu utilizarea lor. Prelucrarea mecanică a materiilor prime are ca rezultat modificarea suprafeţei, inclusiv a zonei aplatizate, striaţii, gropi, cioburi de cristal şi alte modificări, care pot afecta textura pietrei şi geometria sa generală. Investigarea acestor aspecte sprijină interpretarea funcţională finală a uneltelor din piatră.

În plus, scopul cercetării a fost de a crea o colecţie de referinţă pentru a facilita analiza comparativă şi de a răspunde la trei întrebări principale:

- Este posibilă diferenţierea între modelele de urme lăsate de prelucrarea diferitelor organe vegetale?
- Care este impactul caracteristicilor petrografice şi morfologice ale resurselor litice utilizate?

- Durata de utilizare are impact asupra aspectului, morfologiei, dezvoltării şi tipurilor de urme de uzură?

Progresele recente în domeniul tehnologiei imagistice au permis comunității de trasologie să adopte abordări obiective şi cantitative pentru analiza uzurii. Abordarea prezentată aici utilizează o strategie multimodală care implică atât analize morfologice, cât şi cantitative. Pentru a măsura geometria şi textura de suprafață a GST se utilizează tehnici care variază de la scara macro la cea submicronică. Aceste tehnici cuprind:

- Fotogrammetrie: pentru captarea geometriei GST şi crearea unei replici digitale 3D pentru diverse evaluări morfometrice preliminare;
- Microscopie: utilizarea microscoapelor cu rezoluții şi măriri diferite, cum ar fi Dino-Lite, stereomicroscopul, microscopul optic (OM), microscopul digital 3D şi microscopul electronic de scanare (SEM) pentru a obține imagini şi a efectua observații şi evaluări calitative ale caracteristicilor de suprafață;
- Profilometrie: pentru obținerea de date 3D din zonele selectate şi evaluarea microtopografiei pentru a evalua microtopografia suprafețelor GST.

Procedura a fost testată pe plăci şi pietricele selectate, colectate de-a lungul râului Racovăţ, care curge chiar la poalele stâncii, unde se deschide peştera Brînzeni I, şi folosite pentru a prelucra diferite organe vegetale. Pentru a verifica mecanismele tribologice, care au loc în timpul prosecului de transformare şi modelele de uzură aferente, colecția de replicare include, de asemenea, experimente de referință încrucişată efectuate pe pietricele compatibile colectate din râul Fiora (Manciano, Italia). În acest caz, pietrele au fost selectate pe baza similitudinii lor morfometrice şi petrografice cu GST arheologice şi experimentale moldoveneşti. Abordarea combină atât mărirea, cât şi rezoluția în 2D şi 3D pentru a identifica caracteristicile cheie în cadrul urmelor de uzură, permițând discriminarea între prelucrarea diferitelor resurse. Tehnicile 3D facilitează, de asemenea, măsurarea precisă şi interpretarea cantitativă, subliniind în acelaşi timp potențialele erori din literatura de specialitate existentă în ceea ce priveşte metodele de achiziție şi analiză a datelor. Această metodologie integrată, aplicată inițial la uneltele experimentale, a fost extinsă ulterior la o selecție de GST arheologice de la Brînzeni I. Rezultatele au fost apoi comparate cu datele din colecția experimentală pentru a obține informații despre utilizarea lor funcțională.

Analiza demonstrează, că majoritatea obiectelor selectate au fost folosite ca unelte multifuncționale în utilizări secundare concomitente sau secvențiale, care implicau prelucrarea plantelor, dar și diferite resurse non-vegetale precum ocrul. Mai mult, analiza uzurii de utilizare în diferite stadii de dezvoltare pe uneltele experimentale relevă modele distincte asociate cu transformarea unor organe vegetale specifice, care prezintă variații în funcție de stadiul de utilizare a uneltei.

[Per ringraziare i miei familiari, i numerosi amici e i colleghi moldavi e italiani che mi hanno sostenuto durante questo percorso, l'abstract è stato tradotto anche in queste lingue].

Nel corso dell'evoluzione umana gli utensili in pietra sono stati essenziali per la lavorazione meccanica di varie risorse. Tuttavia, identificare queste pietre e riconoscerle come "strumenti" rappresenta spesso una sfida. L'ascesa delle tecnologie litiche nel Pleistocene, e in particolare della scheggiatura, ha ridotto l'attenzione verso gli strumenti macrolitici negli studi sul Paleolitico medio e superiore. Fino ad anni recenti gli strumenti in pietra non scheggiata venivano raramente recuperati negli scavi archeologici, rimanendo così ampiamente sottorappresentati e poco studiati anche a causa di vari vincoli metodologici quali euristica, caratteristiche della strumentazione che, ancora oggi, poco si adatta a questo tipo di materiali e limiti di tempo.

La recente attenzione per quelle tecnologie che possiamo definire "trasparenti", in quanto legate a materiali deperibili - quindi di difficile conservazione in un contesto archeologico e trasparenti all'analisi con la maggior parte dei metodi convenzionali di studio - ha rinnovato l'interesse per gli strumenti litici non scheggiati e per i ciottoli utilizzati come strumenti per frantumare e macinare varie risorse vegetali sin dal tardo Pleistocene.

Un'eccezione degna di nota si può ritrovare già negli anni 60 del secolo scorso, nella meticolosa attenzione e cura dedicata a questi manufatti da Chetraru e Borziac, durante gli scavi condotti nel sito di Brînzeni I.
Brînzeni I è una grotta situata nel distretto di Edinet, nella Moldavia occidentale. Lo scavo del sito ha dimostrato il ruolo chiave svolto dalla grotta, situata in posizione strategica in un bacino idrografico favorevole per l'approvvigionamento di materie prime, l'accesso all'acqua e alle risorse alimentari. Queste caratteristiche l'hanno resa un rifugio ideale per *Homo sapiens* nel periodo di colonizzazione dell'Europa durante il MIS 3 (Stadio Isotopico Marino 3, 60-

25 ka). All'interno del livello più antico del deposito archeologico, attribuito al Paleolitico superiore, sono stati recuperati 114 potenziali strumenti macrolitici, ognuno dei quali è stato documentato e mappato. Dopo il loro ritrovamento, questi strumenti sono stati sottoposti a una prima sommaria pulizia e accuratamente conservati nel magazzino del Museo Nazionale di Storia della Moldavia, dove sono rimasti intoccati fino all'attuale studio. La scelta di utilizzare questo sito come caso di studio è stata dettata dalla particolare attenzione posta durante il loro recupero, dal loro stato di conservazione e dal numero di questi possibili strumenti, che risulta essere senza precedenti in altri contesti del Paleolitico superiore.

L'obiettivo dello studio è stabilire un protocollo di indagine da applicare in modo sistematico, per il riconoscimento e l'identificazione di questi strumenti. Il metodo si basa principalmente su riconoscimento, analisi e quantificazione dell'usura, delle tracce d'uso e di tutti quei cambiamenti nella geometria dell'oggetto legati al loro utilizzo. La lavorazione meccanica delle materie prime provoca alterazioni superficiali della pietra, tra cui aree appiattite, strie, crateri, scheggiature dei cristalli e altri cambiamenti che possono influenzare la geometria degli strumenti e la loro tessitura superficiale. L'indagine di questi aspetti supporta l'interpretazione funzionale degli utensili in pietra.

Inoltre, lo scopo della ricerca è stato quello di creare una collezione di riferimento per facilitare l'analisi comparativa e per rispondere principalmente a tre domande:

- È possibile differenziare le tracce lasciate dalla lavorazione dei diversi organi vegetali?
- Qual è l'impatto delle caratteristiche petrografiche e morfologiche delle risorse litiche utilizzate sullo sviluppo delle tracce d'uso?
- La durata dell'uso ha un impatto sull'aspetto, la morfologia, lo sviluppo e le tipologie delle tracce d'uso?

I recenti progressi delle tecniche di imaging hanno permesso alla comunità degli studiosi di tracce d'uso l'adozione di approcci oggettivi e quantitativi.
Questo studio impiega una strategia multimodale che prevede l'impiego sia delle analisi morfologiche, sia quantitative. Per misurare la geometria e la texture della superficie degli strumenti macrolitici vengono utilizzate tecniche che vanno dalla scala macro a quella submicrometrica. Queste tecniche comprendono:

- La fotogrammetria: per catturare la geometria dei reperti e creare repliche digitali 3D per varie analisi e valutazioni morfometriche preliminari;

- Microscopi con diverse risoluzioni e ingrandimenti: Dino-Lite, stereomicroscopio, microscopio ottico (OM), microscopio digitale 3D e microscopio elettronico a scansione (SEM), utilizzati per ottenere immagini, effettuare osservazioni e valutazioni qualitative delle caratteristiche superficiali;
- Profilometria: per ottenere dati 3D da aree selezionate e valutarne la microtopografia.

La procedura è stata testata su lastre e ciottoli selezionati e raccolti lungo il fiume Racovăţ, che scorre proprio ai piedi della rupe dove si apre la grotta Brînzeni I, e poi impiegati per la lavorazione di diversi organi vegetali. Al fine di verificare i meccanismi tribologici che avvengono durante le operazioni di trasformazione e i relativi modelli di usura, la collezione di riferimento ha considerato anche esperimenti condotti su ciottoli raccolti dal fiume Fiora (Manciano, Italia). In questo caso le rocce sono state selezionate in base alla loro compatibilità morfologica e petrografica con gli strumenti macrolitici moldavi, confrontati sia con i reperti archeologici che con la collezione sperimentale.

L'approccio integra la capacità d'ingrandimento e la risoluzione di tecniche 2D e 3D mirate a identificare le caratteristiche chiave tra le tracce d'uso, consentendo di discriminare tra l'elaborazione di risorse diverse. Le tecniche 3D inoltre, supportano l'interpretazione quantitativa, evidenziando i potenziali errori della letteratura esistente, per quanto riguarda i metodi di acquisizione e le analisi dei dati. Questa metodologia integrata, inizialmente applicata ai soli strumenti sperimentali, è stata successivamente estesa a una selezione dei reperti macrolitici di Brînzeni I. I risultati sono stati poi confrontati con i dati della collezione sperimentale per supportare la loro interpretazione funzionale.

L'analisi ha dimostrato che la maggior parte degli oggetti selezionati sono stati utilizzati come strumenti multifunzionali, impiegati in usi secondari concomitanti o sequenziali, che coinvolgono la lavorazione delle piante ma anche di diverse risorse non vegetali come l'ocra. Inoltre, l'analisi dell'usura degli utensili sperimentali, considerando vari stadi di sviluppo, presenta variazioni legate ai tempi di utilizzo e rivela modelli distinti associati alla trasformazione di specifici organi vegetali.

List of abbreviations and acronyms

AMH   Anatomically Modern Humans
ASO   Aerial Plant Organs
CT scan   Computerised Tomography Scan
DOF   Depth of Field
FEG-SEM   Field Emission Gun – Scanning Electron Microscope
FN   Field Number
FTIR   Fourier-transform infrared spectroscopy
FOV   Field of View
GSD   Ground Sampling Distance
GST   Ground Stone Tool
ICP   Iterative Closest Point
MIS 3   Marine Isotopic Stage 3
NA   Numerical Aperture
OM   Optical Microscopy
OP   Operator
PVS   Vinylpolysiloxane
RCA   Real Contact Area
RMS   Root Mean Square
Sa   Arithmetical Mean Height of the Surface
SEM   Scanning Electron Microscopy
SEM-EDS   Energy Dispersive X-Ray Spectroscopy
SfM   Structure-from-Motion
Sku   Kurtosis of Height Distribution
Sp   Maximum Height of Peaks
Sq   Root Means Square Height of the Surface
Ssk   Skewness of Height Distribution
STEM   Science, Technology, Engineering and Mathematics
Sv   Maximum Height of Valleys
Sz   Maximum Height of the Surface
T   Time (experimental stage)
USO   Underground Plant Organ
WD   Working Distance

1. Introduction

The present study is part of a larger research endeavour that involves multiple research teams with the ultimate aims to explore the potential introduction of starch-rich plants in the dietary habits of Anatomically Modern Humans since their first arrival in Eurasia during Marine Isotopic Stage 3 (MIS 3, 60-25 ka). The working hypothesis, proposed by Professor Laura Longo in the project "Unfolding the complexity of nutrition at the dawn of modern humans in Eurasia" (2015-2018: Longo 2016; Longo et al. 2018), suggests that task-specific Ground Stone Tools (GSTs) were utilised by *Homo sapiens* to transform selected starch-rich organs into highly energetic food.

Within this broad context, the current PhD project aimed to establish a comprehensive and interdisciplinary approach for the identification and analysis of stone pebbles used during the Upper Palaeolithic as ground stone tools. The focus is on determining their function and in particular exploring the tribological mechanisms occurring during their use in task specific activity such as the elaboration of different plant organs. The study involves a review of existing methods and the exploration of new approaches influenced by different disciplines.

The PhD program "Technology Driven Sciences: Technologies for Cultural Heritage" provided the ideal environment for the development of this research, as one of its main aims is to draw influences from various disciplines and encourage their integration. The combination of Science, Technology, Engineering, and Mathematics (STEM) disciplines brings a systematic and analytical approach to the study of archaeological contexts. These disciplines offer tools and methodologies that deepen our understanding of materials, techniques, and cultural contexts of artefacts. Scientific techniques, such as imaging technologies, chemical analysis, and material characterization, have revolutionised the field, enabling researchers to uncover hidden details, identify materials, and gain insights into manufacturing processes.

However, the study of ground stone tools goes beyond the application of scientific techniques alone, emphasising the interdisciplinary nature of the needed approach. A holistic methodology that integrates qualitative and quantitative data was indeed employed, by combining the expertise and support of scholars from diverse disciplines, such as archaeology, physics, conservation science, and engineering.

The present research is the result of this dialogue and exploration in the middle ground where different approaches and languages intersect.

Among numerous sites (almost 30) already sampled along the Pontic Steppe area, the site of Brînzeni I, a cave located in northwest Moldova, was targeted for this research. This site presents the most significant collection of unstudied ground stone tools (GSTs) characterised by limited lithic variability. Following their excavation, the tools were mapped, labelled and underwent a first cleaning. However, the subsequent biography of these tools reveals that they remained stored and untouched in wooden boxes until our survey in 2016 and 2017. These circumstances make Brînzeni I an ideal case study for testing protocols and developing a site-specific reference collection. Since methodological refinement and the development of interdisciplinary-based study protocols are at the core of this research, the creation of the reference collection plays a crucial role. The collection was carefully designed, taking into consideration the operative variability that may influence the experimental replication of tool use with an emphasis on the tribological mechanisms that affect the development of use-wear patterns and geometrical property change at macro to sub-micro scales.

In this regard, this research encompasses multiple objectives. Firstly, it aims to investigate the selection and processing of plant foods during the Upper Palaeolithic specifically focusing on the inhabitants of Brînzeni I and the GSTs recovered from the site. These GSTs provide material evidence of human behaviour and hidden activities related to perishable technologies, contributing to our understanding of an intangible heritage. By investigating the tribological mechanisms involved during plants processing and analysing the wear patterns associated with different plant organs at various stages of tool use, valuable insights can be gained into the techniques, gestures, and strategies employed in plants transformation. The construction of a reference collection of task-specific tools is crucial in this context.

Secondly, the research aims to understand the functional role of the Brînzeni I GSTs and determine if they were used for plants processing tasks. Through a comprehensive analysis of tool geometry, surface texture, wear patterns, comparison with experimental data, and residue analysis (part of a related project, which also add the nanoscale level to the investigation, for detail see Birarda et al. 2020, 2023), the study aims to establish a direct link between the GSTs and their specific functional use. In this perspective the investigation

contributes to the understanding of the cultural and subsistence practices of the Upper Palaeolithic population at Brînzeni I.

Furthermore, the research seeks to assess and improve current methodologies in the study of GSTs, while also identifying and mitigating potential biases. The experimental collection plays a crucial role in this endeavour by serving as a framework to test the approach and obtain feedback about tools transformation during use from a context where tool use-biography is known and traced. The above highlights the significant emphasis that is necessary to place on constructing the reference collection. In the present study the collection serves as a basis for comparative analysis, enabling the study and interpretation of wear patterns observed on archaeological GSTs. Through controlled experiments and replication of tool use scenarios, it is possible to gain a better understanding of the interplay between tool morphology, wear patterns, and specific plant processing activities. That is expressed in the old and natural human gesture of which the GSTs represent the tangible evidence. Reference collection is a valuable resource for identifying and categorising GSTs within the array of the archaeological lithic tools, as well as interpreting their function and the plant resources they were intended to process. Moreover, it allows for the exploration of wear pattern variations and tool use across different contexts, enhancing our knowledge of the cultural and technological practices of past societies.

Methodological considerations, as highlighted by Marsh and Jeffrey (2010), underscore the importance of "experimental" archaeology in confirming findings through reproducible and replicative experiments while preserving unique and non-repeatable original artefacts (it is to notice that in this research term "artefact" is used *sensu lato* encompassing all the object and/or tool utilised or manufactured by human for certain task). These operations are crucial for understanding the nuances of GST usage at different observation scales. At the macroscale, one can disclose the gestures and knowledge of the people who inhabited Brînzeni I cave, knowledge that may have been shared with neighbouring groups. At the microscale, the comprehension of the tribological mechanism behind the deformation of the surface roughness can contribute information on the selection of the raw materials of the stones, on the time involved in the transformed medium (organic or inorganic) and to characterise the mechanically processed substance(s). The controlled replication of our ancestor gestures supports us to recreate the main strategies of use and above all to understand the timing and the interactions that produced the tribological modifications of the surface texture that can be observed on the lithic surfaces. Moreover, it

opens up an interesting perspective for future development: the possibility of displaying such archaeological material alongside its operational use. This would foster a dialogue and enhance the understanding of these non-self-explanatory tools for a broader audience, including non-specialists.

The importance of the reference collection was also driven by various non-scientific factors, including logistical, safety, and geopolitical considerations. The constraints imposed by the Covid-19 pandemic and the ongoing Ukraine-Russia war, which have also affected the territory of Transnistria, have posed significant challenges in terms of safely accessing artefacts in Moldova. As a result, it was not possible to conduct a new sampling at the National Museum of History of Moldova, in Chisinau, where the GTSs are stored.

The present manuscript is structured into five main sections, each containing several chapters that contribute to the conceptual and methodological foundations, as well as the results and discussions derived from the study.

The first section, comprising the current **Chapter**, **Chapters 2** and **3**, lays the foundation for the research. In Chapter 2, terminological issues related to ground stone tools are addressed, as well as kinematics, tribological mechanisms, and wear that occur during tool use are explored. Chapter 3 presents the research design and situates it within the current state-of-the-art. Moreover, the chapter emphasises the significance of parallel residues analysis to enhance the understanding of the tools' function.

The second section comprises **Chapter 4**, offering an insight into the archaeological site of Brînzeni and its GSTs. This chapter also provides a concise account of the sampling campaign conducted prior to this study. Furthermore, initial assessments based on petrographic and morphological characterisation were conducted at the dawn of this PhD research. Their significance is addressed within this chapter, as they formed the foundation for selecting suitable rock types and establishing the morphometric attributes necessary for slabs and pebbles to comprise the replicative collection.

The third section encompasses **Chapters 5** and **6**, centring on the reference collection. In Chapter 5, the construction of the reference collection and the approaches employed are detailed. This includes the data obtained during the Experimental Archaeology dedicated Day organised by the writer in October 2021 at the Physics Department of the University of Turin, which was open to students. Both the program and the data resulting from participants' involvement in this activity were anonymised and are included in

Appendix A. Additionally, the chapter delineates the analysis and results of qualitative and quantitative investigations of the experimental tools' surfaces. Quantitative data arising from the processing of aerial measurements obtained using a confocal profilometer are reported in **Appendix B**.

Additionally, in Chapter 6, the outcomes of a parallel study dedicated to the acquisition and analysis of 3D photogrammetric data are presented. This part is the results of the secondment, supervised by Dr. Fabio Menna from the 3D Optical Metrology Unit at the Bruno Kessler Foundation (FBK), Trento (Italy), which brought to a critical refinement of existing protocols and the development of a custom setup to achieve consistent and repeatable results while addressing potential sources of systematic errors.

The fourth section of the research encompasses **Chapters 7**, where the functional analysis of the archaeological GSTs is presented, involving their examination at macro, micro, and sub-micro scales. This includes the integration and comparison of results obtained from the analysis of archaeological tools and experimental data. Quantitative data resulting from the processing of aerial measurements acquired using a confocal profilometer are documented in **Appendix C**.

The concluding section is represented by **Chapter 8**, which summarises the findings from preceding sections and outlines directions for future research.

2. Ground Stone Tools

2.1. Definitions

The subject of this study focuses on stones, specifically cobbles, river pebbles, and slabs, not modified from their natural shape and utilised by Anatomically Modern Humans during the Upper Palaeolithic for transformative tasks. These duties encompassed the processing of plant organs for various nutritional reasons, such as transforming them into flour and softening them for easier chewing and digestion, or for non-alimentary assignment as separating the fibres to create treats.

Different terms have been used to describe these types of stone tools, such as "non-flint implements", "non-flaked tools", "non-flaked industry" and "non-chipped stone tools". However, these terms primarily focus on what these artefacts are not, rather than providing a comprehensive understanding of their nature and function. Therefore, among the available lexical options, the author of this study prefers the terms "ground stone tools" or "macrolithic tools", as they give to the artefacts the dignity as category per se, not in comparison with other groups of stone implements.

These terms encompass multiple categories of essential domestic tool kit manufactured and/or used in a wide range of daily activities, involving processing of various raw materials for different purposes and retrieved in a large geographical and chronological contest. These activities, include for example, producing mineral pigments, breaking bones, cracking nuts, pounding wood for fibres extraction, grinding plants organs for flour production, preparing leather, polishing ceramic vase, and more activities, which requires percussion, ponding, cracking, grinding, abrasion, polishing, chopping, pecking and softening actions (Rowan and Ebeling 2008; Adams et al. 2009; Dubreuil et al. 2015).

Since this dissertation specifically focuses on the processing of plants, the term "ground stone tools" (GSTs) is preferred as it accurately recalls this function. The word "ground" refers to the action of grinding (in the sense of reducing to powder) and also alludes to the location where the stones were typically placed when processing plants is the case. Additionally, the term specifies that these tools are made of stone and emphasises their active role in various actions as instruments. Indeed, the term GSTs provides a clear and concise description of the tools and their function in plant processing activities but, as have been

already noticed by various scholars (e.g., Wright 1992; Ebeling and Rowan 2004; Hamon 2008; Adams et al. 2009), it seems misnomer when applied to other type of activity that is not implying a transformative task (e.g., prepare leather or polish clay objects). However, when adopting a functional approach, this is the only term that satisfies this requirement. Even "macrolithic tools" highlights other aspects of this object, emphasizing their morphology, which is a secondary characteristic when investigating these artifacts compared to their function.
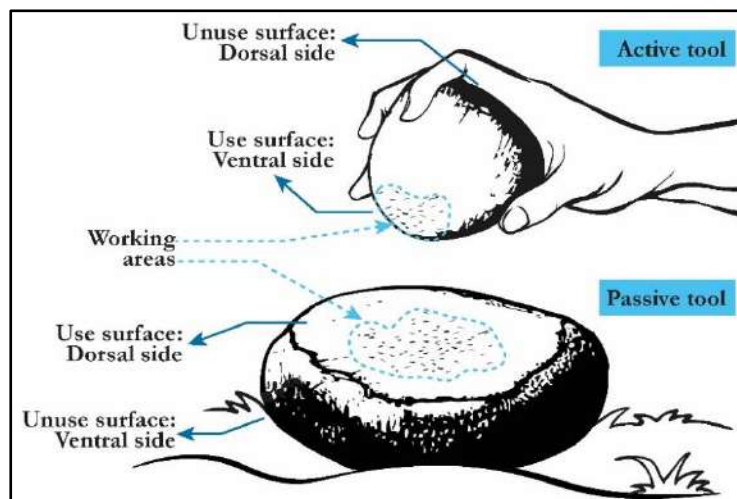
Figure 2. 1. Representation of an active and passive GSTs and related nomenclature. The image also highlights the specific area directly involved in the processing action: the working area. It is also important to note that the edge closer to the operator is called proximal edge, while the farthest is called distal edge.

Upper Palaeolithic GSTs used in plant processing were typically utilised in pairs, consisting of a lower steady passive stone where the material to be processed was placed, and a movable item held in one hand that actively performed the grinding and/or pulverising task (Figure 2.1). As noted by Adams (2002a: 119), active tools often outnumber passive ones in archaeological contexts. This study suggests that this may be due to the tendency of active stones to break more easily and thus be replaced. Furthermore, Adams proposed that pebbles used as active tools could have been selected and accumulated for future use, while passive tools might have been recycled for other purposes, such as being used as building stones or being collected before site abandonment, thereby resulting in a lower number in archaeological contexts. It is also worth considering the potential use of perishable materials such as wood. However, to the best of the author's knowledge, the existence of wooden tools of this kind has not been reported in prehistoric archaeological contexts (although perishable materials are rarely preserved in non-arid archaeological contexts). Kraybill (1977: 492) does mention the use of wooden mortars and pestles in ethnographic examples and classical archaeological contexts, specifically used for producing a desired end product, such as a core flour that would not smash the seeds after breaking the hulls.

2.2. Kinetics and tools typology

This study focuses on specific GSTs used for transforming various plant resources, specifically above and underground storage organs (ASOs and USOs). These resources were processed for nutritional purposes or for non-food-related uses. It is worth noting that some of the resources, especially ASOs, could have been consumed raw, freshly gathered. Despite the time needed for their elaboration, the advantages of processing these resources were diverse. Firstly, it facilitated the separation of desirable components from undesirable ones, serving both food-related and non-food-related purposes (e.g., separating fibre to make thread, but also removing the pericarp from shelled fruit). The processing also resulted in a reduction in resource volume, making them easier to transport and allowing for extended storage periods. Additionally, it made the plants easier to chew, digest, and assimilate nutrients, in particular reducing fibres supports starch assimilation, while also promoting detoxification processes (as one of the needed steps, together with leaching and roasting). Furthermore, the resource elaboration for food consumption led to changes in texture, opens to the possibility of different cooking techniques, which will also impact on digestion as well as on flavour (Stahl 1989; Bofill 2012; Dubreuil and Nadel 2015; Longo et al. 2021a).

To understand the underlying motions and forces that occur during processing, the principles of kinetics, as a branch of mechanics, are applied. These principles serve as a valuable tool for understanding the mechanics behind the visible wear traces. Experimental reproduction through repeated trials, was in this study the primary approach used to gain insights and enhance the understanding of these processes. By replicating and observing the motion and forces involved, researchers can uncover valuable information about the wear patterns and their formation process.

Sophie A. de Beaune, a prominent scholar in the field, conducted a pioneering study on unshaped GSTs (de Beaune 2004). Drawing upon Leroi-Gourhan's classification (*L'homme et la matière* 1943), she distinguished different types of possible action performed with GSTs. Based on her reasoning, the evolution of gestures involved in the processing of organic matter is reported here. According to de Beaune, the first gesture performed by early hominids was cracking hard fruits using an anvil as passive support and a hammerstone as active tool, with a gesture similar to what is performed by modern Chimpanzees. The kinematic required a "thrusting percussion", defined as a single percussive movement where the operator pushes the stone onto the organic matter. From this simple gesture, both

cracking and **knapping** actions (the latter related to flake tool production) emerged. When it comes to processing softer materials such as USOs, leaves, fruits, kernels, phloem, as well as mineral resources like ochre or animal products like meat, fat, and tendons, the "thrusting percussion" gesture is accompanied by a "resting percussion". This involves a more rhythmic back-and-forth movement. The tools used in this manner are known as grinder-pestles, typically in the shape of pebbles. Over time, these tools elongated and increased in weight, taking the form of pestles. Gradually, these tools started to be used solely for "thrusting percussion" in a **pestling** action, in conjunction with deep passive tools initially shaped like shallow quern-mortars, which then gradually deepened to create proper mortars. The thrusting motion is no longer generated by the operator's strength, rather by the weight of the tools. Additionally, grinder-pestles gradually began to be used exclusively for "resting percussion", employing a broad surface. This gave rise to a category of instruments known as grinding stones. These tools, both passive and active, operate through a "diffuse percussion" action, where the entire surface is used, either through perpendicular **pounding** (what in engineer is named an impact motion), horizontal parallel **grinding** (what in engineer is named a sliding motion), or initially a combination of both (Figure 2.2) (Czichos 1987: 103; Dubreuil 2001). The direction of motion could be back-and-forth, circular, random, or oblique. With the advent of cereals, the predominant movement became back-and-forth, performed with the active tool handled with both hands on larger passive tools.
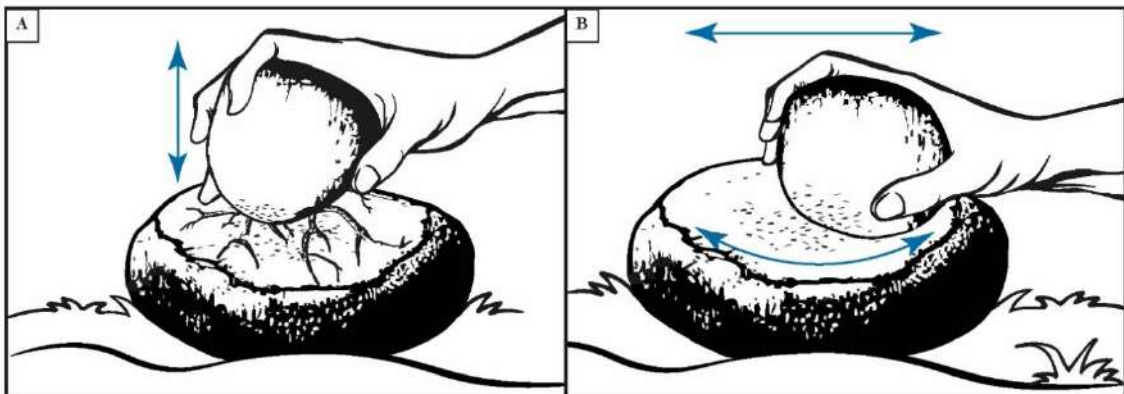
Figure 2. 2. Resting percussion gesture performed for different actions: A) vertical ponding; B) horizontal grinding in back-and-forth and circular motions
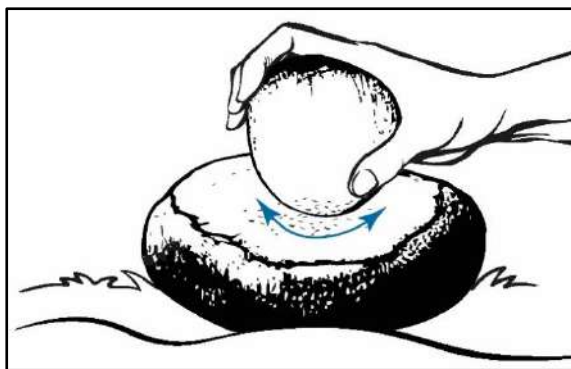
Figure 2. 3. Gesture that combines the rotation and the rhythm of the resting percussion and the strength of the thrusting percussion. It is particularly useful in the final stage of roots processing when the powder stick on the tools working surface.

During the experimental reproduction of vegetal resources elaboration, the writer identified another action that can be very useful when processing roots, a resource that differs greatly in size and consistency from seeds and cereals (Figure 2.3). The gesture implied the axial rotation of the active tool ensuring a stable contact between the tool surface and the resource treated, while applying pressure on it. The rotational resting percussion gesture is combined with the pressure exerted by the wrist that resembles the force applied during a thrusting percussion. The type of contact is not far from the rolling motion seen in engineering applications (e.g., Czichos 1987: 103). This motion is particularly helpful in separating the root fibres. When used for pulverising tasks, it mitigates the issue of root paste sticking to the active tool surface, which would otherwise reduce the tool's efficiency.

Other classifications of tool motion are available in the literature. For example, Adams (2002: 41-42) divided the types of gestures into circular stroke, reciprocal stroke (back-and-forth motion), rocking stroke (for a definition see Haury 1950: 315-316; Morris 1990: 181-182), crushing (utilising the weight of the tool), pounding (utilising the user's strength), pecking, chopping. Another possible classification is provided by Wright (1992), who categorises tool kinematics as grinding, pounding, battering, chopping, cutting, and chiselling. These classifications, which offer different perspectives on the various types of motions involved in tool use, are reported here only as an example of the large variability that is encountered when dealing with the topic.

It is evident that there has been terminological inconsistency in the discourse surrounding the kinematics of slabs and pebbles for performing different actions and the mechanical treatment of various raw materials. This issue has been recognised since the 1970s (e.g., Hole et al. 1969: 170; Kraybill 1977: 487-488; Adams et al. 2009; Hamon 2008), and it is reflected in the confusion surrounding the nomenclature of pounding and grinding tools. Partially, this can be also attributed to the broad geographical and cultural contexts of discoveries, as well as the chronological diversity of the archaeological contexts. As a result, terminology derived from different languages has been introduced into the international

framework, leading to terms such as "*manos*" from Spanish word (e.g., Hayden 1987), which is internationally used to define what can be also called "*molette*", derived from French literature, "*handstone*" or "*grinder*" from English definitions. Moreover, there has been a proliferation of subcategories within these terms, further contributing to the complexity of the nomenclature in the field (e.g., Wright 1992; David 1998; Adams 2002; De Beaune 2004; Hamon 2008; Adams et al. 2009; Dubreuil and Nadel 2015; Dubreuil et al. 2015).

In this dissertation, the description of gestures and actions follows de Beaune's approach, but it has been adapted to suit the specific needs of the study. However, the writer's perspective differs from de Beaune's interpretation of implements used for multiple actions as an intermediate stage in GSTs development. The focus on cereal processing as the pinnacle of GST evolution appears a Eurocentric vision, disregarding the fact that other resources, such as roots, can be also used to produce flour, as still occurred outside Europe and USA as for example in Asia (e.g., the *Colocasia esculenta* roots that is commonly use in India with the name Taro to produce flour). The treatment of these resources requires a completely different kinetics than cereals requiring both pounding and grinding actions. During the period under analysis, the division between gestures and the boundaries between different types of tools are not always clear-cut. The same tool or different faces of it can be used in multiple actions, either through a two-step motion or through contemporary secondary use (for definition see next paragraph). In this dissertation, a strict typological classification is avoided to prevent contributing to the existing nomenclature confusion and to ensure worldwide understanding. Instead, the tools are described according to the base of Leroi-Gourhan's classification, which distinguishes:

- The mode of use, whether the tool is a "**Passive tool**" (the lower, stationary stone where the raw material is placed) or an "**Active tool**" (the movable item handled with one hand) (Figure 2.1);
- The tool's kinematics and the type of gesture involved;
- The type of contact, whether it is linear and mainly involves the tool's edge, punctiform, or diffuse utilising the entire tool surface, as well as the direction of contact.

2.3. GSTs life-cycle and wear formations

Tools biography counts several different phases. According to Dubreuil and colleagues (Dubreuil et al. 2015: 110-111), the life history of a ground stone tool can be divided into seven stages: 1) raw material choice and procurement; 2) manufacture; 3) primary utilisation; 4) secondary utilisation; 5) recycling; 6) discard; and 7) post-depositional processes. However, taking into account the researches of Adams (in particular Adams 2002a: 18-43) and Hayes and colleagues (Hayes et al. 2018), the author prefers to divide the life of a tool into six phases: 1) the design stage, which includes Dubreuil's raw material choice, procurement and manufacture phases; 2) the use phase, which includes Dubreuil's primary utilisation, secondary utilisation and recycling phases; 4) discard; 5) post-depositional processes; and 6) the excavation and curation phases, which were not included in Dubreuil's overview of the tool's life-cycle. Not all stone tools have to encompass all of these phases (e.g., after the design phase the tool could have been discarded without being used). It is important to note that all phases can leave diagnostic wear patterns on the GST surface.

The design stage involves the selection of the lithotype and the acquisition of lithic resources. The raw material used for these tools could have been obtained through quarrying from bedrock or by collecting naturally occurring cobbles and pebbles along the rivers. Stones could have been selected considering their desired durability and efficiency, preferring materials that are resistant and possess surface texture suitable for effectively processing the selected medium. The shape and weight of the stones could have been considered to ensure their effectiveness in performing specific tasks. As a result, stones may have been chosen for their *expedient design* (Adams 2002a: 21; also referred to as *ad-hoc* implements by Dubreuil et al. 2015), utilising their natural shape and properties, or they may have been intentionally shaped and crafted to meet specific functional requirements defined as *strategic design* (Adams 2002a: 21). *Comfort features* (Adams 2002a: 19), which, for instance, aim to improve the ergonomic handling of active tools, may have also been taken into consideration when selecting a stone or incorporating it into the design in the case of later shaping and refinement.

The use phase involves the actual utilisation of the tool and considers the intended scope of its design, as well as any eventual maintenance strategies employed. According to Adams (2002a: 21-25), tools can be designed for *single use* or *multiple uses*. In the latter case, we can talk of *concomitant secondary use* or *sequential secondary use* according to when the non-

principal use is occurring. When the tool is simultaneously employed in multiple functions or different sides of the stone are used for diverse purposes it is possible to talk about *concomitant secondary use*. Additionally, Hamon (2008: 1504) observes that tools can be involved in *two-step tasks*, where the same tool is used for different gestures and kinematics, although the purpose remains the same. If a tool is reused for a different task at a later time, it can be referred to as *sequential secondary use*. This may involve a *redesign* of the tool, which can be remanufactured. Alternatively, the tool may be reused without any change to its shape, or it may have already been altered by repeated use to the point where it is no longer functional for its initial task. The artefact can also undergo *recycling*, defined by Adams (2002a: 23-24) as its employment in a completely different activity without changing its shape. Schiffer in his studies dealt extensively with the concept of *reuse*, a stage of a artefacts' life, which he divided in different typology (Schiffer 2010: 32-34). This includes *lateral cycling*, which implies the sole change of the user, and therefore can be challenging to identify in archaeological contests; *recycling*, which involves intentional changes in the tool's shape and purpose; *secondary use*, which refers to a change in the task without altering the tool's shape. In this study, Adams' definitions are followed, but as in Schiffer's framework, recycling is considered as a possible stage within the use (or reuse) phase of a tool. The concept of recycling here refers to a phase when both the function and the context of utilisation are changed, which may or may not involve a change in artefact shape, either purposefully or accidentally as a result of the new activity. For example, it is not uncommon to see milling stones recycled as building stones in rural areas, which sometimes requires rough reshaping of the implements or used in the new function without any change in the artefacts' geometry.

The discard phase, present also in Dubreuil's framework, occurs when the tool enters the archaeological deposit. This can happen at any stage after the design phase. The tool may be left behind intentionally or inadvertently, or it may be discarded because it has become worn out and is no longer usable or broken during utilisation. In some cases, the tool may be placed in a funerary context, while in other instances, intentional breakage may occur, resulting in the tool being "killed" (Dubreuil et al. 2015: 111).

The post-depositional phase encompasses weathering, chemical and mechanical processes that can occur after the artefact enters the archaeological deposit. This phase encompasses the study of taphonomic processes, which involve biological, chemical, and erosional processes that can alter the geometry, surface texture of the tools, and any

remaining residues from the processed resources found on the lithic surface and within its crevices (Hayes et al. 2018).

The excavation and curation phases are important stages in the life history of a tool that the author would like to point out as fundamental steps in the tool biography. It encompasses all the activities performed with the tool from its discovery and recovery from the archaeological deposit until its musealisation or storage. This stage is crucial as it involves excavation, documentation, cleaning procedures, preservation strategies, transportation, and storage or musealization. These activities can potentially alter the texture of the object, create new wear traces that may modify or obliterate previous ones, as well as contaminate the residues, removing the original and introducing new residues, making the identification of original features extremely challenging (Longo et al. 2022).

Wear – defined as surface damage that occurs at the contact area and resulting from item use (Kapsa 2004) – can occur at any phase of a tool's life-cycle, including instances where it may already be present due to natural processes such as weathering or rolling. However, this study specifically focuses on the use-wear traces, which are here defined as the traces generated by intentional human utilisation of the tool. Despite acknowledging the potential impact of post-depositional processes on use-wear, the primary emphasis of this study remains on the use stage.

Use-wear analysis is based on the principles of tribology, the science and technology of interacting surfaces in relative motion, encompassing the study and application of friction, lubrication, and wear. There is an ongoing and vigorous debate among scientists and engineers regarding the various mechanisms that contribute to wear formation, especially referring to metal artefact and machinery. In the study of GSTs, the investigation of tribological principles underlying wear formations was the primary focus of Adams' works (e.g., Adams 1993, 2002a: 27-41, 2002b, 2014; Adams et al. 2009), which identified and distinguished four main mechanisms that combine mechanical and chemical interactions: fatigue wear, abrasive wear, adhesive wear, and tribochemical wear. It is important to note that in real surface contact, multiple mechanisms are typically at play, with one mechanism often being dominant based on factors such as the tool's characteristics, the nature of the material being treated (media), and external factors such as the type of motion and pressure applied.

Adhesive wear, a mechanism that is still under investigation and not fully understood, has been observed particularly in the absence of a lubricant medium and when the two surfaces are made of stones with similar hardness. It occurs when two surfaces come into contact, resulting in molecular-level interactions. Even in the absence of movement, these interactions lead to an exchange of electrons between the surfaces, creating a local bond (Carollo et al. 2019). As the surfaces separate, the bonds between them break, generating frictional heat and causing loose rock grains. These rock particles can either adhere to the surface and later become dislodged, remain between the moving surfaces, or attach to the opposite surface. Initially, the damage may only be visible under high-power magnification, but as wear progresses, the damage accumulates and interacts with other wear mechanisms (Teer and Arnell 1975: 95-96; Czichos 1978: 119-120; Adams 2002a: 29; Adams et al. 2009: 46-47; Jeyaprakash and Yang 2020: 11-12).

Fatigue wear occurs when excessive pressure or alternating stress is exerted on the contacting surfaces, leading to the deformation and then collapse of the highest elevations that bear the weight and load. This type of damage manifests as cracks, fractures, pits, and impact fractures, visible with both low- and high-power microscopies. As Adams noticed, the accumulation of fatigue wear on lithic surfaces resembles the frosted glass effect. Notably, while fatigue wear has the potential to obliterate damage caused by adhesive wear, it also exposes fresh surface areas where new adhesive bonds can form (Adams 2002a: 30; Adams et al. 2009: 47).

Abrasive wear takes place during sliding contact due to two possible mechanisms: i) in the case of two surfaces with different hardness, the harder grains dig into the softer surface; ii) particles that have been loosened through the adhesive and fatigue wear mechanisms can remain between the surfaces and act as abrasive agents. These processes result in the formation of striations (linear scratches) and gouges (deep and large scratches) on the surface of the softer stone, aligned in the direction of movement (Teer and Arnell 1975: 100; Adams et al. 2009: 47; Adams 2002: 30-31; Jeyaprakash and Yang 2020: 10-11).

Tribochemical wear is the result of chemical processes that occur when two surfaces interact with each other and with the surrounding environment. This process is influenced by frictional energy generated during movement, pressure, and alternating stresses. It leads to the formation of reaction products, such as films and oxides, which can be observed as polished areas visible with microscopic or even macroscopic examinations (Czichos 1978: 123-125; Adams 2002: 31-32). Polish, especially on flint tools, has been extensively studied,

and two main hypotheses exist about their formation mechanisms: the abrasive model and the additive or silica gel model (for a detailed discussion see Schmidt et al. 2020 and the literature therein). According to the abrasive model, polish formation takes place when fatigue wear becomes negligible because the texture of the stone evens out, causing the asperities to no longer scratch each other. Also, the contact of the surfaces with the worked material may lead to a smoothing of the surface texture, resulting in the formation of polish. The additive or silica gel model of polish formation suggests that polish is formed through the deposition of a thin layer or film consisting of amorphous silica. It appears that the flint surface locally transforms into an amorphous gel during the working of wet plant materials, and that the amorphous gel layer traps plant residues. It is worth noting that not all studies support the adhesion of matter in the polish formation process (e.g., Bofill et al. 2013).

All the observed use-wear features (a summary of the detected features and the terminology used in this manuscript is provided in Table 2.1 and shown in Figure 2.4) can be described in terms of their distribution and density, spatial arrangement and orientation on the surface and relative to each other, as well as their morphology, including relevant morphometric characteristics such as length, width, and, if applicable, depth. Additionally, polish is often characterised by its reflectivity, but due to the challenges in parametrically quantifying this characteristic and its subjective nature in qualitative description, it is not addressed in this dissertation.

Table 2. 1. Tribological mechanism, the associate wear traces (according to Adams et al. 2009), and the description of each trace. The definition "Rubbed area" it was introduced by the author to describe a specific pattern extended on large area of the tool surface and visible already with low-power microscopy, which was observed also by other scholars (e.g., Fullagar and Field 1997; Adams et al. 2009, fig. 6.7d; Liu et al. 2010, fig. 4D-E; Dubreuil et al. 2015, fig. 7.13; Longo et al. 2021b)

Tribological mechanism	Observable use-wear traces	Description
Adhesive wear	Debris	Grains extracted from surface
	Pit	The cavity left by grain removal
Fatigue wear	Crack	Refer to visible and localised fissures that can occur also on fractured grains
	Pit	Depression or cavity formed when grains crack
	Fracture	A break that can affect only the crystal or extend into the matrix, potentially resulting in tool breakage
	Step fracture	Specific type of fracture that creates a stair-like pattern on the bulging grains

	Conchoidal fracture	Specific type of fracture characterised by the production of smooth, curved surfaces with concentric radial ridges
	Frosted appearance	Smooth, uneven, reflective surface with the presence of cracks, giving it a frosted or glazed-like appearance
Abrasive wear	Gouge	Deep and wide linear trace
	Striation and micro-striation	Linear trace
	Levelling	Initially, it affects individual grains, lowering them to the level of the matrix. This process can further extend to impact the stone matrix itself, resulting in the flattening of surface waviness
	Grains welded	Smoothing and levelling of the grains at the matrix level that bring to their coalescence or fusion
	Rubbed area	Combination of features that frequently arise during contact with hard or scattered materials, involving repeated contact between the two lithic surfaces. This wear type is marked by a rough surface texture with multiple areas of levelled high topography. Discontinuous polished regions often create a reticular pattern, along with groups of short, parallel striations
	Grain edge rounding	Smoothing of the grain edge generally due to the elaboration of soft and elastic medium
Tribochemical wear	Polish and micro-polish	Highly reflective areas typically connected to levelling and to grains welded together

All use-wear traces have an impact on the surface texture level, with the exception of levelling, which can also modify surface waviness. Additionally, the fracture feature can alter the tool's geometry and potentially result in its breakage. The nature of the material being treated has a significant influence on the development of wear. In general, harder and less flexible materials tend to interact with the higher areas of surface topography, while softer and more pliable resources are more likely to interact also with the lower and medium areas of topography (e.g., Adams 2002: 33; Dubreuil et al. 2015).
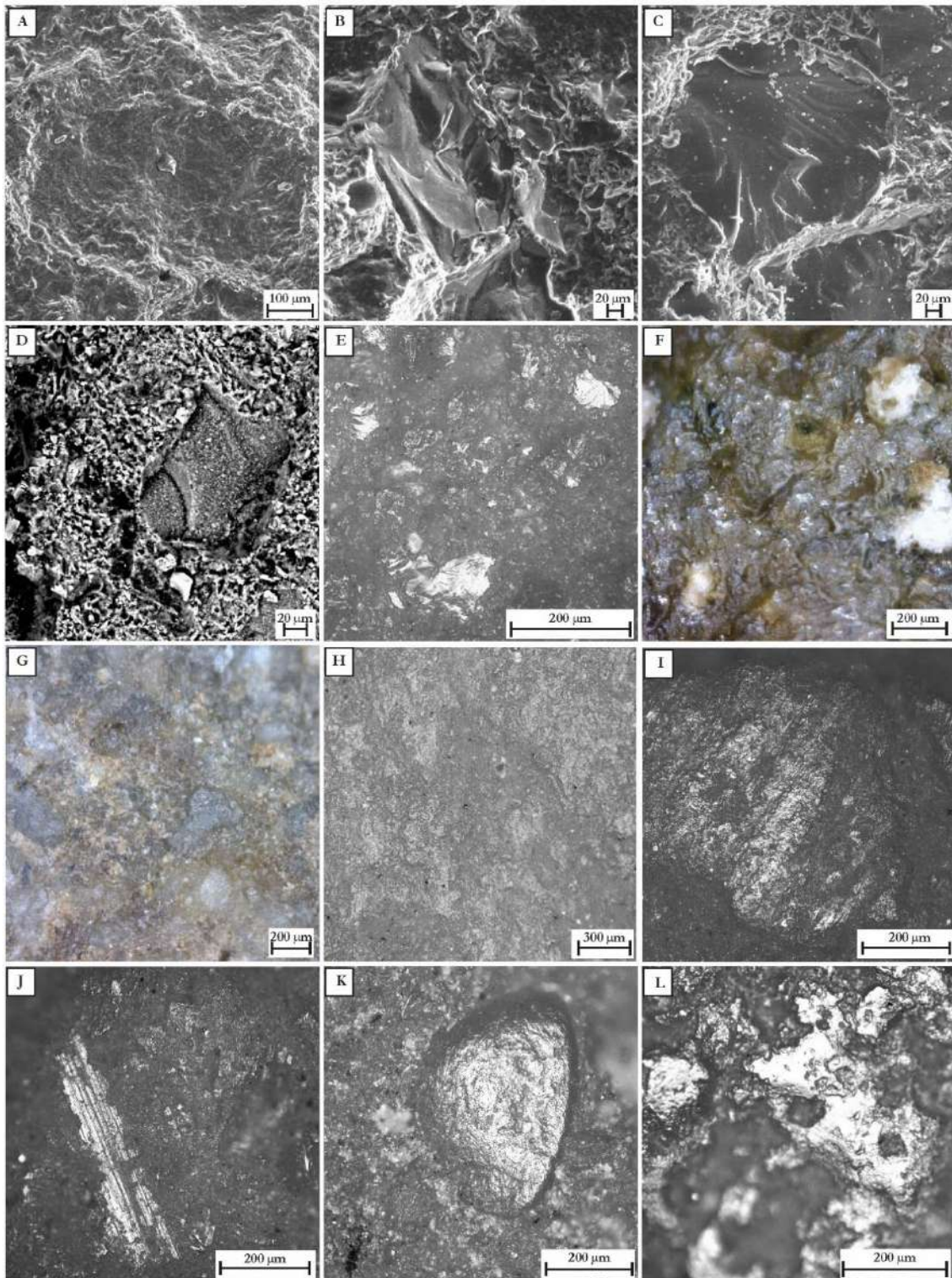
Figure 2. 4. Examples of use-wear traces develop on experimental GSTs depicted with different microscopes: A) SEM image of a flattened area with debris; B) SEM images of a pit, cracks are also visible; C) SEM images of a fractured crystal with superficial cracks; D) SEM images of a step fracture on a crystal edge; E) optical microscope images of a conchoidal fracture; F) portable digital microscope image of an area showing frosted appearance; G) portable digital microscope image of an area characterised by grains levelling at the matrix level that bring to the welding appearance; H) stereomicroscope image of a rubbed area; I) optical microscope image of a micro-pitted type of polish develop on top of a flattened crystal and development of light striations; J) optical microscope image of a group of parallel striations and serrated type of polish; K) optical microscope image of a crystal characterised by edge rounding, flattening and polish development; L) optical microscope image of a deposit type of polish.

3. Research design

3.1. Exploring approaches to functional analysis: a theoretical overview

Functional analysis, as a component of archaeological research, provides valuable insights into the purpose and use-biography of an artefacts. When applied to the analysis of stone tools, it involves examining the traces and wear patterns left on their surfaces to gain a deeper understanding of their functional aspects. By integrating key approaches such as design analysis, traceology and in particular use-wear analysis, researchers can conduct a comprehensive evaluation of the tools' functionality. Additionally, residue analysis can be employed as a complementary method to further enhance our understanding of artefacts utilisation. It is important to note that functional analysis can be based on the establishment of a reference collection, which serves as a valuable resource for studying the formation processes of diagnostic patterns. This collection acts as a proxy for interpreting and deciphering archaeological evidence (e.g., Adams 2002a; 2010; Dubreuil et al. 2015; Marreiros et al. 2020, for a theoretical discussion and insights into these subjects).

Design, when referring to stone tools, pertains to the process of crafting artefacts, with a focus on the deliberate planning to create objects with characteristics that enable them to perform specific functions or purposes. It is worth noting, as mentioned in the previous chapter, that design can also be naturally expedient, whereby items may not be intentionally shaped, but rather selected based on their attributes suitable for the intended tool's utilisation. Therefore, design takes into account socio-cultural constraints, including economic, technological, social, and ideological factors, that influenced the production of these specific objects. Design theory was introduced in ground stone analysis in 1979 by Horsfall, replacing the previous notion of **form**. In contrast, form describes the shape and structure of an artefact, regardless of its constituent material. When applying the concept of form to functional analysis, it must be considered that tools with distinct shapes can be utilized for the same task, and conversely, a single tool can serve various functions. Consequently, it becomes evident that this concept is inadequate for defining tool function. Considerations based on morphology fail to provide a conclusive indication but only offer suggestive clues to potential utilisation(s). Design instead, involves various considerations such as the

selection of raw materials, the tool's morphology, intentional modifications to achieve a desired shape, and considerations of durability and efficiency. When these concepts are not combined with the traceological approach, this method is referred to as techno-functional analysis, which primarily focuses on the morphology of tools and their intentional modifications. Techno-functional analysis is generally supported by ethnographic observations and, to a lesser extent, experimental approaches (Adams 2002a; Marreiros et al. 2020).

<u>Use-wear analysis</u> focuses on examining the traces left on artefacts as a result of their intentional use. It involves identifying surface features that provide valuable insights into the specific activities carried out with the tool, as well as the materials processed and the manner in which they were elaborated. By analysing the working surface(s) of the tool, along with the handling strategy and associated gestures, use-wear studies facilitate a better understanding of how the tool was used, the purpose it served and eventually, providing information about possible length of use.

In a broader perspective, **<u>traceological studies</u>** aim to define the type, location, extent, and distribution of various wear traces on artefacts. This includes not only use-wear, which is the result of intentional human use, but also traces formed during non-use phases throughout the tool's life-cycle. By examining these traces, traceologists can gain insights into the tool biography (Adams 2002a; 2010; Dubreuil et al. 2015; Marreiros et al. 2020).
A well-established practice among traceologists involves the creation of a reference collection based on the methodology inherent to **experimental archaeology**. Experimental archaeology is a research method that follows a hypothetical-deductive process, where hypotheses are tested in order to either be falsified – consequently rejected and substituted by new hypothesis that must be tested according to an iterative process – or validate (Outram 2008, based on Karl Popper's theory). It is very often linked with the concepts of reproduce, replicate, reconstruct, recreate past conditions, process, activities or artefacts (Coles 1979; Mathieu 2002; Outram 2008). However, as Reynolds (1999) pointed out, the past cannot be truly replicated, and evidence of how things truly were, not affected by interpretation, are extremely rare. Given that, stone tools replicative experiment is the act of making and/or using stone specimens to investigate/test methods, inquiry and make hypotheses (Outram 2008; Eren et al. 2016). The replicative use of ground stone tools and the creation of a site-specific reference collection serve as an essential instrument for traceological analysis, to compare the use-wear patterns observed on archaeological artefacts with those found on

artefacts with a known use-biography. This comparative analysis enables researchers to interpret the traces identified on original lithic tools and offers valuable insights into their use and historical significance. By examining similar wear patterns and characteristics, researchers can gain a deeper understanding of how these tools were utilised in the past and contextualise their role within the broader archaeological context.

Traceological analysis traditionally involves the use of different microscopies to qualitatively evaluate the surface texture of tools. However, in recent years, there has been a growing emphasis on quantitative analysis. In this regard, an engineering-based approach to surface texture analysis distinguishes two main methods for inferring tool function (Myshkin and Grigoriev 2013):

- The comparative method, which relies on the expert visual evaluation of the similarity between the object under study and a reference collection.
- The parametric method, which involves the use of various statistical parameters to quantitatively evaluate the surface characteristics.

By employing this latter method, researchers aim to enhance the objective and quantitative aspects of traceological analysis.

In addition to use-wear and traceological studies, **<u>residue analysis</u>** provides a valuable complementary source of evidence. Residues can be defined as fragments of the elaborated resource that become embedded in the tool's lower microtopography (Borel et al. 2014; Fullagar 2014). This highlights their susceptibility to conservation procedures during curation practices (Longo et al. 2022). While use-wear analysis provides insights into the manner and materials processed with a tool, residue analysis plays a crucial role in refuting or confirming, and in this case, specifying hypotheses in greater detail. Through morphological analysis of residues and their characterisation using chemoprofiling techniques, researchers can further enhance their understanding of past societies.

Concluding, it is possible to affirm that functional analysis implies a multidimensional approach that considers a wide range of features associated with the artefact, including tool design, material properties, wear, residues, and cultural context. By integrating these different elements, functional study aims to reconstruct past behaviours, technological choices, and cultural practices of ancient societies.

3.2. Exploring GSTs through multidimensional approaches: the functional analysis perspective

This research has multiple objectives. It aims to explore the transformation process of plant organs during the Upper Palaeolithic through the analysis of GSTs, which were the tools used for these tasks. Specifically, this study focuses on the artifacts retrieved at Brînzeni I, a cave located in NW Moldova, known for its abundant collection of putative GSTs. The investigation of tribological mechanisms involved in plants processing involves analysing wear patterns associated with different plant organs at various stages of tools replicative use. This analysis provides valuable insights into the strategies, techniques, and gestures employed in their transformations.

As a secondary objective of the study, the aim is to comprehend the functional role of the Brînzeni I GSTs and to determine whether they were indeed employed in plant processing tasks. Through a comprehensive analysis of tools design, wear patterns, comparison with experimentally produced data, and residue analysis (as part of a related project, details in Birarda et al. 2020, 2023; Longo et al. 2021a, 2022), this study strives to establish a direct link between the GSTs and their intended function. Thus, the investigation will contribute to the understanding of the cultural and subsistence practices of the Upper Palaeolithic population at Brînzeni I, also marking the inaugural study of its GSTs collection.

Furthermore, the research aims to assess existing approaches to the study of GSTs, refining the methodology used and identifying any potential biases. With this aim in mind, particular emphasis is directed towards the experimental collection, which plays a pivotal role in complementing and enriching our comprehension of the tribological mechanisms underpinning tool use in plants processing activities.

To reach these aims a comprehensive analytical procedure was established. This procedure considers artefact morphometric evaluation, surface texture analysis, the creation of a site-specific experimental collection, and the examination of potential residues trapped in the crevices of the stones. Summarising, the three main research lines are:

- Design analysis, qualitative surface texture evaluation, and parametric analysis;
- Comparison of the GSTs with a reference collection specifically designed for ground stone tools;
- Characterisation of the biogenic residues trapped in the stone cavities.

While the first two points are of primary importance for the present research and are closely interconnected, the third point is not directly part of the present PhD research, but rather a component of Prof. Laura Longo's research and Dr. Clarissa Cagnato's Postdoc study. As mentioned in the previous paragraph, traceological study, and consequently functional analysis, are strongly supported by experimental reference collections, necessary for comparative approach. In this research, the experimental collection played a pivotal role not only as a base for qualitative and quantitative comparison, but also to investigate functional aspects and explore the broader context of tribological mechanisms occurring during the transformation of different plant organs.

To conduct this interdisciplinary research a multiscale approach was implemented encompassing both archaeological and experimental tools. The importance of considering multiple scales of analysis to achieve a holistic functional interpretation is widely recognised (as already highlighted by Adams et al. 2009; Bamforth 2010; Bofill 2012; Dubreuil and Savage 2014; Dubreuil et al. 2015 among other) and applied in the current research considering increasing magnifications from macro to sub-micro scales.

The initial analysis of the archaeological tools involved a macro scale survey to evaluate the design of Brînzeni I GSTs, with a particular focus on morphological aspects. This assessment was complemented by morphometric evaluation and petrographic analysis. The morphometric observations supported the preliminary categorisation distinguishing the active from the passive stones, the identification of putative working areas and providing insights into the potential gestures involved in their use, such as vertical pounding/battering or horizontal grinding. Furthermore, the petrographic composition of the tools was considered providing initial insights into their durability and efficiency.

Residues from selected GSTs were morphologically analysed by Dr. Cagnato using techniques such as optical microscopy (OM) and scanning electron microscopy (SEM). In the framework of the collaboration with Prof. Longo and Dr. Cagnato, the need to characterise these residues led to the applications for beam times at Elettra Synchrotron, which were granted after competitive evaluations (Birarda et al. 2020, 2023). To chemoprofile the residues, FTIR analysis was conducted using synchrotron light, allowing for their investigation to partially determine their attribution and their genuine ancient nature.

The data from residue analysis, morphometric evaluation of archaeological GSTs, and petrographic analysis guided the construction of the reference collection. Furthermore, a comprehensive evaluation of the selected pebbles to be used in replicative experiments,

including petrographic, morphometric, and texture analyses, was conducted before their utilisation.

Various microscopy techniques with progressively higher magnification and resolution capabilities were utilised to examine the surface texture of both archaeological and experimental tools. The latter were analysed at various stages of use, including the unused stage. The combination of these techniques enables the examination of different aspects of surface texture and wear traces, providing a comprehensive understanding of their characteristics, extent, intensity, and direction.

At the sub-micro level, SEM was utilised to examine specific features that were identified in the previous phase. Additionally, the adoption of a confocal profilometer enabled the generation of three-dimensional reconstructions of specific areas of both archaeological and experimental tools. This technique provided detailed insights into the surface topography, enhancing the understanding of the tools' characteristics and wear patterns.

The qualitative evaluations were complemented by parametric approaches conducted at two distinct levels: macro and sub-micro scales. At the macro scale, three-dimensional virtual reconstructions were utilised to facilitate quantitative assessments of the overall tool geometry. Conversely, at the sub-micro scale, more detailed examinations of specific areas of the tools were performed, enabling the calculation of ISO 25178-2 3D surface parameters. While qualitative microscopy analysis remains crucial in the current state of the field (as highlighted by Arroyo and de la Torre 2016; Zupancich et al. 2019), the significance of quantitative evaluation has been increasingly recognised for achieving an objective description and facilitating comparisons. However, it is important to approach quantitative analysis with caution, as many scientific studies on stone tools tend to prioritise measurements without considering the meaningful interpretation of the numerical values (as discussed in a broader context by Comis 2021). Therefore, a comprehensive approach was adopted in this study, which involved the integration of both qualitative and quantitative data. Additionally, a comparative method was employed to analyse both the qualitative and quantitative data, comparing archaeological tools with experimental tools and evaluating the changes in experimental tools at different stages of use and in the unused state. This approach allowed for a more comprehensive understanding of the tools' functional aspects and their transformation over time.

The author now wishes to provide a crucial clarification that is often overlooked in archaeological literature regarding the terms magnification and resolution. While these words are frequently used interchangeably, they have distinct meanings. Resolution refers to the magnitude of measurable geometric features and the resolving power of a microscope, which is its ability to distinguish closely spaced points or lines in an image. On the other hand, magnification relates to a microscope's capacity to produce an image of an object at a larger or smaller scale than its actual size. Magnification allows for the visualisation of finer details that may not be discernible to the naked eye. It is important also to note that accuracy, which refers to the deviation of a measurement from its nominal value, is a separate concept that should be distinguished from magnification and resolution (Barone 2012; DeRose and Doppler 2018).

3.3. The multi-level nature of the tool's morphology and the multi-scale study design

It is well-established that the topography of an object's surface exhibits a multi-scale nature (Vakis et al. 2008). Engineers and tribologists, through the progress in technological instruments to scan surfaces at very fine resolutions, recognised that form, waviness and roughness are key morphological features that should be considered to fully describe contact mechanics interactions between bodies (see Table 3.1 with some of the classical definitions commonly used in the field). Specifically, roughness could go down even to the atomistic scale, provided that no cut-off scales are present. Such cut-off scales are however usually introduced by either material features (grain size, etc.) or by natural or artificial surface treatments (polishing, finishing, etc.) (see Borri and Paggi 2015). Despite this general understanding, there is considerable heterogeneity among scholars (and even among the same scholars in different publications) regarding the specific levels of roughness that should be included in the analysis to correctly describe a specific interface phenomenon.

Table 3. 1. Multiple levels of the artefact morphology according to different archaeologist and engineers.

Adams 2002a: 29; Adams et al. 2009; Dubreuil and Savage 2014; Dubreuil et al. 2015	Description	Leach 2013, 2014; Calandra et al. 2019a, 2019b	Description	Zahouani et al. 2004; Evans et al. 2014	Description	Myshkin et al. 2003	Description
		Surface topography	Overall surface structure and features			Form	$>10^3$ µm
Topography	Describe the **shape** as the general morphology of the tool surface	Surface form	The shape of the object	Form	The overall shape	Form	$>10^3$ µm
Microtopography	Described the **roughness or asperity** in terms of **morphology** and **texture** as visible under magnifications	Surface texture	What remain subtracting form from topography	Waviness	Low frequency **surface topography** (undulations)	Waviness	From 10^3 µm to 10^1 µm
				Roughness	Higher frequency feature characterising the **surface texture** (level to distinguish worn surfaces)	Microroughness	From 10^2 µm to 0.5 µm
						Physical relief or subroughness	0.5 µm to 10^{-3} µm
						Atomic/molecular roughness	$<10^{-3}$ µm

In this study a three-level model is considered for the present investigation concerning archaeological tools:

1. Geometry: This level describes the general shape of the object, its overall morphology. The analysis of this level focus on understanding the shape of the object as a whole. The term "form" is avoided to prevent pre-assumptions about the function of the object based on its shape (see above discussion about Form and Design theory in paragraph 3.1).

2. Surface waviness: This level describes the trend of the surface on a large scale, whether it appears flat, sinuous, undulated, irregular, or with a rugged course.

3. Surface texture: This level considers the spatial organisation of the surface relief, both at the topographical level (observed with naked eye, without magnification) and the microtopographical level (observed with magnification) (*sensu* Adams 2002a: 29). Therefore, it encompasses microscopical roughness, with peaks and valleys forming the topographical reliefs (Adams et al. 2009: 48). Hence, surface texture encompasses characteristics such as the degree of roughness and the morphology of the relief. It involves detailed examination of the surface, including the variations in height, spacing, and distribution of features (Zavarise et al. 2004).

The analytical approach of this study included documenting tool geometry, surface waviness trends, and texture at multiple resolutions and magnification levels, ranging from macro to sub-micro scales. This methodology is original, since it combines a range of instruments and techniques which are usually applied in different fields (topography, 3D models acquisition for reverse engineering purposes, fine scale roughness analysis for mechanical engineering applications), and their combination on archaeological GSTs as well as on a large reference collection is unprecedented. The following methods were employed:

- 3D modelling of the stone geometry was conducted to perform morphometric assessments and determine the main surface undulations. This process involved creating three-dimensional representations of the tools to evaluate their geometric characteristics. Through the testing of various approaches and the subsequent refinement of data acquisition and processing strategies, it also became possible to conduct a preliminary assessment of the surface topography;

- A variety of microscopy techniques, including stereomicroscopes, optical microscopy, digital microscopes, and scanning electron microscopes, were employed to identify, observe, and document surface texture characteristics and use-wear traces. Different levels of magnification and resolution were used to capture a comprehensive to detailed view of the surface features and wear patterns;

- Microtopography 3D reconstruction and measurements of specific areas of interest were conducted using a confocal profilometer. This technique enabled a detailed examination of the surface microtopographical features and facilitated the quantitative evaluation of various surface texture parameters.

The analytical strategy of the study aimed to gather detailed and comparable data on both archaeological and experimental GSTs, enabling a comprehensive analysis of their morphology, surface characteristics, and potential use-related features. For future applications beyond the aims of the present thesis, the acquired morphological features at different scales could also be exploited to create digital twin models of GSTs to simulate damage and wear traces evolutions (Marulli et al. 2023), disclosing the role of the different scales in those phenomena. To ensure data comparability among archaeological and experimental tools, the design of the analytical strategy, the selected equipment, setup, and parameters were kept consistent. Although there were some exceptions due to the inability to directly inspect the archaeological items, the overall approach remained consistent.

The analysis of the tools considers not only the areas that were used but also the unused areas. This differentiation allows for the distinction between use-related wear (hereafter use-wear) and unintentional wear (hereafter wear) that occurs on the surface due to factors such as handling or contact with the ground. Furthermore, the application of multi-scale techniques for the analysis aims to overcome the challenge of identifying and characterising the real contact area (RCA) within the nominal contact area, as this is dependent on resolution and magnification. Indeed, RCA consists of a group of separate contact spots, which in turn are composed of smaller contact spots down to the nanoscale, referred to as the physical contact area (see Myshkin et al. 2003; Paggi and Ciavarella 2010, and references therein). By employing a multi-scale analysis, it becomes possible to capture and understand the hierarchical nature of the surface contact area(s) in GSTs.

3.3.1. Macro scale

At the dawn of the stone tools study, microscopic observation and manual measurements were the main methods used for their analysing (Semenov 1964; Tringham et al. 1974; Odell 1977; Hayden 1979; Keeley 1980). However, with the advent of digital technology and the dawn of "cyber archaeology" or "virtual archaeology" (see Grosman 2016), new opportunities for analysing these artefacts have emerged. In the last decade, 3D reconstruction of stone artefacts has become a prominent method among researchers due to its versatility, precision, and potential for various applications such as analytical, pedagogical, and illustrative purposes. This method has been widely used, with over 200 articles on lithic analysis using 3D techniques published since 2002 (the extensive revision of the employment of 3D techniques for lithic analysis is beyond the scope of this research and have been published in 2022 by Wyatt-Spratt). Several 3D scanning techniques, such as laser, structured light, CT, and photogrammetry, have facilitated the acquisition and virtual reconstruction of complete artefacts. 3D reconstructions have enabled various analyses, such as morphological inspections, texture and volume analysis, quantitative evaluations, and assessment of the operational chain (Shott 2014; Magnani et al. 2020; Wyatt-Spratt 2022). Having a digital model of the artefact is particularly valuable in GSTs analysis, as often the studied items are in foreign museums and not available for direct inspection. This has allowed researchers to investigate stones' morphology, traces of use, and technological aspects effectively, for archaeological, ethnographical, modern primates, and experimentally produced tools (e.g., Caruana et al. 2014; Benito-Calvo et al. 2015, 2018; Longo et al. 2018, 2021b; Zupancich et al. 2019; Caricola et al. 2018; McCartney and Sorrentino 2019; Arroyo and de la Torre 2020; Zupancich and Cristiani 2020; Paixao et al. 2021, 2022; Hayes et al. 2021, 2022).

The use of 3D scanning and photogrammetry has become a common practice in many projects, particularly for documentation purposes. While drawings can be prone to human errors, 3D reproductions offer greater accuracy and provide an objective 360° visualisation. Moreover, in drawings, the expertise and ability of the researcher, as well as their interpretation, play a fundamental role in determining what to include and exclude, as well as other aspects such as the preferred point of view. In this sense, photogrammetry as a substitute for drawing and single pictures, is a valid improvement of a well-established method less prone to operator choices and subjectivity (e.g., Gašparović and Malarić 2012; Magnani et al. 2020).

3D scanners are one way to produce 3D models, employing a light source, such as a laser or structured pattern of light, along with cameras to record the light deformation (Porter et al. 2016). Nonetheless, 3D scanning devices are often expensive and their portability may be limited making it difficult to asset them or adopt them in suboptimal conditions. Alternatively, photogrammetry involves taking sets of overlapping photographs from different angles, identifying reference points, and then using triangulation to create 3D models (Green et al. 2014; Porter et al 2016). Whereas photogrammetry may seem a user-friendly option compared to 3D scanning, which necessitates some technical knowledge before use, it actually calls for more involvement and expertise from the operator to ensure high-quality results. In contrast, 3D scanning requires less intervention once the operator is trained. Therefore, while photogrammetry may seem more accessible, for achieving accurate and reliable results with this technique is mandatory adequate preparation and experience on the part of the operator. On one hand flexibility of photogrammetric methods and the abundance of free and low-cost commercial software make it an attractive option, on the other hand there is currently a lack of standardisation in data acquisition protocols, eventually leading to results that are not always sufficient to provide reliable metrical data. Although photogrammetry can produce visually impressive outcomes suitable for documentation and illustrative purposes, it is crucial to exercise caution when considering analytical needs. The accuracy and resolution of photogrammetric data depend heavily on the collection and processing strategy, which can affect the type of analysis that can be performed. Precise planning of acquisition and processing is crucial for accurate results. Despite its potential, many studies on archaeological stone tools present analyses with little detail on the photogrammetric setup, data acquisition, and processing strategies.

In this study, 3D technology was employed for both qualitative and quantitative evaluations of archaeological and experimental GSTs, serving multiple purposes: i) documentation, replacing drawings and single pictures; ii) evaluation of stone geometry and morphological characteristics, including measurements of height, width, thickness, surface area, and volume. It also supports the extraction of cross sections to assess use-surface shape; iii) for experimental tools, quantification of surface depletion at different stages of replicative use to be used as a proxy for evaluating the geometry of archaeological GSTs. Furthermore, the utilisation of 3D models has proven to be a valuable support in contextualising wear patterns, defining their orientation and assessing their spatial distribution on the tool's surface. This was tested at the outset of the study by the writer, using previously acquired

dataset to reconstruct the 3D model of the limestone passive tool from the Crimean site of Surein I, and published in Longo et al. 2021b. In this perspective, application of 3D modelling techniques provided valuable insights into the relationship between wear patterns, spatial distribution and tool functionality. In a broader sense this macroscale evaluation also supports the kinetics and gesture evaluation.

Initially, photogrammetric techniques based on Structure-from-Motion (SfM) and Multi-View Stereo reconstruction were planned for both archaeological and experimental tools to have comparable data. However, due to safety reasons, it was not possible to access the Moldovan museum and perform the acquisition. Therefore, the analysis of the archaeological materials was conducted on a sample of the selected GSTs using previously acquired 3D models obtained with the handheld 3D scanner based on light technology, Artec3D Space Spider (Longo et al. 2021a). Unfortunately, the resolution of the model was not sufficient to support textural evaluation, and the 3D data were solely utilised to provide a visualisation of the object's geometry and morphometric parameters. Instead, the geometry of the experimental tools was acquired with the photogrammetric technique at various stages of replicative use. Different acquisition setups and elaboration strategies were explored. A critical evaluation of potential sources of bias in data collection and subsequent elaboration were performed, and the methodology was accordingly adjusted thereby enhancing the reliability and validity of the outcome. The results, which are presented in Chapter 6, brought also to the publication of the paper Sorrentino et al. 2023b.

3.3.2.   Micro scale

3.3.2.1. Molds

In order to perform traceological analysis, negative replicas of the GSTs surface texture were created using a high-definition vinylpolysiloxane (or PVS) molding compound (e.g., Longo 1994; Longo et al. 2018, 2021a, 2021b, 2022; Ollé and Vergès 2014; Goodall et al. 2015; Pedergnana and Ollé 2017; Hayes et al. 2018; Macdonald et al. 2018; Zupancich et al. 2019; Cristiani and Zupancich 2020; Sorrentino et al. 2021a, 2021b; 2023a). In this study, molds were taken on representative areas of the archaeological tools to avoid excessive invasiveness caused by the greasiness that PVS material leaves on the stone surface, difficult to be removed. This selective approach allowed for the molding of sample areas on both the used and unused surfaces of the archaeological tools. On the other hand, for the experimental

tools, the analysis encompassed the entire used surface as well as a selected sample area of the unused surface. This approach allowed for a comprehensive examination of the textural features and wear patterns across the entire tool surface. By considering the all surface without preconceived notions or biases, a more accurate assessment of the tool's characteristics could be achieved (for discussion see Van Gijn 2014). This approach provided valuable comparative data for the analysis. Moreover, the utilisation of monochromatic molds facilitates the examination of stone surface topography, enhancing contrast due to morphological characteristics without the misleading effect of colour variations commonly found in stones composed of different minerals. Furthermore, when observed under microscopes, there is reduced light reflection due to the absence of crystal reflectivity.

The decision to employ molds for traceological analysis was driven by four main factors:

- The studied archaeological GSTs cannot be transported to the analytical facility, and the necessary equipment could not be taken to the museum storage room. Therefore, the prudent choice was to create replicas of the items' surfaces;

- Analysing large samples under the microscope objective can be challenging due to the structural characteristics of most microscopes. Moreover, the original size of the stones may not align with the SEM chamber dimensions. Additionally, some samples, such as pestles with typically convex active surfaces, are prone to movement during analysis. In contrast, molds offer advantages, including reduced natural glare and improved colour homogeneity compared to stone surfaces, thereby enhancing the emphasis on textural surface characteristics.

- To ensure data comparability with the archaeological specimens molds were also obtained from replicative tools;

- Molds of the reference collection were taken to establish a permanent comparative reference collection of use-wear traces at different stages of wear development.

The selected molding compound was Provil® Novo L (Hereutz – Kulzer), primarily designed for dental applications because of its ability to create accurate imprints of cavities, crevices, scarring, and undercuts. The two-component compound is supplied in a cartridge, enabling the user to mix and apply the paste at a 1:1 ratio for 1.5 to 2 minutes before the

polymerisation process begins. Once applied to the stone surface, the mold can be easily peeled off the stone surface. The PVS exhibits excellent long lasting dimensional stability, with a deformation under pressure of 3.1% and elastic recovery after deformation of 99.7%, and minimal distortion (linear shrinkage = -0.2%) (Kulzer 2021).

However, the accuracy of the impressions may be limited by the intrinsic texture of the mold material, resulting in a general smoothing of the original surface texture (Goodall et al. 2015; Macdonald et al. 2018; Delgado-Raack et al. 2022). Additionally, the molding process may trap air into the paste, creating circular smooth craters that are easily identified at all scales and techniques. Factors such as the roughness and humidity of the artefact's surface and environmental conditions like room temperature can influence this phenomenon. To mitigate this effect, it is recommended to choose a molding compound with a medium/slow setting time, control the temperature of the PVS material by refrigerating it to reduce the reticulation process time, and ensure that the stone surface is thoroughly dry (Sorrentino et al. 2023). Previous studies (Goodall et al. 2015; Macdonald et al. 2018) have also demonstrated that using a low viscosity compound results in higher level of accuracy in the replicated surfaces.

While the creation of positive copies (casts) from molds is a commonly used method in surface replication (e.g., Longo 1994; Bienenfeld 1995; Banks and Kay 2003; Ollé and Vergès 2014; Pedergnana and Ollé 2017), the inherent linear distortion of PVS, although limited, and the aforementioned challenges, prompted the decision to refrain from using this procedure in order to avoid introducing additional errors and surface feature approximation into the replicated surfaces. Instead, by utilising negative copies, a higher degree of accuracy was achieved in replicating the surface features, taking into account all aspects in reverse, as molds represent the negative reproduction of the surface.

3.3.2.2. Microscopies

As emphasised by Bamforth, the identification and recognition of use-wear patterns depend on both the availability of a reference collection and the ability to effectively highlight relevant features (Bamforth 2010). Different types of use-wear require the application of specific equipment and analytical techniques for their study. By utilising different equipment and techniques, researchers can enhance their ability to accurately identify and interpret different types of wear. Moreover, as recently demonstrated by Calandra and colleagues (Calandra et al. 2019a) not only the equipment, but also its specific settings are determining.

In the absence of a standardised approach for the optimal visualisation of use-wear traces, it is important to provide thorough documentation of the methods and settings employed to meet *preproducibility* criteria, as recommended by Stark (Stark 2018). To address the potential bias introduced by unintentional feature selection, this study utilised multiple instruments considering different magnification and resolution capacity (Table 3.2). By employing a diverse range of instrumentation, the author aimed to mitigate the limitations associated with the selective disclosure of features and enhance the overall reliability of the findings.

In particular molds were first observed with the Leica S9i stereomicroscope, available at the Physics Department of the University of Turin. The instrument is equipped with a LED light ring for vertical illumination and an integrated 10 MP CMOS camera. The magnification ranges from 12× to 110× (10× eyepieces, 2× lens) and a 9:1 zoom. The maximum resolution is 500 lp/mm.

In a second instance molds were investigated with the Olympus BX51 reflected light optical microscope available at the laboratory of the Centro Conservazione e Restauro "La Venaria Reale" (Turin, Italy). The microscopy employs vertical incident light and both dark and light fields, and is equipped with an integrated camera. The magnifications employed were 40×, 100×, and 500× (10× eyepieces) with a polarising filter for the 100× lens. Due to the limited DOF of this equipment and the highly rugged samples surface, capturing a fully focused image required a time-consuming process of data acquisition and post-processing. This involved capturing multiple images of the same area of interest with different focal planes. These images were then combined using the Stack Focuser plugin in the open-source software ImageJ, following a procedure developed based on the principles outlined by Plisson and Lompré (Plisson and Lompré 2008). This stacking technique enabled the creation of a final composite image that may be fully focused, depending on the number of the acquired images.

In the case of the experimental tools, direct observation of the stones surface was also possible thanks to the use of a portable digital microscope Dino-Lite Pro AM413ZTA. The microscope has a 1.3-megapixel sensor, illumination with eight white LEDs, light polariser, and magnification range of 10×, ~50× and 220×.

To determine the lithological type of the stones two samples collected from archaeological GSTs and several experimental samples were selected. Thin sections were prepared from these samples, which were then observed and characterised using the Olympus BX41 optical microscope available at the Department of Earth Sciences of the

University of Turin. The microscope was equipped with transmitted light, polarisers, and phase contrast techniques to enhance the visibility and characterization of the thin sections.

Table 3. 2. Specification for all the employed optical microscopes use in this research. NA = numerical aperture; WD = working distance; FOV = field of view; FN = field number (in case of Leica S9 and Olympus DSX1000, the FN is calculated as: FOV * objective lens magnification); DOF = depth of field. All the parameters are expressed in mm except NA that is unitless.

Microscope	Objective magnification	NA	WD	FOV	FN	DOF
Dino-Lite Pro AM413ZTA	30×	-	21	13 × 10.4	-	1.9
	50×	-	1.9	7.8 × 6.4	-	0.88
	220×	-	Touch	2 × 1.6	-	0.2
Leica S9i	0.6-5.5×	0.167	122	37.6	22.56-206.8	12
Olympus BX41	1.25×	0.04	3.5	17.6	22	0.17188
	4×	0.10	18.5	5.5	22	0.0275
	10×	0.25	10.6	2.2	22	0.0044
	20×	0.40	1.2	1.1	22	0.00172
Olympus BX51	4×	0.10	18.5	5.5	22	0.0275
	10×	0.30	10	2.65	26.5	0.00306
	50×	0.5	10.6	0.53	26.5	0.0011
Olympus DSX1000	XLOB10X: 140×-1400×	0.30	30.0	0.27-2.74	37.8-3836	-

The field of traceology has been characterised since its inception (e.g., Semenov 1964; Tringham et al. 1974; Odell 1977; Hayden 1979; Keeley 1980) by a division between proponents of the low-power approach and advocates of the high-power approach. The low-power approach involves the use of stereomicroscopes and angled light, while the high-power approach utilises metallographic microscopes with incident light and magnification exceeding 200× (for an overview of the discipline's history and main improvement see Longo and Skakun 2008; Van Gijn 2014; Stemp et al. 2016, and literature herein). Traditionally, the examination of GSTs using microscopy involved the use of stereomicroscopes with magnifications up to 80×, while optical microscopes with magnifications ranging from 50× to 500× were commonly employed for focused examination of polish features. However, in the last decade, there has been an increasing trend towards the combined use of both approaches (e.g., Adams 2002a, 2002b, 2010; Dubreuil 2004; Hamon 2008; Bofill et al. 2013; Dubreuil and Savage 2014; Dubreuil et al. 2015; Hayes et al. 2017, 2018, 2022; Caricola et al. 2018; Cristiani and Zupanchic 2020; Longo et al. 2021b, 2022; Paixão et al. 2021, 2022;

Sorrentino et al. 2021a, 2021b, 2023a). It is clear that in this study the wear-trace analysis took the advantage of both low-power and high-power approaches. Optical microscopy is not only valuable for observing polish but also for providing detailed information about the type of traces and specific morphological characteristics, while stereomicroscope is providing an overview of the present features, their density, spatial distribution and orientation. Therefore, the combination of both stereomicroscopy and optical microscopy allows for a more comprehensive analysis of GSTs, enabling researchers to examine and describe various aspects of surface features. Table 3.3 specifies the features that pertain to the use phase of the life history of a GST, which have been analysed by different scholars using both low and high-power microscopy approaches.

Table 3. 3. An overview of the different features observed at both low and high magnification by various authors. The focus is on the use phase of a GST's life history. The table underscores the diversity of focus among different authors, while also noting the presence of terminological discrepancies for certain features.

Features	Visible at low magnification according to:	Visible at high magnification according to:
Topography	Adams 2010; Dubreuil and Savage 2014; Dubreuil et al. 2015; Caricola et al. 2018; Zupanchic et al. 2018; Cristiani and Zupanchic 2020	
Surface levelling	Adams 2010 (**levelled area**); Bofill et al. 2013; Hayes et al. 2017, 2018	
Microtopography	Hamon 2008; Adams 2010; Caricola et al. 2018; Zupanchic et al. 2018;	Dubreuil and Savage 2014; Dubreuil et al. 2015 (**microrelief**)
Intergranular space	Hamon 2008; Adams 2002a: 36; Adams 2010; Zupanchic et al. 2018; Cristiani and Zupanchic 2020	
Trace, shape and/or change on individual grain	Adams 2002a:35, 2002b, 2010; Hamon 2008; Dubreuil and Savage 2014; Dubreuil et al. 2015; Hayes et al. 2017, 2018; Caricola et al. 2018; Cristiani and Zupanchic 2020	Dubreuil and Savage 2014; Dubreuil et al. 2015; Hayes et al. 2017, 2018 (**fracturing and scarring**)
Surface reflectivity	Dubreuil et al. 2015; Dubreuil and Savage 2014	

Abraded areas or abrasion		Dubreuil et al. 2015; Zupanchic et al. 2018; Cristiani and Zupanchic 2020
Linear trace or striation	Adams 2002a: 35, 2002b, 2010; Bofill et al. 2013; Dubreuil and Savage 2014; Dubreuil et al. 2015; Hayes et al. 2017, 2018; Caricola et al. 2018; Zupanchic et al. 2018; Cristiani and Zupanchic 2020 (**macro striation**)	Dubreuil and Savage 2014; Dubreuil et al. 2015; Hayes et al. 2017, 2018 (**micro-striation**); Caricola et al. 2018 (**micro-striation**); Zupanchic et al. 2018 (**micro striation**); Cristiani and Zupanchic 2020 (**micro striation**)
Polish or sheen	Adams 2010; Bofill et al. 2013	Bofill et al. 2013; Dubreuil and Savage 2014; Dubreuil et al. 2015; Hayes et al. 2017; Caricola et al. 2018 (**micro-polish);** Zupanchic et al. 2018; Cristiani and Zupanchic 2020 (**micro polish**)
Impact fracture	Adams 2010	
Cracks	Adams 2002b	
Step fractures	Adams 2002b	
Pit	Adams 2002b; Caricola et al. 2018; Zupanchic et al. 2018; Cristiani and Zupanchic 2020 (**pitting**)	
Fracture	Caricola et al. 2018	

3.3.3.   Micro to sub-micro scales

3.3.3.1. 3D digital microscope

In this study, a 3D digital microscope, the Olympus DSX1000, was also utilised (see Table 3.2 for detail). The microscope was made available to the laboratory of the Centro Conservazione e Restauro "La Venaria Reale" (Turin, Italy) through a temporary permission granted by Olympus Italia Srl. However, due to limited time and access to this equipment, priority was given to the analysis of the archaeological samples. This type of equipment is an effective solution to address the challenges posed by the low vs high power approaches as they typically offer a wide range of magnification options (e.g., Hirox KH-8700 used by the author in previous project, has a magnification range from 18× to 2500×; for detail see Longo et al. 2021b). By employing a 3D digital microscope, several issues commonly

encountered with traditional OMs can be resolved. One significant challenge in analysing large items like GSTs using traditional OMs is the limitation imposed by their WD and structural design, which are primarily optimised for thin samples such as slides. In contrast, digital microscopes, with their adjustable and tiltable stands, it allows to accommodate large samples. Also, the optical head can be optimally oriented relative to the stone surface, facilitating multi-angle observation of large implements, utilising not only zenithal light but also other lighting angles to enhance specific features. Furthermore, digital microscopes commonly feature mechanical stages that enable sample movements and rotations, facilitating inspections without the need for manual adjustments and item manipulations. To address the limited FOV inherent in traditional OMs, digital microscopes offer the capability to create image mosaics through a small motorised console. This feature greatly simplifies the images stitching process, allowing for a broader view of the sample and even enhancing the capacity of the stereomicroscope. Another notable advantage of digital microscopes is their ability to overcome the limited DOF of traditional optical microscopes, particularly when examining surfaces with uneven textures. Digital microscopes achieve this by capturing a series of images at different focal planes and automatically combining them to generate a fully focused image. This feature allows for the visualisation of the fine topography of the item at various magnifications, enhancing the analysis and providing valuable insights. Additionally, it provided the reconstruction of the area's 3D model, further enhancing the understanding of the surface topography.

3.3.3.2. Scanning electron microscopy (SEM)

SEM, along with other techniques capable of reaching sub-micro or nanoscales, has traditionally been employed in lithic studies for small sample sizes or specific research questions, mainly due to limitations in time and budget. As a result, SEM is more commonly used in the examination of flake, flint, quartz, and bone tools (e.g., Stemp et al. 2016, and literature cited within). In contrast, its application in GSTs trace morphological analysis is relatively rare (e.g., Dubreuil 2004; Dubreuil and Grosman 2009; Longo et al. 2018, 2021b; Sorrentino et al. 2023a).

The SEM technique offers several advantages, including the capability to achieve very high magnification. Moreover, it allowed the acquisition of both low and high magnification images for a detailed inspection of surface features at increasing levels.

Unlike light microscopes, SEM, thanks to the electron beams, have a wider depth of field: at the same NA of the final lens, the same DOF can be reach lowering the magnification and the WD, while with a smaller NA a longer WD and lowering the magnification it is possible to increase the DOP facilitating the acquisition of fully focused images that do not need any post-processing (Borel et al. 2014). Additionally, SEM can capture images without interference from sample reflection or the properties of rock crystals, providing clear and accurate morphological information (Ollè and Vergés 2014). This can be useful for the identification of striations, which at OM can be confused with the linear patterns that is reflected by the interaction between lights and specific surface texture (Borel et al. 2014). Also, polished areas are well showed at SEM, as smooth darker areas. Moreover, SEM can also provide valuable insights into the elemental composition of the sample, enabling the detection of residues. Therefore, it is particularly useful for correlating traces and residues in archaeological studies.

However, one constraint of SEM is the limited space within the chamber, which can pose challenges when analysing larger items as GSTs. The employment of molds is a valid solution to this issue (Longo et al. 2020; 2021b).

In this study, SEM was implemented in systematic analysis of both archaeological and experimental tools collections, and used to examine the areas on the molds that were identified as significant during stereomicroscope analysis. In the case of the archaeological tools, attention was also given to residues presence on the surface. The ZEISS EVO60 EP available at the laboratory of the Centro Conservazione e Restauro "La Venaria Reale" (Turin, Italy) was employed in this study, and set in extended pressure mode, operating at 20 kV. Images were captured at magnifications ranging from 65× to 1000×, maintaining a WD of 8.5 or 10 mm and with a resolution of 3072×2304 pixels. The majority of the images were obtained using the secondary electron mode, which is suitable for inspecting the sample's topography. However, some images were acquired using the backscattered electron detector, as it provides information about the composition of the sample, particularly useful in case of residues presence. SEM allowed for the detailed investigation of the mold selected areas, providing valuable insights into the surface features, morphology, and eventual direct correlation with residues.

As already noticed by Borel and colleagues (Borel et al. 2014), the wider DOF of SEM can create the illusion that all the elements visible in the image are located at the same level of the sample's topography, therefore it is important to combine its information with data

acquired from light source microscopy. Additionally, the lower microtopography may appear brighter than higher, which is the opposite of what is typically naturally observed where darker areas represent a lower zone. However, in the present research, this particular characteristic of SEM proved to be extremely useful, since the analysis is performed on mold that are the negative copies of the surface features.

3.3.3.3. Confocal profilometer

Since the 1980s there have been various efforts to achieve an objective and quantitative description of lithic tools surface texture. These efforts involve the use of different techniques for the acquisition of 2D surface profile data or, more recently, 3D aerial data. These enable the creation of detailed topographic maps that capture surface features at the micro- to nano-scale. This development emerged from the need of objective descriptions that avoid subjective terms derived from optical observations and allow for comparisons among different studies. However, these attempts primarily focused on flint artefacts, and the application of these techniques to GSTs was limited. This limitation can be attributed to several factors. Firstly, there has been a relatively lesser emphasis on studying GSTs compared to flaked assemblages. Additionally, GSTs present unique challenges for this type of analysis. While flaked tools generally have a relatively uniform composition and exhibit limited variation in terms of raw materials, tasks, and textural characteristics within the same assemblage, GSTs present a high degree of variability in all these aspects. A GST is typically composed of rock that combines different minerals and exhibits diverse textural characteristics. Within a single GST assemblage, as well as when comparing different assemblages, there is significant variation in types of rocks used, petrographic compositions, texture, and tasks performed. This extensive diversity poses challenges in establishing direct comparisons across different GST samples. Moreover, the wide range of tasks performed using GSTs adds complexity to their surface analysis. Each specific activity leaves behind distinct textural changes on the tool's surface, and when considering tools used for the same task, the variation in lithic composition further leads to a diverse wear pattern (Delgado-Raack et al. 2022). This complexity is further compounded by the possibility of a single artefact being used for multiple concurrent or sequential tasks, resulting in a diverse array of trace types and patterns. Moreover, unlike flaked tools, which typically have a single primary working surface, GSTs can possess multiple working areas, each of them displaying varying levels of use intensity. This adds another layer of complexity to the study of GSTs and

necessitates careful consideration already during the planning phase of data acquisition for quantitative surface analysis.

In this study, the Leica DCM 3D dual-core 3D measuring microscope available in the MUSAM-Lab at the IMT School for Advanced Studies Lucca (Lucca, Italy) was chosen for its wide range of surface measurement capabilities, spanning from several millimetres to a few nanometres, for its capacity of analysing surfaces ranging from smooth to very rough, and its high measurement speed, a feature particularly advantageous when dealing with large sample collections. The Leica DCM 3D profiling systems can analyse the surface in both confocal and interferometry mode. The confocal objectives, with higher NA, enable the measurement of steep slopes up to a maximum local slope of 70 degrees (Table 3.4). In confocal mode, high-resolution measurements in the submicron lateral range and nanometres scale vertical resolution can be achieved. On the other hand, interferometry mode provides large fields of view combined with sub-nanometre Z resolution. Summarising, the confocal mode is suitable for very rough to smooth surfaces, while interferometry mode is more appropriate for the analysis of smooth surfaces (Leica Microsystems 2023).

Given the high variability in roughness, typical of a GST surface, the confocal mode was selected for analysing both the molds obtained from the archaeological tools and from the experimental tools at various stages of use, facilitating comparison. The confocal mode employs a non-contact scanning technique that focuses different wavelengths of light on each point of the surface. By selectively capturing the focused wavelengths and automatically eliminating out-of-focus informations, the microscope can reconstruct the 3D topography of the surface. This process leverages the understanding of the relationship between wavelength and focal point distance to accurately measure roughness heights and generate detailed surface maps (Bofill et al. 2013; Leica Microsystems 2023). The Leica DCM 3D is equipped with a passive vibration isolation base, ensuring equipment stability during measurements. The microscope is equipped with three magnification lenses: 10×, 20×, and 100× (detail in Table 3.4). For the specific research purposes the 10× and 20× objective lenses were mostly utilised.

Table 3. 4. Characteristics of the Leica DCM 3D objective lens 10×, 20×, and 100×.

Objective magnification	NA	FOV (μm)	Optical res. (X/Y) (μm)	Vertical res. (nm)
10×	0.30	1270×950	0.47	<30
20×	0.50	636.61×477.25	0.28	<15
100×	0.90	127×95	0.15	<3

Both microscopy images and topographic maps were acquired. The latter data were elaborated using the open-source software Gwyddion (Nečas and Klapetek 2010). Since the data were acquired from molds, which are the negative copies of the surface, the parameters were inverted and flipped along the x-axis prior to their analysis. This was done to replicate the analysis as if it were on the actual tool surface. Additionally, the average plane was subtracted to eliminate the influence of tool geometry and primary waviness, focusing solely on the surface roughness. Surface maps were then used to calculate sets of standard statistical parameters for profile and areal characterisation (e.g., Astruc et al. 2003; Stemp and Stemp 2003; Evans and Donahu 2008; Delgado-Raack et al. 2009, 2022; Bofill 2012; Bofill et al. 2013; Evans et al. 2014; Stemp 2014; Stemp et al. 2016; Calandra et al. 2019a, 2019b; Caricola et al. 2018; Macdonald et al. 2019; Zupancich and Cristiani 2020; Paixão et al. 2021, 2022; Sorrentino et al. 2023a). In particular in this study the Surface Heights Distribution and the ISO 25178-2 surface texture areal parameters (Table 3.5) were computed.

Table 3. 5. ISO 25178-2 surface texture areal parameters

Sa	Arithmetical mean height of the surface
Sq	Root means square height of the surface
Ssk	Skewness of height distribution
Sku	Kurtosis of height distribution
Sp	Maximum height of peaks
Sv	Maximum height of valleys
Sz	Maximum height of the surface

The **Surface Heights Distribution** can be visualised as a histogram, which shows how many points on the surface have a given height value. This histogram helps to quantify the statistical features of the surface elevations (Blateryron 2013).

The roughness of the surface can be described by the two parameters, Sa and Sq. The **Root Mean Square Roughness** (Sq) provides information on the standard deviation of the surface heights' distribution with respect to the average plane. On the other hand, the

Arithmetical Mean Height (Sa) of the surface expresses the difference in height of each point compared to the average of the surface as an absolute value. The two parameters are related to each other, but Sq is considered more statistically robust and of wide use in contact mechanics. The wear process primarily influences these two parameters, through a modification over time, with surfaces becoming smoother with the depletion of the asperity tips. Conversely, the observation of an increase in Sa and Sq could indicate localised fracture events that expose new rough surfaces of the brittle stone, which are usually rougher than worn asperities (Blateryron 2013; Calandra et al. 2019a; Keyence 2023). Additionally, comparing the time evolution of Sa and Sq for different stones provides information on their wear resistance (Sorrentino et al. 2023a).

The **Skewness** (Ssk) parameter is used to describe the asymmetry of the shape of the height distribution curve. When the majority of the data are located to the right of the mean line and the tail of the graph extends to the left, the height distribution is considered negatively skewed (left-skewed). Conversely, when the bulk of the data are on the left and the tail extends to the right, it is considered positively skewed (right-skewed) (Figure 3.1). Summarising:

- Negatively skewed: Ssk < 0 indicates that there are more valleys or pores with different heights, while relatively few peaks exhibit limited altitude variability.

- Ssk = 0 ± 0.5 indicates a symmetrical distribution around the mean value (Gaussian distribution of the height), indicating a balance between peaks and valleys.

- Positively skewed: Ssk > 0 indicates that there are more peaks of different altitudes, while there are relatively few valleys with limited height variability.
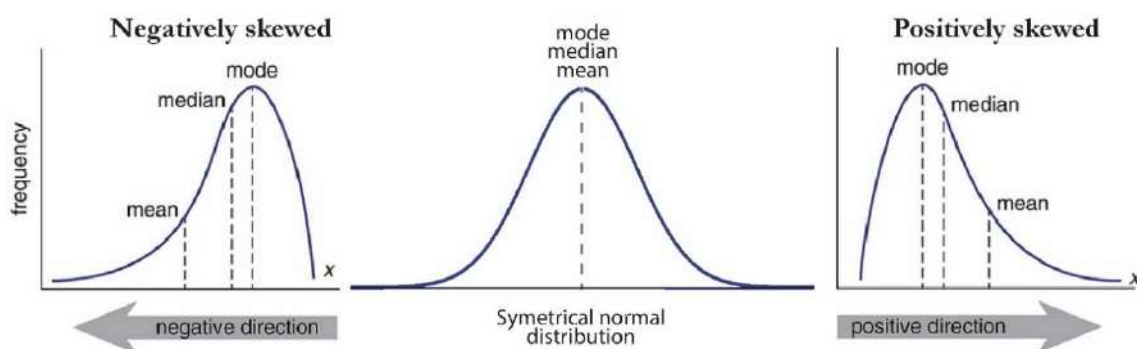
Figure 3. 1. Type of Skewness (modified from Sing 2021).

The degree of skewness is considered approximately symmetric when the Ssk value falls within the range of 0 ± 0.5. It is considered moderate when it ranges from -1 to -0.5 or from 0.5 to 1. Beyond ± 1, the skewness is considered high (Blateryron 2013; Sharma 2020; Sing 2021).

It is important to note that Ssk is strongly influenced by isolated peaks or valleys in the surface roughness profile (Blateryron 2013). Studies conducted on grinding wheels have shown that a combination of peaks and valleys in the surface topography leads to a Ssk value around 0. Grinding wheels with a higher density of abrasive grains tend to exhibit higher Ssk values compared to those with fewer abrasive grains or peaks, and after their utilisation are likely to have a more negative Ssk value (Denkena et al. 2023).

Kurtosis (Sku) is a parameter that measures the sharpness of the distribution and the fatness of the tails (Figure 3.2):

- Sku > 3 named leptokurtic distribution: have a spiky distribution, heavy and long tails representing a higher number of extreme values or outliers;
- Sku = 3 named mesokurtic distribution: is a normal gaussian distribution;
- Sku < 3 named platykurtic distribution: have a dulled height distribution and light and short tails presenting a few extreme values (outliers).

It has been demonstrated that outliers influence the kurtosis value more than the values near the mean (Blateryron 2013; Sharma 2020; Sing 2021; Keyence 2023).

Bofill and colleagues (Bofill et al. 2013) noticed that when kurtosis value is higher than 3 it reflects the formation of surface flattening.
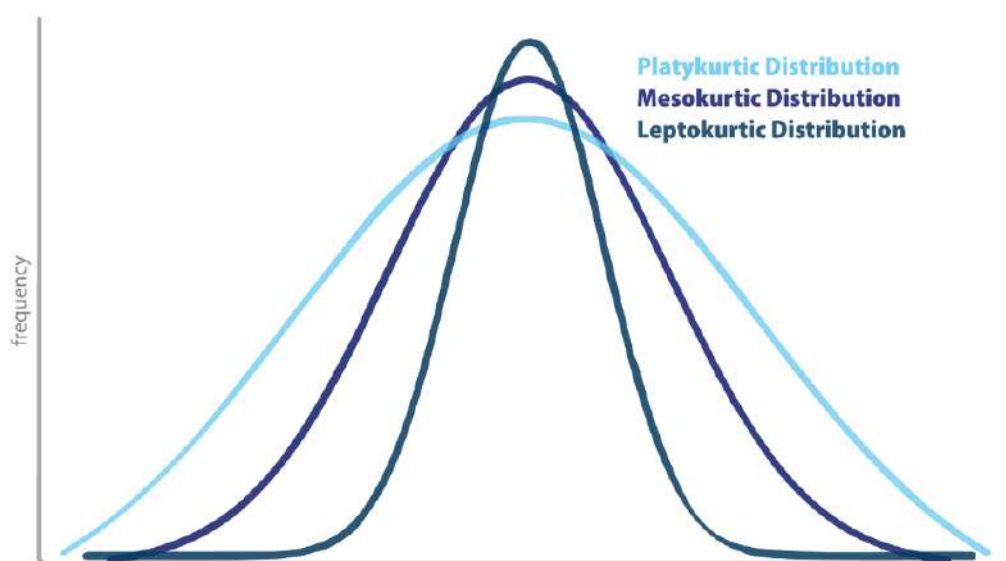
Figure 3. 2. Kurtosis distribution.

It is also important to note that Ssk and Sku parameters may be less mathematically stable than other parameters because they involve higher-order powers in their equations, leading to faster error propagation (Blateryron 2013; Denkena et al. 2023).

The **Maximum Peak Height** (Sp) parameter indicates the height of the highest peak within the analysed area, while the **Maximum Pit Height** (Sv) represents the absolute value of the height of the lowest pit. The **Maximum Height of the Surface** (Sz) parameter is the sum of the absolute values of Sp and Sv, therefore representing the maximum surface amplitude (Blateryron 2013; Keyence 2023).

4. Brînzeni I archaeological site and the recovered Ground Stone Tools

4.1. Brînzeni I archaeological site

The Eurasian Steppe Belt is a vast territory that stretches from the Carpathians to the Urals to the Altai Mountains, extending from the northern Black Sea beaches to the Caspian Sea (Birarda et al. 2020). During the Middle Pleniglacial, Anatomically Modern Humans (AMH) made their appearance in this region prior to 40 cal ka. The predominant biome during the cold phase of MIS 3 (39-36 kya) consisted mainly of grasslands and evergreen taiga, with patches of deciduous forest. The southwestern territories of the East European Plain, including Moldova, were located on the peripheral areas of the harsher climatic conditions, which affected the northeastern latitudes and areas with permafrost (on the broad topic see e.g., Sirenko et al. 1990; Hoffecker 2009; Stepanchuk et al. 2009; Hardy 2010, and literature therein). In particular, the middle basin of the Pruth River was rich in resources, including caves and rock shelters, raw materials for tools production, animals and plants for sustenance. This area is characterised by many caves situated in adjacent river valleys, separated from each other by narrow karstic Sarmatian limestone ridges rising around 200 m in height, formed in Miocene times, and named Toltry. These caves became a favourable refuge for human settlement, as evidenced by the wealth of Upper Palaeolithic archaeological records (Allsworth-Jones et al. 2018a, 2018b).

Figure 4. 1. Brînzeni I cave located in N-W Moldova, in the Edinet region.

Brînzeni I, located within the Edinet district, is a cave situated near the summit of one of the aforementioned limestone ridges, rising 62 m above the eastern bank of the Racovăț River (Figure 4.1). Notably, the Racovăț River, a tributary of the Pruth River, flows directly beneath the cave. Additionally, the Dragiste River intake lies in close proximity to the cave, while the Pruth River is positioned approximately 8 km south of the site. Currently, the cave measures 9 × 18 m, with a height ranging from 0.5 to 4 m. However, it appears smaller compared to its ancient dimensions, as the dripline has receded over time.

The settlement was discovered in 1960 by V.N. Verina and N.A. Chetraru, who conducted two trial trenches in the same year. The excavation continued in the following years (1963-65, 1968, and 1975), always under the direction of N.A. Chetraru, uncovering an area of around 60 m². During these campaigns, the excavation was divided into a grid where each square was 1 m² and named with numbers and letters from the Cyrillic alphabet (Figure 4.2). A detailed documentation of the archaeological deposit and the findings was produced, including a plan that was updated every year (Figure 4.3).
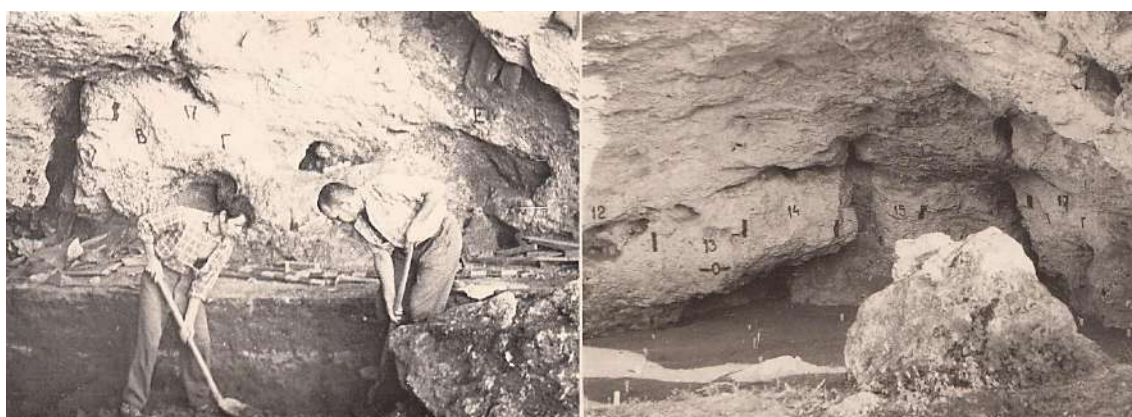
Figure 4. 2. Pictures of the Chetraru excavation in 1960 (courtesy of the National Museum of History of Moldova). The numbering-lettering system is visible on the cave wall.
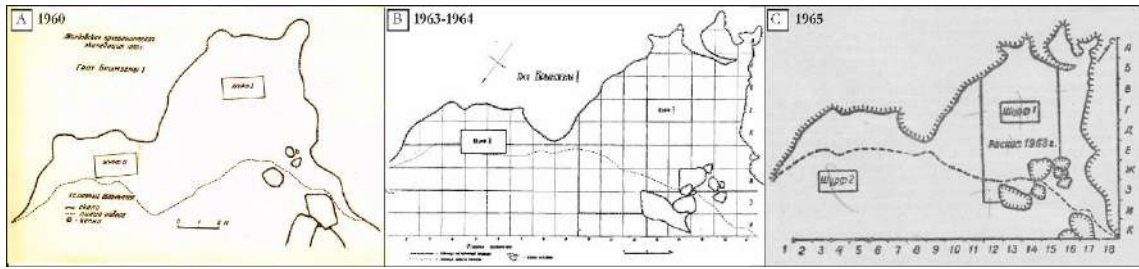
Figure 4. 3. Plans of Brînzeni I from various Chetraru excavation champaigns. A) plan drawn by Chetraru in 1960 (courtesy of the National Museum of History of Moldova); B) plan drawn by Chetraru after the 1963-1964 campaigns (Chetraru 1965b); C) plan drawn by Chetraru after the 1965 campaign (Chetraru 1965a).
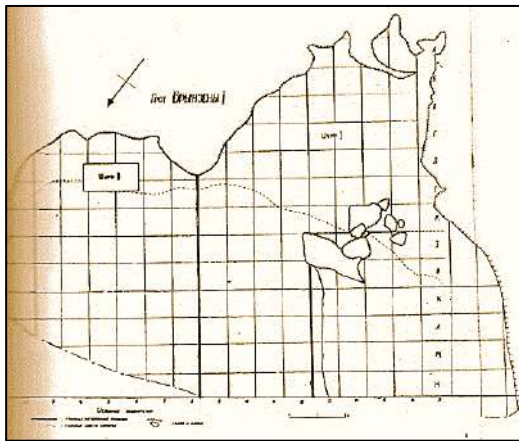
Figure 4. 4. Plan of Brînzeni I cave drown by Chetraru after the 1987 excavation (Borziac 1988)

In 1987, I.A. Borziac extended the excavation and uncovered an area of 22 m², including the terrace of the cave (Figure 4.4), and established the profile section along the 8-9 line. In 1992-1993, the site and the stratigraphy were re-examined by I.A. Borziac, S. Covalenco, and the Belgian expedition, to acquire samples for soil micromorphology study, palynological analysis, and radiocarbon dating (Allsworth-Jones et al. 2018a, 2018b; Noiret 2009).

In 2015, Burlaku and Vishnyatsky conducted a trial trench adjacent to the section established by Borziac; however, this survey was not further pursued (Covalenco personal communication; survey area reported in Figure 4.6).

In 1996, Chirica and colleagues (Chirica et al. 1996) presented a revised version of the Chetraru cave map, presenting a new lettering system, which utilised Latin letters. It is important to note that this new system was not a transliteration of the original Cyrillic lettering but rather a substitution of the lettering system with the Latin alphabet (Figure 4.5). However, this alteration in the lettering system gave rise to certain complexities in both the lettering-numbering system and the cataloguing of findings. As a result, the attribution of the Latin letters became ambiguous, leaving uncertainty as to whether they referred to the transliteration of the Cyrillic letters or were associated with the new lettering-numbering system. In 2018, Allsworth-Jones and colleagues (Allsworth-Jones et al. 2018a) recovered the original Cyrillic lettering-numbering system. Additionally, the drawing of the section established by Borziac shows discrepancies between the two versions. According to Chirica and colleagues the section spans from square Г to К (Chirica et al. 1996), while Allsworth-Jones and colleagues reports the sections from squares Д to Л (Allsworth-Jones et al. 2018a;

both versions are depicted in Figure 4.5). This difference may be due to the resemblance between the graphical symbols in Cyrillic and Latin, which do not always correspond to the same letter. The ambiguity, as discussed in the current study, presents a novel observation and warrants future attention and systematic revaluation. Here, the original Cyrillic reference system is used since most of the artefacts are also registered and catalogued accordingly.
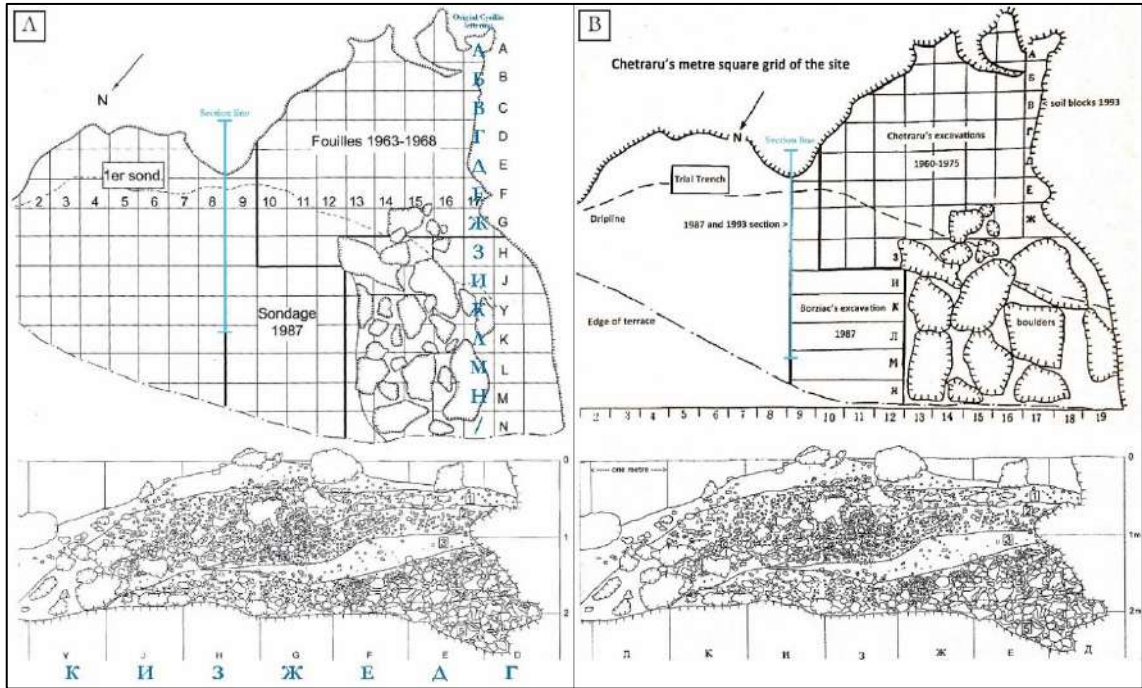
Figure 4. 5. Plans and sections of Brînzeni I cave. It can be observed that there is no correspondence between the Latin lettering and the original Cyrillic lettering (highlighted in dark blue). A) Plan and section modified after Chirica et al. 1996, presenting the Latin lettering system. B) Plan and section from Allsworth-Jones et al. 2018a, presenting the original Cyrillic lettering system.
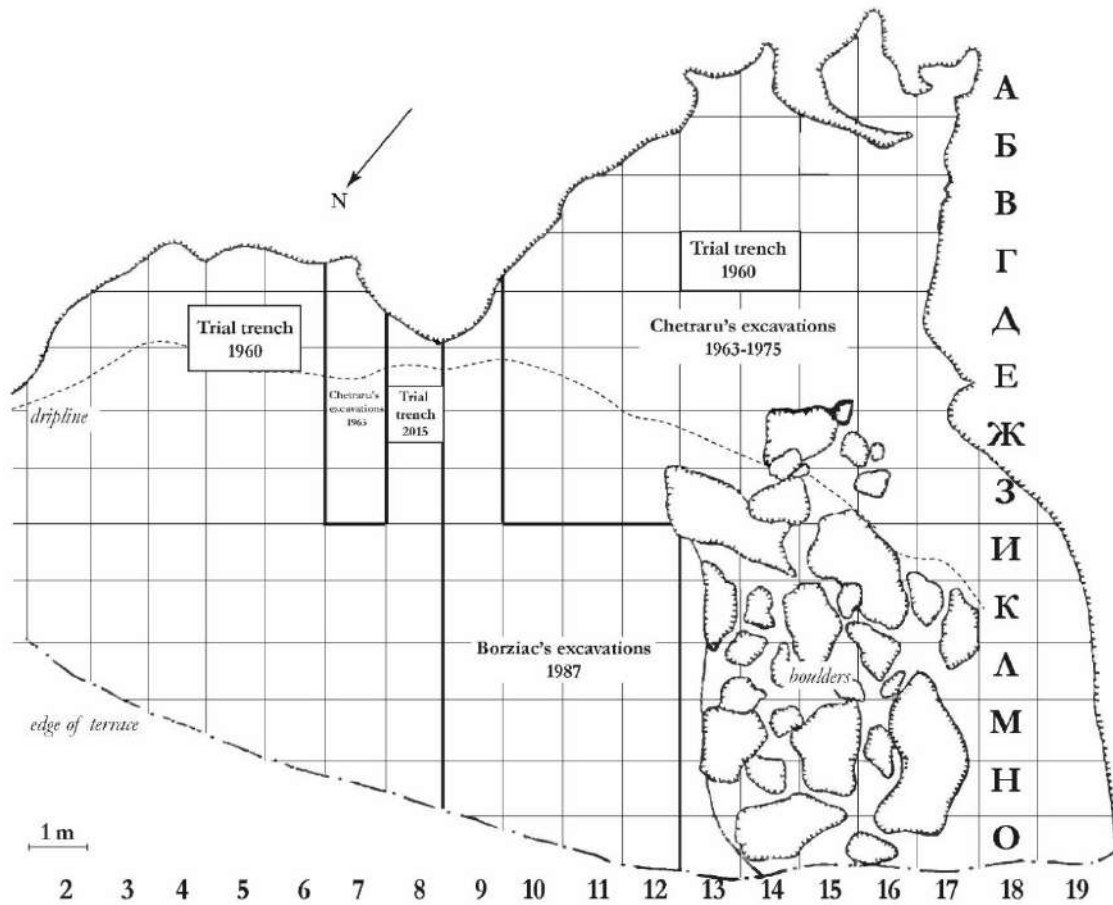
Figure 4. 6. Final plan of Brînzeni I cave, encompassing all excavation and trial trench data, including the 2015 survey. This representation has been adapted from Chirica et al. 1996 and aligned with Allsworth-Jones et al. 2018a, in addition to incorporating insights from communication with researchers from the National Museum of History of Moldova

From a stratigraphic perspective, archaeologists have distinguished five stratigraphic units, which have been attributed to three cultural layers based on the findings. However, there are different interpretations between Chetraru and Borziac regarding their attribution (Allsworth-Jones et al. 2018a). For this dissertation it is important that they agree on the fact that the oldest cultural layer, cultural layer III, has been attributed to an Upper Palaeolithic horizon.

At the base of this layer, a hearth surrounded by stones was uncovered in the central part of the cave (square 13Г), presenting an area of approximately 35-45 cm of burnt soil. Additionally, in other parts of the cave, ashes and burnt animal bones found in close association with flint tools may indicate the presence of other hearths.

A total of 7355 stone artefacts were found in this cultural layer, including 22 unworked nodules, 327 cores, 757 blades, 5160 flakes, 889 debris and ca. 200 retouched tools. The majority, 75% of them, are made of grey and black flint sourced from the Pruth River, while a few quartzite tools are known to originate from the northern area of the Pruth

basin. The retouched tools predominantly represent Upper Palaeolithic production (i.e., burins, end scrapers, side scrapers, bifacial leaf points, and blades). However, some Mousterian (Middle Palaeolithic) tools, such as Levallois points and blades, are also present (Otte et al. 1996; Noiret 2009; Allsworth-Jones et al 2018a).

Relevant to this study, 114 pebbles were also uncovered and classified as 28 quartzite and 86 sandstones, mostly flat slabs interpreted by the archaeologists, who did not study them extensively, as anvils for flint or bone working, or as grinders for the processing of vegetables. In addition to the stone artefacts, a few rare bone artefacts and artworks were discovered at the site, including a mammoth ivory pendant, three fragmented retouched tools made from horse bone, a perforated horse incisor, and a hare bone with polished ends (Chetraru 1970, 1989; Otte et al. 1996; Noiret 2009; David and Pascari 2012; Allsworth-Jones et al. 2018a; Carciumaru et al. 2019). However, these artefacts have not undergone microscopic analysis, and only the ivory pendant was subjected to a dedicated detailed analysis (Carciumaru et al. 2019). During the current research, this artefact underwent a preliminary microscopy survey, and also Raman measurements were performed, revealing the presence of incisions and traces of red ochre.

Based on the study of the artefacts, particularly the lithic assemblages, scholars have proposed different interpretations and attributions for this cultural layer. While an in-depth review of the ongoing debate is beyond the scope of this study, since the site serves primarily as a case study to test the methodological approach, some of the theories are briefly reported here.

In 1973, Chetraru defined Brînzeni cave as the eponymous site of the "Brînzeni culture", which is considered a transitional culture between the Mousterian and Aurignacian, sharing traits with both and with the parallel western Szeletian culture (Chetraru 1973). Borziac further developed this initial classification, and analysing the broader regional context proposed a scheme for the Early Upper Palaeolithic in the area, dividing it into two groups: the first represented by Brînzeni and the second by Gordinesti cave, layer 3 (excavated by Borziac between 1974 and 1976), identified as a new culture that he named the "Pruth culture" (Borziac 1984). The "Brînzeni culture" in this framework represents a transitional phase from the Mousterian to the Upper Palaeolithic (Otte et al. 1996; Borziac et al. 2006: 213-214). Grishchenko, who performed the geological evaluations of the stratigraphy in 1965, suggested that cultural layer III had a long formation period. Therefore, based on micromorphological analysis he suggested to divide cultural layer III into two stratigraphic

layers belonging respectively to the Upper Palaeolithic and to the Mousterian (Grishchenko 1969). However, both Chetraru and Borziac stated that the artefacts distribution within cultural layer III is homogeneous and belongs to one stratigraphic layer. Anikovich suggested the possibility of the occupation during the Stillfried B period based on the presence among the faunal remains of the arctic fox and collared lemming, which are indicators of a cold phase (Anikovich 1992). However, samples were collected for radiocarbon dating in 1993, and the dates obtained revealed a wide range of 12,000 years for cultural layer III, and indicating a substantially later time period than initially expected (see the table reported in Figure 4.7). This long interval seems to align with Grishchenko's analysis of the stratigraphy. Considering scientific dating, Noiret stated that Brînzeni is part of the "Pruth culture", which is identified in the region and extends east to the Carpathians between 30-26 ka (Noiret and Otte 2010). This timeframe aligns with the dating, and locates this Culture between the end of the Aurignacian to the earliest phase of the Gravettian. In this scenario, the early Aurignacian elements among the Brînzeni's tools might be the result of contact with neighbouring sites (Noiret 2009). In more recent years, Allsworth-Jones reviewed the context and concluded that Borziac's scheme is over-complicated, suggesting that in this area, there is a single Early Upper Palaeolithic entity. He also agreed that the range of 12,000 years (31,929-29,964 to 18,232-17,565) for this layer seems too broad. The radiocarbon calibrated dates are younger than what archaeologists supposed based on lithic assemblage analysis. But in light of results obtained elsewhere in the region, it is likely that if these samples or others from the site were re-dated using ultrafiltration, they might turn out to be several thousand years older than present estimates (Allsworth-Jones et al. 2018).

More recently, additional AMS radiocarbon dating on collagen from bone samples (Prof. L. Longo personal communication) suggests that the site can be attributable to the Upper Palaeolithic and to the early presence of *Homo sapiens* in the region.

Lab. No.	Sample	Calibrated date (cal BP)	
OxA-4118	Reindeer tooth	23,624–22,676	
OxA-4119	Horse tooth	27,366–26,230	
OxA-4120	Horse long bone	18,232–17,565	
OxA-4121	Horse long bone	27,179–26,085	Cave
OxA-4122	Reindeer long bone	31,292–29,964	chamber
OxA-4123	Horse tooth	20,445–19,616	
OxA-4124	Horse long bone	31,030–19,597	
OxA-4898	Horse mandible	24,843–23,721	Terrace
OxA-4899	Horse bone	24,425–23,140	
OxA-6999	Horse tooth	24,955–23,995	
OxA-7001	Bone	27,923–27,263	Unknown
Lv-2186	Bone	26,568–25,446	

Figure 4. 7. Brînzeni I plan (modified after Chirica et al. 1996 and according to Allsworth-Jones et al. 2018a version) with the location of the central hearth and the area of sample collection for radiocarbon dating, which are reported on the right (modified from Allsworth-Jones et al. 2018a).

4.2. The GSTs preliminary data acquisitions

This section provides a brief overview of the preliminary analysis conducted at the National Museum of History of Moldova in Chisinau before the beginning of this PhD study. It also outlines the criteria used for selecting the ground stone tools that were studied. Furthermore, the morphometric data and the petrographic analysis conducted in the preliminary stage of the current PhD research are presented here, while the detailed macro-scale analysis and trace study are discussed in Chapter 7.

The morphometric analysis carried out primarily on the 3D models allowed comprehensive exploration of the geometric characteristics of the stone tools. By examining various dimensions, shapes, and features of the tools' surfaces, valuable insights were gained into their potential functions and likely working areas. This analysis was instrumental in defining the basic characteristics to be considered during the selection of items for constructing the reference collection, ensuring that it encompassed a representative range of tool types and possible uses. Moreover, the petrographic analysis provided a deeper understanding of the stone's inherent properties and resistance to wear. By studying the mineral composition and microstructure of the lithic materials, the rocks' characteristics and variations that might have influenced their performance as tools were investigated. The addition of this knowledge proved to be essential in establishing a site-specific reference collection, detailed in Chapter 5, tailored to the archaeological context, and allowed for precise comparisons between wear traces found on the artefacts and experimental tools. In Chapter 7, the detailed wear analysis delves into the examination of patterns and features

observed on the stone tools' surfaces. To validate the findings and interpretations, wear patterns observed on the archaeological artefacts were compared with those produced on the experimental tools. By scrutinising and comparing wear patterns and other signs of tool use, combining them with the results of residue analysis, the aim was to elucidate the specific activities and functions these artefacts were involved in during their life. This comprehensive functional analysis allowed meaningful conclusions to be drawn about the tools' use-biography and the activities performed by the ancient inhabitants of the cave.

4.2.1.   Context and sampling

The 114 putative GSTs were retrieved during multiple excavation campaigns and categorised into 28 quartzite and 86 sandstone artefacts. However, prior to 2016, they had not undergone a detailed examination. Following their retrieval from the archaeological site, the artefacts were roughly washed in the Racovăț River below the cave and later stored in wooden boxes at the National Museum of History of Moldova in Chisinau. These artefacts remained untouched until the 2016-2017 survey conducted by Prof. Longo. This marked the dawn of their investigation aimed at assessing their potential past use as tools. Out of the large number of collected pebbles, 36 putative GSTs were selected by curators as the most promising candidates for further analysis (Longo et al. 2021a).

As described in Longo et al. 2022, the sample strategy was developed and continuously refined over the years through several sampling campaigns, with active participation from the writer of this dissertation. The implementation of this strategy began in the storage room of the museums. Prior to the analysis, the surfaces of the tables were covered with acetate or subjected to a bleaching process. This precautionary measure aimed to prevent contamination from the surrounding environment. Furthermore, the stones were handled with powder-free gloves to minimise the introduction of contaminants. Each stone was photographed and, in some cases, scanned with the handheld 3D light scanner Artec3D Space Spider. Subsequently, the stones were gently blown with a hairdryer to remove any dust or superficial contamination. The pebble surfaces were then surveyed with a stereomicroscope to identify potential areas of use. Many of the pebbles still retained sediment residues adhering to their surfaces, and in addition, a carbonatic crust was present in spots on most of the GSTs. From these areas, samples for starch analysis were collected by carefully removing samples of crust using a clean bistoury. Furthermore, fragments of

rocks, already detached from the surfaces, were collected for different types of analysis, and mainly petrographic characterisation.

The areas of the stones surface identified as potential use surface were sonicated, partially immersing the stones in an ultrasonic tank or pipetting distilled water directly on the surface, and then storing the liquid in vials with ethanol for further residues analysis.

Selected areas on the stone surface were replicated using Provil Novo molding compound. For each area, up to three successive molds were taken. The first two molds were specifically utilised for residues analysis, as they could capture remnants entrapped in the crevices of the stone. The third mold was allocated for trace analysis. These selected areas were strategically chosen for molding to cross-check potential use areas and distinguish possible unused regions. To ensure procedural tracking, the molds were photographed, meticulously numbered, and securely stored in zip bags, ready for subsequent examination of residues and traces (Longo et al 2022).

The current dissertation focuses on 10 GSTs samples primarily selected from the cave chamber, and therefore retrieved during Chetraru excavations, with priority given to the ones found in proximity of hearths (Figure 4.8). These tools are more likely to be associated with plant processing for alimentary purposes. For each item different areas were analysed, distributed on different faces of the lithic tools. A total of 14 putative working surfaces were investigated.

The initial effort was to recover the general information and identify the provenance of each item, considering the uncertainty arising from the transliteration between Cyrillic and Latin letters.
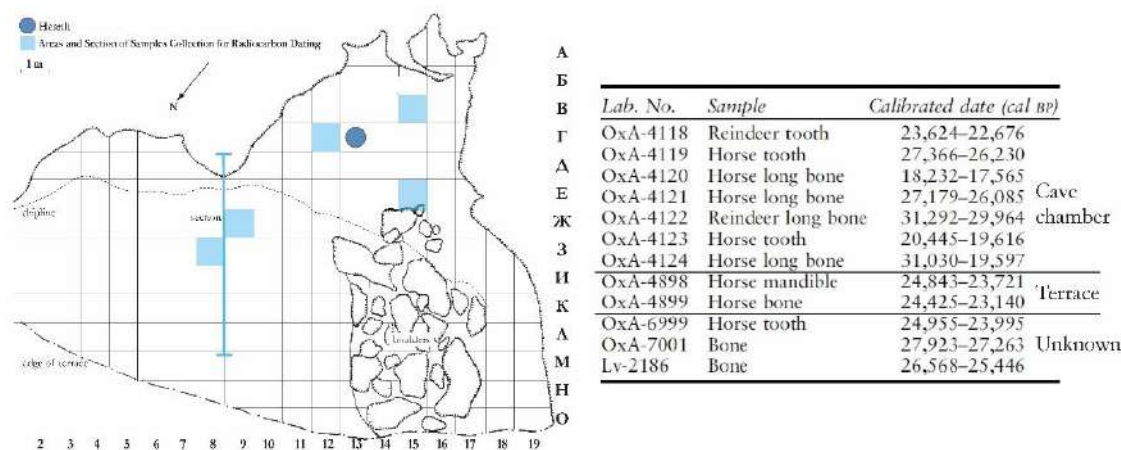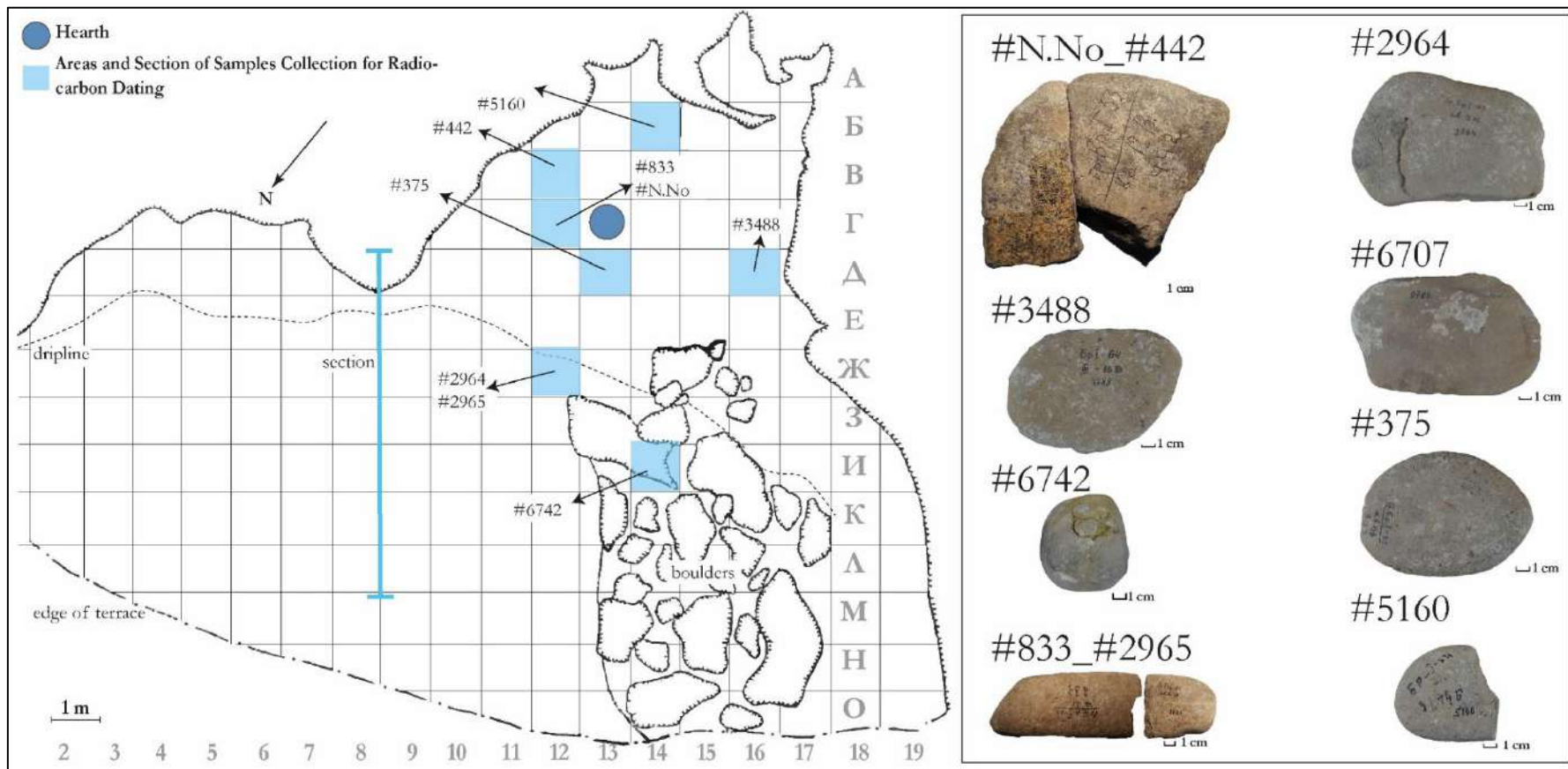
Figure 4. 8. Brînzeni I plan (modified after Chirica et al. 1996 and according to Allsworth-Jones et al. 2018a version), showing the positions of the 10 GSTs analysed in this study. The provenance of BZ#6707 remains unknown. The scale bar for the GSTs is 1 cm, and the tools are displayed in relative proportion to each other.

It is worth noting that during the preliminary analysis conducted at the museum as part of Prof. Longo's sampling campaign in 2016-2017, fragments BZ#442 and BZ#N.No. were found to be refitted as components of the same broken and incomplete tool, despite being retrieved from different squares. Additionally, fragments BZ#833 and BZ#2965 were also refitted as belonging to the same tool, which is now completed except for small missing fragments (Longo et al. 2021a).

4.2.2.   Petrographic analysis

Since the formation of traces on ground stone tools is highly influenced by the raw materials used, the petrography of the stones was carefully considered before analysing the traces and their formation process. This information played a crucial role in selecting the stones to construct the experimental reference collection, as explained in Chapter 5. Due to the limited availability of rock samples from the archaeological tools (due to clear conservative restrictions), the study commenced with an analysis of the geological characteristics of the Edinet district and the regions surrounding the Pruth and Racovăţ Rivers. The geological map of Moldova indicates that the area is characterised by a uniform geological setting, primarily composed of sandstone and limestone formations from the Miocene and lower Pliocene age, with Badenian and Sarmatian stage formations as the closest to the archaeological site (Геологическая карта Молдовы Молдавской; Kováč et al. 2007; Revenco et al. 2016) (Figure 4.9).
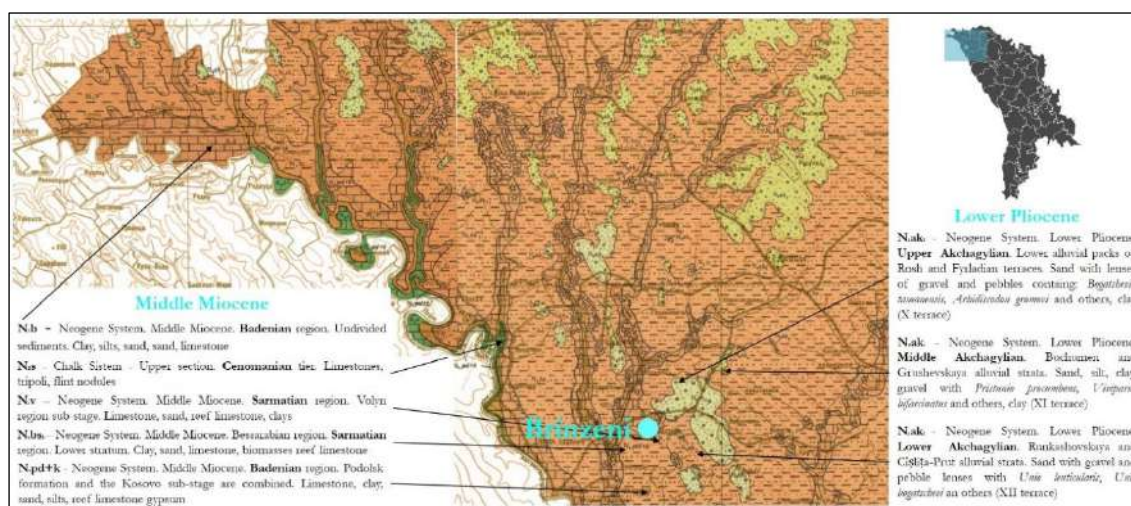
Figure 4. 9. Extract from the geological map of Moldova (Геологическая карта Молдовы Молдавской)

Among the fragments already detached from the GSTs and collected during the 2017 survey, there was a fragment from the pebble BZ#6742. This fragment was used for

petrographic analysis, which was conducted through thin-sections, observed with the Olympus BX41 optical microscope in transmitted light. The microscope is equipped with phase contrast and polarised light, and was used primarily at 40× (Figure 4.10). The sample was classified as quartz-arenite, a sedimentary rock of terrigenous origin. It exhibited homogeneous grains with an average size ranging between 100 μm and 500 μm and consisted of sub-spherical, rounded quartz and quartzite clasts. This sandstone was mostly monomineralic and likely formed by the erosion of granite or granitoid rocks. Additionally, some monocrystalline aggregates of quartz resulting from the dismantling of metamorphic basement rocks were also present. Rare occurrences of carbonates, amphiboles, feldspars, iron oxides, glauconite, and very rare white mica were also detected. The matrix constituted approximately 5% of the rock, and the cement, consisting of calcium carbonate, was less than 5%. The porosity was measured at around 10-15%, and it could be classified as closed, with individual pores not interconnected. This quartz-arenite is hard but also brittle rock, and its closed porosity makes it impermeable. To validate the classification, SEM-EDS analysis was also conducted on a polished sample, coated with a layer of carbon of 15.0 nm thickness and a density of 2.25 g/cm^3. The analysis revealed a composition of more than 99% silicon (Si) and traces of iron (Fe), which was consistent with the previous attribution of the sample to quartz-arenite (Figure 4.10) (Sorrentino et al. 2023a).
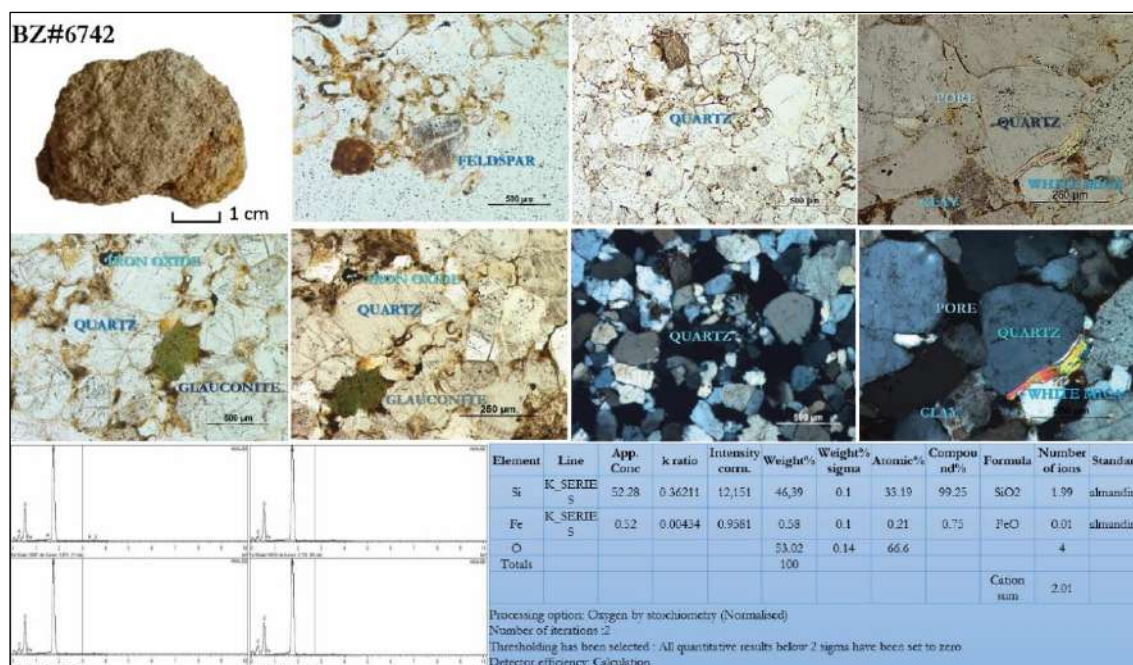
Figure 4. 10. Representative microstructures and mineral assemblages of the quartz-arenite from the archaeological sample BZ#6742 in transmitted and polarising light, as well as SEM-EDS analysis (modified from Sorrentino et al. 2023a)

A second sample, a small fragment originating from the surface of tool BZ#442, was also subjected to SEM-EDS analysis as it was too small for thin-section. Additionally, this sample was included in a selection of samples that underwent µCT analysis using synchrotron light at the Elettra Synchrotron in Trieste, following a competitive evaluation (Proposal number: 20215734 at SYRMEP beamline, proposers: L. Longo, A. Re; participants: G. Sorrentino, L. Vigorelli). The analysis revealed a composition and structure consistent with a calcarenite, a sedimentary rock mainly composed of calcite with traces of manganese (Mn). It exhibited a fine-grained carbonatic matrix, with presence of clay and very fine-grained quartz (Figure 4.11). The sample displayed a high porosity and distinctive tubular voids typical of bioturbation, which affected the carbonatic matrix. Foraminifera were also observed through the µCT analysis (Figure 4.12). According to this data, the rock is soft and prone to react with acidic substances, making it unsuitable for heavy tasks, which aligns with the fact that the GST is broken into several fragments, with only two recognised and refitted. Based on the preliminary evaluation by the curator, it may be a sandstone belonging to the Badenian stage formation (Middle Miocene, see Figure 4.9).
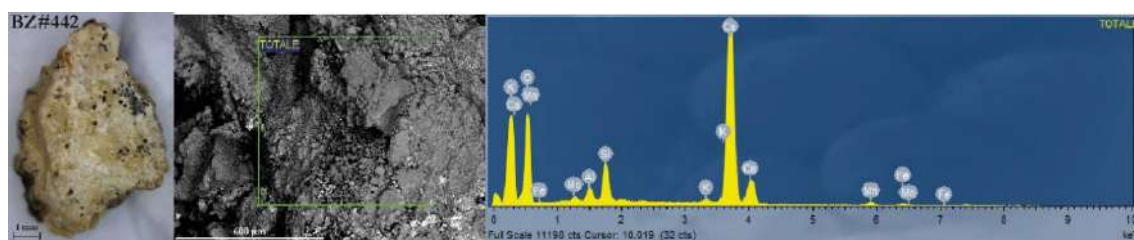
Figure 4. 11 Fragment from BZ#442 and SEM-EDS analysis.
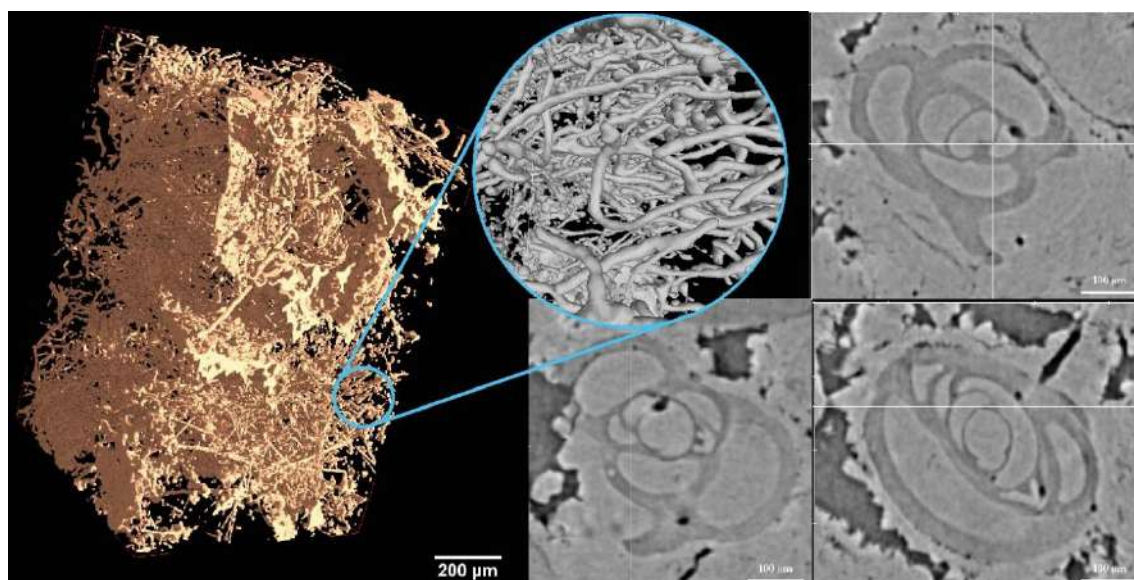
Figure 4. 12 µCT analysis of the sample from BZ#442 using synchrotron light (Elettra Synchrotron, Basovizza, Trieste, Italy). On the left, the 3D model displaying the tubular void structure. On the right, various foraminifera found in the rock.

The curators of the Brînzeni collection, performed a first visual inspection of the other rocks, and indicate the presence of *gres* which is the Moldovan word for sandstone.

Since the availability of archaeological samples suitable for destructive analysis was severely limited due to preservation concerns, the analysis of rocks collected from the Racovăț River, not only played a fundamental role in constructing a compatible and tailored replicative collection but also deepened the understanding of the potential lithotypes present at the site. The analysis confirmed that most of the samples could be attributed to quartz-arenite rocks, such as sample BZ#6742, while other types of sandstone, such as greywackes, were also present as detailed in Chapter 5, corroborating the information communicated by the curator.

4.2.3.   Preliminary morphometric evaluation

An initial morphometric evaluation was conducted on the selected 10 putative GSTs through photographs and 3D models (Figure 4.13). Furthermore, to gain a better understanding of the collection's characteristics, the preliminary geometrical characterisation was performed on a larger sample of 18 GSTs. The primary objectives of this assessment were to gain a basic understanding of the morphological characteristics of the assemblages and to facilitate the selection of comparable pebbles for the construction of the reference collection.

Subsequently, a detailed investigation of the macroscopic characteristics and use-wear traces on the archaeological GSTs was conducted following the production and analysis of the experimental collection. The comparison with the reference collection aimed to enhance the understanding of the natural appearance of the stone and the mechanisms underlying wear development on these types of rocks when they come into contact with various types of raw resources and different gestures for their elaboration. The comprehensive morphometric and textural analysis, along with its comparison to the experimental collection, is presented and discussed in Chapter 7.

As mentioned before, the morphometric characteristics of the selected GSTs were extracted from photographs and 3D models. The latter were obtained with the Artec3D Space Spider light 3D scanner acquired during the 2016-2017 sampling campaigns (Longo et al. 2021a; models available for visualisation at sketchfab.com/ADM-VCH). However, the resolution of the 3D models was not sufficient to perform textural evaluation, therefore they

were solely used for visual examination to gain a basic understanding of the object's geometry, morphometric parameters and main waviness.

It is important to note that not all tools were scanned. For the GSTs where 3D models are available, dimensions were obtained by processing the mesh in Cloud Compare. The software enabled the extractions of sections that allowed measurements of the tools' main axes. Additionally, Cloud Compare functions for volume and surface area calculation were employed, and the corresponding parameters were reported in Table 4.1. In some cases, the weights of tools were available, also included in Table 4.1 for comprehensive documentation. Considering that the morphometric characteristics of tools were the basis for selecting the stones to be used in the replicative experiments, it was important to enhance the variability regarding weight and dimensions to identify the main necessary characteristics of the GSTs. Therefore additional 8 GSTs are included in this part of the study (highlighted in blue in Table 4.1). These tools were selected solely based on data availability, and used for their macroscopic characteristics to improve the statistics.

Table 4. 1 The GSTs analysed in the study are reported. In blue are presented the additional GSTs included to enhance the dimensional variability. The retrieval square, level, and year are reported, as well as the morphometric characteristics such as weight and dimensions. For the GSTs with available 3D models, the volume and surface area were also calculated.

Inventory No.	Square	Level	Year	Weight (g)	Dimensions (mm)	Volume (mm³)	Surface (mm²)
BZ#442	12В	3	1963	935	118.17×129.19×41.15	423371	35663.8
BZ#N.No.	12Г	3	1963	617	138.48×74.4×43.26	268904	26323.5
BZ#2965	12Ж	3	1963	201	62×57×34	-	-
BZ#833	12Г	3	1963	442	126×57×37	-	-
BZ#6742	14И	3	1965	751	100.16×71.39×78.51	331126	25159.5
BZ#375	13Д	3	1963	-	118.34×84.57×48.1	263880	22730.8
BZ#6707	?	3	1965	740	138.15×88.44×36.88	302059	28833.4
BZ#2964	12Ж	3	1963	884	144.58×100.92×48.68	388022	31811.9
BZ#5160	14Б	3	1964	297	79×73×59	-	-
BZ#3488	16Д	3	1964	-	127.92×90.4×34.3	225234	24104.7
BZ#1093	12Д	3	1963	499	115.35×62.36×47.47	212350	19624.7
BZ#N.No.	11Ж	3	1964	421	75.85×92×43.22	182027	17158.9
BZ#N.No.	11Ж	3	1964	1446	175×114×113	-	-
BZ#4292	11Ж	3	1964	243	233.14×184.51×33.85	1055810	90859.6
BZ#3487	16-14Д	3	1964	400	154.21×63×47.08	235068	23675.2
BZ#177	9И	3	1987	1236	152.47×124×75.4	690589	45280.3
BZ#380	13 Д	3	1963	234	78.65×44.89×43.50	-	-
BZ#1376	14Д	3	1963	660	114.22×100.34×36.19	292633	29039.3

Upon initial macroscopic examination, primary characteristics were emphasised:

- The two fragments BZ#2965 and BZ#833 refit into an elongated stone with a final weight of more than 600 g. The edge of both #2965 and #833 fragments are convex and smoothed, but #833 presents a more pointed end.

- BZ#5160 is a fragment resembling in size and fracture the item #2965. The edge is convex but narrower compared to the large surface of the edge of #2965.

- BZ#6742 is characterised by an asymmetrical ellipsoid shape with one side rounded and one side flattened. Moreover, the rounded side exhibits severe fractures with detachments of large fragments.

- BZ#375 is characterised by oval shape, featuring one convex face and another slightly convex face, which also exhibits a slight concavity in the central part, as evident from the section along the length of the instrument.

- BZ#3488 has a flattened sub-discoidal shape, with a convex surface and the opposite slightly concave.

- BZ#2964 presents a sub-rectangular shape, featuring one flat face and one convex.

- BZ#6707 also presents a rectangular shape and flat surfaces one of which slightly is convex.

- The fragments BZ#442 and BZ#N.No. (lacking an inventory number) refit, suggesting a large sub-rectangular incomplete stone. Its weight exceeded 1.5 kg, but the original weight may have been higher, possibly around 2 kg or more.

Based on these preliminary investigations, stones with consistent characteristics were selected to construct the reference collection, which serves as a basis for the wear mechanism analysis (presented in Chapter 5), and to conduct a comparative wear investigation of the archaeological tools (presented in Chapter 7). As detailed in the following chapter, the experimental reproduction using compatible resources provided insights into wear appearance and development, as well as the natural characteristics of the stones, such as their lithic properties and response to mechanical stress. This supports differentiate use-traces from typical pre-existing features that may be mistaken for wear-related patterns.
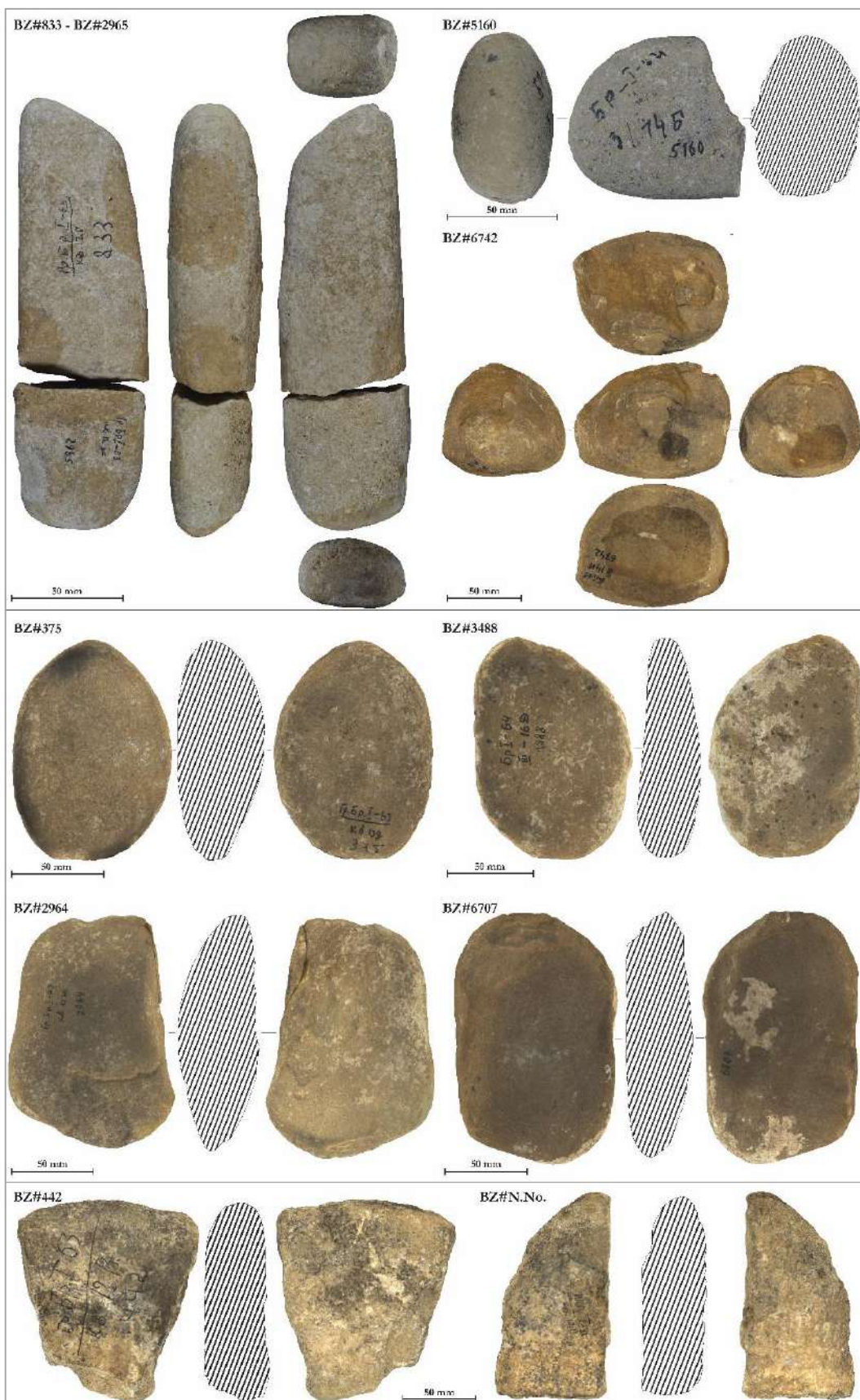
Figure 4. 13. The GSTs analysed in this study. Different views and cross-section are extracted from 3D models, except for #833-#2965 and #5160, for which only high-resolution pictures are available.

5. The reference collection

5.1. The construction of an experimental GSTs replicative collection: a theoretical overview

Stone tool replicative experimentation involves creating and/or using a stone specimen with specific relevant attributes to investigate and test hypotheses, inquiries, and methods (Outram 2008; Eren et al. 2016).

In the field of experimental archaeology, replicating ground stone tools is a critical component of the experimental process, which includes hypothesis formulation, testing, and the application of appropriate analytical methods Establishing an experimental reference collection that replicates the original ancient use of the tools is essential in supporting functional analysis and investigating the formation process of diagnostic patterns of use-wear as a proxy for studying and interpreting archaeological evidence (Coles 1979; Adams 2010; Eren et al. 2016). The aims of a replicative experiment can be:

- validate an analytical approach;
- generate models and predictions through data from scenarios that have been experimentally tested and verified;
- testing a theory or hypothesis.

The experiment can be conducted in an exploratory or confirmatory manner. An exploratory study means to identify issues to be addressed or to establish a baseline for comparison, while testing the consistency of this result is the purpose of a confirmatory research. A thorough study should involve both types of approach. It is also crucial at this point to check for equifinality, performing several trials to determine whether multiple causes can result in the same outcome and if potential alternative causes have to be considered (Adams 2010; Marsh and Jeffrey 2010; Marreiros 2020).

Designing an experimental stone collection, various approaches can be used, which were classified and categorised by scholars according to different parameters. Typically, in GSTs technological investigations two types of settings are designed, according to the research question(s). The so called "laboratory/controlled experiments", are generally conducted in a laboratory setting, characterised by repeatable conditions also obtained

through the employment of mechanical devices for control or measure changes; while the "actualistic/field/natural experiments" involve newly-made replicas of authentic artefacts and mimicking potential past conditions to understand how the tools were manufactured or used to perform certain tasks (Outram 2008; Bamforth 2010; Adams 2010; Marsh and Jeffrey 2010).

Starting from the distinction between natural and lab experiments, Marsh and Jeffrey (Marsh and Jeffrey 2010) focused their dissertation on the role that controlling variables plays in the two types of settings. Laboratory experiments are used for highly controlled investigations that focus on a limited number of variables. Such tests frequently concentrate on the physical and mechanical characteristics of the materials that humans used to make tools, investigating their universal properties beyond the archaeological and cultural background. On the other hand, employing a field setting to potentially recreate realistic use contexts implies loosening variables control to examine aggregate effects at a wide scale.

The variables occurring into an experimental setting can be divided into three categories (Marreiros et al. 2020):

- Independent variables: are the input variables that can be changed to determine the way they affect the outcome. Standardisation is essential, and the experiment's key parameters should remain constant, unless testing them is the goal;

- Dependent variables: are the variables present in the outputs, the one that are measured, connected by a cause-and-effect relationship with the independent variables.

- Cofounding variables: are those variables that are not identified as having an impact on the outcome, and cannot be controlled, tested, or assessed, due to the experimental design itself.

Among all the possible variables, in all types of settings, the human factor is always the most challenging one. Our different behaviours complicate the analysis beyond the straightforward cause-and-effect interactions (Adams 2010). This consideration became even more impactful when trying to replicate skills, goals, perceptions and decision-making processes of people from a different time and culture. To address this matter the anthropologist Raymond Mauldin (1993) during his study of tools efficiency in food processing, involved a Bolivian woman who was more familiar with this type of tasks and tools than a newer scientist. However, who is writing believes that a direct use of the tools by the scientist offers a broader understanding of gestures, kinetics and tools efficiency,

which can guide considerations and further adjustments in experimental settings, as well as influence the overall study approach.

Another way to control the human factor in GSTs experimental replicas is the employment of mechanical setup (Astruc et al. 2003; Calandra et al. 2020; Paixão et al. 2021). This laboratory-controlled arrangement overcomes the limited variables supervision of a more "natural" setting and has the undeniable advantages of being reproducible, having control over factors that are even difficult to monitor, such as the number of percussions, their direction or the pressure delivered (Delgado-Raack et al. 2009; Adams 2010; Caricola et al. 2018; Hayes et al. 2018; Zupancich et al. 2019). Nonetheless, the design of the machinery itself can introduce variables absent in actual activities made by humans and when results are compared with original artefacts could unintentionally lead to misleading interpretations and equifinality issues. In the writer's opinion, a "sentient being" can make decisions and adjust strategies to be more effective while performing a task. These adjustments may include changes in posture, gestures, direction, pressure, and speed, as well as introducing inherent randomness to gestures over time as fatigue accumulates during performance.

The need to change the type of movement, evaluate task outcomes while performing it, and contextually decide on different movements or pressure adjustments can lead to changes in the way tools are held or in determining which stone surface is more effective. These are just some of the considerations that the human operator makes during the experimental reproduction, which surely our ancestors did too, and that the machinery cannot reproduce (Sorrentino et al. 2023b). A stronger analogy with past behaviours may be produced simply by studying the range of variance in selected human-related factors (Marsh and Jeffrey 2010).

In more recent years, Marreiros et al. (2020) revised this classification and moving from Eren and colleagues (2016) theory, proposed three different designed categories to experimental approach:

- <u>First generation experiments.</u> The first generation experiments replicated ancient technologies, techniques, gestures, and examined archaeological tool reproductions to determine their applicability, efficacy, and durability when utilised in a specific activity. These experiments attempted to test initial observations, develop new hypotheses, and determine the main variables that occurred during the replicative tools use.

- <u>Second generation experiments.</u> The second generation experiments did not aim to replicate real human-related activities, but to test general properties and principles not related to any specific archaeological contest. Consequently, the employment of mechanical equipment and automated apparatus to limit experiment variations owing to human subjectivities and individuality is frequently implied. The objective is to investigate general hypotheses, tribological mechanisms occurring during use, physical principles, testing single variables identified during first generation experiment and verifying their cause-and-effect relationship, building models defining units of analysis and measure. The analytical units should provide data to connect identified patterns and the process that produced them, integrating quantitative and qualitative data to improve accuracy, quality and objectivity.

- <u>Third generation experiments</u>. Third generation experiments are designed to test models identified in the second generation experiments within a specific archaeological context. Human individualism and gesture are again represented as variables, and the chosen tools should be replicas of the archaeological ones. However, the experiment should also include "*standard samples*" (Marreiros et al. 2020), as well as blind tests (unknown use of the tools prior to data collection). In data gathering and interpretation, qualitative and statistical approaches are integrated.

Although this model has the advantage of establishing a clear flow between the approaches and the research questions, its hierarchical structure and some of the key concepts are distant from the principles of this research. As already stated, employing machinery to replace human gesture and behaviour performing "hyper-controlled experiments" can result in tools diverging the most from a real artefact and therefore they cannot be considered as a proxy to understand archaeological patterns and models. It is also difficult to overlook the specific archaeological context, as different times and cultures entail varying human behaviours, customs, and traditions unique to their respective contexts (just as an example, the shape of the tools, or the way they were handled). Also, the petrographic and physical characteristics of the employed lithic materials strongly impacts on the experiment and its results. Therefore, it is not possible to talk about "*standard samples*", since stone hardness, density and roughness variability are specific characteristics for the type of rock that strongly influence their responses to mechanical stress.

5.2. A site-specific reference collection for the Brînzeni I GSTs

The replicative experiment approach was used in this study to investigate GSTs use-wear development while processing various types of underground and aerial plant organs (USO and ASO respectively) in order to make them suitable for human consumption. Other information regarding perishable technologies that can be achieved by processing plants (i.e., fibres) has been very briefly touched upon, but it is out of the goal of the present PhD research. Several replicative experiments were planned to clarify the tribological mechanism that occurs during USO and ASO mechanical process and compare use-wear traces occurring on tools with a known biography to those patterns present on the Brînzeni I GSTs. The lithic tools' surfaces were subjected to normal and frictional forces during use, and the presence of a medium between them resulted in deformations, cracks or fractures, striations, smoothing the grain tips, and flattening of the surface (Kapsa 2004) whose development and appearance has to be investigated.

Before performing a replicative experiment, it is fundamental to clearly state the research question(s), accurately planning the experimental setup, possibly considering more than one approach, defining the data collection strategy and the analytical procedures. Nevertheless, in this process not only the research questions played a central role, but also time constraints and laboratory equipment availability have to be considered.

Moving from Eren and colleagues' considerations (Eren et al. 2016) the aims of this experiment were several and of diverse nature:

- Testing theories or hypothesis based on use-wear traces analysis:
  - testing if it was possible to infer that Brînzeni I inhabitant were familiar with different plants organs utilisation;
  - testing if it was possible to infer that Brînzeni I inhabitant were using GSTs for plants organs elaboration;
  - verify if the selected archaeological samples were employed in plants processing;
  - verify the impact of different variables on final use-wear traces patterns;
  - verify the cumulative development of use-wear on GSTs surfaces;
  - verify the wear traces appearance also on unused surfaces of the lithic tools.
- Generate models:

- creating proxies to compare the use-wear traces and related residues on archaeological GSTs;

- characterising the human inflicted modification on selected types of stones when used as tools;

- identifying and characterising differences between use-wear traces produced by treating different types of plants resources;

- recovering the gestures and the know-how of Brînzeni I occupants, a knowledge that might be shared with the nearby groups;

- recreating the main Brînzeni's GSTs strategies of environmental resources usage, timing and interactions.

- Validate an analytical approach:
    - Validate a multiscale and multimodal analytical approach to GSTs, also combining qualitative and quantitative analyses;
    - Validate the use of sequential experimental approach to GSTs study.

For these purposes, seven exploratory experiments were followed by several confirmatory tests (as reported in paragraph 5.3). Variables evaluation had a central role in all the adopted conditions. The setup did not consider the difference between "natural" and "laboratory" settings as a strict boundary, taking advantages from both approaches and in the light of their diverse attitude towards variables. The experiments were indeed performed both openair and in laboratory environment, conducted always by human operators, but consistently considering the possible independent variables occurring during the action, among which:

- The intrinsic properties of the stones, such as their general rock classification, petrographic features, fabric (the organisation of the rock's granular components), and texture properties (namely granularity, cohesion, porosity of the emerging grains). All of these characteristics may influence how the rocks react to mechanical stress and their various abrasive capacities (Adams et al 2009; Delgado-Raack et al. 2009; Dubreuil and Savage 2014);

- The physical characteristics of the pebbles and slabs selected to be used as GSTs: the shape, size, weight, use surface geometry and extension, whose choice is conditioned by the characteristics of the medium to be processed and affects the operator's gestures and positions;

- The kind and physical properties of the different plant organs, which influence the operator's gestures and motion, also affecting the development and morphology of the use-wear traces (Adams 2010);
- The duration of usage and the quantity of the processed material, which also influence wear-traces development, distribution and amount;
- The different sources of contamination, which influence residue analysis and to a certain extent also traces.

In order to address these issues, a petrographic analysis of the archaeological GSTs and geological study of the Edinet region was at the base of the selection of the rocks to be used. The stones were selected based on the archaeological artefact morphology and weight. After the stones collection, they were also sampled for petrographic and compositional analysis (both petrographic and morphological data reported in Chapter 4). They were cleaned and prepared using a defined protocol, to minimise possible contamination (cleaning and surface preparation procedure is detailed in paragraph 5.2.3).

The majority of the items within the Brînzeni I GSTs assemblage exhibit an expedient design (Adams 2002a: 21). This design is characterized by lithic tools that show no intentional preparation of the stones to enhance their effectiveness in tasks or make them easier to hold. Instead, they were selected and used in accordance with their natural rock shape. Hence, the preparation of the stones for the experiment did not involve any shaping or surface treatment, but solely focused on deep cleaning, labelling, weighing, and grid drawing (as explained in paragraph 5.2.3). The grid was necessary to fulfil the requirements, previously pointed out by Calandra and colleagues (Calandra et al. 2019b), for a reference system to accurately relocate the identified features.

Then the stones were coupled and each pair used to treat only one resource. These were selected to encompass the category of USO and ASO, compatible with the biome of MIS 3 in the Pontic Steppe and considering differences in terms of dimension, greasiness, stickiness, wetness, stringiness, brittleness, crunchiness and lightness. Since during the experiment it is not possible to have control on the amount of flour produced and its granularity (dependent variable), to exercise control on the elaborated resources and results it was chosen to control and keep constant the amount of the processed material and the duration of the experiment.

To control contamination all materials were handled with powder-free gloves. The stones were stored in plastic zip-bag and when used isolated from both natural and lab

surfaces using plastic wrap, avoiding the use of any paper sheet since it leaves fibres. After their utilization, in order to minimize bacterial, fungal, and lichen colonization, which not only contaminates the residues but also affects the compactness of the rock and changes its roughness, the stones were stored in a refrigerator at 4°C.

Human factor was uncontrolled, but monitored with videos and notes. To avoid introducing further variability, the first seven explorative experiments were performed only by the author, to maintain constant the physicality of the operator and the approach to the task. Nevertheless, it has to be considered that in the beginning of this study, the writer was new to this task and the gesture, position, pressure and speed may have changed from the first to the last experiment due to increasing experience. The confirmatory experiments instead were performed by multiple operators with various degrees of experience and different physical characteristics to investigate the impact of the human variable in the use-wear development.

It had to be stated that, while aware of the influence of the post-depositional process on lithic surfaces (e.g., Bamforth 2010; Pergeter 2013; Hayes et al. 2018; Caricola et al. 2018), the investigation of these putative alterations was beyond the scope of this study, but it will be addressed in future research.

Considering that wear-traces have a cumulative development, studying the lithic surface only in the end of the experimental process entails losing knowledge about the mechanisms underlying the generation and modification of the traces. Sequential experiments made it possible to analyse the lithic surface both before and after each cycle of usage, tracing the gradual transformation of the texture as well as how the specific raw material responds to mechanical stress (Ollé and Vergès 2014; Calandra et al. 2019b; Marreiros et al. 2020). The topography of the surface of natural stone plays a critical role in use-wear development. Therefore, tribological analyses typically include examination of an unmodified area of the stone adjacent to the active surface. However, even on the same stone, different surface areas can exhibit distinct topographic features (Ollé and Vergès 2014; Calandra et al. 2019b). As a result, in recent years, it has become more common to study with different degree of detail and accuracy the surface before and after the experimental use for comparison (e.g., de la Torre et al. 2013; Arroyo et al. 2016; Benito-Calvo et al. 2018; Caricola et al. 2018; Zupancich et al. 2019; Arroyo and de la Torre 2020; Cristiani and Zupancich 2020; Zupancich and Cristiani 2020; Paixão et al. 2021). A sequential approach that considers also intermediate stages of wear formation is generally used for flint and/or

flaked industry traceology, particularly in relation to polish formation (e.g., Tringham et al. 1974; Brink 1978; Fullagar 1991; Lerner 2007; Ollé and Vergès 2014; Pedergnana and Ollé 2017), but has been rarely employed in GSTs study (Hamon 2008; Benito-Calvo et al. 2017; Hayes et al. 2018; Sorrentino et al. 2021a, 2023a). In this project, the surfaces were not only documented before and after use, but also during different phases of the experiment, which was structured into cycles lasting 30 minutes each and labelled as T: T_0 (unused), T_1 (30 minutes of processing), T_2 (60 minutes of processing), T_3 (90 minutes of processing), and so on.

In agreement with Bamforth concerns (Bamforth 2010), more "natural" field experiments were incorporated with a strict laboratory setting for data collection and sample analysis. Therefore, a multiscale analytical strategy from macro to sub-micron scales was applied to record the GSTs surfaces before, during and after each experimental cycle. It includes: weight, pictures acquisition for photogrammetric 3D elaboration, Dino-Lite observation of the unused and used surfaces, reproduction of the surface roughness by taking vinylpolysiloxane (PVS) negative impressions (molds). The molds are then examined under microscopes with progressively higher magnification: first with stereomicroscope to provide a general perspective of the distribution of traces on the surface, followed by OM and SEM to detail individual features.

To track the gradual modifications of a specific area, a 0.5 cm^2 square was drawn directly on the stone surface in the centre of the used area as a control square to be punctually examined at each experimental phase (T_{0-5}). The creation of a reference feature on the sample was essential in order to accurately track the changes over time. Since modifying the surface texture was not an option, drawing the square with a permanent ink was chosen as the least invasive reference feature. Unlike other methods such as scratching the sample (Stemp and Stemp 2003; Martisius et al. 2018) or sticking ceramic beads reference points (Calandra et al. 2019b), the ink did not alter the stone's surface. To ensure quantitative evaluation, the square was measured using a confocal profilometer and underwent statistical elaboration. This approach ensured the integration of qualitative and parametric approaches (Myshkin and Grigoriev 2013).

The use of stone tools to process different media is a destructive activity that constantly modifies the stone surface texture. Hence, properly documenting the features during the replicative experiment through 3D reconstructions and by molding surfaces taken at predetermined times has, in a way, "crystallized" the effects of friction on the surface

roughness at specific points in time. This allowed the analyst to monitor and make comparisons with the unused original stone surface at any stage of the replicative experiment (T_1-T_5), enabling a detailed analysis of the natural features present on the surface (e.g., cracks, polish, striations, crystal roundness). This ensures that these natural features, which also develop further during the tool's use, are not mistaken for use-related patterns caused by human intentional activity.

The design of the experimental replicas, the microscopy data, and their evaluations have been partially published in the articles Sorrentino et al. 2021a and Sorrentino et al. 2023. These topics are extensively discussed in the following paragraphs. Additionally, an explanatory video presenting the experimental tool's preparation and performance is available in the presentation Sorrentino et al. 2021b at the EXARC 2021 conference.

5.2.1. Resources selection

In consideration of how the petrographic characteristics of stones and the nature of the processed media can affect tools' response to mechanical stress and the development of use-wear, careful attention was paid to the selection of raw materials for the experimental usage. Pebbles and slabs were chosen and collected based on their similarity in shape, size, weight and petrographic attributes to the archaeological tools. To achieve this, the geological characteristics of the Edinet district and the regions surrounding the Pruth and Racovăţ Rivers up to 50 km from the cave were studied, and lithic material was selected accordingly. As already discussed, the geological map of Moldova indicates that the area is characterised by a homogeneous geological setting, consisting of sandstone and limestone of Miocene and lower Pliocene formation (Геологическая карта Молдовы Молдавской; Kováč et al. 2007; Revenco et al. 2016) (Figure 5.1).

The inhabitants of Brînzeni I likely considered the Racovăţ River, which flows in the valley near the cave, a satisfactory source of lithic material procurement, easy to collect and requiring a very limited cost of manufacture. These lithic resources had already been transported, rolled, and shaped by the river, facilitating their selection and collection without requiring a long journey to reach the outcrop sources or a long preparation before use. Constraints such as distance to the material sources and difficulty of manufacture often dictated satisfactory choices rather than optimal solutions (Adams 2010). Based on this hypothesis, the pebbles and slabs to be used in the replicative experiment were collected from the Racovăţ River, 6 km north of the cave (Figure 5.1). During the Covid-19 pandemic

emergency, the colleagues of the National Museum of Ethnography and Natural History of Moldova (Chisinau, Moldova) managed to collect and deliver 27 river pebbles to Turin.

The characteristics of GSTs vary according to cultural and temporal factors. Increasing the experimental items including also raw material coming from different geographical locations, can be useful to determine the extent of the outcomes, if they are locally specific. This approach can also supports determine the applicability of the resulting models to different contests (Jolie and McBrinn 2010). Therefore, to broadening the rock variability in terms of hardness, density and roughness characteristics, and also to increase the number of experimental tools, additional 65 slabs and pebbles were collected in Italy near Manciano (Tuscany, Grosseto) along the middle basin of the Fiora River. This area is similar in lithological terms to the Edinet region (Moldova), and characterised by sandstones of Miocene formation (Carta Geologica d'Italia) (Figure 5.2).

The gathered stones were subsequently designated and numbered using the acronyms M# for those acquired from the Racovăț River and GS# for those sourced from the Fiora River.
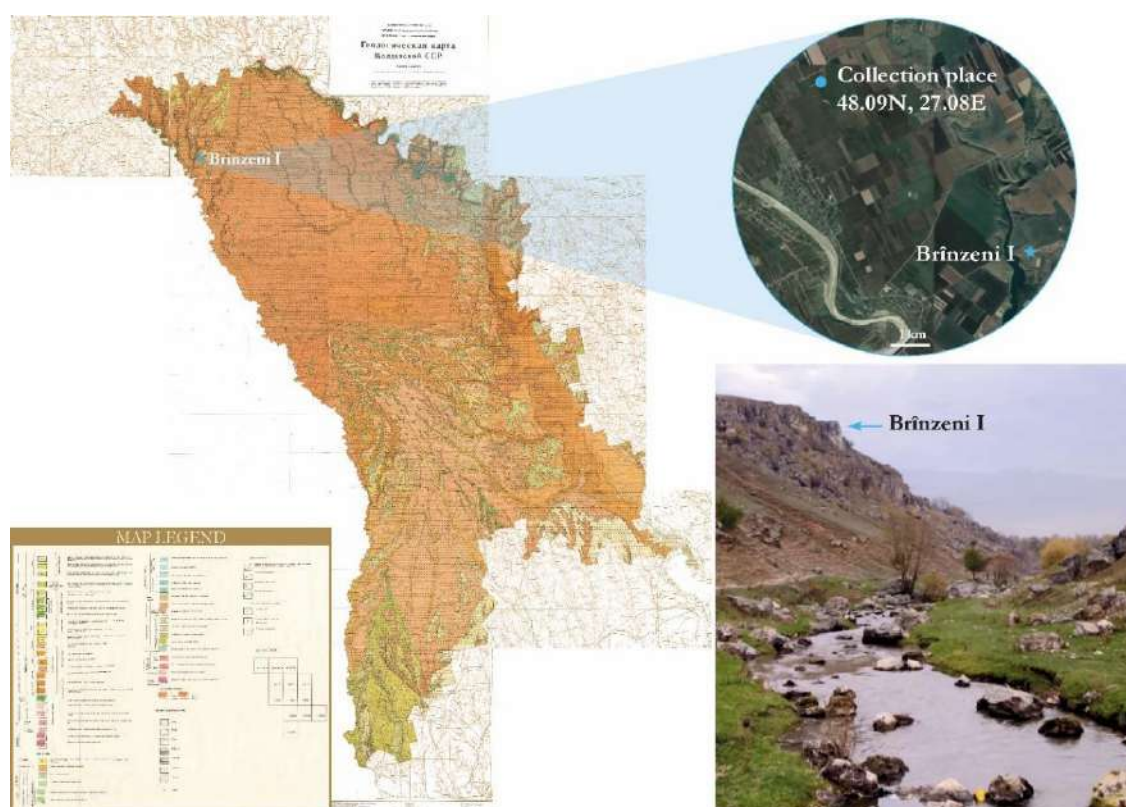
Figure 5. 1. Geological map of Moldova (modified and translated from Геологическая карта Молдовы Молдавской) with the position of Brînzeni I cave. On the right are aerial views (modified from Google Maps, accessed on the 22nd of February 2023) and drone views (modified from Tkachuk 2017) of the areas selected for stone collections.
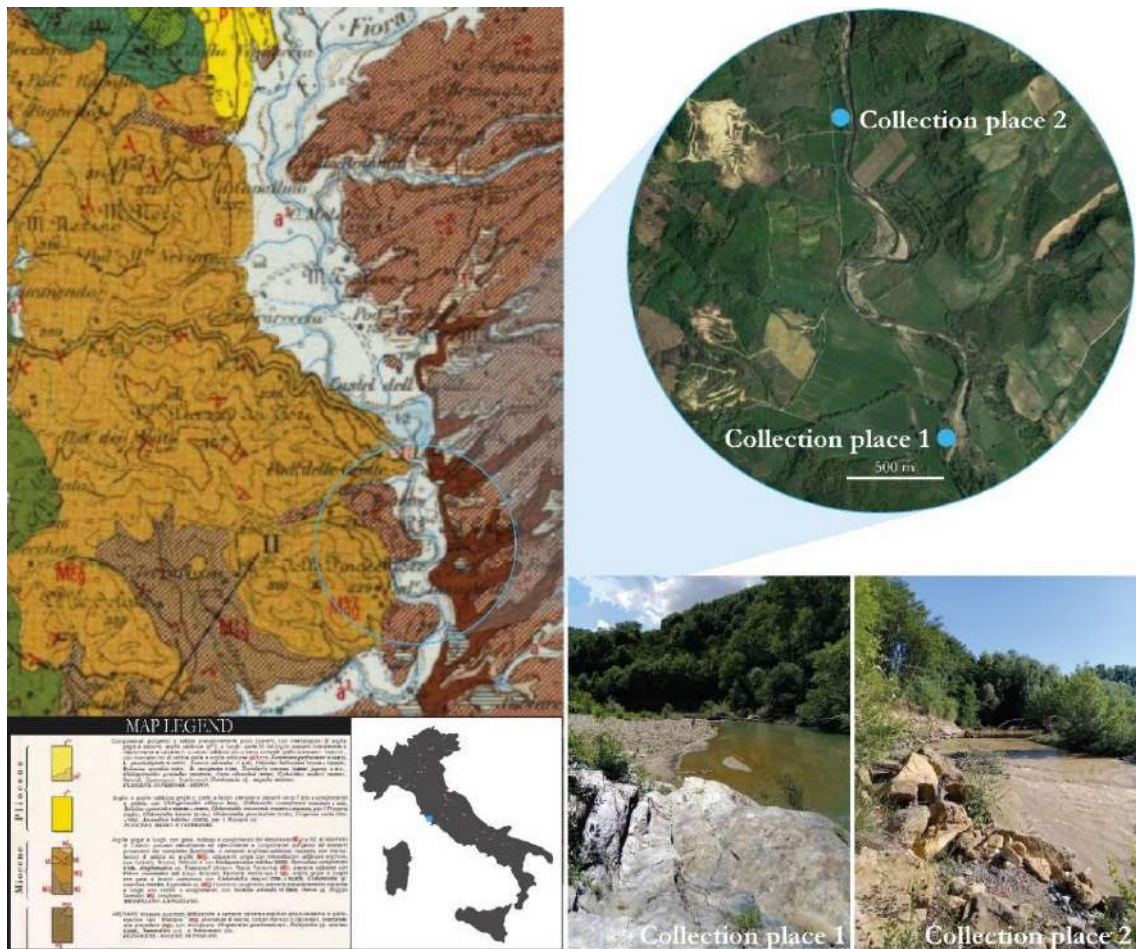
Figure 5. 2. Geological map of the middle basin of the Fiora River (modified from Carta Geologica d'Italia) and the positions of the collection places for the stones used in replicative experiment.

In terms of the plants to be processed, selection was based on palynological analyses conducted in 1987 by S. Medyanik, who collected samples from Borziac's excavation of the cave (Allsworth-Jones et al. 2018a), on plants compatible with the biome of this area (Hardy 2010), and/or those that have been identified through starch and residue analyses of artefacts from MIS 3 Eurasian sites (e.g., Zupancich et al. 2019; Birarda et al. 2020; Longo et al. 2021a; 2022). It is rare to find preserved remains of plants in archaeological contests, especially for so far periods. Furthermore, the fact that many vegetable resources selected for consumption may be eaten raw, thus leaving no traces on the stone tools, limits their potential to be detected in archaeological records, a factor that must be taken into consideration. Based on this concern, parts of plants were selected that may need pre-treatment prior to consumption, like tenderisation, chopping, grinding, peeling etc., activities that leave traces on the tools used for their preparation (Hardy 2010). Nonetheless even other plant organs are considered in the replicative experiments like phloem and fibres or mineral pigments like ochre. Of particular importance for this study are the characteristics of the media processed during the

replicative usage such as dimension, greasiness, stickiness, wetness, stringiness, brittleness, whereas in the distribution and dispersion of the residues even crunchiness and lightness (e.g., achenes), played a significant role in wear-traces development and gesture kinematics. The processed starch-rich organs serve not only for the functional interpretation of archaeological GSTs, but they are also key to the development of a database for the different types of plant resources that could have been collected and transformed during MIS 3 in the Pontic Steppe (Birarda et al. 2020; Longo et al. 2021a). Both underground storage organs (USOs) – roots, rhizomes, tubers and bulbs – and above surface storage organs (ASOs) – fruits, kernel, seeds and leaves – are being considered. Prior to the use, the resources were prepared with different procedures, summarised in Table 5.1, in order to be dried or roasted or row frozen in order to preserving their water content.

Table 5. 1. The USOs (in blue) and ASOs (in white) involved in this research and their preparation strategy.

Specie	Genus	Family	Organ	Preparation
Armoracia rusticana	*Armoracia*	Brassicaceae	Root	Oven dried (40°C for 6 h)
Pastinaca sativa	*Pastinaca*	Apiaceae	Root	Oven dried (40°C for 6 h)
Daucus carota	*Daucus*	Apiaceae	Root	Oven dried (40°C for 6 h)
Cichorium intybus	*Cichorium*	Asteraceae	Root	Air dry for 3 months
Pinus nigra	*Pinus*	Pinaceae	Phloem	Air dry for 7 days
Rumex crispus	*Rumex*	Polygonaceae	Achene	Removed from the steams and air dry for 3 months
Chenopodium album	*Chenopodium*	Amaranthaceae	Achene	Removed from the steams and air dry for 3 months
Corylus avellana	*Corylus*	Betulaceae	Hazelnut	Husk removed and air dry for several months with the nutshell
Pinus sp.	*Pinus*	Pinaceae	Pine nut	Air dry with the nutshell
Quercus sp.	*Quercus*	Fagaceae	Acorn	Pericarp and kernel removed and frosted. Defrosted before the use
Quercus ilex	*Quercus*	Fagaceae	Acorn	Pericarp removed and dried in the oven (40°C for multiple cycles of 2 hours within 7 days)
Echinochloa crus-galli	*Echinochloa*	Poaceae	Seed	Oven dried (40°C for 6 h)
Morus nigra	*Morus*	Moraceae	Barrie	Oven dried (40°C for 6 h)
Trapa natans	*Trapa*	Lythraceae	Fruit	Oven dried (40°C for 6 h)
Ceratonia siliqua	*Ceratonia*	Fabaceae	Pod	Oven dried (40°C for 6 h)

5.2.2.   Petrographic analysis

Thanks to the support of the Geological and Earth science Department of the University of Turin, four Moldovan and seven Italian pebbles were sampled, cut, and polished to obtain thin sections for petrographic analysis (Figure 5.3; Table 5.2) and to confirm raw materials coherence compared to the archaeological samples. The thin sections were observed with the optical microscope Olympus BX41 equipped with transmitted light, polarizer and phase contrast (Department of Earth science, University of Turin). The analysis of the Moldovan rocks also enhances the understanding of lithic variability within the site, considering the limited availability of samples for destructive analysis from the archaeological context.

M7, M17, M23: they are sedimentary rocks of terrigenous nature classifiable, on the basis of the mineralogical composition and the grain size, as quartz-arenites as is the case for the archaeological sample BZ#6742. The rocks are constituted mainly by subspherical and rounded quartz grains of dimension between 1 mm and 250 µm. They are characterised by a high compactness with a low porosity (<5%) that can be considered closed, as single pores not in communication. These characteristics imply that the original sediment has undergone a long-distance transportation from their primary deposit and the rock shows a high mineralogical and structural maturity. The cement is absent; however, a fine clayey matrix surrounds the quartz grains and appears interstitial. Other accessory minerals are present, such as feldspar, very rare white mica and rare glauconite. The latest, in percentage around 1-2%, it is an autigenous mineral, diagnostic of marine depositional environment with low sedimentation rates and poor in oxygen, characteristics of the continental shelf conditions.

M22: the rock can be classified as a graywacke. Compared to the previous samples, M22 is characterised by a high portion (around 65%) of a very fine matrix (10 µm), which enveloped sub-millimetric subspherical and angular quartz grains. The matrix is constituted by quartz and a fibrous mineral possibly clayey in nature. Widespread opaque minerals of 10-20 µm (5-10%) are present as well as glauconite (5-10%). The porosity degree is low, below 5%.

GS1, GS6: they are terrigenous sedimentary rocks classified as a sublitharenite. They are composed of 80% of sub-spherical and sub-rounded quartz grains, characterised by a rather homogeneous size, spanning from 1 mm to 100 µm. These characteristics indicate a high textural and compositional maturity. Opaque minerals and argillite granules are also

present as well as very rare feldspar. The rocks also show a fine clayey matrix, while the cement is absent. Porosity is poorly developed (< 5%). Among the stone collected from Fiora River GS1 and GS6 are the one more similar to BZ#6742 and differs only in a greater amount of matrix, while the mineralogical composition and texture are comparable. In sample GS1 there is also a rare carbonate between the clasts and the matrix which is also slightly more abundant.

GS2: it is a sedimentary rock of terrigenous nature classifiable as a sandstone. It is constituted by 40% of very well rounded and subsferic quartz grains of homogeneous size (around 500 μm) immersed in an abundant carbonate cement (50%), while the matrix is absent. The porosity is around 10%. Among the secondary minerals, opaque and bioclastic minerals (fragments of fossil shells) are detected.

GS3, GS4, GS5, GS7: they are sedimentary rocks of terrigenous nature, classifiable as calcarenites, similar to the archaeological sample BZ#442. They are characterised by abundant carbonate cement and grains of heterogeneous mineralogical composition, mainly consisting of quartz, but also by abundant calcite veins, bioclasts, quartzites, limestones, opaque minerals, epidote and rare white mica. The grain size is heterogeneous with calcite crystals reaching the millimetre, while the quartz of a few hundred microns. The matrix is absent, and the porosity is below the 5%.

Table 5. 2. Summary of the characteristics of the rocks used in the replicative experiments. Stones marked with an asterisk (*) were exclusively used for thin sections (modified from Sorrentino et al. 2023a)

Sample	Rock type	Porosity	Cement	Matrix	% Quartz	Quartz grains characteristics	Other minerals
M7	Quartz-arenite	Closed <5%	Absent	<5%	95%	1000-250 μm; subspherical and subrounded	Feldspar 1 % White mica 2 % Glauconite 1-2%
M17*	Quartz-arenite	Closed <5%	Absent	<5%	95%	1000-250 μm; subspherical and subangular	Feldspar 1% White mica 2% Glauconite 1-2%
M22*	Graywacke	1-2%	Absent	55%	30%	sub-millimetric subspherical and angular	Opaque 5-10%; Glauconite 5-10%
M23	Quartz-arenite	Closed <5%	Absent	<5%	95%	1000-250 μm; subspherical and rounded	Feldspar 1% White mica 2% Glauconite 1-2%
GS1*	Sublitharenite	<5%	10%; carbonate	20	50%	1000-100 μm; subspherical and subangular	Opaque 10% Clay 20% Feldspar 5% Calcite 5%
GS2*	Sandstone	Closed <5%	40%; carbonate	<5%	30%	500 μm; rounded and subspherical	Opaque 10% Bioclast 10% Clay 10%
GS3	Calcarenite	1-2%	30%; carbonate	<5%	40%	300-100 μm; angular and subspherical	Bioclasts 2% Clay 15% Opaque 5% White mica 3%
GS4*	Calcarenite	Closed <5%	30%; carbonate	<5%	45%.	500-100 μm; angular and subspherical	Calcschist 15% Opaque 5% Epidote 2% White mica 3%
GS5*	Calcarenite	Closed 5-10%	25%; carbonate	<5%	40%	500-100 μm; angular and subspherical	Quartzites 15% Slate 15% Opaque 5% White mica 3%
GS6	Sublitharenite	Closed <5%	Absent	<5%	75%	1000-100 μm subspherical and subrounded	Opaque 10% Clay 10% Feldspar 5%
GS7	Calcarenite	Closed 10%	15%; carbonate	<5%	25%	300-100 μm subspherical and angular	Bioclasts 10% Calcite 30% Opaque 5% Clay 15%
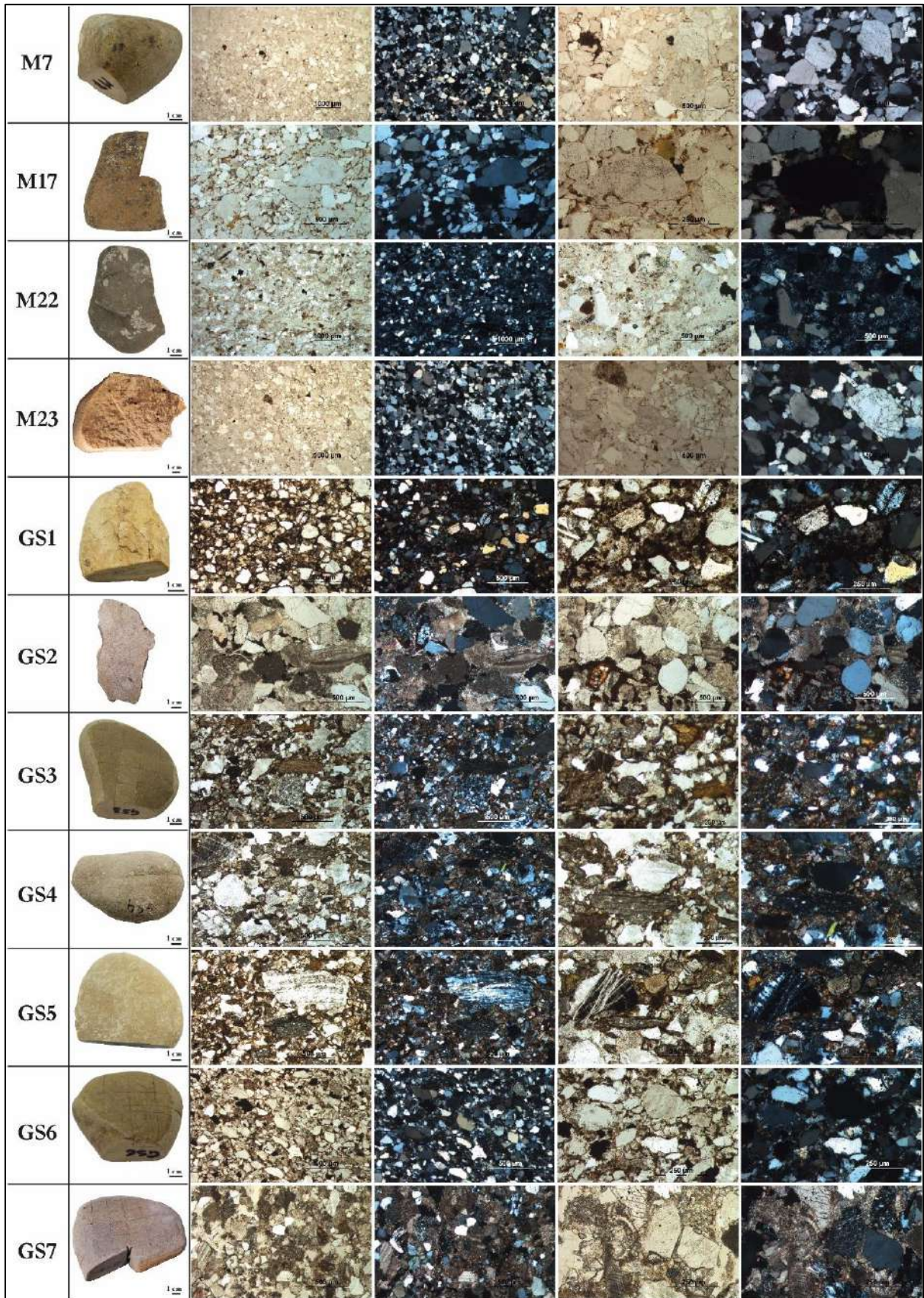
Figure 5. 3. The stones selected for thin section, their microstructures and mineral assemblages in transmitted light at single polarizer and at crossed polarised.

5.2.3. Stones preparation – Time zero (T$_0$)

Prior to the replicative use, two stones for each resource were selected to be used in pairs: one as passive tool and one as active tool. Then they have been cleaned, first with running water and brushing, and in a second time a more in-deep cleaning in an ultrasonic tank was performed. The stones were placed in a zipped bag filled with demineralised or deionized water (according to the availability in the lab) and immersed for 30 minutes in the ultrasonic bath (Elmasonic S15H present in the laboratory of the Physics Department of the University of Turin) set in sweep mode to disperse the waves more evenly on the samples. Despite the fact that there are more efficient methods to clean the surface using chemical solvents, they were avoided due to their corrosive or caustic effect that may reduce the rock's surface compactness (Banks and Kay 2003). The residues adhering to the stones were so removed and gathered in the bag, then put into test tubes (50 ml) with a few drops of Ethanol 96% and preserved in a refrigerator to serve as a reference to document original contaminations. The stones, which were always handled wearing powder-free gloves, were rinsed with running deionized water and then dried in a lab oven at 37°C (Binder FD23), weighed with a laboratory scale with readability of 0.1 g and maximum capacity of 5 kg (Orma electronic model BC), labelled and finally stored in the refrigerator in separated zip bag.

Stones were individually evaluated for *comfortable features* (Adams 2002a: 19) and in particular for their size, weight, handy shape to hold, surface texture, roughness and geometry of each face to design the active side of the tool (the side directly involved in the use). In this experiment the working surface was only one. On the used surface of both passive and active stones a 2×2 cm grid was drawn with India ink (Pelikan), which has a given composition and it does not affect the residue analysis (Figure 5.4). The central square of the utilised areas was additionally subdivided, and a 0.5 cm^2 control square was delineated (clearly visible on the ventral side of the active tool in Figure 5.5 B) to enable the detailed examination of the cumulative behaviour of use-wear formations. This also facilitated the integration of quantitative data collection with qualitative evaluation. Moreover, on the unused ventral surface of the passive tool (the face in contact with the soil) was also drawn a 2 cm^2 square to evaluate if on this surface wear develops as a consequence of the blows and recoils absorbed during the processing ongoing on the active face of the tool.

Figure 5. 4. The stones were ladled, a grid drawn, negative impressions of the surface were taken using high-definition molds, stored in separated zip bags (from Sorrentino et al. 2021a).

At the unused stage, named "time zero" (T_0), the stones' surfaces were observed with a Dino-lite$^©$ portable digital microscope (Pro AM413ZTA) and zenithal pictures of each square of the grid acquired at fixed magnification: 30×, 50× and 220×. Negative replicas of the surface texture were taken using high-definition molds, made with Provil Novo L (Hereutz – Kulzer; information available at Kulzer Mitsui 2021). The molds were stored in separated zip bags (Figure 5.4), waiting to be observed under microscopes, and to perform profilometer measurements on specific areas. In order to partially remove the traces of PVS that stack on the surface, the stones were washed again with running demineralised water and lightly brushed.

To document the geometry and the macroscale texture of the T_0, a series of pictures of the stones, at different angles and high were acquired for 3D photogrammetric reconstruction. The entire procedure is displayed at this link (Sorrentino et al. 2021b).

5.3. The replicative experiments design

In line with Marsh and Jeffrey suggestions (Marsh and Jeffrey 2010) (see paragraph 5.1), four different approaches to replicative use of GSTs were tested (Table 5.3). These approaches varied in the degree of variable control and were designed to test different parameters:

1. <u>First scenario</u>: is characterised by exploratory sequential experiments that aim to establish the stage, nature, and characteristics of wear trace formation when different types of lithic material are used for a single resource elaboration. The design closely resembles a "natural experiment", conducted in open-air settings (Figure 5.5 A, B);

2. <u>Second scenario</u>: as the previous one, is characterised by exploratory sequential experiments aimed at establishing the times, nature and the characteristic of wear

traces formation when a specific type of lithic material is used for different resources elaboration. Unlike the previous one they were carried out in controlled laboratory conditions (Figure 5.5 C, D);

3. <u>Third scenario</u>: is characterised by 3 exploratory sequential experiments that consider active and passive tools made of different materials, and in particular active stone tools and passive wooden plate (Figure 5.5 E-G);

4. <u>Fourth scenario:</u> is characterised by several confirmatory sequential experiments, which also involved more resource types, plants, operators, and tools concomitant and sequential secondary use (Adams 2002a: 21-25) (Figure 5.6).

In the first three exploratory experiments, stones were used to treat single resource, selected among USOs and ASOs to be representative of the different characteristics as dimension, greasiness, stickiness, wetness, stringiness, brittleness, crunchiness, lightness and also in consideration of the behaviours that they have when coming into contact with the tools surface, as scattering on the passive tool surface in case of achenes of stick on both tools active face in case of roots.

Moreover, in these explorative experiments, at the end of each used cycle, the GSTs were cleaned and gently brushed with demineralized water in a graduated beaker to remove the adhering residues (Sorrentino et al. 2021a, 2021b). The solution was then collected in test tubes (50 ml), stabilised with a few drops of ethanol (96%) and kept in a refrigerator for latter residues analysis (not part of this study). Then stone's detailed surface documentation strategy was applied as reported in paragraph 5.4.

Table 5. 3. The ground stone tools, the operators that performed the replicative use (OP-01 indicate who is writing, while the other codes are explained in Table 5.4), the plants storage organs involved in this research at the various times of the experiment (T_1, T_2…T_5), and the total duration of the experiment. In blue: 1st scenario, explorative experiments in a natural field setting; in grey: 2nd scenario, explorative experiments in a lab setting; in yellow: 3rd scenario, explorative experiments involving a wooden plate and active stone tools; in red: 4th scenario, confirmatory experiments (modified from Sorrentino et al. 2023a).

T	Duration	Passive stones	Active stones	Resources	Experimenter
		GS7	GS8		
T_1	30'			*Rumex crispus* achenes	OP-01
T_2	30'			*Rumex crispus* achenes	OP-01
T_3	30'			*Rumex crispus* achenes	OP-01
T_4	30'			*Rumex crispus* achenes	OP-01
		M12	M9		
T_1	30'			*Rumex crispus* achenes	OP-01
T_2	30'			*Rumex crispus* achenes	OP-01
		GS17	GS18		
T_4	120'			*Rumex crispus* achenes	OP-01
		M23	M2		
$T_{0.1}$	30'			*Quercus* sp. acorn (fresh)	OP-01
T_1	30'			*Quercus* sp. acorn (defrosted)	OP-01
T_2	30'			*Quercus* sp. acorn (defrosted)	OP-01
T_3	30'			*Quercus ilex* acorn (oven dried)	OP-01
		M25	M3		
T_1	30'			*Cichorium intybus* roots	OP-01
T_2	30'			*Cichorium intybus* roots	OP-01
T_3	30'			*Cichorium intybus* roots	OP-01
		Wood plate	GS9		
T_1	30'			*Rumex crispus* achenes	OP-01
T_2	30'			*Rumex crispus* achenes	OP-01
T_3	30'			*Rumex crispus* achenes	OP-01
		Wood plate	M8		
T_1	30'			*Armoracia rusticana* roots	OP-11
T_2	30'			*Armoracia rusticana* roots	OP-09
T_3	30'			*Armoracia rusticana* roots	OP-10
		Wood plate	M7		
T_1	30'			*Corylus avellana* hazelnuts	OP-12
T_2	30'			*Corylus avellana* hazelnut	OP-02
T_3	30'			*Corylus avellana* hazelnut	OP-01

		GS14	GS6		
T₁	30'			*Echinochloa crus-galli* seeds	OP-10
T₂	30'			*Echinochloa crus-galli* seeds	OP-12
T₃	30'			*Echinochloa crus-galli* seeds	OP-02
T₄	30'			*Morus nigra* berries	OP-13
T₅	30'			*Morus nigra* berries	OP-07
		GS3	M5		
T₁	30'			*Chenopodium album* achenes	OP-08
T₂	30'			*Chenopodium album* achenes	OP-03
T₃	30'			*Ceratonia siliqua* pods	OP-05
T₄	15'		broken	*Quercus ilex* acorn (oven dried)	OP-06
		GS16	GS12		
T₁	30'			*Pinus* sp. pine nuts	OP-05
T₂	30'			*Pinus* sp. pine nuts	OP-06
T₃	30'			*Pinus* sp. pine nuts	OP-07
T₄	30'			*Corylus avellana* hazelnuts	OP-04
T₅	30'			*Corylus avellana* hazelnuts	OP-09 - OP-11
		GS15	GS13		
T₁	30'			*Daucus carota* roots	OP-04 - OP-07
T₂	30'			*Pastinaca sativa* roots	OP-04
T₃	30'			*Pastinaca sativa* roots	OP-11
T₄	30'			*Trapa natans* fruits	OP-09 - OP-11
T₅	30'			*Trapa natans* fruits	OP-10
		GS10	M1		
T₁	30'			Ochre	OP-02
T₂	30'			Ochre	OP-13
T₃	30'			Ochre	OP-08
T₄	30'			*Pinus nigra* phloem	OP-03
T₅	30'			*Pinus nigra* phloem	OP-05
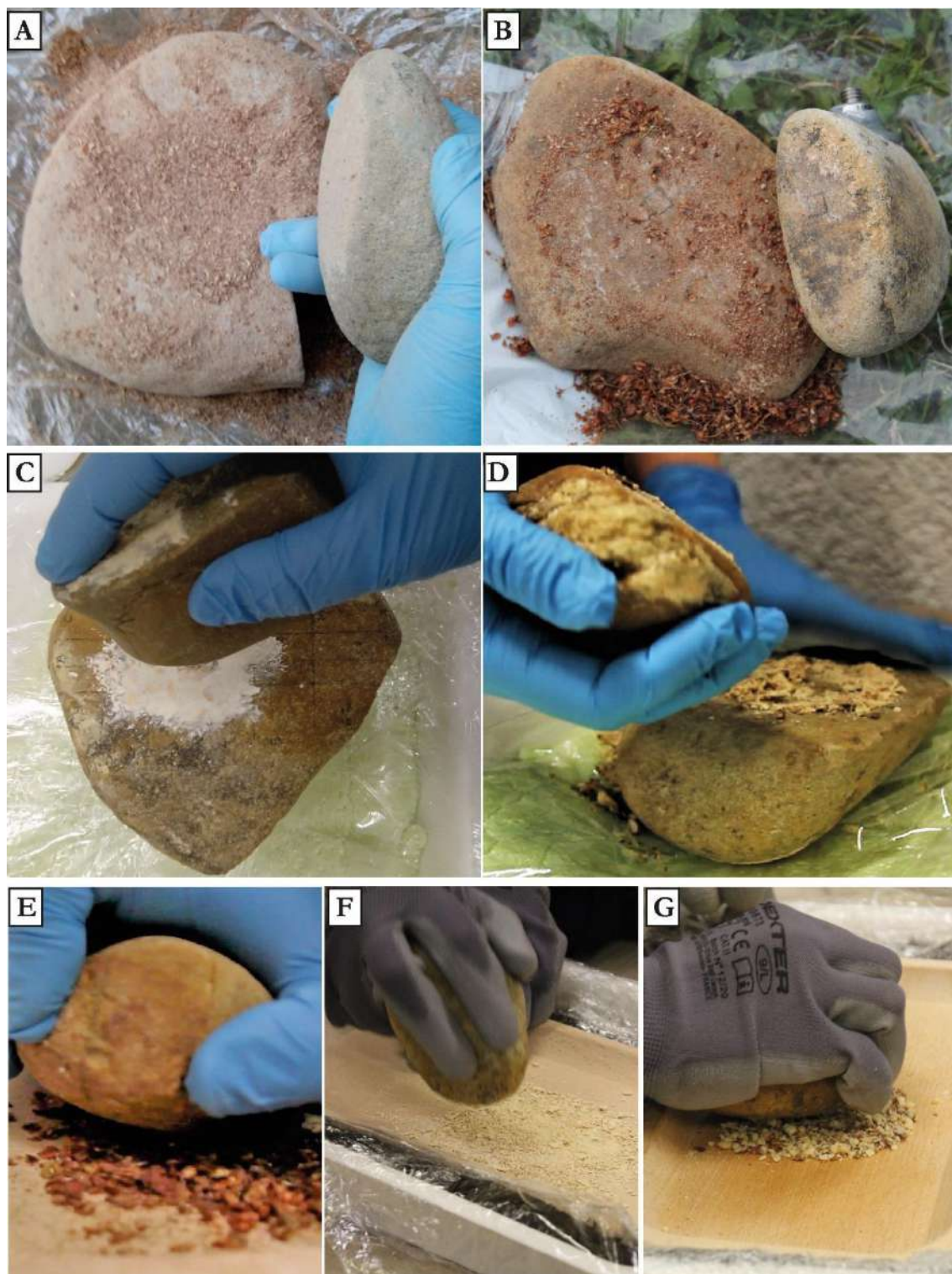
Figure 5. 5. Different approaches to GST replicative use: 1st (A and B), 2nd (C and D) and 3rd scenarios (E, F and G). A: GS7 and GS8 (collected from Fiora River), depicted during T₁ grinding process; B: M9 and M12 (collected from Racovăț River) depicted during T₁ grinding process. C: M25 and M3 depicted during T₁ Cichorium intybus roots transformation into flour; D: M23 and M2 depicted during T₁ Quercus sp. acorn (fresh frosted and defrosted prior to utilisation) pounding. E, F and G: active stone tools paired with wooden plate; E: GS9 (collected from Fiora River), depicted during T₁ while processing Rumex crispus achenes; F: M8 (collected from Racovăț River) depicted during T₁ while processing Armoracia rusticana roots; G: M7 (collected from Racovăț River) depicted during T₁ while processing Corylus avellana hazelnuts.
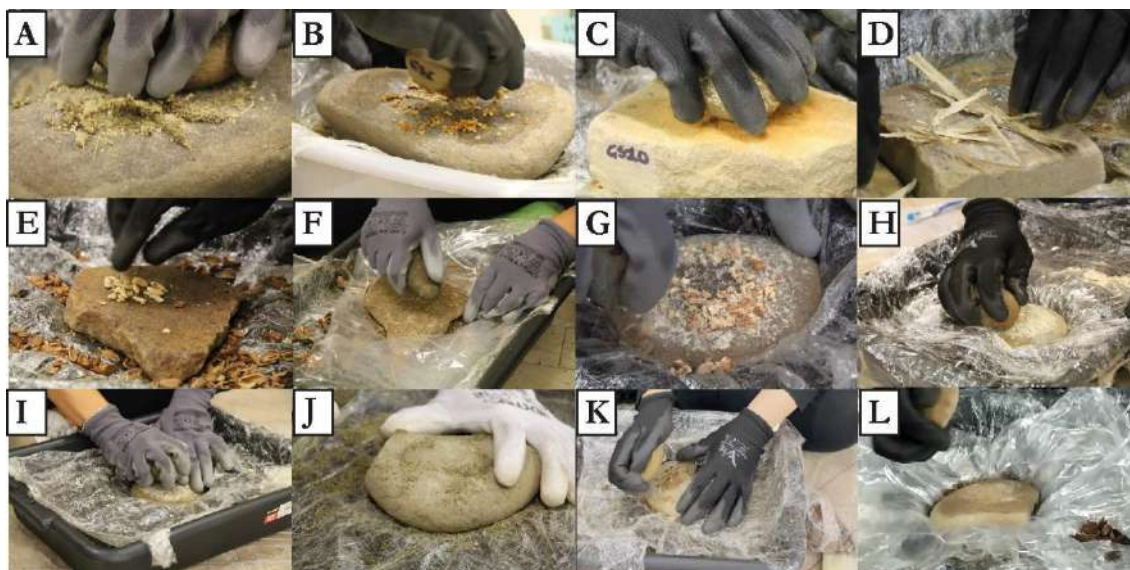
Figure 5. 6. The 4th scenario approach to GSTs replicative use. A: GS14 and GS6 depicted during T₁ Echinochloa crus-galli seeds processing; B: GS14 and GS6 depicted during T₄ Morus nigra berries processing; C: GS10 and M1 depicted during T₁ hematite and goethite processing; D: GS10 and M1 depicted during T₄ Pinus nigra phloem processing; E: GS16 and GS12 depicted during T₁ Pinus sp. pine nuts processing; F: GS16 and GS12 depicted during T₄ Corylus avellana hazelnut processing; G: GS15 and GS13 depicted during T₁ Daucus carota roots processing; H: GS15 and GS13 depicted during T2 Pastinaca sativa roots processing; I: GS15 and GS13 depicted during T₄ Trapa natans fruits processing; J: GS3 and M5 depicted during T₁ Chenopodium album achenes processing; K: GS3 and M5 depicted during T₃ Ceratonia siliqua pods processing; L: GS3 and M5 depicted during T₄ Quercus sp. acorn processing.

5.3.1. First scenario

The first scenario was set up as an actualistic experiment, while always attempting to avoid contaminations and variables monitoring/control. The passive tool was placed on the ground in a shallow depression with a plastic wrap in between to collect the flour while the active stone was held in one hand always wearing powder-free gloves (plastic wrap and gloves as part of the compromise between natural experiment and variable control). Each pair of tools was used to treat only one resource in order to evaluate the nature, shape, distribution and time of occurrence of use-wear traces produced by one single resource. The same intermediate substance, namely *Rumex crispus* achenes, was treated with stones from both Fiora and Racovăţ Rivers to evaluate the impact of rock types on the task and to verify if the outcome is regionally specific or applicable to different contests (Jolie and McBrinn 2010) (Figure 5.5 A, B).

Pounding, threshing, crashing and grinding of achenes were carried out by the writer (OP-01) and the process was documented through videos, pictures, drawings and notes. This strategy was chosen to build confidence in the activities, particularly with the gestures and motions to enact in order to achieve an effective grinding. As well, important decisions were made to find the optimal body positions, selecting the best face of the stones for the kind of

actions to obtain the required grain size of the flour. Additionally, using a single operator reduces the variability that multiple operators might introduce into the task, such as different ways to handle the tools and the position, a different reasoning and adjustment regarding the gesture and the part of the stone to be used for an effective grinding to achieve the size of the flour grain, as well as differences in body proportion and applied strength. The sequential process was organised in cycles of 30 minutes (named T_1, T_2, T_3, T_4), repeated up to 4 times (up to 120 min of vegetal treatment), and processing 15 g of resource as a fixed amount for each cycle.

GS17 and GS18 were an exception, used to elaborate 60 g of *Rumex crispus* achenes for 120 minutes consecutively with documentation of the surface only at T_0 and in the end. This exploratory experiment was set up for a specific aim reported in Chapter 6 (Sorrentino et al. 2023).

5.3.2.   Second scenario

Considering that residues analysis can be prone to several contaminants present in the air, soil, etc. (Crowther et al. 2014; Dozier 2016), hance to further limit the contamination, the second experimental phase was carried out in controlled laboratory conditions. The passive tool was placed in a plastic box, previously filled with polystyrene compound and with a plastic wrap in between to separate the stone from the polystyrene (Sorrentino et al. 2021a; 2021b). The experiments performed during this scenario aimed at completing the exploratory research started with the first scenario, adding roots and fruits to the elaborated resources (Figure 5.5 C, D).

The replicative use was conducted by OP-01 and documented through videos, pictures, drawings, and notes. The sequential process followed the established protocol, organized into cycles of 30 minutes each (named T_1, T_2, T_3), repeated 3 times for a total of 90 minutes. Each cycle involved processing 15 g of resource as a fixed amount. Regarding the pairs of stones (M23 and M2) used for acorn processing, an additional step was considered, labelled as $T_{0.1}$. This step is not considered a grinding cycle, as it was solely dedicated to removing the pericarp through a light stroke.

5.3.3.   Third scenario

The third scenario also reproduces the condition that the active and passive tools were made of different materials such as stone for the former and wood for the latter (Sorrentino et al. 2023a).

The replicative use was conducted by the writer (OP-01) for what concerns GS9, and by multiple operators, including the writer, for M7 and M8 (Figure 5.5 E-G; Table 5.3). The documentation strategy included videos, pictures, notes and detailed drawings. The mechanical process was organised in cycles of 30 minutes (named T_1, T_2, T_3), repeated 3 times (total of 90 minutes) (Sorrentino et al. 2023a). Various strategies were employed in order to monitor the quantity of the processed media:

- GS9, utilised to grinding *Rumex crispus* achenes by the writers: 15 g of resource was processed each cycle (Figure 5.5 E);

- M8, utilised to crush and ground *Corylus avellana* hazelnuts by OP-12 and OP-02 at T_1 and T_2, while at T_3 by OP-01 (Figure 5.5 F). The resource was weight at T_0, T_2 and T_3:
    - at T_1 and T_2 48.90 g of hazelnuts with shells were process (an average of 24.45 g each T),
    - at T_3 36.80 g of hazelnuts with shells were processed (the writer was performing experiments for several months while OP-12 and OP-02 were new to this task).

- M7, utilised to pound and ground *Armoracia rusticana* roots by multiple operators (OP-11, OP-09, OP-10) (Figure 5.5 G). The resource weight at T_0 was 90 g, while at T_3 was 60 g, meaning that 30 g of resources were utilised, an average of 20 g each T.

After each cycle, only the active lithic tools were cleaned using the aforementioned procedure, while the wooden base was dry brushed.

5.3.4.   Fourth   scenario: "Experimental archaeology day" (4th October 2021)

The fourth scenario was designed as a confirmatory test, leading to an increase in the number of replicative experiments. Consequently, a broader range of variables was considered, encompassing various stones that exhibited differing shapes and sizes. The

involvement of multiple operators, utilisation of diverse plant organs such as phloem, berries, and pods, incorporation of a higher variety of plant species (as detailed in Table 5.3), and the inclusion of a non-vegetal resource were also part of this scenario. Specifically, the non-vegetal resources were hematite and goethite pieces collected at Ponte di Veja (Verona, Italy) employed for ochre pigment production (Figure 5.6 C).

For these purposes, on October 4th, 2021, this thesis author organised the "Experimental archaeology day" at the Physics Department of the University of Turin (see program in Appendix A). For this dedicated day, twelve colleges were selected among PhD and other students (Table 5.4). An introduction to replicative experiments in GSTs research was followed by a practical session. The introduction was delivered by two invited speakers:

- Lara Comis (in remote mode): "Introduction to experimental research in archaeology";
- Laura Longo (in presence): "The relevance of deductive reference collection for Ground Stones".

In the hands-on session, the participants were split into couples: alternately one person was processing the raw resources while the other was documenting the activity (participants role shifting every T). The record includes photos, videos, and an *ad hoc* created form to be filled out with notes and drawings (both the form structure and the filled forms are provided in Appendix A). The day was closed by the discussion and a Question-and-Answer session.

The stones preparation followed the same procedure described in paragraph 5.2.3 and applied also to all stones involved in the first, second and third experimental scenarios. The ten employed stones were paired by this research author, who also made a preselection of the used and unused surface and drew on them a 2×2 cm grid.

During the replicative experiment the passive tools were lodged in plastic boxes, previously filled with soil and with a plastic wrap in between.
The participants, 4 males and 8 females (Table 5.4), were always wearing gloves. The process was repeated 5 times and each grinding cycle lasted 30 min (up to 150 min, named T_1, T_2, up to T_5). The treated resources were weighed before and after the experiment to estimate the amount of resource that was processed during each experimental cycle (Table 5.5).

Table 5. 4. Participants to the "Experimental archaeology day" that performed the replicative use of the GSTs. The experimenters are identified by a code and personal data are reported for statistical and scientific reasons. Moreover, in respect of privacy high and weight are reported as body mass index (BMI) which is calculated dividing the weight by the height in metres squared.

Participant ID	Gender	Age	BMI	Notes
OP-02	F	35	19.03	
OP-03	F	30	18.82	
OP-04	M	39	27.78	
OP-05	F	28	25.18	Athlete
OP-06	M	26	24.21	
OP-07	F	23	18.75	
OP-08	F	37	18.82	
OP-09	F	31	26.22	
OP-10	F	31	21.77	Athlete
OP-11	M	32	26.22	Archaeologist
OP-12	F	34	22.84	Athlete
OP-13	M	28	30.68	

Considering the hypothesis that the analysed archaeological GSTs might have been used for various purposes rather than just one resource elaboration, each pair of stones was utilized for processing multiple resources (Figure 5.6). Both concurrent and sequential secondary uses were taken into account (Adams 2002a: 21-22). Specifically, four pairs were employed to process various resources (Table 5.3): one resource type from T_1 to T_3; subsequently, the residues were collected, and the surfaces were dry-brushed in preparation for the processing of a different resource type from T_4 to T_5. Instead, the stone pair GS3 and M5 were utilized to process various resource types, such as achenes, pods, and acorns (Table 5.3, Figure 5.6 J-L). The objective of treating different plant organs with varying characteristics in terms of hardness, greasiness, and wetness with the same lithic surfaces was to verify whether the gradual formation of traces and their subsequent modification would be influenced by the different characteristics of the media leading to different patterns compared to the processing of individual resources. Furthermore, ochre was also included (Figure 5.6 C), since the microscope observation of the archaeological stone fragment BZ#442 revealed the presence of red spots later attributed to hematite after Raman analyses (reported in Chapter 7).

At T_3, prior to the processing of the second resource, the surfaces of the stones were documented by taking up to 3 molds for each area of the stone's used face. These molds were utilized not only for recording surface texture but also for thorough cleaning of any residues present. Upon completion of the experiment (T_5), the stones were cleaned using

demineralized water, and their surfaces were documented using photogrammetric acquisition, molds, and observations made with various microscopes as described in the next paragraph.

Table 5. 5. Table of the weight of the used plant organs expressed in g.

Resource	Weight before use	Weight after use	Amount of resource utilised	Number of Cycle	Amount of resource utilised every T
Pastinaca sativa roots	68.90	43.70	25.20	2	12.60
Daucus carota roots	44.60	37.50	7.10	1	7.10
Pinus nigra phloem	20.20	20.20	20.20	2	10.10
Chenopodium album achenes	180.70	169.80	10.90	2	5.45
Corylus avellana hazelnuts	167.60	100.80	66.80	2	33.40
Pinus sp. pine nuts	358.70	180.90	177.80	3	59.27
Quercus ilex acorns	119.10	103.40	15.70	1	15.70
Echinochloa crus-galli seeds	58.80	50.60	8.20	3	2.73
Morus nigra berries	100.00	100.00	100.00	2	50.00
Trapa natans fruits	310.60	290.00	20.60	2	10.30
Ceratonia siliqua pods	100.50	48.80	51.70	1	51.70

5.4. The sequential experiments documentation strategy

The documentation strategy applied to the replicative GSTs used in the experiments of the first three scenarios considers acquiring data at each sequence of the replicative experiment to track changes in the overall stone geometry, surface texture, and use-wear formation process. This multiscale documentation was applied in order to create a use-biography including natural stone surface before its use (T_0) until the last phase of the processing. Otherwise, the stones involved in the fourth scenario replicative experiments

were documented with the here presented documentation strategy only at T_0 and at the end of the use (T_5), while molds were taken also at T_3 after 90 minutes of use to track the surface texture at an intermediate stage of the replicative experiment.

After use, each stone was cleaned with demineralized water in a separate beaker to remove adhering residues. The solution was stabilised with a few drops of ethanol (96%) and collected in 50 ml test tubes, which were kept in a refrigerator. The GSTs were then let to dry in the laboratory, avoiding the use of the lab-oven at this stage to prevent alteration of the stones' structures and possible residues still adhering to the surface. When needed, the grid and reference square were refreshed. Negative impressions (molds) of the entire use-surface of the GSTs were taken following the grid and stored in single zip bags. Additional molds were taken of the control square alone and when needed, it was also highlighted on the mold surface. Moreover, at T_0 and in the final stage of the replicative experiments, molds of one square of the ventral face of the passive tools were taken to verify wear formation due to blows and recoils absorbed during the mechanical processing ongoing on the dorsal side. At the end of all the experimental uses the GSTs were weighed and compared with the original weight at T_0 to verify the material depletion as reported in Table 5.7.

The documentation strategy also implies the documentation of the surface modifications at multiple magnification scales and resolutions, as schematized in Figure 5.7.
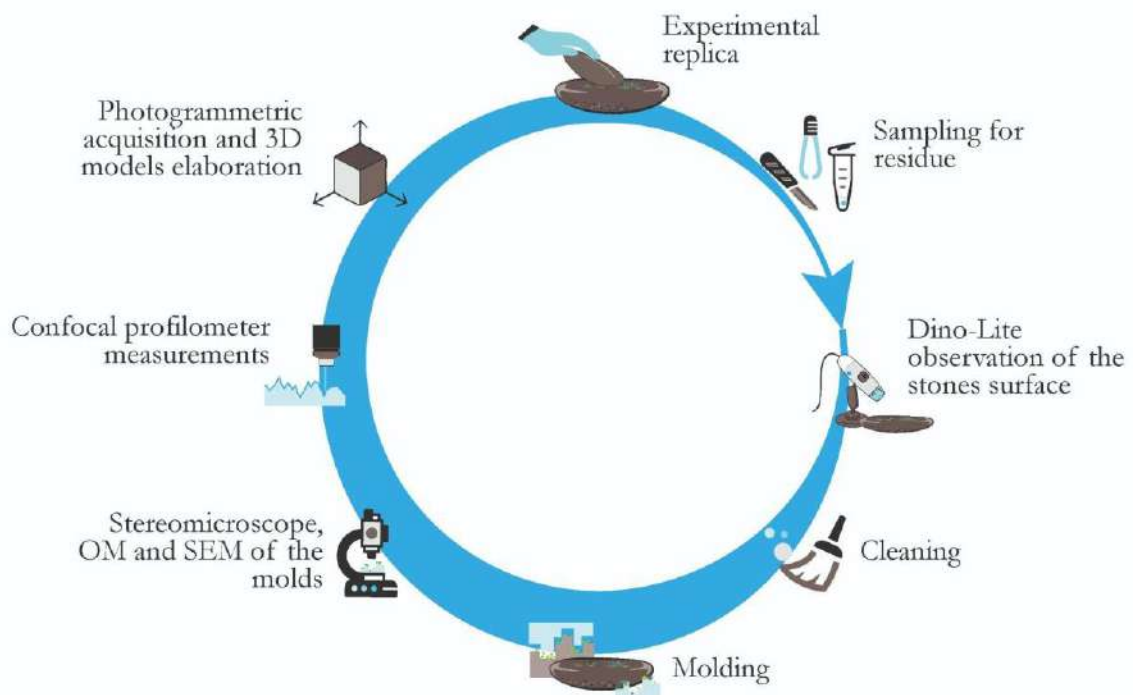
Figure 5. 7. Scheme of the various steps and techniques involved in the documentation and analysis of the experimental GSTs
(from Sorrentino et al. 2023a)

5.4.1. Macro to Micro scales documentation

As detailed in Chapter 3, this study utilised photogrammetric techniques based on Structure-from-Motion (SfM) and Multi-View Stereo reconstruction to create 3D models of the experimental tools. These models served various purposes: i) documentation, providing an alternative to drawing and individual pictures where the researcher's expertise and interpretation play a critical role in determining what to incorporate or omit, selecting the viewpoint, and executing the process. In this sense, photogrammetry is a valid improvement of a well-established method (e.g., Gašparović and Malarić 2012; Magnani et al. 2020). ii) to evaluate stone geometry and calculate morphometric characteristics as height, width, thickness and volume to be compared with the archaeological GSTs; iii) macrotopography evaluation and support the identification and orientation of use-wear pattern highlighted at the microscale using different microscopes (Longo et al. 2021b); iv) determine surface depletion at different stages of the replicative experiment.

The formation and development of wear over time, was analysed through the reconstruction of each tool in 3D at the T_0 stage, which was later compared with the virtual model obtained after each experimental cycle. The data acquisition process followed established guidelines for digitising stone tools, as outlined in relevant literature (e.g., Magnani et al. 2016, 2020; Porter et al. 2016; Benito-Calvo et al. 2018; Caricola et al. 2018; Zupancich et al. 2019; Zupancich and Cristiani 2020; Cristiani et al. 2021).

The GSTs were placed individually and horizontally on a rotating plate, accompanied by a scale bar, and they were evenly illuminated against a neutral-coloured background. A camera (initially a Canon D1100 with various lenses) was employed with specific settings, including an ISO value of 100, a F-stop of 16, and the shutter speed adjusted as necessary. The zoom was not maintained consistently. Photographs were taken by rotating the plate every 15-degree interval and adjusting the camera's position and tilt at three different heights. Subsequently, the object was flipped to capture images of the other side, resulting in two sets of approximately 75-110 photographs (totalling around 150-220 pictures) for each experimental stage. Both raw and .jpg image formats were acquired (Figure 5.8).

Figure 5. 8. Setup for photogrammetric acquisitions.

The data obtained were processed using Agisoft Metashape software. The initial steps involved masking the background of the images to ensure their correct orientation, a time-consuming procedure on large datasets. In some cases, the images of the two sides of the stone had to be oriented in separate chunks, which were later merged into a single point cloud. Following this, the sparse cloud was computed. Then, the project was scaled through the manual collimation of markers on the scale bar, which enabled the transfer of known length to the 3D models. Subsequently, the dense cloud was computed, followed by the creation of a mesh and the application of texture.

From the outcomes, it became apparent that the photogrammetric technique can be susceptible to common errors and limitations that could significantly impact the analysis:

- Scale factor errors: During photogrammetric data acquisition, a scale bar is typically included in the scene to transfer its known length to the 3D model. However, manual measurement of the scale bar can introduce human errors on the order of several micrometres. Scale factor errors were already highlighted also by various scholars as Benito-Calvo et al. 2018 and Magnani et al. 2016;

- Different camera parameters: The use of different camera parameters within the same dataset can lead to misalignments, poor image matching, distortions, and inconsistencies in the reconstructed 3D model;

- Lights and shadow distortion: Rotating or flipping the object to reveal its hidden side can alter the direction of shadows, resulting in changes to the appearance of the texture. This effect is further exacerbated by the highly uneven surface and porosity of the objects, negatively impacting the photogrammetric process (Sapirtstain 2018);

- Lack of consistent reference and spatial orientation: An evident issue arose during the comparison of pre- and post-usage models due to the lack of consistent reference and spatial orientation among all the acquisitions for each stone at different steps of the replicative use (T). The distance between the compared models was mainly due to misalignment rather than surface depletion.

To address these challenges, a dedicated parallel study was conducted as part of a collaboration with the 3D Optical Metrology Unit of the Bruno Kessler Foundation (FBK), in Povo, (Trento, Italy). This study resulted in a thorough revision and refinement of existing protocols, aiming to achieve highly consistent and repeatable results by addressing potential sources of systematic errors. After conducting multiple trials, it became evident that in order to achieve accurate results, which are crucial when employing this technique for analyses that extend beyond the subcentimetric level of conventional applications, a customized approach was necessary. As a result, a specific setup was developed and tested on four experimental GSTs: M9, M12, GS17, and GS18. An overview of this study is presented in Chapter 6 and detailed in Sorrentino et al 2023b.

5.4.2.   Micro scale documentation

It has been demonstrated by Calandra and colleagues (Calandra et al. 2019a) that the microscope and the settings used in use-wear analysis are a key factor, as their choice determine which features are highlighted. Unfortunately, there is currently no defined standard for the best disclosure of use-wear traces. Therefore, the authors recommend carefully reporting all settings used in order to meet *preproducibility* criteria (Stark et al. 2018). Furthermore, to mitigate the effect of unintentional selection of features to disclose, this research adopted multiple instrumentation that can reach different scales and resolutions.

The surface of the experimental GSTs was examined using direct observations of the stones and the molds of the surface under various microscopes and settings (as discussed in Chapter 3 and detail for each microscope reported in Table 3.2).

For stones involved in the first and second scenarios, direct observation of the surfaces was facilitated using the portable digital microscope Dino-Lite Pro AM413ZTA with polarized light. The microscope was positioned on a tabletop stand (Dino-Lite RK-06A) and connected via USB to a PC with DinoCapture 2.0 software installed. Images of each square, into which the surface was divided were examined at T0 and after each replicative use cycle, using fixed magnifications of 30×, 50×, and 220×.

Molds were first examined with the Leica S9i stereomicroscope to record the spatial distribution of use-wear. The stereomicroscope is equipped with a LED light ring for vertical illumination, and a magnification range from 12× to 110× was employed.

The morphological characteristics of the traces on the mold surfaces were then analysed, and the presence of micro-traces and polished areas was confirmed. This analysis was performed using an Olympus BX51 reflected light optical microscope with vertical incident light, which was equipped with an integrated camera. The magnifications used were 40×, 100×, and 500× (10× eyepieces) with a polarising filter. Due to the limited depth of field (DOF ranging from 1.1 µm to 27.5 µm), multiple images (up to 15) of the same area were captured at various focal planes. These images were subsequently combined using the Stack Focuser plugin in the open-source software ImageJ, following the procedure principles established by Plisson and Lompré (Plisson and Lompré 2008).

The use of both low-power (using a stereomicroscope) and high-power approaches (using an OM) allowed for the observation of patterns at different magnifications and resolutions. With stereomicroscope, surface topography, grains, striation patterns, pits, and battering marks were highlighted, while with OM at higher magnification, polishes, abrasion, and micro-striation, grain rounding or fracturing were observed (Dubreuil et al. 2015; Hayes et al. 2018; Zupancich et al. 2019). However, due to the time-consuming nature of the OM data acquisition process, most of the samples were only observed with the stereomicroscope and the SEM. The utilised stereomicroscope effectively highlighted the surface topography, the presence of rubbed areas, levelling, striations, pits, and fractures. Additionally, as noted by Hayes and colleagues (Hayes et al. 2018), polishes are more developed and form faster on smoother surfaces, such as the Moldovan stones used in this study. Therefore, these features are already visible at low magnification and, in some cases, even with the naked eye.

Meanwhile, the SEM, used at both low and high magnification, provided information on surface texture, grains, intergranular space, striation and micro-striation, pits, chipped, flattened and polished areas. It should be noted that the degree of shine of the polish was not evaluated in this study as it is too dependent on the specific setting used. Therefore, the combination of these two techniques provides both an overview and in-depth imaging of the analysed areas and specific feature morphology. To overcome this issue for the archaeological samples, a 3D Digital Microscope was employed (see paragraph 3.3.3.1). This instrument can automatically and within a few seconds combine several images taken by the digital camera at different focal planes, allowing for the visualization of the fine topography of a large area and the building of a 3D image (Longo et al. 2021b). Unfortunately, this equipment was only available for a limited time period at the laboratory of the Centro Conservazione e Restauro "La Venaria Reale", and therefore it was not possible to use it to analyse the entire experimental collection, and priority was given to the archaeological sample.

5.4.3. Micro to sub-micro scales documentation

An accurate scanning of specific features identified through the stereomicroscope and highlighted on the molds with an ink marker, as well as of the control areas, was achieved using the SEM ZEISS EVO60 EP in extended pressure mode. Images were acquired at magnifications ranging from 65× to 800×. The WD was maintained at 10 mm, and the SEM operated at a 20 kV acceleration voltage, capturing images at 3072×2304 pixels. This technique was selected for the capability to overcome the DOF limitation, a structural constraint for light/optical microscopes. Moreover, SEM provides the advantage of focusing on sample morphology without being impacted by light reflection from the sample itself, thus avoiding blurring.

The established protocol for the analysis incorporated the utilization of the profilometer. This technique enabled the examination of the out-of-plane geometry of the surface, an aspect that cannot be evaluated through SEM imaging. Furthermore, it allowed the quantification of surface texture within the sampled area and enabled the calculation of various roughness standard parameters following ISO 25178-2 guidelines. The surface microtopography of the control squares was acquired using a confocal profilometer on molds after each cycle of the replicative process. This procedure produced images of the areas and their subsequent 3D reconstruction over time. The confocal profilometer Leica DCM3D

available at the MUSAM-Lab of the IMT School for Advanced Studies Lucca, was employed. The 10× lens was employed to scan approximately 25 areas of 850 μm² within the reference square positioned at the centre of each tool-use surface, in addition to the unused surfaces of the three passive tools. For tools involved in the first and second scenarios these areas were measured at each stage of the replicative use, including T_0, while for third and fourth scenarios were recorded only at T_0 and at final stage of the replicative use. Out of the 25 areas sampled, a subsample of 9 areas were processed and analysed using the open-source software Gwyddion (Nečas and Klapetek 2010). In order to characterise the scanned surfaces and provide quantitative data on tribological features, the parameters were inverted prior to analysis and flipped along the x-axis to account for the fact that molds are a negative copy of the surface. Additionally, the average plane was subtracted to avoid the influence of mold and tool geometries and to analyse only the surface roughness. The surface height distribution and the seven ISO 25178-2 height parameters were calculated (Blateryron 2013; Calandra et al. 2019a; Zupancich and Cristiani 2020; Paixão et al. 2021, 2022; Keyence 2023). Additionally, the 3D image of the areas was displayed and false colour applied, with higher peaks displayed in red and lower depressions/pits in blue.

5.5. Experimental GSTs data analysis and results

The data collected with the described protocol underwent processing and analysis for morphometric and wear-trace studies aimed at determining the degree of surface depletion and tracking the evolution and modifications of wear patterns over time. It should be noted that this documentation strategy also allowed for the permanent documentation of the tools' use-biography, including the natural stone surface before its use (T_0) and up to the last phase of processing. This is particularly important given that the nature of the experiment is destructive, and pre-existing features are modified, erased, and overwritten each time a tool is used. While molds can permanently document the micro and sub-micro scales of specific areas of tool surface texture at the unused stage (T_0) and through all experimental cycles (up to T_5), the 3D models enabled a macro to micro scale analysis of the overall artefact, revealing changes not only at punctual areas of the surface but also to the tool's entire geometry. This approach allowed for the characterization and quantification of surface depletion, as well as the development of pre-existing features such as cracks and fractures, even on the unused stone faces.

5.5.1.   Macro scale analysis

5.5.1.1. *Morphological consideration*

As mentioned earlier (paragraph 5.4.1), the 3D models obtained according to established literature guidelines (e.g., Magnani et al. 2016, 2020; Porter et al. 2016; Benito-Calvo et al. 2018; Caricola et al. 2018; Zupancich et al. 2019; Zupancich and Cristiani 2020; Cristiani et al. 2021) were inadequate for assessing surface depletion. Only the experimental tools M9, M12, GS17, and GS18, which had their geometry acquired through the *ad hoc* setup, were suitable for comparing the unused and used stages. The results of this comparison are presented in Sorrentino et al. 2023b and briefly summarised in the next chapter.

All other models were used for documentation purposes, providing a basis for extracting essential morphometric information such as dimensions, shape, and cross-sections (Tables 5.6). Additionally, as depicted in Figure 5.10, they offer information about the extent and position of surface depletion for all tools. Moreover, they demonstrate suitable to map the distribution and direction of use-wear identified under microscope, as performed in the testcase of the passive limestone tool from Surein I (Crimea), as mentioned in paragraph 3.3.1 and published in Longo et al. 2021b.

Table 5. 6. Summary of the dimensions of the experimental tools, extracted from 3D models and expressed in mm. L = length, W = width, T = thickness, expressed in mm; surface unit is mm²; volume unit is mm³

Passive Tools	L	W	T	Surface	Volume
GS7	144.3	114.5	43.7	36996	429724
M23	118	155.7	50.1	49311.9	746493
M25	143	115.8	66	51052.6	800818
GS14	234.1	164.6	82.6	84159.8	1781060
GS3	107	96.4	30.8	23623.7	248683
GS16	143.5	147.1	33.6	39362.6	404625
GS15	116.7	102.9	36	23858.1	247612
GS10	167.3	118.7	48.9	54610.4	789801
AVERAGE	134.7	126.9625	48.9625	45371.89	681102
DEV.ST.	58.26716485	23.74131	16.5252	18302.12	468356.3

Active Tools	L	W	T	Surface	Volume
GS8	95.4	63.5	44.5	13847.7	126022
M2	74.5	60.4	44.5	13816.6	132613
M3	88.2	43.9	50.2	13570.1	114696
GS6	87.6	78.5	32	15808.3	140316
M5	73.2	58.8	44	11413.7	103436
GS12	119.3	62.5	38.9	16217.1	150419
GS13	78.9	59.7	44.6	12615.6	119662
M1	93.8	70.1	50.1	18861.2	204161
GS9	81.3	58.1	39.7	11990.7	100607
M7	61.9	68.3	56.2	13997.2	117204
M8	90.7	52.3	45.3	13944.7	131212
AVERAGE	85.89090909	61.46364	44.54545	14189.35	130940.7
DEV.ST.	14.26008125	8.696318	6.121997	2007.03	27156.14

GS7-GS8: Wear is notably pronounced in this pair, as it was employed to process a hard medium (Rumex crispus achenes) involving frequent stone-on-stone contact. The stone variety used in this instance is softer compared to the majority of Moldovan stones, but it aligns with the archaeological sample BZ#442. On the passive tool, at a macro scale, the exposure of new surface areas over time is noticeable, along with the formation of gouges and striations. These features show a predominant direction running along the longitudinal axis. The intensity of these use-wear is particularly prominent in the central region and on the distal edge. Notably, the surface forms a convexity that becomes more distinct and extends across the width during T_3 and T_4. The active tool exhibits noticeable flattening of the initially slightly convex surface. In T_1, this flattening extends near the distal edge and along the left side of the use surface. As the use cycles continue, the wear gradually spreads towards the right side and along the longitudinal axis, becoming more pronounced from T_3 onwards. By T_4, the entire width of the use surface is extensively flattened due to the protracted use.

M23-M2: Regarding M23, no significant changes are noticeable. However, for the active tool M2, there is a noticeable reduction in the natural stone roughness at $T_{0.1}$ (phase related to the removal of acorn pericarp). At T_1 the roughness increases compared to $T_{0.1}$, followed by a slight decrease at T_2, while at T_3 remains relatively constant (Figure 5.9). This observation is further supported by the confocal profilometer data. Additionally, it is evident that the naturally present fractures on the surface are extended by the use, even in the unused

regions, further supporting the idea that the entire tool geometry undergoes morphological changes while performing the transformative tasks.
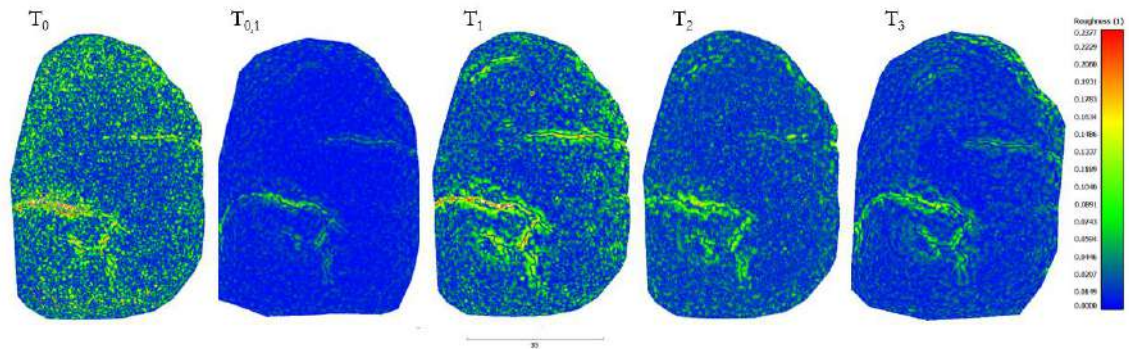
Figure 5. 9. Progression of use surface roughness for M2 computed through 3D models using the Cloud Compare Roughness function calculation, with a radius of 1 mm.

M25-M3: For the passive tool M25, even though the wear is minimal, it remains discernible in the 3D model. At T_1, the wear is localised at the top of the dashed circle visible in Figua 5.10. With the advancement of the replicative use cycles, the wear progresses toward the proximal side affecting the central part of the circled area along. By T_3, it extends further covering the entire area of the circle. Regarding M3, the primary macroscopic feature is the accumulation of root flour residues within the surface pores of the tool.
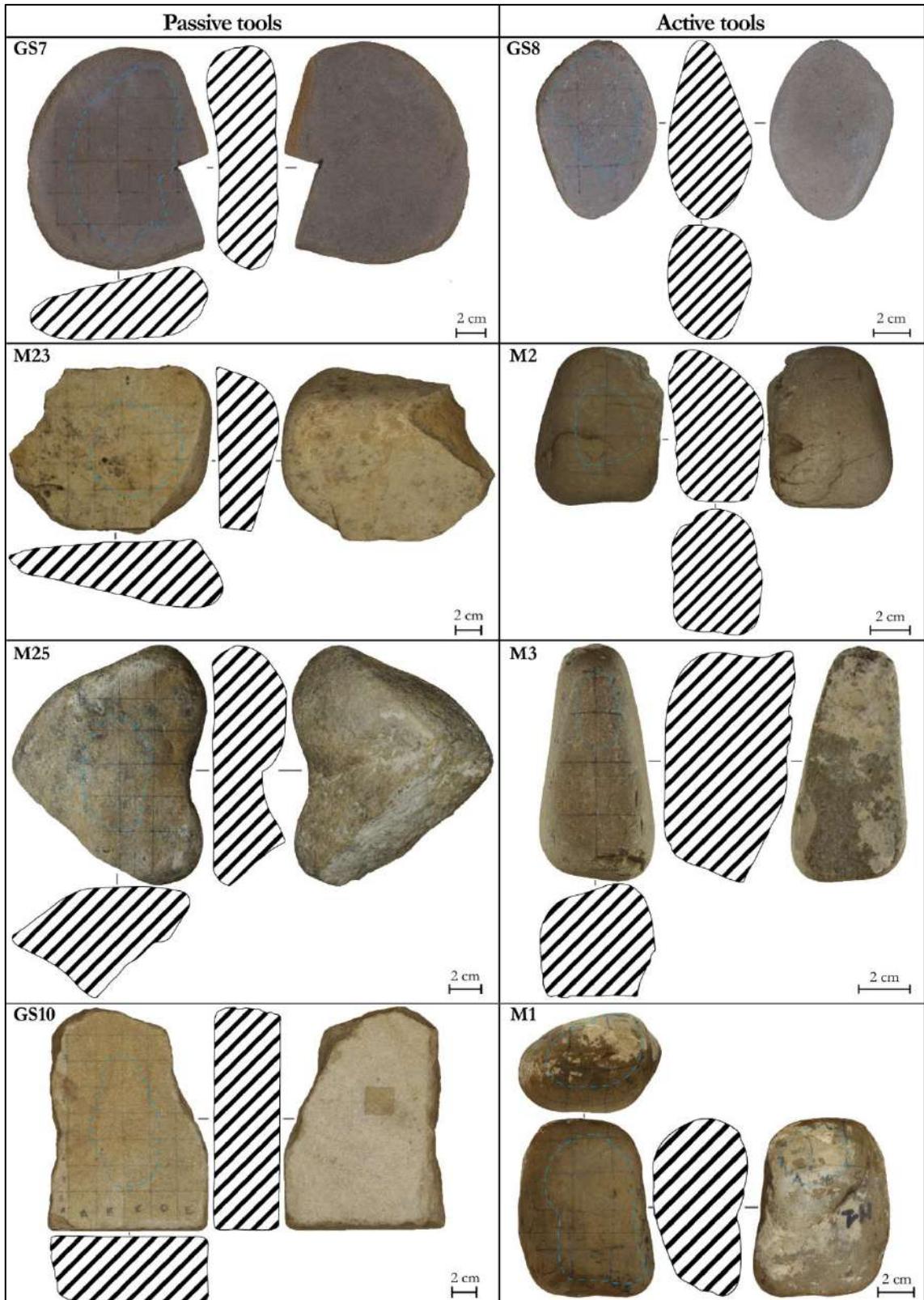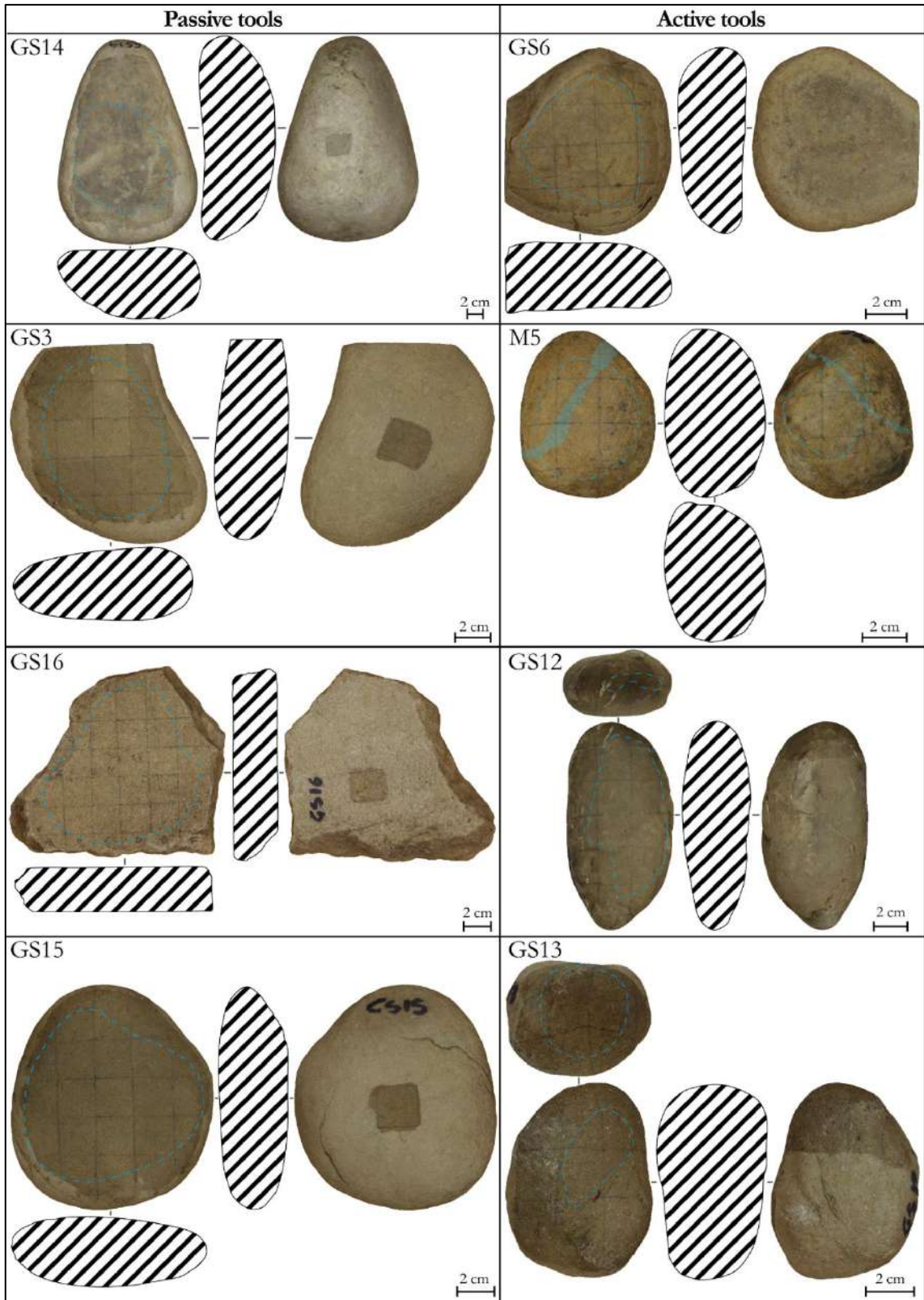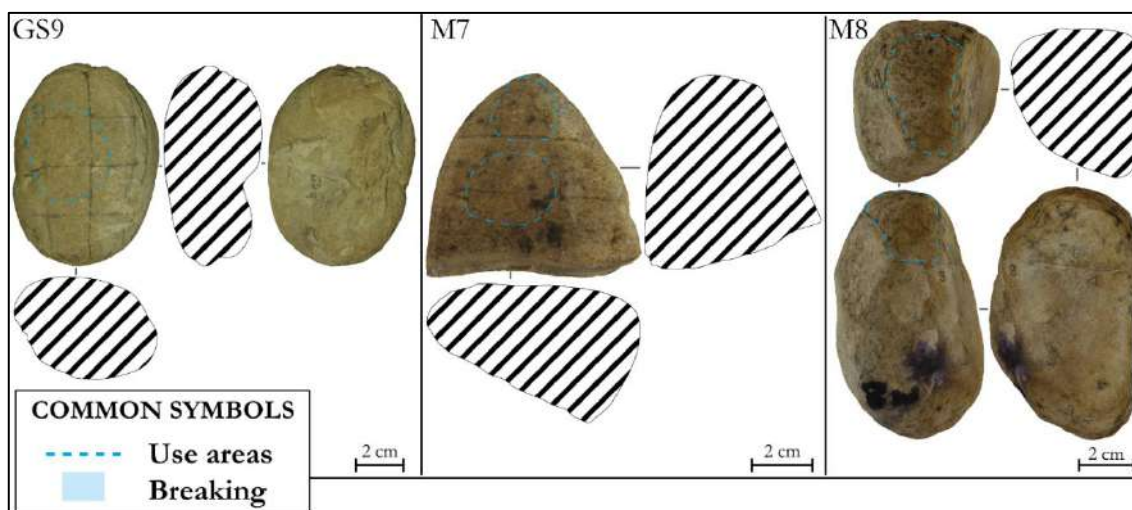
Figure 5. 10. The 3D models of the GSTs investigated in this study are shown. The ventral and dorsal surfaces of the tools are displayed, and sections are extracted from the models. In cases where it is feasible, the proximal edge is positioned towards the bottom of the image. The blue dashed lines indicate the areas directly involved in the task, in its extension at the last cycles of the replicative experiment. In the case of M5, the filled blue area represents the fracture and the lost material that occurred during T4.

The stones were all weighed both before (T₀) and after the experimental use to assess the mass loss resulting from surface depletion (Table 5.7). However, due to the potential impact of environmental and climatic conditions on measurements (both stones and instruments are sensitive to climate and humidity variations), this analysis, even though conducted in a controlled lab environment, should be regarded as a semi-quantitative evaluation. As a result, it proves valuable for comparing the depletion of tools among themselves, but not for establishing their absolute weight values.

Table 5. 7 Table of experimental GSTs weights before and after the use (T0 - T-final). The values reported are the average of 10 consecutive measurements for each tool. The value of the mass lost for each cycle is calculated dividing the loss for the number of experimental cycles and propagating the error. The values are expressed in grams (modified from Sorrentino et al. 2023a).

Plant resource	Achenes		Acorns	Nut fruits	Roots + Fruits	Roots	Seeds + Fruits	Ochre + Phloem
Passive tool	**GS7**	**M12**	**M23**	**GS16**	**GS15**	**M25**	**GS14**	**GS10**
T₀ (±0,2)	1026.5	427.5	1103.6	1043.9	648.6	1091.3	4767.0	1997.4
T-final (±0,2)	1012.4	427.5	1101.4	1042.4	647.2	1091.1	4760.5	1992.8
Lost (±0,3)	14.1	0.0	2.2	1.5	1.4	0.2	6.5	4.6
No. of T	4	1	3	5	5	3	5	5
Ca. lost for each T	3.53 ±0.07	0.00 ±0.3	0.73 ±0.09	0.30 ±0.06	0.28 ±0.06	0.07 ±0.09	1.30 ±0.06	0.92 ±0.06

Active tool	GS8	GS9	M9	M2	M7	GS12	GS13	M3	M8	GS6	M1
T_0 (±0,2)	338.4	252.3	215.9	334.9	330.6	394.7	302.1	322.3	326.8	360.8	522.3
T_{-final} (±0,2)	336.1	249.4	215.9	334.5	330.6	394.6	301.1	322.1	326.4	359.8	521.0
Lost (±0,3)	2.3	2.9	0.0	0.4	0.0	0.1	1.0	0.2	0.4	1.0	1.3
No. of T	4	3	1	3	3	5	5	3	3	5	5
Ca. lost for each T	0.57 ±0.07	0.97 ±0.09	0.00 ±0.3	0.13 ±0.09	0.00 ±0.09	0.02 ±0.06	0.20 ±0.06	0.07 ±0.09	0.13 ±0.09	0.20 ±0.06	0.26 ±0.06

The selected stones exhibit natural comfort features (Adams 2002a). In particular, the ones selected as active tools demonstrate homogeneity in their area, volume and dimensions and compatibility with the archaeological tools (see Table 4.1). The width is not exceeding 80 mm and the average thickness around 45 mm, allowing for comfortable handling with one hand. They have an average weight of around 350 g, providing efficiency without causing additional fatigue to the operator. While these tools exhibit variations in shape, they all feature a large, flat, or slightly convex use surface that is appropriate to perform "*diffuse percussion*" (de Beaune 2004). However, there are exceptions among tools GS13, M3, and M8, where the chosen primary use surface is narrower and demonstrates a distinct convexity. This shape of the use surface was selected to perform repeated "*punctiform*" pounding actions (de Beaune 2004), chosen to suit the specific nature of the treated media (roots). In the case of tools GS12, M1, M5, and M7, both the convex narrow surface and the large flat/slightly convex surface are utilised. The former is most suitable for crushing the resource into large pieces, while the latter is preferred for pulverising it into flour.

The passive tools were selected to have a length and width ranging from 100 to 170 mm, with the exception of GS14, which has a length exceeding 230 mm in line with the dimension estimated for BZ#442 and BZ#4292. This longer length for the experimental stone was chosen to minimize the issue of achenes scattering onto the tool's surface, ensuring that they remain on the stone and do not get lost in the ground, as previously observed using GS7. All passive tools feature a large, flat, or slightly convex use surface. The utilised area is primarily centred and enlarged on the use surface, except for M25 and GS10, where an oval area along the length is predominantly used, and M23, where a circular area in the flatter zone (on the right side of the use surface) is the most utilised (Figure 5.10).

It is noteworthy that passive tools exhibit a higher amount of mass loss compared to active ones. Among all the tools, those used for grinding achenes show the highest level of depletion, followed by stones used for treating seeds/fruit and ochre/phloem. However, it

is also clear that not only the medium processed but also the lithic type of the GST is important for the tools' responsiveness to mechanical stress. Indeed, tools used to treat the same medium but with a different provenience and geological characteristics (Italy or Moldova) show very different responses to mechanical stress, with stones from Fiora showing a higher mass depletion compared to those from Moldova (e.g., GS7 and GS8 compared to M12 and M9 or GS15 and GS13 compared to M25 and M3). These differences in response may be attributed to variations in the stone structure and petrographic characteristics of the rocks, which can affect their toughness, density, and other tribological properties.

5.5.1.2. Gesture analysis and residues distribution

The kinematics employed for different resources processing were adjusted based on the medium's resistance to mechanical transformation, which also influenced the selection of the GSTs' morphology. In the experiments, human intervention played a crucial role in achieving flour as the final functional goal.

To transform the resources, out of the 15 g employed for each replicative experimental cycle, a small amount of raw material was placed on the passive tool surface at a time and processed with the active stone until it was reduced into flour. Therefore, while maintaining a constant amount of resource and length of elaboration, the grain size of the obtained flour could vary based on the operator's perception, characteristics, gestures, and the properties of the treated resource.

For their transformation, the media were treated with horizontal linear or circular movements, and/or vertical motion and applying different pressure. The different characteristics such as resistance, wetness, greasiness, and fibrousness of the media were taken into consideration. The descriptions that follow are extracted from video, picture, notes of the writer and of the participants to the "Experimental Archaeology Day" (see forms in Appendix A).

Achenes. For achenes – dry fruits with a shelled pericarp containing a single seed – which are quite resilient, the predominant grinding movement is horizontal, bidirectional, and sometimes circular. Due to their small and rounded shape, they scatter onto the passive stone surface as soon as they come into contact with the active tool, requiring frequent gestures to group and re-group them using either the free hand or the active tool itself.

During the processing of this material, the contact between the active and passive tools is continuous and only partially mediated by the presence of the processed material.

The flour residues on the passive stone are scattered all around the used surface and even on the stone rim. Interestingly, the central area of the used surface, which exhibits more intense wear, tends to be relatively cleaner (area indicated by the blue line in Figure 5.10). In contrast, the active tool displays fewer residues on its surface, and the ones present are of a finer grain.

Shelled fruits and pods. For oily resources such as acorns, hazelnuts, pine nuts, and pods, which maintain their greasy characteristic even when dry, light pounding with vertical movements is the predominant gesture. This involves fast and repeated contact between the stones and the worked material, which can also result in direct friction of the two stones. In this context, horizontal movements are also needed, although to a lesser extent, to transform the small particles of resources into flour. For pine nuts, circular movements are used, while for hazelnuts, circular and linear bidirectional movements are used, and for dry pods, linear monodirectional movements are applied.

The obtained flour is not scattered all over the stone's surface but stays grouped closer to the contact areas of both stones due to their consistent adhesion.

To grind fresh acorns, the gesture begins with vertical light pounding and then changes into horizontal movements with linear motion while applying pressure with the wrist on the active stone. During $T_{0.1}$, which is dedicated to the removal of pericarps, a visible shine develops on the surface that can be observed with the naked eye. It is worth noticing that, even after washing, residues of acorn flour can still stick in the crevices of the active tool.

Roots. Dry roots are processed using a short, fast, and repeated vertical battering movement, interspersed with axial rotation of the active stone on the root and wrist pressing in place to separate the fibrous portion. Towards the end of the process, horizontal linear movements are employed to powder the obtained chunks. As occurs also for nuts, the contact between the stones surface is strongly mediated by the fibres and/or by the paste that derives from the processing and adheres to the surface, making the treatment of these resources more challenging.

The particles spread more compared to the acorn flour, but due to its wet nature compared to achenes, it tends to adhere to the used area of the active tool. On the passive tool, the area directly involved in the pounding maintained cleaned, forming a distinct circle

where the pounding action is performed, while a ring of larger particles is visible around it (as clearly depicted in Figure 5.6 G).

<u>Berries</u>. For dried berries, the grinding gesture involves horizontal, bidirectional, and circular movements with no direct contact between the surfaces of the stones due to the berries' moistness, which results in a wet paste.

<u>Phloem</u>. In the processing of phloem from *Pinus nigra*, which is used to obtain fibres, effective gestures involve alternating vertical and horizontal unidirectional movements.

<u>Pigments</u>. In the case of ochre, the effective gesture involves shifting between vertical, horizontal linear, and circular motions.

In the third scenario, the use of a wooden base with a light rim provides better control over small size media such as achenes and seeds, reducing their scattering onto the passive surface. Additionally, greasy resources like hazelnuts and roots do not stick to the wood surface. However, due to the smoothness and plasticity of wood, it has a lower friction compared to stone, which reduces its effectiveness in transforming hard resources as achenes, resulting in a longer process and less uniform powder. As a result, the gestures applied are different, primarily involving vertical motions with pressure imposed by the wrist as it comes into contact with the achenes, followed by short horizontal motions. Both the flat and convex faces of the active stone are involved.

For what concerns the dry hazelnuts, after the removal of the pericarp with one stroke, the nuts are lightly pounded with the flat part of the active tool obtaining small crumbs. Finally, linear unidirectional and circular movements with the narrow part of the active tool are used for powdering the nuts into flour, with the wrist transitioning from a flat position to a downward tension.

For roots treatment, the wooden base is particularly efficient, and the motion is primarily vertical with some linear and circular movements, resulting in an easier achievement of the desired result.

5.5.2.   Micro and sub-micro scales analysis

As explained in Chapter 3, various microscopy techniques were utilised to enhance the visibility of wear-related features and provide a comprehensive qualitative description of the observed wear. Part of this analysis has been published in Sorrentino et al. 2021b, 2023a.

Implements involved in achenes and small dry seeds processing. Several tools were implied in achenes and small seeds processing (GS7-GS8; M12-M9; GS14-GS6 up to T_3; GS3-M5 up to T_2; GS9).

In particular the pairs GS7-GS8 is the one that have been more carefully examined considering 4 use-cycles and the unused stage (Figure 5.12). It is noticeable that at T_0 both the grains and the matrix are clearly visible. At T_1 the grains start losing definition on both the GSTs, getting levelled on the active tool, whereas the first fine striations appear on the passive tool. At T_2 and T_3, groups of striations and micro-striations developed on the passive tool and at T_2 the surface shows a rubbed appearance, while at T_3 the striations are less abundant but longer and better defined than at T_2. Also, serrated polish develops, and the entire microtopography seems levelled, a process that continues through T_4, when abraded areas and groups of shorter striations increased as compared to T_3. This process, which is clear on the central part of the stone, where its use is quite intense, is even more evident on the peripheral areas of the used surface where the active tool ends its motion and the depletion of the surface is less intense (Figure 5.11).

The active tool GS8, presents a gradual lowering of the matrix from T_0 to T_4 associated with the levelling of the grains. Groups of micro-striations, mostly iso-oriented, appear since T_1 on the surface of the grains, decreasing in their quantity and in length at T_4, while since T_3 the appearance of a few small polished areas is also detected (Figure 5.13).

Regarding M12 and M9, the pair of stones from Moldova, their natural surfaces are flatter and smoother than the previous pairs. However, the wear trend is very similar, albeit developing at a slower pace. Moreover, there are preexisting features on their natural surfaces that can be mistaken for use-related traces, such as polish areas and conchoidal fractures. On the passive tool, flattened areas and patches of rubbed areas become visible at T_1, which then extend to T_2, exhibiting the same trend as seen in GS7 (Figure 5.14). The active tool displays more intense wear patterns, with large rubbed areas already evident at T_1 that extend significantly by T_2. Notably, the appearance of the first striations at T_2, oriented in the direction of the length of the use surface, is a result of the back-and-forth linear horizontal grinding movement (Figure 5.15).

The analysis of the other tools used in achenes and small dry seeds processing, confirm these observed trends.

GS9, the active tool paired with the wooden base, at T_3 displays a slightly levelled surface and a homogeneously smoothed low microtopography. Additionally, SEM

inspections reveal the presence of very light groups of parallel micro-striations (Figure 5.16).
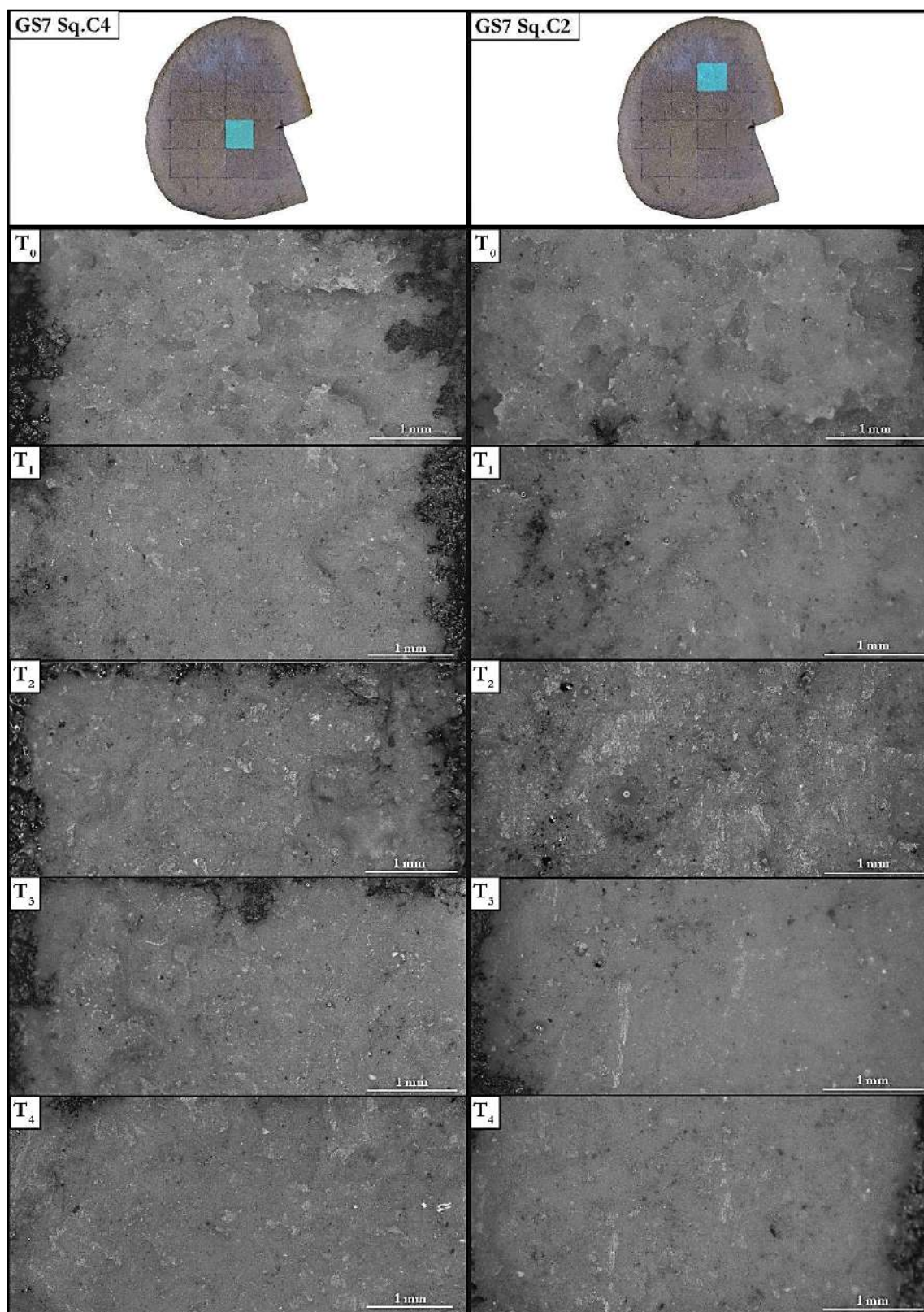
Figure 5. 11. GS7: molds of the surface of the passive tool used to process Rumex crispus achenes at different T and imaged with stereomicroscope. Left: square C4, depicted from T₀ to T₄. Right: square C2 from T₀ to T₄ (from Sorrentino et al. 2023a).
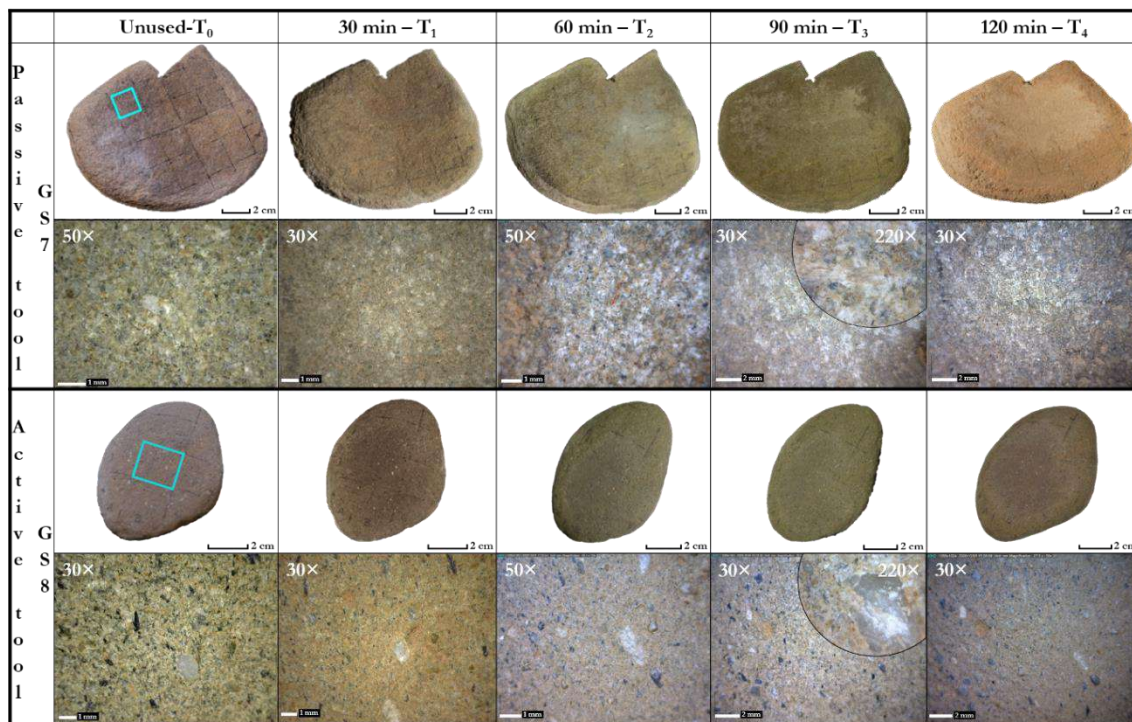
Figure 5. 12. GS7 and GS8 original surface. 3D models and Dino-Lite micrographs of the same area at different stage of the replicative use are presented (modified from Sorrentino et al. 2021a).
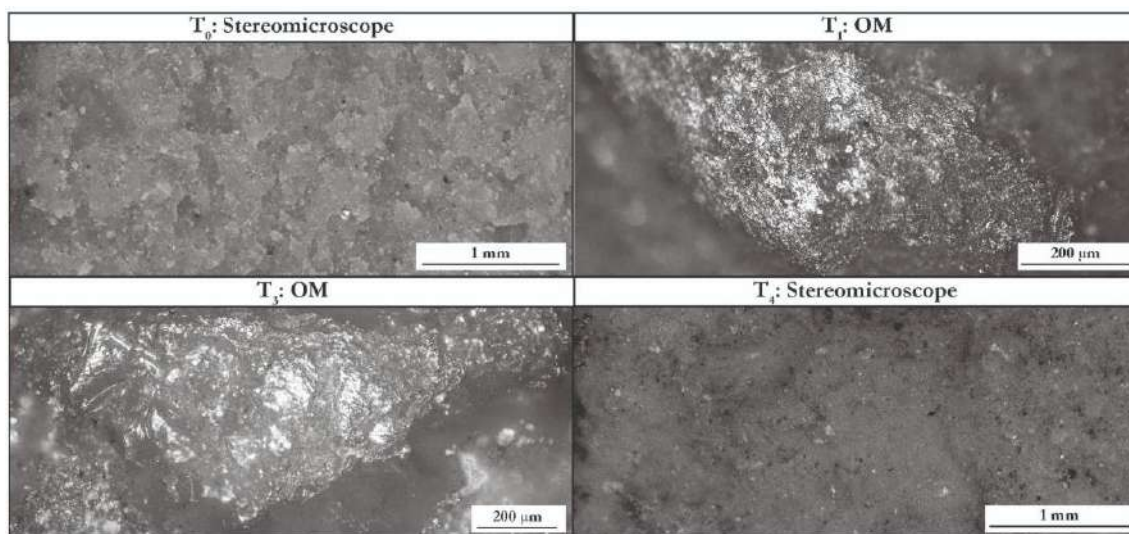
Figure 5. 13. GS8: molds of the surface of the active tool used to process Rumex crispus achenes depicted at T₀, T₁, T₃ and T₄ with stereomicroscope and OM (from Sorrentino et al. 2023a).
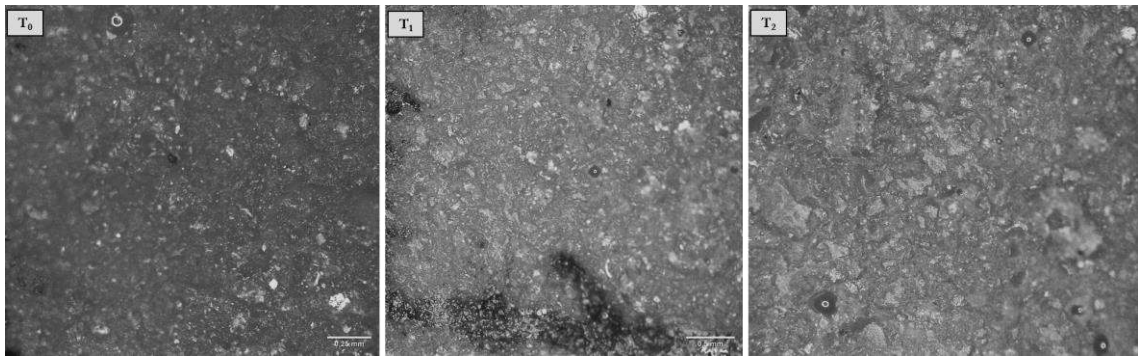
Figure 5. 14. M12: molds of the surface of the passive tool used to process Rumex crispus achenes at different T and imaged with stereomicroscope
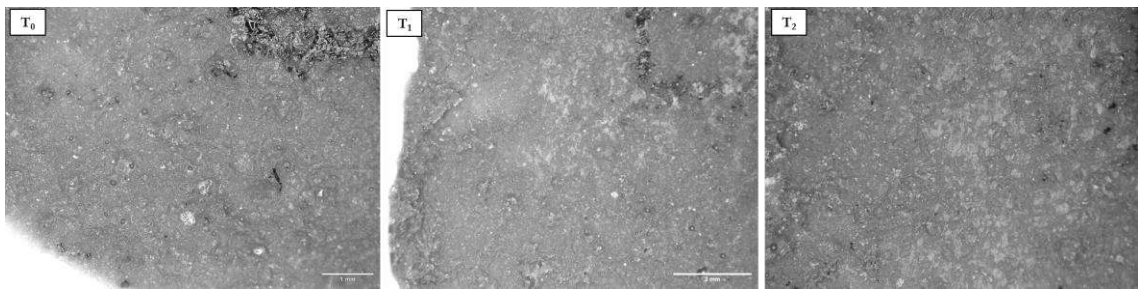
Figure 5. 15. M9: molds of the surface of the active tool used to process Rumex crispus achenes at different T and imaged with stereomicroscope

Figure 5. 16. GS9: molds of the surface of the active tool paired with the wooden base used to process Rumex crispus achenes at T_0 and T_3. Left: the same area at T_0 and T_3 acquired at the stereomicroscope; Right: the same feature at T_0 and T_3 acquired at SEM (from Sorrentino et al. 2023a).

<u>Implements involved in acorns processing</u>. The tools used to process acorns, M23 and M2, exhibit a natural shine. In the case of M23, the passive stone, no significant changes are observed at the macroscale. However, when magnification is increased starting from $T_{0.1}$, the surface develops a frosted appearance as defined by Adams (Adams et al. 2009). By T_1, large and well-defined rubbed areas become evident in the region where the processing takes

place. Additionally, small polished spots, conchoidal fractures, and very light striations can be observed. Moving to T_2, the abraded zones become smaller and less distinct. Upon reaching T_3, the surface levels out, exhibiting a smooth appearance with large areas of intense polish characterising the use-surface, (Figure 5.17 and 5.18).

The use-surface of the active stone, M2, appears to be less affected by the processing, with the main observed change being a light gradual flattening of the surface. (Figure 5.19). In phase $T_{0.1}$, large areas of intense polish become noticeable. Additionally, some natural cracks are seen to propagate through use.

Furthermore, the implements GS3-M5 were also used during T_4 to process acorns. However, the active tool broke after approximately 15 minutes of pestling the oven-dry acorns, in an attempt to reduce them into smaller fragments for later grinding

The pair GS16-GS12 were used to treat pine nuts (90 minutes) and hazelnuts (additional 60 minutes) showing a pattern very different from the one detected on M23-M2. The passive tool presents a highly rough and irregular surface that is not flattened during use, but rather undergoes slight smoothing of both low and high topography with the rounding of crystal edges. By T_3, short groups of light striations become visible, and their different direction indicating circular grinding motions. Large areas of residue accumulate on the surface, which undergoes only dry cleaning (fourth experimental scenario). At T_5, short groups of light parallel striations with a loose density on the surface, are still evident, showing a preferential direction due to prevailing linear grinding. Moreover, micropitted polish areas develop, likely due to contact with greasier resources like hazelnuts. Additionally, some cracks and fractured crystals are visible, likely a result of the crushing process of hazelnut shells (Figure 5.20).

The active tool GS12 initially possesses a flat surface, which by T_3 becomes highly irregular with several prominent rubbed areas and some light striations, along with large micropitted polish areas. While large areas of residue accumulate on the surface, their quantity is lower compared to the active tool. The surface pattern undergoes a significant change after T_3, presenting a levelled and regular appearance, possibly due to the smoothing effect of the greasiness from the hazelnuts. Additionally, some cracks and conchoidal fractures are detected, likely resulting from the crushing of hazelnut shells (Figure 5.21).

M7, the active tool paired with the wooden base used for hazelnuts, exhibits a levelling and smoothing effect on the low microtopography. Additionally, flattened grains with rounded edges are observed. These patterns seem commonly to stone that have contact

with wood and are well highlighted under SEM. However, some conchoidal fractures are also visible, likely resulting from the impact with nutshells during the crushing process (Figure 5.22).
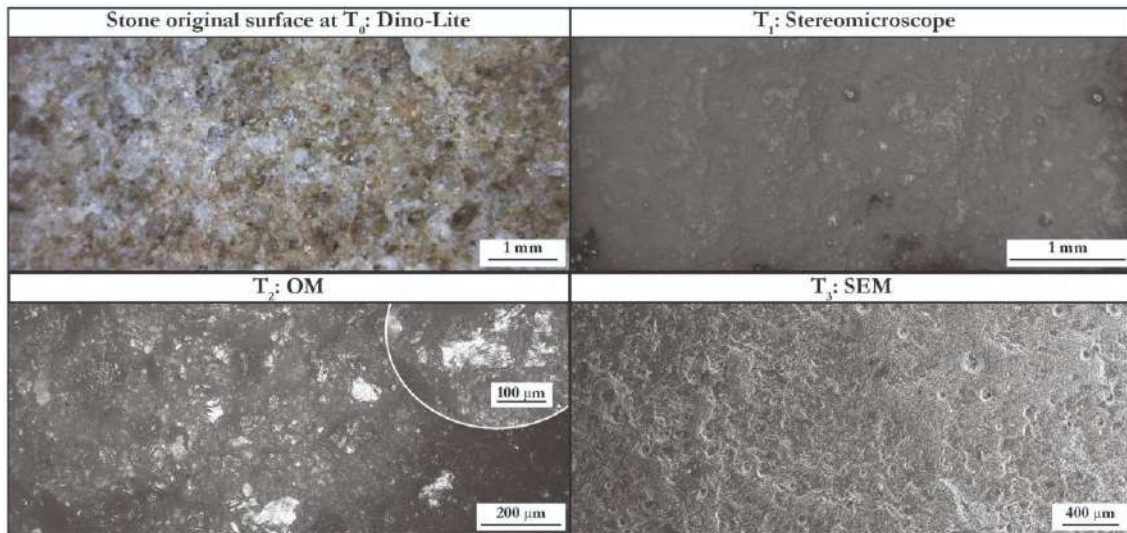
Figure 5. 17. M23: stone surface (T₀ original stone) and molds of the passive tool used to treat acorns at different T. Surface details imaged with different microscopes: T₀: Dino-Lite, T₁: stereomicroscope, T₂: OM, and T₃: SEM, highlight the different scrutiny capacity of each microscope, magnification and resolution (from Sorrentino et al. 2023a).
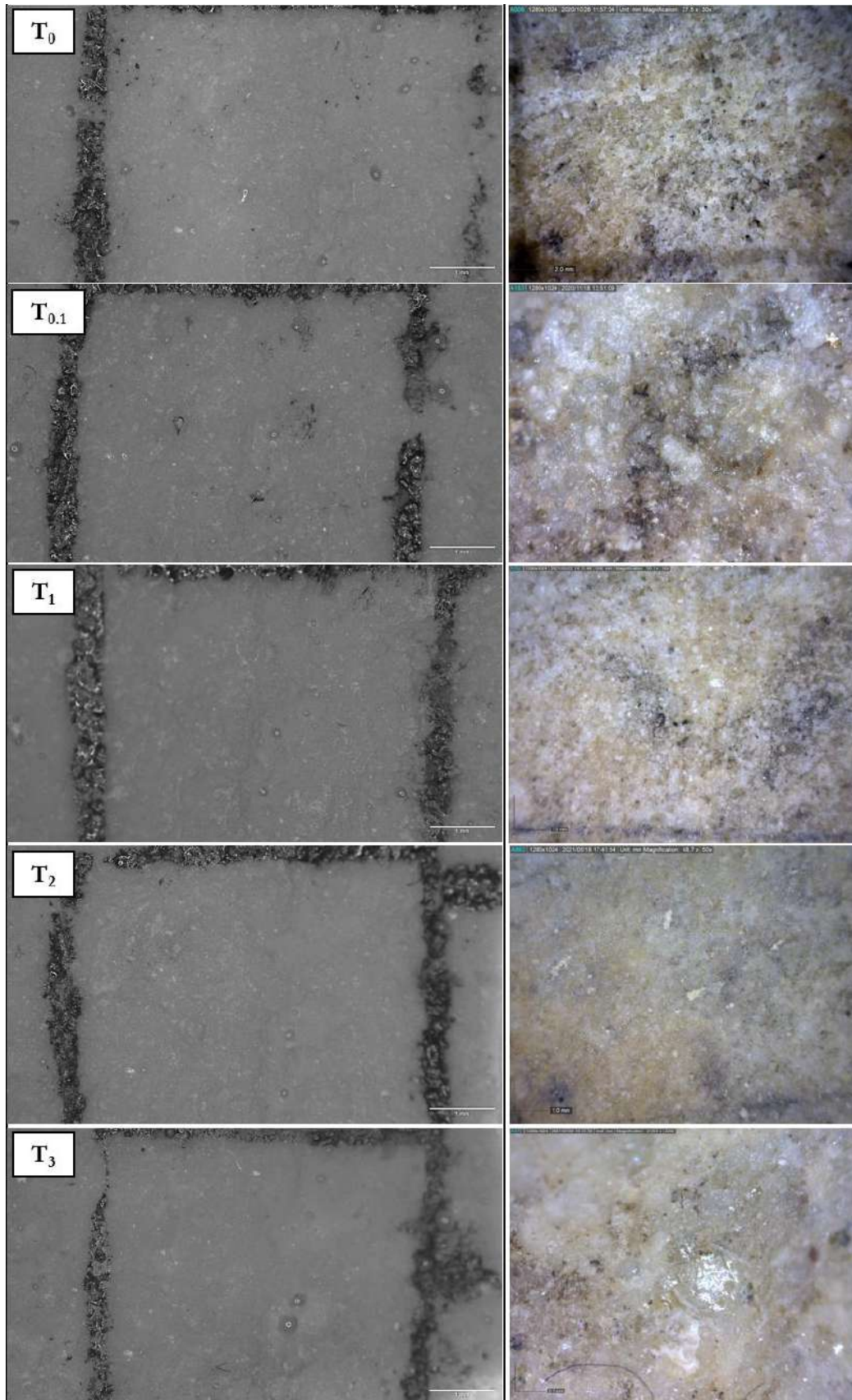
Figure 5. 18. M23: molds and original surface of the same square on the passive tool used to process acorns at different T and imaged with stereomicroscope (on the left) and Dino-Lite (on the right).
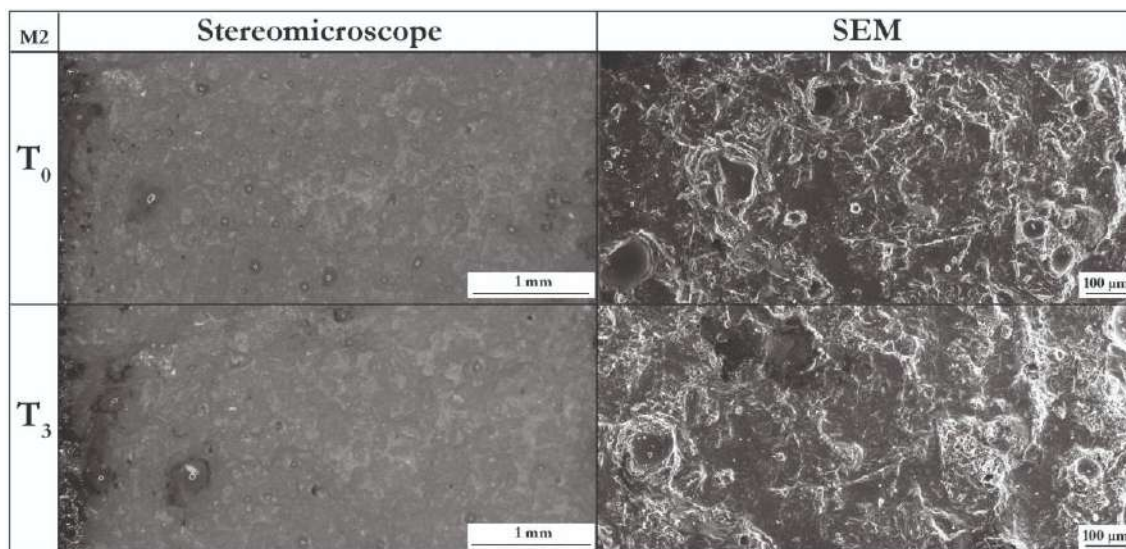
Figure 5. 19. M2: molds of the surface of the active tool used to process acorns at T_0 and T_3. Left: the same area at T_0 and T_3 acquired at the stereomicroscope; Right: the same area at T_0 and T_3 acquired at SEM (from Sorrentino et al. 2023a).
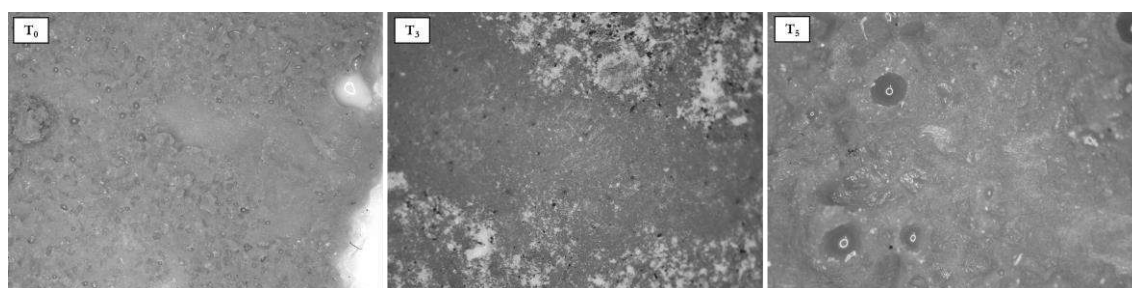
Figure 5. 20. GS16: molds of the surface of the tool, under stereomicroscope and depicting T_0, T_3 and T_5.
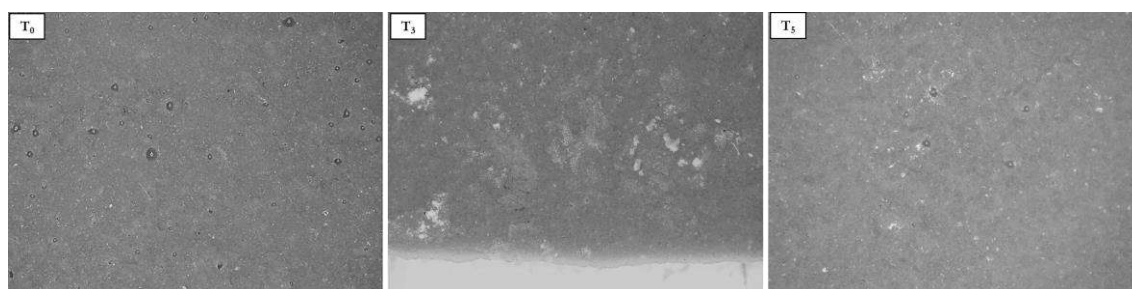
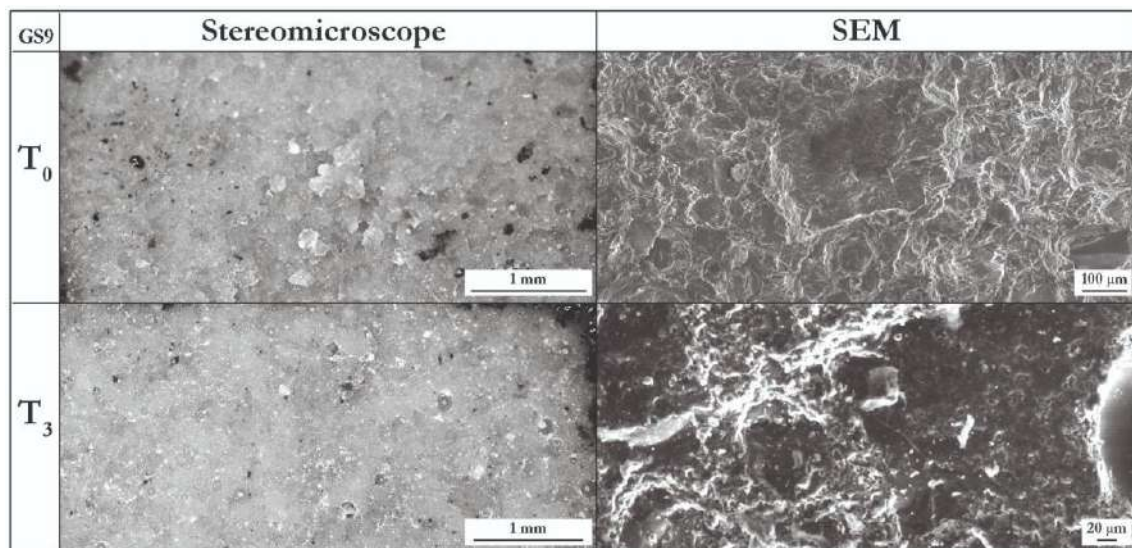*Figure 5. 21. GS12: molds of the surface of the tool, under stereomicroscope and depicting T_0, T_3 and T_5.*
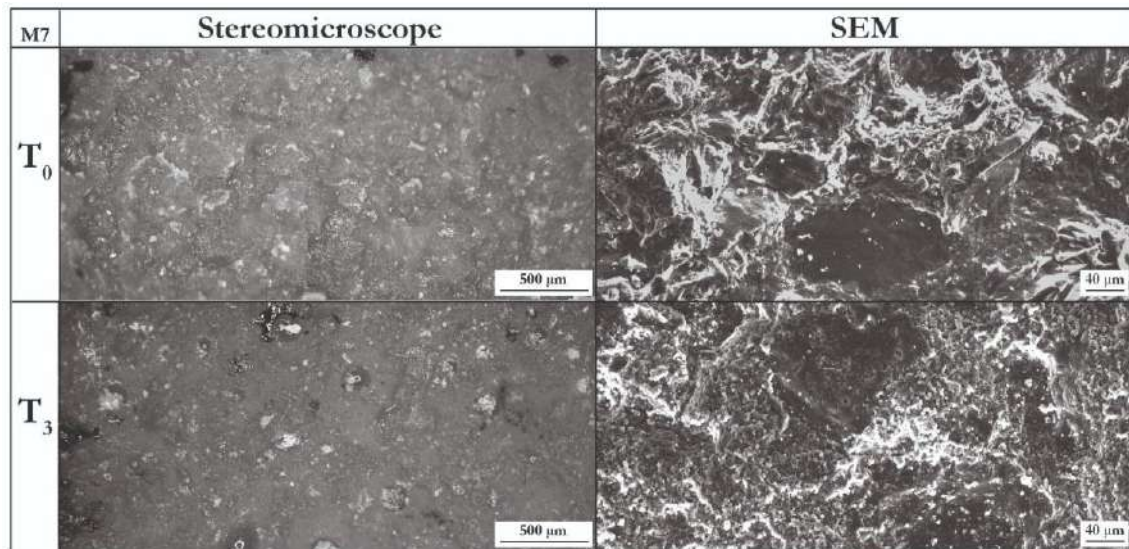
Figure 5. 22. M7: molds of the surface of the active tool paired with the wooden base used to process hazelnuts at T_0 and T_3. Left: the same area at T_0 and T_3 acquired at the stereomicroscope; Right: two different surface details within the same area at T_0 and T_3 acquired at SEM (from Sorrentino et al. 2023a).

Implements involved in roots processing. The stones used to process the USOs (M23-M2; M8; GS15-GS13 up to T_3); seems to be very lightly affected by the processing. On the Moldovan tools M25 and M3, areas characterised by polish are evident at high magnification and intensify through time. On the passive stone M25 very light striations are detected (Figure 5.23). SEM inspections confirm that the surface shows very little change, but at T_3 areas that were smooth in the original surface exhibit a light roughness at the micro-topographical level, which is more intense in the active tool, M3, whose working surfaces show broken grains, battering marks, and polish. Moreover, roots debris are visible since the paste gets easily trapped on the cavity of the stone, even more on the active tools (Figure 5.24).

Regarding the pair from Fiora River, GS15-GS13, wear becomes more apparent. The surface of the passive tool shows a general smoothing effect along with scattered areas of micropitted polish and rare polished deposits. Some fractured crystals and conchoidal fractures are also visible (Figure 5.25). As for the active tool, observations were restricted to naked eye observation during the experiment (forth replicative scenario), and molds were not taken at T_3. This limitation was due to the presence of *Dacus carota* root residues that adhered to the tool surface, making it impossible for the mold to replicate the stone's surface features.

M8, the active tool used with the wooden base, when compared with M3, shows more appreciable changes in the surface morphology and at T_3 the lowering of the surface is

evident, as well as the increasing of the rubbed and polished areas; the inspection at SEM revealed some broken grains (Figure 5.26).
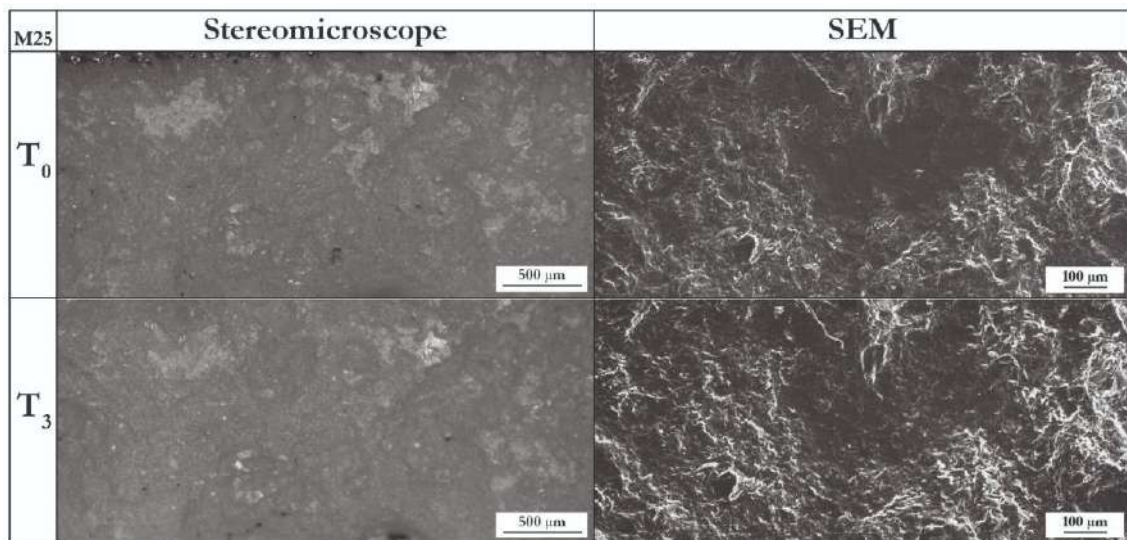
Figure 5. 23. M25: molds of the active tool surface used to process Cichorium intybus roots at T_0 and T_3. Left: the same area at T_0 and T_3 acquired at the stereomicroscope; Right: the same area at T_0 and T_3 acquired at SEM. In T_0 a naturally polished area is visible, while in T_3 this polish becomes slightly coarse (from Sorrentino et al. 2023a).
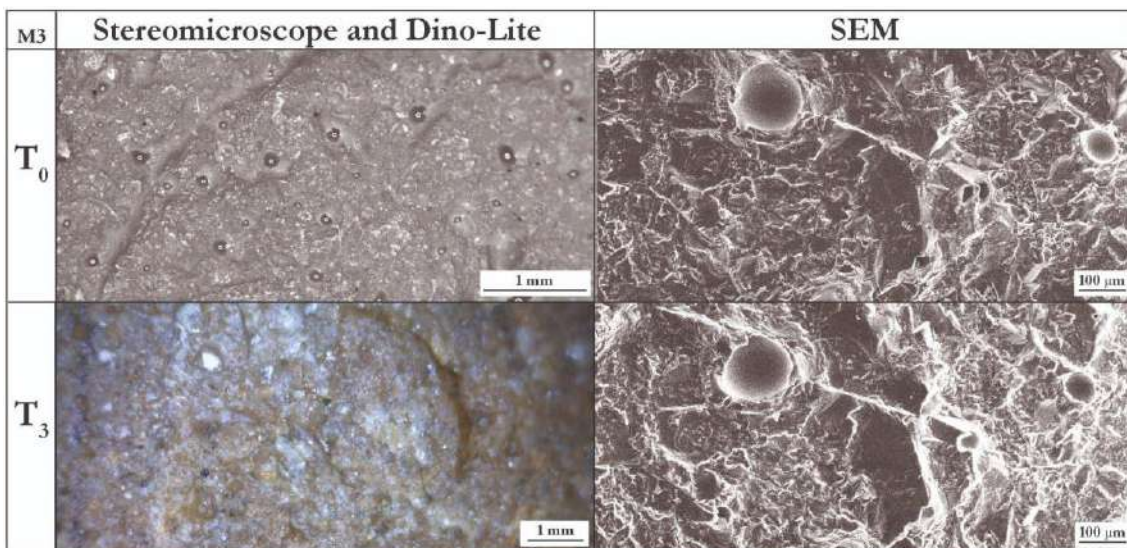
Figure 5. 24. M3: stone surface (T_3 on the left original stone) and molds of the active tool at T_0 and T_3. Left: T_0 image acquired at the stereomicroscope and depicting the same area of T_3 acquired with Dino-Lite; Right: the same area at T_0 and T_3 acquired with SEM. In T_0 naturally polished areas are visible while in T_3 the area of this polish increased (from Sorrentino et al. 2023a).
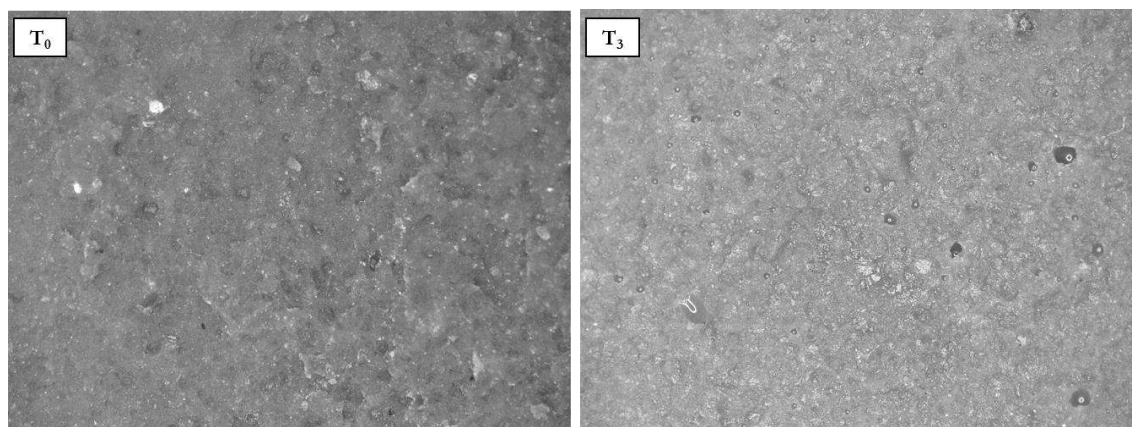
Figure 5. 25. GS15: molds of the surface of the passive tool, under stereomicroscope and depicting T$_0$ and T$_3$
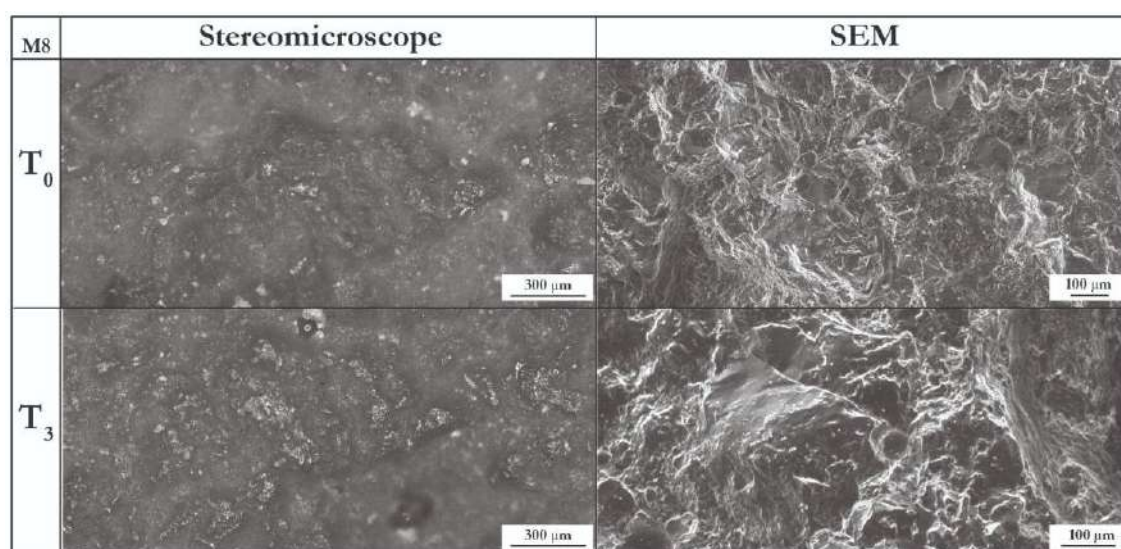
Figure 5. 26. M8: molds of the surface of the active tool paired with the wooden base used to process Armoracia rusticana roots at T$_0$ and T$_3$. Left: the same area at T$_0$ and T$_3$ acquired at the stereomicroscope; Right: two different surface details within the same area at T$_0$ and T$_3$ acquired at SEM (from Sorrentino et al. 2023a).

Implements involved in ochre processing. The tools used to treat ochre present totally different patterns. The passive stone, GS10 at T$_3$, is characterised by levelling of the surface, the presence of broken grains and conchoidal fractures, visible already at low magnification (Figure 5.27).

Furthermore, the ventral side of selected experimental GSTs was also analysed. GS10 ventral side at T$_5$ is here reported as an example (lower portion of Figure 5.27). Microscopy analysis of this side of the tool reveal traces that affected the matrix, resulting in a uniform wear pattern. The harder grains protruding from the surface were flattened, and in some instances, they displayed slight polishing on their tops or other phenomena as edge chipping and fracturing. These changes were a consequence of the impacts and soil rebounds experienced during the mechanical processing carried out on the active surface.

The active stone M1 at T$_3$ also displays a levelling and smoothing of the matrix and rubbed areas. The stone initially exhibits a natural uniform polish, which becomes mostly diminished with use, appearing only in small patches and displaying a less uniform appearance in the form of micropitted polish (Figure 5.28).
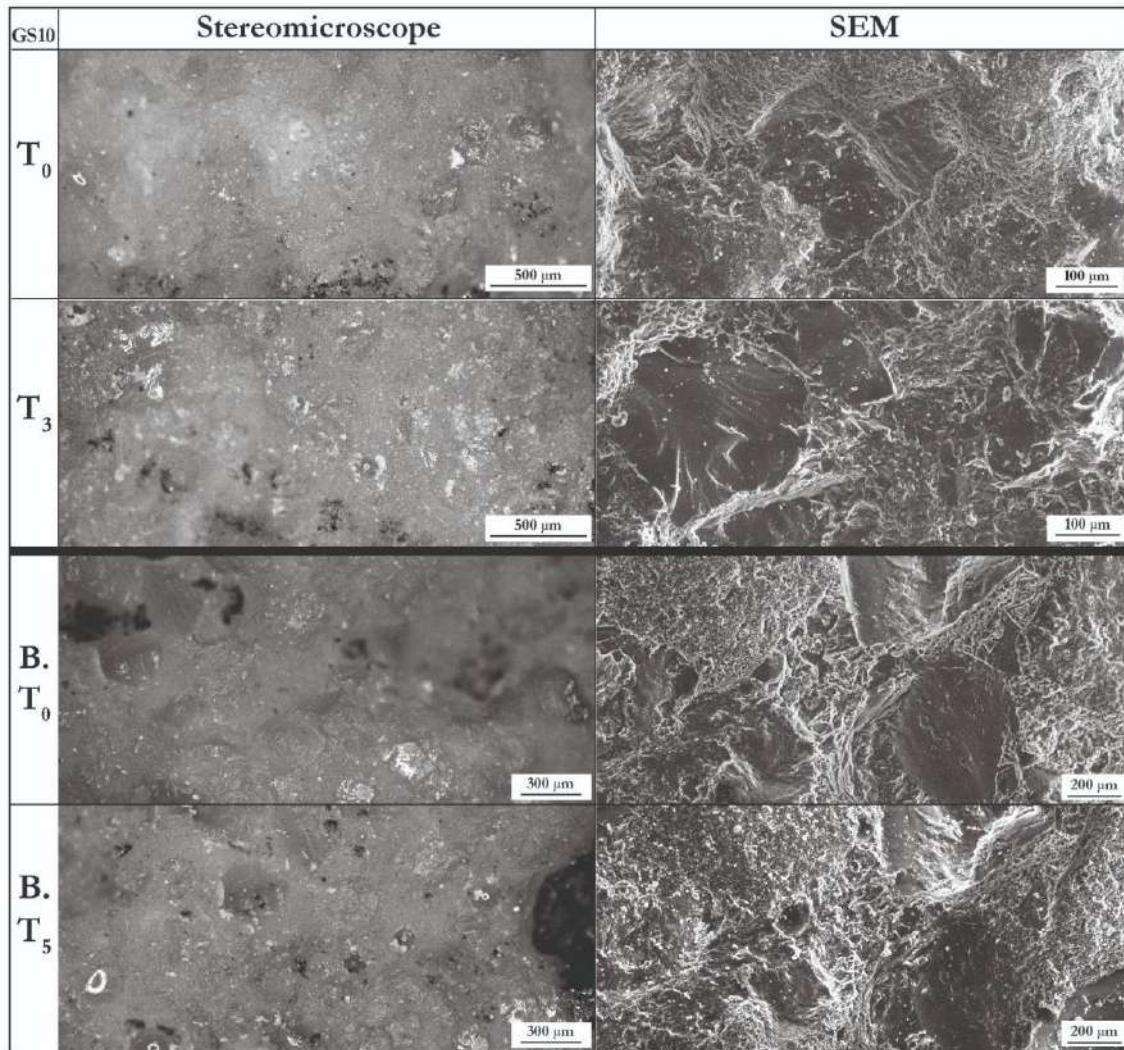
Figure 5. 27. GS10: molds of the surfaces of the passive tool used to process ochre. Above: images of the same area of the used surface at T$_0$ and T$_3$ acquired at the stereomicroscope (on the left), and at SEM (on the right); Below: images of the same area of the bottom side of the tool (B., lying on the ground during processing) at T$_0$ and T$_5$ acquired at the stereomicroscope (on the left) (from Sorrentino et al. 2023a).
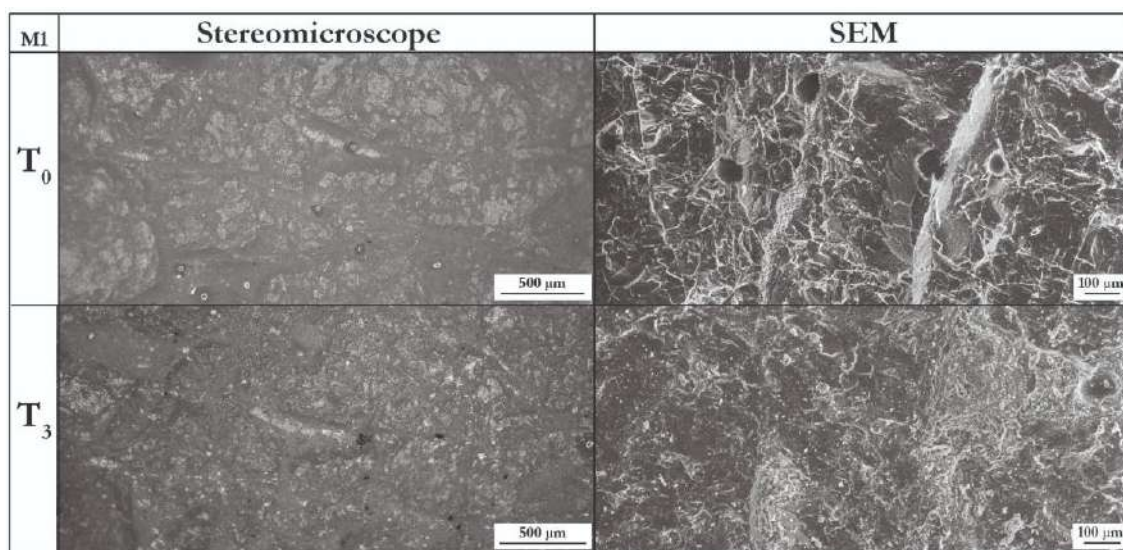
Figure 5. 28. M1: molds of the active tool surface used to process ochre at T_0 and T_3. Left: the same area at T_0 and T_3 acquired at the stereomicroscope; Right: the same area at T_0 and T_3 acquired at SEM (from Sorrentino et al. 2023a).

Implements involved in phloem processing. The same pair of stones, GS10 and M1, was used from T_4 to T_5 to process *Pinus nigra* phloem. Consequently, the wear resulting from the processing of this resource accumulates on preexisting features. These features were not natural but rather derived from ochre processing.

The passive tool GS10, exhibits extensive and intense rubbed areas, along with both large groups of short and well-defined linear striations showing varying oblique directions. Additionally, there are large patches of pronounced micropitted polish and some areas displaying a serrated polish (Figure 5.29).

The active stone M1 at T_5 present large and diffuse polished areas mainly of micropitted type but also small deposit type on top of the high topography (Figure 5.30).
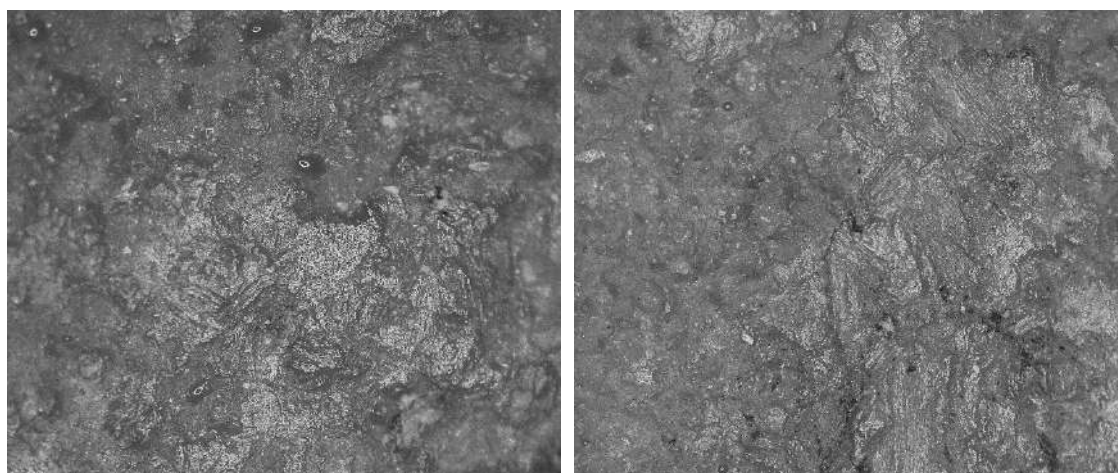
Figure 5. 29. GS10: mold of the surfaces of the passive tool used to process phloem.
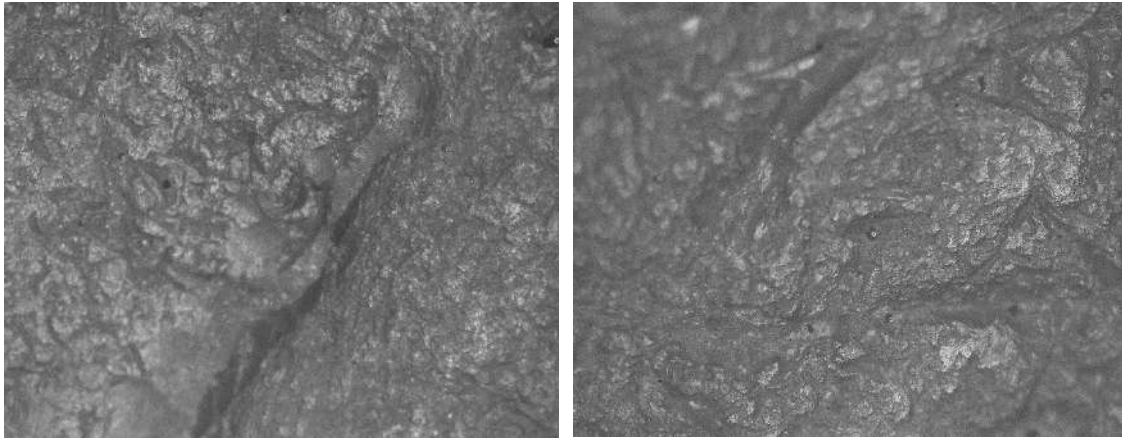
Figure 5. 30. M1: mold of the surfaces of the active tool used to process phloem.

5.5.3.   Parametric approach

In the central square of the use-surface of each tool, a 0.5 cm² control square(s) was drawn that were recorded on molds using a Leica DCM3D confocal profilometer. Twenty-five areas of 850 µm² within the reference squares were measured with a 10× lens, and nine were then sampled for data elaboration and analysis.

By recording the same areas throughout the various cycles of the replicative process, this allowed to gather data on wear formation and development, as well as quantitative information for statistical tribological analysis. Confocal profilometry enabled the calculation of the high distribution and also of the ISO 25178-2 surface texture areal parameters. It has to be noticed that Gwyddion software is not calculating the Kurtosis (Sku), but the Excess Kurtosis value by considering a Gaussian data distribution as zero (Nečas and Klapetek 2012). Therefore, to obtain the Sku, 3 needs to be added (hence, the Sku boxplot in Figure 5.32 reports data as Sku values minus 3).

These objective measurements of the surface features of the stones, allowed accurate and detailed understanding of the wear patterns resulting from different processing tasks.

The analysis was performed on the active tools paired with the wooden base GS9, M7, M8; the active tools GS8, M2, M3, M1 and their coupled passive tools GS7, M23, M25, GS10. Moreover, the roughness descriptors Sa and Sq were calculated also for the unused surface of the passive tools GS10, GS3 and M12. The measured values for the experimental GSTs, are here plotted and discussed, while the data are reported in Appendix B. The Sa and Sq parameters are plotted in Figure 5.31, while data for Ssk and Excess kurtosis (Sku -3) are shown in Figure 5.32. Figure 5.33 collects Sp, Sv and Sz values, and finally the scatter plot hight distribution is shown in Figures 5.34 to 5.44.

The analysis clearly demonstrates that initially, all the stones from the Fiora River had higher roughness compared to the Moldovan ones. This is likely because the raw material of the stones from the Racovăt River is primarily quartz-arenite with a few greywackes, while the Fiora River pebbles are made out of sandstones, sublitharenites and calcarenites. As a result, the wear mechanism for the Fiora River stones is characterised by a rapid, progressive smoothing of the asperities over time, leading to a significant reduction of Sq and Sa in particular after the first utilisation cycle.
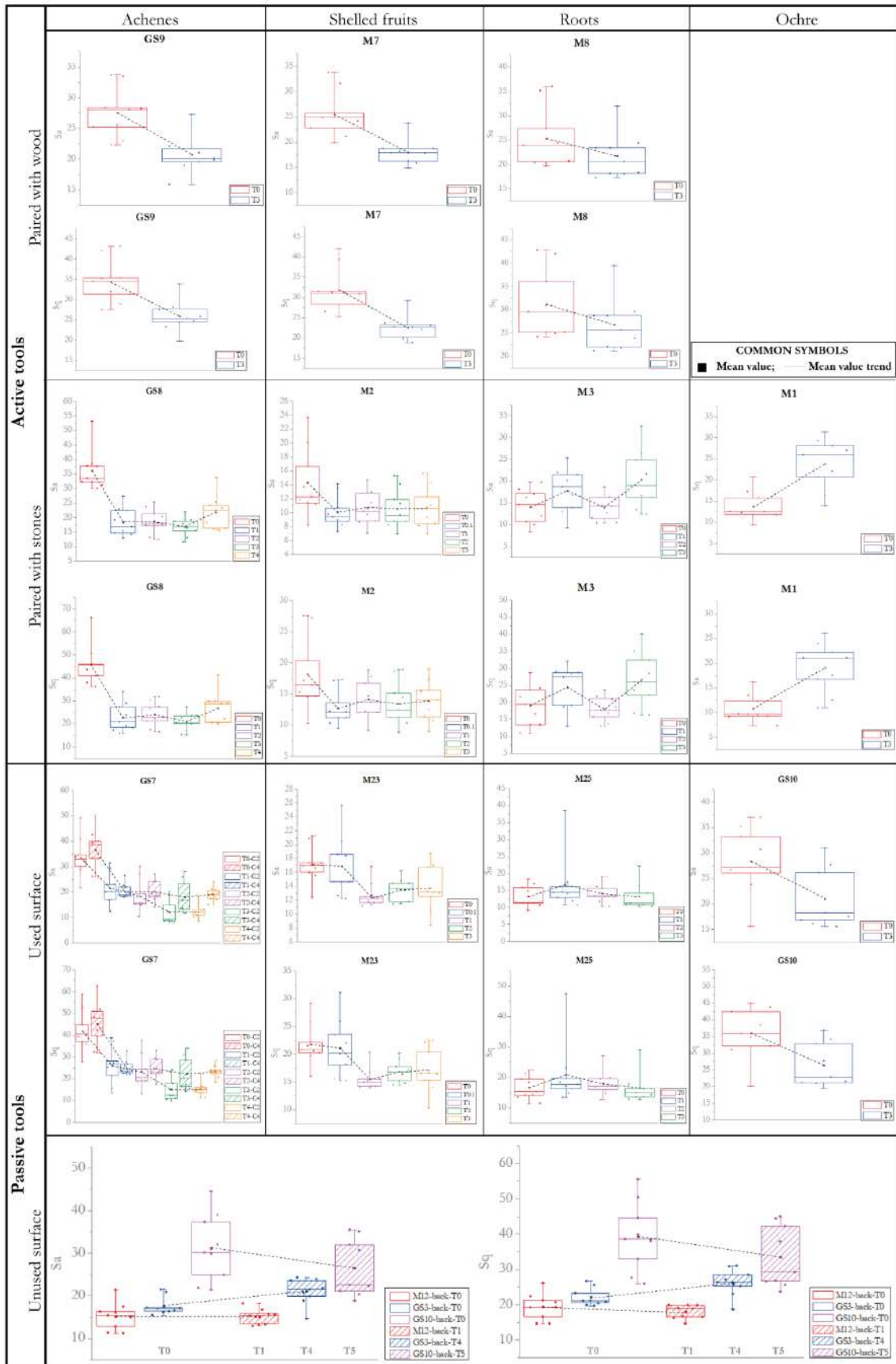
Figure 5. 31. Boxplot of the Sa and Sq parameters of the analysed experimental GSTs.
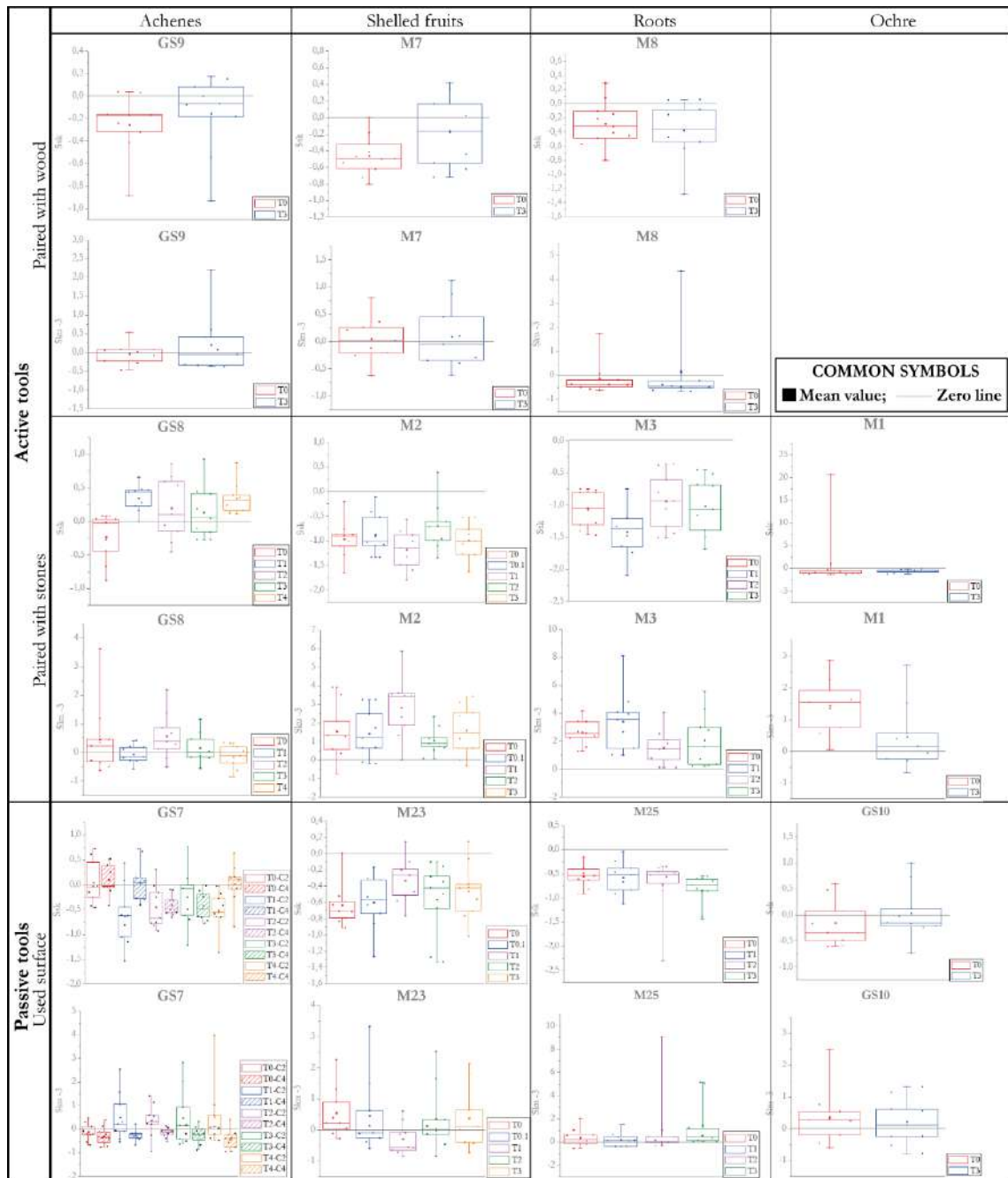
Figure 5. 32. Boxplot of the Ssk and Excess Kurtosis (Sku-3) parameters of the analysed experimental GSTs
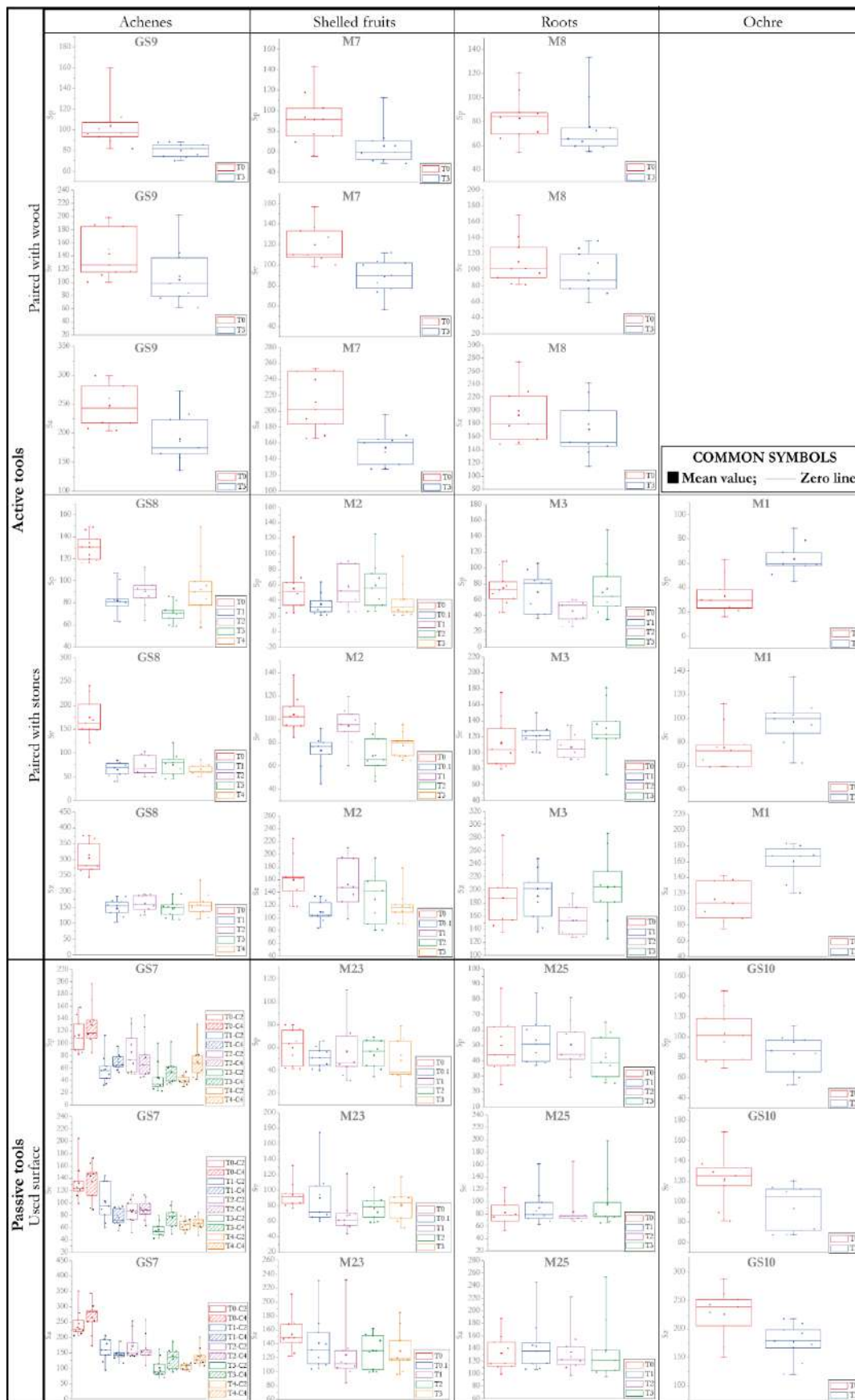
Figure 5. 33. Boxplot of the Sp, Sv and Sz parameters of the analysed experimental GSTs

GS7-GS8. For the passive tool GS7 two different squares on the use surface were analysed: C4 located at the centre of the use surface and C2 located at the peripheral area of the same surface. It is noteworthy that the two squares exhibited different behaviours. After an initial decrease in Sa and Sq parameters, which is more pronounced in the central square, the roughness in C4 becomes relatively constant with small non-monotonic oscillations, likely due to alternating cycles of levelling and wear pattern formation. On the other hand, C2 accumulates fatigue and the roughness value decreases over time. This phenomenon is also clearly evident in the microscopy analysis.

The analysis of height distributions (Figure 5.34) reveals that, from T_0 to T_1, the amplitude of the tails decreases, with a more significant reduction observed in square C4 compared to C2. This observation is consistent with the smoothing of surface asperities, as indicated by the evolution trend in the Sa and Sq parameters. As the experiments progress, distinct patterns emerge in the two squares. In C4, the distribution remains relatively similar until T_4, while in C2, the mode of the distribution shifts towards positive values particularly evident in T_1 as demonstrated also by the moderate negative Ssk. Moreover, a gradual decrease in the amplitude of the tails is observable. A closer examination reveals that the distribution is symmetrical, with a skewness around 0 ± 0.5, which tends to decrease and become slightly negative after the initially minimal positive value at T_0. Additionally, all the distributions exhibit a negligible deviation from the kurtosis of the Gaussian distribution, which is 3, as shown in Fig. 5.32 by plotting the value of Sku - 3. Furthermore, the wear process is accompanied by a reduction in the maximum peak height, particularly evident in the early stages of the test (T_1). Subsequently, Sp oscillates between 30 and 80 µm, with the more pronounced variations observed in square C2. The Sv parameter for square C2 decreases until T_3, with two significant drops between T_0 and T_1 and between T_2 and T_3, while an increase is noticeable at T_4. In square C4, the trend of Sv is mainly influenced by the dip observed between the T_0 and T_1 stages. Subsequently, it fluctuates between 60 and 100 µm. The Sz values decrease after T_0, then it remains relatively constant, and decreases again between T_2 and T_3.

In the case of GS8, the Sa and Sq parameters exhibit a trend similar to what was observed for GS7 in square C4. The height distributions (Figure 5.35) are evenly distributed around zero and follow a Gaussian shape. Comparing these parameters at the different times reveal a general trend where the tails gradually diminish in amplitude. This phenomenon is attributed to the progressive formation of wear, which smooths out the peaks and valleys of

the surfaces. The Ssk tends to increase and becomes slightly positive from the initial negative value at T_0, the opposite trend if compared to its paired tool GS7. Similar to GS7, all the distributions exhibit a negligible deviation from the kurtosis of a Gaussian distribution. Again, as in GS7, a reduction in the maximum peak height is observed especially at the beginning of the test (see T_1 compared to T_0) and then it oscillates from 60 to 90 μm for later times. This validates the periodic pattern of wear progression wherein crystal fractures are followed by dulling and surface levelling. The maximum pit height is also primarily affected by the change between T_0 and T_1, and then it remains almost constant. The sum of Sp and Sv leads to Sz, which corresponds to the maximum surface amplitude, that also follows the trends observed for the previous parameters.
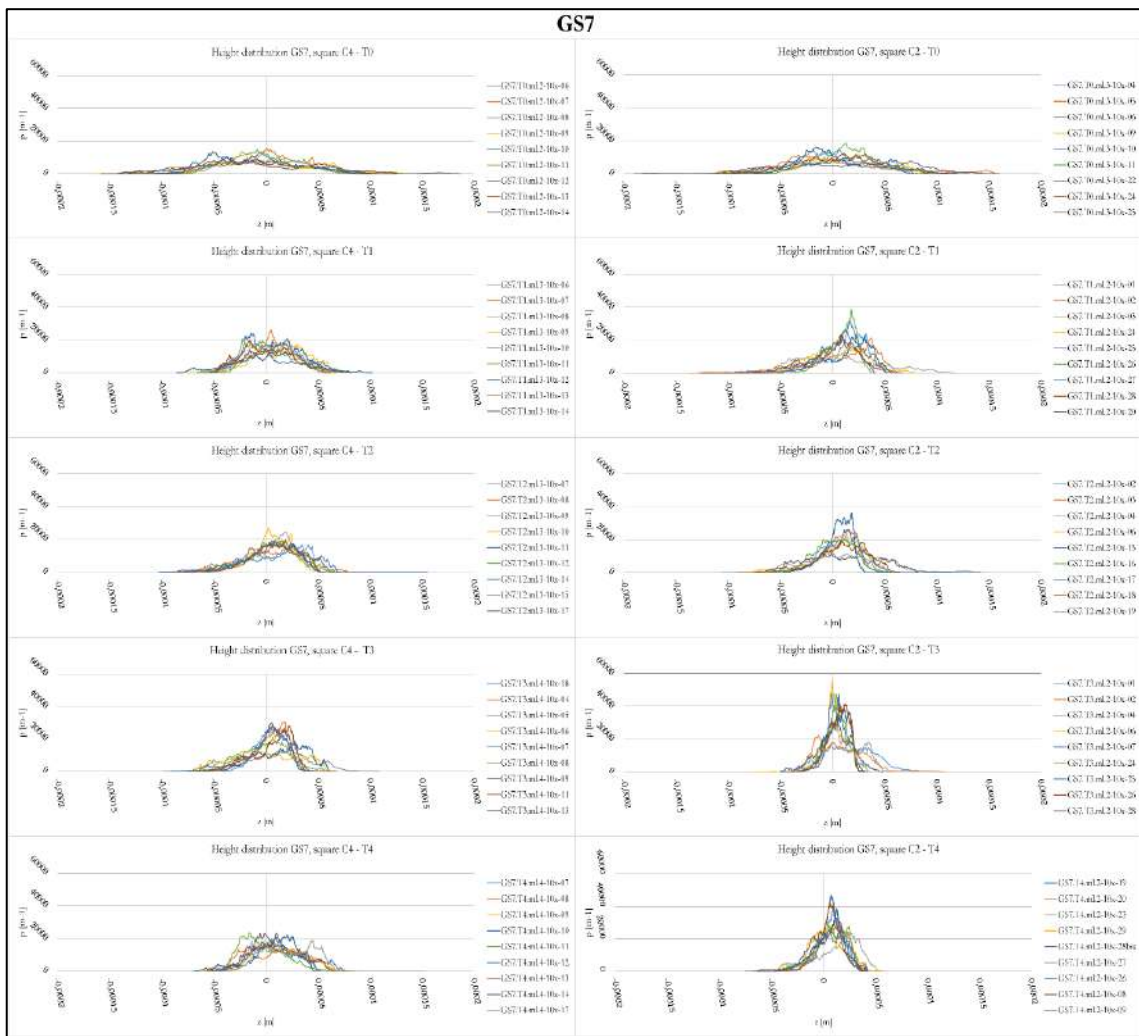
Figure 5. 34. GS7: high distributions of the two control squares C2 and C4.
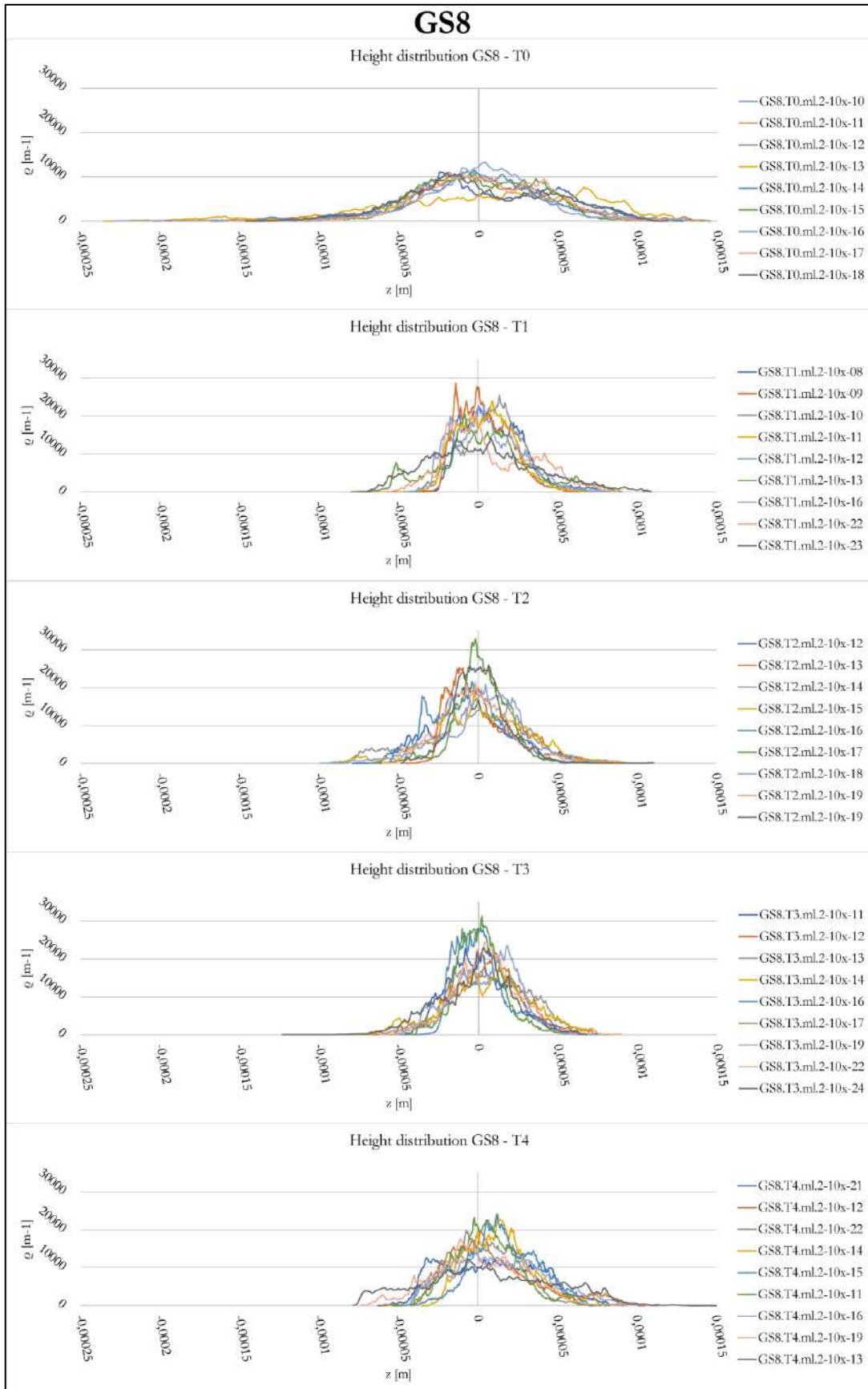
Figure 5. 35. GS8: height distributions

M23-M2. The tools M23 and M2, were used in acorns processing through different steps, the $T_{0.1}$ phase used to remove the pericarp implying vertical motion, and from T_1 to T_3 used to produce flour through vertical and horizontal movements. Acorns are a source of moisture and fat, which can lead to smoothing of the tools surface during grinding. Indeed, after the first use cycle, M2 exhibited a significant decrease in the Sa and Sq values, indicating a surface smoothing effect. However, after T_1, there was an increase in these parameters, followed by a relatively consistent pattern throughout the subsequent use cycles (refer to Figure 5.31). This suggests that the surface roughness reached a relatively stable state after an initial smoothing.

In contrast, the passive tool M23 demonstrated a minimal initial roughness decrease, as the pounding action primarily affected a small area of the surface. However, a drastic reduction in the Sa and Sq values occurred from $T_{0.1}$ to T_1, similar to the behaviour observed in GS7 from T_0 to T_1. After this initial decrease, there was a slight increase in the roughness parameters.

The height distributions analysis confirms the observed trend. For M23 (Figure 5.36), there is a slight enlargement of the curve from T_0 to $T_{0.1}$, followed by a reduction in the tails primarily between $T_{0.1}$ to T_1. The distributions then remain relatively constant. This is also evident from the excess kurtosis, which values were slightly above 0 at T_0, and becomes slightly negative at T_1, before reaching positive values again at T_2. The modes of the curves are minimally shifted towards positive values, while the tails extend in the negative side of the graphs. Indeed, the skewness values are negative, indicating asymmetry in the surface texture. The maximum pit height hows the most significant reduction between $T_{0.1}$ to T_1. On the other hand, the maximum peak height remains relatively stable and presents lower values compared to the Sv. The Sz values decrease until T_1 and then stabilises for the later cycles. The height distributions of M2 (Figure 5.37) clearly exhibit a spike shape with long tails at all use cycles, characteristic of a positive kurtosis. Moreover, the tails present a noticeable difference between T_0 and $T_{0.1}$, with a decrease in their amplitude, followed by their expansion in subsequent use cycles. The skewness values for M2 are negative and exhibit non-monotonic oscillations. As for M23, the Sp parameter remains relatively stable for all used cycles varying from 40 to 80 μm, while a higher non-monotonic oscillation is noticeable for the Sv parameter. Similarly, the Sz parameter follows the same non-monotonic trend. Both M23 and M2, when compared to GS7 and GS8, show narrower height distributions since T_0, suggesting a limited range of height variation on their surfaces.
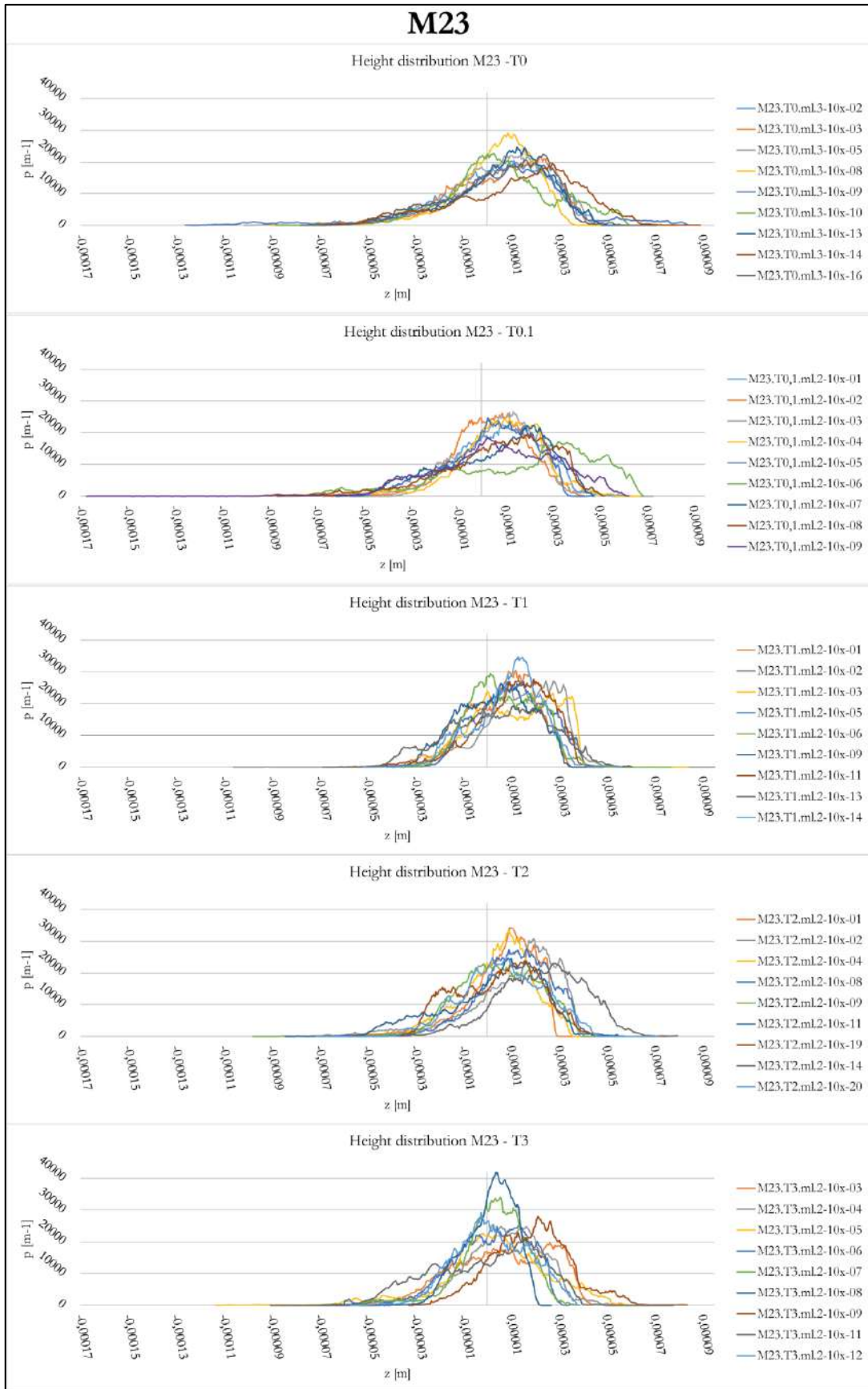
Figure 5. 36. M23: height distributions
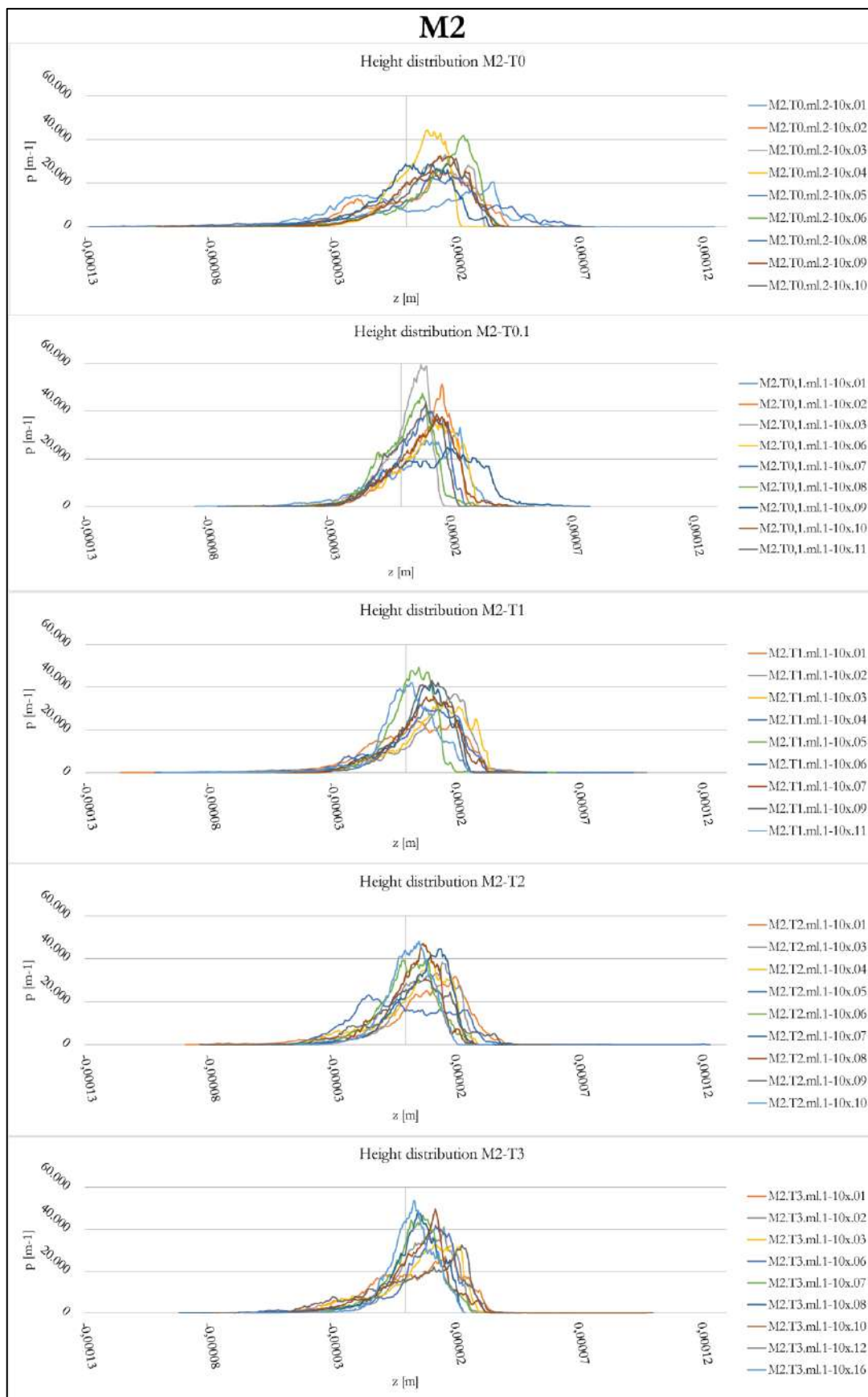
Figure 5. 37. M2: height distributions

M25-M3. M25 and M3, like M23 and M2, are also Moldovan stones; however, they were employed for the elaboration of dry roots primarily through pounding actions. This task could lead to the formation of cracks and the exposure of new surfaces, resulting in an increase in Sa and Sq values at certain time intervals. The trend over time for these parameters is non-monotonic, especially noticeable in the case of the active tool M3. Compared with the above-described tools, their behaviour is opposite, with an initial increase of roughness followed by a subsequent decrease.

The height distribution of M25 (Figure 5.38) can be described as a Gaussian distribution, centred around the mid-plane, slightly shifted towards positive values. This indicates that the surface texture is relatively symmetrical, with the skewness values close to 0 or slightly negative, and the kurtosis values around 3, which is typical of a mesokurtic distribution. However, for T_2 and T_3, the height distributions take a more spiked shape with longer tails, indicating a higher value of Sku (>3) and a moderate Ssk. The Sp and Sv parameters for M25 do not exhibit significant oscillations during the different use cycles. Additionally, the maximum surface amplitude also shows minimal variation, ranging from 110 to 150 μm.

For the active tool M3, the height distributions (Figure 5.39) are particularly spiked and have long tails (Sku > 3), indicating the presence of outliers. The distributions are highly skewed with the modes towards the positive value (negative Ssk parameters, mostly below -1). The different Sp and Sv ranges demonstrate that pits extend higher than peaks. Moreover, if compared with the active tools GS8 and M2, the Sp and Sv values do not exhibit significant oscillation, ranging from 40 to 80 μm for Sp and 90 to 130 μm for Sv. Consequently, the maximum surface amplitude (Sz) also shows minimal variation across the different use cycles.
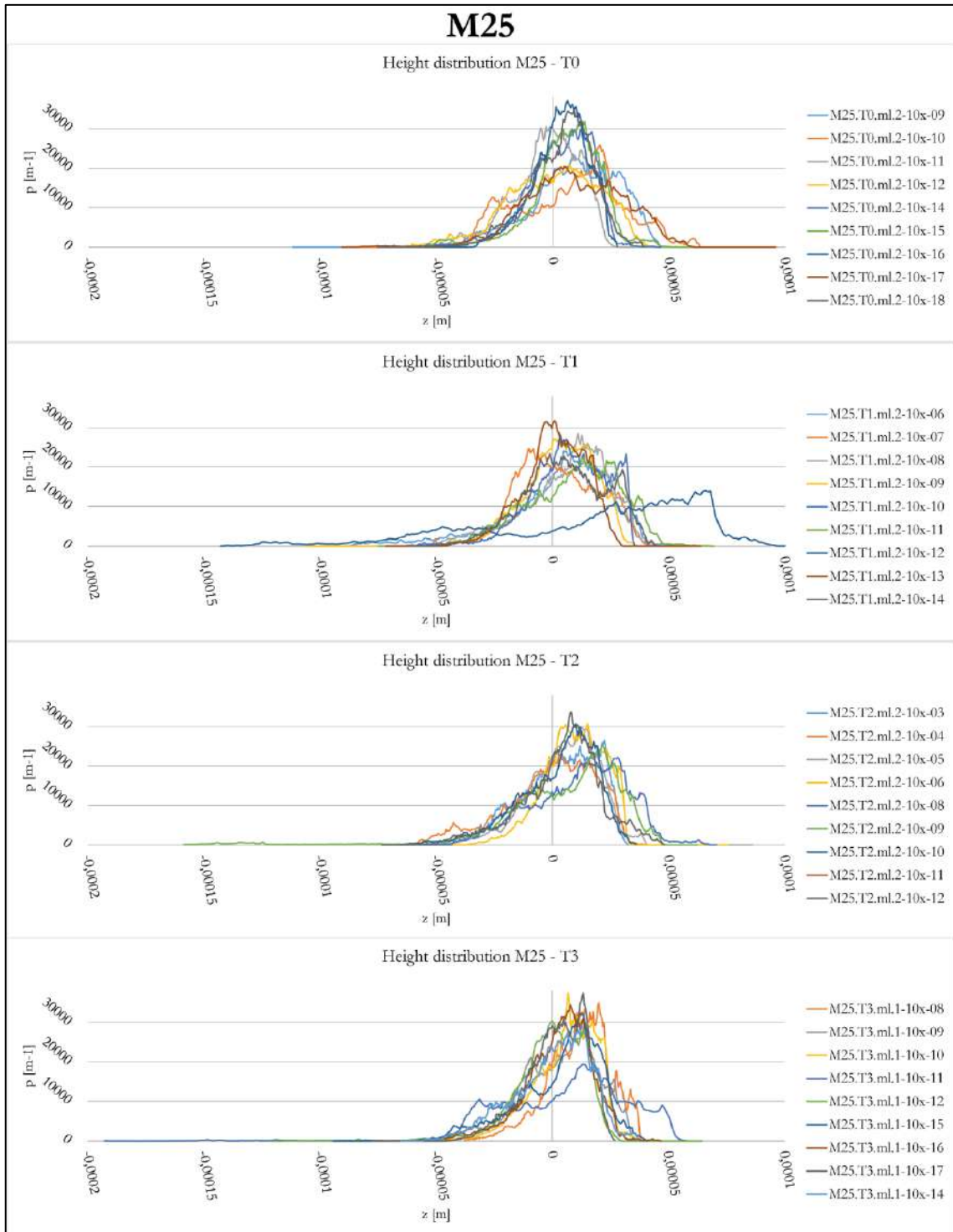
Figure 5. 38. M23: height distributions
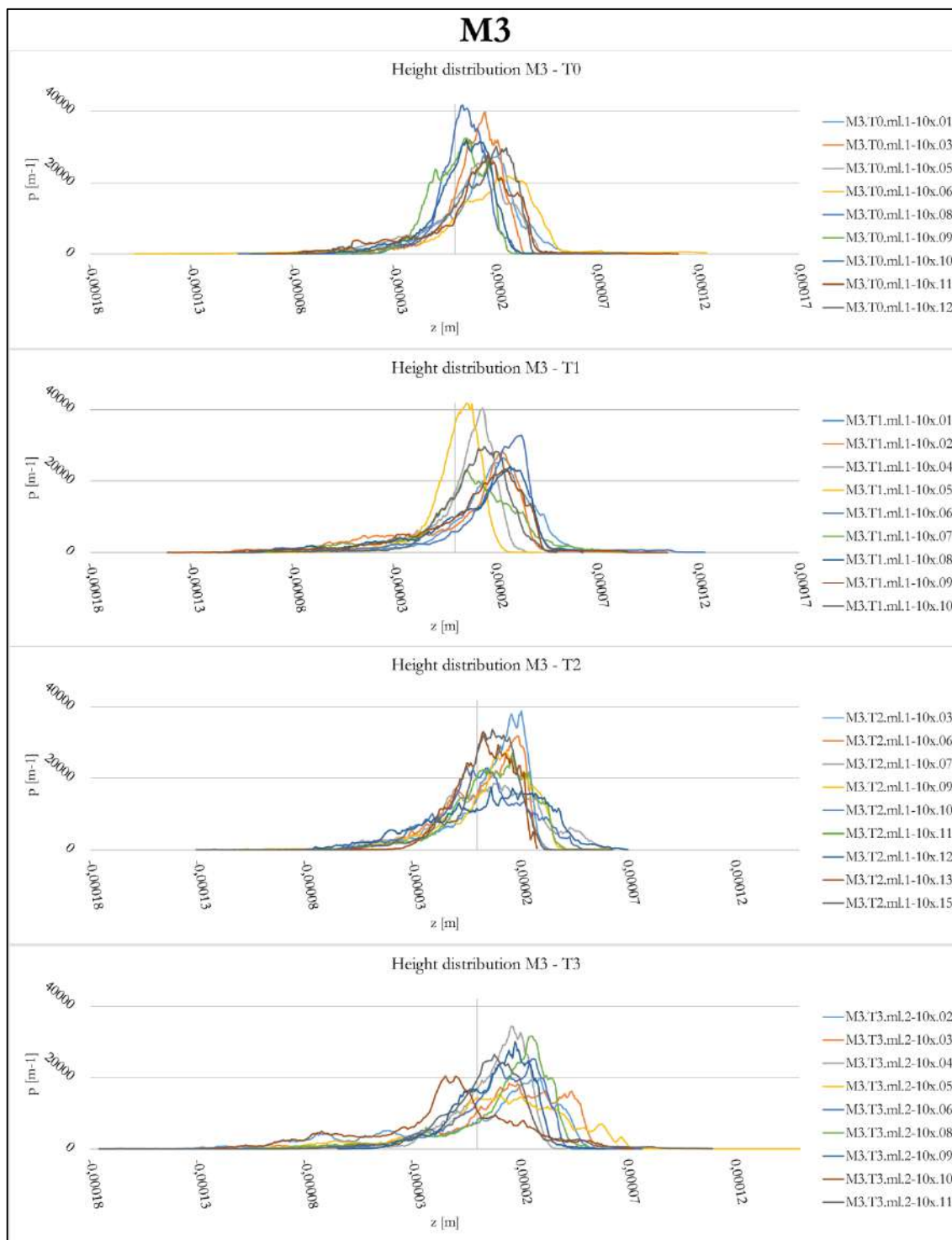
Figure 5. 39. M3: height distributions

GS10-M1. The active tool M1 and the passive tool GS10 were used for ochre pigment elaboration and exhibited contrasting trends. M1, a Moldovan stone, showed an increase in roughness similar to M3, another Moldovan stone used in a process involving a non-fatty resource that can lead to the formation of crystal cracks and fractured surfaces. On

the other hand, the passive tool GS10, an Italian stone, showed a noticeable decrease in roughness similar to GS7, which was also involved in processing a non-moisture resource. To ascertain whether this difference in trend is due to the petrographic dissimilarity between the active and passive stones or to the different role of the two tools, further tests are required.

The height distributions of GS10 (Figure 5.40) follow a Gaussian distribution with an Ssk value around 0 and a Sku value around 3. The amplitudes of the tails in the initial distribution decrease due to progressive wear formation, which smooths out peaks and valleys. This is evidenced by the decrease in both the Sp and Sv parameters, as well as a reduction in the maximum surface amplitude (Sz), which decreases from 200-250 µm to 150-200 µm.

For the active tool M1, the height distributions (Figure 5.41) exhibit a slight shift towards positive values, as indicated by the Sku values. The excess kurtosis, initially positive, tends to decrease towards zero. The elongation of the tails in both directions is also confirmed by the Sz values, which increases due to the presence of crystal crashing and battering marks resulting from the process. Specifically, the Sq parameter, which initially ranges from 20-40 µm, increases to 60-70 µm, while the Sv parameter increases from 60-80 µm to 85-100 µm.
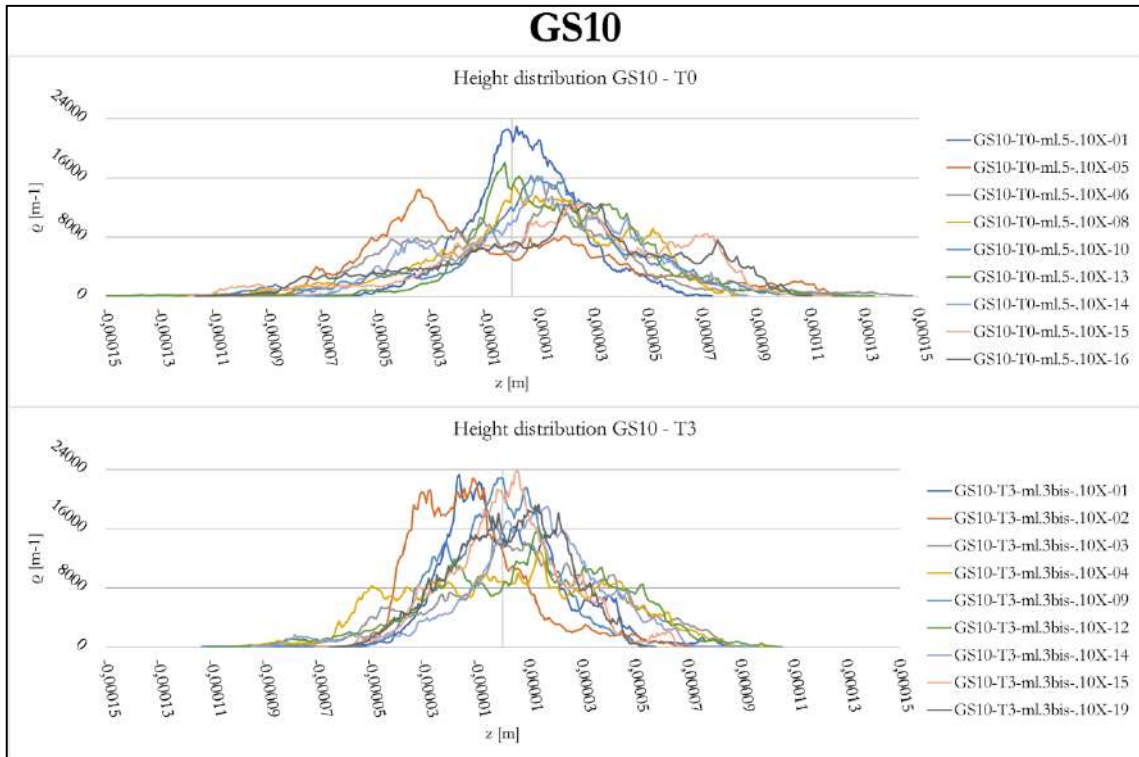
Figure 5. 40. GS10: height distributions
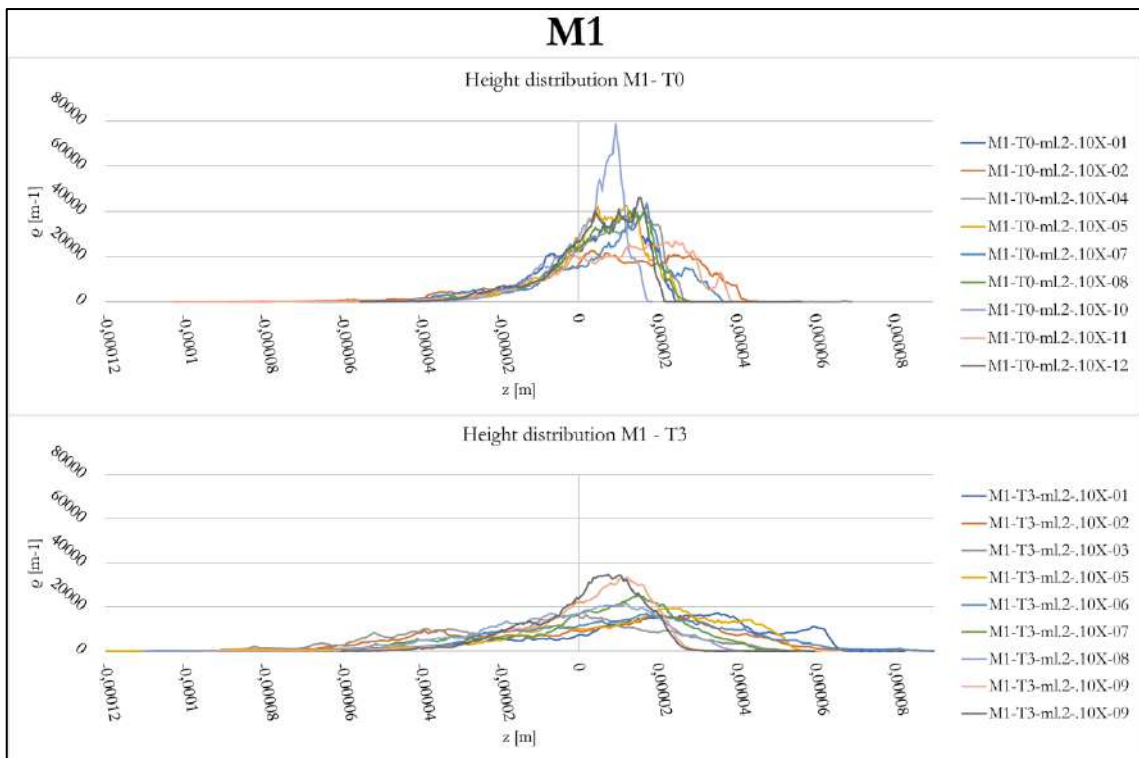
Figure 5. 41. M1: height distributions

Unused surface. The analysis also revealed that on the passive tools, the side of the stone that is not used in mechanical processing and is in contact with the ground, undergoes

transformation as a result of the blows and recoil absorbed during the processing ongoing on the use-surface. Stone M12, which is made of resistant quartz-arenite and was used for only 30 minutes to process achenes, showed very little decrease in roughness. In contrast, GS10, made of less resistant sandstone and used for 150 minutes, exhibited a significant decrease in roughness. However, the calcarenite GS3, which was used for 105 minutes to process various resources such as achenes, pods, and acorns, showed the opposite trend. It is difficult to determine whether this difference is due to the lithology, the processed media, or the operators involved, and further samples need to be studied to draw conclusions.

Active stones use with wooden plate. Finally, the analysis of the active tools used in conjunction with wooden plates revealed a reduction in roughness from T_0 to T_3, which was more pronounced in GS9 and M7, and less significant in M8. Although M7 and M8 have similar lithology, M7 exhibited a trend more similar to GS9. This suggests that the material being processed and the corresponding gestures have a significant impact on the extent of roughness reduction. Moreover, while M3, the active tool used to treat roots, shows an increase in roughness due to the pounding of the resource against a harder surface (the stone surface of M25), M8, which is used for the same task but in conjunction with a more flexible surface (wooden plate), exhibits a smoothing of the surface. This observation demonstrates a different wear mechanism between the two tools.

The height distributions of all tools (Figures 5.42, 5.43 and 5.44) exhibit a Gaussian shape, with the Sku values around 3, except for M8, which shows a slightly platykurtic shape and the Sku values slightly below 3. Moreover, all height distributions are slightly shifted towards positive values, with a more pronounced shift in M7, as indicated by the negative Ssk values. The decrease in the Sp and Sv values from T_0 to T_3 confirms the formation of wear, which smoothest out peaks and valleys. This trend is more pronounced for M7 and GS9. The Sz parameter follows the observed trends for the other quantities.
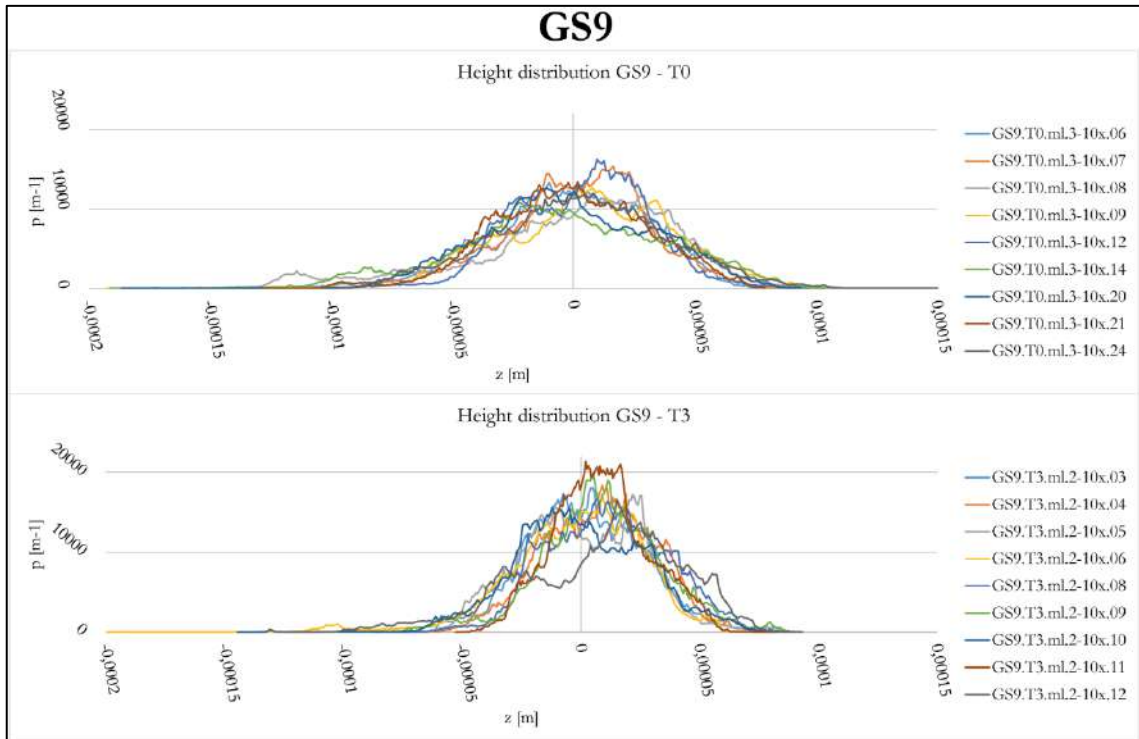
Figure 5. 42. GS9: height distributions
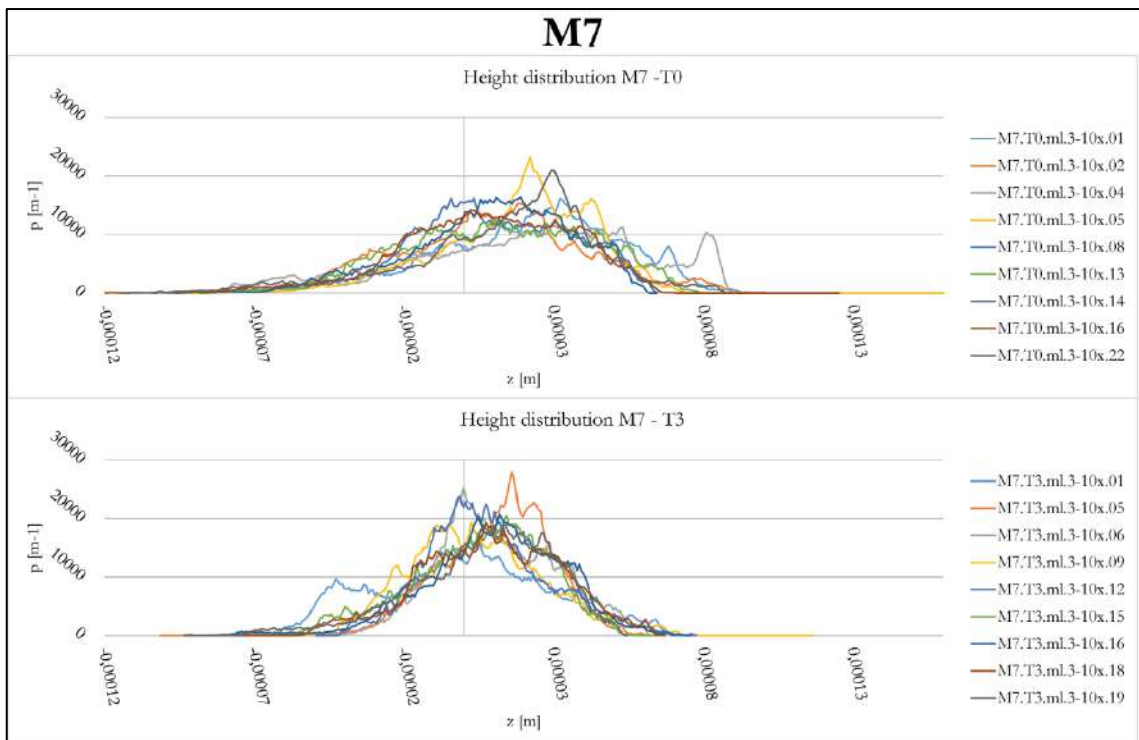
Figure 5. 43. M7: height distributions
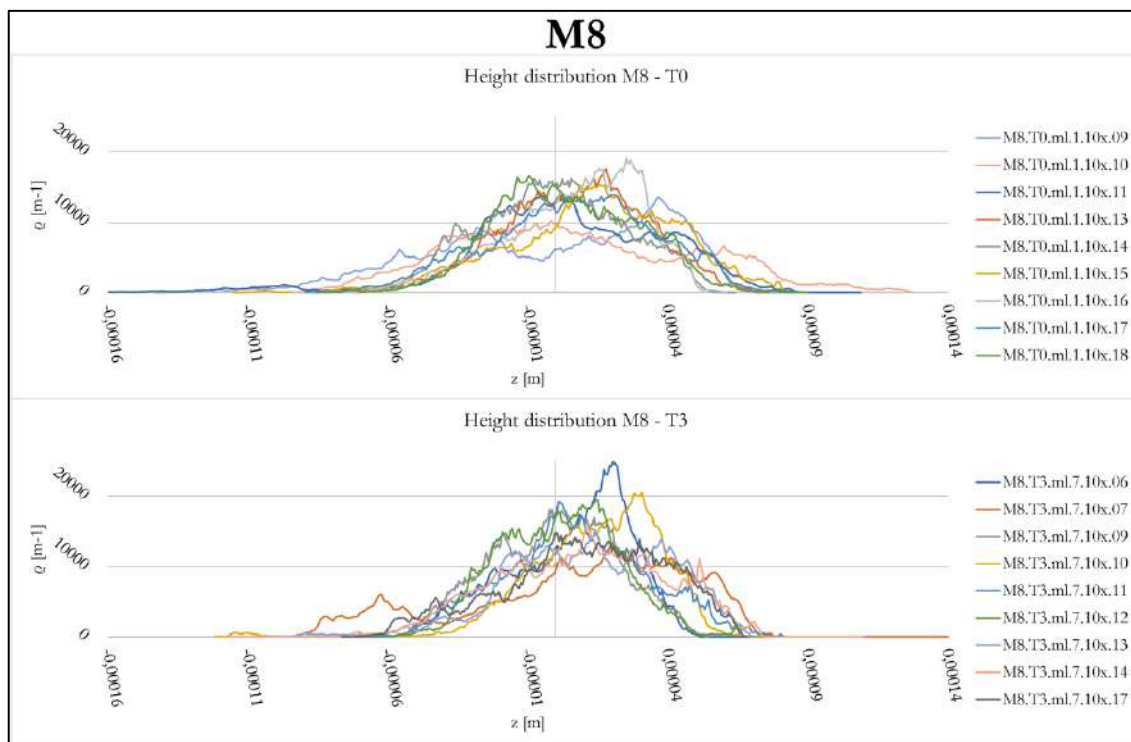
Figure 5. 44. M8: height distributions

5.6. Conclusions

The presented site-specific sequential replicative experiment introduces a novel protocol designed to systematically document and analyse the morphological and textural alterations of selected lithic surfaces subjected to mechanical stress associated with the processing of various plant organs. Furthermore, these experiments serve as controlled proxies that enhance the interpretation of the wear traces observed on the sampled GSTs retrieved from cultural layer III of the Brînzeni I cave.

The stones and their surface characteristics were meticulously documented in their natural state, referred to as phase T_0, which represents the state before any utilisation. This documentation encompassed petrographic analysis, geometric documentation, microscopy examination of the entire tool texture, profilometry data acquisition and their statistical analysis for specific controlled areas. Subsequently, the modifications undergone by the lithic surfaces throughout successive use cycles (ranging from T_1 up to T_5) were permanently recorded. The emergence and development of specific use-related patterns were correlated with the intensity and duration of usage. By identifying, selecting, and controlling variables within the experimental framework, which included factors like lithic resource properties, the medium processed, duration of transformative activities, and the amount of elaborate

vegetal material, a comprehensive assessment of the impact of different plant organs on the formation and progression of use-wear patterns was achieved. Despite the impact of the human factor in the experimental design, endeavours were undertaken to standardise both the reference collection design and the documentation protocol. This standardisation was guided by parameters systematically monitored at specific intervals and varying scales, spanning from macro-level observations through the construction of a digital 3D collection based on photogrammetric techniques, to sub-microscopic analyses relying on the contribution of different microscopy and profilometry. The systematic scrutiny of human variability also served to elucidate human gestures, delineating the most efficient movements for the particular transformative tasks, and highlighting potential deviations stemming from individual perceptual variations.

The utilisation of stone tools implied an inherently transformative process that progressively alters both surface texture and, to a certain degree, the geometric attributes of the stone. As a result, in order to systematically capture and analyse the qualitative and quantitative aspects of use-related changes, 3D reconstructions and vinylpolysiloxane molds were obtained at consistent and repeated time intervals. This documentation approach establishes a lasting depiction of the evolving alterations the tools experience, along with the progression and development of surface depletion and wear patterns. This methodological framework facilitated a synchronic examination of surface alterations across the array of implemented GSTs. Significantly, this comprehensive documentation of multiple stages in the progression of tool wear constitutes a pioneering advancement in the field, supporting ongoing and future qualitative and quantitative comparative analyses.

The design and the analysis of the replicative experiments revealed qualitative and quantitative indicators that serve as proxies for identifying comparable characteristics on the archaeological GSTs. One key aspect highlighted by the analysis is the recurring pattern of use-wear development. This cyclical pattern is evident for most of the elaborated resources, with a more pronounced effect observed in the case of achenes grinding. Here the wear progression creates periodic patterns wherein grains fracture, exposing new surfaces. This results in an increase in roughness, followed subsequent phases of flattening and decrease in roughness associate also with traces exhibiting different morphological and distribution characteristics. Moreover, it demonstrates that certain features develop only in contact with specific types of resources that possess distinct characteristics. For instance, large and intense polish areas do not develop in contact with dry, small and hard resources as achenes and

small seeds (except for serrated polish type). Among the considered media, small and/or hard resources such as ochre and achenes give rise to linear traces like striations or gouges. This could be attributed to the resource size, which leads to repeated stone-on-stone contact during processing, and to a lesser extent, to the resistance of these resources. The parametric analysis also reveals that roots leave a distinctive wear trend, which contrasts with the trends observed for all the analysed vegetal resources. This trend can be detected on both active and passive tools. It is interesting to note that the motion used to process acorns is more similar to that used for processing roots. Thus, a more similar wear pattern would be expected. However, the parametric data show a closer trend to achenes grinding. Even in the case of active tools used in conjunction with a wooden base, those used for processing roots exhibit very different use-wear parametric characteristics compared to those used for acorns and achenes. Furthermore, all the tools used in conjunction with the wooden base show a general smoothing of the low microtopography, which is clearly perceptible under SEM.

The systematic use of SEM to analyse the entire extent of tool used surfaces demonstrates the capability of this technique to highlight alterations in both low and high microtopography. This approach avoids the interference of lighting and the limited DOF of OM, providing a fundamental tool for comparison with archaeological surfaces.

The replicative use exclusively targeted one side of the passive tools, specifically to assess also the transformative processes taking place on the unused ventral surface. This strategic approach provided valuable insights that enhance the ability to interpret specific wear patterns evident on the archaeological GSTs with greater nuance. Notably, these insights encompassed the effects of blowing and recoiling, manifesting as the levelling of the matrix and the dulling of the crystals, which also undergo flattening. Quantitative data stemming from confocal profilometer analysis further supports the understanding of this transformational process, which generally results in a reduction of stone roughness attributed to an overall surface smoothing phenomenon. However, it is important to highlight that in one out of three instances, an increase in roughness was detected. To gain a comprehensive understanding of the underlying causes of this variability, future studies will require a larger sample size.

In all its complexity, this protocol is unprecedented as it allows analysts to monitor, permanently record, and ponder the tools use-biography across the different stages of their *mise en place*. The use of pebble stones for processing plants opened the view on at least some

of the perishable materials that were used and transformed by *Homo sapiens*; the GSTs are informative regarding our intangible knowledge of sapient gestures.

6. A tailored approach for macroscale analysis of experimental GSTs

As reported in the previous chapter, photogrammetric techniques based on Structure-from-Motion (SfM) and Multi-View Stereo reconstruction were employed in this study for various purposes. One crucial aim was to create 3D models of the experimental tools to explore at the macroscale the formation and development of wear over time investigating the effects at the level of the tool's geometry and waviness. After testing several setup and processing following literature available indication (e.g., Magnani et al. 2016, 2020; Porter et al. 2016; Benito-Calvo et al. 2018; Caricola et al. 2018; Zupancich et al. 2019; Zupancich and Cristiani 2020; Cristiani et al. 2021) it was clear that to reach the accuracy needed by the research question, a tailored setup was needed. Consequently, a dedicated study was undertaken during a secondment period at the 3DOM research unit of the Bruno Kessler Foundation (FBK) in Trento to further investigate and overcome all the issues occurred during the experimental collection of photogrammetric data, both acquisition and elaboration (detailed in paragraph 5.4.1). The collaboration resulted in a thorough revision and refinement of existing protocols, aiming to achieve highly consistent and repeatable results by addressing potential sources of systematic errors. This comprehensive approach led to the development of a custom setup specifically tailored to address the research questions of the study.

The findings and results of this study have been documented and extensively published in Sorrentino et al. 2023b. An excerpt of the article is presented below, providing a glimpse into the details of this part of the research. Additionally, to ensure transparency and reproducibility of the analysis conducted, the raw dataset required for replicating the analysis of one testcase (GS17), has been made publicly available and can be accessed as an open access resource (Sorrentino 2023).

6.1. The samples

Pilot tests were conducted using two pairs of ground stone tools, allowing the testing and fine-tuning of the methodology. Specifically, the tools under investigation were the M9 active tool and M12 passive tool, two quartz-arenite pebbles collected from the Racovăț River, as well as GS18 active tool and GS17 passive tools, respectively a calcarenite and a sandstone collected from the Fiora River, softer stones than previous pair of tools (Figure 6.1). The selected stones were utilised for processing *Rumex crispus* achenes, chosen for its small, hard, and rounded pericarp that imply repeated direct contact between the two lithic surfaces during grinding, as a result of achenes scattering onto the passive tool. As demonstrated in the previous chapter, these characteristics of achenes determine a fast and intense stones surface depletion. M9 and M12 were utilised for a duration of 30 minutes (T_1) resulting in a limited surface depletion. Consequently, GS17 and GS18 were employed for a longer duration, a total of 2 hours (T_4) to ensure an appreciable consumption of the surface.
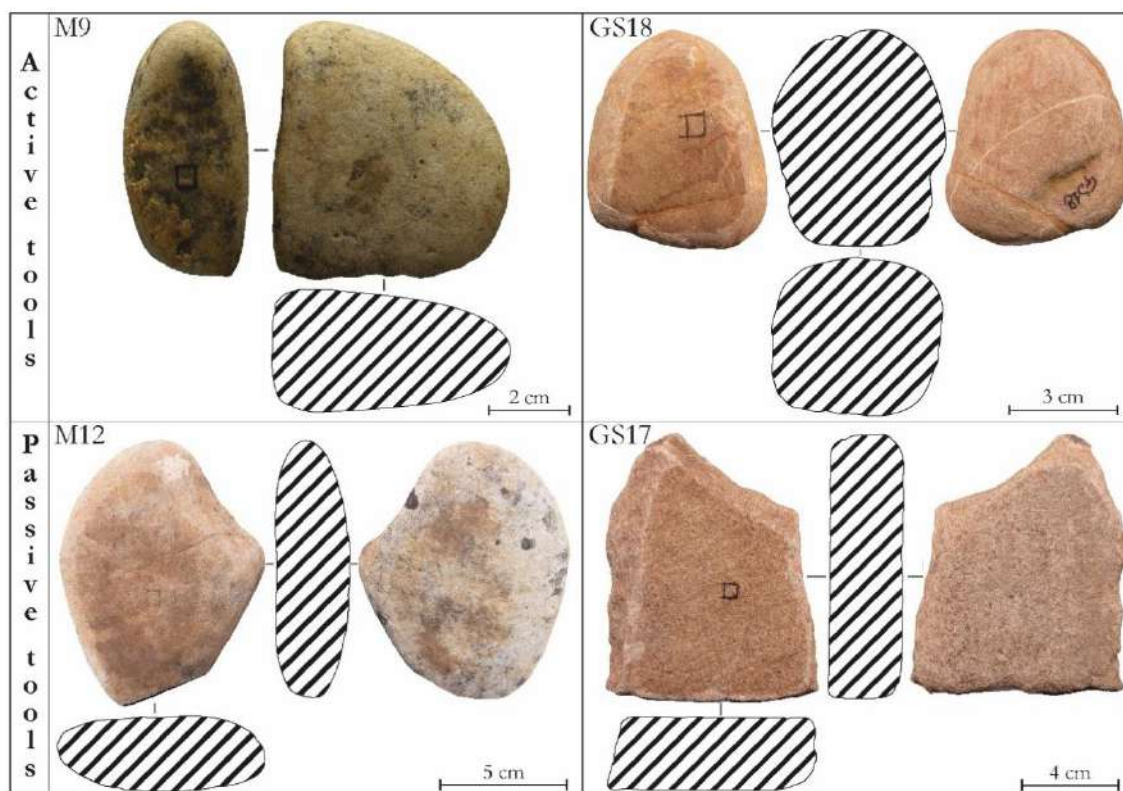
Figure 6. 1. The GSTs involved in the pilot study. The 3D models show both the used and unused surfaces, while the cross-sections are calculated from the 3D models, highlighting the trend of the use surface (modified from Sorrentino et al. 2023b).

6.2. The development of an *ad hoc* setup

An *ad hoc* setup was constructed after conducting a critical review of existing protocols. A graded turntable was adopted to capture the GSTs from different angles (Porter et al. 2016; Nicolae et al. 2014), and markers were fixed at various heights on the turntable (Figure 6.2 A, B). Each GST was individually placed on the turntable in an upright position (Figure 6.4 B). Previous studies have demonstrated that photographing an object in its vertical position increases the overlap between sets of pictures, resulting in improved image orientation accuracy (Porter et al. 2016; Sapirstein 2018; Magnani et al. 2020; Antinozzi et al. 2022) and reducing the likelihood of gaps or multiple overlapping points in the processed point cloud. This phenomenon occurs particularly at the narrow edge of the object, where the conjunction of the two faces' point-clouds occurs. This has a significant impact, for example, when studying flaked tools, where diagnostic features are often located at the edges of the artefacts. In order to place the object vertically, previous studies have proposed expedients such as using a metal wire (Magnani et al. 2016) or putty-like substance (Magnani et al. 2016; Porter et al. 2016; Sapirstein 2018). These are not feasible for heavy or geometrically complex objects where the barycentre is not easy to centre. Moreover, these expedients cannot be safely applied as the stability of the object is not guaranteed when the table is rotated. Therefore, a more complex and invasive solution was adopted.

In this study two distinct metrological kinematic bases, manufactured by ThorLabs, were utilised: the KB1X1 and KB2X2. Each base comprises two plates: one with three spherical earth magnets and the other with three V-grooves, which allow for the top plate to be positioned on the base plate on the same location and orientation with high precision and repeatability (Table 6.1).

Table 6. 1. ThorLabs Kinematic Bases used in the study, along with minimum and maximum errors at angular repeatability test, as provided by the manufacturer (ThorLabs 2023).

Kinematic base model	Dimension	Holding	Minimum error	Maximum error
KB1X1	25 mm^2	1633 g	0.58 µrad	26.72 µrad
KB2X2	50 mm^2	2835 g	3.60 µrad	30.96 µrad

The base KB1X1 was employed for the active stones while the KB2X2 for the passives (Figure 6.2 C). Each stone was perforated to a depth of approximately 0.5 cm, and thread-to-thread adapters manufactured by Edmund Optics for optomechanical

applications, were inserted and fixed in place with a two-component epoxy metal glue. The opposite ends of each adapter were attached to the top plates of the kinematic bases and secured with hot melt glue, while the bottom plates were fixed to the turntable (Figure 6.2 B). This guarantees that the stones can be placed and removed from the turntable each time a replicative experiment is performed, and then repositioned on it with high precision, ensuring always the same position and orientation of the stone (within the uncertainty defined by the manufacturer). The procedure of flipping the object 180 degrees to capture the hidden side, typically employed in photogrammetric acquisition of stone tools, was deliberately avoided. This approach, while providing additional information about the part of the stone attached to the adapter (note that this is a non-diagnostic side), can introduce challenges in the merging process, affecting the accuracy of image orientation (Magnani et al. 2020; Porter et al. 2016; Sapirstein 2018; Nicolae et al. 2014) and resulting in gaps or multiple overlapping points in the processed point cloud. By refraining from this step, the number of required pictures was reduced, saving time and computer processing resources, and eliminating the need for the time-consuming pre-alignment elaboration that involves outlining the object's silhouette (masking) to ensure picture orientation.
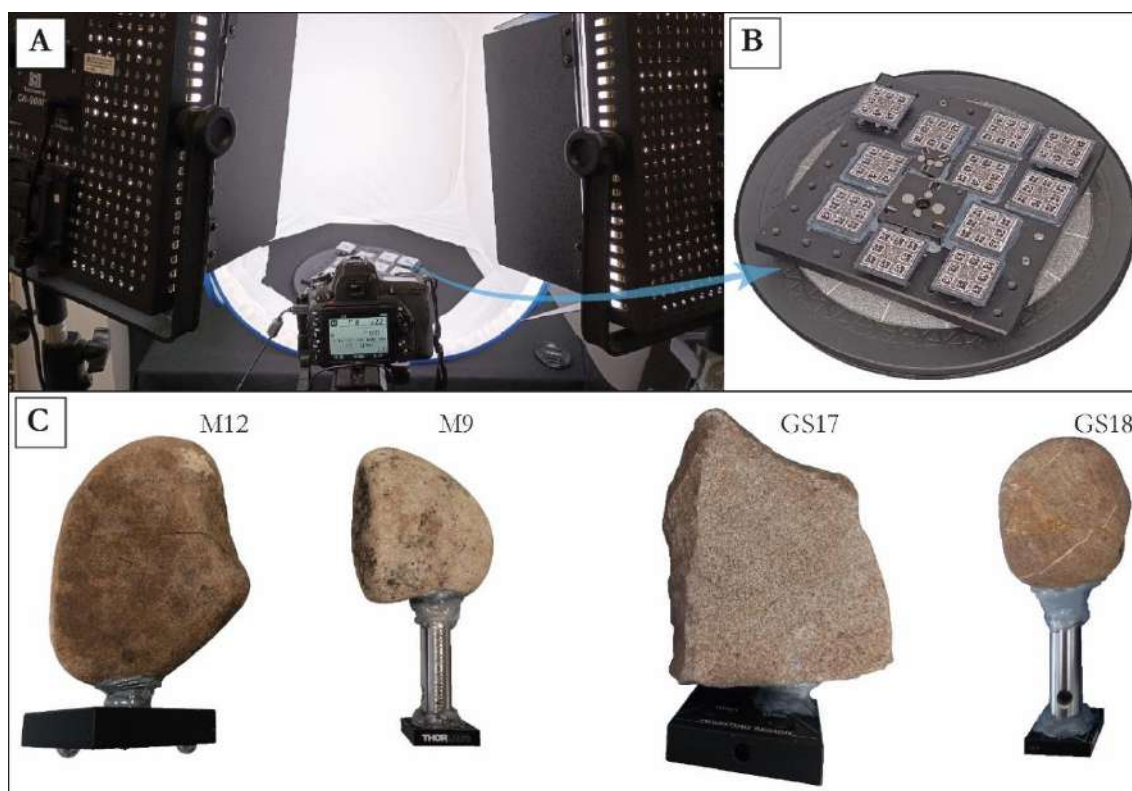
Figure 6. 2. The photogrammetric acquisition setup in the FBK lab. A) The light box, two symmetrically placed led light panels and the Nikon D750 camera in the middle with camera settings displayed. B) The turntable, equipped with fixed markers and with the bottom plates of the kinematics bases. C) The GSTs involved in the study, supplied with the bottom plates of the kinematics bases (from Sorrentino et al. 2023b).

The impact of lighting was also addressed, as moving/flipping the object position can significantly modify the appearance of uneven surfaces (Sapirstein 2018; Karami et al. 2022) (Figure 6.3) thus creating problems with the orientation of the images. By avoiding overturning the object, this issue was mitigated and further minimised by using a lightbox that homogeneously distributes the light coming from two symmetrically placed LED light panels (Figure 6.2 A).

Figure 6. 3. Example of the dependency of the local texture on the shades casted by directional lighting when moving/flipping over the stone on the acquisition space. The same area of the stone rim is depicted A) with the use surface facing up and B) with the use surface leaning on the turntable C) on the 3D model mesh (modified from Sorrentino et al. 2023b).

During image acquisition, the camera setup, as shown in Table 6.2, was kept constant to ensure accurate and consistent parameters throughout the tests. The setup and camera parameters were calibrated to achieve a ground sampling distance (GSD) between 0.0413 and 0.0548 mm. The camera was fixed on a tripod placed in front of the table and between the two lights (Figure 6.2 A).

Table 6. 2. Details about the camera equipment and settings used for acquiring the photographs during this pilot tests

Camera Model	Nikon D750
Lens	AF-S Micro NIKKOR 60 mm
Camera Parameters	Manual settings
ISO	100 (native value)
Aperture	F-stop of 22 (to maximise depth of field without diffraction effects)
Shutter Speed	Approximately 1/8 of a second
Image Format	Raw format (.nef)
Additional Precautions	Remote shutter, raise and lock mirror, focus ring locked with hot melt glue

Pictures were captured by rotating the table at intervals of 10-degrees (or less in proximity to the narrow edges of the stones) and adjusting the position and tilt of the camera towards the object at three different heights. Additional photographs were taken of complex, top and/or narrow areas of the items resulting in an average of 100-120 images.

To assess the repositioning error, each GST acquisition was conducted three times for each experimental stage (T) to verify the repeatability and estimate the uncertainty associated with the acquisition method. After the first acquisition, the tool was temporarily removed from the turntable and then replaced and acquired again for two more times. However, for M12 at T_0, it was acquired also three additional successive times without removing it from the turntable to prevent any repositioning error caused by the operator or the kinematic base (the number of the acquisition for each experimental cycle are schematised in Figure 6.6).

In order to calibrate the camera parameters, consistently oriented the models of the stones at different T to a shared spatial coordinate system, and ensure a resolute and consistent model scaling, a separate calibration project was carried out, which involved acquiring the setup without any samples. For scaling purposes, a low thermal expansion scale bar (Brunson 803-MCL Length Reference Kit) was fixed to the rotating plate. This tool, made of Invar alloy (FeNi36), provides a thermally stable reference length of 224.9998 mm (Brunson 2023) (Figure 6.4 A). During this process, images of the turntable with the markers were captured at 20-degree intervals. The camera was adjusted to obtain images at three different heights, and was also rotated horizontally to the left and right (i.e., both portrait and landscape orientation), following standard protocols of a self-calibration imaging network (Fraser 1997). Although camera calibration can be part of the SfM process and is regularly used in many 3D digitisation projects carried out using photogrammetry, an *ad hoc* project for camera calibration ensures that the most suited camera network is realised. This is in particular important for high accuracy projects where the imaging network is not optimised for calibration but for the 3D digitisation of the object of interest.
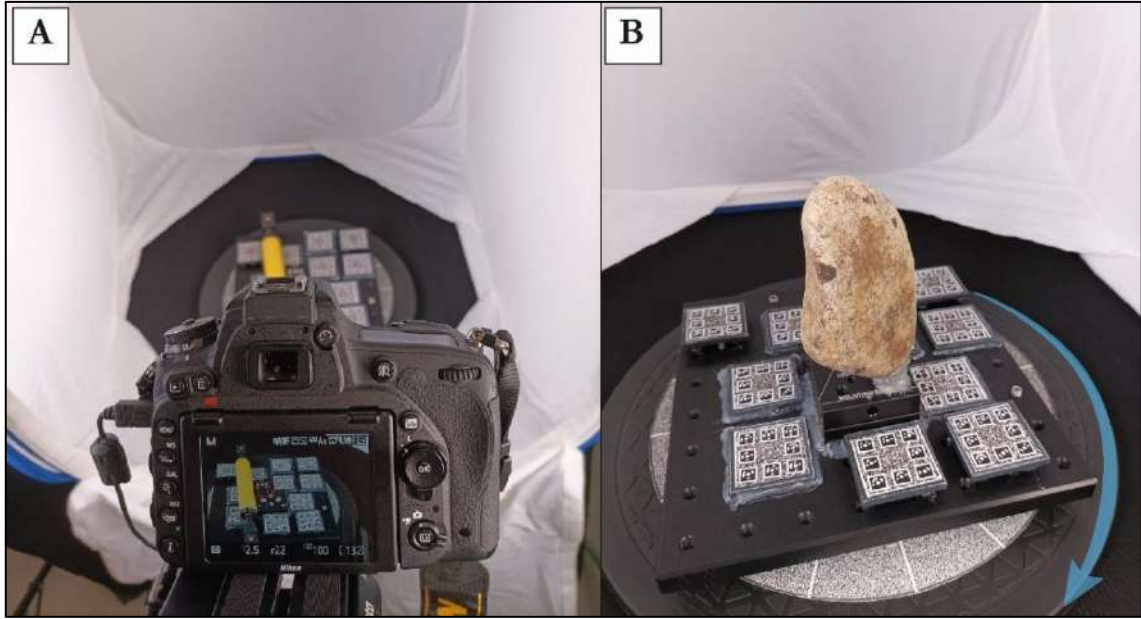
Figure 6. 4. The ad hoc setup. A) Data acquisition for the creation of the calibration project, which involved acquiring the setup without any sample. For scaling purposes, a low thermal expansion Brunson 803-MCL Length Reference was fixed to the rotating plate. B) The GSTs acquisition, with the item fixed on the turntable employing the kinematic base and pictures acquired rotating the plate every 10-degree and adjusting the position of the camera at three different heights.

The digital raw pictures were converted to .jpg files using NxStudio, and then processed using Agisoft Metashape software to generate the 3D models following the workflow schematised in Figure 6.5.
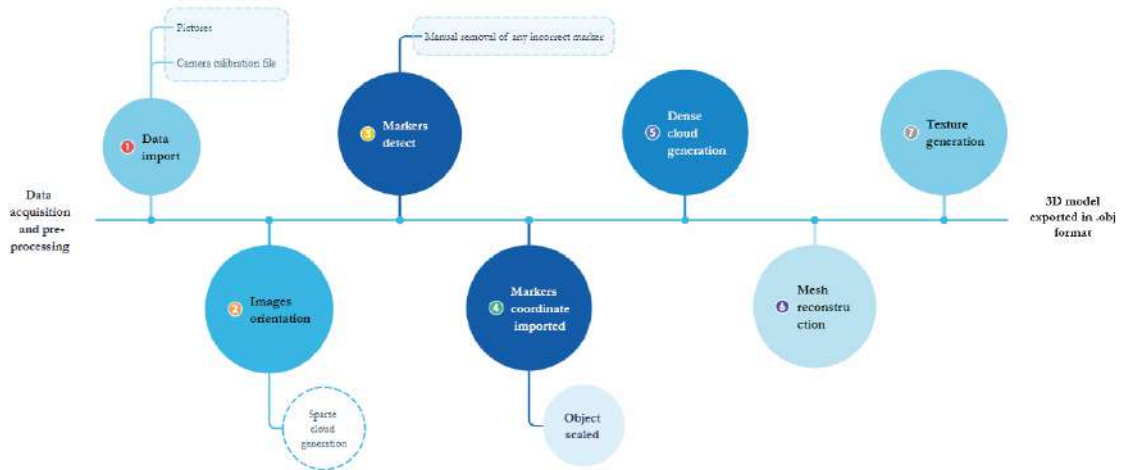
Figure 6. 5. Workflow for the 3D elaboration: 1) pictures were uploaded into one Metashape chunk (no needs for masking or elaborate the images into different chunks to be later merged). Also, camera calibration parameters were imported. 2) The images were oriented and sparse-cloud compute. 3) The markers present on the turntable were automatically detected and (4) their coordinate system was imported to ensure consistent spatial orientation and object scaling across all projects. 5) The dense cloud was generated, followed by (6) the mesh that was finally (7) texturized to produce the 3D model, which was exported in .obj.

As summarised in Figure 6.6, in the end of the data processing for each of the four GSTs three 3D models for T_0 (named acquisition 1, 2, and 3) and three for T_1/T_4 (named

acquisition 5, 6 and 7) were obtained, except for M12 at T_0 which count three more 3D models, obtained without removing the object from turntable (named acquisition a, b, c).
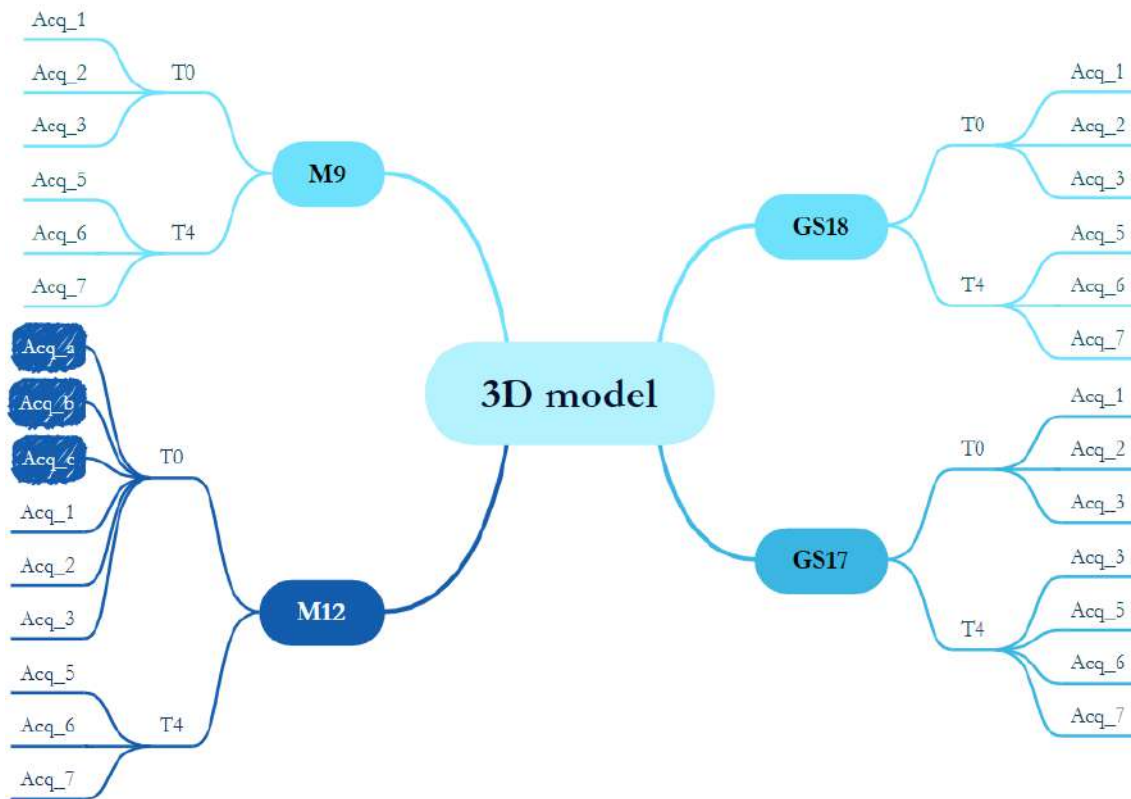
Figure 6. 6. Summary of the obtained 3D models. The acquisitions highlighted in dark blue (a, b and c) were captured consecutively without removing the object from the turntable.

6.3. 3D data processing

Each .obj files were imported into the open-source software CloudCompare to be analysed. The dimension, shape and cross section of the tools was computed and reported in Figure 6.1 and Table 6.3.

Table 6. 3. GSTs morphometric informations. The dimension, overall tool shape and selected use surface description are reported (from Sorrentino et al. 2023b)

Stone	Dimension (mm)	Tool overall shape	Use surface shape
GS17 (passive tool)	107.36×84.09×29.97	Flat trapezoidal prismatic shape	Flat profile
GS18 (active tool)	58.96×42.27×43.17	Spherical shape	Convex profile
M12 (passive tool)	100.38×80.57×29.5	Irregular shape	Concave profile
M9 (active tool)	62.73×29.81×57.67	Ovoidal shape (flattened)	Flat surface

The Cloud-to-Mesh Distance function was utilised to compare the GSTs at T_0, which were used as the reference, with the T_1/T_4 meshes. This function calculates the distance between the vertices of the compared mesh and the triangles of the reference mesh.

To assess the repeatability of the implemented photogrammetric process and evaluate the acquisition and repositioning errors, multiple comparisons were conducted among models acquired at the same T. Since there is no surface depletion among the models acquired at the same T, any observed variation should primarily result from acquisition errors. The analyses are presented in false-colour, where a gradient ranging from red to dark blue is used, including intermediate tones such as orange, yellow, green, and light blue. The values in the red, orange, and bright yellow regions indicate a positive distance, with a maximum of 100 μm represented in red. The yellow and acid green tones indicate no distance, while the shades of green, turquoise, and blue represent a negative distance, with a maximum of -400 μm depicted in dark blue. Any distance exceeding the reference range of 100 μm to -400 μm is presented in a uniform shade of grey.

To verify the acquisition error independent from repositioning variance by the operator and/or the kinematic base, the three acquisitions M12 at T_0 a, b and c were compared among each other. The results showed a high level of overlap with only a few singular spots showing an absolute distance of up to 28 μm due to acquisition noise (Figure. 6.7).
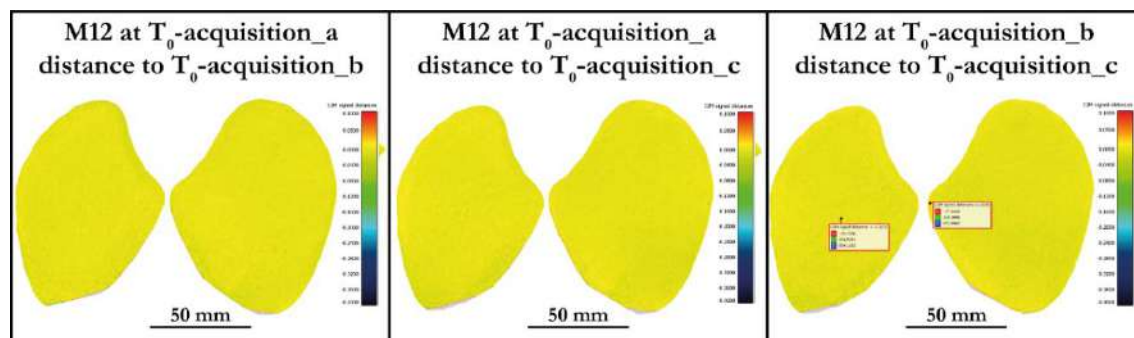
Figure 6. 7. M12 at T_0 acquisition a, b, c compared among them. This test was necessary to verify the acquisition error unrelated to the kinematic base repositioning variances (modified from Sorrentino et al 2023b)

Then, to verify the repositioning error of the kinematic bases acquisition 1, 2, and 3 of all GSTs were compared among them (Figure 6.8). To improve statistical significance, also acquisition 5, 6, and 7 were compared among them (Figure 6.9). The outcomes indicated a substantial degree of overlap among the compared models, with an average absolute distance of approximately 40 μm (represented by green and orange areas) and a maximum of 80 μm (represented by red and darker green areas).
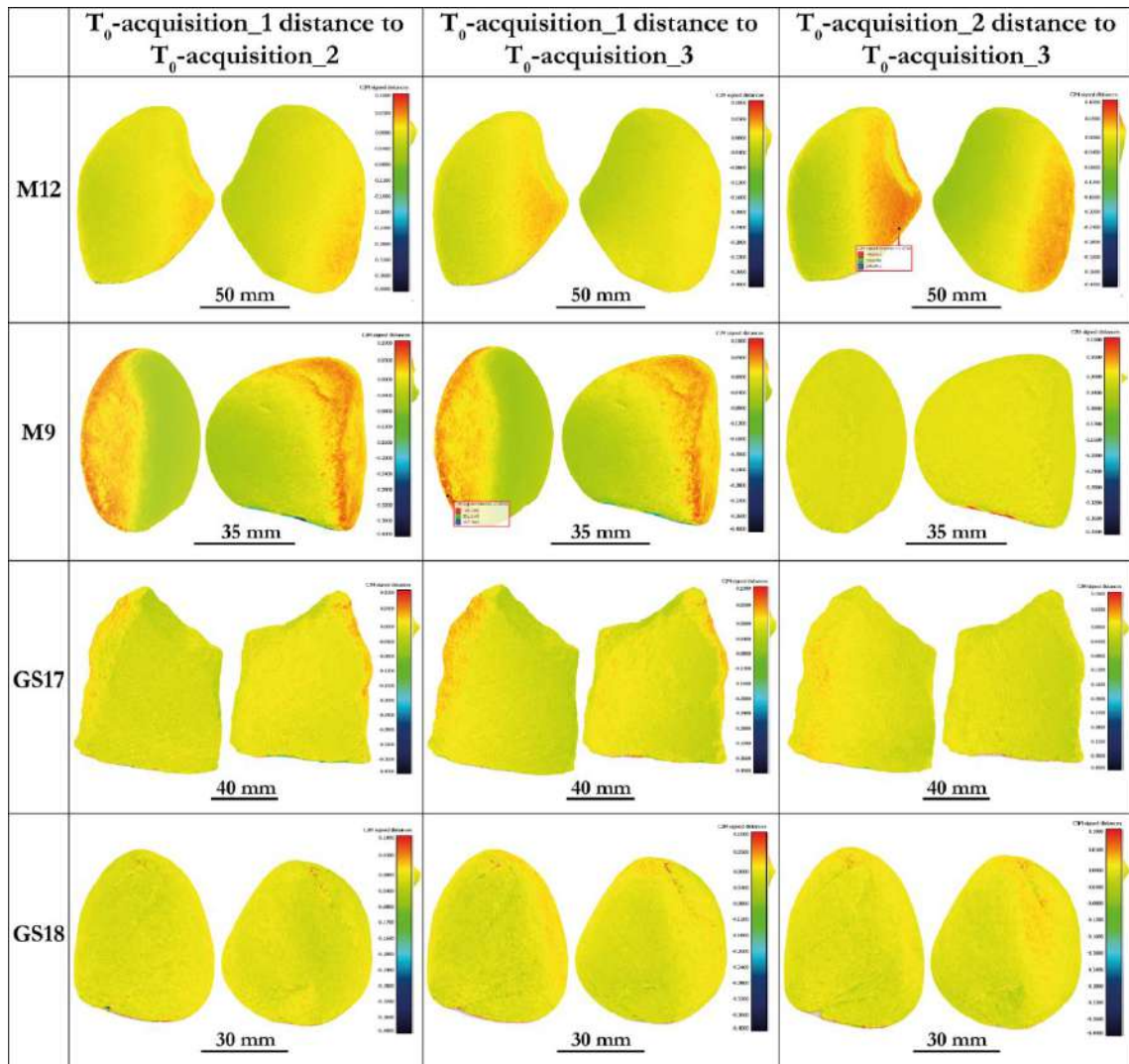
Figure 6. 8. All the involved GSTs at T_0 acquisitions 1, 2, and 3 compared among them. The analysis showed a high degree of overlap between the compared models, with an average absolute distance of approximately 40 μm. Only in rare cases, such as when comparing M9 between acquisition 1 and 3, as well as 1 and 2, and M12 between acquisition 2 and 3, was a maximum distance of 80 μm observed (modified from Sorrentino et al. 2023b)
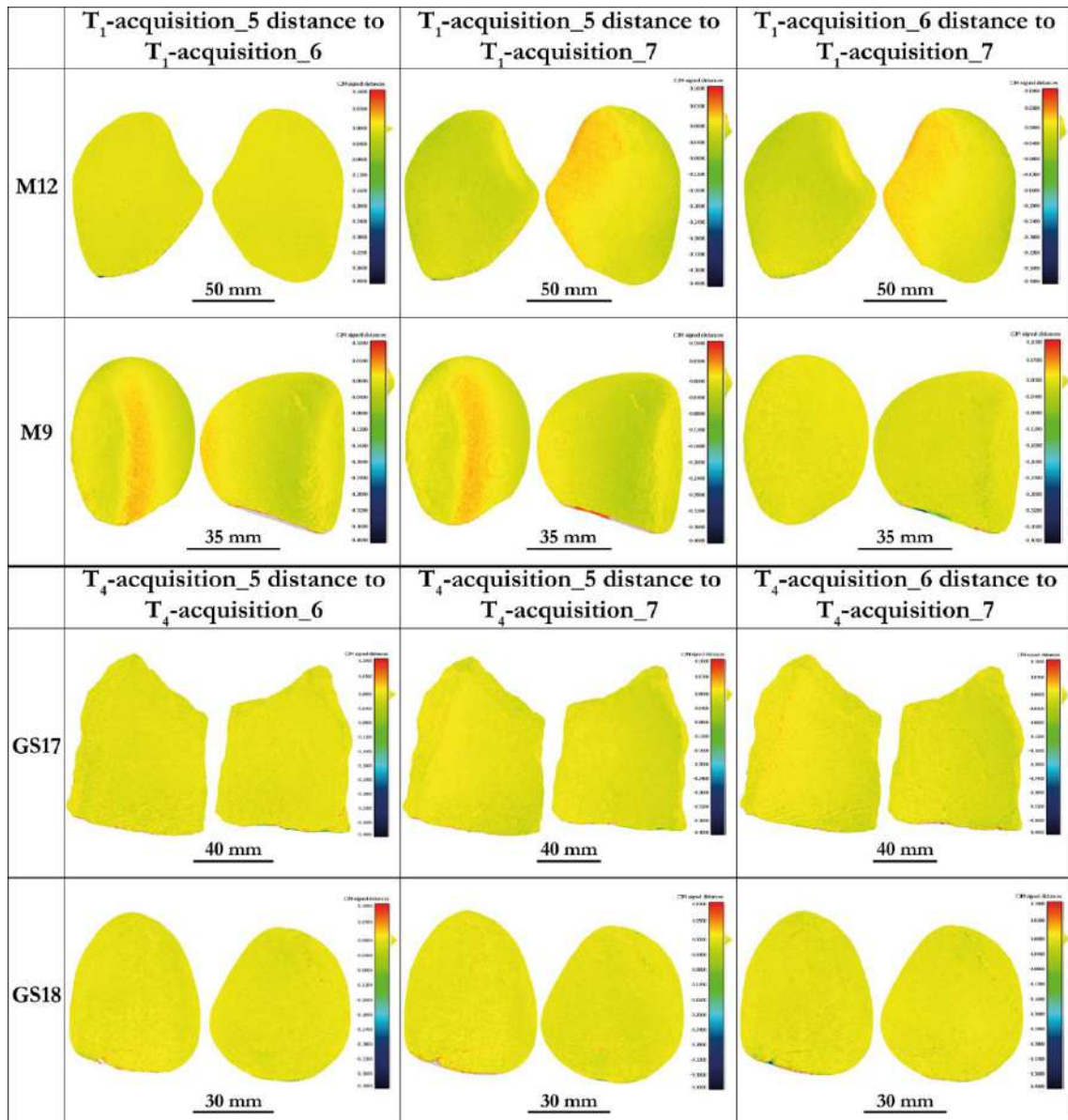
Figure 6. 9. All the involved GSTs at T_1/T_4 acquisitions 5, 6 and 7 compared among them. The results indicate a high degree of overlap between the compared models, suggesting a significant level of repeatability in the repositioning of the items achieved through the use of kinematic bases (modified from Sorrentino et al. 2023b).

To analyse and quantify surface depletion after GSTs' utilisation in processing *Rumex crispus* achenes, considering the impact on the overall tool, the T_0 models were all compared with the T_1/T_4 models. As presented in Chapter 2, the use leads to a gradual loss of material through subtractive wear mechanisms, such as adhesive, fatigue, and abrasive wear (e.g., Adams 1993, 2002a, 2002b, 2014; Hamon 2008; Adams et al. 2009; Dubreuil et al. 2015). Therefore, it is expected that the differences between T_0 and T_1/T_4 should be zero or negative in the real contact areas of the working surface.

Comparing models based on the alignment provided by the kinematic bases has proven to be effective in highlighting and measuring wear patterns (Figure 6.10). However, the positioning inaccuracy, in particular the rotation of the kinematic bases may result in distances between models that exceed 100 μm in absolute value, even in areas unmodified by the replicative tool usage. In some cases, these errors can be greater than the mesh distance due to surface depletion. This was observed in the case of M12 T_0 acquisition 3 when compared to T_1 acquisition 6, where the repositioning error resulted in a distance of up to 103 μm in absolute value, which is greater than the -30, -40 μm variation observed on the working surface. Similar results are observable in the comparison between M9 at T_0 acquisition 2 and T_1 acquisition 5. Otherwise, the distance caused by repositioning errors did not exceed 100 μm for GS17 and 50 μm for GS18, and did not overlap with the wear patterns observed.

To overcome the repositioning error of the kinematic base, a subsequent attempt was performed involving the Iterative Closest Point (ICP) function of CloudCompare. This is a fine registration algorithm that iteratively aligns two entities. In this case the T_0 acquisitions were used as the reference files and the T_1/T_4 models translated and rotated to match the reference. The ICP algorithm attempts the alignment of the two entities until the difference in error between two iterations falls below a predefined threshold that was set to 95% (5% difference was estimated due to use-related morphological change). Furthermore, to improve computational efficiency, the Random Sampling Limit was set to 500000, which subsampled the data cloud at each iteration, and the Enable Farthest Point Removal option was enabled to discard possible points that are too distant from the model cloud and thus may represent potential blunders.

Again, the models T_0 acquisitions 1, 2, and 3 of each GSTs were compared with the models T_1/T_4 acquisitions 5, 6, and 7.

Applying the ICP fine registration algorithm to the already well-aligned models further minimises the distance errors, improving the recognition of the actual distance due to wear mechanisms (Figure 6.11).
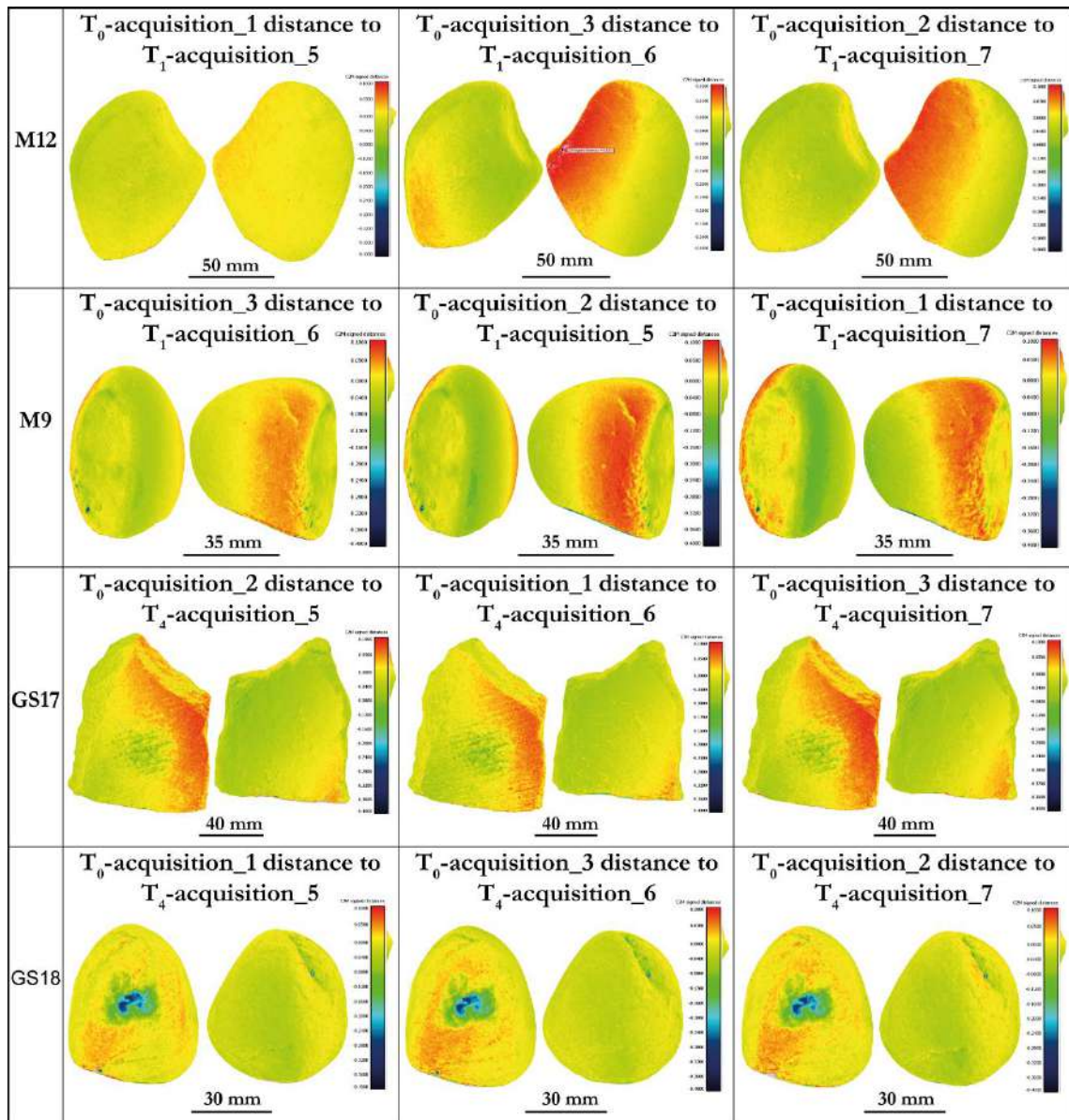
Figure 6. 10. The acquisitions 1, 2, and 3 of all GSTs at T_0 compared with the acquisitions 5, 6, and 7 of the same GSTs at T_1/T_4. The false colour images were utilised to depict the distance between the mesh of the unused items and the mesh of the tools after use, with the aim of highlighting distinct wear patterns. The analysis revealed that wear patterns were particularly noticeable in the central region of the working surface of the tools GS17 and GS18, which are made of a softer rock type and were utilised for a duration of 2 hours (modified from Sorrentino et al. 2023b).
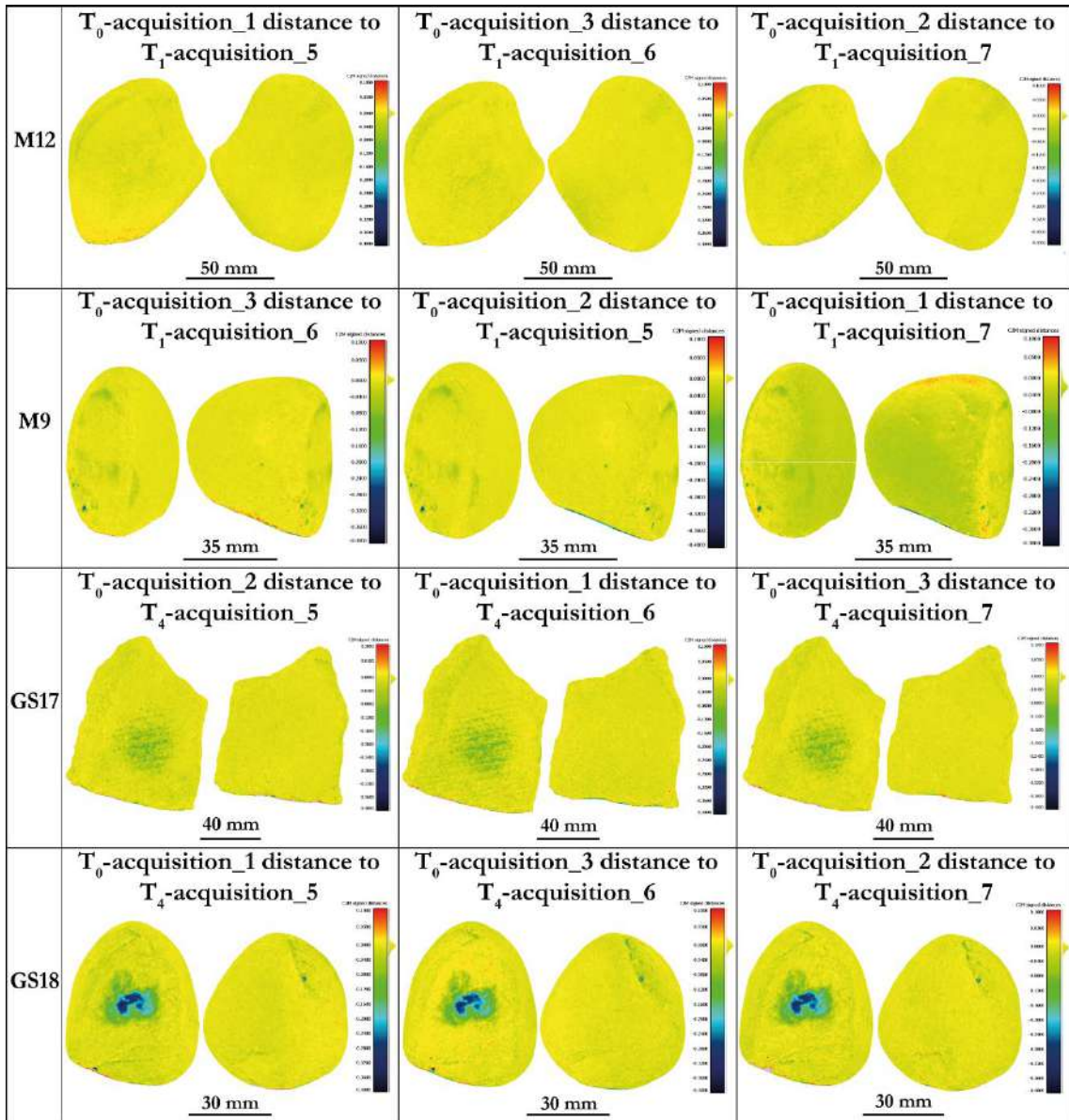
Figure 6. 11. The acquisitions 1, 2, and 3 of all GSTs at T_0 compared with the acquisitions 5, 6, and 7 of the same GSTs at T_1/T_4 applying the ICP algorithm. False-colour images were utilised to display the distance between the mesh of the unused items and the mesh of the tools after use. The application of the ICP fine registration algorithm further enhanced the visibility of wear patterns, including those on M12 and M9, which had less intense depletion due to their shorter utilisation periods (modified from Sorrentino et al. 2023b)

Moreover, as previously mentioned, every photogrammetric survey needs a scaling procedure. To create 3D models, a scale bar or a ruler of a known length is included in the scene and used to scale the model. The end points of the reference are typically materialised by photogrammetric targets (i.e., circular coded, cross type) or by other signs as the graduation in the case of the ruler. However, the process of collimating these points on the scale bar during data processing, especially when done manually, can introduce human errors of several micrometres. As an example, Benito-Calvo and colleagues (Benito-Calvo et al.

2018: 613) report a scale factor of 0.86 in their photogrammetric model compared to models acquired with a scanner. To verify the impact of even smaller factors, 8 tests on GS17 and GS18 were performed, simulating a relative scaling error of 2‰ and 5‰, corresponding to a measurement error of ± 0.2 mm and ± 0.5 mm on a 100 mm scale bar. Models acquired at T_0 were used as reference items and kept unaltered, while to the T_4 models were applied 4 different scale factors: 0.998; 0.995; 1.002 and 1.005. Based on the analysis it is evident that even a few micrometres of errors when determining the scale factor can invalidate the results (Figure 6.12). In all the tests the co-registration errors were distributed across the entire surface of the objects, with errors within 100 μm in absolute value for the analysis using a scale factor of 0.998 and 1.002, but reaching up to approximately 450 μm in absolute value for those with a scale factor of 0.995 and 1.005. Additionally, the extension and depth of the wear trace patterns also changed, with noticeable differences already present in the models with a scale factor of 0.998 and 1.002, while the changes became dramatically evident in the case of 0.995 and 1.005.
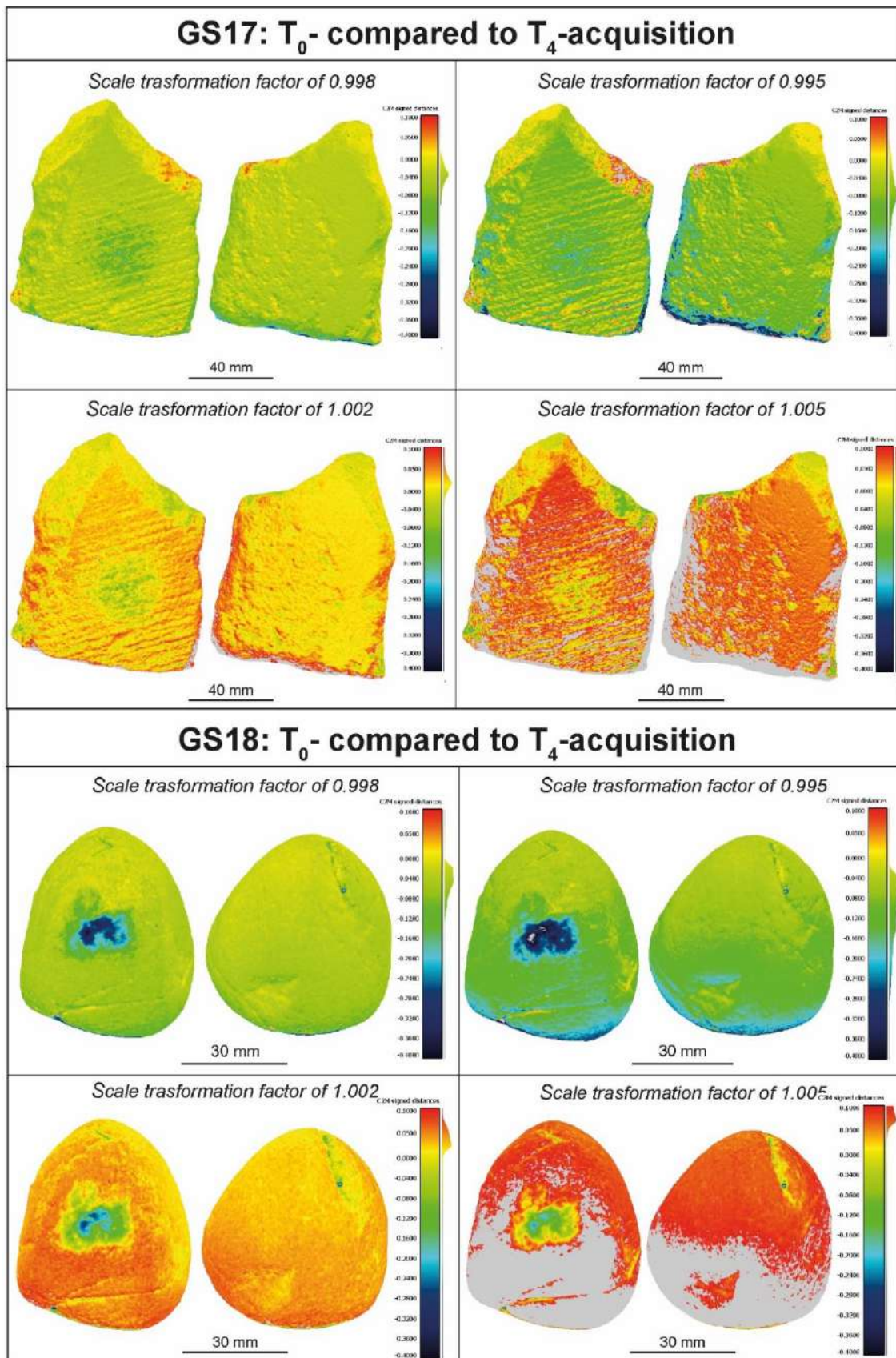
Figure 6. 12. GS17 T₀ acquisition 1 compared to T₄ acquisition 7, and GS18 T₀ acquisition 3 compared to T₄ acquisition 5. Different scale factors were applied (modified from Sorrentino et al. 2023b).

6.4. Results and conclusions

From the analysis, and as highlighted in Figure 6.11, it is evident that M12, which is made of a rock type particularly resistant to mechanical stress and used only for 30 minutes, displayed changes in the working surface barely appreciable. Indeed, the distance between T_0 and T_1 models are up to -40 μm, primarily along the working surface's edges and a superficial but widespread wear pattern is also apparent in the central region.

On the other hand, the active tool M9, made of the same rock type, at T_1 displayed more pronounced wear patterns compared to M12, particularly in the convex and protruding areas of the use surface (green areas displaying a distance to T_0 up to -70 μm). Additionally, few battering marks were also detected, presenting a maximum depth of -370 μm, represented in the false-colour analysis as dark blue spots.

As expected, the pair of tools GS17-GS18, made of stones coming from the Fiora River and employed for a longer period of 2 hours, presented a more intense wear pattern. GS17 at T_4 displayed a large depletion area in the centre of the used surface, whose distance from T_0 was up to -170 μm (dark green region). The active tool GS18 at T_4 presented the most defined and intense wear pattern, extending on the protruding area of its convex use surface. The distance to T_0 for this area reached up to -360 μm. Additionally, fractures were observed on the unused dorsal surface (the side held in the hand), which deepened after stone utilisation, confirming that the entire tool underwent a morphological change during utilisation.

Lastly, despite the cleaning process that each tool underwent after their utilisation, all exhibited flour residues of *Rumex crispus* embedded in surface craters, depicted in the analysis as isolated red dots. The attribution of these positive distance spots to flour residues is also confirmed by microscopic observations.

Figure 6. 13. Example of Rumex crispus residues entrapped in the pits (highlighted by the arrows) on the surface of M12 at T1.

Based on the presented results, this preliminary study has effectively demonstrated the capability of close-range photogrammetry and the custom setup to trace and measure morphological changes in experimental ground stone tools at different stages of their replicative use, providing valuable insights for quantitative analysis. From a methodological perspective, the conducted tests underscore the significance of designing an acquisition setup that aligns with the research objectives and emphasises the necessity of (pre)determining the metrical requirements specific to answer the research questions. Additionally, this approach identified and addressed potential sources of errors that may arise from existing methods, thereby minimising the risk of misleading interpretations.

To ensure highly consistent and repeatable results, a thorough refinement of existing protocols was undertaken to address potential sources of systematic errors. This meticulous process begins during the design stage of the experimental setup, enabling the identification and mitigation of potential issues. However, it is important to highlight that the implementation of the kinematic base, due to its invasive nature, is not suitable for archaeological artefacts. Instead, the primary, fulfilled focus of this study was on developing a reliable and accurate approach to measure use-wear patterns resulting from the tribological mechanisms during the intentional use of experimental GSTs, considering the tool's entire geometry. This approach enables a comprehensive understanding of the mechanisms that occur during tool utilisation, not only at the contact area level but considering the object as a single system where actions have consequences on its entire geometry. Furthermore, expanding the 3D collection of experimental tools, acquired using the proposed method and considering intermediate stages of tool utilisation, can serve as a valuable proxy for comparison in the analysis of archaeological GSTs. In the archaeological context, access is limited to only one step of tool usage, lacking information about the other stages along the functional biography of the stone tools. Therefore, the models generated from these sequential replicative experiments play a pivotal role in enhancing the comprehensive understanding of the archaeological evidence, serving as a valuable resource for approximating the missing stages of tool usage and contributing to a more accurate interpretation of the archaeological record.

7. The analysis of the Brînzeni I GSTs

7.1. The multiscale comparative approach

As presented in Chapter 3, the methodology applied to the investigation of the archaeological GSTs closely mirrored the approach utilised for the experimental tools. This approach demonstrated its effectiveness in enabling functional analysis and facilitating the comparison of data between archaeological and experimental tools. The methodology encompasses observations of tools morphology and texture at various scales, examination of different facets of the stone, and considering the information obtained from residue analysis.

To conduct morphometric analysis, a combination of pictures and 3D models was employed. In the case of the archaeological GSTs, digital models were generated using the 3D light scanner Artec3D Space Spider, which were acquired during the 2016-2017 sampling campaign (Longo et al. 2021a; data are accessible for visualisation at sketchfab.com/ADM-VCH). However, it is noteworthy that the resolutions of these models were inadequate for conducting textural evaluations. Consequently, they were exclusively employed for visual inspection, facilitating a comprehensive understanding of the object's geometry, primary waviness, and overall morphometric characteristics.

The analysis of traces was conducted on molds, which were also obtained during the 2016-2017 sampling campaign. Molds were collected from various regions of the stone surfaces, and for this study, an average of two distinct areas were examined for each tool. Various microscopy techniques were employed for this purpose, including a stereomicroscope (Leica S9i), a reflected light microscope (Olympus BX51), a 3D digital microscope (Olympus DSX1000), a scanning electron microscope (ZEISS EVO60 EP), and a confocal profilometer (Leica DCM 3D), with specific settings outlined in Tables 3.2 and 3.4. Furthermore, for BZ#442, Raman analysis was conducted on some red areas visible on a fragment of the original GSTs, as reported in paragraph 7.1.8.

SEM images were primarily captured using secondary electrons, with an accelerating voltage of 20.00 kV and a WD of 8.5 mm. Furthermore, some samples underwent analysis with the

Zeiss Supra 40 high-resolution FEG-SEM available at IOM-CNR in Basovizza (Trieste, Italy). This instrument is equipped with a third-generation Gemini column, the Everhart-Thornley secondary electron detector, and a high-efficiency in-lens detector.

The employment of diverse microscopes aimed at improving the readability of use-wear traces and facilitating a comprehensive qualitative assessment.

The Leica DCM 3D confocal profilometer was employed to analyse a 0.5 cm^2 area on each examined side of the sample GSTs, following the approach tuned for the experimental tools. The confocal microscopy function was utilised to visualise these areas, while the profilometer function was applied to reconstruct their microtopography in 3D. This reconstruction facilitated the calculation of parametric data, elaborated, presented, and compared with experimental collection data in paragraph 7.2.

The analysis of the site-specific experimental collection has yielded valuable insights into rock characteristics, variability, and responses to mechanical stress in particular correlated with different plant organs elaboration and gesture. These insights have proven pivotal for interpreting the archaeological evidence. Furthermore, the inclusion of stones gathered directly from the Racovăț River in the collection has contributed valuable information about the natural aspects of the rocks. This aids in distinguishing genuine use-wear patterns from naturally occurring ones, enabling a more precise interpretation of the past use and activities associated with the archaeological artefacts.

The figures in the next paragraphs illustrate the following:

- The mesh (when available) of the analysed tools;
- The examined molds with their specific positions on the GSTs surfaces and the locations of the micrographs labelled with Latin letters. Notably on all molds, the area named "A" indicates the 0.5 cm^2 squares selected for confocal profilometer microtopographic analysis;
- Different microscope images captured at various magnifications;
- False-colour confocal profilometer maps of the analysed squares within area A. The analysed areas measure 850 μm^2, and the false-colour gradient depict higher peaks in red, while lower depressions and pits in blue.

It is worth mentioning that the microtopographic false-colour maps were elaborated with Gwyddion software, which allowed for the visualisation of real surface topography by inverting the parameters and performing the analysis as if on the actual surface rather than the negative copy (molds).

7.1.1. BZ#2965 and BZ#833

Figure 7. 1. High-resolution images depicting various sides of the refitting fragments BZ#833 and BZ#2965.

BZ#2965 and BZ#833 fragments (Figure 7.1) were found to refit into an elongated active stone, resulting in a final weight exceeding 600 g and a length measuring approximately 188 mm. Upon close examination of high-resolution pictures, it becomes evident that the edge of #2965 exhibits a convex shape and displays a levelled and smoothed surface. These characteristics may indicate its use. Likewise, the edge of #833 appears pointed and smoothed, indicating potential utilisation as well. Moreover, this specific edge shows a few pecking marks, which may have been made to shape the tools into pointed ends.

The opposite end of the #833 fragment, where the fracture occurred, displays noticeable smoothing on one edge of the fracture. This characteristic is consistent with the possibility that the tool continued to be used even after it broke into two pieces. The hypothesis of utilising either one or both fragments as independent tools could also provide an explanation for their retrieval in different squares in the archaeological site, separated by a distance of approximately 3 m.

Figure 7. 2. High-resolution images of BZ#833 and BZ#2965, clearly indicating the positions of the molds.

Two molds were examined from this tool: mold 5, acquired from the narrow lateral side of #833, and mold 3, acquired from the convex face of #2965 (Figure 7.2).

On mold 5, large levelled areas can be observed (e.g., Figures 7.3 and 7.4, areas: A.3, D.2, E; Figure 7.5, areas: A.1, A.7, A.8, A.9) along with various groups of long striations mainly in the direction of the main axes of the tool (e.g., Figures 7.3 and 7.4, areas: A.5, B.1, B.2, D.1; Figure 7.5, areas: A.6, A.8, A.9). Additionally, micropitted and deposit types of polish are also visible (e.g., Figures 7.3 and 7.4, areas: A, C, E) as well as serrated (e.g., Figures 7.3 area: A.5).

Mold 3 was cut into two parts during the analysis to better fit into the SEM chamber for analysis. Diffuse levelling with grains welded and flattened areas are visible (e.g., Figure 7.7, areas: A.6, B.1, B.2; B.1, B.2, C.1,

C.2, C.3, C.4; Figure 7.7 areas: A.2, A.5, A.6, A.7, A.9). Several groups of short striations with a loose distribution on the surface are also observed, exhibiting connected density (e.g., Figure 7.7, areas: A.1, A.3, A.4, A.5, B.2). The linear traces display varying orientations (as clearly visible in Figure 7.7, area: A.1; Figure 7.8, area: A.7; Figure 7.8, areas: A.5 and A.6). Serrated polish type is evident in several areas, as seen in Figures 7.6 and 7.7 (areas A), as well as flattened polished regions in B.2, C.3, and C.4.
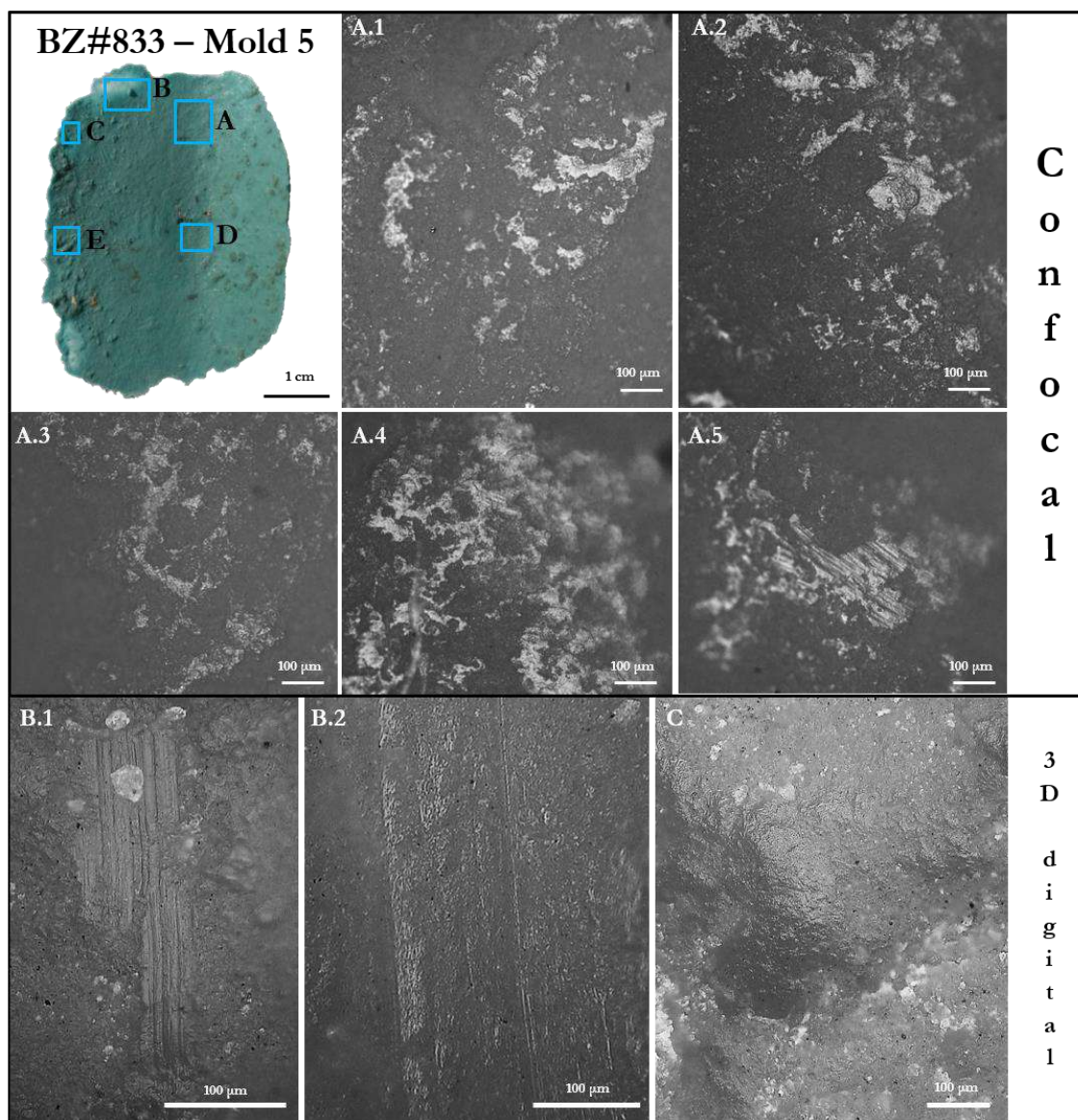
Figure 7. 3. Different microscopes images of different areas on BZ#833 - Mold 5 are shown. In the top left corner, is depicted the mold with indications of the areas depicted in the micrographs. The first row shows pictures acquired with the confocal profilometer, while below pictures acquired with the 3D digital microscope.
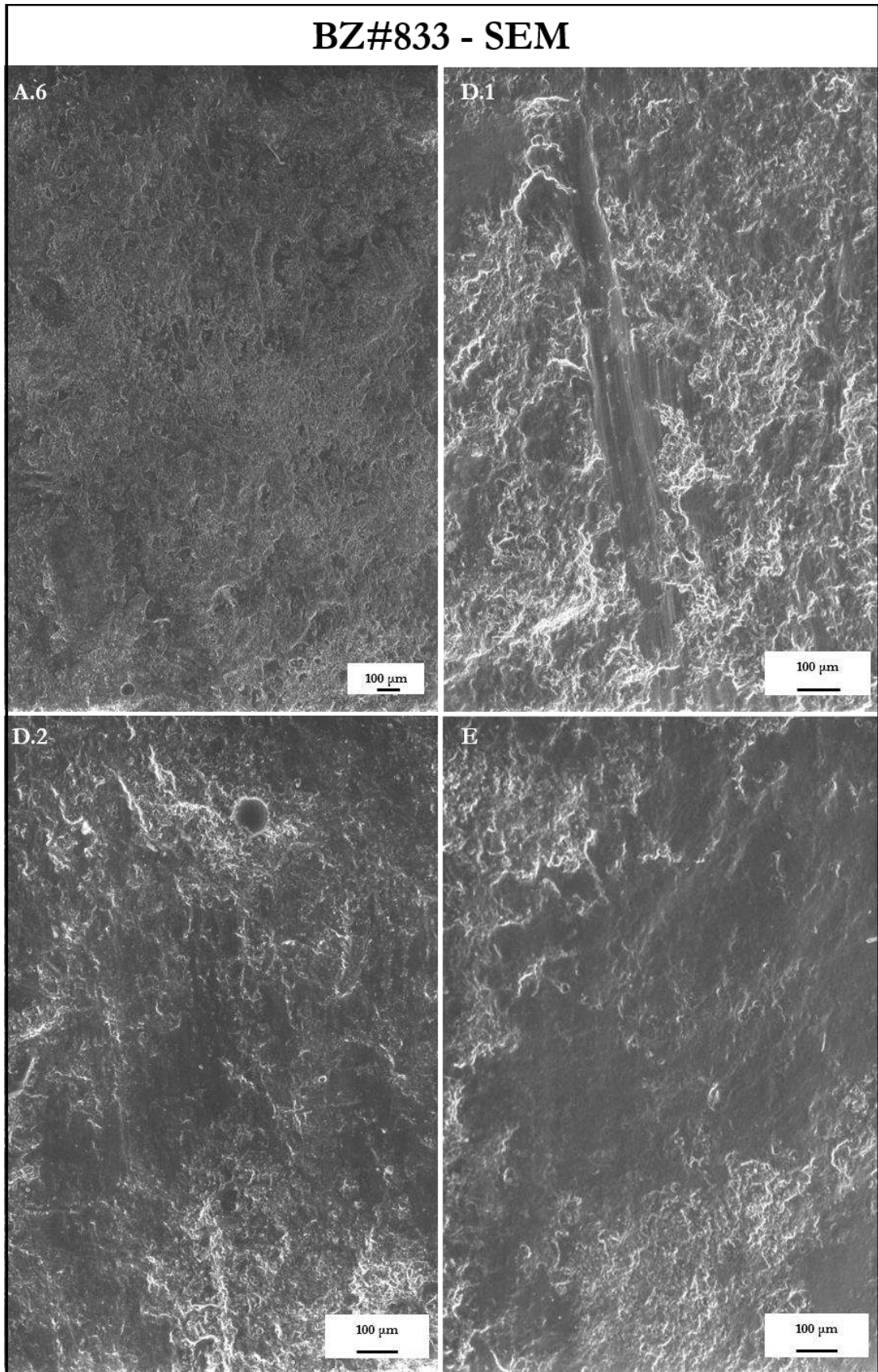
Figure 7. 4. SEM images acquired on area A, D and E of BZ#833 - Mold 5.

BZ#833 – Mold 5
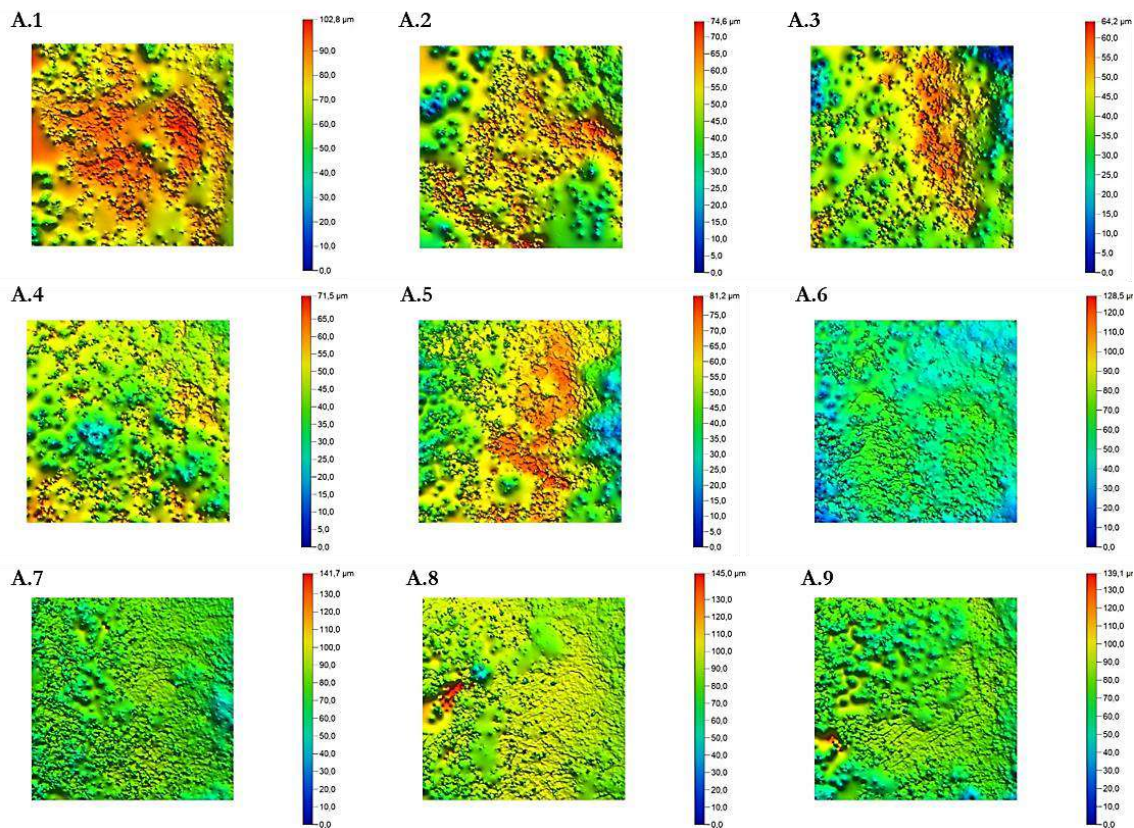
Figure 7. 5. BZ#833, mold 5: False-colour microtopographic maps of the analysed squares within area A. Large flattened area and striations are visible
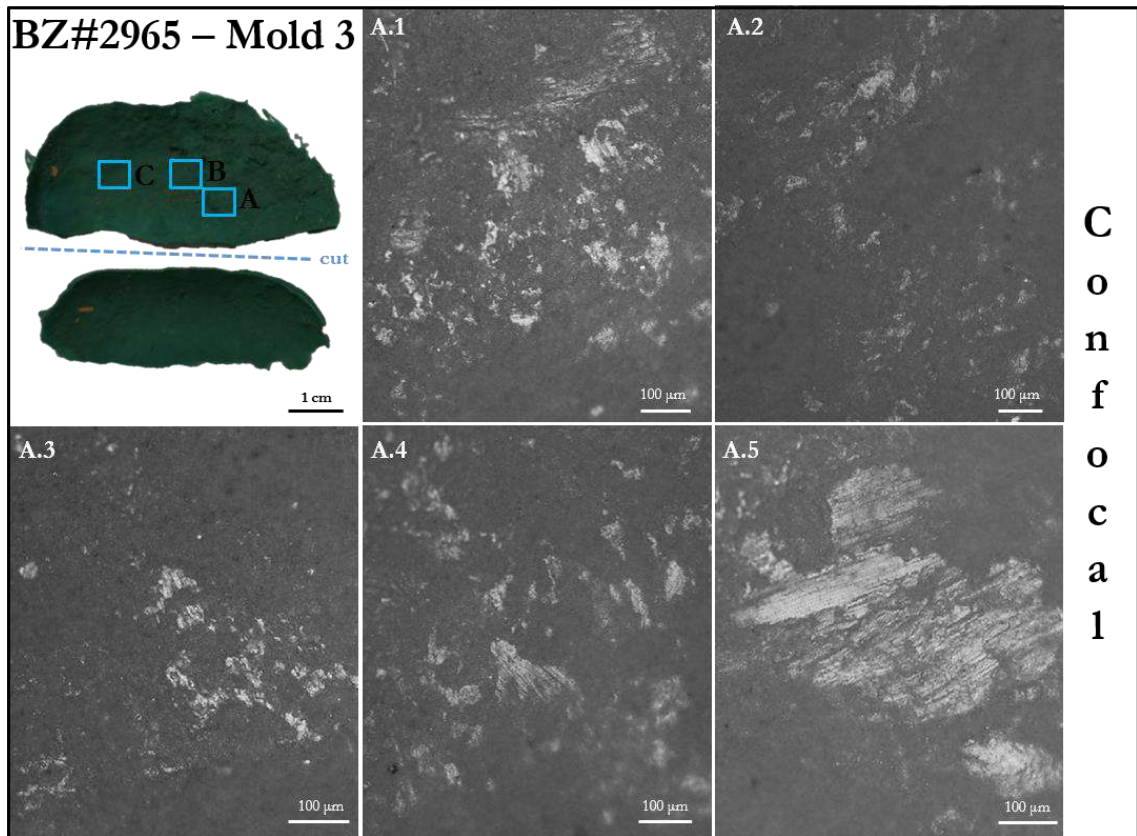
Figure 7. 6. Confocal profilometer images of differet areas on BZ#2965 - Mold 3 are shown. In the top left corner, is presented the mold with indications of the areas depicted in the micrographs. The first row shows pictures acquired with the confocal profilometer.
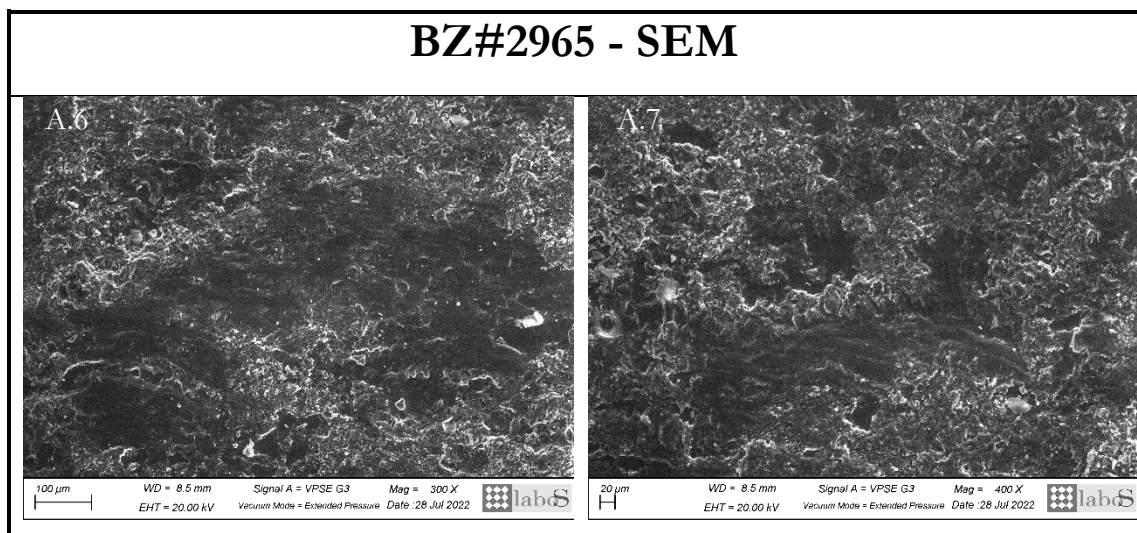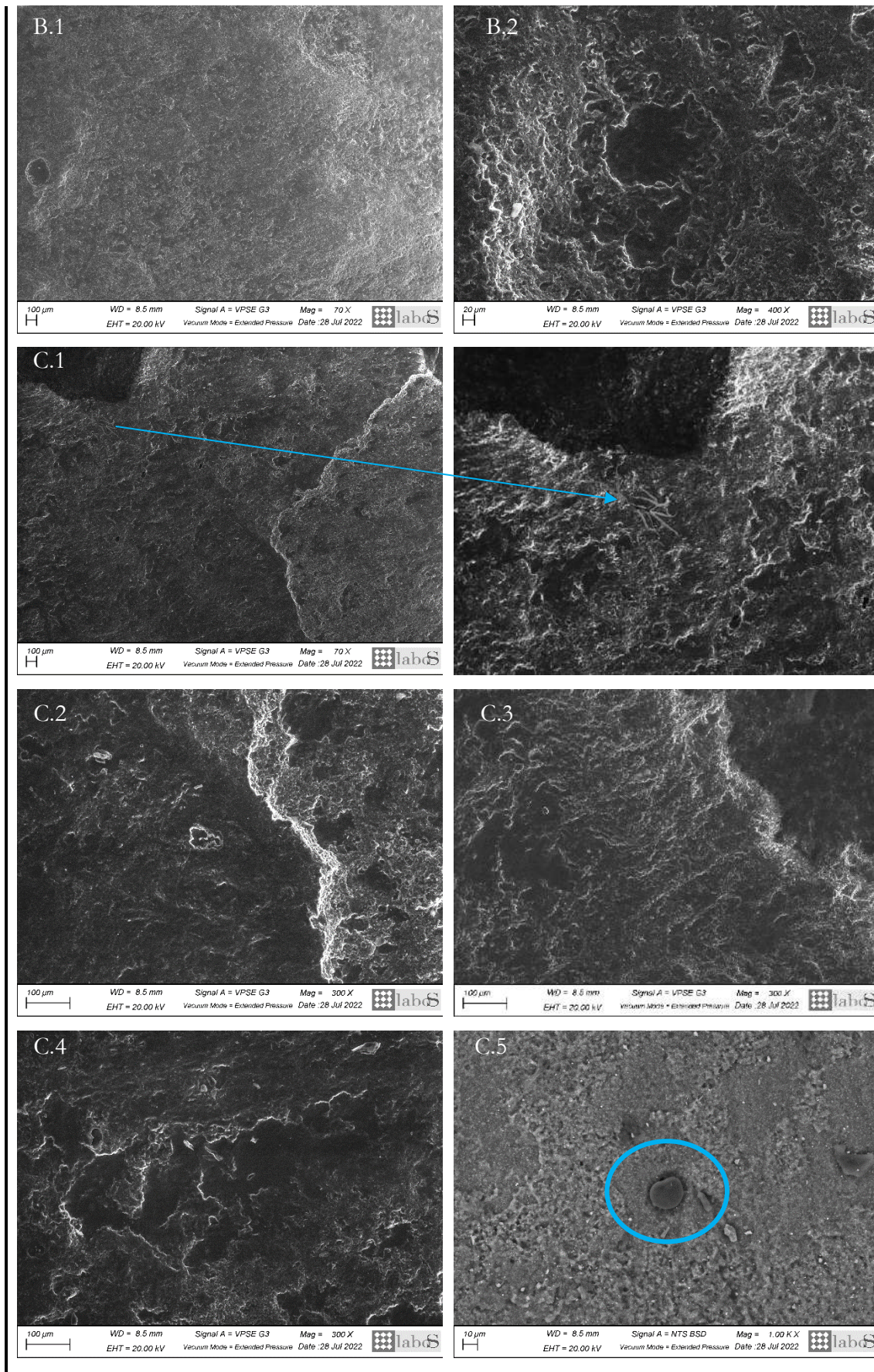
Figure 7. 7. SEM images acquired with secondary electrons at ETH 20.00 kV and WD 8.5 mm, except image C.6 that is acquired in back scattered to enhance the presence of residues, as the presented putative starch granule.

BZ#2965 – Mold 3
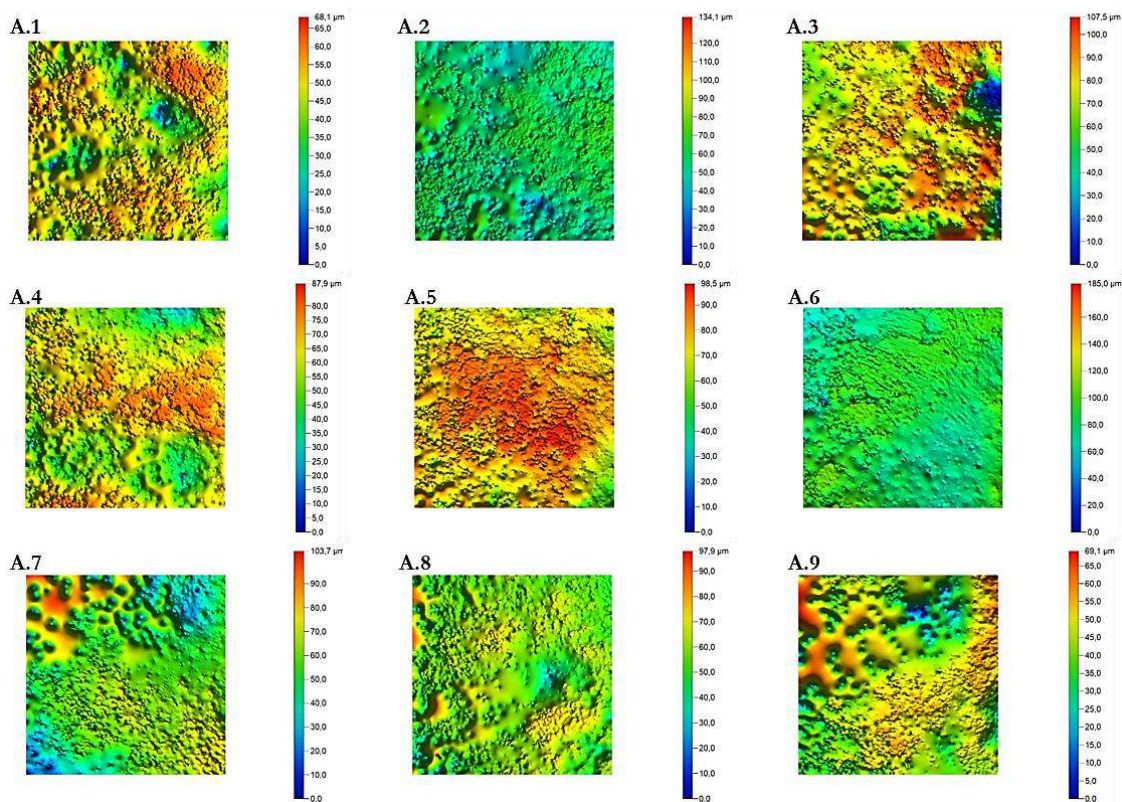
Figure 7. 8. BZ#2965, mold 3 area A: False-colour microtopographic maps of the analysed squares within area A. large flattened area and striations are visible.

The analysis of the experimental tools reveals that quartz-arenite, a highly resistant rock, displays noticeable changes only after extended periods of use. Particularly, wear patterns like striations become apparent only upon contact with harder materials or smaller particles, resulting in repeated interactions between the two lithic surfaces. For instance, M9, an active tool employed for grinding *Rumex crispus* achenes, and M5, utilised for *Chenopodium album* achenes, both display light striations due to their interaction with this type of resource. Indeed, the specific morphology of #2965, coupled with the orientation and nature of the use-wear patterns, strongly suggests the application of a circular grinding motion, compatible with the processing of a resistant resource such as achenes. The presence of starch granules, detected on mold by the writer (e.g., Figure 7.7 area C.5, blue circle) and confirmed by residue analysis (unpublished results by Dr. Irina Pantukina and Dr. Clarissa Cagnato), is in line with
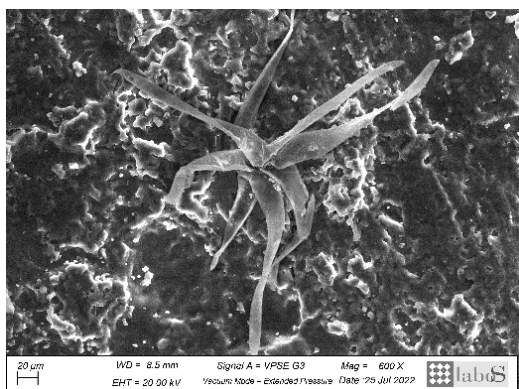
Figure 7. 9. Fiber detected on GS3 at T₃ after treating Chenopodium album achenes and Ceratonia siliqua pods

this hypothesis. Additionally, other plant residues were identified, such as the fibre highlighted in Figure 7.7 area C.1, resembling a residue found on GS3 at T_3 after 30 minutes of *Ceratonia siliqua* pods crushing and grinding, and 60 minutes of *Chenopodium album* achenes grinding (Figure 7.9).

Residue analysis also highlighted the presence of a fragment of plant vascular tissue, characteristic of xylem and phloem, which treatment may have contributed to the uniform surface smoothing visible to the naked eye and under SEM at low magnifications (see Figure 7.7 areas: B1, C.1).

Regarding the fragment #833, there are evident indications that this portion of the tool was also employed, coming into contact with a hard and resistant resource. The wear patterns observed on this fragment align with a back-and-forth movement. The consistent orientation of long groups of striations, distributed along the main axes of the tool, recalls the behaviour of a pestle when used alongside a mortar. However, within the Brînzeni GSTs collection, there is no item or fragment that presents the concavity of a mortar. Remarkably, starch granules and fragments of plant tissue were also identified on this fragment, further supporting the hypothesis of its active role in processing plant resources.

7.1.2.   BZ#5160

Figure 7. 10. Pictures representing the different sides of the fragment BZ#5160

BZ#5160 (Figure 7.10) is a fragment of a flattened and convex-ended cylinder. It shares similarities in size, shape, and fracture pattern with fragment #2965, suggesting its potential use as an active tool. Its convex edge is narrower compared with the broader edge of BZ#2965.
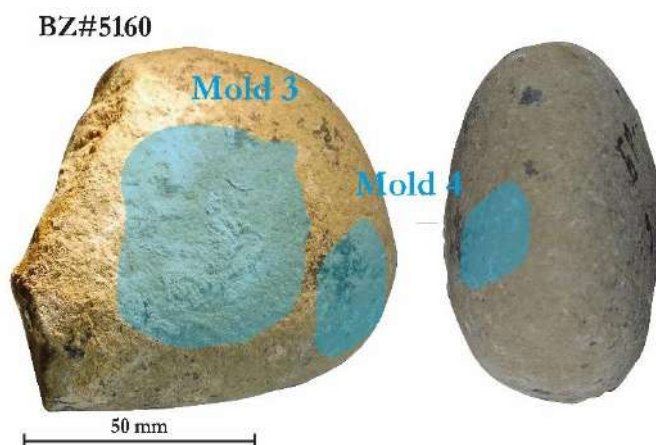
Figure 7. 11. Images depicting BZ#5160, highlighting the positions of the molds.

Two molds underwent analysis: mold 3, covering the larger surface, and mold 4, positioned adjacent to the convex edge (Figures 7.11). Both molds were acquired following the removal of the carbonatic crusts that were covering the surface. These crusts were successfully dislodged by immerging the stone in carbonated water for several hours, facilitating its gentle detachment through friction and revealing the underlying original tool surface.

On mold 3 (Figure 7.12), the micrographs obtained under confocal profilometer revealed the presence of micropitted polished areas, along with small serrated polished areas visible on the highest points of the surface elevation. Examination with the 3D digital microscope highlighted the presence of several long and connected striations (Figure 7.12, Areas: B.1 and C.2). These features appear to be well-preserved and clearly defined, likely preserved from post-depositional processes by the crust that formed on the surface, possibly as a consequence of the post-depositional process itself. Most probably these crusts have effectively shielded the surface and its associated features. Therefore, upon their removal the utilised surface became exposed. The 3D reconstruction demonstrates that these wear features are concentrated predominantly on the high and middle surface microtopography, depicted as blue and green regions in the false-colour 3D map (Figures 7.12, areas C.1, C.3; note that the topography is reversed in accordance with the data acquired from molds). SEM images were captured using backscattering mode to enhance residue visibility, which can be observed in the form of fibres (e.g., Figure 7.12 areas: A.4, E.2, E.4) and other sub-circular particles. The micrograph taken in area D.2, displaying striations, was acquired in secondary electron mode utilising the FEG-SEM available at IOM-CNR in Basovizza (Birarda et al.,

2020). The SEM micrographs illustrated in Figure 7.12 validate the presence of flattened regions frequently accompanied by groups of striations. Some crystals also exhibit fractures, step fractures, and pits, the existence of which is confirmed by the false-colour microtopographic maps (Figure 7.13). These maps effectively portray substantial variability in heights, but also numerous small-levelled areas and few micro-striations.

The same configuration of wear patterns observed on mold 3 extends towards the convex edge, encompassing the region of mold 4 (Figure 7.14). However, a close examination of the microtopographic maps (Figure 7.15) reveals that in this area, the surface displays a more pronounced roughness.

From the pattern, it seems that this tool was employed in a back-and-forth horizontal grinding motion on a resistant resource, such as achenes, and to a lesser extent, in a vertical action. This is evident as flattened areas and striations exhibit a greater extent than pits and cracks.

The use of this tool in the processing of vegetal resources is further supported by the analysis of one of the crust samples (Figure 7.16). The area of the crust that was in contact with the lithic surface was examined using FEG-SEM as well as by the writer under optical microscope, revealing the presence of vegetal residues, including starch granules and other plant fibres.

While the tool's shape, fractures, and the presence of distinct groups of elongated striations recall similarities with the tool composed by the fragments #833-#2965, the distribution of the wear pattern suggests a different type of motion, as well as a significantly more pronounced intensity of use for the #833-#2965 tool. Further investigation is required to fully understand the function(s) of this BZ#5160. It is essential to determine whether the convex face, characterised by a shape suitable for pounding activity, indeed signifies such a use.
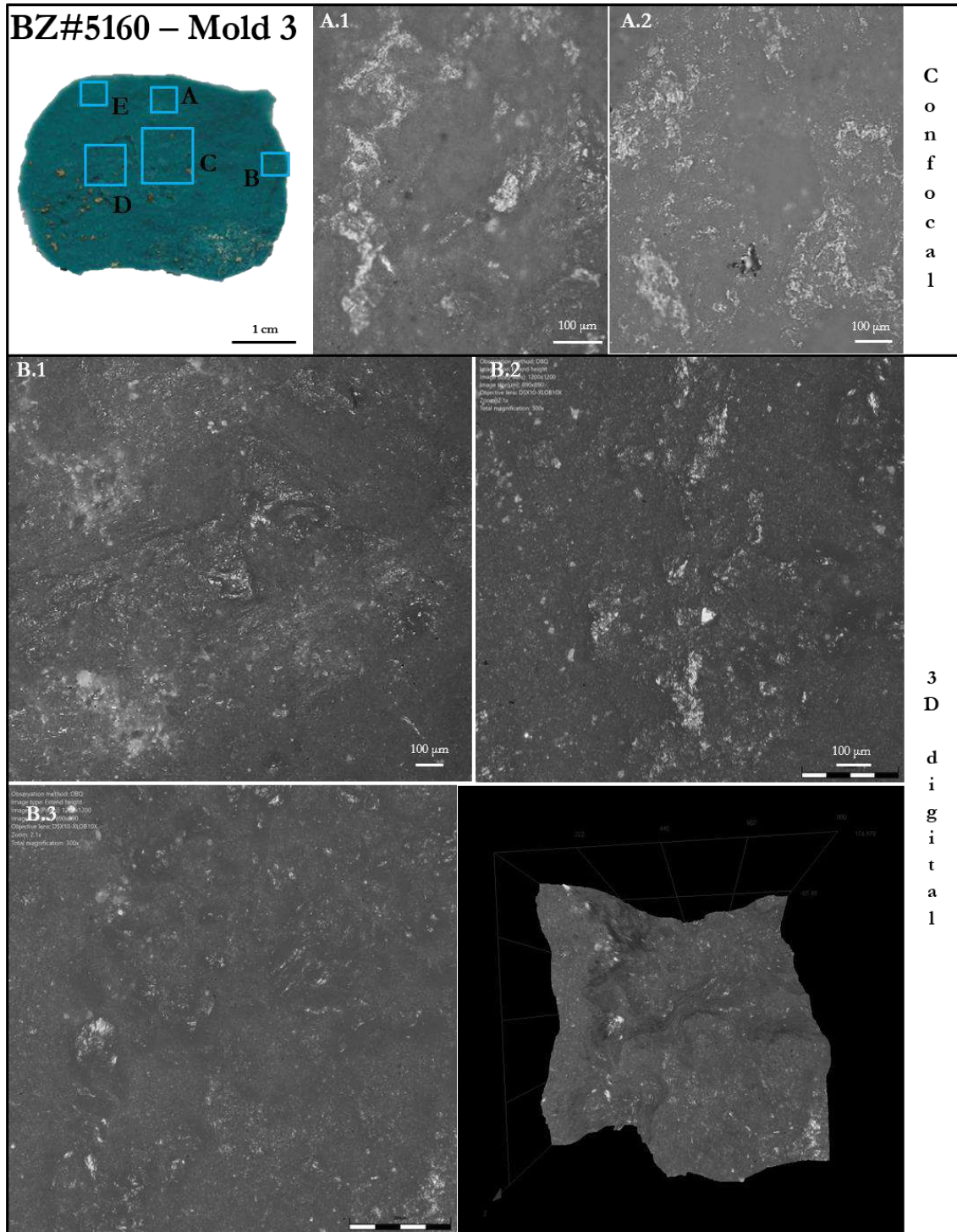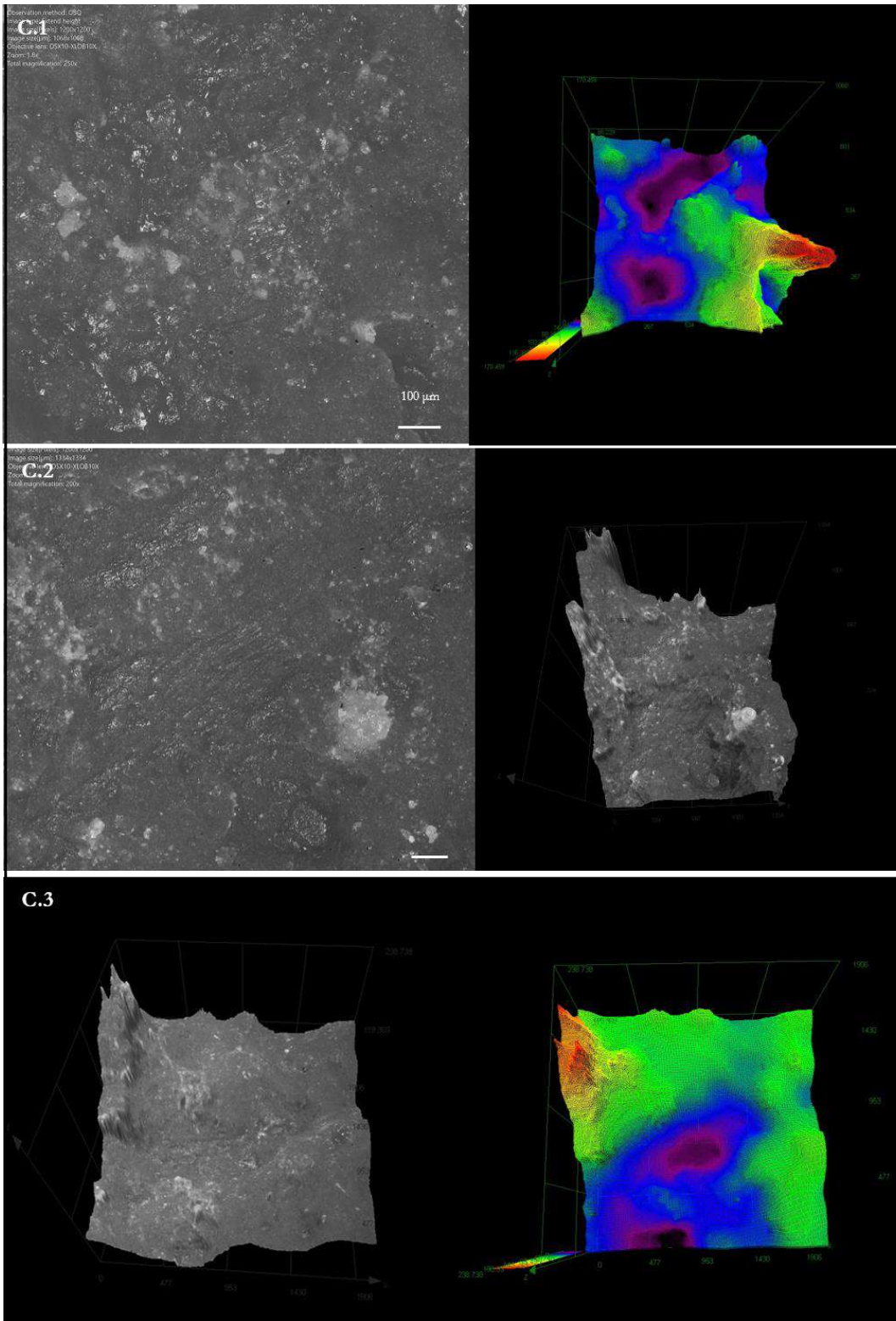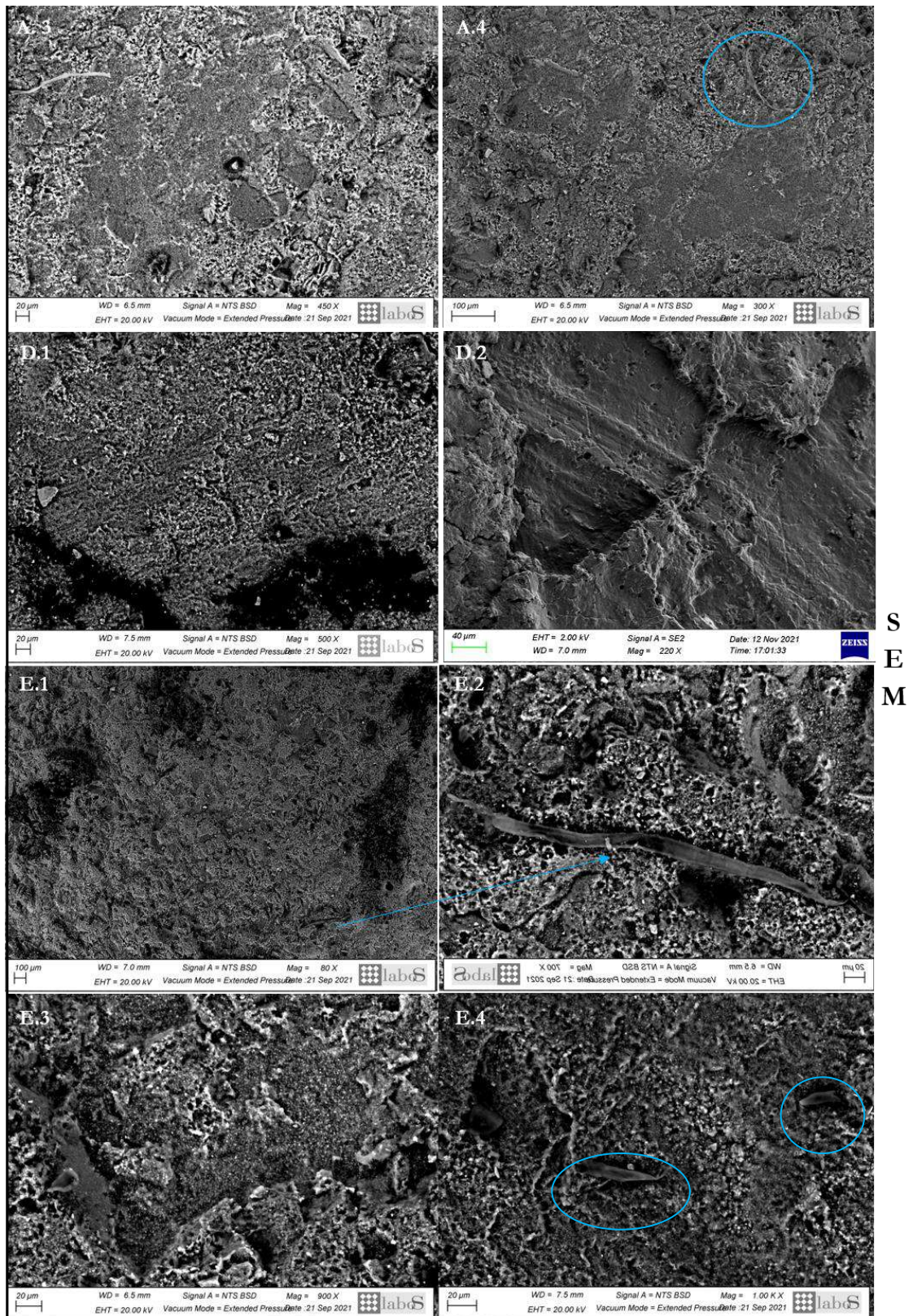
Figure 7. 12. Various microscopes images of different areas on BZ#5160 - Mold 3 are presented. In the top left corner, the mold is depicted, with designated regions corresponding to the micrographs. On top: images obtained through the stereomicroscope; middle: images captured with the 3D digital microscope; on bottom: SEM images. Notably, the micrograph for areas B.1, C.1, C.2, and C.3 is accompanied by corresponding 3D models and/or false-colour 3D models, emphasising the relationship between use-wear traces and surface topography (it should be noted that the topography is reversed as the data was acquired from molds).

The SEM images reveal several plant fibre fragments, highlighted in blue. Additionally, area E.2 was captured using FEG-SEM.

BZ#5160 – Mold 3

Figure 7. 13. BZ#5160, mold 3: False-colour microtopographic maps of the analysed squares within area A. The regions exhibit a large variability in heights but also small levelled areas, as well as pits, and micro-striations.
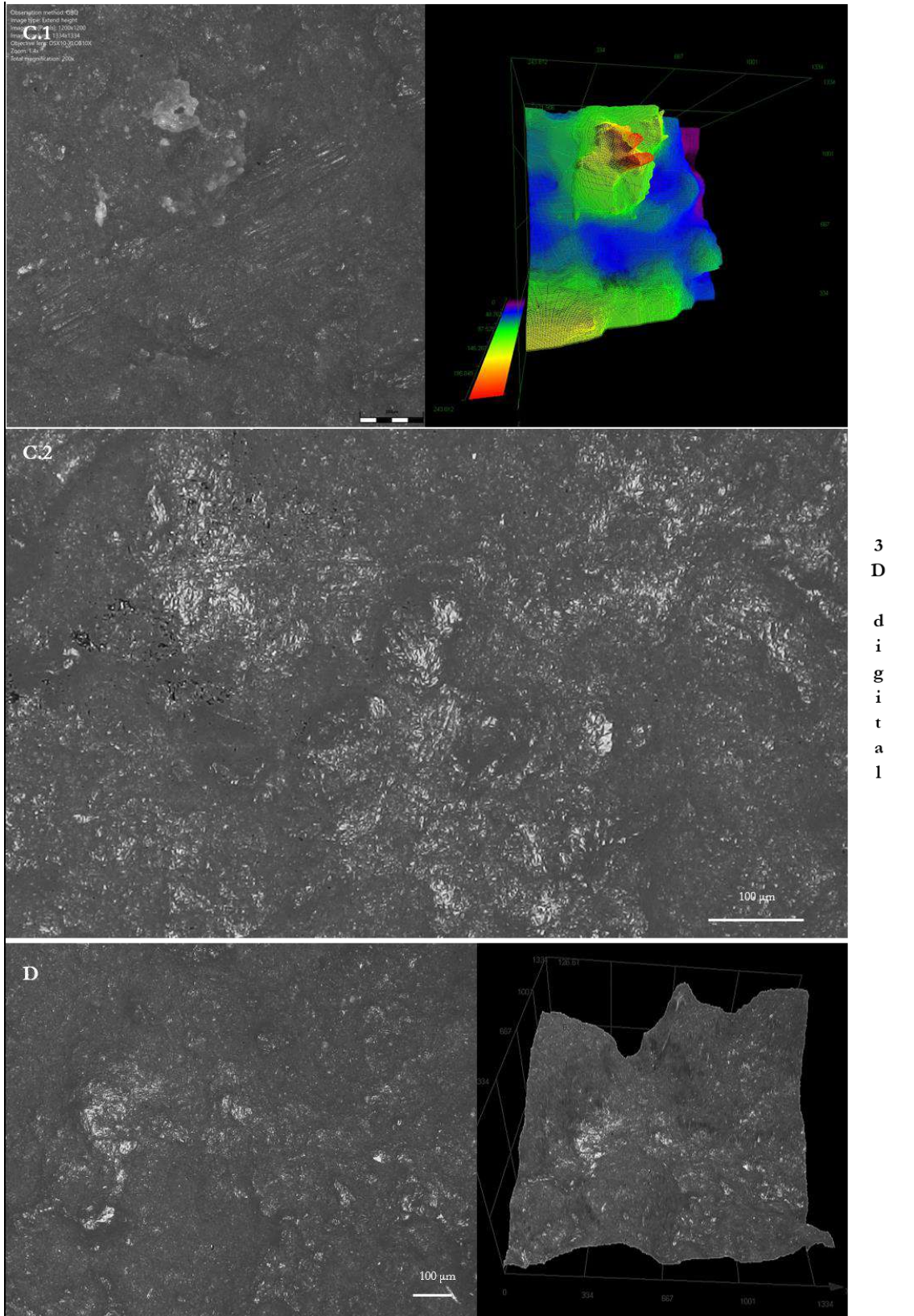
Figure 7. 14. 3D digital microscope images of BZ#5169-Mold 3. Notably, the micrograph for areas A, B, C.1, and D are accompanied by corresponding 3D models and/ or false-colour 3D models, emphasising the relationship between use-wear traces and surface topography (it should be noted that the topography is reversed as the data was acquired from molds).

BZ#5160 – Mold 4

A.1

A.2

A.3

A.4

A.5

A.6

A.7

A.8

A.9
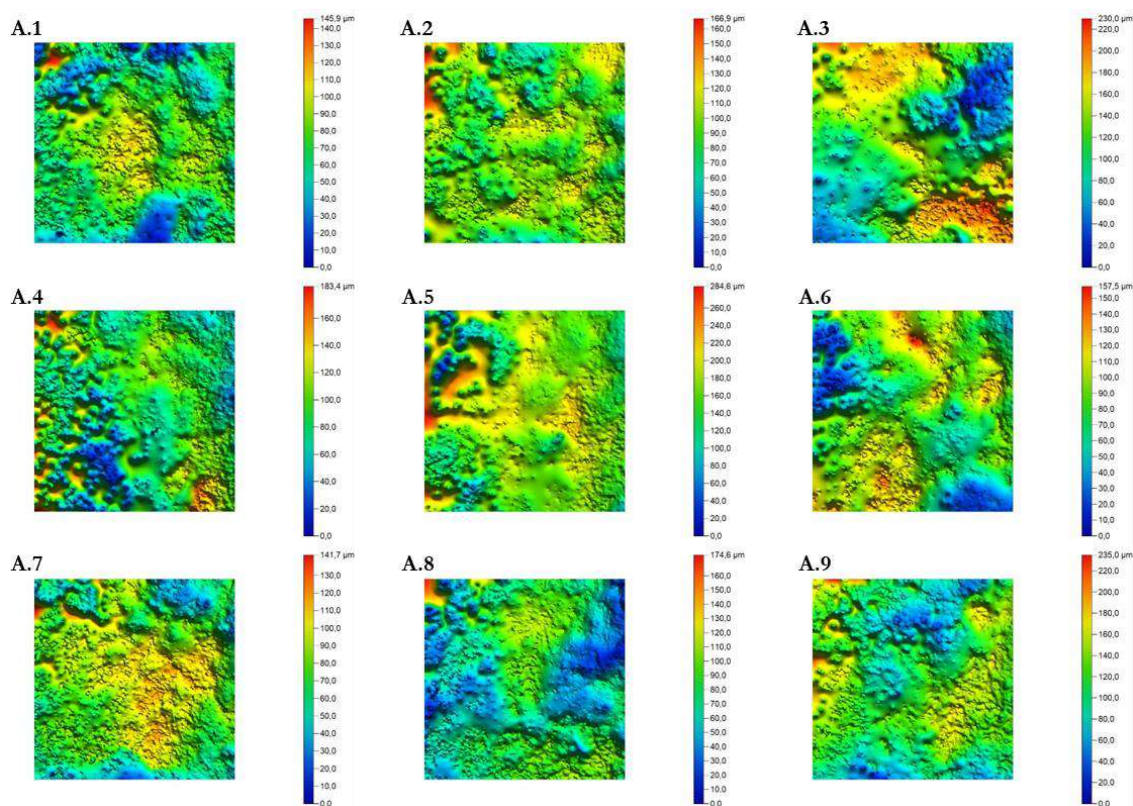
Figure 7. 15. BZ#5160, mold 4: False-colour microtopographic maps of the analysed squares within area A. The areas exhibit a large variability in heights and large presence of low topography.

BZ#5160 - Crust sample

SEM

OM
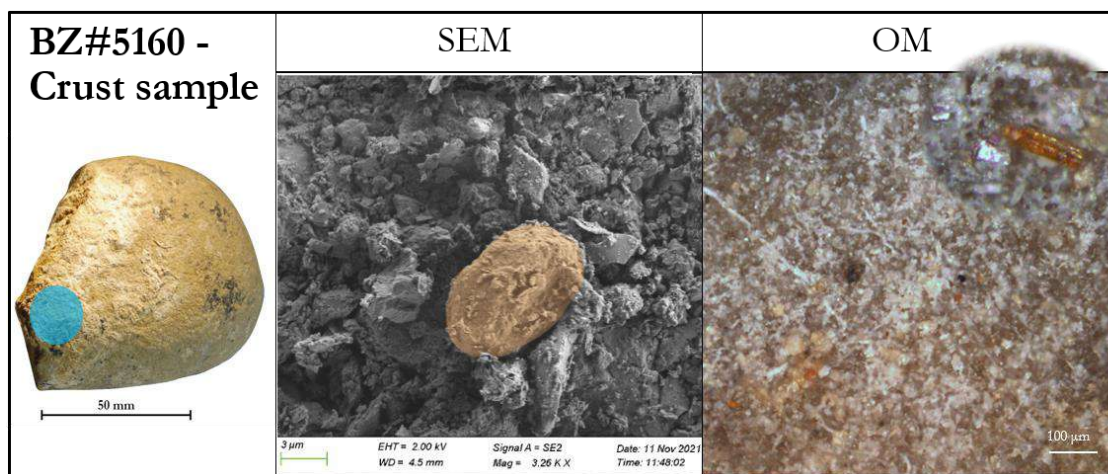
Figure 7. 16. The carbonatic crust sampled from the surface of BZ#5160 (blue circle indicating the sampling area): the side in contact with the lithic surface was analysed. The image includes a SEM image where a starch granule has been highlighted using orange colour.and an OM micrograph depicting some vegetal residues.

7.1.3.   BZ#6742
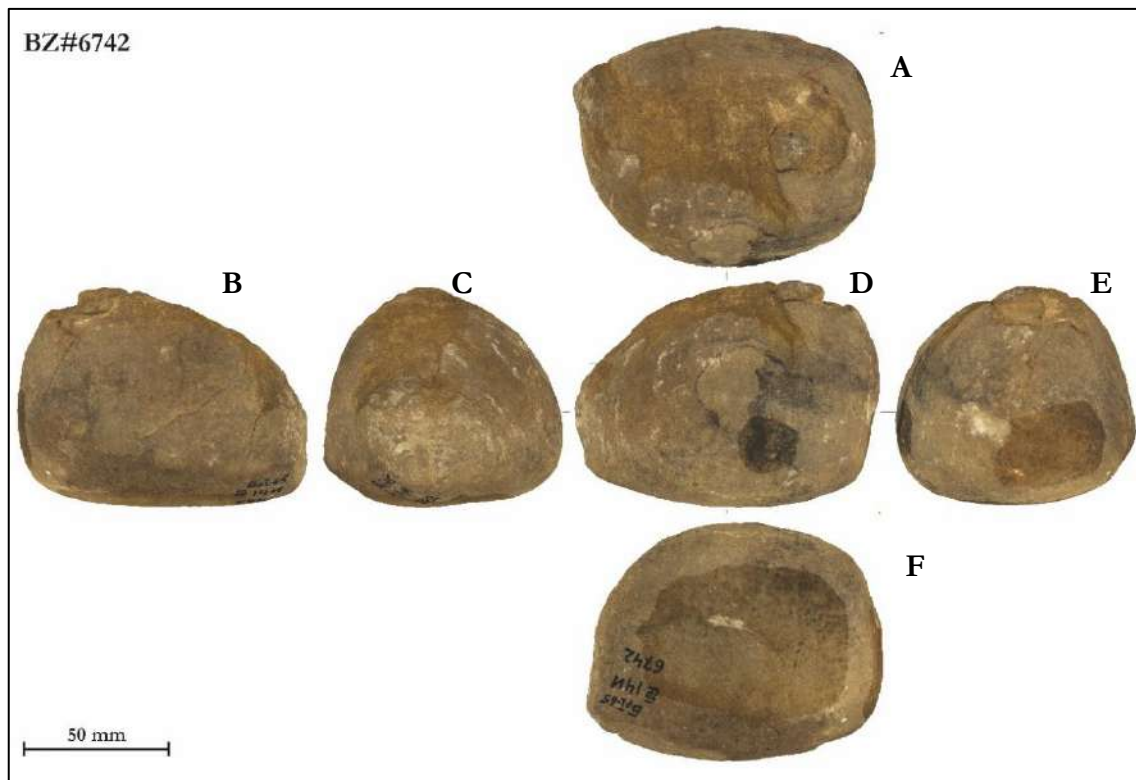
Figure 7. 17. Images extracted from the 3D model showing various surfaces of BZ#6742.

BZ#6742 (Figure 7.17) is characterised by dimensions and shape that resemble those of an active stone tool intended for horizontal grinding activities. It presents an asymmetrical ellipsoidal shape with one side rounded (face A) and another side flattened (face F). Furthermore, face A exhibits pronounced fractures that led to the detachment of substantial fragments. It is likely that these severe damages occurred after recovery or during excavation, given the fresh appearance of the fractures without adhering earth. Numerous minor damages are visible on the surface, including a pronounced pit on face E. On face D, a dark area exhibits characteristics resembling the effect of the exposure to fire.

Three molds underwent analysis (Figure
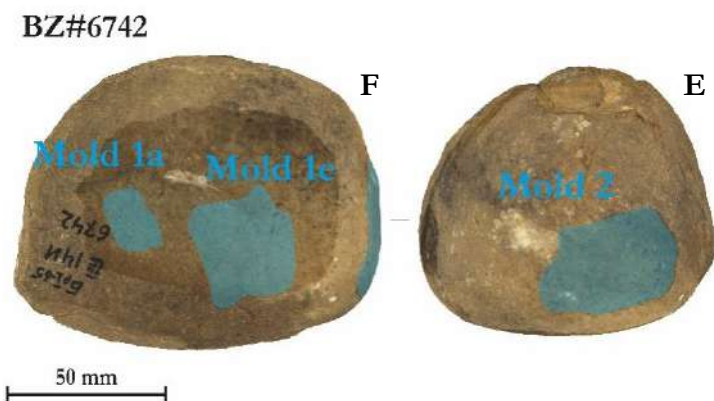
Figure 7. 18. Images depicting BZ#6742, highlighting the positions of the molds.

7.18): mold 1a and 1e, taken from the flat side F, and mold 2, taken from the convex face E. Microscopy observations on the latest side revealed the presence of several conchoidal fractures (Figure 7.19, areas: A.2, B and C). The grains are well distinguishable from the matrix, as evident from the microtopographic maps in Figure 7.20. Nonetheless, the elevated tips exhibit cracks and distinct levelling but retaining their unsmoothed nature and sharp edges.

Molds 1a and 1e (depicted in Figures 7.21 to 7.24) also reveal conchoidal fractures and pits. The fractured crystals exhibit increased reflectivity, accompanied by small surface cracks (Figure 7.21, areas: A.4, B, C.1; Figures 7.23, areas: B.1, B.2, C, D1, D3, D.1, D.2, D.4). The more pronounced modifications are primarily visible on the high microtopography clearly discernible in the false colour 3D models (Figure 7.23, areas: C and D4). A significant number of grains exhibit smooth and rounded edges (Figure 7.21, areas: A.1, A.4, B; Figure 7.23, areas: A, D4). However, flattening is either limited or absent, as visible from the microtopographic maps (Figures 7.22 and 7.24). The co-occurrence of smoothed surfaces, cracks, and fractured crystals result in the frosted appearance described by Adams et al. 2009 (clearly observed in Figure 7.21, area C, and Figure 7.23, area B).

On both examined surfaces, the grains are clearly distinguishable from the matrix, a feature also apparent in the microtopographic maps (Figures 7.20, 7.22, 7.24). However, on face F, a notable degree of smoothed areas can be observed. Furthermore, a variety of residues have been identified on the surface, having been dislodged from the lithic substrate by the mold. Upon examination under polarised light, starch grains displaying the distinctive Maltese cross pattern were identified (e.g., Figure 7.23, area D.3).

Based on tool shape and traces it is conceivable to hypothesise that the tool was used for vertical actions. Its usage may have encompassed multiple faces of the tool, with face F emerging as the predominant use surface. While this face appears to have been potentially involved in pounding resistant, yet not hard, vegetal resources (such as USOs or more likely fruits with soft kernels, given the absence of fibres and other plant tissues – although deeper residue analysis is required), face E seems to have served in a secondary use for a more challenging task, such as cracking hard kernels but probably use less intensively. The hypothesis of its involvement in heavy tasks is further reinforced by the tool's weight, which exceeds the average weight for the Brînzeni active tools.

The presence of black spots, resembling the effects of proximity to fire, may indicate the item's recycling in a different task that potentially involved exposure to flames. Nonetheless,

the artefact's compromised state of preservation hinders further progress beyond the realm of hypothesis.
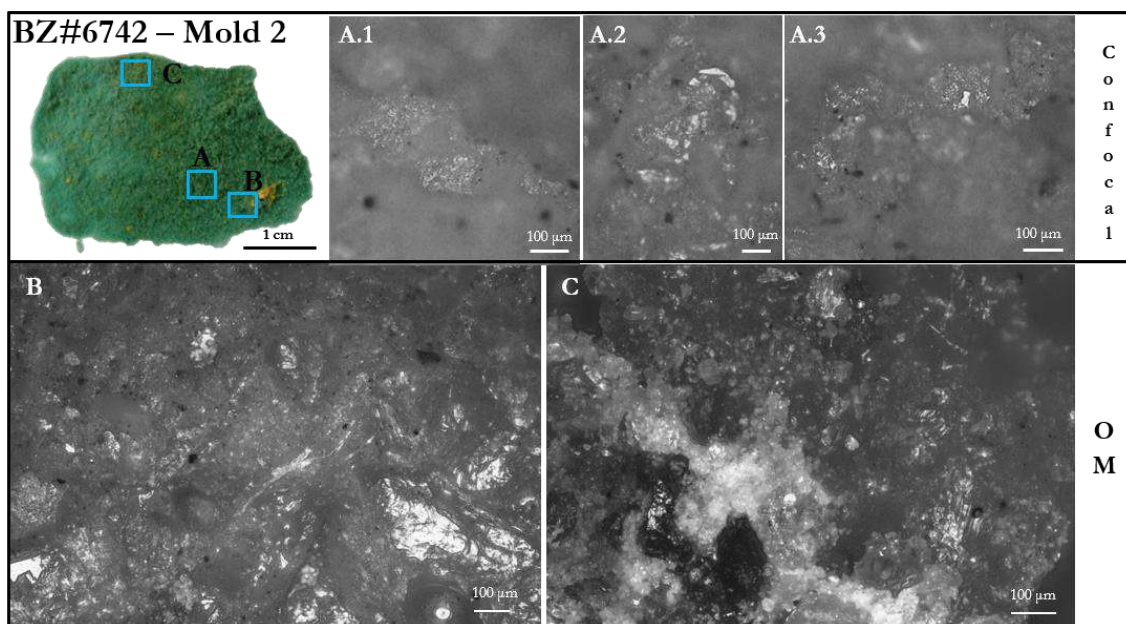
*Figure 7. 19. Confocal and OM micrographs of different areas on BZ#6742- Mold 2.*

BZ#6742 – Mold 2
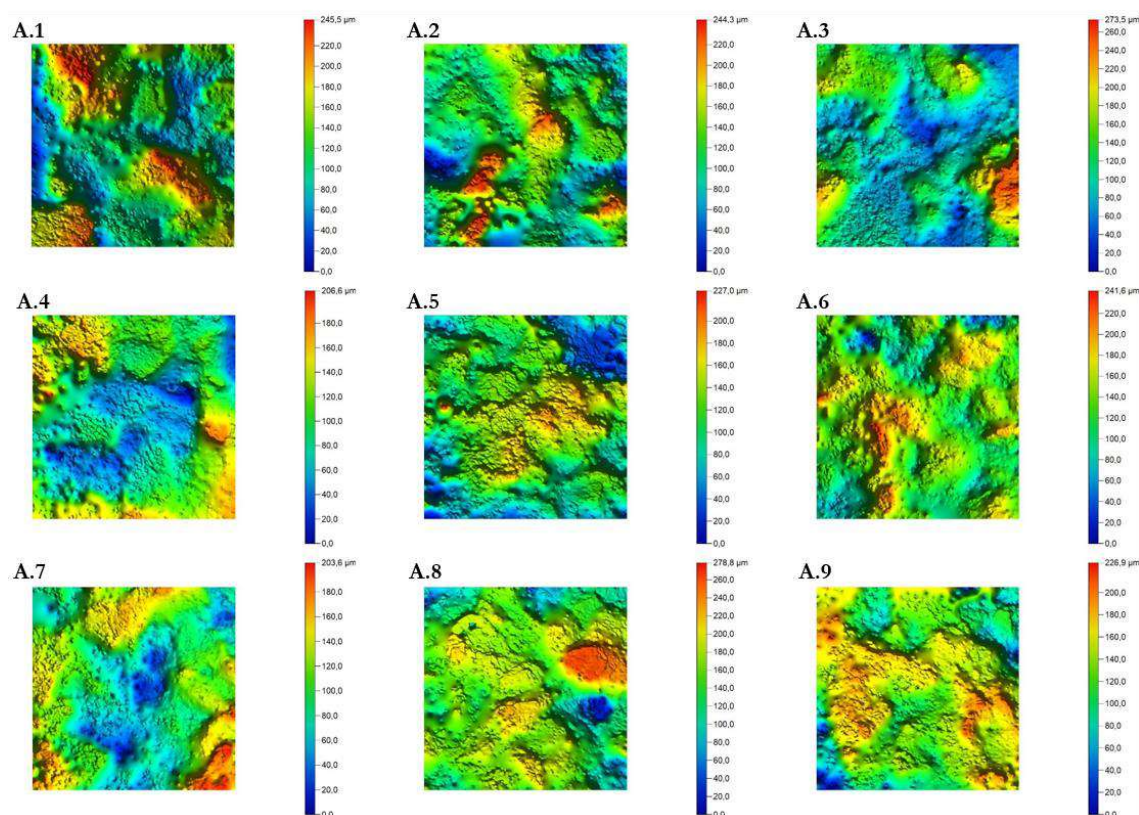
Figure 7. 20. BZ#6742, mold 2: False-colour microtopographic maps of the analysed squares within area A. Some flattened areas are visible.

Figure 7. 21. Confocal profilometer and optical microscopes micrographs of different areas on BZ#6742-Mold 1a

BZ#6742 – Mold 1a
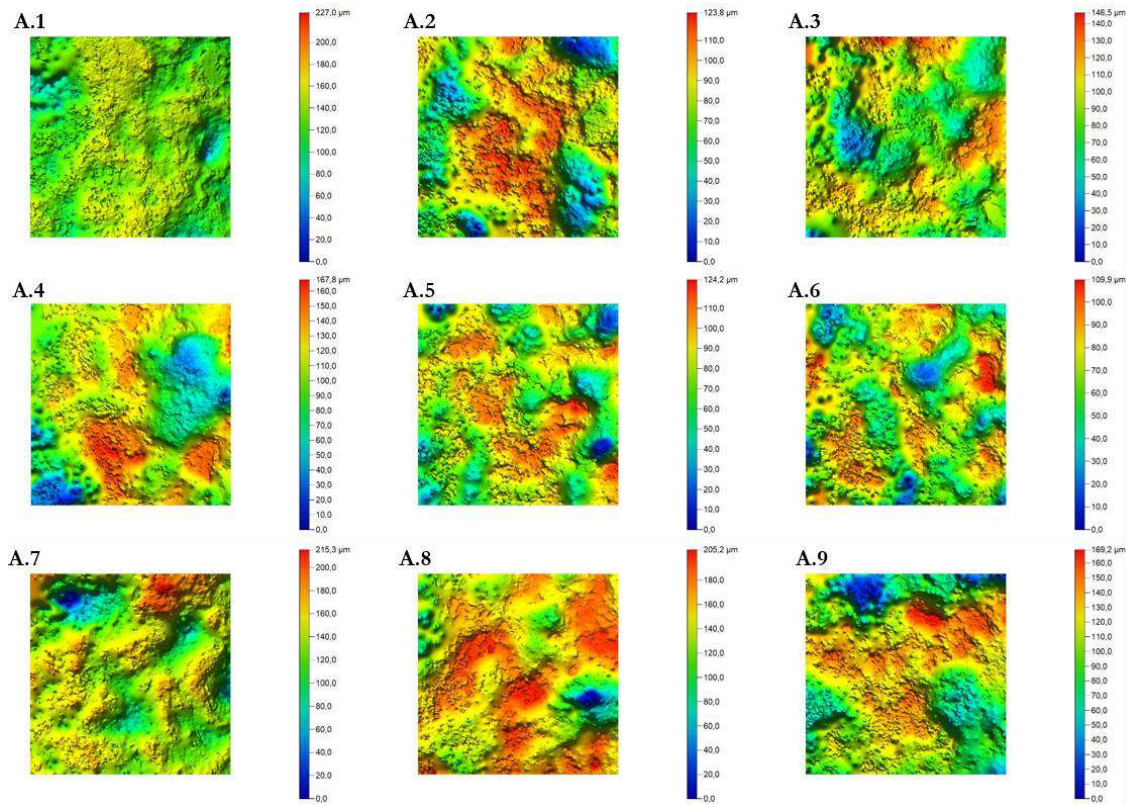
Figure 7. 22. BZ#6742, mold 1a: False-colour microtopographic maps of the analysed squares within area A.
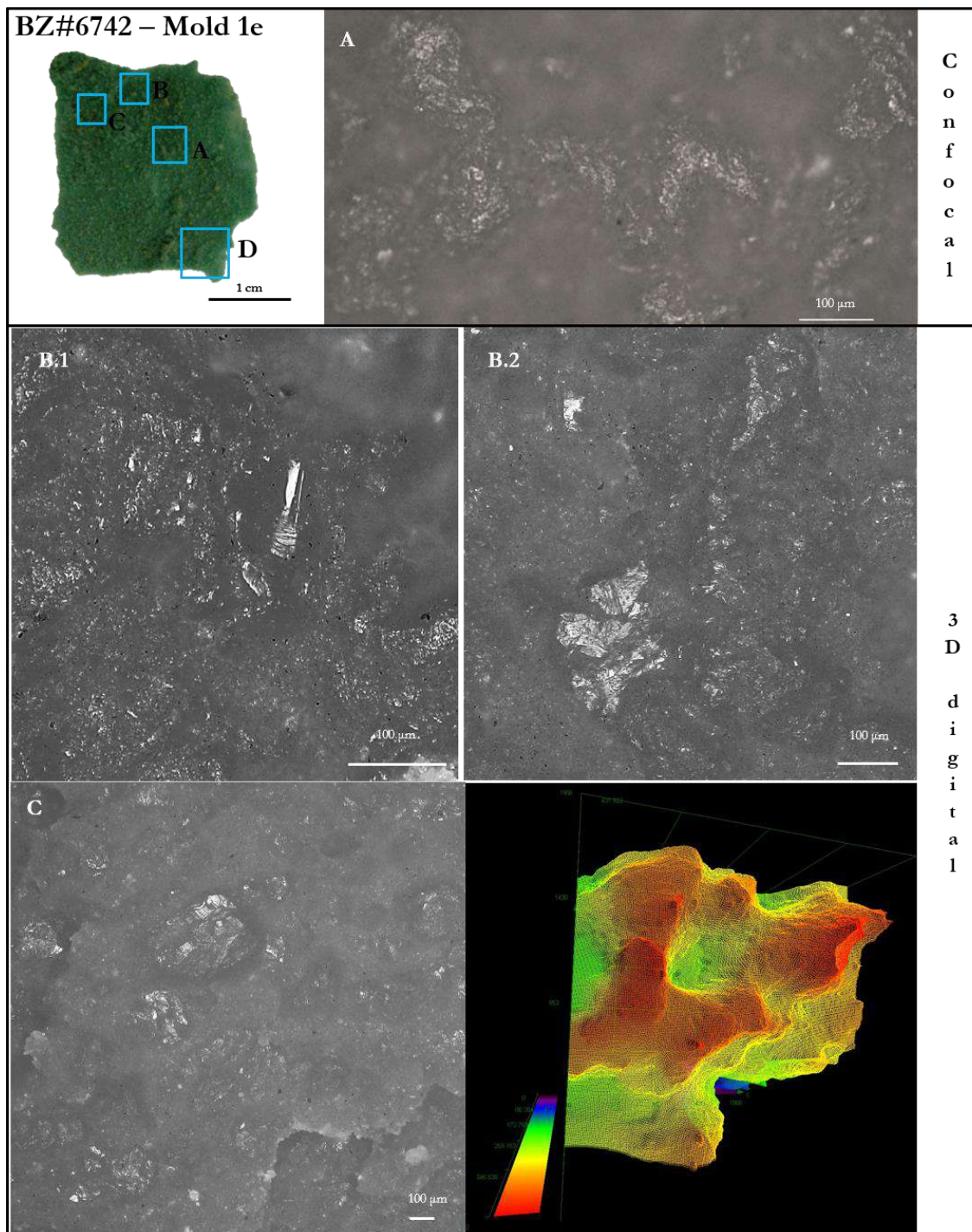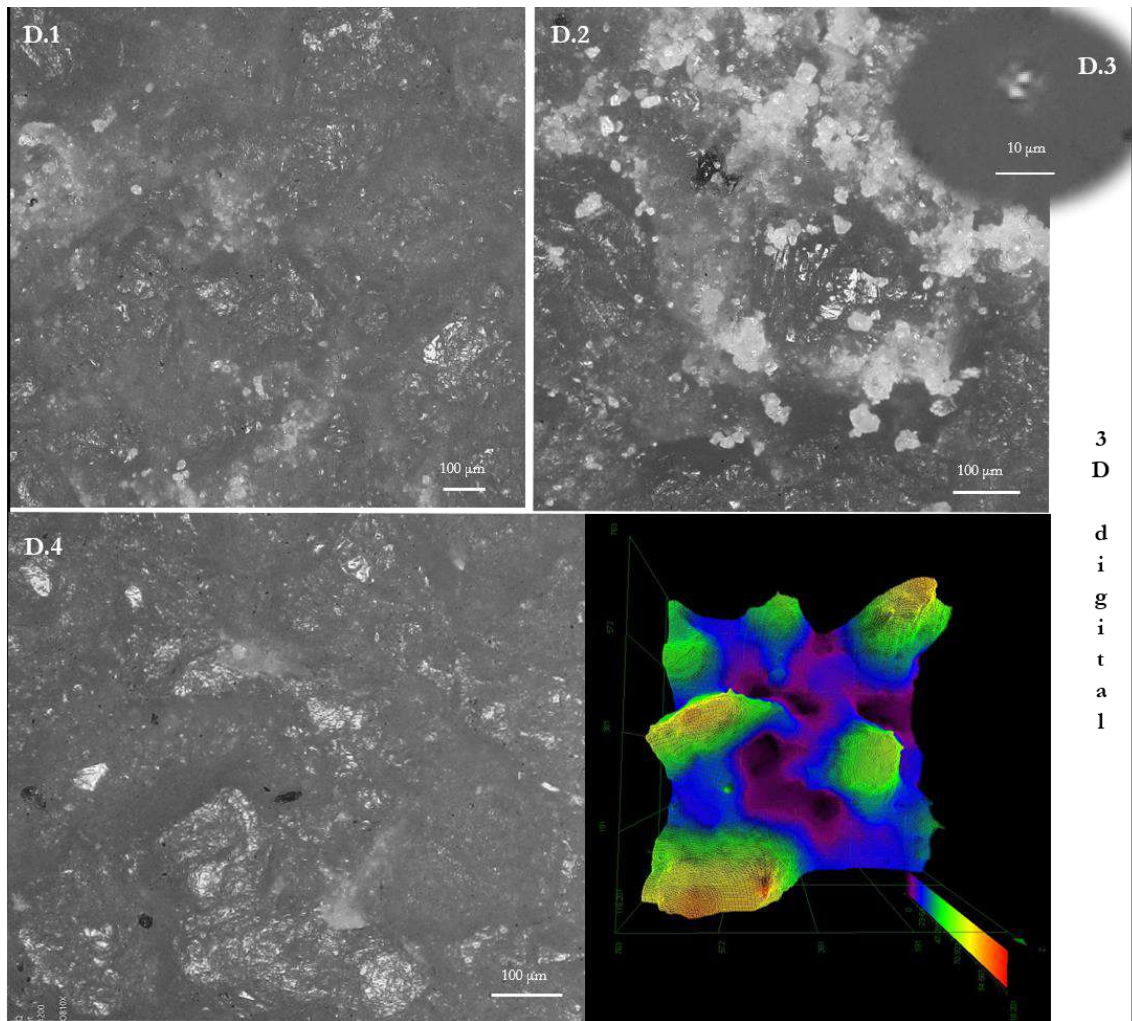
Figure 7. 23. Confocal profilometer and 3D digital microscope images of BZ#6742 - Mold 1e. Also, false-colour 3D of areas C and D5 showing the location of wear-feature on the surface relief and the well distinguishable surface crystal that bulge from the matrix.

BZ#6742 – Mold 1e
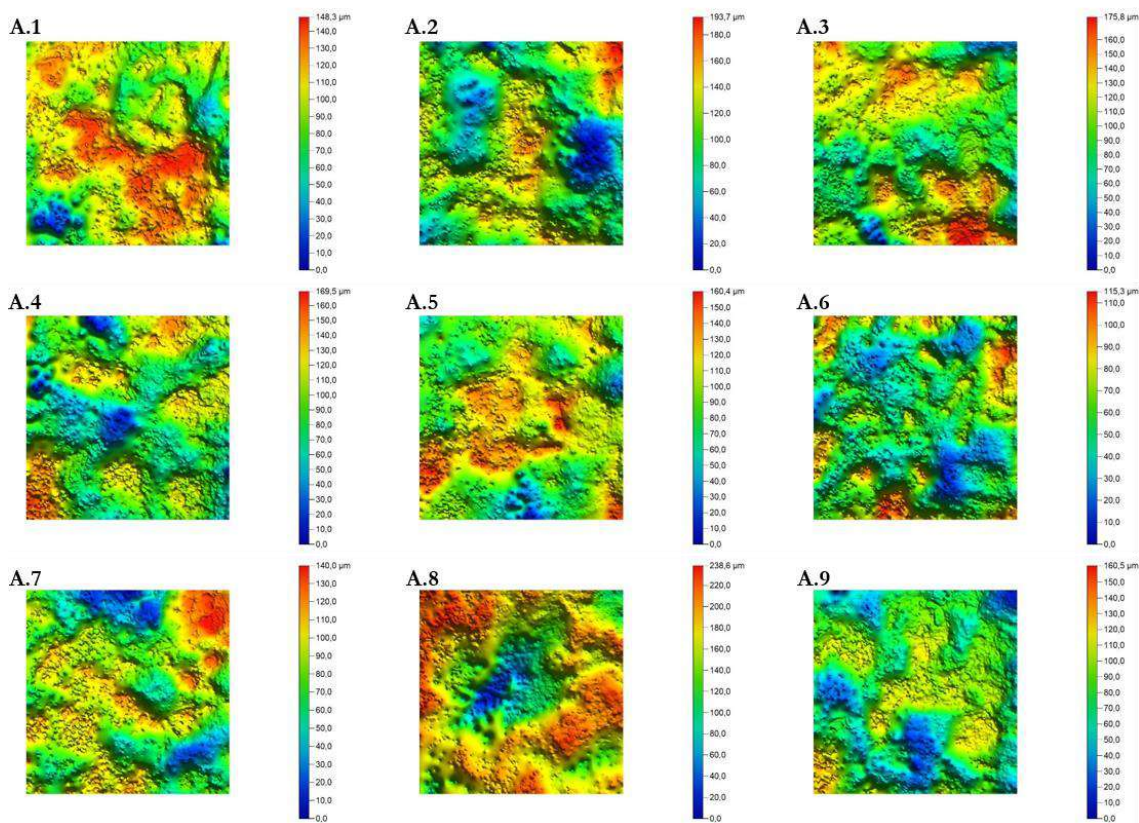
Figure 7. 24. BZ#6742, mold 1e: False-colour microtopographic maps of the analysed squares within area A.

7.1.4.   BZ#375
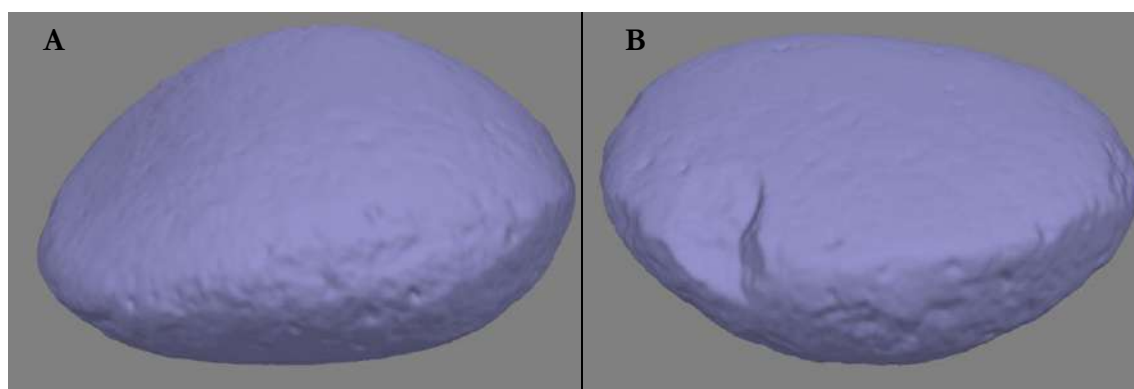
Figure 7. 25 Mesh of the two main side of BZ#375

BZ#375 exhibits an oval shape with one face being convex (face A), while the opposite face is flat or slightly convex (Face B), featuring a slight concavity in the central part (Figure 7.25). The convex side displays a distinct dark red spot, resembling a pigment trace. The overall shape suggests that the tool probably functioned as an active tool for grinding activities. Despite its shape, its dimensions of about 12 cm in length and 8.5 cm in width

make it rather bulky for use as a grinder/pestle. However, its shape and thickness of nearly 5 cm are in line with the comfort features of such tools.
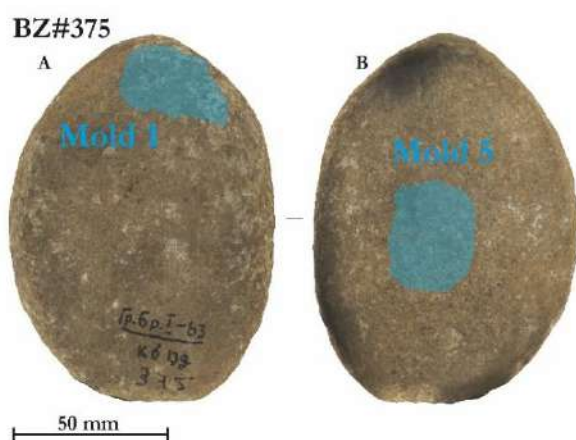
Figure 7. 26. Images extracted from the 3D model depict BZ#375, highlighting the positions of the molds.

Two molds were subjected to analysis: mold 1, taken from a marginal area of the large convex face A, and mold 5, taken from the central area of the expansive flat face B (Figure 7.26).

Mold 1 displays light smoothing of the surface (Figure 7.27, areas: A.1, A.3), along with a few wear patterns, including small flattened areas (Figure 7.27, areas: A.3, A.4, A.5), and micropitted polish (Figure 7.27, area A.2), distributed across the high asperity. False colour confocal profilometer maps reveal significant height variations in this region, as well as subtle striations (Figure 7.28, areas: A.3, A.5, A.7).

Mold 5 displays several use-wear features, such as pits, broken crystals with microfractures, and conchoidal fractures, along with a few step fractures (Figure 7.29). Additionally, flattened areas on the highest elevation are present and clearly depicted in the microtopographic maps (Figure 7.30).

Face A displays a limited number of use-related features; however, it is essential to acknowledge that the mold was obtained from the periphery of a potentially utilised region. Thus, the presence of only a few traces is justifiable and does not preclude the prospect of use within the more convex portion of this area. Conversely, mold 5 corresponds to the central area of face B, where evidence of vertical pounding activity is evident through the presence of numerous fractured crystals, pits, step fractures, and conchoidal fractures. Furthermore, clear indications of horizontal movement are observable, as inferred from the flattened tips of the asperities.

Upon comparing the data with that of the experimental collection, a notable resemblance is evident with the active tool M8 at T_3, used in USOs processing. However, the absence of polish and the presence of putative pigment may imply a putative engagement in pigments processing; nevertheless, it is noteworthy that residue analysis of this tool has not been undertaken to date, and the coloured mark could potentially stem from contamination.

The shape of the object, with its convex face, along with the nature of the wear traces, suggests an active tool that bears resemblance to the shape of the experimental tool named GS8. However, this particular tool is smaller and more easily manageable by hand. If we postulate a handling akin to that of GS8, the polish observed on mold 1 may be attributed to contact with the palm of the hand.
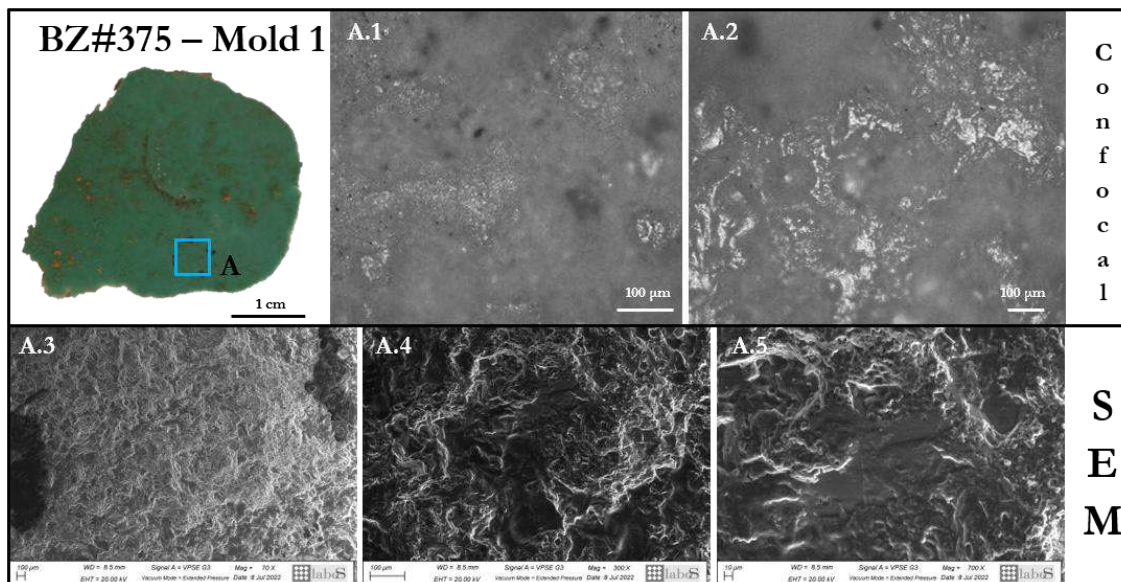
Figure 7. 27. Confocal microscopy and SEM micrographs of area A on BZ#375-Mold 1

BZ#375 – Mold 1
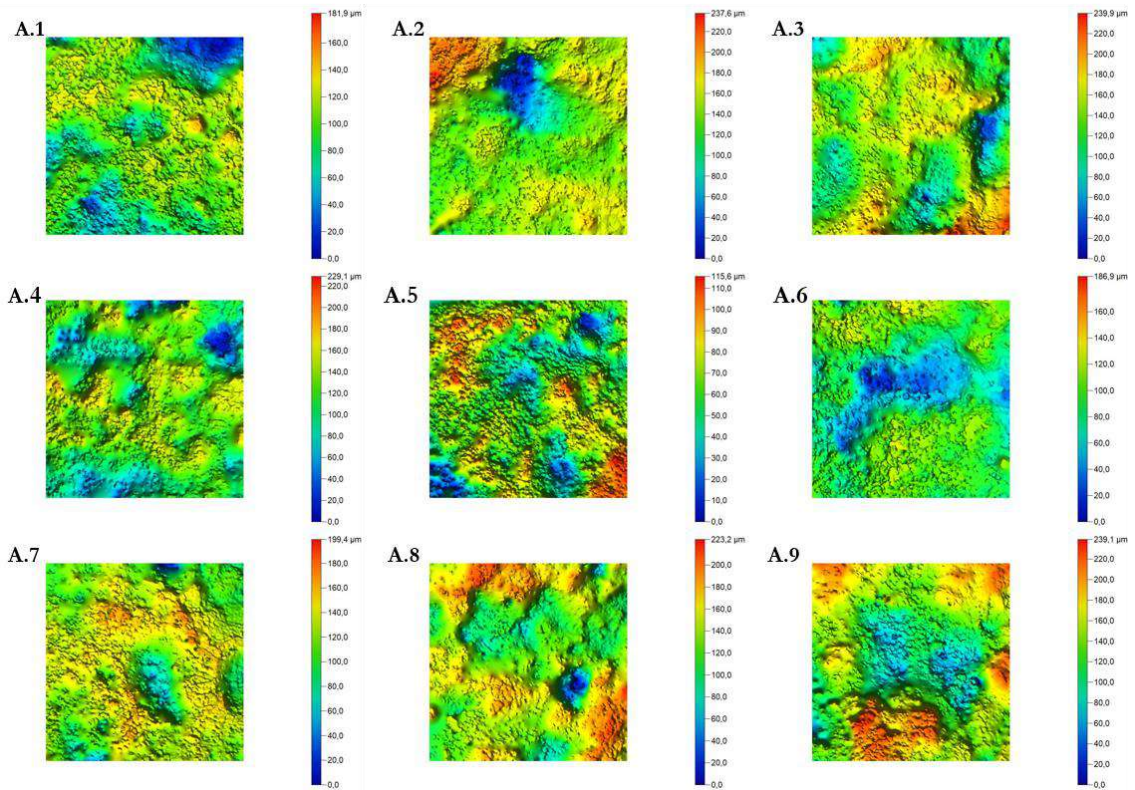
Figure 7. 28. BZ#375, mold 1: False-colour microtopographic maps of the analysed squares within area A. The areas exhibit a large variability in heights.
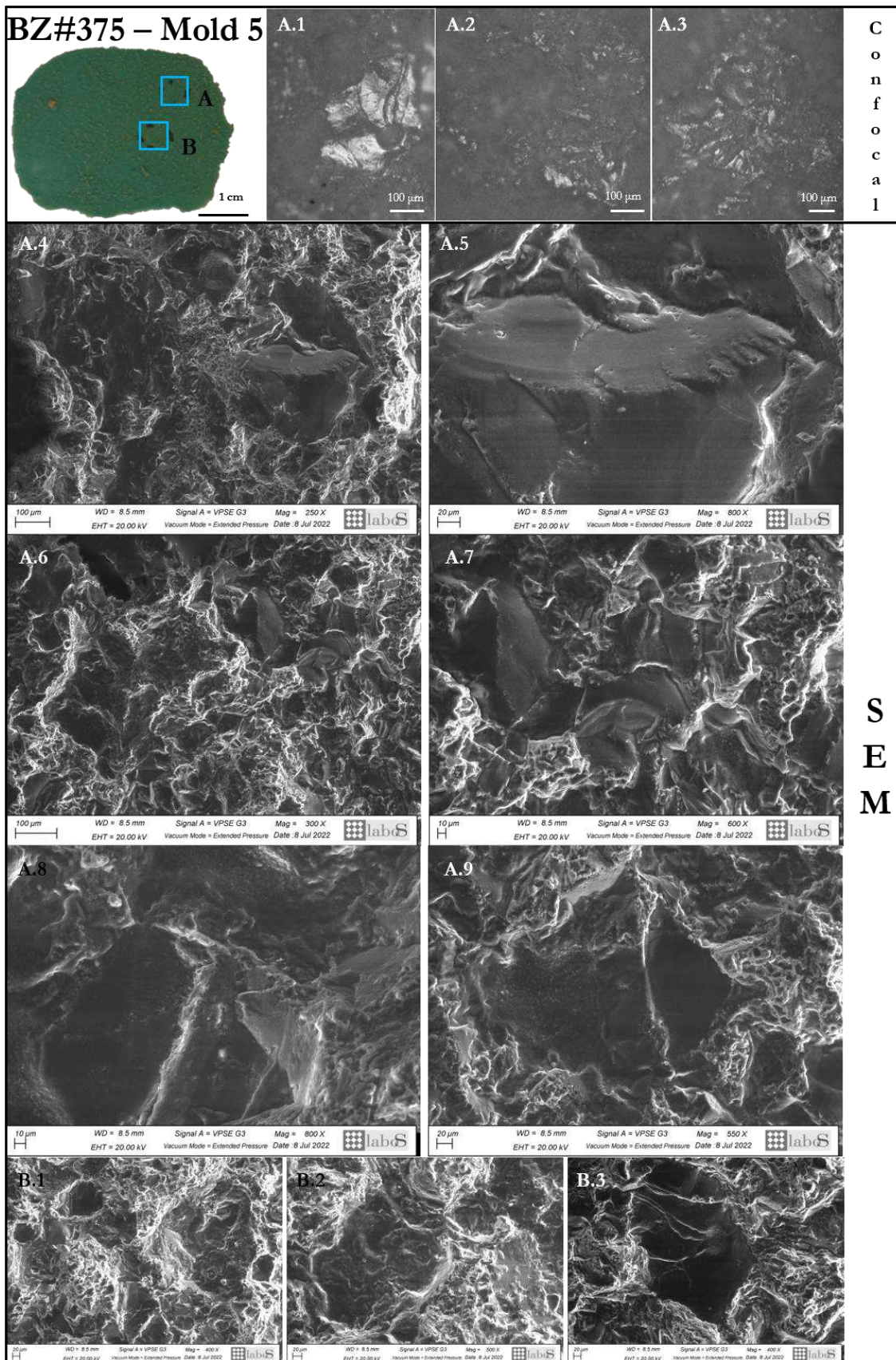
Figure 7. 29. Confocal microscopy and SEM micrographs of areas on BZ#375-Mold 5

BZ#375 – Mold 5
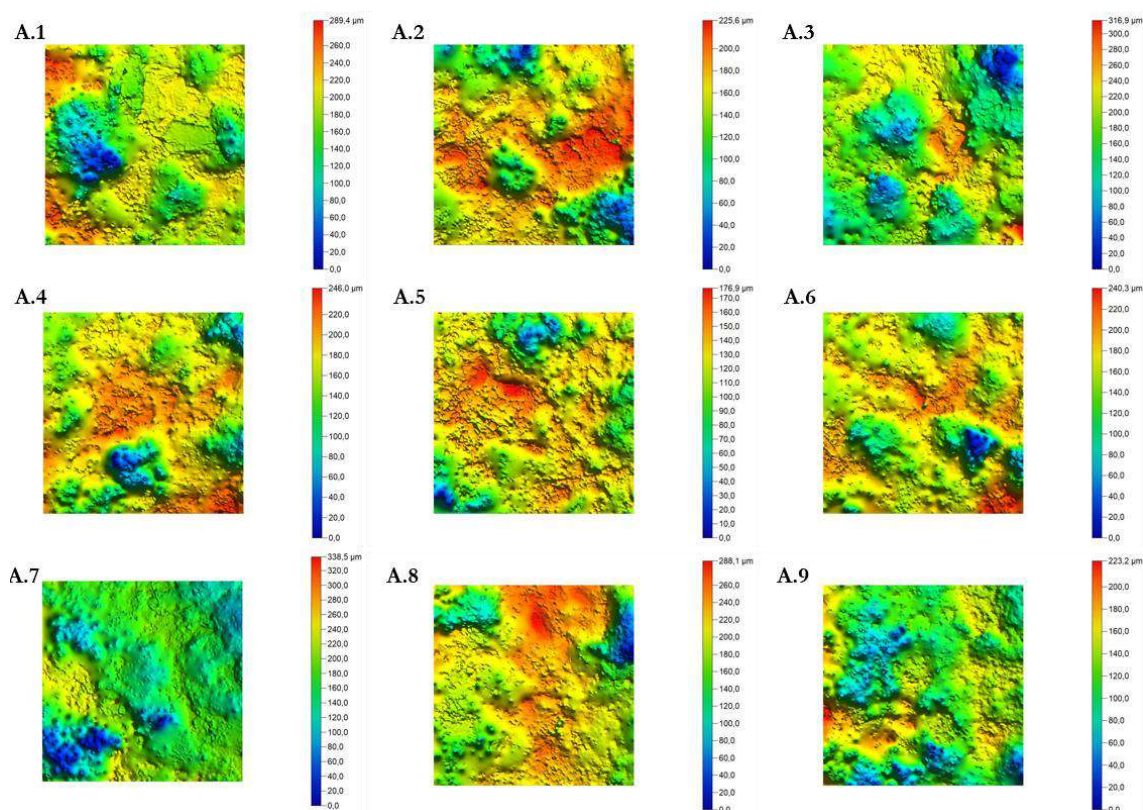
Figure 7. 30. BZ#375, mold 5: False-colour microtopographic maps of the analysed squares within area A. Small levelled areas are displayed.

7.1.5.   BZ#3488
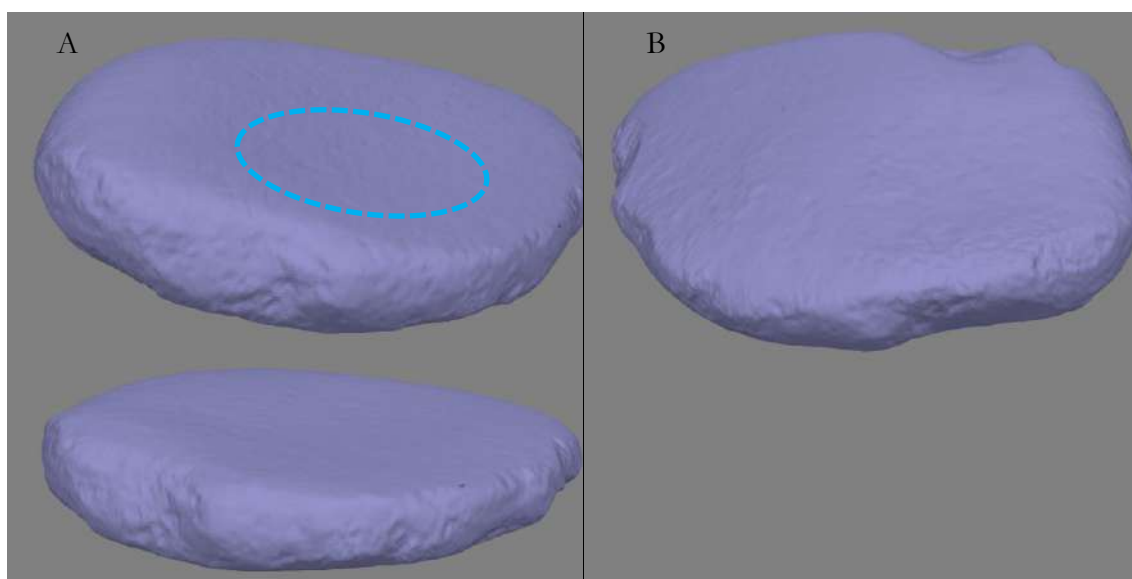
Figure 7. 31. Mesh of the two main faces of BZ#3488. Two different views are displayed for face A, and the concavity in the centre of the face is highlighted by the blue dashed circle.

BZ#3488 displays a flattened sub-discoidal shape, with one side (face A) being flat/slightly concave, and the opposite side (face B) being convex (Figure 7.31). The shape and dimensions align with those of a passive tool. Moreover, the 3D model indicates a more pronounced concavity in the central area of face A, which could potentially signify surface depletions from hypothetical use. Therefore, one large mold taken from the central area of face A (Figure 7.32) was selected for the analysis.

Figure 7. 32. Image extracted from the 3D model depict BZ#3488, highlighting the positions of the mold.

Mold 1 was divided into two parts during the analysis to better fit into the SEM chamber (Figures 7.33). Microscopy examination reveals the presence of extensive rubbed areas (Figure 7.33, area A.2), which are also supported by microtopographic false-colour maps (Figure 7.34). The asperity displays levelling, resulting in patches of flat areas (Figure 7.33, areas: A.3, A.4, A.7, B, C.1, C.2), and this is also visible in the false-colour maps (Figure 7.34, areas: A.4, A.5, A.9). Some areas exhibit micropitted polish (Figure 7.33, area A.1). Moreover, while the grains retain their distinct shapes, a degree of general smoothing is evident, particularly visible upon SEM inspection. Additionally, SEM analysis reveals the presence of starch granules, such as the one indicated by the blue arrow in Figure 7.33, area A.7. At the macroscale, a large dark red spot at the centre of face A resembles pigment trace; however, a detailed trace analysis has not been conducted yet.

The tool displays features that suggest an initial stage of use, as evidenced by the extensive rubbed areas that the experimental replicas demonstrate to be associated with early phases of utilisation. It is worth noticing that these rubbed areas lack linear traces, diminishing the likelihood of them arising from the processing of seeds or achenes. Moreover, the presence of few pits implies pestling activities although not intense. Furthermore, a general smoothing effect is visible on the surface. In light of comparative analysis with experimental data, the hypothesis is of a passive tool used for the elaboration of a woody resource.
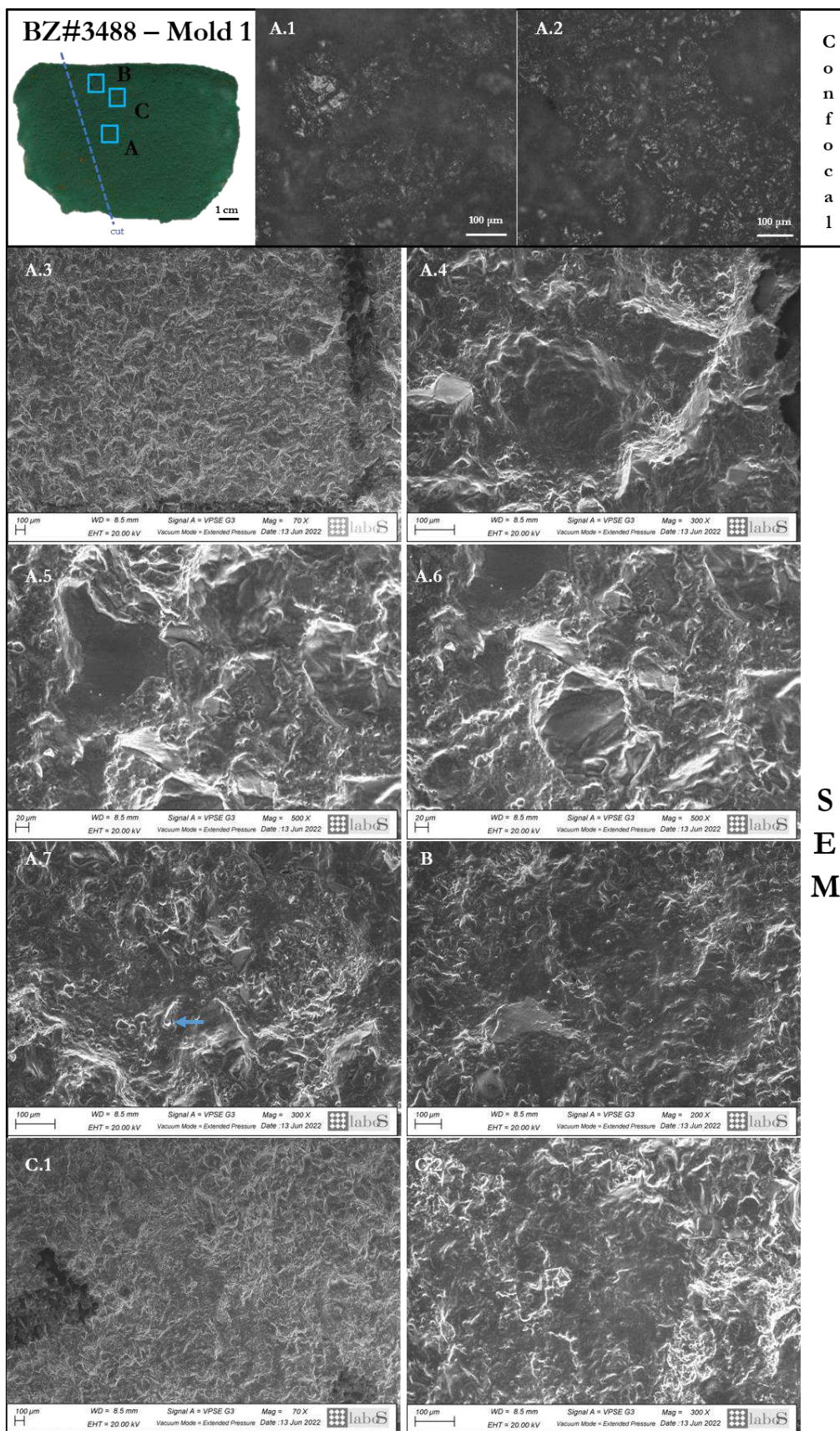
Figure 7. 33. Confocal and SEM micrographs of areas on BZ#3488-Mold 1. The blue arrow in image A.7 indicate a putative starch granule.
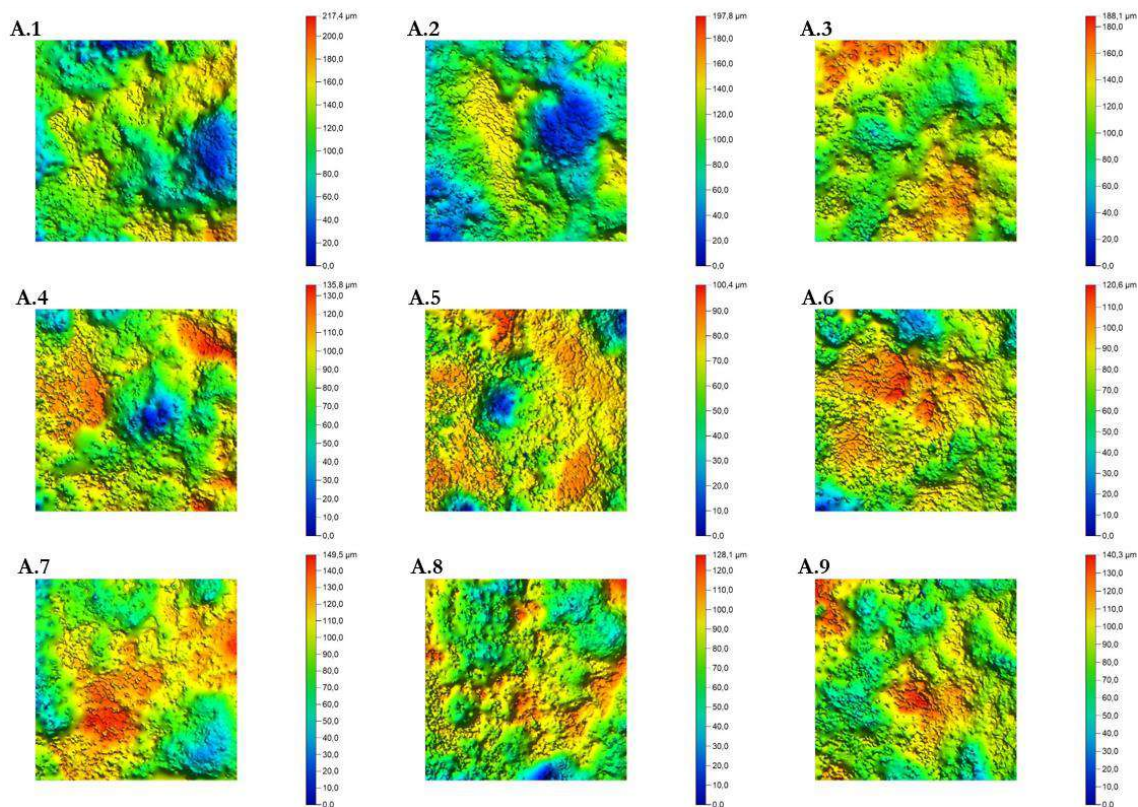
BZ#3488 – Mold 1
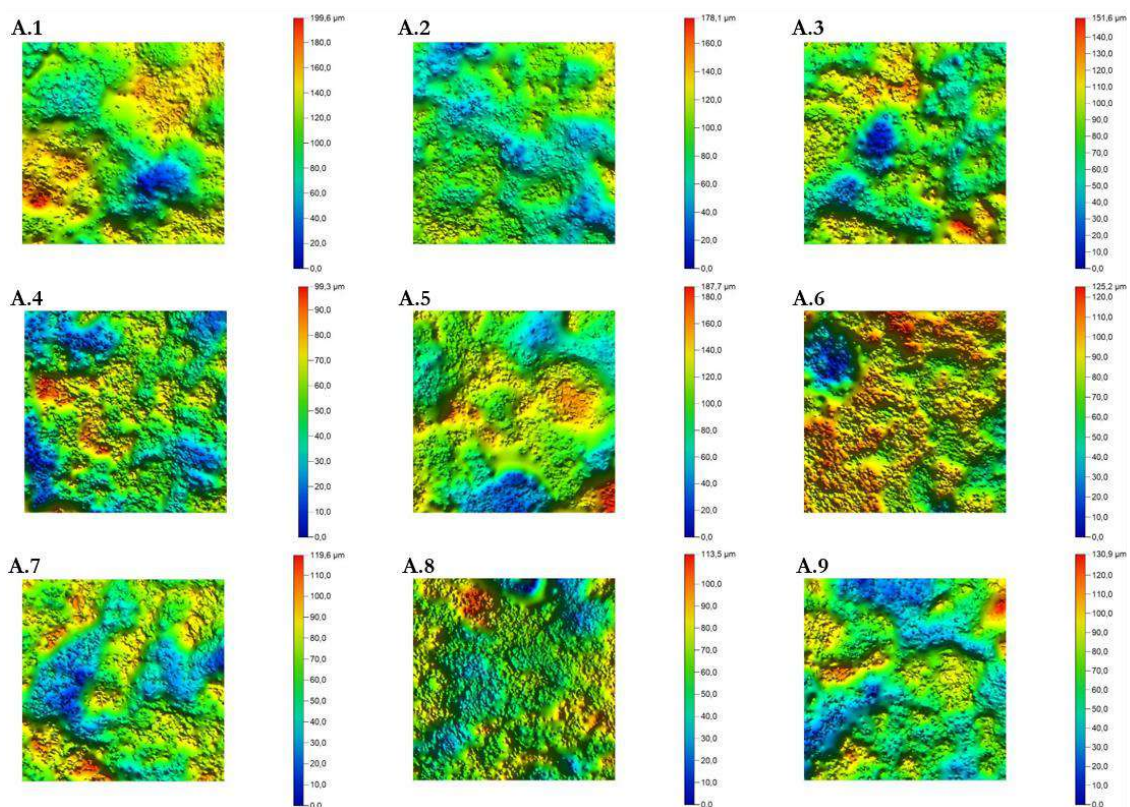
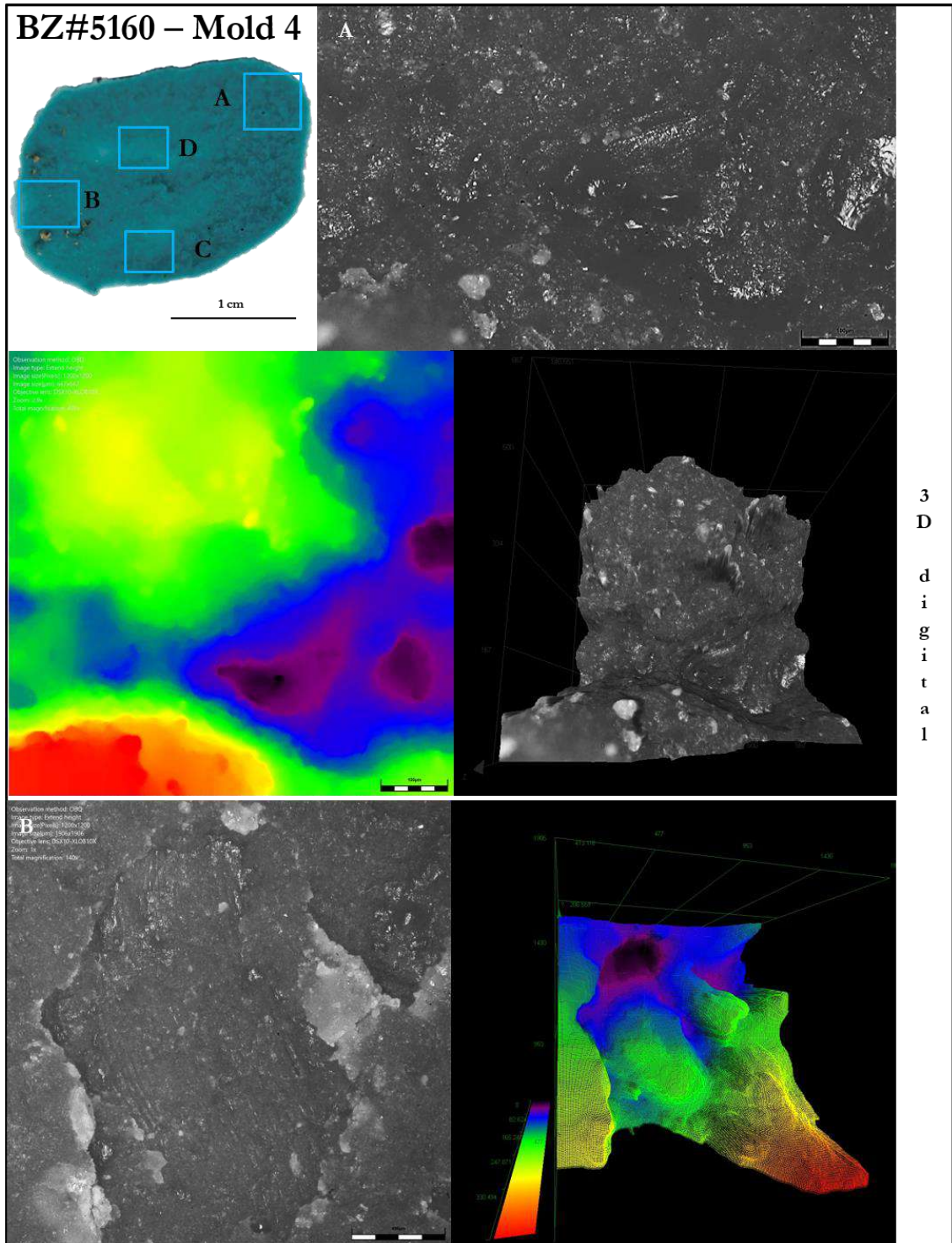*Figure 7. 34. BZ#3488, mold 1: False-colour microtopographic maps of the analysed squares within area A. The areas exhibit a large variability in heights.*

7.1.6.   BZ#2964
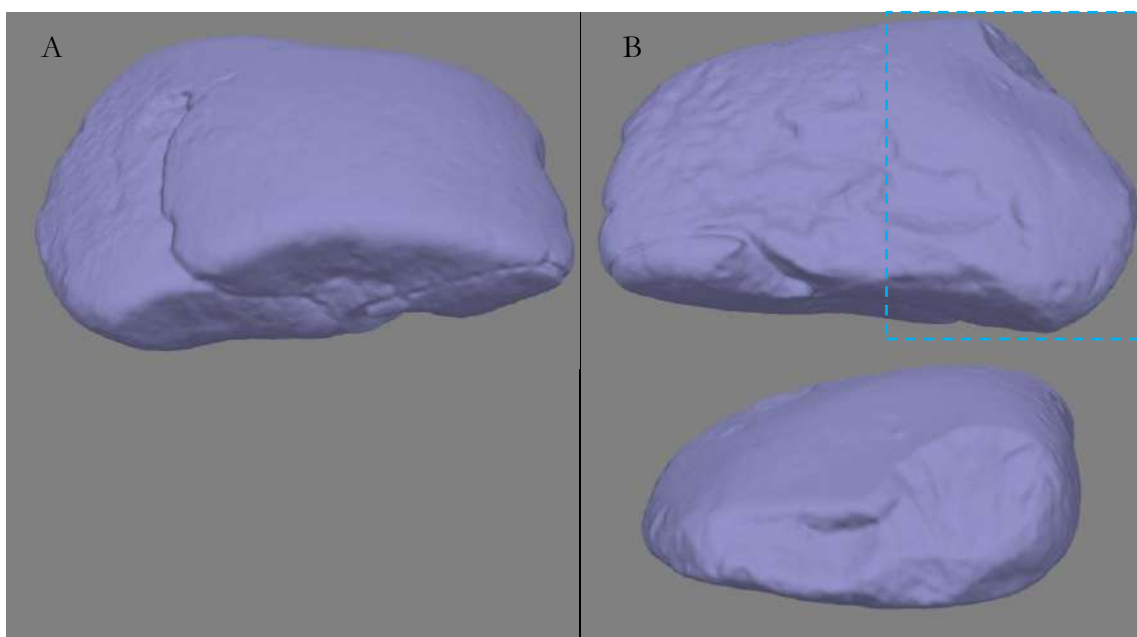
Figure 7. 35. Mesh of the two main faces of BZ#2964. Two different views are displayed for face B.

BZ#2964 displays a sub-rectangular shape with two convex large surfaces, of which face B is less convex and relatively flatter compared to face A (Figure 7.35). Face A shows a deep fracture that led to the detachment of a large fragment from the lateral side. The surface of this face appears smoothed, whereas face B is more irregular and displays several damages likely occurred in ancient time. On this side, a significant detachment on the edge suggests an attempt of intentional shaping (area in the dashed rectangle in Figure 7.35).

Figure 7. 36. Image extracted from the 3D model depict BZ#2964, highlighting the positions of the mold.

The analysis was conducted on one mold taken from face A (Figure 7.36).

Mold 1 presents a smoothed surface, which is particularly noticeable at low magnification and predominantly affecting the areas of low topography (Figure 7.37: areas A.2, A.3). The grains are clearly distinguishable from the matrix and exhibit a few wear patterns, which include flattened tips (Figure 7.37: areas A.4, A.5, A.7, B.1) and micropitted polish distributed on top of the crystals (Figure 7.37: area A.1). False-colour confocal profilometer maps (Figure 7.38) present a significant variation in heights and occasional small flattened areas, as in areas A.8 and A.9.

Based on the analysis, the comparison with the reference collection, and the shape of the tool, this is a passive stone, and face A appears to be the ventral unused surface. This surface, which was in contact with the ground, shows evidence of smoothing, likely resulting from the impact and recoil forces that must have been intense, given the noticeable unevenness of face B, clearly visible from 3D and pictures inspection (Figure 7.35 face B). The residues analysis has indeed demonstrated the presence of a few starch grains. Notably, these starch grains, unlike those retrieved from the other GSTs, do not exhibit a damaged appearance (or to a lesser extent). This observation supports the hypothesis that the analysed side was not actively utilised. The presence of starch grains on the non-use surface can plausibly be attributed to the inherent dispersal of the resource from the surface experiencing active use. However, to further confirm this hypothesis, the analysis of the other side of the tool is necessary.
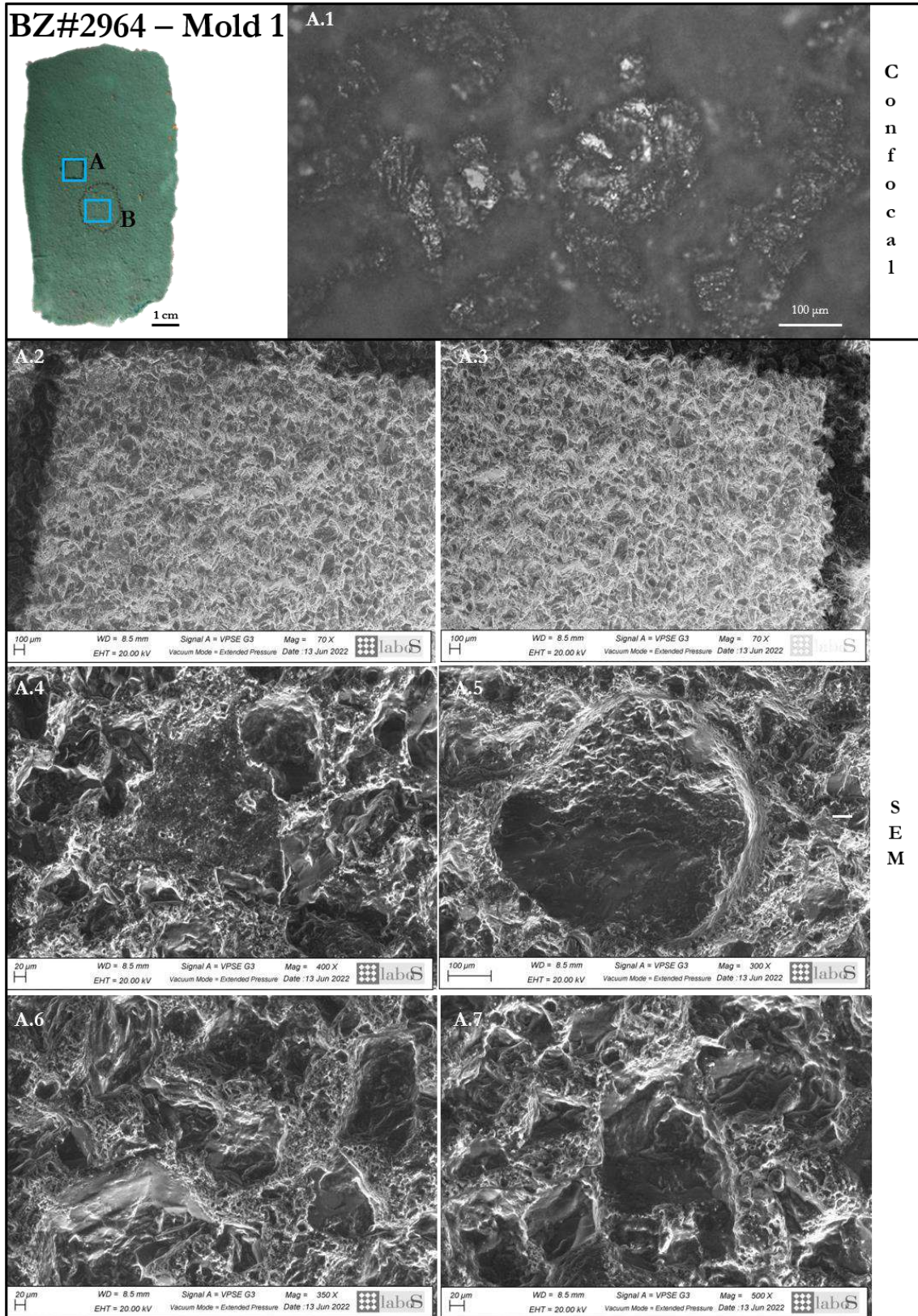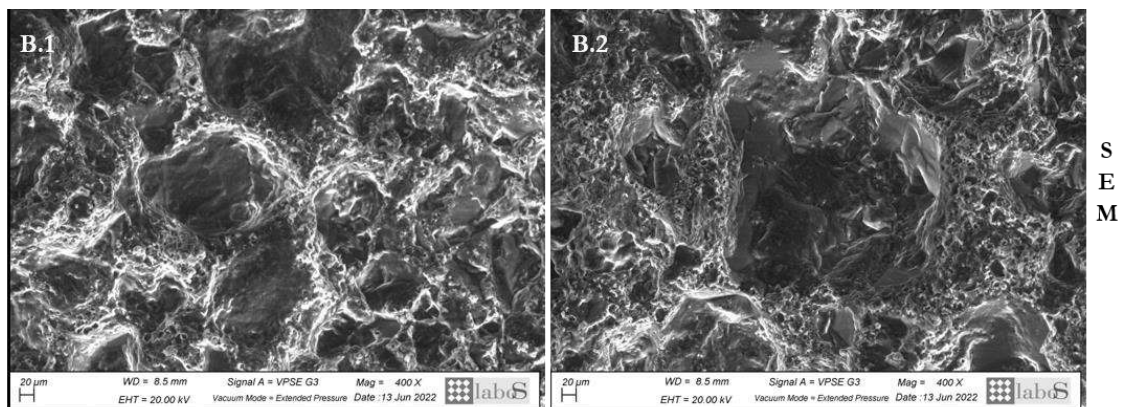
Figure 7. 37. Confocal microscopy and SEM micrographs of different areas on BZ#2964-Mold 1.

BZ#2964 – Mold 1
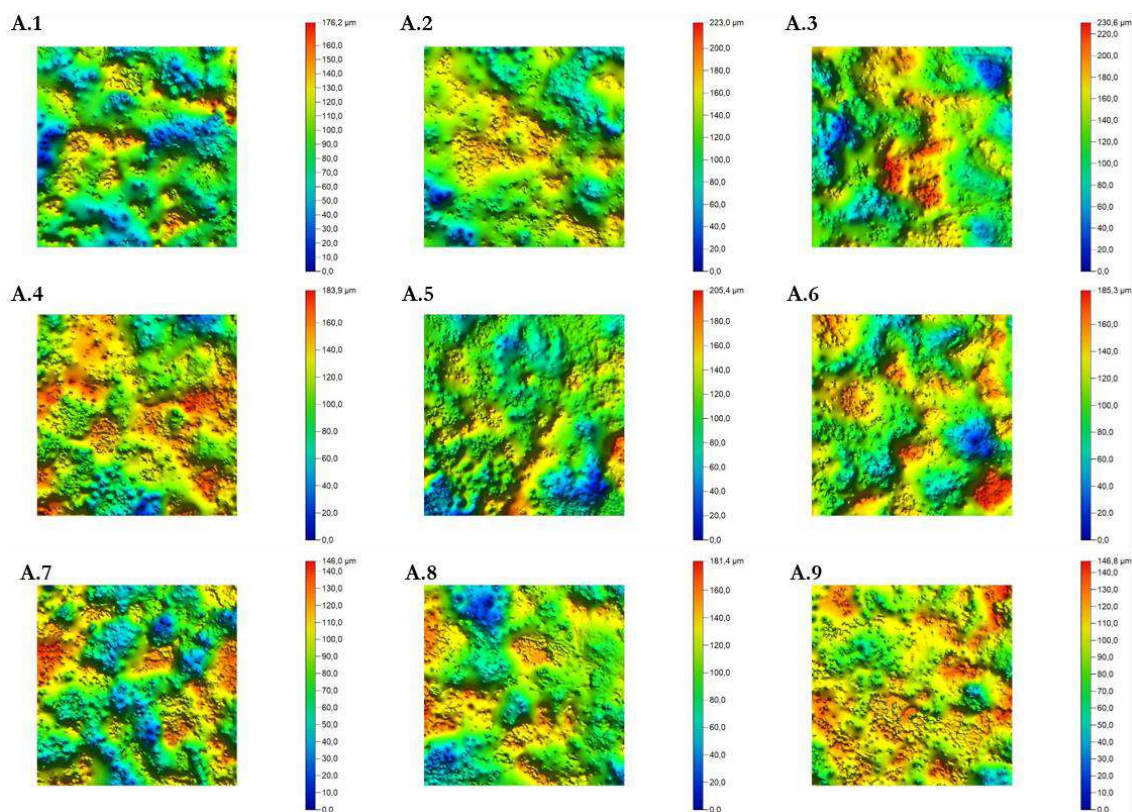
Figure 7. 38. BZ#2964, mold 1: False-colour microtopographic maps of the analysed squares within area A. The areas exhibit a large variability in heights.

7.1.7.   BZ#6707
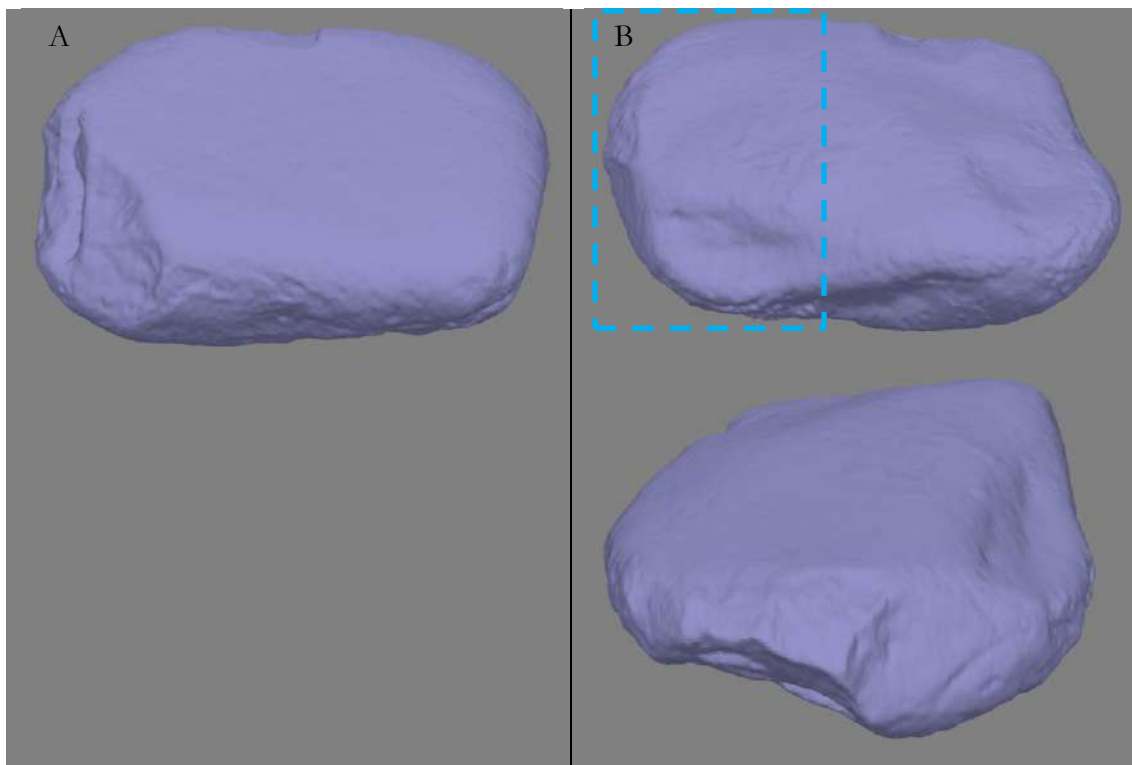
Figure 7. 39. Mesh of the two main faces of BZ#6707. Two different views are displayed for face B.

BZ#6707 exhibits a rectangular shape with flat surfaces, one of which is slightly convex (Face B). Notably, on this side, the presence of some detachments may indicate an intentional shaping (as highlighted within the dashed rectangle in Figure 7.39).
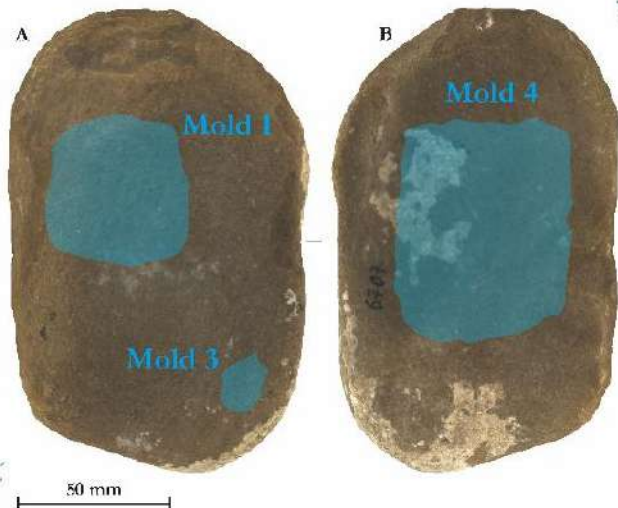
Figure 7. 40. Images extracted from the 3D model depict BZ#6707, highlighting the positions of the molds.

Three areas were analysed: mold 1, from face A; mold 3, from a marginal region of the same face; and the larger mold 4, taken from the central area of face B (Figure 7.40).

Mold 4 exhibits evident signs of wear (Figures 7.41), with extensive rubbed areas and flattening of significant portions of the surface, as highlighted by the topographic maps (Figures 7.42). In contrast with mold 1 and 3, in mold 4 the grains are no

longer distinguishable from the matrix, having reached the same level. The presence of micropitted and deposit types of polish are clearly visible (Figures 7.41).

Mold 1 (Figures 7.43) and mold 3 (Figures 7.44) display high roughness and elevation variability, as illustrated in the topographic maps (Figures 7.45). The protruding grains are prominently visible and distinguishable from the matrix (Figures 7.43: areas C and D), and their sheen is attributed to both their natural reflectance and initial flattening. Additionally, limited rubbed areas are evident (Figures 7.45: areas B and D; Figure 7.44). SEM investigation validates the substantial irregularity of the surface, characterised by well-defined grains and a significant presence of rounded residues, likely starch granules (Figures 7.43: area E).

Based on the observed wear patterns and tool morphology, it is evident that this stone served as a passive implement. On face B, the distinct trace patterns featuring large flattened areas, as well as the absence of linear traces, closely resemble the patterns observed on experimental tools used for processing USOs. The residue analysis further confirms the SEM observations, revealing a substantial presence of starch grains. These residues have been identified as originating from tubers and the *Poaceae* family (commonly known as grasses, Birarda et al. 2020), in addition to other unidentified sources. Notably, many of these starch grains exhibit damage typical of exposure to high temperatures, reminiscent of processes such as roasting or other techniques aimed at making the plant organs softer and more easily digestible.
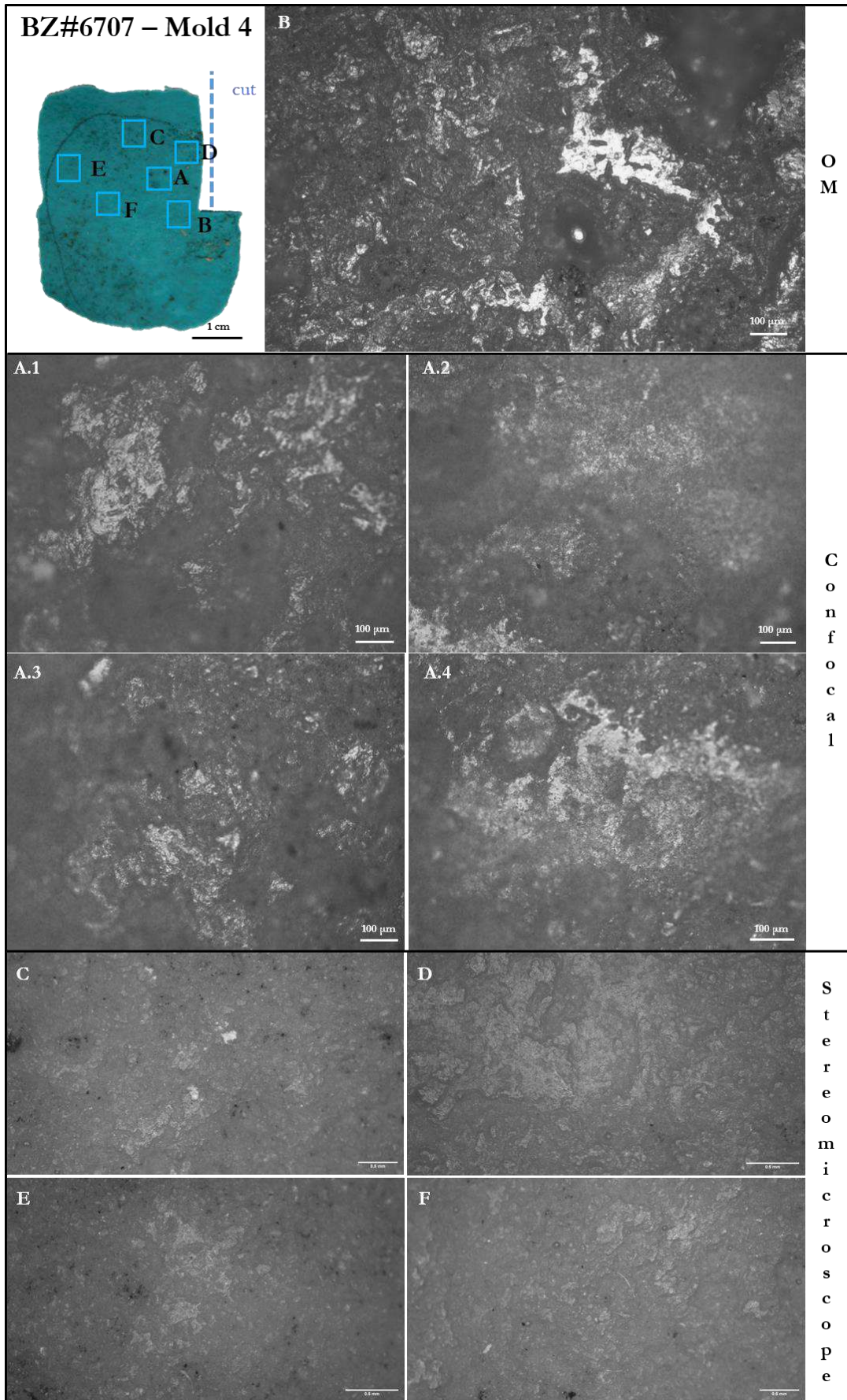
Figure 7. 41. Different microscopes images of several areas on BZ#6707 - Mold 4 are shown. In the top left corner, is depicted the mold with indications of the areas depicted in the micrographs acquired. The first row shows an OM image; the second row shows pictures acquired with the confocal microscopy; the third row shows stereomicroscope images.
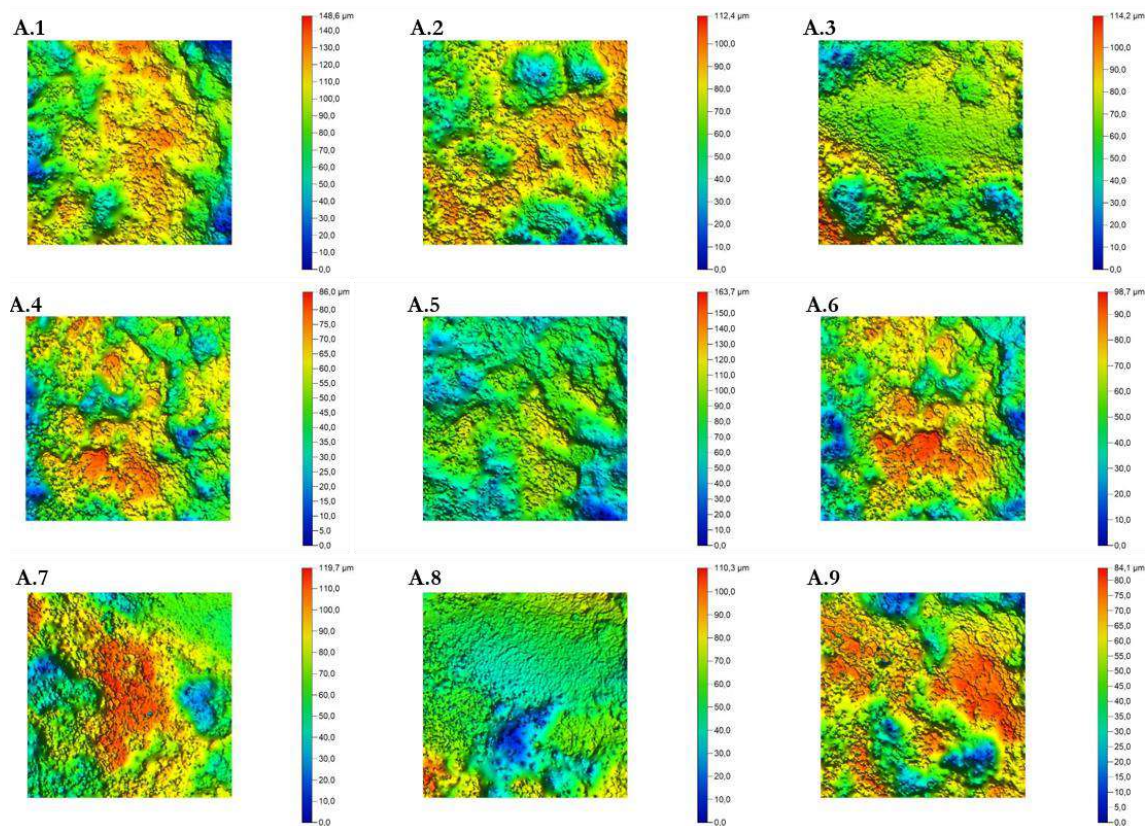
Figure 7. 42. BZ#6707, mold 4: False-colour microtopographic maps of the analysed squares within area A. Large flattened areas are clearly visible.
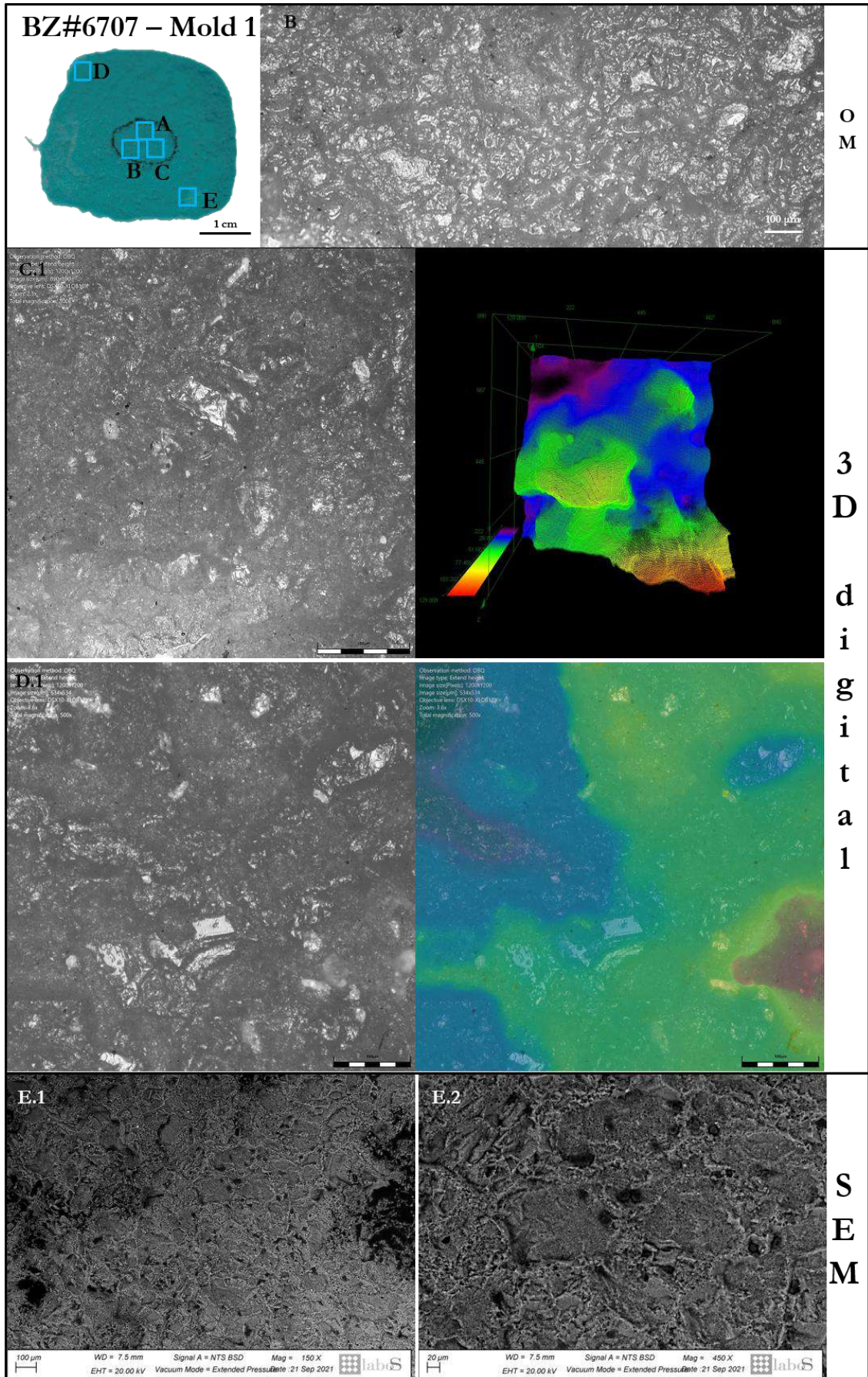
Figure 7. 43. Different microscopes images of several areas on BZ#6707 - Mold 1 are shown. In the top left corner, the mold with indications of the areas depicted in the micrographs acquired. The first row displays OM images. In the central part of the pictures, there are images and 3D models acquired with the 3D digital microscope. Notably, the false-colour 3D image of area C.1 highlights the location of wear features on the surface relief. For area D.1, the false colour map is overlapped onto the microscope image to emphasise the location of the specific features detailed in the image on the left. The bottom of the figure shows SEM images acquired with a backscattered electrons detector.
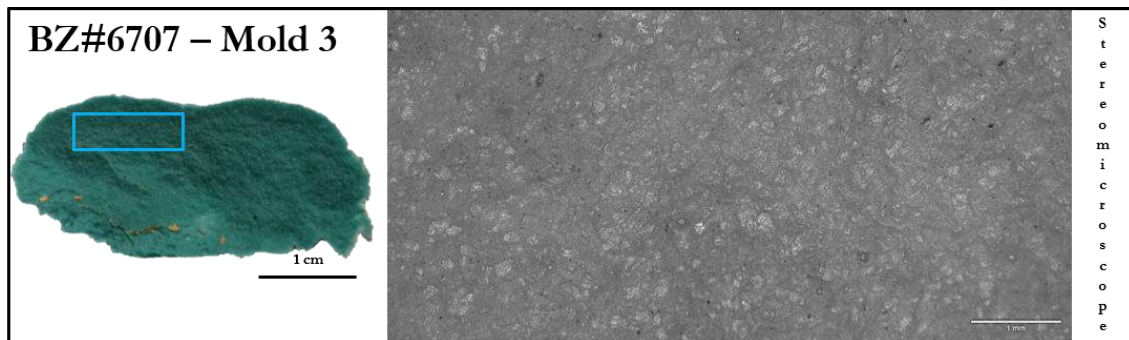

Figure 7. 44. Stereomicroscope micrograph of an area of BZ#6707-Mold 3.

BZ#6707 – Mold 1
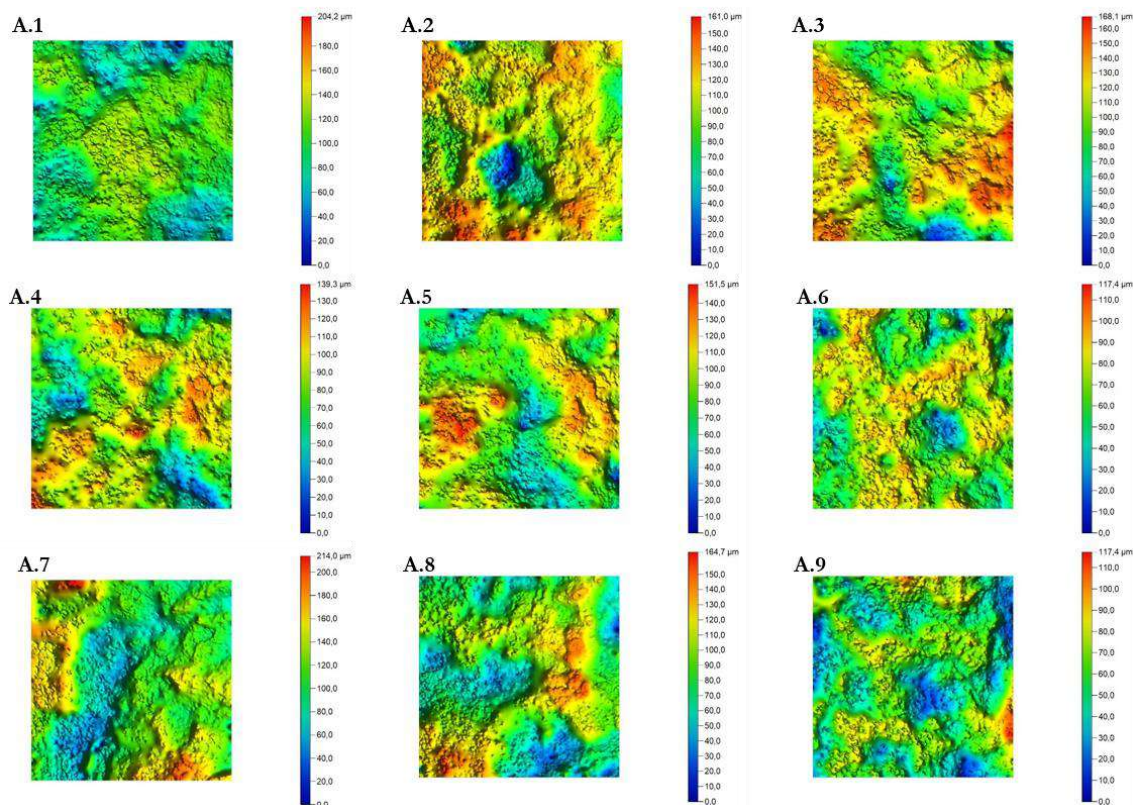
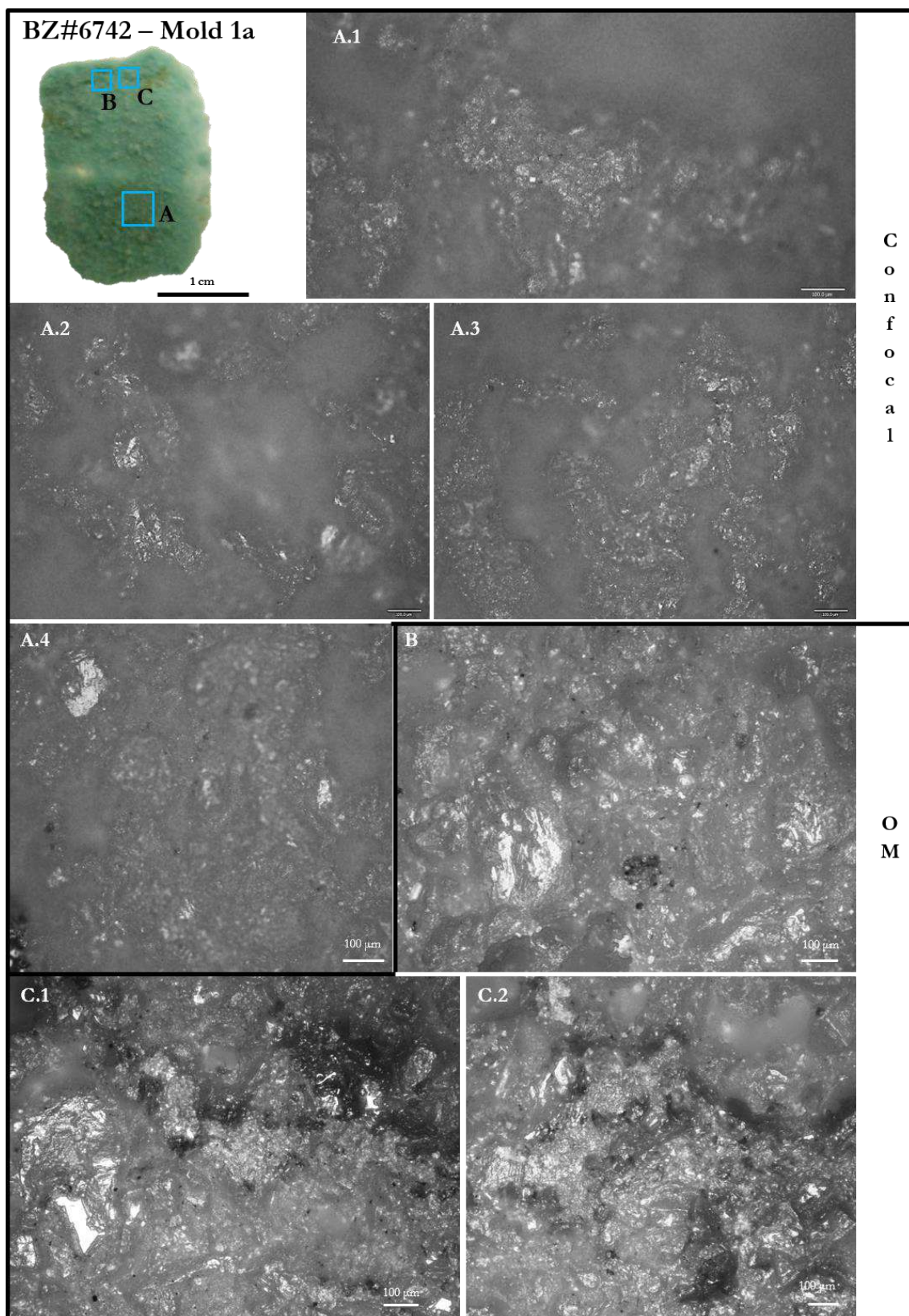*Figure 7. 45. BZ#6707, mold 1: False-colour microtopographic maps of the analysed squares within area A. The areas exhibit a large variability in heights but also small flattened areas on top of the asperity.*

7.1.8.   BZ#442 and BZ#N.No.
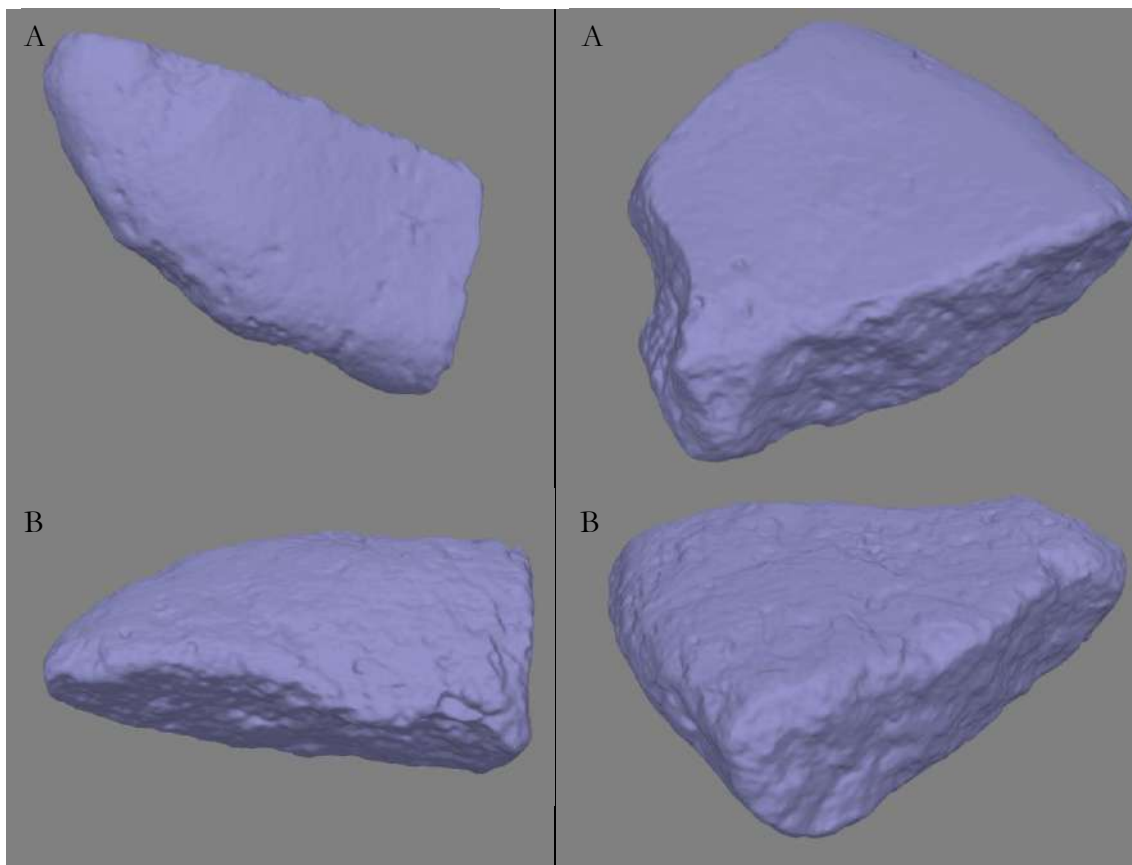
Figure 7. 46. Mesh of the two main sides of BZ#N.No. (on the left) and BZ#442 (on the right).

The fragments BZ#442 and BZ#N.No. refit suggesting a large sub-rectangular incomplete passive tool with flat surfaces. Its weight exceeded 1.5 kg, but the original weight may have been higher, possibly around 2 kg or more, and its size exceeds 14 cm in height,
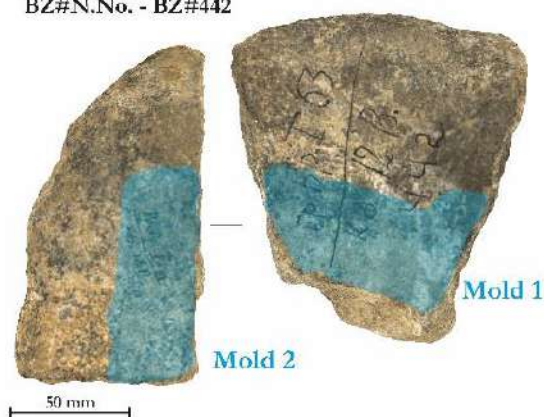
Figure 7. 47. Images extracted from the 3D model depict BZ#442 and BZ#N.No, highlighting the positions of the molds.

with a length of more than 20 cm and a maximum thickness of around 4-5 cm. Both fragments present a smooth face A and a coarse texture of face B (Figure 7.46).

For the analysis of this implement, two molds were examined, one for each face A of the two refitted fragments: mold 1 taken from fragment #442, and mold 2 from #N.No. (Figure 7.47). Additionally, a detached fragment from the surface of

BZ#442 was also analysed for both traces and residues. This fragment, as presented in Chapter 4, was also used to study the stone composition and volume.

The microscopy analysis clearly indicates that the stone has undergone significant usage, leading to the development of diffuse and intense wear traces (Figures 7.48, 7.49, 7.50). It is noteworthy that this stone is softer compared to the ones previously analysed (as highlighted in Chapter 4), which results in more evident use-wear traces and developing faster than on quartz-arenite. The grains are fully welded with the matrix, reached a point where their distinction is no longer possible (Figures 7.48 and 7.50). Notably, visible flattened areas with long striations are evident in both microscopy examinations and microtopographic maps (Figure 7.49). These striations are generally arranged in small yet elongated clusters, often accompanied by gouge as visible in the micrographs of the stone fragment (Figure 7.50). Diffuse polished areas are present, encompassing serrated (Figure 7.49, areas: C, F, D.2, D.3, G.2, G.4), micropitted (Figure 7.49, areas: B.1, B.2, G.6, G.7, I), and deposit types (Figure 7.49, areas: B.1, G.2, G.5, G.6, I). While the preferential orientation of the striations is along the length of the tool in a slightly oblique manner (Figure 7.49, areas: C, F, D.2, D.3, G.1, G.3, G.4, G.5, G.6, H; Figure 7.51, areas: A.5, B.1, B.2, B.4), the diffuse polished areas exhibit a preferential circular orientation (Figure 7.49, areas: D.1, E, B.1, B.2, I). This suggests that this passive tool was utilised in grinding activities involving both linear and circular motions.

The residue analysis uncovered the presence of a limited quantity of starch grains, all exhibiting signs of damage, potentially attributed to resource processing. As outlined in Birarda et al. 2020, the analysis of starch grains demonstrates an 80% probability of belonging to rhizomes (type of USO), aligning with the presence of extensive levelled and polished regions.

Additionally, the microscopy analysis performed by the writer on the fragment detached from the surface of BZ#442, revealed a distinct red area and several small spots (Figure 7.51). To further investigate this aspect, micro-Raman spectroscopic measurements were conducted by the author with the support of Dr. Alessia Giordana at the Earth Science Department of the University of Turin. The analysis was performed with a Horiba JobinYvon HR800 spectrometer, equipped with an Olympus BX41 microscope, CCD detector cooled (-70 ° C), 600 lines mm$_{-1}$ diffraction grating, and two polarised lasers: red HeNe laser (wavelength 633 nm, power 20 mW) and Nd solid state green laser (wavelength 532 nm, power 250 mW). In this case the green laser was employed. The obtained data were

processed by the author using Crystal Sleuth software (Laetsch and Downs 2006). The results showed clear resemblance with the hematite reference spectra for the red areas and calcite spectra for the rock matrix (Figures 7.51, 7.52, 7.53).

Hematite is the primary mineral in red ochre, which can exist in a highly pure form. However, it is more common for red ochre's composition to include a diverse range of additional minerals such as quartz, clays, gypsum, micas, feldspars, and various others according to provenience (Eastaugh et al. 2008: 285-286).

Combining this information, it is possible to hypothesise that this tool was utilised as a passive tool in vegetal resources processing, particularly USOs, which contributed to the development of the extensive polished areas. Additionally, sequential secondary uses for ochre processing are likely, accounting to the well-defined linear traces observed. While the experimental replicas did not exhibit linear traces associated with ochre, it is important to consider that both the quartz-arenite and quartz-rich sandstone utilised in the experiment are more resistant to mechanical stress compared to calcarenite. Based on the writer's previous experience (McCartney and Sorrentino 2019) and a review of available literature (e.g., Hodgskiss 2010; Rifkin 2012; Rosso et al. 2016), grinding ochre typically produces distinct groups of striation, micro-striation and grooves, oriented parallel to one another. This implies a repetitive back-and-forth motion that can cause particularly pronounced linear traces depending on factors such as stone hardness, ochre resistance, and intensity of use.
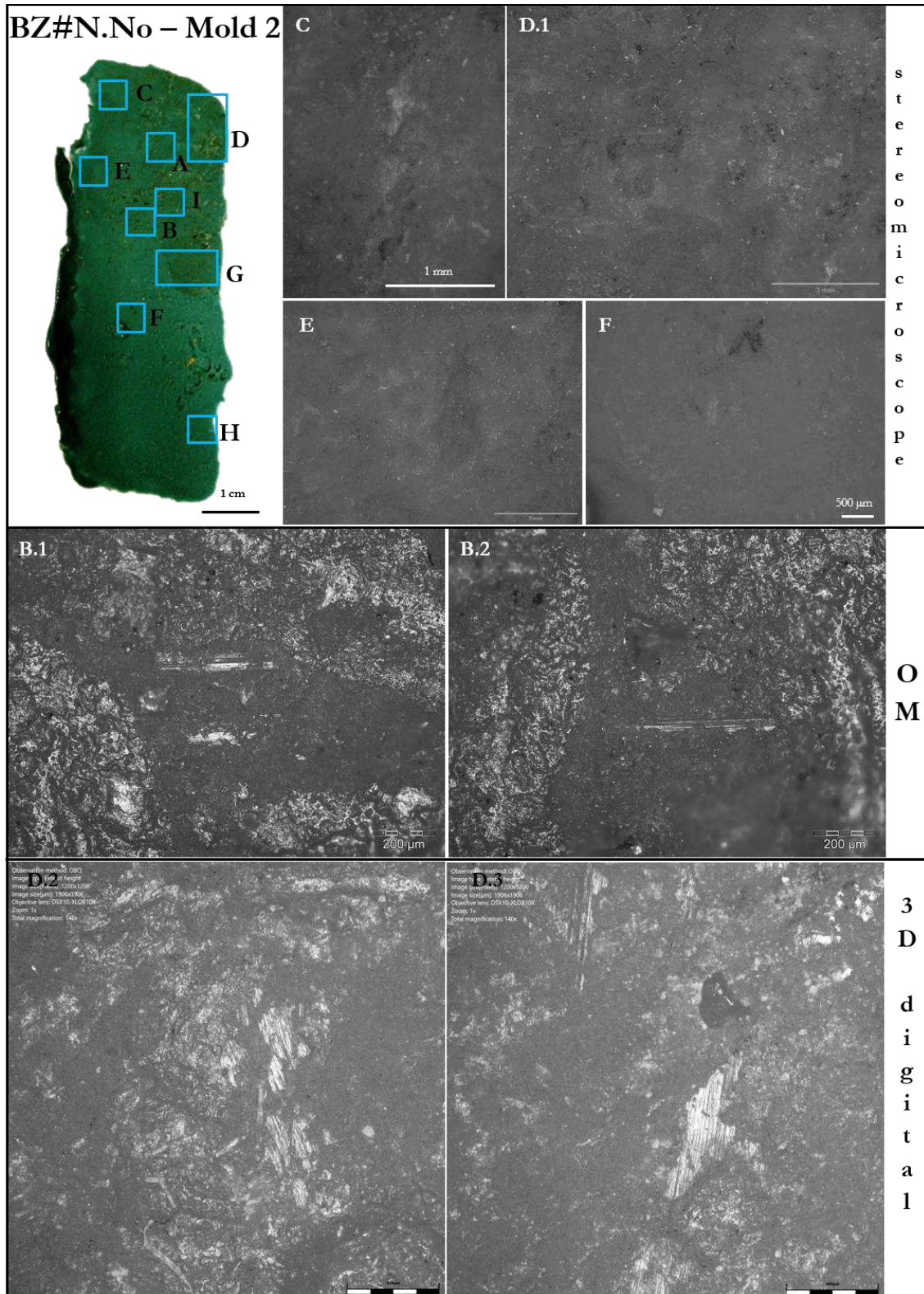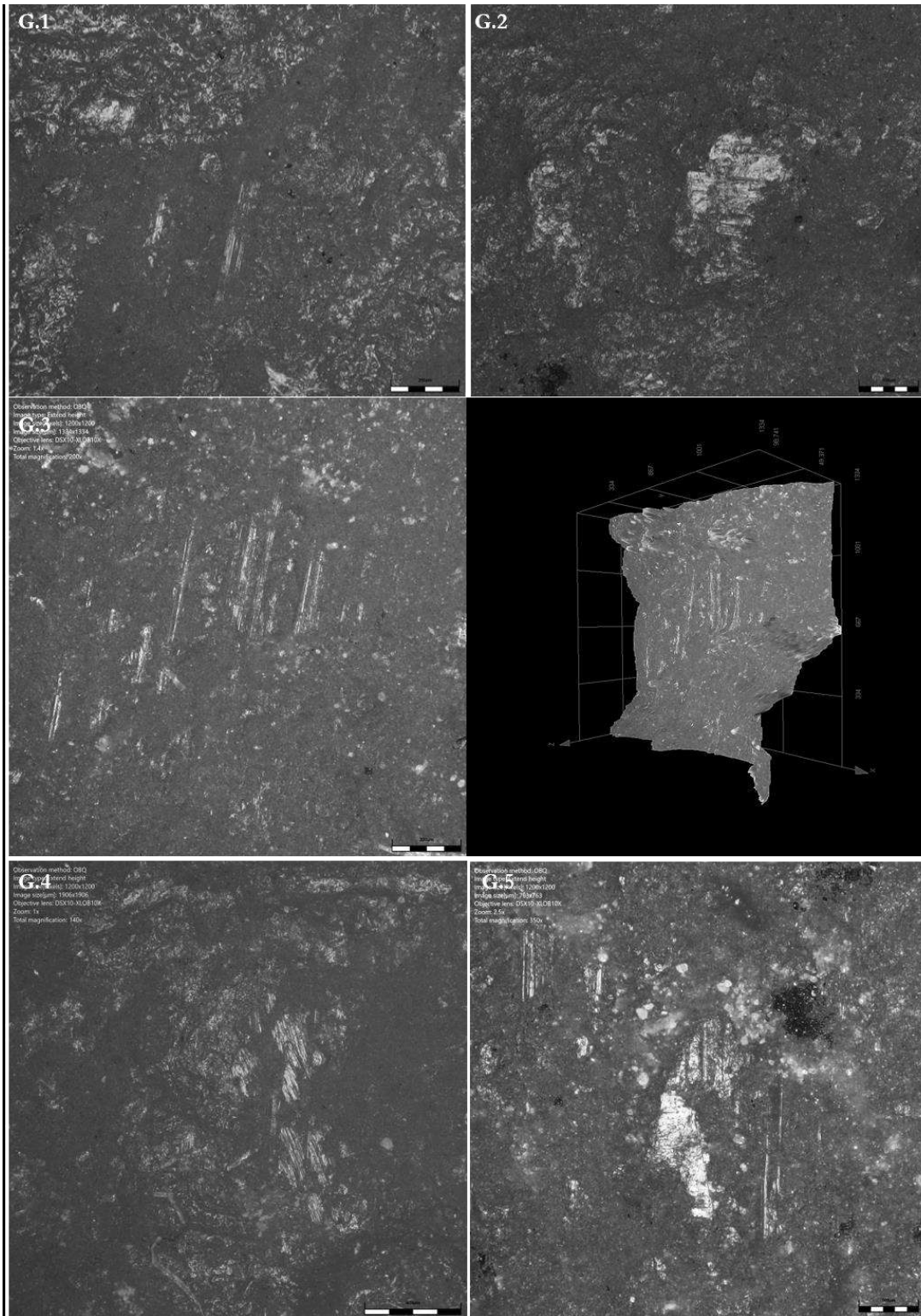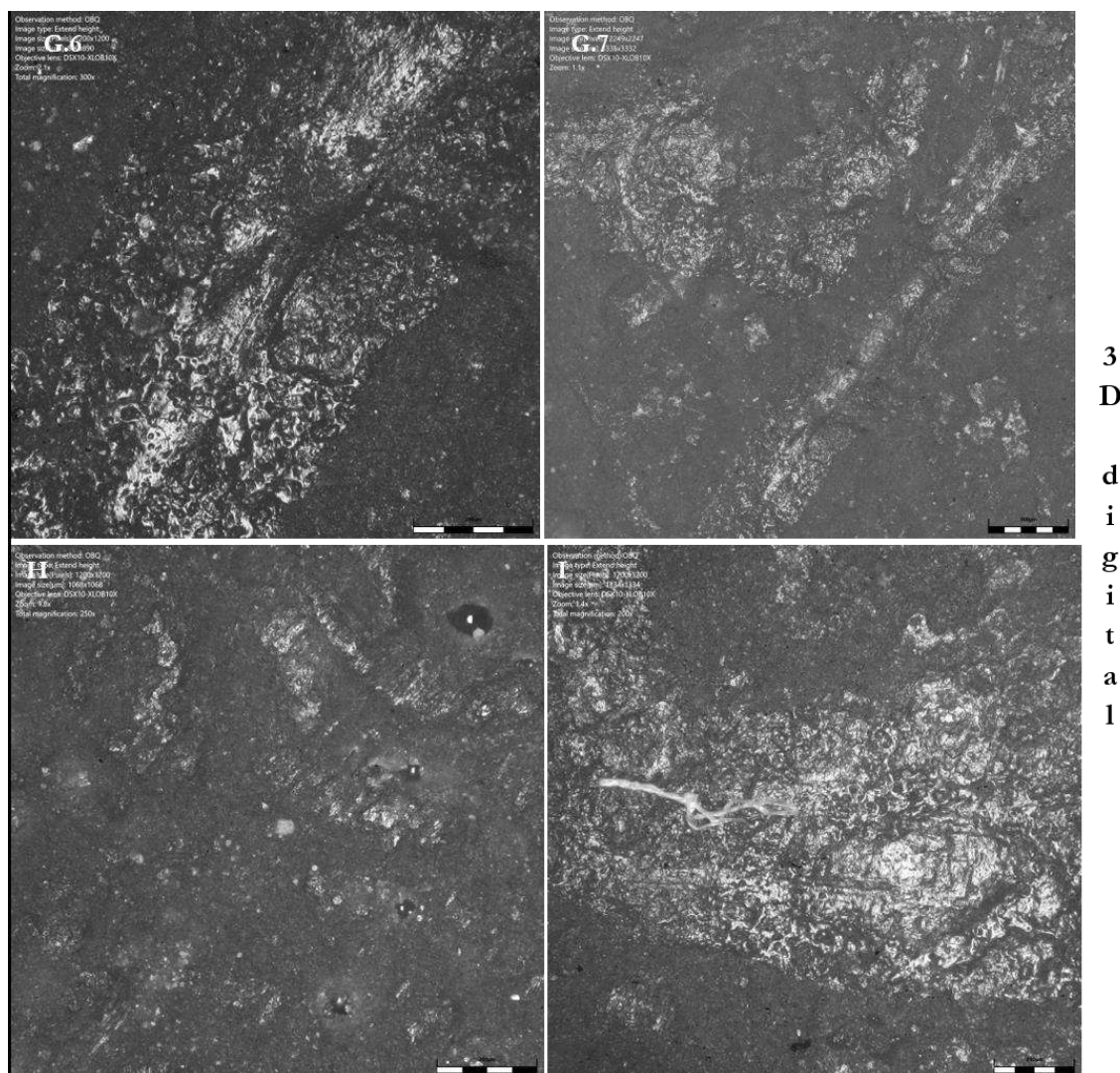
Figure 7. 48. Various microscope images of different areas on BZ#N.No. - Mold 2 are presented. In the top left corner, the mold is shows with the indications of the depicted areas in the micrographs. The first section features stereomicroscope images, followed by images acquired with OM in the second section. Subsequently, micrographs and a 3D model acquired using the 3D digital microscope are included.

BZ#N.No-Mold 2
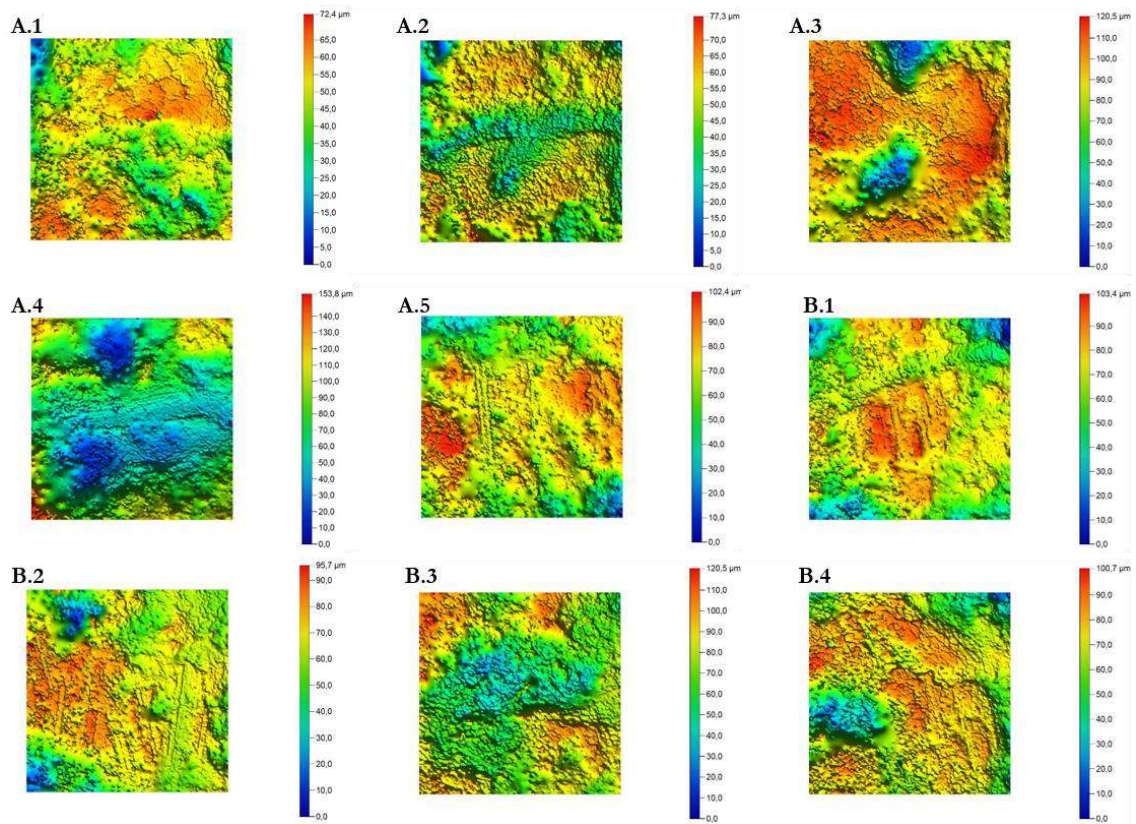
Figure 7. 49. BZ#N.No., mold 2: False-colour microtopographic maps of the analysed squares within areas A and B. Large flattened areas are clearly visible often associated with groups of striations, mainly oriented in the direction of the tool length.
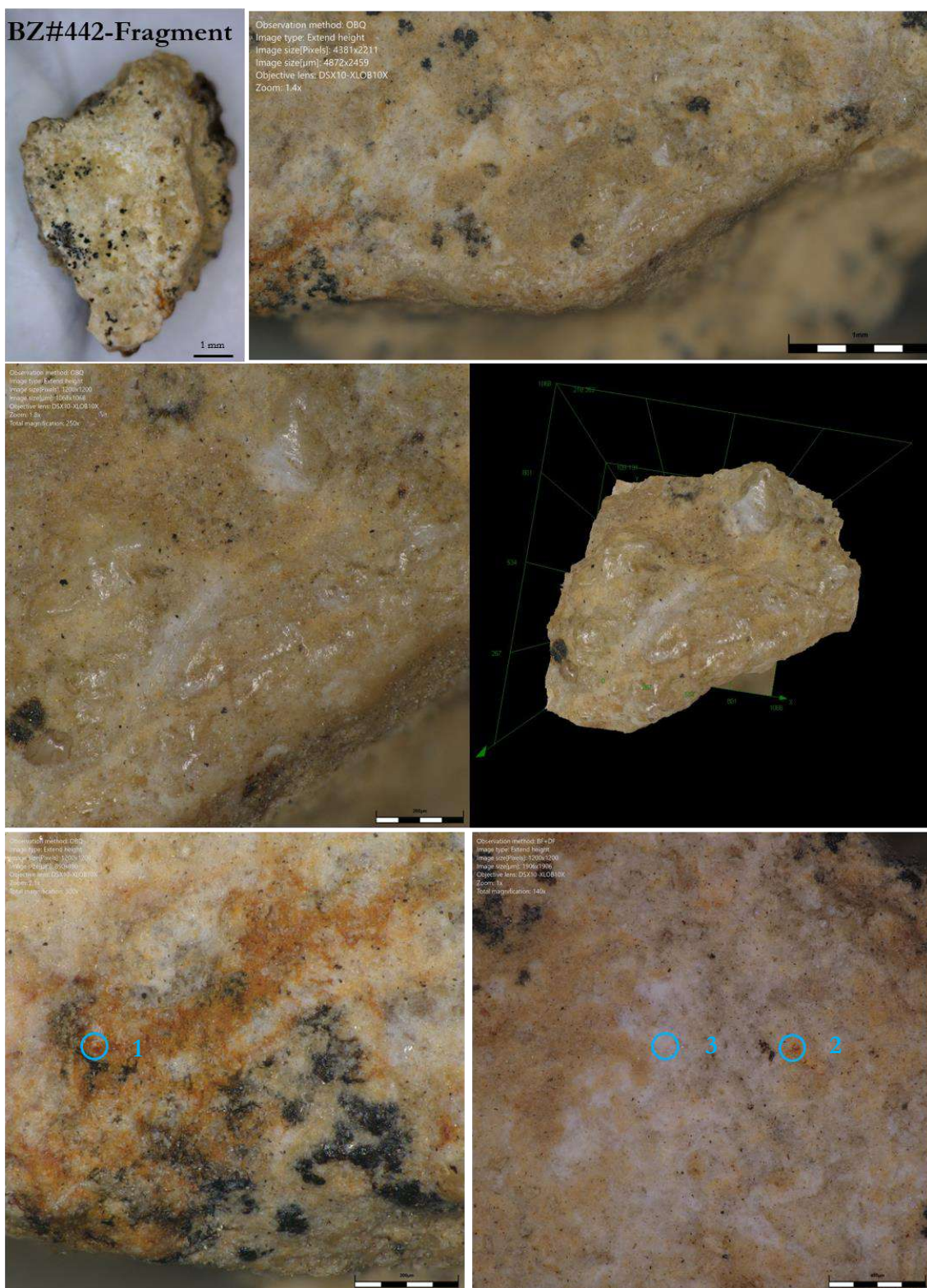
Figure 7. 50. BZ#442 fragment: The upper left corner displays an overview captured with Dino-Lite. The remaining images were obtained using the 3D digital microscope. The regions circled in blue indicate the areas that underwent Raman analysis.
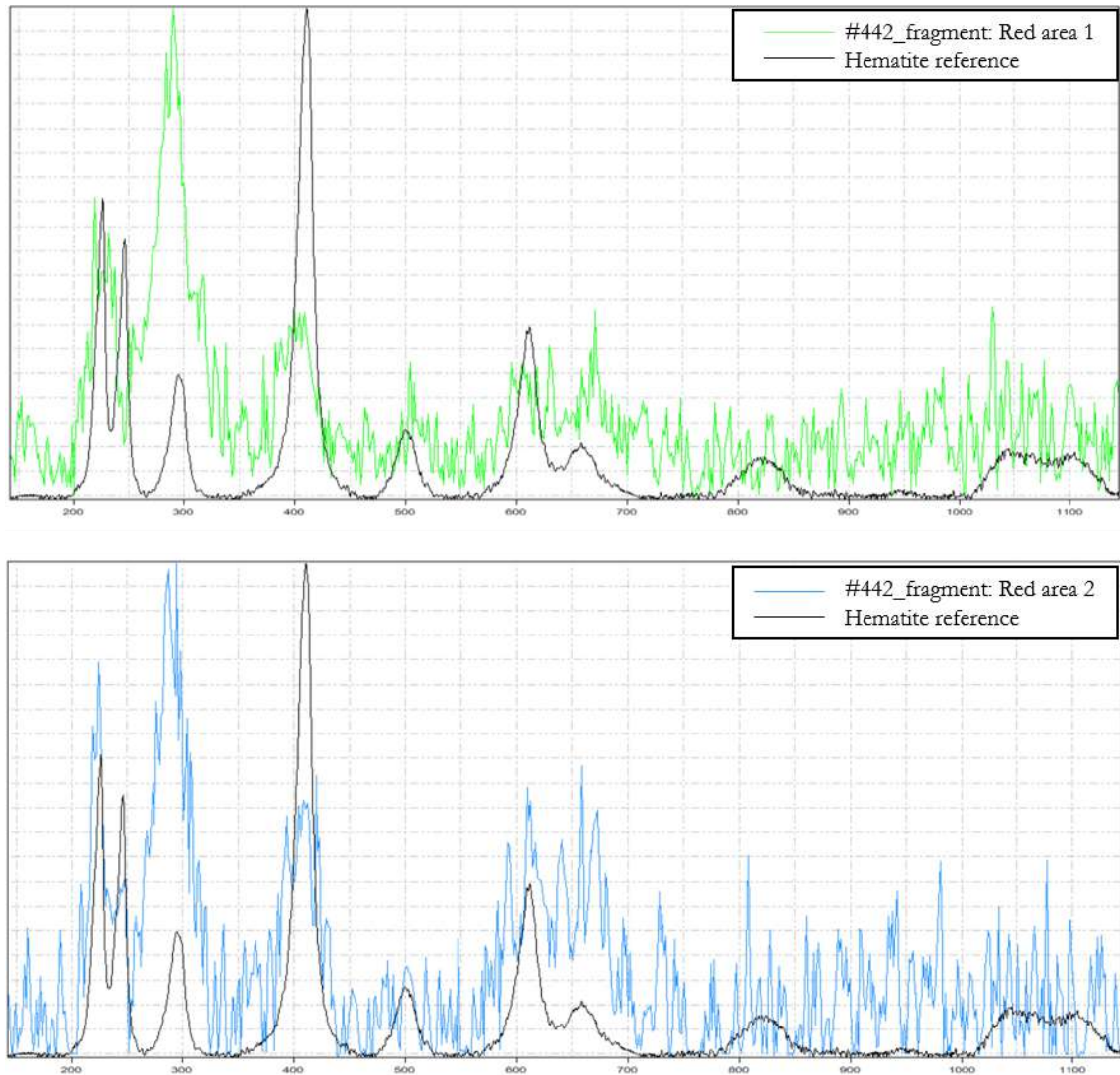
Figure 7. 51. Raman spectra of the two red spots (points 1 and 2 circled in Figure 7.50) analysed on fragment #442. The coloured lines represent the acquired spectra, while the black line corresponds to the hematite reference from the RRUFF project database (Lafuente et al. 2015).
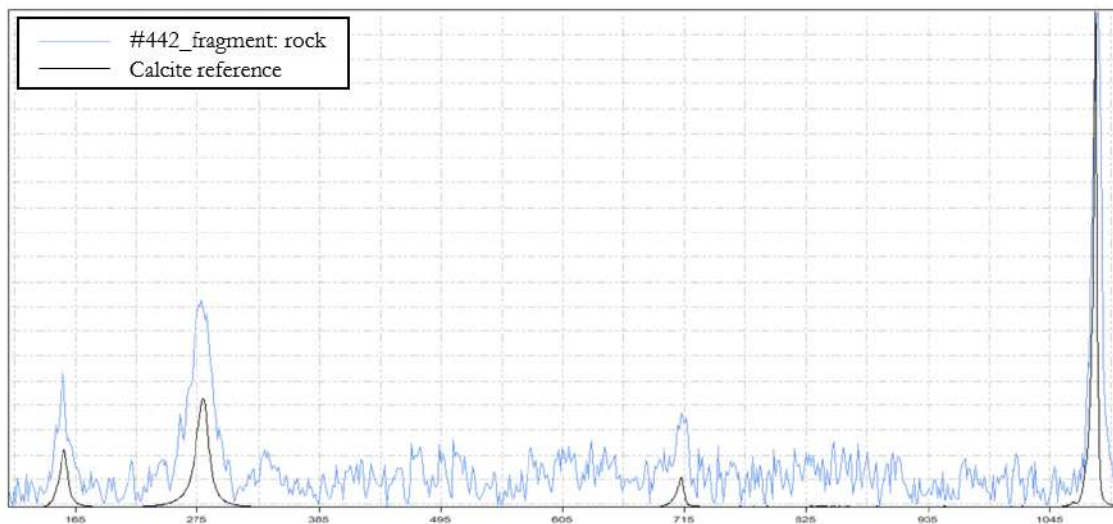
Figure 7. 52 Raman spectra of fragment #442 rock matrix are presented (point 3 circled in Figure 7.50). The blue line represents the acquired spectra, while the black line corresponds to the calcite reference from the RRUFF project database (Lafuente et al. 2015).
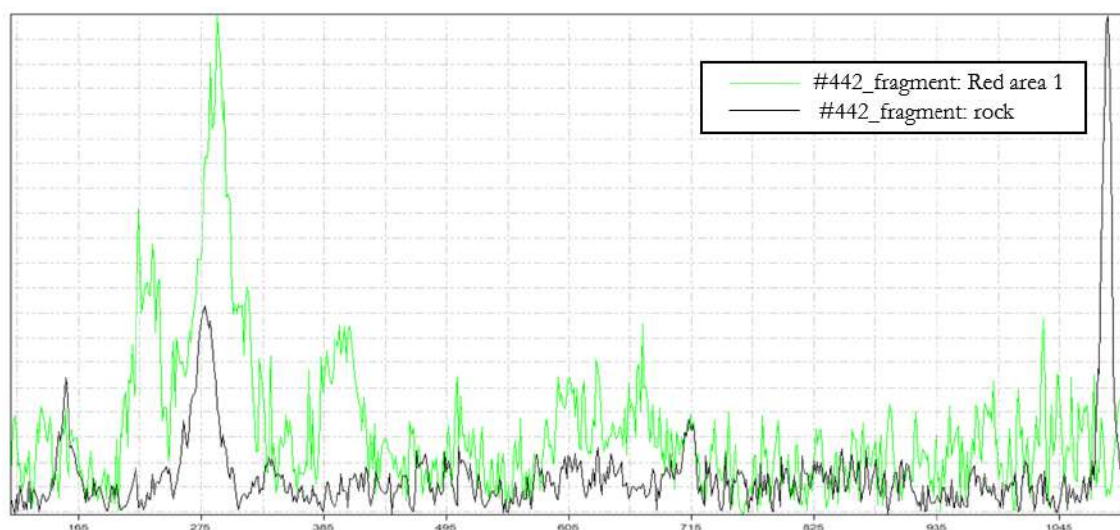
Figure 7. 53 Comparison of the Raman spectra between the red spot 1 (green line) and the background calcite (black line) reveals that the intense peak around 290 cm^{-1} in the green spectra may be attributed to the presence of calcite in the background.

7.2. Statistical analysis

On each mold, a 0.5 cm^2 square was drawn and recorded using the Leica DCM3D confocal profilometer. Within these reference squares, twenty-five areas of 850 µm2 were measured using a 10× lens, and nine areas were then selected for data elaboration and analysis. As described earlier, the confocal microscopy function of the instrument was used to depict these areas, and microtopographic maps were acquired with the profilometer function. The data were processed using Gwyddion software, which allowed for the

calculation of the height distribution and the ISO 25178-2 height parameters for each measured area.

These objective measurements of the stone surface allowed for the evaluation of the surface statistical parameters and facilitated a comparison with the reference collection, minimising potential influence from the analyst's perception and experience.

Given the unavailability of a direct comparison of the measured features with the natural state of the archaeological stone tools, the average values of ISO 25178-2 height parameters are also reported and discussed here for the experimental GSTs in their natural, unused stage (T_0) (Table 7.1), providing a closer approximation to the natural state of the archaeological GSTs. From the data, it is evident that the roughness of these stones in their natural state is relatively modest, with an average Sa of 17±6 μm and Sq of 21.8±7 μm. The distribution of heights demonstrates a Gaussian or leptokurtic distribution (Sku = 3 or Sku > 3) with a symmetrical shape, yielding Ssk values around 0 or moderate negative skewness (with the exception of M1, which exhibits positive Ssk). The Sp, Sv, and Sz values exhibit considerable variability. Moreover, a comparison between Sp and Sv reveals that valley values consistently exceed peak values.

Table 7. 1. Average for the considered ISO25178-2 surface texture areal parameters for all the experimental tools at unused stage.

SAMPLE	Mean roughness (Sa)	RMS roughness (Sq)	Skew (Ssk)	Excess kurtosis	Max.height of peaks (Sp)	Max. height of valleys (Sv)	Max. height of the surface (Sz)
M7- T_0	25.43935556	31.82513333	-0.481259832	0.049643956	91.85455556	119.986	211.8406667
M8- T_0	25.35075556	31.18522222	-0.266306011	-0.128750356	82.966	110.0332222	192.9993333
M2- T_0	14.34654444	18.18318889	-0.962340667	1.547992222	55.66311111	104.2303333	159.8938889
M3- T_0	14.09433333	19.07566667	-1.070842111	2.64646	74.874	113.0832222	187.9571111
M1- T_0	10.74776778	13.76051556	1.361519111	1.439918	33.20591111	75.76993333	108.9759556
M23- T_0	17.15611111	21.79437778	-0.632533727	0.552450956	60.02955556	93.74111111	153.7706667
M25- T_0	13.31696667	16.69748889	-0.548365222	0.410982456	50.28806667	82.12297778	132.4109333
AVERAGE	**17.20740492**	**21.78879905**	**-0.371446923**	**0.931242462**	**64.12588572**	**99.85239999**	**163.9783651**
DEV.ST.	*5.899434453*	*7.068204536*	*0.812820215*	*0.991300194*	*20.31124294*	*16.50695515*	*36.17237579*
Max.	25.43935556	31.82513333	1.361519111	2.64646	91.85455556	119.986	211.8406667
Min.	10.74776778	13.76051556	-1.070842111	-0.128750356	33.20591111	75.76993333	108.9759556

The measured values for the archaeological GSTs, are here discussed and plotted in boxplots, while the data are reported in Appendix C. In Figure 7.54, the Sa values are plotted, while in Figure 7.55, the Sq are presented. Moving on to Figure 7.56, the data for Ssk and in Figure 7.57 the Excess kurtosis (Sku - 3) are shown. Additionally, Figures from 7.58 to 7.60

displays the values for Sp, Sv, and Sz. Finally, Figures from 7.61 to 7.68 show the scatter plots for the height distribution.

BZ#833 and BZ#N.No. display notably low Sa and Sq values, which are not comparable to any of the experimental tools and are also lower than those observed in any other analysed archaeological GSTs. Additionally, their internal variability is quite minimal. For instance, BZ#2965 displays Sa: 7.6126 ± 1.8488 and Sq: 9.8445 ± 2.5967, while BZ#833 shows Sa: 6.9794 ± 1.201 and Sq: 9.0108 ± 1.3714, indicating a notably smooth surface. The distributions of heights (Figure 7.61) for both analysed areas are similar, with a leptokurtic distribution characterised by a spiky curve and elongated tails. Remarkably, the excess kurtosis value exceeds 0, indicative of a flattened surface texture, as highlighted by Bofill and colleagues (Bofill et al. 2013). Furthermore, the heights distribution curves present their modes around zero or slightly shifted above 0. Indeed, the skewness degree is symmetric or moderately negative, illustrating that the surfaces feature slightly more heights variability for the valleys than for the peaks that present more uniform altitude, compatible with the high microtopography flattening observed in the microscope analysis. Comparative evaluation of Sp, Sv, and Sz values for the two areas reveals similar patterns, with pit depths exceeding peak heights (for detailed values, refer to Appendix C).

BZ#5160. The comparison of the Sa and Sq values between the two analysed areas reveals a slight difference. Specifically, on mold 4, these values are higher than for mold 3 and display a more scattered distribution. This pattern aligns with trends observed in experimental data, where tools primarily used for grinding tasks undergo a reduction in roughness, leading to the flattening of the surface. As a result, the Sa and Sq values are lower in the used areas, while the roughness is more pronounced and data variability is greater in unused areas (T_0). However, it is important to note that when comparing the values for mold 3 with those reported in Table 7.1, which shows the average values for the natural unused surface of the experimental tool, there is a substantial degree of overlap. As explained in the previous section, this finding confirms the need to consider additional areas to gain a further insight into the functional attributes of the tool.

The height distribution (depicted in Figure 7.62) exhibits a slightly leptokurtic Gaussian shape for mold 3, consistent with microscopy observations that suggest the presence of flattened areas, likely attributed to grinding tasks. The excess kurtosis value is approximately zero, with some measurements for mold 3 slightly exceeding this value. The mode of the

height curves in both cases is slightly shifted above 0. The degree of skewness approaches symmetry for mold 4, indicating a balance between valleys and peaks on the surface. In contrast, mold 3 exhibits a more dispersed distribution, notably skewed towards the negative direction. This analysis is consistent with microscopy observations that indicate the high and middle microtopography of this item experiences the most pronounced wear, resulting in a narrower range of heights for the peaks compared to the valleys. Furthermore, when considering Sp and Sv values, mold 4 demonstrates comparability (Sp: 93.472 ± 21.542; Sv: 97.59 ± 31.376). However, for mold 3, the valleys are higher than the peaks. The Sz value is higher for mold 4, confirming a more pronounced distance between peaks and valleys.

BZ#6742. The Sa and Sq measurements for the three analysed areas reveal that face E exhibits the most pronounced roughness. In contrast, the data for molds 1a and 1e, both from face F, are comparable. Among these, mold 1e demonstrates slightly higher roughness values and a more scattered distribution. When compared to the data from the experimental collection, these data align with observations made for the tools involved in the pounding task, which led to the increase of roughness due to the formation of cracks and fractures. Notably, the central area (mold 1e) displays higher values than mold 1a, including more outliers. Data for mold 2 seems to confirm the hypothesis of a more heavy-duty task, such as cracking nuts for this side of the tool, presenting the higher values among all the analysed archaeological tools.

The height distribution, as depicted in Figure 7.63, displays a Gaussian shape for all the analysed areas. However, mold 1a exhibits a slight tendency towards a leptokurtic distribution, as also evidenced by the excess kurtosis values that, in a few instances, exceed 0. The mode for the height distributions of mold 2 is centred around 0, and the Ssk values are symmetrically distributed, falling within the range of 0 ± 0.5. This indicates a balance between peaks and valleys. Similarly, for mold 1e, the mode falls within the range of 0 ± 0.5, only slightly shifted towards positive values. In a few measurements, the tails of the distribution extend towards the negative direction, indicative of a moderate negative skewness. This demonstrates higher variability in valley altitudes and limited variability in peak altitudes. This feature is more pronounced in mold 1a, which presents moderately to significantly negative skewed values.

Comparing the Sp and Sv values for the three areas, it becomes evident that data for molds 1a and 1e are comparable, with higher values for the maximum depth of the valley. In contrast, mold 2 has higher values for both parameters, and the Sp and Sv values are similar.

In line with this data, the amplitude of the surface (Sz) for molds on face F is nearly the same, while for face E, it is substantially higher.

Comparing the data for all values with the averages reported in Table 7.1, it becomes evident that face E, which could be attributed to the heavy task hypothesis, is the one that deviates the most from the potential values of the natural unused rocks. However, as previously mentioned, the compromised conservation state of the tool limits any interpretation to the realm of the hypothesis.

BZ#375. Sa and Sq measurements for the analysed areas reveal that mold 5 exhibits the most pronounced roughness compared to mold 1. Assuming a vertical motion with face B as the working surface and face A as the dorsal side, the increase in roughness from unused to used areas aligns with experimental data exemplified by M3, used for pounding roots, and M1, involved in pounding and grinding ochre. This correlation is further supported by the presence of putative pigment residues observed on the surface. However, the microscopy analysis revealed a notable resemblance with the wear pattern observed on M8, where in this instance, the roughness is higher in the unused stage.

The heights distribution, as shown in Figure 7.64, displays a more pronounced leptokurtic shape for mold 5, with excess kurtosis values higher than 0 for both molds. However, it also displays a notable internal variability among the individual measurements within the same mold, a characteristic more pronounced for mold 1. The heights distribution curve modes for both areas are shifted towards positive values with long tails in the negative direction, particularly pronounced for mold 5. The Ssk values demonstrate a moderate degree of skewness. A closer comparison with experimental tools presents similarity with M1, while M3 exhibits a more pronounced negative Ssk, and M8 displays a slightly platykurtic distribution. The amplitude of the surface (Sz) is substantially higher for mold 5, as also the maximum height of the valleys (Sv), while Sp is comparable for the two analysed areas, but mold 5 exhibits higher internal variability.

BZ#3488. Microscopic observations suggest that this tool had contact with a woody resource. Upon comparing the selected ISO parameters with the data from the experimental collection, the closest resemblance is found with M7. Although M7 is an active tool and was used in conjunction with a wooden base for grinding and pounding activities, there is a

parallel in terms of contact material and motion between M7 and the presumed function of #3488, which however is interpreted as a passive tool.

The Sa and Sq average values are closely comparable to the data of #6707. The heights distribution (Figure 7.65) exhibits a Gaussian shape, with an average excess kurtosis around 0. The Ssk values are also around 0, with a few moderately negatively skewed outliers.

The Sp and Sv values are comparable, with the maximum depth of the valleys slightly higher than the height of the peaks. The Sz average value is approximately 145 ± 35.8 μm.

BZ#6707. The analysis was performed on mold 1, taken from face A, and mold 4 from face B. Upon comparing the Sa and Sq values for the two areas, it is evident that face B, which is presumed to be the utilised surface based on the microscope analysis, exhibits a lower roughness. This characteristic is consistent with experimental data, indicating that passive tools experience a generally lowering of the roughness values during use. Notably, this trend can be opposed during the initial 30 minutes when elaborating specific resources as roots. However, the visible traces as observed under the different microscopes suggest a more prolonged period of utilisation, likely beyond the experimental stages T_4.

The heights distribution of mold 1 (Figure 7.66) suggests a slight tendency towards a platykurtic shape, with most measurements having Sku values distributed slightly below 3. The modes of the curves are centred around 0, with the exceptions of one outlier that displays high negative skewness. The heights distribution for mold 4 (Figure 7.66) displays a Gaussian shape, with Sku values slightly above and below 3. The modes of the curves are centred around 0, and a few measurements are moderately negatively skewed.

The Sz values for mold 4 are lower than for mold 1, consistent with the wear experienced by the surface. Additionally, in both areas, the Sv values are higher than the Sp values.

BZ#2964. The analysed area exhibits elevated Sa and Sq values compared with the other archaeological passive tools, indicating the possibility that this face either remained unused or experienced minimal utilisation. The heights distribution (Figure 7.67) demonstrates a Gaussian shape, with Sku values concentrated around 3 and characterised by symmetrical to moderately negative skewness. Remarkably, the average value of Sz is the highest observed for archaeological passive tools and is comparable to the upper range of values recorded for the experimental stones at T_0. It is worth noting that in passive tools, there is usually a decrease in this parameter after use, a trend that is evident from

experimental data. The Sv values are higher than the Sp parameters, both of which reflect similar data dispersion.

BZ#N.No. This tool exhibits the lowest Sa and Sq values among all the archaeological passive GSTs. The Sa and Sq values are comparable to that of #6707 mold 4, albeit with a slightly greater dispersion. The heights distribution, as depicted in Figure 7.68, presents a highly variable shape. While the majority of measurements yield Sku values exceeding 3, giving a leptokurtic shape to the distribution, some measurements also present Sku values around or below 3. Notably, the Ssk values display considerable dispersion, primarily falling below 0, signifying a moderate to high negative skewness. This suggests a markable variability in valley heights, with fewer peaks displaying limited altitude variations. The surface amplitude ranks as the lowest among archaeological passive tools, comparable only to that of #6707 mold 4. The Sp values are lower than the corresponding Sv values, marking the lowest among all the analysed GSTs.

These data support the pronounced wear patterns observed after microscopes investigation. Upon comparing the data with the experimental collection, a significant similarity is apparent with GS7 across all the measured parameters, especially pronounced with square C2 and from T_3 onwards. This resemblance gains significance when considering that both tools serve a passive function and share a comparable composition and structure as calcarenites. This similarity, further confirmed by microscopic use-wear analysis, lends support to the hypothesis that tool BZ#442-BZ#N.No. was employed for processing small/hard resources as achenes, similarly to the task performed by GS7.
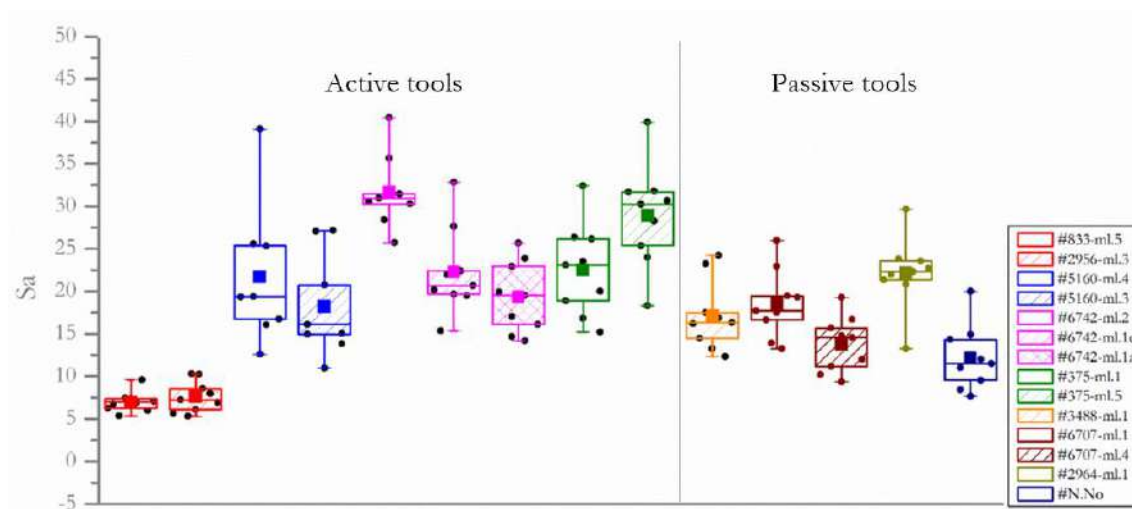
Figure 7. 54. Boxplots of the Arithmetical mean heights of the surface (Sa) for the analysed archaeological GSTs.
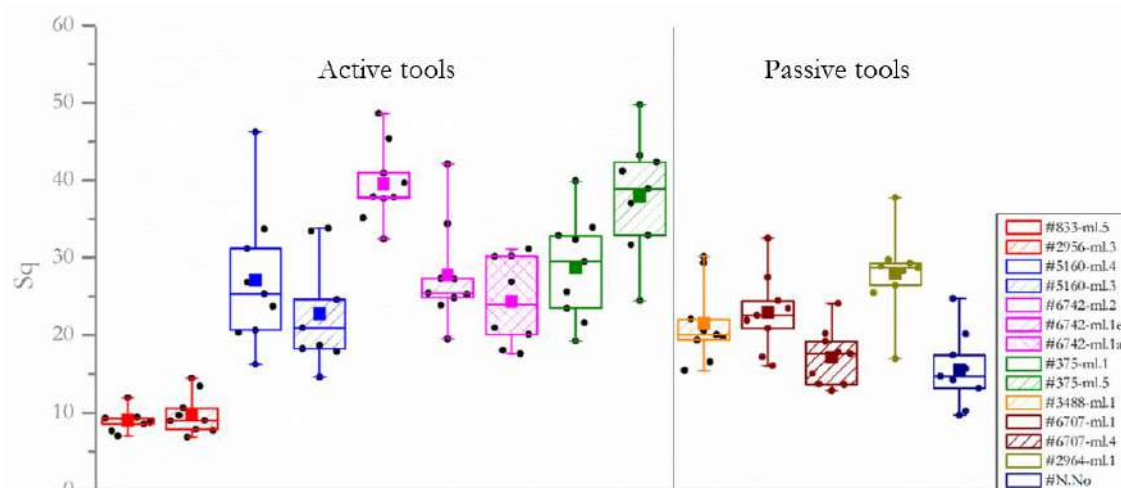
Figure 7. 55. Boxplots of the Root means square heights of the surface (Sq) for the analysed archaeological GSTs.
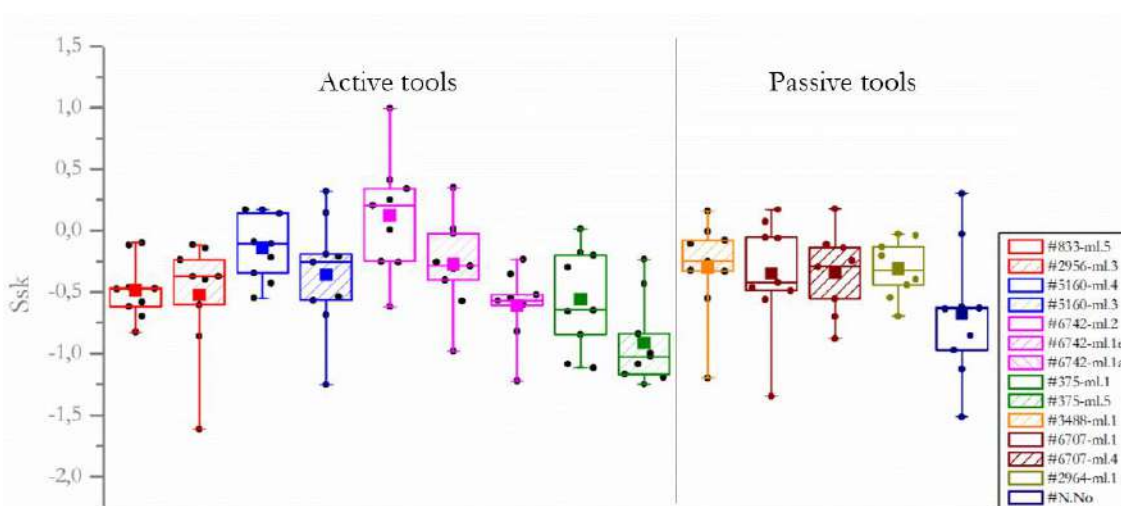
Figure 7. 56. Boxplots of the Skewness of the heights distribution (Ssk) for the analysed archaeological GSTs.
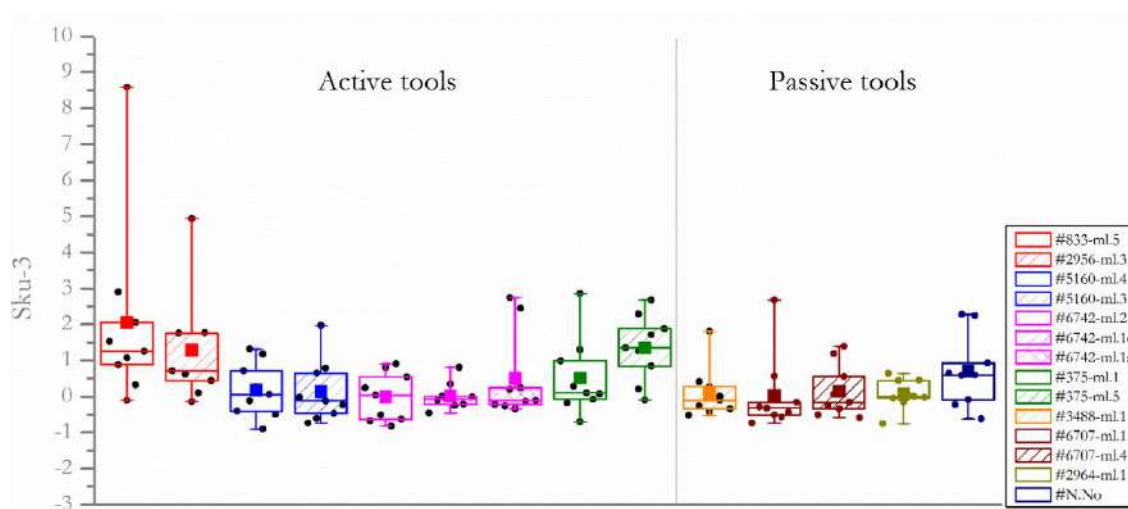
Figure 7. 57. Boxplots of the Excess Kurtosis of the height distribution for the analysed archaeological GSTs.
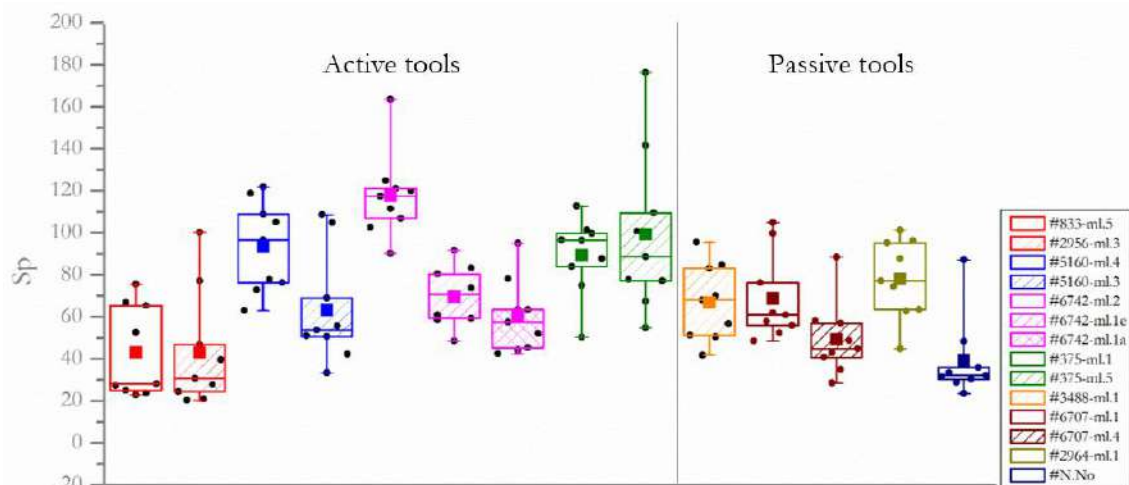
Figure 7. 58. Boxplots of the Maximum height of the peaks (Sp) for the analysed archaeological GSTs.
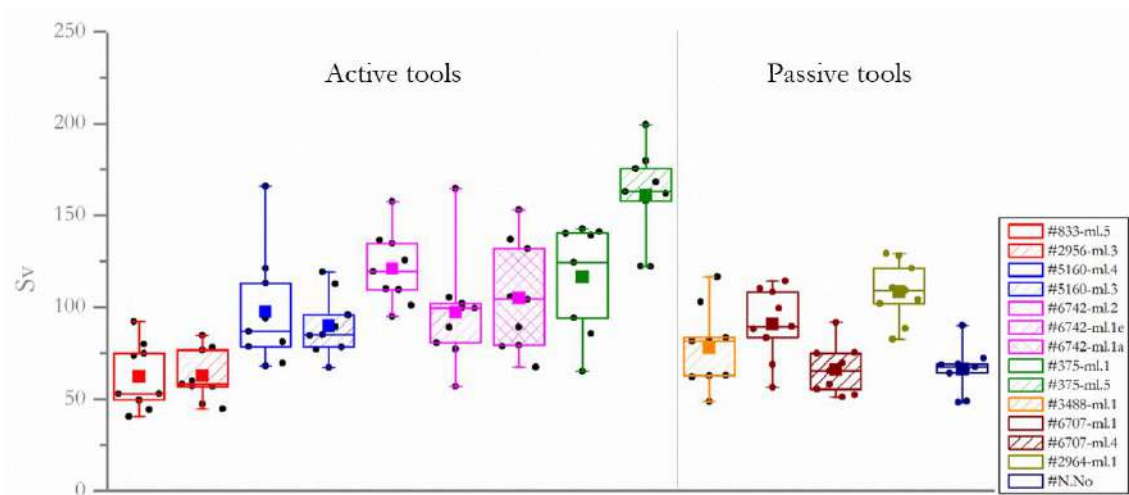
Figure 7. 59. Boxplots of the Maximum height of the valleys (Sv) for the analysed archaeological GSTs.
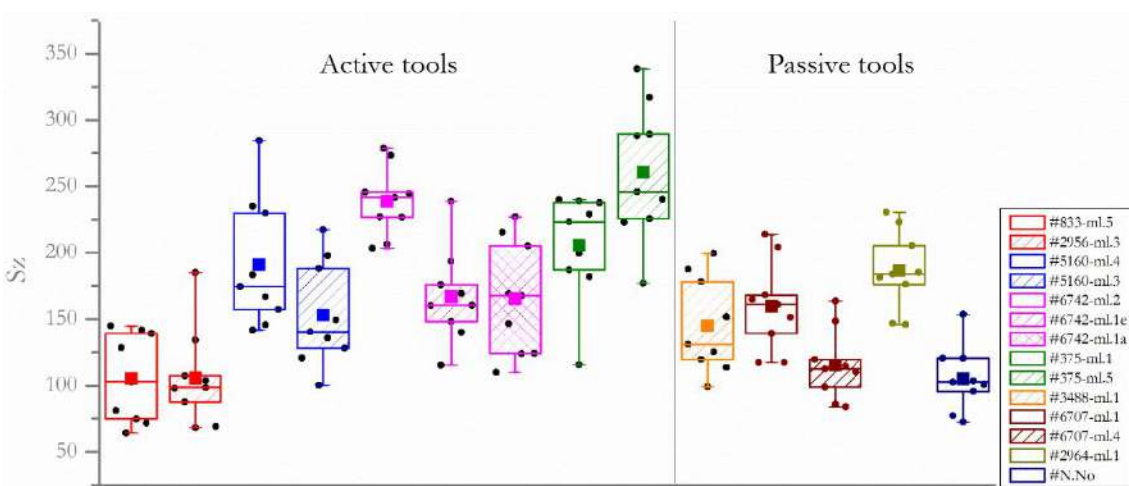
Figure 7. 60. Boxplots of the Maximum heights of the surface (Sz) for the analysed archaeological GSTs.
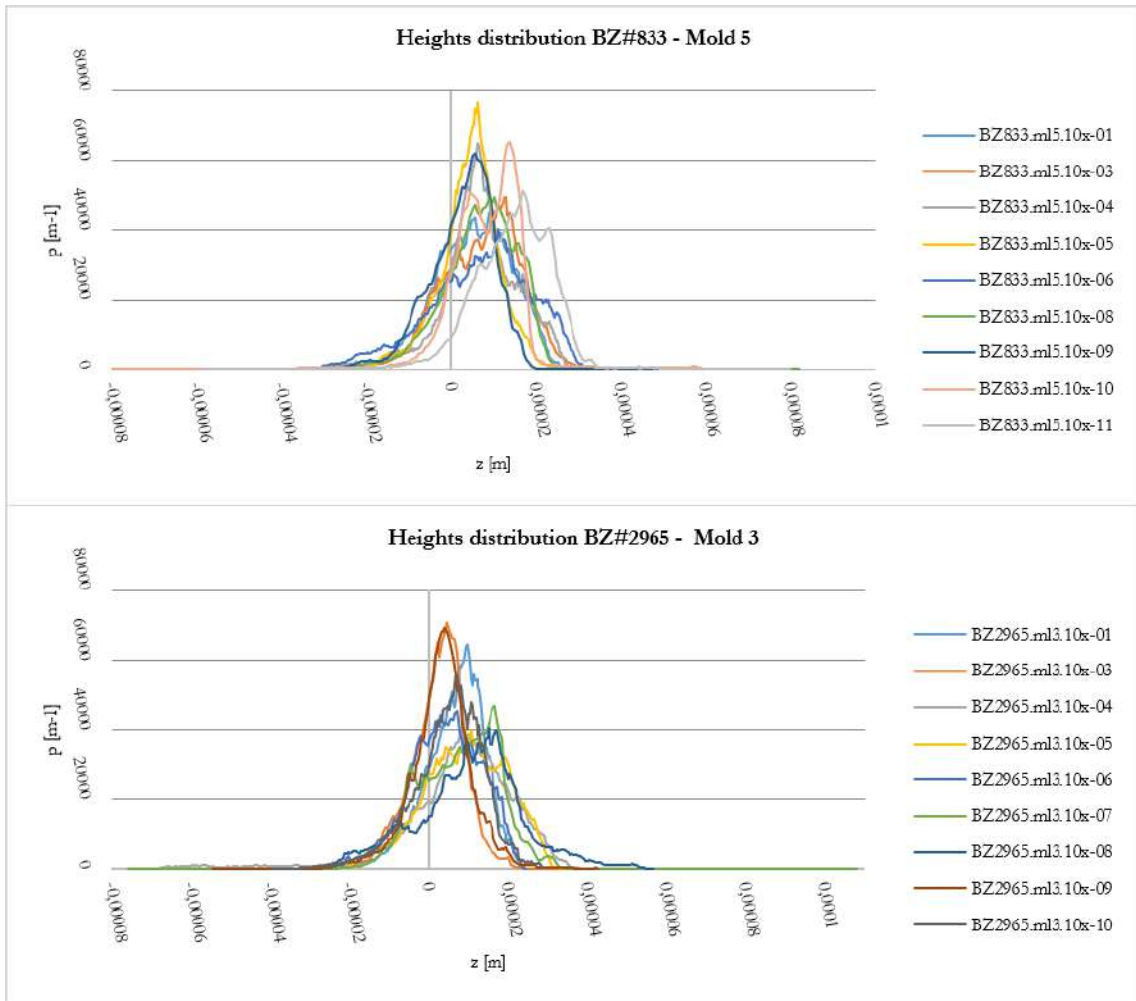
Figure 7. 61. Heights distribution for BZ#2965 molds 3 and 5.
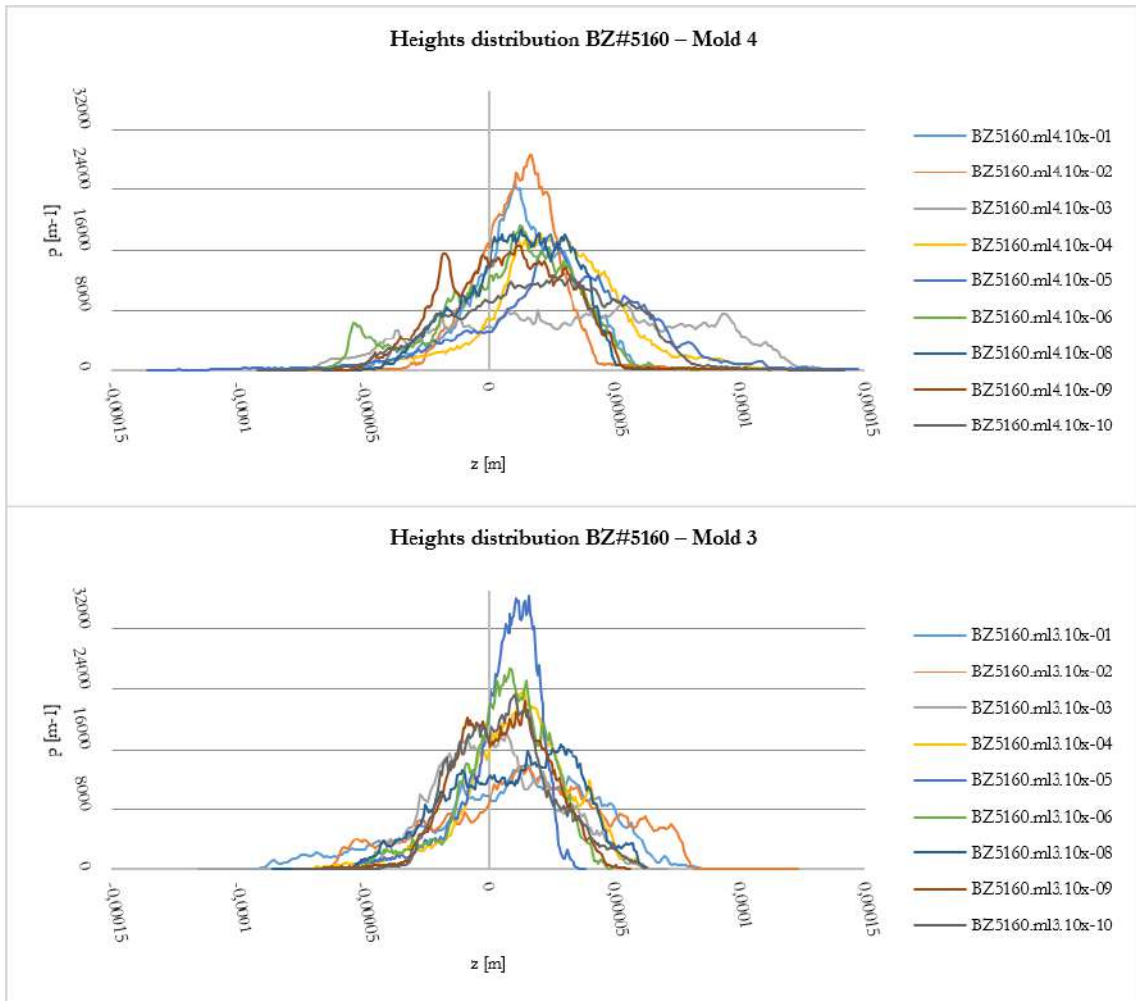
Figure 7. 62. Heights distribution for BZ#5160 molds 3 and 4.
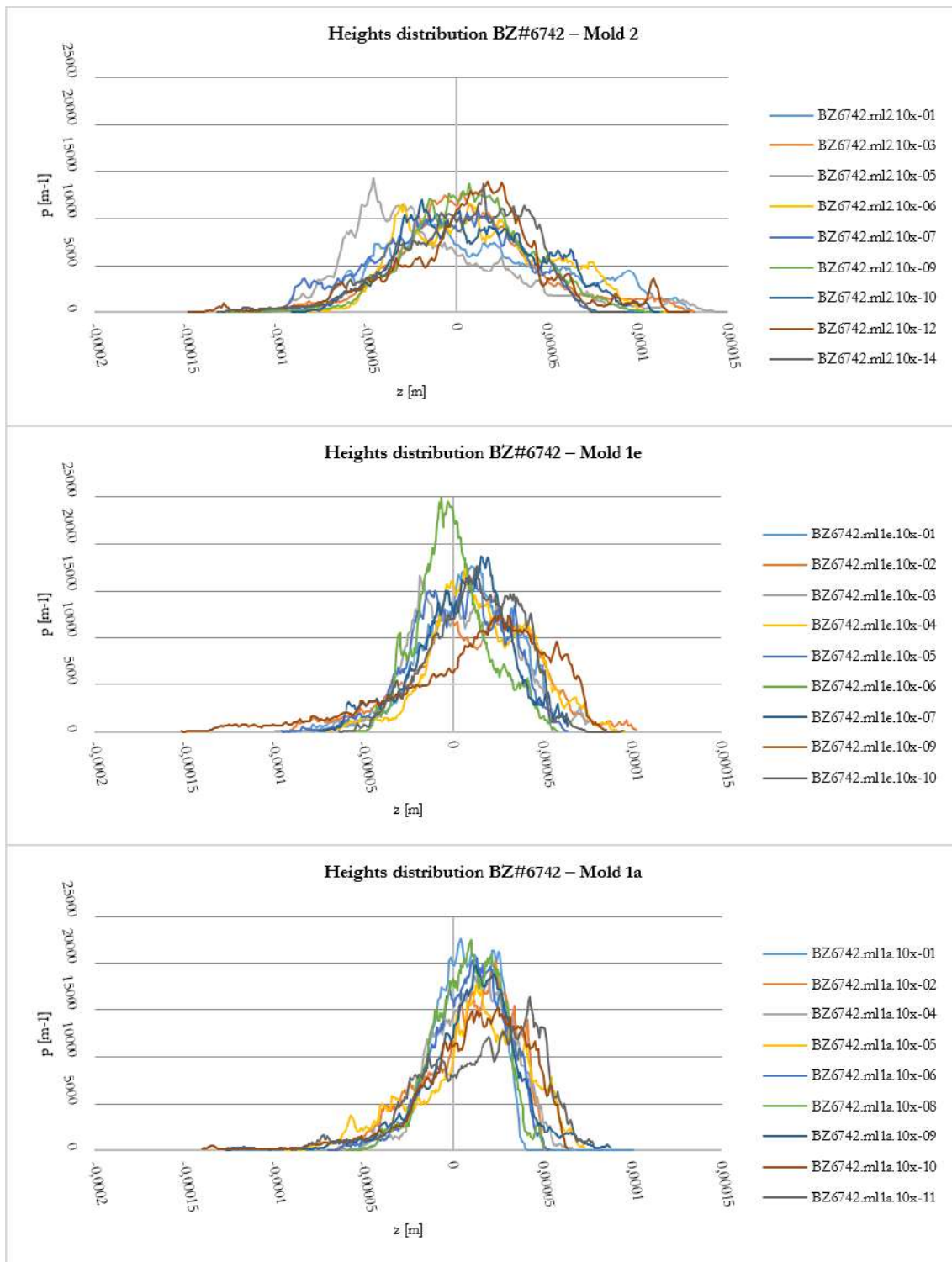
Figure 7. 63. Heights distribution for BZ#6742 molds 1a, 1e, and 2.
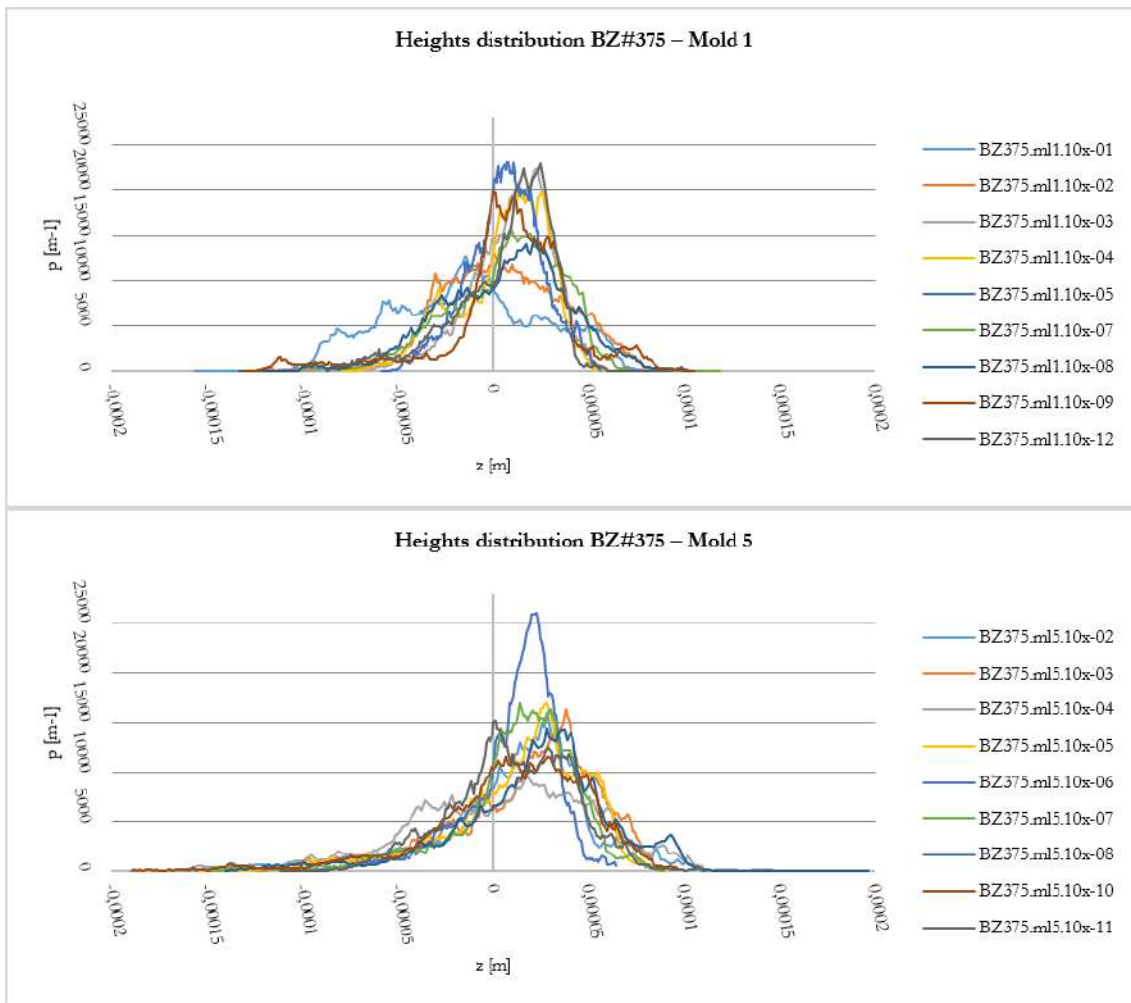
Figure 7. 64. Heights distribution for BZ#375 molds 1 and 5.
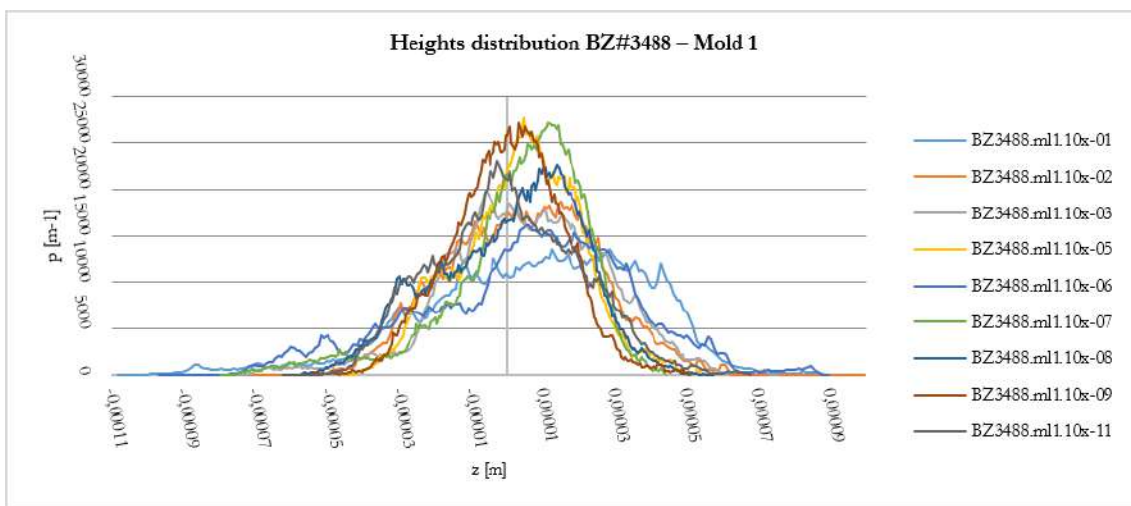
Figure 7. 65. Heights distribution for BZ#3488 molds 1 and 5.
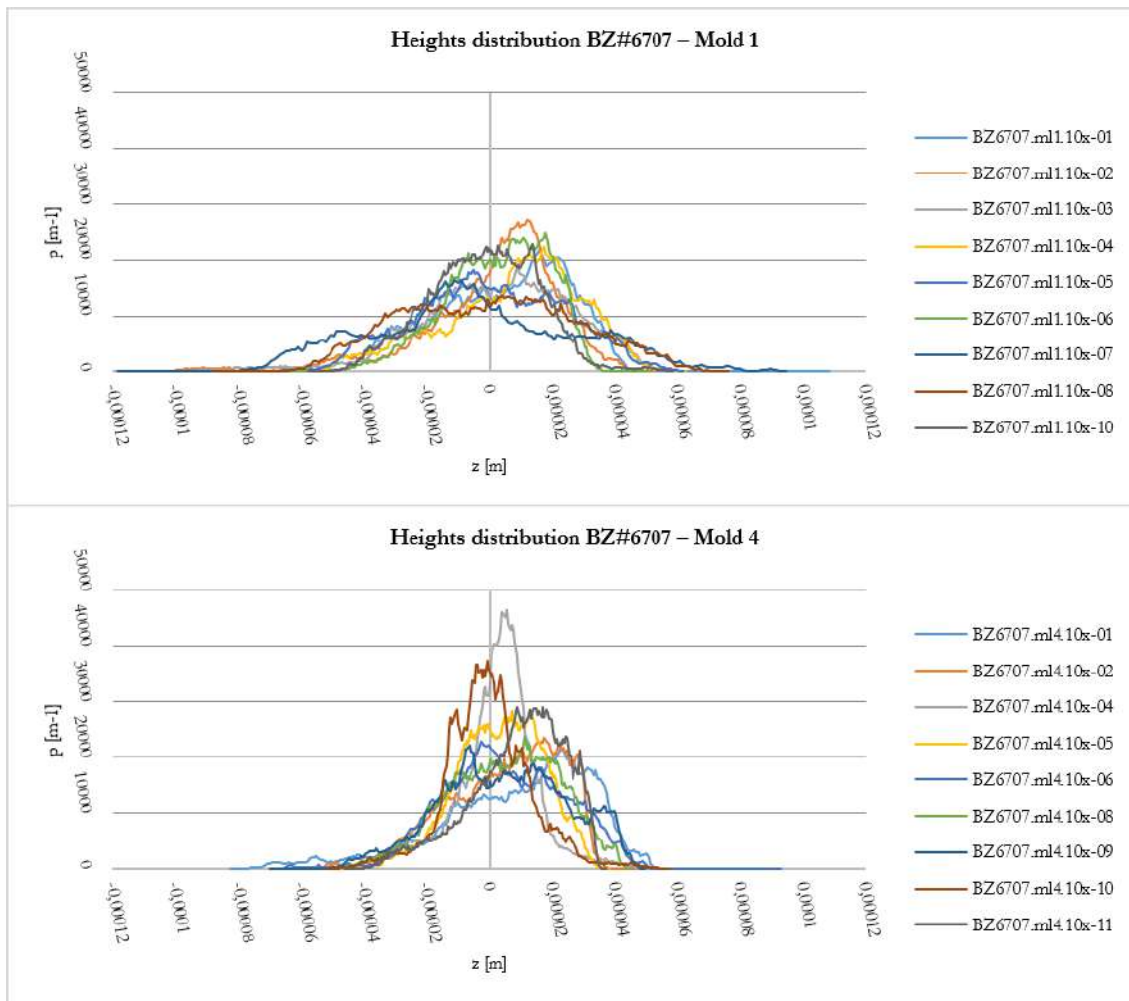
Figure 7. 66. Heights distribution for BZ#6707 molds 1 and 4.
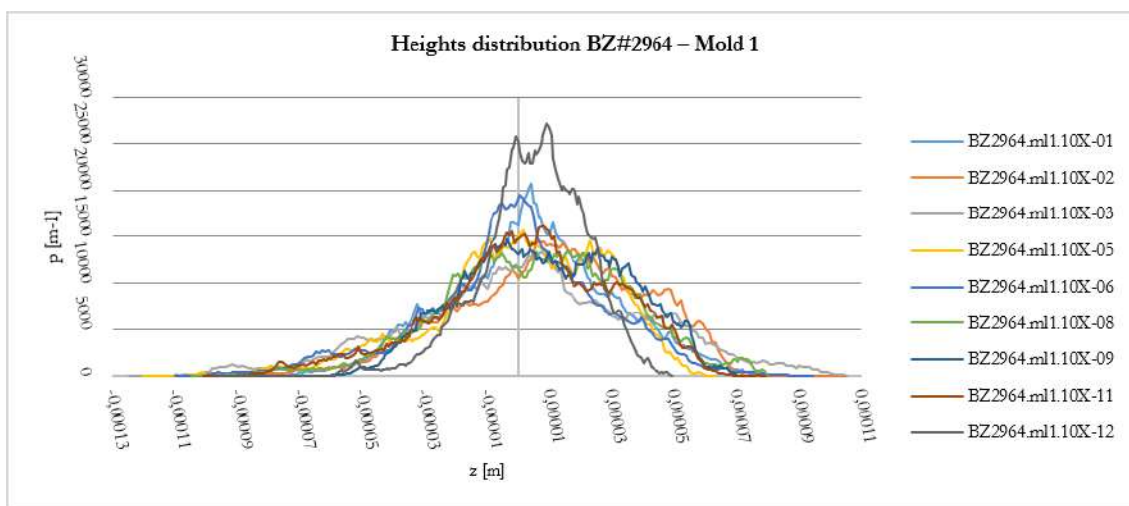
Figure 7. 67. Heights distribution for BZ#2964 mold 1.
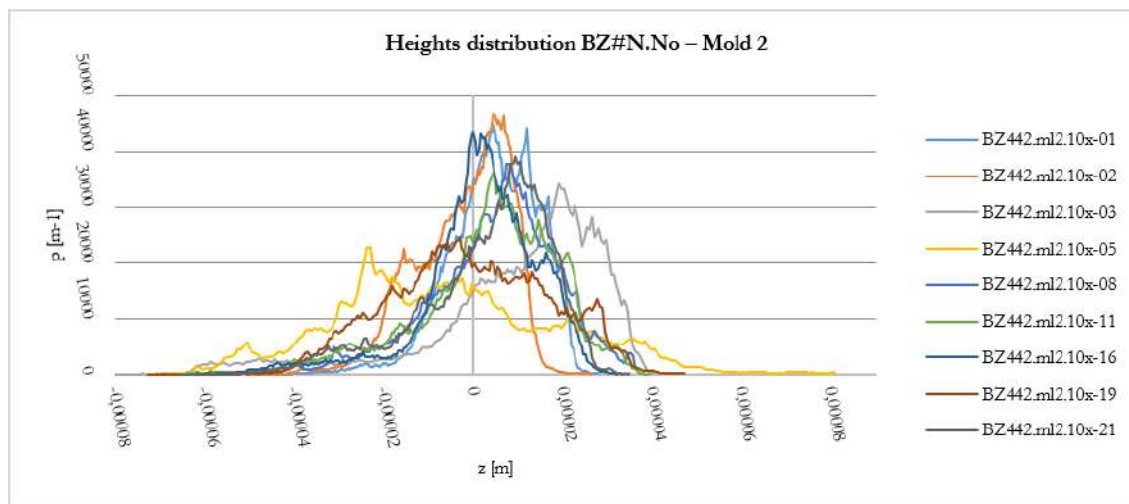
Figure 7. 68. Heights distribution for BZ#N.No. mold 2.

7.3. Conclusions

In conclusion, this chapter focused on the analysis of ground stone tools sourced from the Brînzeni I cave. The primary focus has been on the items retrieved within the cave chamber, therefore during Chetraru's excavation campaigns. Priority has been given to tools located in close proximity to hearths, as they are more likely to have been used for processing food resources. The scrutiny of the tools encompasses the evaluation of their overall geometry, accompanied by the examination of their morphological characteristics, and, for 18 GSTs, morphometric attributes. A more comprehensive analysis was conducted on a subset of 10 items, focusing on trace and functional assessments. Multiple areas of each item were examined, distributed across various faces of the lithic tools, resulting in a total of 14 potential working surfaces being investigated.

Drawing from the petrographic characteristics observed in the analysed GSTs, as well as insights gleaned from the experimental collection, it is supposed that the stones used as tools were likely sourced from the immediate vicinity of the cave. The shapes and smooth surfaces of the majority of the artefacts suggest a potential origin from river benches, possibly collected near the cave. The area is indeed rich in rivers such as the Racovăț, Dragişte, and Pruth Rivers, which flow in close proximity to the cave, with the Pruth River reaching a maximum distance of 8 km from the cave. During the design phase, the presence of rocks in the site area, characterised by good resistance to mechanical stress, high scratch resistance due to their predominantly quartz composition, suitable surface textures for processing tasks, and appropriate dimensions and shapes for easy handling facilitated by river transport and

rolling, collectively renders the notion of extensive procurement journeys unlikely. The limited sample examined for the petrographic analysis, although constrained, does appear to support this hypothesis, as it reveals the same rock types between the archaeological artefacts and newly collected stones from Racovăț River used for experimental purposes.

Most of the stones do not show signs of shaping (or to a very limited extent) and appear to have been selected for their inherent expedient design (Adams 2002a: 21), chosen for their dimensions, shapes, and weights suitable for to be used as tools in transformative tasks.

Upon examining the Brînzeni I GSTs assemblages and conducting a morphometric evaluation of 18 samples, reveals a discernible distinction in the collection, with four distinct main shapes being identified. The similarities in terms of morphometric characteristics indicate a meticulous preselection of the pebbles and slabs prior to their use. The selected tools were divided into five groups (as reported in Table 7.2 with average for the reported parameter as well as standard deviation): elongated active tools (referred to as group 1 in the table); small broken active tools with a convex edge (referred to as group 2 in the table); ellipsoidal active tools with at least one rounded edge (referred to as group 3 in the table); large passive tools with flat sub-rectangular shapes consistently exhibiting breakage (referred to as group 4 in the table); and smaller passive tools with sub-circular/sub-oval shapes (referred to as group 5 in the table).

Table 7. 2. The 18 GSTs consider for morphometric evaluation, divided according to their characteristics, displaying the average of the measured dimensions in blue, and the corresponding standard deviations in light blue.

Group	Item	Weight (g)	Dimensions (mm)			Volume (mm³)	Surface (mm²)	Condition
1	BZ#2965+BZ#833	643	188	57	37	-	-	broken and refitted
	BZ#1093	499	115.35	62.36	47.47	212350	19624.7	broken, a small part is missing
	BZ#3487	400	154.21	63	47.08	235068	23675.2	
	AVERAGE	**514**	**152.52**	**60.7866 6667**	**43.85**	**223709**	**21649.95**	
	DEV.ST.	*122.192 4711*	*36.3544 729*	*3.29492 5391*	*5.93547 8077*	*16064.051 85*	*2864.136 017*	
2	BZ#5160	297	79	73	59	-	-	broken, incomplete
	BZ#380	234	44.89	78.65	43.5	-	-	broken, incomplete
3	BZ#6742	751	100.16	71.39	78.51	331126	25159.5	
	BZ#375	-	118.34	84.57	48.1	263880	22730.8	
	BZ#N.No.	421	75.85	92	43.22	182027	17158.9	
	AVERAGE	**586**	**98.1166 6667**	**82.6533 3333**	**56.61**	**259011**	**21683.06 667**	
	DEV.ST.	*233.345 2378*	*21.3185 7015*	*10.4378 2704*	*19.1222 6713*	*74668.656 88*	*4101.915 277*	

4	BZ#442+BZ#N.No.	1552	256.65	203.59	43.26			broken and refitted, but incomplete
	BZ#N.No.	1446	175	114	113	-	-	broken, incomplete
	BZ#4292	243	233,14	184.51	33.85	1055810	90859.6	broken and refitted
	BZ#177	1236	124	75.4	152.47	690589	45280.3	broken, incomplete
	AVERAGE	**1119.25**	**197.1975**	**144.375**	**85.645**	**873199.5**	**68069.95**	
	DEV.ST.	*598.7438935*	*59.6575 3955*	*59.9928 4874*	*56.8421 4076*	*258250.24 57*	*32229.43 211*	
5	BZ#1376	660	114.22	100.34	36.19	292633	29039.3	
	BZ#3488	-	127.92	90.4	34.3	225234	24104.7	
	BZ#2964	884	144.58	100.92	48.68	388022	31811.9	
	BZ#6707	740	138.15	88.44	36.88	302059	28833.4	
	AVERAGE	**761.333 3333**	**131.217 5**	**95.025**	**39.0125**	**301987**	**28447.32 5**	
	DEV.ST.	*113.513 5822*	*13.2464 3946*	*6.52566 9825*	*6.53662 1834*	*66784.595 86*	*3197.824 528*	

The collection of GSTs includes numerous fragments of broken active tools resembling BZ#5160, BZ#2965, and BZ#380 (referred to as group 2 in the table). Experimental replicas have shown that active tools are more prone to breaking, especially when engaged in pounding or cracking tasks. Fragment BZ#2965, which was found to refit and belongs to the group of elongated active tools, suggests the possibility that other fragments from group 2 may share the same shape. However, this attribution remains speculative, and only through an increased number of analysed tools and a broader residue analysis it will be possible to shed light on this aspect.

The presence of recurring specific features within each identified group, such as the propensity of larger passive tools (group 4 in table) to break, could imply a shared common function. However, in order to ascertain whether these variations in form correspond to distinct functional tasks, requires an expansion of the analysed sample through comprehensive geometric, trace, and residue analyses.

Trace analysis and functional evaluations were conducted on the selected 10 items, employing a methodology that entailed both comparative and parametric analyses. This approach was contextualised within the established framework derived from the reference collection. Preliminary observations of the Moldovan stones chosen for inclusion in the reference collection, in their pristine and unutilized state, unveiled inherent characteristics and distinct attributes. Indeed, these stones often exhibit a naturally polished surface and presence of other features as cracks, fractures and pits. Consequently, when these features are observed on archaeological tools, their presence may not necessarily indicate utilisation.

Moreover, these stones possess a low inherent roughness and display a good resistance to mechanical stress. These attributes make this rock type particularly suitable for pounding activities, a characteristic that might have been recognized by the cave occupants who likely selected them precisely for this purpose. The visible traces, indeed, indicate a predominant pounding motion, which is consistent with the results of residue analysis (Birarda et al. 2020). This analysis revealed a prevalence of starch granules originating from USOs, which typically involve a predominantly vertical motion during processing.

The presence of quartz enhances their scratch resistance, requiring stone-to-stone contact to develop striations, a use- wear feature commonly associated with back-and-forth linear grinding processes. Interestingly, experimental replication involving ochre, a substance known from literature reviews and the author's prior studies to produce distinct linear traces, in this contest fails to produce such wear marks. Consequently, when microscopic examinations of the Brînzeni I GSTs reveal occurrences of linear traces, it prompts the hypothesis that these tools were utilised for processing small, resilient resources, such as seeds or achenes. The scattering of these materials on the passive tool surfaces would imply direct contact between active and passive tools, thus explaining the presence of linear traces. Only tools BZ#833-BZ#2965, BZ#5160 and BZ#442-BZ#N.No. exhibit such traces, while the majority of the collection display marks consistent with different plant organs pestling and contact with woody resources.

Residues analysis conducted independently from this thesis (encompassing six items BZ#833, BZ#2965, BZ#442, BZ#N.No., BZ#6707, BZ#2964), confirmed by additional OM and SEM inspections carried out by the author, have revealed the presence of different plant residues. These were identified by Dr. Cagnato and Pantukina as starch granules, plant vascular tissue and fibres. Additionally, ochre was also identified through the author's OM observation and Raman analysis. As a result, future analyses should incorporate a broader range of resources and integrate them into the experimental framework to enable meaningful cross-comparisons. In this direction a first step has already been taken by including ochre among the processed media in the experimental replicas.

8. Conclusion

      A primary objective of this study was to conduct a thorough assessment of existing methods and techniques in Ground Stone Tool study, subjecting them to critical scrutiny in order to establish a calibrated overall approach for their analysis. Beyond its achievements, this research serves also to illuminate biases and unresolved inquiries, which warrant future exploration as a subsequent phase of this research endeavour.

Furthermore, this study assumes a pivotal role as the inaugural dedicated investigation into the Brînzeni I GSTs collection.

      The originality of the employed methodology resides in its interdisciplinary character, synthesising concepts and methodologies from the realms of both humanities and STEM disciplines. This integration encompasses a diverse array of approaches, to explore various aspects of the tools' characteristics span across multiple dimensions, ranging from macro to submicron scales. This thorough investigation endeavours to examine the modifications in stone geometry and surface texture that occur when these tools are used for plant transformative tasks.

The approach was developed and validated on replicative tools employed across four distinct experimental scenarios, encompassing both natural and laboratory settings. A meticulous consideration was given to the variables that exert an influence on the experiment influencing the appearance and development of surface modifications of GSTs. Furthermore, this approach was also implemented to archaeological tools, constituting an instance of its application to real case-study. This reference collection was specifically designed to address inquiries concerning the 114 pebbles retrieved from the lowest cultural layer of the Brînzeni I cave. Preliminary traceological and residue analyses on a sample of 36 items hinted at their potential utilisation as ground stone tools in plant processing. Part of the results of the parallel residues investigation and the strict relationship with traceological analysis has been published in:

Birarda G., Cagnato C., Cefarin N., Stani C., Pantyukhina I., Badetti E., Covalenco S., Marcomini A., Obada T., Sava E., **Sorrentino G**., Skakun N., Vaccari L., Longo L. (2020). Direct morpho-chemical characterisation of elusive plant residues from Aurignacian Pontic Steppe ground stones: supper's ready for Homo sapiens. *BioRxiv.*

DOI: doi.org/10.1101/2020.07.23.212324;

Longo L., Altieri S., Birarda G., Cagnato C., Cefarin N., Graziani V., Obada T., Pantyukhina I., Ricci P., Skakun N., **Sorrentino G.**, Terekhina V., Tortora L., Vaccari L., Lubritto C. (2021). A Multi-Dimensional Approach to Investigate Use-Related Biogenic Residues on Palaeolithic Ground Stone Tools. *Environ. Archaeol.* DOI: doi.org/10.1080/14614103.2021.1975252;

Longo L, Birarda G., Cagnato C., Badetti E., Covalenco S., Pantyukhina I., Skakun N., Vaccari L., Terekhina V., **Sorrentino G**. (2022). Coupling the beams: How controlled extraction methods and FTIR-spectroscopy, OM and SEM reveal the grinding of starchy plants in the Pontic steppe 36,000 years ago. *J. Archaeol. Sci. Rep.*, 41. DOI: doi.org/10.1016/j.jasrep.2021.103333.

Birarda G., Badetti E., Cagnato C., **Sorrentino G.**, Pantyukhina I., Stani C., Dal Zilio S., Khlopachev G., Covalenco, Obada T., Skakun N., Sinytsin N., Terekhina V., Marcomini A., Lubritto, Vaccari E., Longo L. (submitted). Morpho-chemical characterization of individual ancient starches from Palaeolithic Pontic Steppe ground stones.

To assemble the reference collection, pebbles and slabs were collected from the Racovăţ River and employed for pounding and grinding activities involving various plant organs. Notably, the replicative collection also encompassed comparative experiments involving cobbles from the Fiora River in Italy. Selection was based on congruence in terms of morphometric and petrographic attributes with the Moldovan archaeological and experimental GSTs. This expansion aimed to enrich the scope of the collection beyond the Edinet region and provide insights into how stones respond to mechanical stress after different periods of use.

As demonstrated by this study, establishing a tailored reference collection prior to functional analysis is far from redundant. The inherent attributes of the stone hold a pivotal role over the formations, temporal patterns, categories of traces, distributions, and wear progressions, taking into account its cumulative/destructive nature. The methodological enhancement encompasses the development of a sequential reference collection that covers multiple stages of tool utilisation. This collection traces the evolution of wear patterns that underlie the distinct behaviours exhibited by different lithic types, highlighting their

association with specific processed plant organs and their appearance and extent at various stages. The insights garnered emphasise the importance of this foundational phase in understanding the use of archaeological ground stone tools.

Through the integration of various methods and examinations in both two-dimensional and three-dimensional domains, the presented approach effectively identifies crucial features within wear patterns. The inclusion of three-dimensional techniques not only facilitates precise measurements and quantitative analysis but also reveals potential biases that could emerge already during the data collection stage of a research.

The multimodal strategy tested on experimental GSTs encompasses the utilisation of photogrammetric techniques to capture stones geometry and generate 3D models at predetermined moments of the experimental process. This serves a dual purpose: to ascertain the stones depletion throughout their usage and to reconstruct an approximation of the missing stages of the archaeological tools use-biography. Various approaches were explored, including established methods from the literature, shedding light on inherent biases and common errors associated with photogrammetric techniques. The results, which are partially reported in this dissertation, have been published in:

Sorrentino G., Menna F., Remondino F., Paggi M., Longo L., Borghi A., Re A., Lo Giudice A. (2023). Close-range photogrammetry reveals morphometric changes on replicative ground stones. *PLOS ONE*. DOI: 10.1371/journal.pone.0289807.

Furthermore, the implementation of microscopy observations spanning varying scales and resolutions, such as Dino-Lite, stereomicroscopy, optical microscopy (OM), 3D digital microscopy, and scanning electron microscopy (SEM), allowed for the acquisition of images depicting the tool's surface. By employing diverse microscopy techniques, the analysis could focus on increasingly smaller areas with heightened resolution, enhancing the ability to scrutinise finer surface details without losing the overall contest. Additionally, preliminary tests were conducted at the beginning of this research during the peak of the COVID-19 pandemic on previously acquired data from the Crimean archaeological site of Surein I. The below-reported publication includes the results of this preliminary investigation.

Longo L., Skakun N.N, Pantyukhina I.E., Terekhina V.V, **Sorrentino G.** (2021). Aurignacian grinding stone from Surein I (Crimea): "trace-ing" the roots of starch-based diet. *J. Archaeol. Sci.Rep.*, 38, 102999. DOI: doi.org/10.1016/j.jasrep.2021.102999.

Instead, the methodology and rationale underpinning the creation of the reference collection, was published in two articles (the latest also selected as the issue cover story by the Heritage journal) and a YouTube video, which served as contributions to the EXARC 2021 conference:

Sorrentino G., Lo Giudice A., Re A., Borghi, A., Longo L. (2021). Più di un semplice ciottolo: Un protocollo sperimentale per la comprensione del ruolo di strumenti macrolitici nella trasformazione delle risorse vegetali nel Paleolitico Superiore in Eurasia. Archeologie sperimentali. Temi, metodi, ricerche, 2, pp. 24-40. DOI: doi.org/10.13135/2724-2501/2_2021;

Sorrentino G., Lo Giudice A., Re A., Borghi, A., Longo L. (2021). Replicate Plant Processing REVEALs Ground Stones complex Biography. EXARC, EAC12 World Tour: Session 13. Available at: https://youtu.be/vvJLDTX13Fo;

Sorrentino G., Longo L., Obada T., Borghi A., Re A., Paggi M., Lo Giudice A. (2023). Tracing Old Gestures: A Multiscale Analysis of Ground Stone Tools Developed on Sequential Lab-Controlled Replicative Experiments. *Heritage*, 6, pp. 4737–4767. DOI: doi.org/10.3390/heritage6060252.

The qualitative investigations were integrated with confocal profilometry analysis, which were instrumental in obtaining 3D data for specific areas (several 850 µm² squares), enabling a comprehensive examination of the microtopography of both experimental and archaeological GST surfaces. This approach provided objective parameters for description, and the comparison of such data between the experimental collection and archaeological tools allowed for a parametric-based comparative analysis. However, it is important to note that functional interpretation of this type of data cannot stand alone; rather, it necessitates a robust foundation rooted in microscopy observations. Moreover, considering that different types of stones respond to mechanical stress in distinct ways, it is even more evident the necessity of constructing a tailored reference collection in all contexts including parametric study.

The application of quantitative methods to delineate distinct phases of surface depletions has revealed a recurring cyclic pattern of surface roughness. This pattern often encompasses alternating phases of roughness increase and decrease, oscillating between flattening of the surface texture and phases characterised by more pronounced traces. This

recurring phenomenon has been discerned through the sequential dataset, offering valuable insights when examining the potential function of archaeological ground stone tools.

The presented integrated approach establishes a reliable and quantitative path for use-wear analysis, facilitating precise data collection and promoting informed interpretation. This robust methodology allows for a comprehensive understanding of the functional biography of ground stone tools, shedding light on their past applications and highlighting potential associated dynamics.

Having established robust methodologies and a comprehensive reference collection, analysed from various perspectives and scales, the research is poised to move further to a level where the emphasis will shift from methodological questions towards addressing archaeological inquiries. This trajectory entails an enlargement in the sample archaeological ground stone tools subject to analysis, as well as the inclusion of further areas on the tools that warrant examination. This broadening of focus encompasses the exploration of previously overlooked side of the artefacts, including the less frequently utilised lateral sides, which holds the promise of providing greater insights into the original appearance of the stones for comparative purposes. In this context, the investigation of experimental stones, originating from the same collection area and sharing identical raw materials as the archaeological tools, offers a valuable glimpse into the potential pre-utilisation characteristics of the studied GSTs. Furthermore, the incorporation of the ventral face of the passive tools (the surface in contact with the ground) within the examined areas provides valuable insights to distinguish between utilised and unused surfaces. It is important to note that even areas not directly engaged in processing undergo transformation and exhibit distinct wear trace patterns.

The aspiration to broaden the scope of investigation is further reflected in the intent to encompass the scrutiny of diverse resources beyond the vegetal realm, thus enhancing the narrative surrounding tool utilisation practices. Already, the inclusion of ochre in this direction has provided a useful avenue for comparison. Furthermore, the systematic utilisation of the same methods and a consistent array of techniques for both experimental and archaeological tools provide a robust framework for comparative assessment, encompassing both qualitative and quantitative data. However, for robust comparison the dataset of quantitative experimental data needs to be increased.

The temporal dimension has been pivotal in this study. Exploring various phases of tool use within the tools' lifecycle offers a unique vantage point for comprehending the

dynamic evolution of usage traces over time. Looking ahead, a future avenue of development will delve into the influence of post-depositional effects. This underscores the necessity for continued investigation, delving into the potential impact of burial and environmental factors on the discernible signatures of tool usage.

References

Adams J.L. (1993). Mechanism of wear on ground stone surfaces. PCAS Quarterly, 29(4), pp. 61-74.

Adams J.L. (2002a). Ground Stone Analysis: a technological approach. The University of Utah Press, pp. 336. ISBN: 0874807166.

Adams J.L. (2002b). Mechanism of wear on ground stone surface. In: Moudre et broyer. Procopiou H., Treuil R. (Eds.). Éditions CTHS, Paris, pp. 57-69.

Adams J.L. (2010). Understanding Grinding Technology through Experimentation. In: Designing Experimental Research in Archaeology, Examining Technology through Production and Use. Ferguson J.R. (Ed), University Press of Colorado, Boulder, pp. 129-151. ISBN: 978-1-60732-022-7.

Adams J.L. (2014). Graund stone use-wear analysis: a review of terminology and experimenal methods. J. Archaeol. Sci., 48, pp. 129-138.

Adams J.L., Delgado-Raack S., Dubreuil L., Hamon C., Plisson H., Risch R. (2009). Functional analysis of macro-lithic artefacts: a focus on working surface. In: Non-flint raw material use in prehistory old prejudices and new direction, Proceedings of UISPP congress, Lisbon, Portugal, September 2006, Sternke F., Eigeland L., Costa L.J. (Eds.), BAR-IS, pp. 43-66. ISBN: 978 1 4073 0419 9.

Allsworth-Jones P., Borziac I.A., Chetraru N.A., French C.A.I., Medyanik S.I. (2018a). Brînzeni: A Multidisciplinary Study of an Upper Palaeolithic site in Moldova. Proceedings of the Prehistoric Society, 84, pp. 41–76. DOI: https://doi.org/10.1017/ppr.2018.3.

Allsworth-Jones P., Borziac I.A., Chetraru N.A., French C.A.I., Mihailescu C.D., Medyanik S.I. (2018b). The Middle Palaeolithic Site of Buzdujeni in Moldova: Establishing the Archaeological and Environmental Record. J. Paleolit. Archaeol., 1, pp. 129–177. DOI: https://doi.org/10.1007/s41982-018-0009-7.

Anikovich M.V. (1992). Early Upper Palaeolithic Industries of Eastern Europe. Journal of World Prehistory, 6(2), pp. 205-245.

Antinozzi S., Fiorillo F., Surdi M. (2022). Cuneiform Tablets Micro-Surveying in an Optimized Photogrammetric Configuration. Heritage, 5(4), pp. 3133-3164.

Arroyo A., de la Torre I. (2016). Assessing the function of pounding tools in the Early Stone Age: A microscopic approach to the analysis of percussive artefacts from Beds I and II, Olduvai Gorge (Tanzania). J. Archaeol. Sci., 74, pp. 22-24. DOI: https://doi.org/10.1016/j.jas.2016.08.002.

Arroyo A., de la Torre I. (2020). Pitted stones in the Acheulean from Olduvai Gorge Beds III and IV (Tanzania): A use-wear and 2D approach. J. Hum. Evol., 145, 102837. DOI: https://doi.org/10.1016/j.jhevol.2020.102837.

Arroyo A., Hirata S., Matsuzawa T., de la Torre I. (2016). Nut cracking tools used by captive chimpanzees (pan troglodytes) and their comparison with early stone age percussive artefacts from Olduvai Gorge. PLoS One, 11, e0166788. DOI: http://dx.doi.org/10.1371/journal.pone.0166788.

Astruc L., Vargiolu R., Zahouani H. (2003). Wear assessments of prehistoric instruments. Wear, 255, pp. 341–347. DOI: https://doi.org/10.1016/S0043-1648(03)00173-X.

Bamforth D.B. (2010). Conducting experimental research as a basis for microwear analysis. In: Designing Experimental Research in Archaeology, Examining Technology through Production and Use. Ferguson J.R. (Ed), University Press of Colorado, Boulder, pp. 92 - 109. ISBN: 978-1-60722-022-7.

Banks W.E., Kay M. (2002). High-Resolution Casts for Lithic UseWear Analysis. Lithic Technology, 28(1), pp. 27-24. DOI: 10.1080/01977261.2002.11721000.

Barone S. (2012). Rilievo 3D a luce strutturata. In: Archeometria e restauro. L'innovazione tecnologica. Siano S. (Ed.), Nardini editore, pp. 19-26.

Benito-Calvo A., Arroyo A., Sánchez-Romero L., Pante M., de la Torre I. (2017). Quantifying 3D Micro-Surface Changes on Experimental Stones Used to Break Bones and Their Implications for the Analysis of Early Stone Age Pounding Tools. Archaeometry, 60, pp. 419-436. DOI: http://dx.doi.org/10.1111/arcm.12325.

Benito-Calvo A., Carvalho S., Arroyo A., Matsuzawa T., de la Torre I. (2015). First GIS analysis of modern stone tools used by wild chimpanzees (Pan troglodytes verus) in Bossou, Guinea, West Africa. PLoS ONE, 10(2), e0121612.

Benito-Calvo A., Crittenden A.N., Livengood S.V., Sánchez-Romero L., Martínez-Fernández A., de la Torre I., Pante M. (2018). 3D 360° surface morphometric analysis of pounding stone tools used by Hadza foragers of Tanzania: A new methodological approach for studying percussive stone artefacts. J. Archaeol. Sci. Rep., 20, pp. 611-621. DOI: https://doi.org/10.1016/j.jasrep.2018.06.003.

Bienenfeld P. (1995) Duplicating Archaeological Microwear Polishes with Epoxy Casts. Lithic Technology, 20(1), pp. 29-39.

Birarda G., Badetti E., Cagnato C., Sorrentino G., Pantyukhina I., Stani C., Dal Zilio S., Khlopachev G., Covalenco, Obada T., Skakun N., Sinytsin N., Terekhina V., Marcomini A., Lubritto, Vaccari E., Longo L. (submitted). Morpho-chemical characterization of individual ancient starches from Palaeolithic Pontic Steppe ground stones. Sci. Rep.

Birarda G., Cagnato C., Cefarin N., Stani C., Pantyukhina I., Badetti E., Covalenco S., Marcomini A., Obada T., Sava E., Sorrentino G., Skakun N., Vaccari L., Longo L. (2020). Direct morpho-chemical characterization of elusive plant residues from Aurignacian Pontic Steppe ground stones: supper's ready for Homo sapiens. BioRxiv.

Blateryron F. (2013). The areal field parameters. In: R. Leach (ed.), Characterisation of Areal Surface Texture. Springer-Verlag Berlin Heidelberg. DOI: 10.1007/978-3-642-36458-7_2.

Bofill M. (2012). Quantitative analysis of use-wear patterns: a functional approach to the study ogf grinding stones. In: Broadening Horizon. Conference of young researchers working in the Ancient Near East. Universitat Autònoma de Barcelona, Belleterra, pp. 63-84.

Bofill M., Procopiou H., Vargioluc R., Zahouanic H. (2013). Use-wear analysis of Near Eastern prehistoric grinding stones. In: Regards croisés sur les outils liés au travail des végétaux. An interdisciplinary focus on plant-working tools. XXXIIIe rencontres internationales d'archéologie et d'histoire d'Antibes. P. C. Anderson, C. Cheval et A. Durand (Eds), Éditions APDCA, Antibes, pp. 220-226.

Borel A., Ollé A., Vergès J.M., Sala R. (2014). Scanning Electron and Optical Light Microscopy: two complementary approaches for the understanding and interpretation of usewear and residues on stone tools. J. Archaeol. Sci., 48, pp. 46-59. DOI: http://dx.doi.org/10.1016/j.jas.2013.06.031.

Borri C., Paggi M. (2015). Topological characterization of antireflective and hydrophobic rough surfaces: are random process theory and fractal modeling applicable? J. Phys. D: Appl. Phys., 48(4), 045301. DOI: 10.1088/0022-3727/48/4/045301

Borziac I. (1988). Report Dniester expedition about field research in 1987. Academy of sciences of the Moldovan SSR, Department of archaeology of ethnography and art, Department of archaeology (in Russian). Отчет. Днестровской экспединии о полевых исследованиях в 1987 году. Академия наук Молдавской ССР. Отдел археологии этнографии и искусствоведения. Отдел археологии.

Borziac I., Chirica V., Valeanu M.C. (2006). Culture Et Sociétés Pendant Le Paléolithique Supérieur À Travers L'espace Carpato - Dniestréen. Iasi, Bucarest. ISBN: 973-716-495-4.

Borziac I.A. (1984). Verkhnepaleoliticheskaya stoyanka Gordineshty I v Poprut'ye. Stiinta, Chisinau, Moldova (in Russian).

Brink J.W. (1978). The role of abrasives in the formation of lithic use-wear. J. Archaeol. Sci., 5, pp 363-371. DOI: https://doi.org/10.1016/0305-4403(78)90055-9.

Brunson (accessed in May 2023). Scale Bar for laser trackers. Available online from: https://www.brunson.us/products/laser-tracker-products/metrology-3d-measurement-smr-target-holders-scale-bars.html.

Calandra I., Gneisinger W., Marreiros J. (2020). A versatile mechanized setup for controlled experiments in archeology. Sci. Technol. Archaeol. Res., 6, pp. 30-40. DOI: https://doi.org/10.1080/20548923.2020.1757899.

Calandra I., Schunk L., Bob K., Gneisinger W., Pedergnana A., Paixao E., Hildebrandt A., Marreiros J. (2019a). The effect of numerical aperture on quantitative use-wear studies and its implication on reproducibility. Sci Rep 9, 6313. DOI: https://doi.org/10.1038/s41598-019-42713-w.

Calandra I., Schunk L., Rodriguez A., Gneisinger W., Pedergnana A., Paixao E., Pereira T., Iovita R., Marreiros J. (2019b). Back to the edge: relative coordinate system for use-wear analysis. Archaeol Anthropol Sci, 11, pp. 5937-5948. DOI: https://doi.org/10.1007/s12520-019-00801-y.

Caricola I., Zupancich A., Moscone D., Mutri G., Falcucci A., Duches R., Peresani M., Cristiani C. (2018). An integrated method for understanding the function of macro-lithic tools. Use wear, 3D and spatial analyses of an Early Upper Palaeolithic assemblage from North Eastern Italy. PLoS ONE, 13(12), pp. 1-46. DOI: https://doi.org/10.1371/journal.pone.0207773.

Carta geologica d'Italia 1:100.000, Foglio 136 (accessed on 22nd February 2023). Available online from: sgi.isprambiente.it/geologia100k/mostra_foglio.aspx?numero_foglio=136.

Caruana M.V., Carvalho S., Braun D.R., Presnyakova D., Haslam M., Archer W., Bobe R., Harris J.W.K. (2014). Quantifying traces of tool use: a novel morphometric analysis of damage patterns on percussive tools. PLoS ONE, 9(11), e112856.

Charciumaru M., Nitu E.C., Obada T., Cirstina O., Covalenco S., Lupu F.I., Leu M., Nicolae A. (2019). Personal ornaments in the Mid Upper Palaeolithic east of the Carpatians. Paleo, 30(1), pp. 80-97.

Chetraru N.A. (1965a). Investigations of paleolithic groths in the north-west of moldova. In: Nature protection in Moldova. Academy of Sciences of the Moldovan SSR commission for nature protection, vol. 3, pp. 60-78 (in Russian). Исследование палеонтологических гротов северо-запада Молдавии. Охрана природы молдавии. Академия наук молдавской сср комиссия по охране природы; выпуск 3.

Chetraru N.A. (1965b). Report on field studies of the Paleolithic district of the Prut-Dniester and Moldavian archaeological expeditions in 1963-1964, at the village Buteshty. Chisinau, Archive of the National Museum of the History of Moldova, 23 (in Russian).

Chetraru N.A. (1970.) Unikal'nyi predmet paleoliticheskogo iskusstva iz grota Brynzeny I. In: Okhrana Prirody Moldavii, 8, pp. 133–138 (in Russian).

Chetraru N.A. (1973). Pamyatniki Epokh Paleolita i Mezolita.Stiinta, Chisinau, Moldova (in Russian).

Chetraru N.A. (1989). Amulet iz pozdnepaleoliticheskoi stoyanki v grote Brynzeny I. In: Pamyatniki drevneishego iskusstva na territorii Moldavii. Borziac I.A. (ed.) Stiinta, Chisinau, Moldova, pp. 5–10 (in Russian).

Chirica V., Borziac I., Chetraru N. (1996). Les Gisements du Paléolithique Supérieur Ancien entre le Dniestr et la Tissa. Iași: Helios.

Coles J. (1979). A theory. In: Experimental Archaeology. Coles J. (Ed.) Accademic press, London, pp. 1-7.

Comis L. (2021). L'archeologia sperimentale e il contributo delle scienze sociali. Una proposta filosofica per l'integrazione dei metodi e la disseminazione. Archeologie sperimentali. Temi, metodi, ricerche, 2, pp. 1-10. DOI: https://doi.org/10.13135/2724-2501/2_2021.

Corollo V., Paggi M., Reinoso J. (2019). The steady-state Archard adhesive wear problem revisited based on the phase field approach to fracture. Int. J. Fract.215, pp.39–48. DOI: https://doi.org/10.1007/s10704-018-0329-0.

Cristiani E., Zupancich A. (2020). Sandstone Ground Stone Technology: a Multi-level Use Wear and Residue Approach to Investigate the Function of Pounding and Grinding Tools. J. Archaeol., 28, pp. 704-725. DOI: 10.1028/s41598-020-72276-0.

Cristiani E., Zupancich A., Duches R., Carra M., Caricola I., Fontana A., Flor E., Fontana F. (2021). Non-flaked stones used in the Mesolithic Eastern Alpine Region: A functional assessment from Romagnano Loc III and Pradestel sites. J. Archaeol. Sci: Rep., 31, 102928. DOI: https://doi.org/10.1016/j.jasrep.2021.102928.

Crowther A., Haslam M., Oakden M., Walde D., Mercader J. (2014). Documenting contamination in ancient starch laboratories. J. Archaeol. Sci., 49, pp. 90-104. DOI: https://doi.org/10.1016/j.jas.2014.04.0223.

Czichos H. (1978). Tribology: A Systems Approach to the Science and Technology of Friction, Lubrication, and Wear. Tribology Series 1. Elsevier Scientific Publishing Co., New York, p. 399.

David A., Pascari V. (2012). Recifele de la Brinzeni: Monument natural valoros si unical din Republica Moldova. Modul ambient, 6(66), pp. 13-17.

David N. (1998). The Ethnoarchaeology and Field Archaeology of Grinding at Sukur, Adamawa State, Nigeria. African Archaeological Review, 15 (1), pp. 13-63.

de Beaune S.A. (2004). The invention of technology: Prehistory and cognition. Current Anthropology, 45(2), pp. 139-162.

de la Torre I., Benito-Calvo A., Arroyo A., Zupancich A., Proffitt T. (2012). Experimental protocols for the study of battered stone anvils from Olduvai Gorge (Tanzania). J. Archaeol. Sci., 40(1), pp. 313-332. DOI: https://doi.org/10.1016/j.jas.2012.08.007.

Delgado-Raack S., de Tobaruela J.M., Bettinardi I., Soldevilla J.A., Risch R. (2022). Surface roughness as a quantitative approach to use-wear on macrolithic tools: A comparative analysis. J. Archaeol. Sci. Rep., 46, 102645.

Delgado-Raack S., Gómez-Gras D., Risch R. (2009). The mechanical properties of macrolithic artifacts: a methodological background for functional analysis. J. Archaeol. Sci., 36(9), pp. 1823-1831. DOI: https://doi.org/10.1016/j.jas.2009.03.033.

Denkena B., Bergmann B., Raffalt D. (2023). Sharpening of graded diamond grinding wheels. SN Appl. Sci. 5, 145. DOI: https://doi.org/10.1007/s42452-023-05362-3.

DeRose J., Doppler M. (2018). What Does 30,000:1 Magnification Really Mean? Some useful guidelines for understanding magnification in today's new digital microscope era. Available online from: https://www.leica-microsystems.com/science-lab/applied/what-does-300001-magnification-really-mean.

Dozier C. (2016). Airborne Starch Dispersal from Stone Grinding: Experimental Results and Implications. J. Archaeol. Sci. Rep., 8, pp. 112–115. DOI: 10.1016/j.jasrep.2016.05.057.

Dubreuil L. (2001). Functional studies of Prehistoric Grindingstones: A methodological research. Bulletin du Centre de recherche francais à Jérusalem, 9, pp. 73-87.

Dubreuil L. (2004). Long-term trends in Natufian subsistence: a use-wear analysis of ground stone tools. J. Archaeol. Sci., 31, pp. 1613-1629. DOI: 10.1016/j.jas.2004.04.003.

Dubreuil L., Grosman L. (2009). Ochre and hide-working at a Natufian burial place. Antiquity, 83, pp. 935–954. DOI: 10.1017/S0003598X00099269.

Dubreuil L., Nadel D. (2015). The development of plant food processingin the Levant: insights from use-wear analysis of Early Epipalaeolithic ground stone tools. Phil. Trans. R. Soc. B, 370, 20140357.

Dubreuil L., Savage D. (2014). Ground stones: a synthesis of the use-wear approach. J. Archaeol. Sci. 48, pp. 139-153. DOI: 10.1016/j.jas.2013.06.023.

Dubreuil L., Savage D., Delgado-Raack S., Plisson H., Stephenson B., De La Torre I. (2015). Current analytical frameworks for studies of use– wear on ground stone tools. In: Use-

wear and residue analysis in archaeology; João Manuel Marreiros, Juan F. Gibaja Bao, Nuno Ferreira Bicho, Eds. Springer Cham, pp. 105–158.

Eastaugh N., Walsh V., Chaplin T., Siddall R. (2008). Pigment Compendium, a Dictionary and Optical Microscopy of Historical Pigments, Butterworth-Heinemann, Italy.

Ebeling J.R., Rowan Y.M. (2004). The Archaeology of the Daily Grind: Ground Stone Tools and Food Production in the Southern Levant. NEA, 67(2), pp. 108-117.

Eren M., Lycett S., Patten R., Buchanan B., Pargeter J., O'Brien M. (2016). Test, model, and method validation: the role of experimental stone artifact replication in hypothesis-driven archeology. Ethnoarcheology, 8(2), pp. 103–136. DOI: https://doi.org/10.1080/19442890.2016.1213972.

Evans A.A., Donahu R.E. (2008). Laser scanning confocal microscopy: a potential technique for the study of lithic microwear. J. Archaeol. Sci., 35, pp. 2223-2230. DOI: 10.1016/j.jas.2008.02.006.

Evans A.A., Macdonald D.A.; Giusca C.L.; Leach R.K. (2014). New method development in prehistoric stone tool research: evaluating use duration and data analysis protocols. Micron, 65. pp. 69-75. DOI: 10.1016/j.micron.2014.04.006.

Fraser C.S. (1997). Digital camera self-calibration. ISPRS Journal of Photogrammetry and Remote sensing, 52(4), pp. 149-159.

Fullagar R. (2014). Residues and Usewear. In: Archaeology in Practice: A Student Guide to Archaeological Analyses. Balme J., Paterson A. (Eds). Malden: Blackwell Publishing, second edition, pp. 232-263.

Fullagar R., Field J. (1997). Pleistocene seed-grinding implements from the Australian arid zone. Antiquity, 71(272), pp. 300-307. DOI: 10.1017/S0003598X00084921.

Fullagar R.L.K. (1991). The role of silica in polish formation. J. Archaeol. Sci., 18(1), pp. 1-24. DOI: https://doi.org/10.1016/0305-4403(91)90076-2.

Gašparović M., Malarić I. (2012). Increase of readability and accuracy of 2D models using fusion of close-range photogrammetry and laser scanning. In: ISPRS - International Archives of the Photogrammetry Remote Sensing and Spatial Information Sciences. Shortis M, Mills J. (Eds), Vol. XXXIX-B5. XXII ISPRS Congress, 25 August – 01

September 2012, Melbourne, Australia. DOI: 10.5194/isprsarchives-XXXIX-B5-93-2012.

Геологическая карта Молдовы Молдавской 1:200000, 1985 г.

Goodall R., Darras L., Purnell, M. (2015). Accuracy and Precision of Silicon Based Impression Media for Quantitative Areal Texture Analysis. Sci Rep., 5, pp. 10800. DOI: https://doi.org/10.1038/srep10800.

Green S., Bevan A., Shapland M. (2014). A comparative assessment of structure from motion methods for archaeological research. J. Archaeol. Sci., 46, pp. 172-181.

Grishchenko M.N. (1969). Materialy po geologicheskoi kharakteristike nekotorykh arkheologicheskikh pamyatnikovv peshcherakh i grotakh Severo-Zapadnoi Moldavii. Okhrana Prirody Moldavii, 7, pp. 135–146.

Grosman L. (2016). Reaching the point of no return: the computational revolution in archaeology. Annu. Rev. Antrophol., 45, pp. 129-145.

Hamon C. (2008). Functional analysis of stone grinding and polishing tools from the earliest Neolithic of north-western Europe. J. Archaeol. Sci. 35, pp. 1502-1520. DOI: 10.1016/j.jas.2007.10.017.

Hardy B.L. (2010). Climatic variability and plant food distribution in Pleistocene Europe: implications for Neanderthals diet and subsistence. Quat. Sci. Rev., 29, pp. 662-679. DOI: https://doi.org/10.1016/j.quascirev.2009.11.016.

Haury E.W. (1950). The Stratigraphy and Archaeology of Ventana Cave, Arizona. University of Arizona Press, Tucson, Arizona, p. 325.

Hayden B. (1979). Lithic Use-Wear Analysis. New York: Academic.

Hayden B. (1987). Lithic studies among the contemporary Highland Maya. University of Arizona Press, Tucson, p. 387.

Hayes E.H., Field J.H., Coster A.C.F., Fullagar R., Matheson C., Florin S.A., Nango M., Djandjomerr D., Marwick B., Wallis L.A., Smith M.A., Clarkson C. (2021). Holocene grinding stones at Madjedbebe reveal the processing of starchy plant taxa and animal tissue. J. Archaeol. Sci. Rep., 25, 102754.

Hayes E.H., Fullagar R., Field J.H., Coster A.C.F., Matheson C., Nango M., Djandjomerr D., Marwick B., Wallis L.A., Smith M.A., Clarkson C. (2022). 65,000-years of continuous grinding stone use at Madjedbebe, Northern Australia. Sci. Rep., 12, 11747.

Hayes H.E., Cnuts D., Lepers C., Rots V. (2017). Learning from blind tests: Determining the function of experimental grinding stones through use-wear and residue analysis. J. Archaeol. Sci. Rep., 11, pp. 245–260. DOI: http://dx.doi.org/10.1016/j.jasrep.2016.12.001.

Hayesa E., Pardoe C., Fullagara R. (2018). Sandstone grinding/pounding tools: Use-trace reference libraries and Australian archaeological applications. J. Archaeol. Sci. Rep., 20, pp. 97-114. DOI: https://doi.org/10.1016/j.jasrep.2018.04.021.

Hodgskiss T. (2010). Identifying grinding, scoring and rubbing use-wear on experimental ochre pieces. J. Archaeol. Sci., 37(12), pp. 3344-3358. DOI: https://doi.org/10.1016/j.jas.2010.08.003.

Hoffecker J.F. (2009). Neanderthal and Modern Human dietin Eastern Europe. In: The evolution of Hominin diet: Integrating Approaches to the Study of Paleolithic Subsistence, Hubin J.J. and Richards M.P. (Eds.), Springer science, pp. 87-98. ISBN: 9781402096982.

Hole F., Flannery K.V., Neely J.A. (1969). Prehistory and human ecology of the Deh Luran plain: an early village sequence from Khuzistan, Iran. University of Michigan Press, p. 514.

Horsfall G.A. (1979). A Design Theory Perspective on Variability in Grinding Stones. Master of Arts Thesis at the Department of Archaeology, Simon Fraser University, Burnaby, p. 122.

Jeyaprakash N., Yang C.H. (2020). Friction, Lubrication, and Wear. In Tribology in Materials and Manufacturing. Patnaik A., Singh T., Kukshal V. (Eds). IntechOpen. DOI: 10.5772/intechopen.93796.

Jolie P.M., McBrinn B.S. (2010) Experimental Zooarcheology: Research Direction and Methods. In: Designing Experimental Research in Archaeology, Examining Technology through Production and Use. Ferguson J.R. (Ed), University Press of Colorado, Boulder, pp. 241-258. ISBN: 978-1-60732-022-7.

Kapsa P. (2004). Généralités sur l'usure. In: La tribologie. Comment la science fait parler les vestiges archéologiques. Georges J.M, Zahouani H., Kapsa P., Vargiolu R. (Eds). Dossiers d'archéologie, 290, Faton, pp. 8-9. ISBN: 5552001555140.

Karami A., Menna F., Remondino F., Varshosaz M. (2022). Exploiting light directionality for image-based 3d reconstruction of non-collaborative surfaces. The Photogrammetric Record., 37(177), pp. 111-138.

Keeley L.H. (1980). Experimental Determination of Stone Tool Uses: A Microwear Analysis. Chicago: University of Chicago Press.

Keyence (2023). Area Roughness Parameters (acccessed on 11th May 2023). Available online from:
https://www.keyence.com/ss/products/microscope/roughness/surface/parameters.jsp.

Kováč M., Andreyeva-Grigorovich A., Bajraktarević Z., Brzobohatý R., Filipescu S., Fodor L., Harzhauser M., Nagymarosy A., Oszczypko N., Pavelić D., Rögl F., Saftić B., Sliva U., Studencka B. (2007). Badenian evolution of the Central Paratethys Sea: paleogeography, climate and eustatic sea-level changes. Geologica Carpathica, 58(6), pp. 579-606.

Kraybill N. (1977). Pre-Agricultural Tools for the Preparation of Foods in the Old World. In: Origins of Agriculture. Reed C.A. (Ed.). World Anthropology, De Gruyter Mouton, Berlin, New Yorkton, pp. 485-522. DOI: https://doi.org/10.1515/9783110813487.

Kulzer Mitsui chemicals group (2021). Provil novo: Informazione prodotto (acccessed on 16th Februray 2023). Available online from: kulzer-dental.it/IT/downloads/further_products_2/provil_1/Provilnovo_ProdInfo_Logo_Kulzer.pdf.

Laetsch T., Downs R. (2006) Software for identification and refinement of cell parameters from powder diffraction data of minerals using the RRUFF Project and American Mineralogist Crystal Structure Databases. Abstracts from the 19th General Meeting of the International Mineralogical Association, Kobe, Japan, 23-28 July 2006.

Lafuente B., Downs R.T., Yang H., Stone N. (2015) The power of databases: the RRUFF project. In: Highlights in Mineralogical Crystallography, Armbruster T., Danisi R.M. (eds.) Berlin, Germany, W. De Gruyter, pp. 1-30.

Leach R. (2013). Introduction to surface topography. In: Charactreization of areal surface texture. Leach R (Ed.), Springer, Berlin, pp. 1-13.

Leica microsystem (2023). Leica DCM 3D. Aveilable from: www.leica-microsystems.com.

Lerner H. (2007). Digital image analysis and use-wear accrual as a function of raw material: an example from Northwestern New Mexico. Lithic Technol., 32, pp. 51-67. DOI: https://doi.org/10.1080/01977261.2007.11721043.

Liu L., Field J., Fullagar R., Bestel S., Chen X., Ma X. (2010). What did grinding stones grind? New light on Early Neolithic subsistence economy in the middle Yellow River Valley, China. Antiquity, 84, pp. 813–833. DOI: 10.1017/S0003598X00100249.

Longo L, Birarda G., Cagnato C., Badetti E., Covalenco S., Pantyukhina I., Skakun N., Vaccari L., Terekhina, V., Sorrentino, G. (2022). Coupling the beams: How controlled extraction methods and FTIR-spectroscopy, OM and SEM reveal the grinding of starchy plants in the Pontic steppe 36,000 years ago. J. Archaeol. Sci. Rep., 41. DOI: https://doi.org/10.1016/j.jasrep.2021.103333.

Longo L. (1994). Le industrie litiche. L'analisi delle tracce d'uso. In: Le industrie litiche del giacimento paleolitico di Isernia la Pineta. La tipologia, le tracce di utilizzazione, la sperimentazione. Peretto C. (Ed). Cosmo Iannone, Isernia, pp. pp. 355-404. ISBN: 8851600031.

Longo L. (2016). Gestures from the Past: Grinding Stones and Starchy Food Processing at the Dawn of Modern Humans. In: Proceedings of 22nd International Conference on Virtual System & Multimedia (VSMM), Kuala Lumpur, Malaysia, 17-21 Oct. 2016, pp. 1-7. DOI: 10.1109/VSMM.2016.7863149.

Longo L., Altieri S., Birarda G., Cagnato C., Cefarin N., Graziani V., Obada T., Pantyukhina I., Ricci P., Skakun N., Sorrentino G., Terekhina V., Tortora L., Vaccari L., Lubritto C. (2021a). A Multi-Dimensional Approach to Investigate Use-Related Biogenic Residues on Palaeolithic Ground Stone Tools. Environ. Archaeol. DOI: https://doi.org/10.1080/14614103.2021.1975252.

Longo L., Iovino M.R., Lemorini C. (2000). L'analisi funzionale per lo studio delle industrie litiche. Rivista di scienze preistoriche, LI, 2000-2001, pp. 389-454.

Longo L., Skakun N.N. (2008) Introduction "Prehistoric Technology" 40 years later: functional studies and the Russian Legacy Interpreting Stone Tools. In: Proceedings of the International Congress. Longo L., Skakun N. (Eds.), Prehistoric Technology' 40 Years Later: Functional Studies and the Russian Legacy. Verona (Italy), 20 - 23 April 2005. BAR Int., 1783, Oxford, pp. ix-xiii.

Longo L., Skakun N.N., Pantyukhina I.E., Terekhina V.V, Sorrentino G. (2021b). Aurignacian grinding stone from Surein I (Crimea): "trace-ing" the roots of starch-based diet. J. Archaeol. Sci.Rep., 38, 102999. DOI: https://doi.org/10.1016/j.jasrep.2021.102999.

Longo L., Skakun N.N., Sorrentino G., Vassallo V., Abate D., Terekhina V., Sinitsyn A., Khlopachev G., Hermon S. (2018). Les gestes retrouves: A 3D visualisation approach to the functional study of Early Upper Palaeolithic grinding stones. In: Exploring Oceans of Data. Matsumoto, M., Uleberg, E. (Eds.). CAA 2016, Oslo. Archaeopress, Oxford, pp. 447–455. ISBN: 9781784917302.

Macdonald D., Harman R., Evans A.A. (2018). Replicating surface texture: preliminary testing of molding compound accuracy for surface measurements. J. Archaeol. Sci. Rep., 18, pp. 839-846. DOI: https://doi.org/10.1016/j.jasrep.2018.02.033.

Macdonald D.A., Liye X., Gallo T. (2019). Here's the dirt: First applications of confocal microscopy for quantifying microwear on experimental ground stone earth working tools. J. Archaeol. Sci. Rep., 26, 101861. DOI: https://doi.org/10.1016/j.jasrep.2019.05.026.

Magnani M., Douglass M., Porter S.T. (2016). Closing the seams: resolving frequently encountered issues in photogrammetric modelling. Antiquity., 90(354), pp. 1654–1669. DOI: https://doi.org/10.15184/aqy.2016.211.

Magnani M., Douglass M., Schroder W., Reeves J., Braun D.R. (2020). The digital revolution to come: photogrammetry in archaeological practice. Am. Antiq., 85(4), pp. 737-760. DOI: https://doi.org/10.1017/aaq.2020.59.

Marreiros J., Calandra I., Gneisinger W., Paixão E., Pedergnana A., Schunk L. (2020). Rethinking Use-Wear Analysis and Experimentation as Applied to the Study of Past Hominin Tool Use. J. Paleolit. Archaeol., 3, pp. 475–502. DOI: https://doi.org/10.1007/s41982-020-00058-1.

Marsh E.J., Jeffrey R.F. (2010). Introduction. In: Designing Experimental Research in Archaeology, Examining Technology through Production and Use. Ferguson J.R. (Ed), University Press of Colorado, Boulder, pp. 1-12. ISBN 978-1-60732-022-7.

Martisius N.L., Sidéra I., Grote M.N., Steele T.E., McPherron S.P., Schulz-Kornas E. (2018) Time wears on: assessing how bone wears using 3D surface texture analysis. PLoS One, 13, e0206078. DOI: https://doi.org/10.1371/journal.pone.0206078.

Marulli M.R., Sorrentino G., Menna F., Paggi M. (2023). Digital twin models of replicative ground stones: insight into simulating usage of Upper Paleolithic tools. Sci. Rep. DOI: https://doi.org/10.1038/s41598-023-45425-4.

Mathieu J.R. (2002). Introduction. In: Experimental Archaeology: Replicating Past Objects, Behaviors, and Processes. Mathieu J.R. (Ed.) BAR international series, 1035, Archaeopress, Oxford, pp. 1-4. ISBN: 1-84171-415-1.

Mauldin R.P. (1993). The Relationship between Ground Stone and Agricultural Intensification in Western New Mexico. Kiva, 58(3), pp. 317–330. DOI: 10.1080/00231940.1993.11758212.

McCartney C., Sorrentino G. (2019). Ayia Varvara a preliminary analysis of stone tools used in pigment processing and tanning with ochre. In: Astruc L., McCartney C., Briois F., Kassianidou V. (Eds.). Near Eastern Lithic Technologies on the Move. Interactions and Contexts in Neolithic Traditions, Studies in Mediterranean Archaeology, 150, pp. 63-78. ISBN: 978-9925-7455-3-1.

Morris D.H. (1990). Changes in Groundstone Following the Introduction of Maize into the American Southwest. J. Anthropol. Res., 46(2), pp. 177-194. DOI: https://www.jstor.org/stable/3630071.

Myshkin M.K., Grigoriev A.Ya., Chizhik S.A., Choi K.Y., Petrokovets M.I. (2003). Surface roughness and texture analysis in microscale. Wear, 254, pp. 1001-1009. DOI: :10.1016/S0043-1648(03)00306-5.

Myshkin N.K., Grigoriev A.Ya. (2013). Roughness and texture concept in Tribology. Tribology in Industry, 35(2), pp. 97–103.

Nečas D., Klapetek P. (2012). Gwyddion: an open-source software for SPM data analysis. Cent. Eur. J. Phys., 10, pp. 181–188.

Nicolae C., Nocerino E., Menna F., Remondino F. (2014). Photogrammetry applied to problematic artefacts. In: Remondino F., Menna F. (Eds.), ISPRS Archives XL-5, pp. 451–456.

Noiret P. (2009). Brynzeni I. In: Le Paléolithique supérieur de la Moldavie, Noiret P. (Ed.), Liège, pp. 425–470. ISBN: 978-2-920495-06-4.

Noiret P., Otte M. (2010). Aurignacian and Gravettian occupation in Eastern Europe between 33.00 and 23.000 uncal BP. OIS 3 Conference.

Odell G.H. (1977). The application of micro-wear analysis to the lithic component of an entire prehistoric settlement: methods, problems, and functional reconstructions. PhD Thesis, Harvard University, Cambridge.

Ollé A., Vergès J.M. (2014). The use of sequential experiments and SEM in documenting stone tool microwear. J. Archaeol. Sci., 48, pp. 60-72. DOI: https://doi.org/10.1016/j.jas.2013.10.028.

Otte M., Lopez-Bayon I., Noiret P., Borziac I., Chirica V. (1996). Recherchess ur le Paléolithique supérieur de la Moldavie. Anthropologie et Préhistoire, 107, pp. 45-80.

Outram A.K. (2008). Introduction to experimental archeology. World Archeology, 40(1), pp. 1–6. DOI: https://doi.org/10.1080/00438240801889456.

Paggi M., Ciavarella M. (2010). The coeffecent of proportionality $\varkappa$ between real contact and load with new asperity models. Wear, 268, pp. 1020-1029.

Paixão E., Marreiros J., Dubreuil L., Gneisinger W., Carver G., Prévost M., Zaidner Y. (2022). The Middle Paleolithic Ground Stones Tools of Nesher Ramla Unit V (Southern Levant): A multi-scale use-wear approach for assessing the assemblage functional variability. Quat. Int. 624, pp. 94-106. DOI: 10.31219/osf.io/gyvw8.

Paixão E., Pedergnana A., Marreiros J., Dubreuil L., Prévost M., Zaidner Y., Carver G., Gneisinger W. (2021). Using mechanical experiments to study ground stone tool use: Exploring the formation of percussive and grinding wear traces on limestone tools. J. Archaeol. Sci. Rep., 37. DOI: https://doi.org/10.1016/j.jasrep.2021.102971.

Pargeter J. (2012). Rock Type Variability and Impact Fracture Formation: Working Towards a more Robust Macrofracture Method. J. Archaeol. Sci., 40, pp. 4056–4065. DOI: 10.1016/j.jas.2012.05.021.

Pedergnana A., Ollé A. (2017). Monitoring and interpreting the use-wear formation processes on quartzite flakes through sequential experiments. Quat. Int, 427, pp. 25-65. DOI: http://dx.doi.org/10.1016/j.quaint.2016.01.052.

Plisson H., Lompré A. (2008). Technician or researcher? A visual answer. In: Proceedings of the International Congress. Longo L., Skakun N. (Eds.), Prehistoric 'Technology' 40 Years Later: Functional Studies and the Russian Legacy. Verona (Italy), 20 - 23 April 2005. BAR Int., 1783, Oxford, pp. 497 - 501.

Porter S.T., Roussel M., Soressi M. (2016). A simple photogrammetry rig for the reliable creation of 3D artifact models in the field. Adv. Archaeol., 4(1), pp. 71-86. DOI: 10.7183/2326-3768.4.1.71.

Revenco M., Castraveţ T., Nicu I.C. (2016). Microzona Saharna. Caracterizare geografică. In: Evoluţia habitatului din microzona Saharna in epoca Fierului. Niculiþă I., Zanoci A., Băþ M. (Eds.), Chişinău, pp. 9-18. ISBN: 978-9975-80-903-0.

Reynolds, P.J. (1999). The nature of experiment in archaeology. In: Experiment and Design: Archaeological Studies in Honour of John Coles. Harding A.F. (Ed.). Oxbow Books, Oxford, pp. 156-162.

Rifkin R.F. (2012). Processing ochre in the Middle Stone Age: Testing the inference of prehistoric behaviours from actualistically derived experimental data. J. Anthropol. Archaeol., 31(2), pp. 174-195. DOI: https://doi.org/10.1016/j.jaa.2011.11.004.

Rosso D.E., Pitarch Martí A., d'Errico F. (2016). Middle Stone Age Ochre Processing and Behavioural Complexity in the Horn of Africa: Evidence from Porc-Epic Cave, Dire Dawa, Ethiopia. PLoS ONE, 11(11), e0164793. DOI: https://doi.org/10.1371/journal.pone.0164793.

Rowan Y.M., Ebeling J.R. (2008). Introduction: The Potential of GroundStone Studies. In: New Approaches to Old Stones. Recent Studies of Ground Stone Artifacts. Rowan Y.M., Ebeling J.R. (Eds.). Ebeling Equinox Publishing Ltd, London; pp. 1-15. ISBN 1 84553 044 6.

Sapirstein P. (2018). A high-precision photogrammetric recording system for small artifacts. J. Cult. Herit., 31, pp. 33–45. DOI: https://doi.org/10.1016/j.culher.2017.10.011.

Schiffer M.B. (1976). Behavioral Archeology. Academic Press, New York, p. 222.

Schmidt P., Rodriguez A., Yanamandra K., Behera R.K., Iovita R. (2020). The mineralogy and structure of use-wear polish on chert. Sci Rep., 10, 21512. DOI: https://doi.org/10.1038/s41598-020-78490-0.

Semenov S.A. (1964) Prehistoric Technology. 1st ed. New York: Barnes and Noble.

Sharma A. (2020). Skewness & Kurtosis Simplified. What is Skewness and how do we detect it? Available online from at: towardsdatascience.com/skewness-kurtosis-simplified-1338e094fc85

Shott M. (2014). Digitalizing archaeology: a subtle revolution in analysis. World Archaeol., 46(1), pp. 1-9.

Sing A.K. (2021). Interpretation of Measures of Shape: Skewness & Kurtosis. Available online from: https://ashington.medium.com/interpretation-of-measures-of-shape-skewness-kurtosis-b8b87c72c65.

Sirenko S.A., Mel'nichuk I.V., Turlo S. I. (1990). Progress in study and reconstruction of Anthropogenic paleo landscapes of the Ukraine. Development of Geography in Ukrainian SSR, Naukova dumka, Kiev, pp. 50-63. (In Russian).

Sorrentino G. (2023). Raw Data Examples for Close-Range Photogrammetry of Replicative Experiments on Ground Stone Tools (Data set). PLOS ONE. Zenodo. https://doi.org/10.5281/zenodo.8196541.

Sorrentino G., Lo Giudice A., Re A., Borghi, A., Longo L. (2021a). Più di un semplice ciottolo: Un protocollo sperimentale per la comprensione del ruolo di strumenti macrolitici nella trasformazione delle risorse vegetali nel Paleolitico Superiore in Eurasia. Archeologie sperimentali. Temi, metodi, ricerche, 2, pp. 24-40. DOI: https://doi.org/10.13135/2724-2501/2_2021.

Sorrentino G., Lo Giudice A., Re A., Borghi, A., Longo L. (2021b). Replicate Plant Processing REVEALs Ground Stones complex Biography. EXARC, EAC12 World Tour: Session 13. Available online from: https://youtu.be/vvJLDTX13Fo.

Sorrentino G., Longo L., Obada T., Borghi A., Re A., Paggi M., Lo Giudice A. (2023a). Tracing Old Gestures: A Multiscale Analysis of Ground Stone Tools Developed on Sequential Lab-Controlled Replicative Experiments. Heritage, 6, pp. 4737–4767. DOI: doi.org/10.3390/heritage6060252.

Sorrentino G., Menna F., Remondino F., Paggi M., Longo L., Borghi A., Re A., Lo Giudice A. (2023b). Close-range photogrammetry reveals morphometric changes on replicative ground stones. PLOS ONE, 18(8), e0289807. DOI: //doi.org/10.1371/journal.pone.0289807.

Stahl A. (1989). Plant-food processing: implications for dietary quality. In: Foraging and Farming: The Evolution of Plant Exploitation. Harris D.R., Hillman G.C. (Eds). Unwin Hyman, London, pp. 171-194.

Stark P.B. (2018). Before reproducibility must come preproducibility. Nature, 557, pp. 612. DOI: https://doi.org/10.1028/d41586-018-05256-0.

Stemp W.J. (2014). A review of quantification of lithic use-wear using laser profilometry: a method based on metrology and fractal analysis. J. Archaeol. Sci., 48, pp. 15-25. DOI: http://dx.doi.org/10.1016/j.jas.2013.04.027.

Stemp W.J., Stemp M. (2003) Documenting stages of polish development on experimental stone tools: surface characterization by fractal geometry using UBM laser profilometry. J. Archaeol. Sci., 30, pp. 287-296. DOI: https://doi.org/10.1006/jasc.2002.0837.

Stemp W.J., Watson A., Evans A.A. (2016). Surface analysis of stone and bone tools. Surf. Topogr.: Metrol. Prop., 4(1), 013001. DOI: 10.1088/2051-672X/4/1/013001.

Stepanchuk V.N, Sapozhnikov I.V., Gladkikh M.I., Ryzhov S.N. (2009). Ukrainian Upper Palaeolithic between 40/10.000 BP: current insights into environmental-climatic change and cultural development. Proceedings of the XV World Congress of the International Union for Prehistoric and Protohistoric Sciences, Archaeopress, Oxford, England, pp. 63-74.

Teer D.G., Arnell R.D. (1975). Wear. In: Principles of Tribology. Halling, J. (Ed.), Palgrave, London, pp. 94–127. DOI: https://doi.org/10.1007/978-1-349-04138-1_5.

ThorLabs (accessed in May 2022). Kinematic Bases. Available online from: https://www.thorlabs.com/NewGroupPage9_PF.cfm?Guide=10&Category_ID=12&ObjectGroup_ID=1546.

Tkachuk M.E. (archived in 2017). NewsMaker. Available online from: newsmaker.md.

Tringham R., Cooper G., Odell G.H., Voytek B., Whitman A. (1974). Experimentation in the formation of edge-damage: a new approach to lithic analysis. J. Field Archaeol., 1, pp. 171-196. DOI: https://doi.org/10.1179/jfa.1974.1.1-2.171.

Vakis A.I., Yastrebov V.A., Scheibert J., Nicola L., Dini D., Minfray C., Almqvist A., Paggi M., Lee S., Limbert G., Molinari J-F, Anciaux G., Aghababaei R., Restrepo S.E., Papangelo A., Cammarata A., Nicolini P., Putignano C., Carbone G., Stupkiewicz G., Lengiewicz J., Costagliola G., Bosia F., Guarino R., Pugno N.M., Müser M.H., Ciavarella M. (2008). Modeling and simulation in tribology across scales: An overview. Tribol. Int., 125, pp. 169-199: DOI: 10.1016/j.triboint.2018.02.005

Van Gijn A.L. (2014). Science and interpretation in microwear studies. J. Archaeol. Sci., 48, pp. 166-169. DOI: http://dx.doi.org/10.1016/j.jas.2013.10.024.

Wright K. (1992). A classification system for grinding stone tools from the Prehistoric Levant. Paléorient, 18(2), pp. 53-81.

Wyatt-Spratt S. (2022). After the revolution: a review of 2D modelling as a tool for stone artefact analysis. JCAA, 5(1), pp. 215-227.

Zahouani H., Vargiolu R., Sidorof F. (2004). Le topographie des surfaces. La tribologie, 290, pp. 10-11.

Zavarise G., Borri-Brunetto M., Paggi M. (2007). On the resolution dependence of micromechanical contact models. Wear, 262(1-2), pp. 42-54. DOI: 10.1016/j.wear.2006.03.044

Zupancich A., Cristiani E. (2020). Functional analysis of sandstone ground stone tools: arguments for a qualitative and quantitative synergetic approach. Sci. Rep., 10(1), pp. 1-12. DOI: 10.1028/s41598-020-72276-0.

Zupancich A., Mutri G., Caricola I., Carra M.L., Radini A., Cristiani E. (2019). The application of 2D modeling and spatial analysis in the study of groundstones used in wild plants processing. Archaeol Anthropol Sci. 11, pp. 4801–4827. DOI: https://doi.org/10.1007/s12520-019-00824-5.

Appendix A: The experimental archaeology day

On October 4th, 2021, the writer invited a group of 12 PhD and MA students on the University of Turin to participate in a dedicated day of experimental archaeology. The activity began with the presentations by. Lara Comis, an expert in ethical considerations and Citizen Science, and. Laura Longo, a specialist in palaeoanthropology and functional analysis. Their lectures were titled "Introduction to Experimental Research in Archaeology" and "The Significance of Deductive Reference Collection for Ground Stones", respectively. Following the theoretical introductions, two practical sessions were conducted, involving controlled laboratory experiments that were meticulously documented. The day concluded with a discussion and a Q&A session.

During the practical sessions, the students worked in pairs. Each pair was provided with two stones — one as an active tool and the other as a passive tool — for processing different plants organs as reported in Chapter 5. Although the focus of the experiment was on vegetal resources, ochre was also considered due to the presence of ochre detected on BZ#442.

Each pair of students took turns, with one person mechanically processing the material for 30 minutes while the other documented the activity. Documentation included specific questions about the operator's positions, gesture, and perceptions during the experiment. Participants were also asked to record their partner's activities through notes, photographs, videos, and drawings. A specifically designed form was provided to participants for the purpose of the experiment. The day program, the form, as well as the completed forms submitted by the participants, are presented below. Personal data has been obscured to ensure privacy.

The program

Program:

9.00 – 10.30 Introduction by invited speakers:

- Lara Comis (in remote mode): Introduction to experimental research in archaeology
- Laura Longo: The relevance of deductive reference collection for Ground Stones
- Giusi Sorrentino: Introduction to the activity

10.30-11.00 Coffee break

11.00-13.00 Experimental activities and data collections

13.00-14.30 Break

14.30-16.00 Experimental activities and data collections

16.00-17.00 Q&A and closing of the day

A total of 12 colleagues working in couples:

- Each couples: one mechanically processes the material for 30 min and one documents the activity (alternatively)
  Each couples will be provided with a base and a pestle to be used to process the given material.
  Gloves and protective glasses will be also provided.
- Mechanical process: ponding and grounding different materials: roots, seeds, shelled fruits and ochre
- Documentation: pictures, videos, drawing and notes of the activities during the experiment. Please bring with you your self phone although some cameras, video camera, and tripods are available at the department.

University of Turin, Physics Department
Via Pietro Giuria 1, Torino
For info contact Giusi Sorrentino:
Email: giusi.sorrentino@unito.it

The form

Documentation form

Name: .... Degree: ....

Experimenter Data:

Name: .... Age: .... ☐F ☐M

Approx. height and weight: .... Degree: ....

Experiment Data:

GST ID:

Stone tools ☐ or Wood base and stone pestle ☐   Time: ....

Resource treated: ....

Position of the operator:

....

....

....

....

....

Hand movements:

☐ Vertical (pestling)

☐ Horizontal (grinding):

   ☐ circular

   ☐ linear monodirectional

   ☐ linear bidirectional

Describe: ....

....

....

Workshop_4th October 2021

GS6-GS14: The filled forms

Experiments for Upper Palaeolithic
Ground Stone Tools:
building a deductive reference collection

Documentation form

Name: ... OP-12 .... Degree: ... .

Experimenter Data:

Name: .. OP-10 .... Age: .... ☒ F ☐ M

Approx. height and weight: ....

Experiment Data: GS6 GS14

Sone tools ☒   or   Wood base and stone pestle ☐   Time: ... T1 ......

Resource treated: ECHINOCADA ....

Position of the operator:

inginocchiata e talvolta
seduta
la posizione varia tra le 3
illustrate in modo ciclico
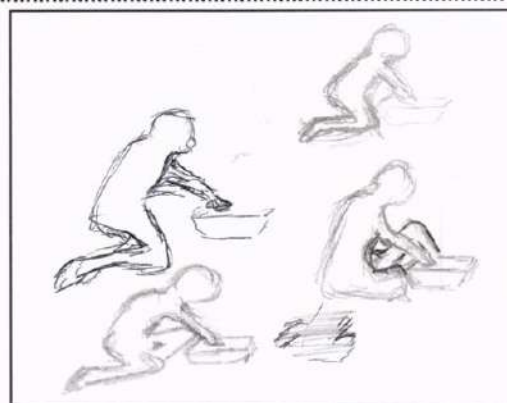
Hand movements:

☐ Vertical (pestling)

☒ Horizontal (grinding):

   ☒ circular

   ☐ linear monodirectional

   ☒ linear bidirectional

Describe: ... circolare (~60-90) ...
alternato a movimenti lineari
Con la mano si impugna perfettamente
la pietra *

*Si e' osservato che movimento
migliore e' lineare bidirezionale
e infine circolare

Workshop_4th October 2021

263

Experiments for Upper Palaeolithic Ground Stone Tools: building a deductive reference collection

Documentation form

Name: ...... OP-10 .... Degree: ... .

Experimenter Data:

Name: .... OP-12 .... Age: ☒F ☐M

Approx. height and weight: .:

Experiment Data: GS6 GS14

Stone tools ☒ or Wood base and stone pestle ☐   Time: ..... T2 ......

Resource treated: .... ECHINOCLOA

Position of the operator:

Seduta di fronte alla bacinella, la
pietra di base i mator piatto di
180° rispetto alla posizione T1.
Inizia battendo con l'autra pietra
sui vegetali per poi compiere
movimenti lineari avanti e indietro
con la mano DX macina e con la
SX tiene la pietra di base.
Dopo aver macinato un po' la pianta
viene raccolta nuovamente al centro
per riprendere la macinatura.

Per rompere i pezzi
più duri (es. semini
attaccati a 'rametti'
+ spessi) si fanno
movimenti lineari
unidirezionali.

Hand movements:

☐ Vertical (pestling)

☒ Horizontal (grinding):

   ☒ circular

   ☒ linear monodirectional

   ☒ linear bidirectional

Describe: Principalmente movimenti
direzionali avanti e indietro.
Anche i volte movimenti circolari
alternati a quelli lineari soprattutto
all'inizio il macinato durante + fine.

Documentation form

Name: ... **OP-13** .... Degree: ....

Experimenter Data:

Name: .... **OP-2** .... Age: .... ☒F ☐M

Approx. height and weight: .

Experiment Data: GS6 GS14

Stone tools ☒ or Wood base and stone pestle ☐   Time: ....T.3.....

Resource treated: ...ECHINOCLOA CRUS GALLI 2019

Position of the operator:

GAMBE INCROCIATE; INIZIA CON IL TOLLERE A MANO I SEMI. PROCEDE CON MOVIMENTI DI SFREGAMENTO LONGITUDINALI IN DUE DIREZIONI ↕; MOVIMENTO ROTATORIO (↻) ANYA ESTARE, PER MACINARE
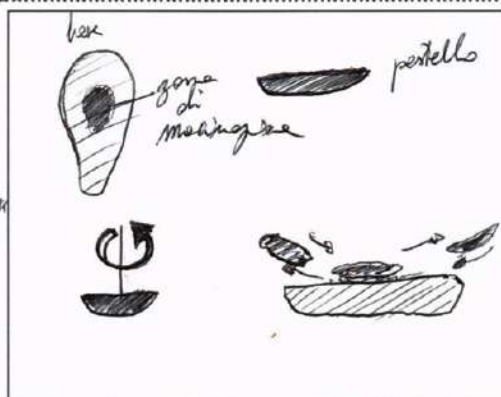
Hand movements:

☐ Vertical (pestling)

☒ Horizontal (grinding):

   ☐ circular

   ☐ linear monodirectional

   ☒ linear bidirectional

Describe: MOVIMENTI LONGITUDINALI PER RACCOGLIERE DAI BORDI, ROTAZORIO ALL'INIZIO PER DISTRUGGERE I PEZZI GROSSI

Workshop_4th October 2021

1) GAMBE INCROCIATE   2) IN GINOCCHIO

MACINA CON MANO DX

RACCOGLIE SEMI SPARSI CON

MANO DX (TENENDO LA PIETRA

RASTRELLO CON SX)
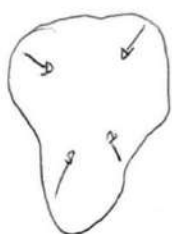
movimenti radiali
emidirezionali per recuperare
i semi sparsi.
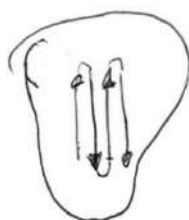
movimenti longitudinali
bidirezionali per macinare.
L'entità dello spostamento è di
circa 3-4 cm, sfruttando il
massimo spazio possibile
dell'incavatura

3) sedute   con braccio sx teruter appoggiar

Experiments for Upper Palaeolithic Ground Stone Tools: building a deductive reference collection

Documentation form

Name: ... **OP-2** .... Degree: .

Experimenter Data:

Name: **OP-13** .... Age: .... ☐F ☒M

Approx. height and weight: ...

Experiment Data: $GS6$ $GS14$

Stone tools ☒ or Wood base and stone pestle ☐   Time: ...T4....

Resource treated: MORE DI GELSO ESICCATE

Position of the operator:

In ginocchio. Sta facendo
un movimento rotatorio
pressante. (Preme e gira)
Tiene la base con l'altra
mano (la sinistra)

Una volta snappolata il
movimento diventa lineare
monodirezionale, e Luca si
sposta (mettendosi a gambe
incrociate)

Hand movements:

☐ Vertical (pestling)

☐ Horizontal (grinding):

    ☐ circular

    ☐ linear monodirectional

    ☐ linear bidirectional

Describe: ....
....
....

Mentre sta continuando
alterna il movimento
lineare monodirezionale
a un movimento rotatorio
con pressione

② Quando si è creato uno
strato uniforme di
"scroppo" sulla pietra
e sul pestello, diventa
mollo + lavorabile come
pasta → Movimenti lineari
bidirezionali e si ottene
un rotolo

Workshop_4th October 2021

267

pestello

MOVIMENTO
ROTATORIO
con pressione
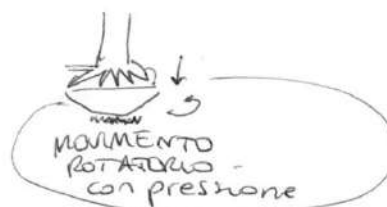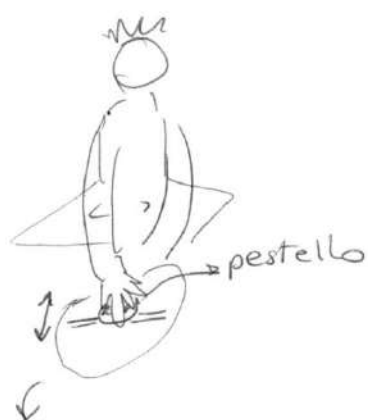
Raccogliamo e mettiamo nuove more.

1) In GINOCCHIO, MOVIMENTO ROTATORIO CON PRESSIONE

Non afferra neanche la pietra. Con la mano aperta
preme e gira
seduto a gambe incrociate

Raccoglie con la pietra, mettendo al centro della
base, dove è più cava, e alterna il movimento
rotatorio pressante a lineare monodirezionale, più
qualche movimento verticale.

2) Col movimento lineare bidirezionale si ottiene un
sigaro.
il prodotto di macinazione è molto appiccicoso

Nuova macinazione (3)
Sembrano più secche e si ~~spappolano~~ rompono invece
di spappolarsi.
Non è stato necessario mettersi in ginocchio ~~ma solo~~
e il movimento è lineare bidirezionale.
Cambio di mano → macinazione con mano sinistra

Per staccare da base → movimento lineare monodirezionale
Per macinare → lineare bidirezionale +
verticale.

Experiments for Upper Palaeolithic Ground Stone Tools: building a deductive reference collection

Documentation form

Name: | OP-4 | .... Degree: . ...

Experimenter Data:

Name: | OP-7 | .... Age: .... ☒F ☐M

Approx. height and weight: .... Degree: .. ..

Experiment Data: ꞡS 6
ꞡ S 14

Sone tools ☐ or Wood base and stone pestle ☐   Time: ......T5....

Resource treated: ..More di gelso...

Position of the operator:

....

....

....

....

....

....

Hand movements:

☒ Vertical (pestling)

☐ Horizontal (grinding):

   ☐ circular

   ☒ linear monodirectional

   ☐ linear bidirectional

Describe: 1). crashing the more di gelso

.2). grinding to gather the gelso.

....

Workshop_4th October 2021

Tech T4 Culture
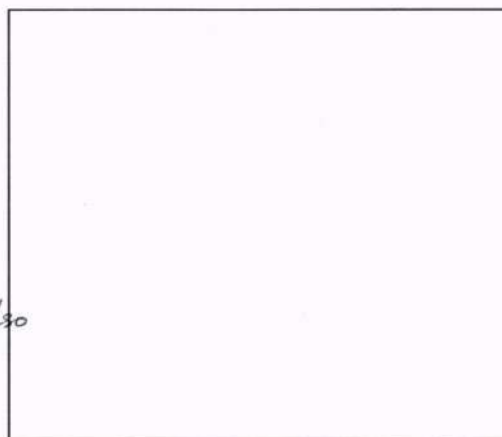
GS12-GS16: The filled forms

Documentation form

Name: ... OP-6 .... Degree:

Experimenter Data:

Name: .... OP-5 .... Age: .   ☒ F ☐ M

Approx. height and weight:

Experiment Data: GS 12
                        GS 16

5one tools ☒   or   Wood base and stone pestle ☐   Time: ....T.1.....

Resource treated: ..PINENUTS...

Position of the operator:
                                    with her legs crossed
First she is sitting ~~mentally~~ and

crushing the pinenuts to get the seeds.

She takes the pestle with her right hand.
She craussed 1st 15 pinenuts, in order to get a big
To obtain the powder she was.   amount.

sat in the same position.
then she needed more pinenuts, so she
crussed more pinenuts to get the
powder but this time two pinenuts
at a time. Also 1st she colpire the
Hand movements: nuts several times
                    and now with 1
1st ☒ Vertical (pestling)   or 2 colpi she do
                            that.
2nd ☒ Horizontal (grinding):

   ☒ circular

   ☐ linear monodirectional

   ☐ linear bidirectional

Describe: To get the seeds the movement

was vertical and to obtain the

powder was circular.
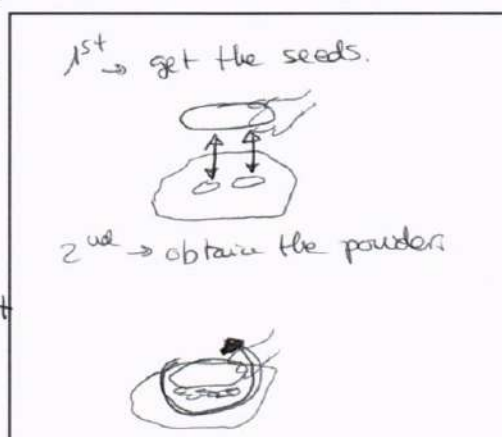
1st → get the seeds.

2nd → obtain the powder

Workshop_4th October 2021

Experiments for Upper Palaeolithic Ground Stone Tools: building a deductive reference collection

Documentation form

Name: ..... | OP-5 | .... Degree: ....

Experimenter Data:

Name: ... | OP-6 | .... Age: .. . ☐F ☒M

Approx. height and weight: ..

Experiment Data: *GS 12* *GS 16*

Stone tools ☒   or   Wood base and stone pestle ☐   Time: ......*T.2*......

Resource treated: ......*PINENUTS*......

Position of the operator:

① POSITIONE SULLE GINOCCHIA ....

....
....
....
....
....
....

Hand movements:

☒ Vertical (pestling) (*PER ROMPERE + MACINAZIONE IL GUSCIO) DOPO*

☒ Horizontal (grinding): (*PER LA MACINAZIONE) PRIMA*

  ☒ circular

  ☐ linear monodirectional

  ☐ linear bidirectional

Describe: *ROMPE UN PINOLO ALLA VOLTA* *UNICO COLPO SECCO, POI PELA IL PINOLO. PERCHE' VUOLE TENERE IL SEME IL PIU' INTERNO POSSIBILE (*)*

Experiments for Upper Palaeolithic Ground Stone Tools: building a deductive reference collection

Documentation form

Name: ..... | OP-5 | .... Degree: ....

Experimenter Data:

Name: .. | OP-6 | .... Age: .. ☐F ☒M

Approx. height and weight: ..

Experiment Data: *GS 12*
GS 16

Sone tools ☒ or Wood base and stone pestle ☐ Time: ....T.2......

Resource treated: ......PINENUTS......

Position of the operator:

① POSIMONE SULLE RINOCCHIA..........
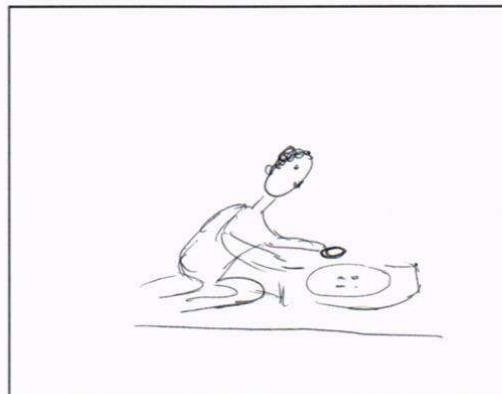
Hand movements:

☒ Vertical (pestling) (PER ROMPERE + MACINAZIONE
IL GUSCIO) DORO

☒ Horizontal (grinding): (PER LA MACINAZIONE)
PRIMA

☒ circular

☐ linear monodirectional

☐ linear bidirectional
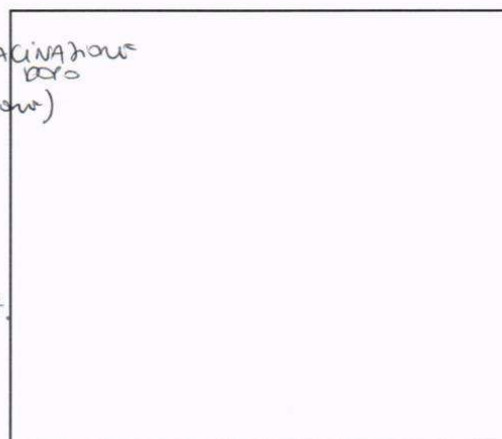
Describe: ROMPE UN PINOLO ALLA VOLTA,
UNICO COLPO SECCO, POI PELA IL PINOLO.
PERCHE' VUOLE TENERE IL SEME IL PIU'
INTERO POSSIBILE (＊)

(★) HA DETTO CHE HA "IMPARATO" DAI MIEI MOVIMENTI.

PER LA MACINAZIONE HA UTILIZZATO PER PRIMA UN MOVIMENTO
CIRCOLARE (COME AVEVA VISTO DA ME), SUCCESSIVAMENTE
HA PREFERITO UN MOVIMENTO VERTICALE + SUCCESSIVO MOVIMENTO
CIRCOLARE.

A METÀ HA CAMBIATO POSIZIONE: PER IL DISPESO CON LE BRICCECHE
PIEGATE (NON SI È TROVATO)
    ↳ Allego foto.
HA RICOMINCIATO SULLE GINOCCHIA.

QUANDO SI TIRURA IL PINOLO RIMANE NEL RESIDUO SUL "PESTELLO"
LO RIMUOVE CON LE DITA

Experiments for Upper Palaeolithic Ground Stone Tools: building a deductive reference collection

Documentation form

Name: OP-4 .... Degree: ..

Experimenter Data:

Name: OP-7 .... Age: .. ☒F ☐M

Approx. height and weight:

Experiment Data: ᐸS12 CS16

Sone tools ☒ or Wood base and stone pestle ☐   Time: ...T3.....

Resource treated: *Pinenuts*..

Position of the operator:

.... cRossed legs.....................................

....

....

....

....

....

Hand movements:

☒ Vertical (pestling)

☐ Horizontal (grinding):

   ☒ circular

   ☐ linear monodirectional

   ☐ linear bidirectional

Describe: 1). crash the hard part of

Pinenuts 2) grind the seeds by

small movement.....................................

Experiments for Upper Palaeolithic Ground Stone Tools: building a deductive reference collection

Documentation form

Name: .. OP-7 .... Degree: ....

Experimenter Data:

Name: OP-4 .... Age: ☐ F ☒ M

Approx. height and weight: .

Experiment Data: { BASE AND. GS PISTLE 12 + 16 }

~~Stone tools~~ ☐ or Wood base and stone pestle ☐   Time: ...T.G.....

Resource treated: ..(CAUCASUS GEORGIA 2017.).......
NOCCIOLE

Position of the operator:

CROSSED legs..................

Hand movements:

☐ Vertical (pestling)

☐ Horizontal (grinding):

☒ circular

☐ linear monodirectional

☒ linear bidirectional

Describe: ..1) ~~PRESS~~ THE HARD.....
PRESSING IN ORDER TO PULL OUT

SHELL WITH A STRONG KNOCK.

2) GRINDING WITH LINEAR + CIRCULAR
BIdirectional movements

Experiments for Upper Palaeolithic Ground Stone Tools: building a deductive reference collection

Documentation form

Name: OP-9 .... Degree: ....

Experimenter Data:

Name: OP-11 .... Age: .... ☐ F ☐ M

Approx. height and weight: ...

Experiment Data: GS12 GS16

Sone tools ☑ or Wood base and stone pestle ☐   Time: T5

Resource treated: .... shelled fruts ....
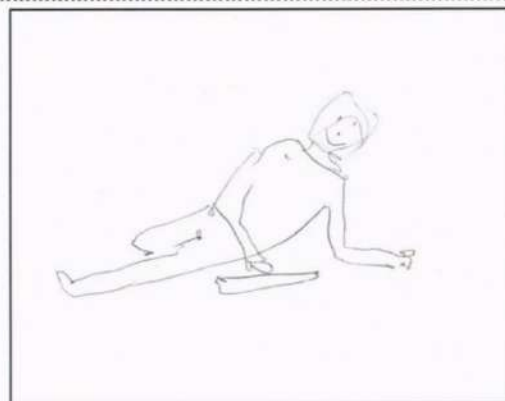
Position of the operator:

....

....

....

....

....

....

Hand movements:

☑ Vertical (pestling)

☑ Horizontal (grinding):

☐ circular

☐ linear monodirectional

☑ linear bidirectional

Describe: for 10 minutes

we used the opposte side of

the pistels ... sorry !!

we used small side

Workshop_4th October 2021

GS13-GS15: The filled forms

Documentation form

Name: **OP-7** .... Degree: ..

Experimenter Data:

Name: **OP-4** .... Age: ... ☐ F ☒ M

Approx. height and weight: .

Experiment Data: GS 15 GS 13   10 MINUTI

Stone tools ☐ or Wood base and stone pestle ☐   Time: ...T.1......

Resource treated: ..DAUCUS CAROTA (RAW 350 g)..............

Position of the operator:

..CROSSED LEGS................................

....

....

....

....

....

Hand movements:

☒ Vertical (pestling)

☐ Horizontal (grinding):

    ☐ circular

    ☐ linear monodirectional

    ☒ linear bidirectional

Describe: .1) pressure with..............

VERTICAL BIDIRECTIONAL movements ★ ....

PESTLING SOFTLY..............................

1) DA CVS CAROTA

        → Soft pieces of wood   →   IT DIVIDED INTO 2 parts

2) COLOR CHANGES → from brown to ORANGE

3) L'operatore tiene fisso con una mano il petto più grande e con l'altra mano libera usa maximment[i?] verticali lineari bidirezionali (GRINDING) → polvere arancione

    Seduto a gambe INCROCIATE

Documentation form

Name: [OP-4] .... Degree: ...

Experimenter Data:

Name: [OP-7] .... Age: ... ☒F ☐M

Approx. height and weight: ....

Experiment Data: { BASE GS 15 / PESTLE GS 13   20 MINUTI

Stone tools ☐ or Wood base and stone pestle ☐   Time: .....T 2.......

Resource treated: ..DAUUS...CAROTA...............

Position of the operator:

.....SEDUTO...SULE..GINOCCHIA...............

....

....

....

....

....

Hand movements:

☒ Vertical (pestling)

☐ Horizontal (grinding):

　☐ circular

　☐ linear monodirectional

　☒ linear bidirectional

Describe: *The material is not well dry*

Sag we use the stones for making

Them safter

Experiments for Upper Palaeolithic Ground Stone Tools: building a deductive reference collection
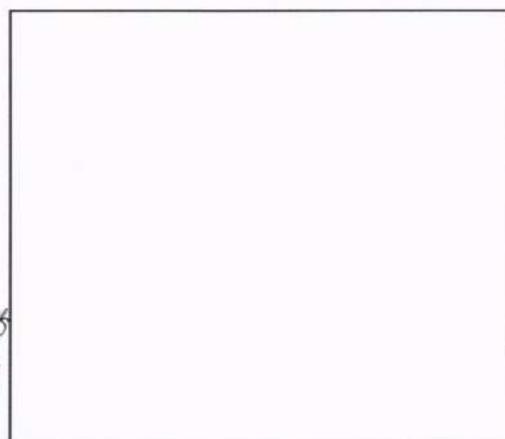
Documentation form ① T1 + T2 ⟶ DACUS CAROTA
(10') (20 MINUTES)

② T3 → PASTINACA

Name: OP-7 .... Degree: ...

Experimenter Data:

Name: OP-4 .... Age: .... ☐ F ☒ M

Approx. height and weight: ....

Experiment Data: { BASE GS 15
PESTLE GS 13

Stone tools ☐ or Wood base and stone pestle ☐ Time: ...T3...

Resource treated: ...PASTINACA...

Position of the operator:

CROSSED LEGS
....
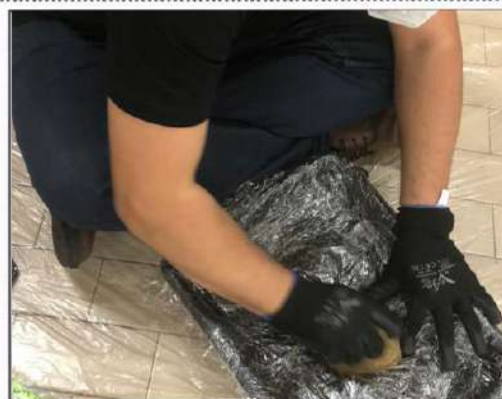
Hand movements:

☒ Vertical (pestling)

☐ Horizontal (grinding):

   ☒ circular

   ☒ linear monodirectional

   ☒ linear bidirectional

Describe: ① FIRSTLY PESTLING bet
MAKING little
fragments ② THEN GRINDING
WITH CIRCULAR + LINEAR BIDIRECTIONAL
MOVEMENTS

③ ALTERNATION of
PESTLING AND
CIRCULAR GRINDING IN
A CONTINUOUS WAY

Workshop_4th October 2021

280

Documentation form

Name: OP-9 .... Degree: ....

Experimenter Data:

Name: OP-11 .... Age: .... ☐ F ☒ M

Approx. height and weight: ..

Experiment Data: GS15
GS13

Sone tools ☒ or Wood base and stone pestle ☐   Time: T5

Resource treated: .... Pastinaca ....

Position of the operator:

....

....

....

....

....

....

Hand movements:

☒ Vertical (pestling)

☐ Horizontal (grinding):

☐ circular

☐ linear monodirectional

☐ linear bidirectional

Describe: .... little rotations ....
.... rotating + pressing ....

....

Workshop_4th October 2021

Experiments for Upper Palaeolithic Ground Stone Tools: building a deductive reference collection

Documentation form

Name: .. **OP-9** .... Degree: ....

Experimenter Data:

$c_5 - 13$ 15 min + 15 min AБNAHM

Name: ...... **OP-9** - TRAPA NATANS Age: ,   ☑F ☐M

Approx. height and weight: ....

Experiment Data: GS 15
GS 13

Stone tools ☑   or   Wood base and stone pestle ☐   Time: ... T5 ....

Resource treated: .... TRAPA NATANS

Position of the operator:

A lot of the residues sticky to the surface of the pestle,

Hand movements:

☑ Vertical (pestling)

☐ Horizontal (grinding):

  ☑ circular

  ☐ linear monodirectional

  ☑ linear bidirectional

Describe: ....

....

....

Workshop_4th October 2021

Experiments for Upper Palaeolithic Ground Stone Tools: building a deductive reference collection

Documentation form

Name: **OP-12** .... Degree: ....

Experimenter Data:

Name: **OP-10** .... Age: .... ☒ F ☐ M

Approx. height and weight: ....

Experiment Data: GS15 / GS13

Sone tools ☒ or Wood base and stone pestle ☐   Time: T6

Resource treated: TRAPA NATANS (castagna d'acqua)

Position of the operator:

Seduta e inginocchiata

seduta con una gamba piegata in avanti e l'altra gamba "in alto" affianco a vaschetta

(marginal notes) seduta con gamba sx piegata davanti al corpo e gamba dx piegata vicino vaschetta

seduta gambe inginocchiate

Hand movements:

☒ Vertical (pestling)

☑ Horizontal (grinding):

☐ ▱ circular

☐ ▱ linear monodirectional

☐ linear bidirectional

Describe: inizialmente movimenti verticali e poi movimenti circolari e lineari monodirezionali per rendere più fine la grana

(marginal note) impugnatura sempre la stessa

Workshop_4th October 2021

M1-GS10: The filled forms

MANO SX TIENE FERMO BASAMENTO.

MANO DX USA IL MORTAIO.

LE PRIME 3 DITA AGGANCIANO
IL MORTAIO; le ALTE
DUE (MIGNOLO + ANULARE)
LO TENGONO
LATERALMENTE

← mortaio

SEDUTA, GAMBE
INCROCIATE

mortar
verticle,
3 dita aggancio,
due tengono lateralmente

+

MOVIMENTO ANTIORARIO

Experiments for Upper Palaeolithic Ground Stone Tools: building a deductive reference collection

Documentation form

Name: OP-2 .... Degree: ....

Experimenter Data:

Name: OP-13 .... Age: .... ☐F ☒M

Approx. height and weight: ....

Experiment Data: H1 GS10

Stone tools ☒ or Wood base and stone pestle ☐   Time: T2

Resource treated: OCRA 1 - Ponte di Veja (VR) - heated 180° per 10 min 230° per 20'

Position of the operator:

IN GINOCCHIO, TIENE IL FRAMMENTO CON LE MANO SINISTRA E LO ROMPE CON LA PIETRA TENUTA A DESTRA.

TIENE IL PESTELLO CON TUTTA LA MANO

① ROMPE IL FRAMMENTO

LA MANO AVVOLGE LA PIETRA, CON TUTTE LE DITA
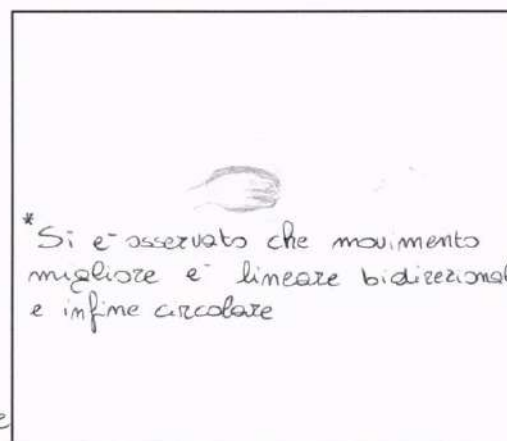
MOVIMENTO VERTICALE

POSIZIONE INGINOCCHIATA

Hand movements:

☒ Vertical (pestling) FIRST

☒ Horizontal (grinding): THEN

☐ circular

☐ linear monodirectional

☐ linear bidirectional

Describe: ....
INIZIALMENTE ROSSA, MACINANDO SI NOTA ETEROGENEITÀ (PIÙ scura all'esterno che all'interno), E POLVERIZZATA È POCO PIÙ SCURA DEL CAMPIONE PRECEDENTE

② POLVERIZZA

POSIZIONE A GAMBE INCROCIATE. TIENE SEMPRE UNA MANO SULLA BASE

ORA TIENE IL PESTELLO CON 3 DITA (POLLICE, INDICE E MEDIO)

Workshop_4th October 2021

Tech4Culture

286

③ MACINA

LA PIETRA NON È PIÙ IN VERTICALE, MA IN ORIZZONTALE,
CON MOVIMENTI ROTATORI ALTERNATI A VERTICALI

IN SEGUITO SI PASSA A MOVIMENTI
LINEARI MONODIREZIONALI ALTERNATI
A ROTATORI E A MOVIMENTI
VERTICALI (MODESTI) PER ROMPERE
FRAMMENTI ANCORA PRESENTI

DATA LA FORMA DELLA PIETRA ~~VENGONO~~ VIENE USATO
ANCHE UN MOVIMENTO DEL POLSO, PER DARE
ANDAMENTO ONDULATORIO AL PESTELLO

USA DITA PER RACCOGLIERE
AL CENTRO

④ CAMBIO POSIZIONE → TORNA IN GINOCCHIO,
MOVIMENTO LINEARE ~~ALTRO~~ BI DIREZIONALE, USATO
ANCHE PER RACCOGLIERE, TORNA A USARE
LA PIETRA IN VERTICALE

Documentation form

Name: .. | OP-3 | .... Degree: ....

Experimenter Data:

Name: .... | OP-8 | .... Age: .... ☒ F ☐ M

Approx. height and weight: ....

Experiment Data: $^{65}_{n} \, ^{10}_{1}$

~~S~~one tools ☒ or Wood base and stone pestle ☐ Time: ...T.3.....

Resource treated: ......OCRA ROSSA..

Position of the operator:

Kneeling ⟶ crossed legs
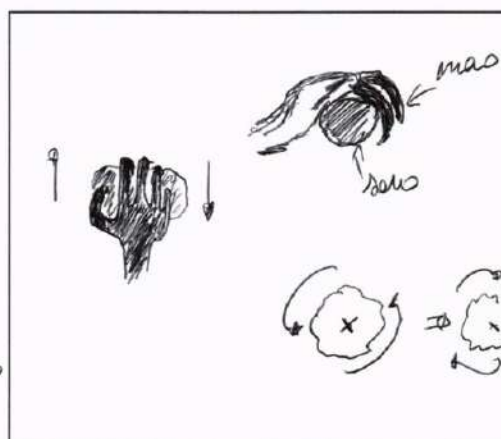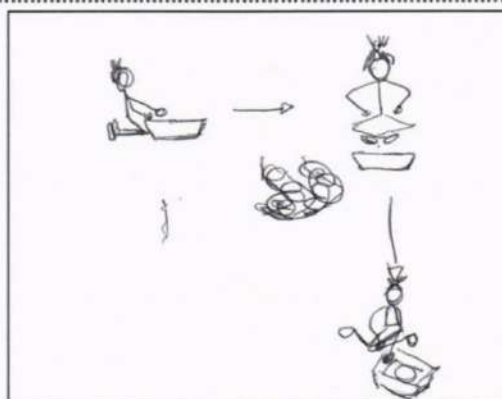

Hand movements:

☒ Vertical (pestling)

☐ Horizontal (grinding):

☐ circular

☐ linear monodirectional

☐ linear bidirectional

Describe: ......Starts pestling with flat surface, then with one lateral face – Small shots without too much force (using the weight of the stone)

Workshop_4th October 2021

The earth environment provides an "elastic" response on [Comments on T3] the hit (you can see small pieces of ochre jumping up)

At ~ 1mm granulometry movement change as <u>horizontal bidirectional</u>

At 5 min ochre is pulverized – At this point position is changed from sitting on the heels to crossed legs

Also, we collect this material and then we move to another fragment

Again vertical movements with a strong hit to break the big fragment

Experiments for Upper Palaeolithic Ground Stone Tools: building a deductive reference collection

Documentation form

Name: **OP-8** .... Degree: ....

Experimenter Data:

Name: **OP-3** .... Age: ..:........ ☒F ☐M

Approx. height and weight: ....

Experiment Data: H1
GS10

Stone tools ☐   or   Wood base and stone pestle ☐   Time: ....T.5.....

Resource treated: ...Floem.A.....................................

Position of the operator:

...SAT WITH CROSSED LEGS.............

....

....

....

....

....
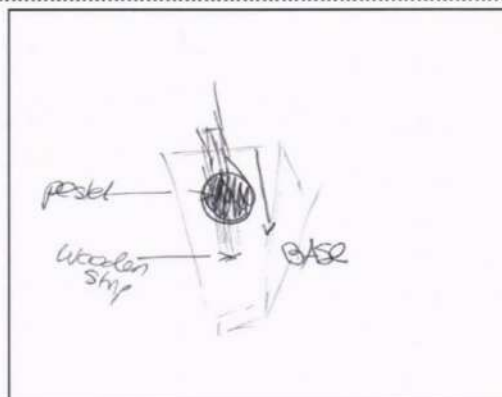
Hand movements:

☐ Vertical (pestling)

☒ Horizontal (grinding):

　☐ circular

　☒ linear monodirectional

　☐ linear bidirectional

Describe: ...the work on the...........

wooden strips begins

with the wider part of
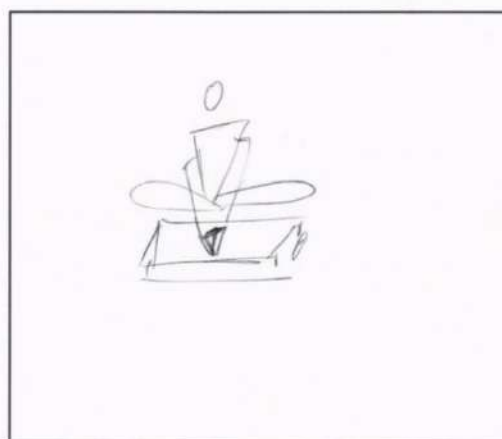
the pebble → long and regular movement
Then outward

after few minutes, ▮▮▮▮ changes strategy
using the pestel Q_i by the smaller part (hammering)

~~and then~~

~~And then she regularly (in cycle) changes from hammering to slicing.~~

LAURA sta alternando una lavorazione a cicli
→ 1° fase movimenti lineari lenti e lenghi
da sé verso l'esterno
→ 2° martellando
→ 3 di nuovo movimenti "liscianti" verso l'esterno

Documentation form

Name: **OP-6** .... Degree:

Experimenter Data:

Name: ..**OP-5**.. Age: .... ☒F ☐M

Approx. height and weight: .

Experiment Data: GS10
M1

Sone tools ☒ or Wood base and stone pestle☐   Time: ....T.S....

Resource treated: ~~FLOCLA~~ PINO NERO ....

Position of the operator:

She is sitting with her legs open.
1st step she was sliding the stone
with a linear movement but it wasn't
effective so she changed to a combination
of plashing and linear monodirectional
movements. The movements follow
the direction of the fibers
The stone is in vertical
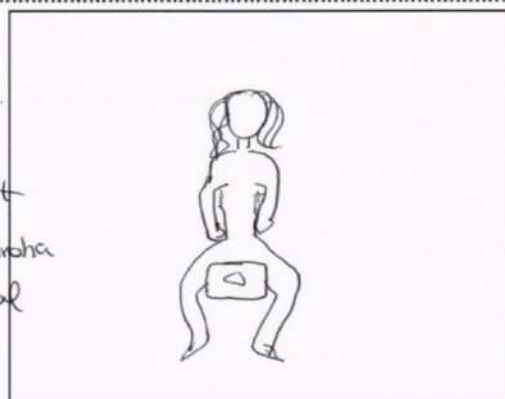
Hand movements: ⬡↑↓

☒ Vertical (pestling)

☒ Horizontal (grinding):

   ☐ circular

   ☒ linear monodirectional

   ☐ linear bidirectional
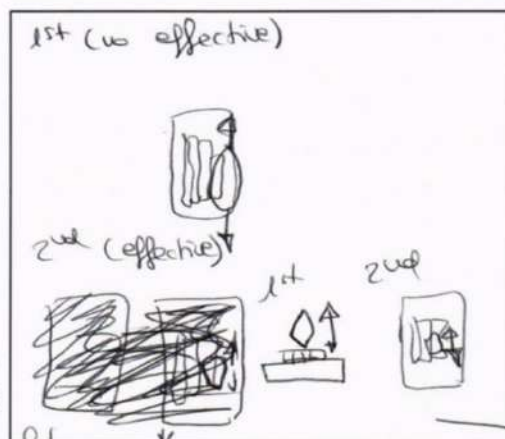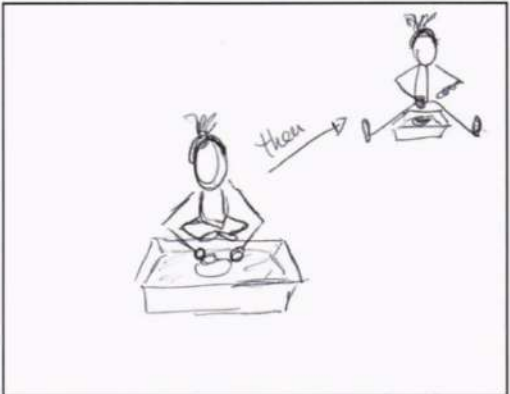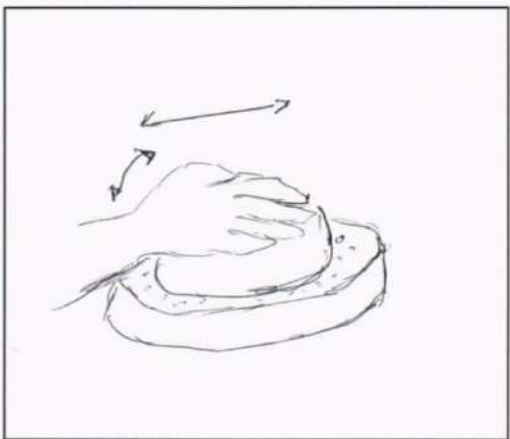
Describe: .She.combines.plashing.with
linear.monodirectional., ~~and the~~
~~~~ she also uses
~~to separate~~ her hands .the fibers. *

1st (no effective)

2nd (effective)↓

1st   2nd

Workshop_4th October 2021

(*) ULTIMI 5 MINUTI ABBIAMO CAMBIATO OPERATORE

M5-GS3: The filled forms

Experiments for Upper Palaeolithic Ground Stone Tools: building a deductive reference collection

Documentation form

Name: ..... OP-3 ..... Degree: ....

Experimenter Data:

Name: ..... OP-8 ..... Age: .... ☒F ☐M

Approx. height and weight: ....

Experiment Data: M5 GS3

Stone tools ☒ or Wood base and stone pestle ☐ Time: ...T1...

Resource treated: ..... Chenopodium .....

Position of the operator:

Crossed-legs, curve on the tools, right-handed (for changes see comments, page 2)

Hand movements:

☐ Vertical (pestling)

☒ Horizontal (grinding):

   ☒ circular → after 10 min

   ☐ linear monodirectional

   ☒ linear bidirectional

Describe: ..... movements also of the wrist, a little bit like making dough

Comments on T1:

After 10 min : more flour-like, starting circular
movements but the seeds goes everywhere

Every 5 seconds we put again on the base the seed
circular movements seems better at this point
↳ not too small circle

After 15 minutes the legs moved from crossed to
stretched keeping the basin in between.

After ~ 5 minutes the legs are back to crossing

Now the "refilling" on the stone is less frequent...

And we are back to horisontal linear bidirectional movements
with wrist movements up and down

By the end of 30 min we have a mix of circular and
horisontal

Experiments for Upper Palaeolithic Ground Stone Tools: building a deductive reference collection

Documentation form

Name: | OP-8 | .... Degree: ..

Experimenter Data:

Name: .. | OP-3 | .... Age: | | ... ☒ F ☐ M

Approx. height and weight: .. ..

Experiment Data: HS
GS3

Stone tools ☐ or Wood base and stone pestle ☐ Time: ...T2.....

Resource treated: ...... Chenopodium ......

Position of the operator:

S/T IN FRONT OF THE set

AFTER 5' change of POSITION:
SIT ON THE HEELS
AFTER 8' change of POSITION:
SIT ON THE SIDE

Hand movements:

☐ Vertical (pestling)

☒ Horizontal (grinding):

   ☐ circular

   ☐ linear monodirectional

  ①☐ linear bidirectional

Describe: ....

Grinding movements
are short and rapid.

OP-3 says that ~~the~~ she doesn't ~~feel~~ unfortable with the circular movement for grinding.

After 15' the grinding movement becomes slower ritmic & constant.

Experiments for Upper Palaeolithic Ground Stone Tools: building a deductive reference collection

Documentation form

Name: **OP-6** .... Degree: [   ]

Experimenter Data:

Name: **OP-5** .... Age: [   ] ☒ F ☐ M

Approx. height and weight: [   ]

Experiment Data:

M5
GS3

Stone tools ☒ or Wood base and stone pestle ☐   Time: ...T3....

Resource treated: ....CARRUBA...

Position of the operator:
she is sat in one leg. First she used
the most rough side of the stone
to cnish. Then she used the
other side of the stone (noe
smooth and polish) to obtain
the smaller fragments. The material
is oiled and sticky.
        buther its more spained
After a time she changed the
leg folded
she left the fragments out of the
stone and then picked them up.

Hand movements:

1st ☒ Vertical (pestling)

2nd ☒ Horizontal (grinding):

☐ circular

☒ linear monodirectional

☐ linear bidirectional

Describe: To broke the carruba the
movement is vertical with rough side
and to obtain
smaller fragments is linear
monodirectional with the smooth
side

Documentation form

Name: OP-5 .... **Degree:** ...

Experimenter Data:

Name: OP-6 .... **Age:** .... ☐ F ☒ M

Approx. height and weight: ....

Experiment Data:
MS
453

Sone tools ☒ or Wood base and stone pestle ☐   **Time:** ....T4......

Resource treated: ...... GHIANDA ARROSTITA ....

Position of the operator:

(1) SULLE GINOCCHIA

(2) SULLE GINOCCHIA PIU' MANO
APPOGGIATA AL SUOLO

Hand movements:

☒ Vertical (pestling)

☐ Horizontal (grinding):

   ☐ circular

   ☐ linear monodirectional

   ☐ linear bidirectional

Describe: (1) PICCOLI COLPI VERTICALI
LA ROCCIA FA USCIRE LA MORBIDA
PARTE DEL MATERIALE *

Workshop_4th October 2021

(✳) UNA GHIANDA PER VOLTA, I COLPI SONO SECCHI E CON MOLTA FORZA. UNA VOLTA OTTENUTI I PEZZI PIÙ PICCOLI, LI MACINA CON ALTRI COLPI MENO POTENTI. UTILIZZA LA PARTE PIÙ LISCIA DELLA ROCCIA

~~LA PARTE DELLA GHIANDA UMBIATA~~

CURVA

LA GHIANDA VIENE MESSA CON LA PARTE PIANA A TOCCARE LA ROCCIA IN MODO DA FACILITARE LA POLVERIZZAZIONE (PRIMA ~~HA~~ TROVATO L'OPPOSTO MA ERA PIÙ DIFFICOLTOSA LA POLVERIZZAZIONE

A 10 MIN SI È ROTTA LA PIETRA.

M7 with wooden base: The filled forms

Experiments for Upper Palaeolithic Ground Stone Tools: building a deductive reference collection

Documentation form

Name: .... **OP-10** .... Degree: ....

Experimenter Data:

Name: .... **OP-12** .... Age: ..... ☒F ☐M

Approx. height and weight: .

Experiment Data: M7

☐ Stone tools ☐ or Wood base and stone pestle ☒ Time: ..T.1......

Resource treated: .... NOCCIOLE ....

Position of the operator:

L'operatore è in posizione seduta sulle ginocchia di fronte alla bacinella, alterna due posizioni.
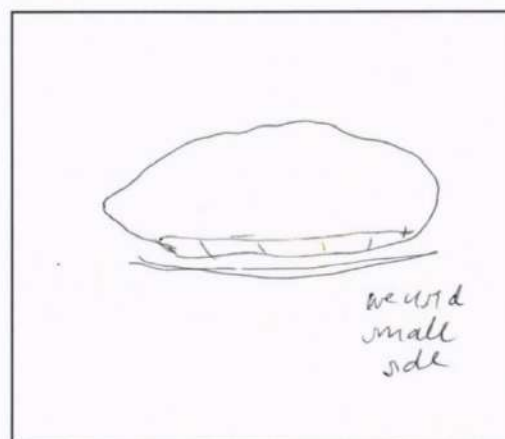
Alterna con movimenti circolari quando la nocciola è più abbastanza tritata

Hand movements:

☒ Vertical (pestling)

☐ Horizontal (grinding):
  ☒ circular
  ☐ linear monodirectional
  ☐ linear bidirectional

Describe: Movimenti verticali fatti x spaccare il guscio e x tritare il frutto interno. Il frutto rimane un po' grossolano

Tech4Culture

Documentation form

Name: .... | OP-2 | .... Degree: . _____ ....

Experimenter Data:

Name: ... | OP-13 | .... Age: . ____ . ☒F ☐M

Approx. height and weight: .: _____ ....

Experiment Data: M7

Sone tools ☐ or Wood base and stone pestle ☒   Time: ....T2....

Resource treated: ....Nocciola...

Position of the operator:

GINOCCHIO.; CURVA SUL

BANZ OL LAVORO. OSEDUTA DI LATO.

RACCOLVE AL CONTRO COM IL DITO.;

④ GAMBE INCROCIATE Deduto

....

....

Hand movements:

☒ Vertical (pestling)

☒ Horizontal (grinding):

☒ circular

☐ linear monodirectional

☐ linear bidirectional

Describe: MONIMANTO VERTICALE

MEZZO PER SPEZZARE.; VERTICALE

DOLCEE PER CHINOIDARE

Workshop_4th October 2021

Documentation form

Name: ..... | OP-2 | .... **Degree:** . ...

Experimenter Data:

Name: ... | OP-13 | .... **Age:** . . ☒F ☐M

Approx. height and weight: .: ....

Experiment Data: M7

$\overline{S}$one tools ☐ or Wood base and stone pestle ☒ **Time:** ....T2.....

Resource treated: ....Nocciola

Position of the operator:

GINOSSMIO; CURVA SUL

BANZ AL LAVORO; OSEDUTA DI LATO;

RACCOLIK AL CONTAR COM IL DITO;

① GAMBE INCROCIATE seduta

Alexia peste cou le parte piatte

rompere i gusci

Hand movements:

☒ Vertical (pestling)

☒ Horizontal (grinding):

   ☒ circular

   ☐ linear monodirectional

   ☐ linear bidirectional

Describe: MOVIMENTO VERTICALE

MEZZO PER SPEZZARE; VERTICALE

DOLCE PER CHINOZZARE

sminuzzare le nocciole

Tento undo per gottare le noci

mainto veloce per sminuzzere

punta e bordo

Workshop_4th October 2021

mano: destra

usa di più le punte quando
deve triturare le nocciole sgusciate

M8 with wooden base: The filled forms

Experiments for Upper Palaeolithic Ground Stone Tools: building a deductive reference collection

Documentation form

Name: .... OP-11 .... Degree: ....

Experimenter Data: .... OP-9 ....

Name: .... Age: .... ☒ F ☒ M

Approx. height and weight: .   ...

Experiment Data: M8

Stone tools ☒ (No!) òr Wood base and stone pestle ☒   Time: ....T.1......

Resource treated: .... Armoraua Rusticana Horsradish..............................

Position of the operator:

....
....
....
....
....
....

Hand movements:

☒ Vertical (pestling)

☐ Horizontal (grinding):

  ☐ circular

  ☐ linear monodirectional

  ☐ linear bidirectional

Describe: ....After pestling.................
.... some little rotations
.... onto the base

Workshop_4th October 2021

304

Documentation form

Experiments for Upper Palaeolithic Ground Stone Tools: building a deductive reference collection

Name: ... OP-9 .... Degree: ....

Experimenter Data:

Name: ... OP-9 .... Age: .... ☑F ☐M

Approx. height and weight: ..

Experiment Data: M 8

Stone tools ☑ or Wood base and stone pestle ☑   Time: ...T2.....

Resource treated: ...Armorana Rusticana Horse Radish

Position of the operator:

....
....
....
....
....
....
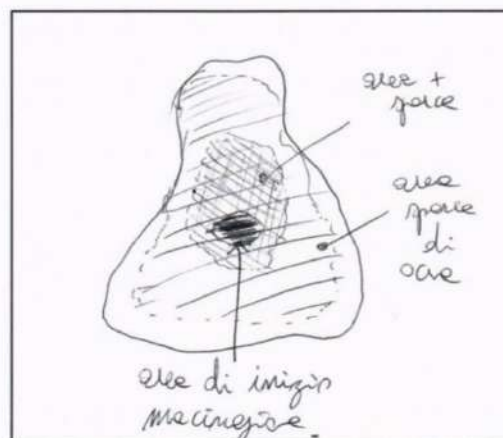

Hand movements:

☑ Vertical (pestling)

☑ Horizontal (grinding):

   ☑ circular

   ☐ linear monodirectional

   ☐ linear bidirectional

Describe: ....
....
....

Workshop_4th October 2021

Documentation form

Name: .... OP-12 .... Degree: . ...

Experimenter Data:

Name: .... OP-10 .... Age: .... ☒F ☐M

Approx. height and weight: ....

Experiment Data: M8

Stone tools ☐ or Wood base and stone pestle ☒ Time: ...T3....

Resource treated: ...Armoracia.. Rusticana. - Horseradish.....................

Position of the operator:

...mainocchiata e seduta in......
modo "alternato".................
....
....
....
....

Hand movements:

☒ Vertical (pestling)

☐ Horizontal (grinding):

   ☐ circular

   ☐ linear monodirectional

   ☐ linear bidirectional

Describe: .pestato e ogni tanto....
sfregamento rotatorio e lineare
bi direzionale............................

Workshop_4th October 2021

306

Appendix B: Experimental GSTs Area Roughness Measurements

Confocal profilometer areal measurements were processed using the open-source software Gwyddion to calculate the seven ISO 25178-2 surface texture areal parameters for the experimental tools. The results are presented in the main text in Chapter 5, plotted in box charts, and the detailed data are provided below. It is important to note that in this section the decimal separator is indicated by the comma. For each experimental stage (T), the same square of 0,5 cm² were analysed, and 9 sub-regions of 850 µm² each were examined. The average value for each parameter was calculated (and reported in blue in the tables) based on the data from all 9 analysed areas, along with their corresponding standard deviation (in light blue).

Acronym	Parameter	Unit of Measurement
Sa	Arithmetical mean height of the surface	µm
Sq	Root means square height of the surface	µm
Ssk	Skewness of height distribution	unitless
Sku	Kurtosis of height distribution	unitless
Sp	Maximum height of peaks	µm
Sv	Maximum height of valleys	µm
Sz	Maximum height of the surface	µm

GS9: Active tool used for processing achenes, paired with a wooden base

SAMPLE	Mean roughness (Sa)	RMS roughness (Sq)	Skew (Ssk)	Excess kurtosis	Max.height of peaks (Sp)	Max. height of valleys (Sv)	Max. height of the surface (Sz)
GS9.T$_0$.ml.3-10x.06	25,559	31,9433	-0,411787	0,00937136	89,295	115,44	204,735
GS9.T$_0$.ml.3-10x.07	23,008	28,9548	-0,321633	0,0763794	107,366	111,37	218,737
GS9.T$_0$.ml.3-10x.08	33,5026	43,1856	-0,885248	0,533074	93,325	150,244	243,57
GS9.T$_0$.ml.3-10x.09	28,3426	35,3499	-0,241013	0,072348	96,699	198,572	295,271
GS9.T$_0$.ml.3-10x.12	22,3465	27,5507	-0,171267	0,0506837	100,761	117,021	217,782
GS9.T$_0$.ml.3-10x.14	33,6911	42,0213	-0,159917	-0,287993	112,232	187,111	299,343
GS9.T$_0$.ml.3-10x.20	28,0678	34,5114	0,0295573	-0,469365	96,102	185,119	281,221
GS9.T$_0$.ml.3-10x.21	25,2212	31,3815	-0,169363	-0,0757088	81,683	126,338	208,021
GS9.T$_0$.ml.3-10x.24	28,2331	35,2671	0,0358869	-0,226664	159,741	100,752	260,493
AVERAGE-T$_0$	**27,55243333**	**34,46284444**	**-0,254975978**	**-0,035319371**	**104,1337778**	**143,5518889**	**247,6858889**
DEV.ST.C -T$_0$	*4,055906597*	*5,345697444*	*0,277354472*	*0,284389112*	*22,74975016*	*37,67493639*	*37,73050697*
GS9.T$_3$.ml.2-10x.03	19,5375	24,4001	0,17114	0,070554	85,066	78,601	163,667
GS9.T$_3$.ml.2-10x.04	18,9848	23,2941	-0,0678978	-0,361382	73,783	83,606	157,389
GS9.T$_3$.ml.2-10x.05	21,0602	25,4094	0,0805649	-0,349899	88,165	75,884	164,049
GS9.T$_3$.ml.2-10x.06	21,7082	28,1557	-0,932126	2,19194	69,96	202,199	272,159
GS9.T$_3$.ml.2-10x.08	20,1765	24,7402	-0,00156072	-0,383778	76,072	98,436	174,508
GS9.T$_3$.ml.2-10x.09	19,8672	25,8471	-0,181249	0,604828	81,884	103,658	185,542
GS9.T$_3$.ml.2-10x.10	22,1303	27,627	-0,0769719	0,406588	87,69	144,918	232,608
GS9.T$_3$.ml.2-10x.11	15,8747	19,8046	0,154005	-0,328577	74,292	61,364	135,656
GS9.T$_3$.ml.2-10x.12	27,2902	33,8307	-0,544636	-0,0500025	85,641	137,378	223,019
AVERAGE-T$_3$	**20,73662222**	**25,90098889**	**-0,155414613**	**0,200030167**	**80,28366667**	**109,5604444**	**189,8441111**
DEV.ST.C -T$_3$	*3,065026105*	*3,852752976*	*0,362455083*	*0,828505872*	*6,833529048*	*44,51627199*	*43,73082918*

M7: Active tool used to process hazelnuts, paired with a wooden base

SAMPLE	Mean roughness (Sa)	RMS roughness (Sq)	Skew (Ssk)	Excess kurtosis	Max.height of peaks (Sp)	Max. height of valleys (Sv)	Max. height of the surface (Sz)
M7.T$_0$.ml.3-10x.01	24,9314	31,0829	-0,467827	-0,123842	77,031	107,043	184,074
M7.T$_0$.ml.3-10x.02	24,8733	31,2221	0,00324351	-0,250546	91,712	98,531	190,243
M7.T$_0$.ml.3-10x.04	31,6032	39,3946	-0,497979	-0,206903	102,579	136,961	239,541
M7.T$_0$.ml.3-10x.05	19,8838	25,2696	-0,61942	0,363285	143,467	109,924	253,391
M7.T$_0$.ml.3-10x.08	33,7733	42,1106	-0,725681	0,259664	93,51	156,846	250,356
M7.T$_0$.ml.3-10x.13	25,7019	30,9336	-0,185171	-0,630459	69,392	100,056	169,448
M7.T$_0$.ml.3-10x.14	21,1591	26,5495	-0,543824	0,0201136	55,789	110,045	165,834
M7.T$_0$.ml.3-10x.16	22,8023	28,3712	-0,493053	0,208798	118,104	133,362	251,466
M7.T$_0$.ml.3-10x.22	24,2259	31,4921	-0,801627	0,806685	75,107	127,106	202,213
AVERAGE-T$_0$	25,43935556	31,82513333	-0,481259832	0,049643956	91,85455556	119,986	211,8406667
DEV.ST.C -T$_0$	4,551185247	5,563777184	0,252088891	0,416887286	26,8704331	19,68988478	36,72742014
M7.T$_3$.ml.3-10x.01	23,7375	29,1894	0,0244814	-0,615557	73,35	89,943	163,293
M7.T$_3$.ml.3-10x.05	14,8953	18,8421	-0,620119	1,11616	52,489	112,107	164,596
M7.T$_3$.ml.3-10x.06	16,25	19,8034	0,165933	-0,39879	51,225	77,111	128,336
M7.T$_3$.ml.3-10x.09	18,1842	22,6851	0,339161	-0,0537839	112,662	83,017	195,679
M7.T$_3$.ml.3-10x.12	15,9076	20,1878	0,414331	0,100786	70,607	56,949	127,555
M7.T$_3$.ml.3-10x.15	17,8824	22,0783	-0,441991	-0,293146	59,657	73,852	133,509
M7.T$_3$.ml.3-10x.16	17,741	22,7595	-0,547771	0,868475	65,939	103,815	169,754
M7.T$_3$.ml.3-10x.18	18,7339	23,1095	-0,163087	-0,351127	58,733	101,874	160,606
M7.T$_3$.ml.3-10x.19	18,766	23,7127	-0,71919	0,455444	48,724	100,058	148,782
AVERAGE-T$_3$	18,01087778	22,48531111	-0,172027956	0,092051233	65,93177778	88,74733333	154,6788889
DEV.ST.C -T$_3$	2,530756971	3,017984592	0,428992893	0,601191473	19,5092987	17,59127878	22,44031354

M8: Active tool used to process roots, paired with a wooden base

SAMPLE	Mean roughness (Sa) (µm)	RMS roughness (Sq) (µm)	Skew (Ssk)	Excess kurtosis (Sku)	Max.height of peaks (Sp)	Max. height of valleys (Sv)	Max. height of the surface (Sz)
M8.T_0.m1.10x.09	36,0209	41,969	-0,48693	-0,616406	87,671	141,378	229,049
M8.T_0.m1.10x.10	35,1994	42,7632	0,294402	-0,5616	120,729	101,497	222,227
M8.T_0.m1.10x.11	27,3708	36,0649	-0,800158	1,74614	106,044	168,363	274,407
M8.T_0.m1.10x.13	20,3504	24,9163	-0,1474	-0,385114	69,45	81,389	150,839
M8.T_0.m1.10x.14	20,4379	25,1286	-0,106747	-0,483716	66,171	82,335	148,506
M8.T_0.m1.10x 15	24,4322	30,9111	-0,450782	0,0909378	71,396	128,184	199,579
M8.T_0.m1.10x.16	19,7018	24,1806	-0,570577	-0,186938	54,601	101,266	155,867
M8.T_0.m1.10x.17	23,9157	29,5623	-0,211495	-0,368333	83,886	95,851	179,738
M8.T_0.m1.10x.18	20,7277	25,171	0,0829329	-0,393724	86,746	90,036	176,782
AVERAGE-T_0	**25,35075556**	**31,18522222**	**-0,266306011**	**-0,128750356**	**82,966**	**110,0332222**	**192,9993333**
DEV.ST.C. -T_0	*6,327070166*	*7,399977764*	*0,342645657*	*0,734111979*	*20,61280695*	*29,69163894*	*42,42517034*
M8.T_3.ml.7.10x.06	18,0352	21,7958	-0,54287	-0,485195	72,452	76,774	149,226
M8.T_3.ml.7.10x 07	31,9761	39,4228	-0,633881	-0,444558	133,663	108,421	242,085
M8.T_3.ml.7.10x.09	18,1698	22,0362	-0,0861928	-0,657685	55,071	59,381	114,451
M8.T_3.ml.7.10x.10	18,3482	23,8438	-1,2817	4,3502	63,345	136,251	199,595
M8.T_3.ml.7.10x 11	20,5733	25,647	0,0617965	-0,389722	74,929	76,482	151,411
M8.T_3.ml.7.10x.12	17,2747	21,1226	0,0541963	-0,221999	65,682	70,531	136,212
M8.T_3.ml.7.10x.13	23,4016	28,7226	-0,475027	0,188003	59,693	119,579	179,272
M8.T_3.ml.7.10x.14	24,3804	29,5888	-0,153018	-0,61447	100,664	127,006	227,669
M8.T_3.ml.7.10x.17	23,4186	28,7033	-0,374743	-0,494592	58,55	86,683	145,233
AVERAGE-T_3	**21,73087778**	**26,76476667**	**-0,381271**	**0,136664667**	**76,00544444**	**95,67866667**	**171,6837778**
DEV.ST.C. -T_3	*4,698451743*	*5,749537598*	*0,423474083*	*1,600017464*	*25,54927465*	*27,65378644*	*43,41099149*

GS8: Active tool used to process achenes

SAMPLE	Mean roughness (Sa)	RMS roughness (Sq)	Skew (Ssk)	Excess kurtosis	Max.height of peaks (Sp)	Max. height of valleys (Sv)	Max. height of the surface (Sz)
GS8.T$_0$.ml.2-10x.10	38,6119	45,9352	-0,0245914	-0,62103	119,867	150,042	269,909
GS8.T$_0$.ml.2-10x.11	37,7424	50,594	-0,442324	1,20943	148,568	202,368	350,935
GS8.T$_0$.ml.2-10x.12	32,4135	40,9953	0,0769413	0,341206	146,459	169,147	315,606
GS8.T$_0$.ml.2-10x.13	53,2426	66,2445	-0,675409	0,22715	134,32	241,47	375,791
GS8.T$_0$.ml.2-10x.14	33,4858	43,6664	-0,269743	0,463825	130,625	150,612	281,236
GS8.T$_0$.ml.2-10x.15	30,0189	36,2466	0,0813208	-0,331923	123,561	121,229	244,789
GS8.T$_0$.ml.2-10x.16	32,2753	46,0672	-0,87977	3,62664	137,906	229,068	366,974
GS8.T$_0$.ml.2-10x.17	31,1916	38,0808	0,0323101	-0,276712	116,266	162,411	278,677
GS8.T$_0$.ml.2-10x.18	37,6086	45,7277	0,0356247	-0,497552	118,547	148,163	266,71
AVERAGE-T$_0$	36,28784444	45,95085556	-0,229515611	0,460114889	130,6798889	174,9455556	305,6252222
DEV.ST.C. -T$_0$	7,079539004	8,798728552	0,360544462	1,318759747	12,02600984	40,48541731	48,2851305
GS8.T$_1$.ml.2-10x.08	15,3661	18,9788	0,656261	0,42103	80,967	56,002	136,968
GS8.T$_1$.ml.2-10x.09	12,9668	15,7537	0,474106	-0,292321	62,762	40,315	103,077
GS8.T$_1$.ml.2-10x.10	14,6495	18,3554	0,162196	0,21062	76,66	78,549	155,209
GS8.T$_1$.ml.2-10x.11	14,1984	17,3103	0,276882	-0,280622	63,327	55,861	119,188
GS8.T$_1$.ml.2-10x.12	19,2116	23,826	-0,0018822	0,18217	101,256	69,207	170,463
GS8.T$_1$.ml.2-10x.13	22,3484	28,8309	0,226114	0,107186	82,217	84,88	167,096
GS8.T$_1$.ml.2-10x.16	16,8379	20,7788	0,451943	-0,15982	80,024	53,153	133,177
GS8.T$_1$.ml.2-10x.22	22,8803	27,2896	0,464589	-0,565319	83,479	74,29	157,768
GS8.T$_1$.ml.2-10x.23	27,3612	34,0295	0,434308	-0,176205	106,772	78,076	184,849
AVERAGE-T$_1$	18,42446667	22,79477778	0,349390756	-0,061475667	81,94044444	65,59255556	147,5327778
DEV.ST.C. -T$_1$	4,86702455	6,143195439	0,199878407	0,310778248	14,7432907	14,85261082	26,36793708
GS8.T$_2$.ml.2-10x.12	21,3087	27,4262	0,540851	0,386063	111,931	75,913	187,844
GS8.T$_2$.ml.2-10x.13	18,0361	22,2425	0,862071	0,115822	85,994	49,693	135,687

GS8.T$_2$.ml.2-10x.14	25,2855	31,8386	-0,318507	-0,180885	92,079	94,417	186,496
GS8.T$_2$.ml.2-10x.15	23,7625	30,2665	-0,148852	0,287968	92,62	97,765	190,385
GS8.T$_2$.ml.2-10x.16	17,3483	21,2319	0,107116	-0,50687	63,962	60,891	124,853
GS8.T$_2$.ml.2-10x.17	12,4619	16,4643	-0,0569771	1,3764	77,94	67,013	144,953
GS8.T$_2$.ml.2-10x.18	20,2859	26,6119	-0,454194	0,676096	84,479	103,016	187,495
GS8.T$_2$.ml.2-10x.19	17,6902	22,8328	0,592149	0,86189	95,807	58,828	154,635
GS8.T$_2$.ml.2-10x.20	13,1524	17,3391	0,669851	2,18246	109,629	50,229	159,858
AVERAGE-T$_2$	**18,81461111**	**24,0282**	**0,199278656**	**0,577660444**	**90,49344444**	**73,085**	**163,5784444**
DEV.ST.C. -T$_2$	*4,347085218*	*5,391362144*	*0,477262404*	*0,820774482*	*14,91196427*	*20,69548936*	*25,30551174*
GS8.T$_3$.ml.2-10x.11	16,5373	20,4289	0,40627	-0,112706	81,814	79,719	161,533
GS8.T$_3$.ml.2-10x.12	17,9886	22,7174	0,04995	0,0105498	69,36	78,772	148,132
GS8.T$_3$.ml.2-10x.13	19,2059	23,509	-0,16215	-0,166936	58,758	92,53	151,287
GS8.T$_3$.ml.2-10x.14	21,8899	27,3611	-0,104996	-0,185392	72,126	86,211	158,337
GS8.T$_3$.ml.2-10x.6	13,0633	16,8523	0,922912	0,706296	73,174	55,446	128,621
GS8.T$_3$.ml.2-10x.17	11,6726	15,2564	0,442716	1,16685	66,235	45,388	111,623
GS8.T$_3$.ml.2-10x.19	16,9459	20,3677	-0,268499	-0,543516	59,671	56,258	115,929
GS8.T$_3$.ml.2-10x.22	15,4761	19,9244	0,184578	0,467552	85,69	67,269	152,96
GS8.T$_3$.ml.2-10x.24	18,6844	23,6642	-0,2731	0,0389418	70,466	121,898	192,364
AVERAGE-T$_3$	**16,82933333**	**21,12015556**	**0,133075667**	**0,153515511**	**70,81044444**	**75,94344444**	**146,754**
DEV.ST.C. -T$_3$	*3,137427153*	*3,686993906*	*0,399060346*	*0,529017083*	*8,960344945*	*23,26788658*	*25,01747318*
GS8.T$_4$.ml.2-10x.11	15,6831	19,905	0,355199	0,199807	77,763	59,535	137,297
GS8.T$_4$.ml.2-10x.12	22,5847	28,7155	0,870379	0,319442	95,622	72,203	167,825
GS8.T$_4$.ml.2-10x.13	33,801	41,2545	0,113011	-0,618886	149,434	86,313	235,747
GS8.T$_4$.ml.2-10x.14	16,2406	20,5277	0,523494	0,0561439	62,466	50,135	112,601
GS8.T$_4$.ml.2-10x.15	16,4152	20,2631	0,123222	-0,359174	57,356	60,23	117,586
GS8.T$_4$.ml.2-10x.16	24,3008	29,8066	0,386759	-0,311727	99,213	59,522	158,735
GS8.T$_4$.ml.2-10x.19	23,244	29,1306	0,316454	0,342522	113,547	75,404	188,951

SAMPLE	Mean roughness (Sa)	RMS roughness (Sq)	Skew (Ssk)	Excess kurtosis	Max.height of peaks (Sp)	Max. height of valleys (Sv)	Max. height of the surface (Sz)
GS8.T$_4$.ml.2-10x.21	25,2386	29,8205	0,160654	-0,855423	83,475	71,645	155,119
GS8.T$_4$.ml.2-10x.22	18,2077	22,2563	0,240854	-0,11325	89,977	58,835	148,812
AVERAGE-T$_4$	**21,74618889**	**26,85331111**	**0,343336222**	**-0,148949456**	**92,09477778**	**65,98022222**	**158,0747778**
DEV.ST.C. -T$_4$	*5,863029137*	*6,950089348*	*0,239362489*	*0,420793842*	*27,79372049*	*11,13262075*	*37,60863472*

M2: Active tool used to process acorns

SAMPLE	Mean roughness (Sa)	RMS roughness (Sq)	Skew (Ssk)	Excess kurtosis	Max.height of peaks (Sp)	Max. height of valleys (Sv)	Max. height of the surface (Sz)
M2.T$_0$.ml.2-10x.01	23,6627	27,2552	-0,20615	-0,750002	121,889	102,626	224,515
M2.T$_0$.ml.2-10x.02	16,6584	20,3825	-0,770248	0,36781	62,712	102,188	164,9
M2.T$_0$.ml.2-10x.03	11,3963	14,5499	-1,01563	1,54634	24,361	93,525	117,886
M2.T$_0$.ml.2-10x.04	8,2091	10,282	-0,897154	1,34644	49,232	94,949	144,182
M2.T$_0$.ml.2-10x.05	20,0778	27,5345	-1,11326	2,10155	63,236	138,017	201,254
M2.T$_0$.ml.2-10x.06	12,2913	16,47	-1,6467	3,53056	24,542	117,011	141,553
M2.T$_0$.ml.2-10x.10	13,722	17,1679	-0,857378	0,574682	69,524	94,444	163,969
M2.T$_0$.ml.2-10x.08	11,8662	15,3491	-0,879906	1,28474	34,035	84,402	118,438
M2.T$_0$.ml.2-10x.09	11,2351	14,6576	-1,27464	3,92981	51,437	110,911	162,348
AVERAGE-T$_0$	**14,34654444**	**18,18318889**	**-0,962340667**	**1,547992222**	**55,66311111**	**104,2303333**	**159,8938889**
DEV.ST.C -T$_0$	*4,89645494*	*5,859208703*	*0,39087735*	*1,484963182*	*29,9173198*	*15,99196297*	*35,35665115*
M2.T$_{0,1}$.ml.1-10x.01	13,5146	17,3186	-1,10686	1,73091	31,837	92,16	123,997
M2.T$_{0,1}$.ml.1-10x.02	8,971	11,1967	-0,916209	0,674826	28,408	79,958	108,366
M2.T$_{0,1}$.ml.1-10x.03	7,31766	9,50163	-1,3364	2,49123	25,686	76,853	102,539
M2.T$_{0,1}$.ml.1-10x.06	10,6898	13,6019	-1,01867	1,20519	23,602	80,139	103,742
M2.T$_{0,1}$.ml.1-10x.07	9,4226	12,2466	-1,33053	3,27064	21,522	81,509	103,031
M2.T$_{0,1}$.ml.1-10x.08	8,2982	10,3412	-0,516542	0,642945	35,934	59,9889	95,9229
M2.T$_{0,1}$.ml.1-10x.09	14,1068	17,1501	-0,106424	-0,194682	63,801	70,264	134,064

M2.T$_{0,1}$.ml.1-10x.10	9,8222	12,1549	-0,419663	-0,115902	39,4158	44,5826	83,9984
M2.T$_{0,1}$.ml.1-10x.11	8,7646	11,254	-1,07904	3,26513	50,396	76,677	127,073
AVERAGE-T$_{0,1}$	**10,10082889**	**12,75173667**	**-0,870037556**	**1,441143**	**35,62242222**	**73,57016667**	**109,1925889**
DEV.ST.C -T$_{0,1}$	*2,308778739*	*2,796677269*	*0,427849204*	*1,334212485*	*13,85279708*	*13,91335211*	*16,12810501*
M2.T$_1$.ml.1-10x.01	14,6901	18,8701	-0,87715	1,88104	90,975	119,282	210,257
M2.T$_1$.ml.1-10x.02	12,9894	17,7587	-1,59195	3,48377	88,838	104,432	193,27
M2.T$_1$.ml.1-10x.03	11,4463	14,6822	-1,00683	1,35481	35,134	81,075	116,209
M2.T$_1$.ml.1-10x.04	12,7528	16,7771	-1,32199	3,59391	87,682	107,296	194,978
M2.T$_1$.ml.1-10x.05	7,09604	9,22595	-0,813731	2,33323	59,229	89,556	148,785
M2.T$_1$.ml.1-10x.06	10,2044	13,711	-1,4828	3,47112	52,775	94,812	147,587
M2.T$_1$.ml.1-10x.07	9,7791	12,2502	-0,56232	0,0166078	37,815	60,2691	98,0841
M2.T$_1$.ml.1-10x.09	8,6637	12,0875	-1,79118	5,87178	41,233	95,578	136,811
M2.T$_1$.ml.1-10x.11	8,8337	12,0442	-1,14423	3,56272	26,007	99,5	125,507
AVERAGE-T$_1$	**10,71728222**	**14,15632778**	**-1,176909**	**2,840998644**	**57,74311111**	**94,64445556**	**152,3875667**
DEV.ST.C -T$_1$	*2,440346058*	*3,14688576*	*0,402130861*	*1,67514517*	*25,4522682*	*16,87835026*	*38,87988407*
M2.T$_2$.ml.1-10x.01	14,1327	18,954	-1,34438	2,36298	68,83	96,168	164,997
M2.T$_2$.ml.1-10x.03	9,6976	12,4127	-0,959669	1,21401	81,388	60,392	141,78
M2.T$_2$.ml.1-10x.04	11,3444	14,4499	-0,988895	0,539184	74,476	83,125	157,601
M2.T$_2$.ml.1-10x.05	15,31	18,6661	0,386306	1,18709	125,246	68,698	193,944
M2.T$_2$.ml.1-10x.06	8,7672	11,2448	-0,677889	0,903674	30,9144	51,1622	82,0766
M2.T$_2$.ml.1-10x.07	8,7912	11,2695	-1,10196	1,85476	42,214	65,208	107,422
M2.T$_2$.ml.1-10x.08	8,2354	10,3561	-0,71478	0,742725	26,2163	64,4177	90,634
M2.T$_2$.ml.1-10x.09	11,8867	15,18	-0,336995	0,0946003	55,76	87,191	142,951
M2.T$_2$.ml.1-10x.10	7,01077	8,87126	-0,607547	0,694064	34,2619	46,6905	80,9524
AVERAGE-T$_2$	**10,57510778**	**13,48937333**	**-0,705089889**	**1,065898589**	**59,92295556**	**69,22804444**	**129,1508889**
DEV.ST.C -T$_2$	*2,801503282*	*3,583137917*	*0,506031228*	*0,692027315*	*31,59516738*	*16,55870917*	*40,52347408*
M2.T$_3$.ml.1-10x.01	14,3431	17,3063	-0,518537	-0,296283	42,04	68,221	110,261

M2.T₃.ml.1-10x.02	9,3856	12,4667	-1,27783	2,55277	61,172	68,465	129,637
M2.T₃.ml.1-10x.03	12,3427	15,6467	-1,00361	0,641184	31,344	89,425	120,769
M2.T₃.ml.1-10x.06	11,0995	15,4889	-1,62936	3,44378	27,886	80,929	108,814
M2.T₃.ml.1-10x.07	8,1645	10,7705	-0,859072	1,48658	25,7674	64,7795	90,5469
M2.T₃.ml.1-10x.08	8,468	11,3745	-1,27108	3,12818	21,255	95,288	116,543
M2.T₃.ml.1-10x.10	10,5773	14,062	-1,06468	2,40424	96,911	81,796	178,707
M2.T₃.ml.1-10x.12	15,6326	19,0332	-0,770945	0,00848678	40,484	79,784	120,268
M2.T₃.ml.1-10x.16	6,96543	8,97989	-0,528012	1,16529	21,7934	69,6246	91,418
AVERAGE-T₃	**10,77541444**	**13,90318778**	**-0,991458444**	**1,614914198**	**40,96142222**	**77,59023333**	**118,5515444**
DEV.ST.C -T₃	*2,90495047*	*3,278492229*	*0,366949244*	*1,348026247*	*24,47010909*	*10,52104863*	*26,07083136*

M3: Active tool used to process roots

SAMPLE	Mean roughness (Sa)	RMS roughness (Sq)	Skew (Ssk)	Excess kurtosis	Max.height of peaks (Sp)	Max. height of valleys (Sv)	Max. height of the surface (Sz)
M3.T_0.ml.1-10x.01	17,0984	23,6643	-1,46582	3,39938	77,558	145,825	223,383
M3.T_0.ml.1-10x.03	10,0161	13,4204	-1,27492	2,58528	56,01	79,423	135,433
M3.T_0.ml.1-10x.05	16,3024	21,6491	-1,30682	2,69537	72,276	131,145	203,421
M3.T_0.ml.1-10x.06	19,7379	28,6683	-0,769601	4,15835	108,41	175,666	284,076
M3.T_0.ml.1-10x.08	8,3299	10,9233	-0,805458	2,39754	44,187	111,261	155,448
M3.T_0.ml.1-10x.09	10,6742	13,3894	-0,809764	1,57629	61,527	83,664	145,19
M3.T_0.ml.1-10x.10	12,0221	16,5442	-0,749986	3,46298	82,751	104,341	187,092
M3.T_0.ml.1-10x.11	18,0838	24,1271	-1,04854	1,30109	103,576	100,028	203,604
M3.T_0.ml.1-10x.12	14,5842	19,2949	-1,40667	2,24186	67,571	86,396	153,967
AVERAGE-T_0	14,09433333	19,07566667	-1,070842111	2,64646	74,874	113,0832222	187,9571111
DEV.ST.C -T_0	*3,996213443*	*5,941873091*	*0,295572325*	*0,915593153*	*21,07571877*	*32,16315963*	*47,14143323*
M3.T_1.ml.1-10x.01	16,8127	24,2743	-1,47749	3,9497	80,758	121,317	202,075
M3.T_1.ml.1-10x.02	25,3075	32,0001	-1,18668	1,02921	84,299	127,644	211,943
M3.T_1.ml.1-10x.04	13,9	19,1189	-1,73535	3,56477	35,944	100,066	136,01
M3.T_1.ml.1-10x.05	9,2893	12,8725	-1,64696	4,83552	41,491	100,721	142,212
M3.T_1.ml.1-10x.06	18,7295	28,4849	-1,20578	4,06883	105,84	128,844	234,683
M3.T_1.ml.1-10x.07	20,1924	27,4464	-0,746499	1,04597	85,439	116,41	201,849
M3.T_1.ml.1-10x.08	21,9784	28,6969	-1,33117	1,501	54,663	126,875	181,538
M3.T_1.ml.1-10x.09	21,4567	29,0095	-1,37342	2,66818	97,839	150,275	248,115
M3.T_1.ml.1-10x.10	13,0238	18,7444	-2,09418	8,10423	41,424	118,297	159,721
AVERAGE-T_1	17,85447778	24,51643333	-1,421947667	3,418601111	69,74411111	121,161	190,9051111
DEV.ST.C -T_1	*5,06436987*	*6,285819315*	*0,38287377*	*2,243543524*	*26,55623857*	*15,30900073*	*39,24488292*
M3.T_2.ml.1-10x.03	12,7429	16,8485	-1,43928	2,0937	35,8	91,537	127,337

M3.T$_2$.ml.1-10x.06	14,3782	17,6775	-0,938316	0,674574	31,971	100,642	132,612
M3.T$_2$.ml.1-10x.07	18,6773	23,6179	-0,355669	0,132361	59,38	93,933	153,313
M3.T$_2$.ml.1-10x.09	16,328	21,7783	-1,33391	2,54472	56,96	116,506	173,466
M3.T$_2$.ml.1-10x.10	16,4182	20,9709	-0,377479	0,117515	55,364	122,784	178,148
M3.T$_2$.ml.1-10x.11	14,2841	18,5847	-1,05961	1,85482	52,837	105,023	157,86
M3.T$_2$.ml.1-10x.12	10,4547	13,6547	-0,804722	1,42657	37,205	91,82	129,024
M3.T$_2$.ml.1-10x.13	10,4897	12,9884	-0,603884	0,790576	25,378	109,802	135,181
M3.T$_2$.ml.1-10x.15	11,544	15,7452	-1,51205	4,03437	60,123	134,443	194,566
AVERAGE-T$_2$	**13,92412222**	**17,98512222**	**-0,936102222**	**1,518800667**	**46,11311111**	**107,3877778**	**153,5007778**
DEV.ST.C -T$_2$	*2,868360512*	*3,631706353*	*0,438036265*	*1,272859506*	*13,39958393*	*14,93205759*	*24,41080045*
M3.T$_3$.ml.2-10x.02	32,5807	40,0467	-1,06805	0,253594	57,033	171,82	228,853
M3.T$_3$.ml.2-10x.03	21,6263	28,5847	-1,15859	1,61423	63,928	117,763	181,691
M3.T$_3$.ml.2-10x.04	12,4517	16,2596	-1,49111	4,30775	35,18	117,923	153,103
M3.T$_3$.ml.2-10x.05	24,8348	32,5206	-0,706621	0,709708	148,391	123,281	271,672
M3.T$_3$.ml.2-10x.06	16,7445	22,1688	-1,39399	2,7891	69,24	135,829	205,069
M3.T$_3$.ml.2-10x.08	19,012	26,0021	-1,68496	2,99568	44,475	139,107	183,582
M3.T$_3$.ml.2-10x.09	13,4385	16,7169	-0,686646	0,353859	51,947	73,019	124,966
M3.T$_3$.ml.2-10x.10	26,3855	34,9357	-0,516056	0,208227	89,389	118,139	207,527
M3.T$_3$.ml.2-10x.11	16,2963	23,5657	-0,452826	5,53569	104,876	181,844	286,72
AVERAGE-T$_3$	**20,37447778**	**26,75564444**	**-1,017649889**	**2,085315333**	**73,82877778**	**130,9694444**	**204,7981111**
DEV.ST.C -T$_3$	*6,606139153*	*8,084488846*	*0,448668645*	*1,941623016*	*35,35700148*	*32,15864923*	*52,20043489*

M1: Active tool used to process ochre

SAMPLE	Mean roughness (Sa)	RMS roughness (Sq)	Skew (Ssk)	Excess kurtosis	Max.height of peaks (Sp)	Max. height of valleys (Sv)	Max. height of the surface (Sz)
M1.T_0.ml.2-10x.01	9,5353	11,6691	-0,690126	0,055133	24,2471	59,6213	83,8684
M1.T_0.ml.2-10x.02	16,2386	20,6809	20,6809	0,748188	38,282	99,114	137,396
M1.T_0.ml.2-10x.04	9,6262	12,2845	-0,947596	1,91557	63,02	72,813	135,833
M1.T_0.ml.2-10x.05	9,3135	12,4944	-1,33791	2,86571	21,2384	75,885	97,1234
M1.T_0.ml.2-10x.07	12,3315	15,7714	-0,882866	0,565471	29,567	78,166	107,733
M1.T_0.ml.2-10x.08	9,6766	12,5208	-1,14737	1,55071	23,2176	65,1527	88,3703
M1.T_0.ml.2-10x.10	7,32501	9,33574	-1,21767	1,63966	16,2201	59,2474	75,4675
M1.T_0.m.2-10x.11	13,5235	17,2936	-1,1112	2,26781	30,023	112,647	142,67
M1.T_0.ml.2-10x.12	9,1597	11,7942	-1,09249	1,35101	53,038	59,283	112,322
AVERAGE-T_0	**10,74776778**	**13,76051556**	**1,361519111**	**1,439918**	**33,20591111**	**75,76993333**	**108,9759556**
DEV.ST.C. -T_0	*2,750724508*	*3,492056747*	*7,247302617*	*0,877880019*	*15,58483509*	*18,83374102*	*24,98827575*
M1.T_3.ml.2-10x.01	22,2032	28,1571	-0,700104	0,157279	63,993	103,094	167,087
M1.T_3.ml.2-10x.02	26,1398	31,2951	-0,268269	-0,671118	88,696	87,753	176,449
M1.T_3.ml.2-10x.03	23,9782	29,338	-0,374513	-0,296438	68,947	99,896	168,844
M1.T_3.ml.2-10x.05	21,1045	26,9668	-1,0727	1,52353	45,077	135,276	180,353
M1.T_3.ml.2-10x.06	21,035	25,9435	-0,0768186	-0,23258	78,853	104,655	183,508
M1.T_3.ml.2-10x.09	12,5031	16,2996	-1,25066	2,71536	59,479	94,52	153,999
M1.T_3.ml.2-10x.10	10,942	13,8496	-0,745723	0,569444	58,131	62,402	120,532
M1.T_3.ml.2-10x.07	17,5428	22,1227	-0,707816	-0,0514459	50,681	79,708	130,389
M1-T3-ml.2-10x.08	16,7324	20,6831	-0,642623	0,39887	58,982	108,666	167,648
AVERAGE-T3	**19,13122222**	**23,85061111**	**-0,648802956**	**0,456989011**	**63,64877778**	**97,33**	**160,9787778**
DEV.ST.C. -T3	*5,10932232*	*6,002346528*	*0,371596859*	*1,055810613*	*13,55270861*	*20,28540912*	*22,04058295*

GS7: Passive tool used to process achenes

For this tool, two areas were analysed: C2, located in a peripheral area of the utilized surface (indicated in the table in light grey), and C4, situated in the central area of the utilized surface (indicated in the table in dark grey).

SAMPLE	Mean roughness (Sa)	RMS roughness (Sq)	Skew (Ssk)	Excess kurtosis	Max.height of peaks (Sp)	Max. height of valleys (Sv)	Max. height of the surface (Sz)
GS7.T$_0$.sq.C2-10x.04	30,0482	37,1229	-0,0394849	-0,235355	108,634	119,637	228,27
GS7.T$_0$.sq.C2-10x.05	41,056	52,7149	0,729426	0,481962	158,705	121,694	280,399
GS7.T$_0$.sq.C2-10x.06	34,4958	44,7806	0,458205	0,296233	131,713	125,316	257,029
GS7.T$_0$.sq.C2-10x.09	32,8524	40,5322	-0,460896	-0,207024	82,235	151,955	234,189
GS7.T$_0$.sq.C2-10x.10	33,9728	40,4396	-0,425515	-0,678279	89,626	123,736	213,363
GS7.T$_0$.sq.C2-10x.11	21,6646	27,6832	-0,15178	0,102273	85,766	134,855	220,621
GS7.T$_0$.sq.C2-10x.25	49,3255	58,8787	-0,251687	-0,549132	146,922	204,741	351,663
GS7.T$_0$.sq.C2-10x.24	31,6166	39,331	-0,0382243	-0,205431	112,083	111,743	223,826
GS7.T$_0$.sq.C2-10x.22	28,7736	35,9842	0,610112	-0,0748257	108,181	98,963	207,144
AVERAGE-T$_0$	**33,75616667**	**41,94081111**	**0,047795089**	**-0,118842078**	**113,7627778**	**132,5155556**	**246,2782222**
DEV.ST.C -T$_0$	*7,797926056*	*9,247022253*	*0,443928941*	*0,372667784*	*27,06989673*	*30,75920661*	*45,59810575*
GS7.T$_0$.sq.C4-10x.06	40,011	51,941	-0,415403	0,383933	116,371	172,739	289,11
GS7.T$_0$.sq.C4-10x.07	25,8721	31,9094	-0,127313	-0,568761	84,597	88,951	173,548
GS7.T$_0$.sq.C4-10x.08	38,5901	47,7338	-0,0452409	-0,220763	170,97	112,141	283,112
GS7.T$_0$.sq.C4-10x.09	39,3515	48,2971	0,519599	-0,362706	137,7	164,536	302,236
GS7.T$_0$.sq.C4-10x.10	33,1411	42,3351	-0,0261106	0,119094	107,259	146,889	254,148
GS7.T$_0$.sq.C4-10x.11	26,1814	32,2994	0,246408	-0,38731	108,483	143,67	252,153
GS7.T$_0$.sq.C4-10x.12	33,4043	39,5935	0,384357	-0,774376	115,349	91,999	207,349
GS7.T$_0$.sq.C4-10x.13	42,549	50,9276	-0,0362152	-0,736331	134,73	149,232	283,962
GS7.T$_0$.sq.C4-10x.14	50,1587	62,6162	0,402284	-0,102439	196,838	146,877	343,715

AVERAGE-T_0	**36,58435556**	**45,29478889**	**0,100262811**	**-0,294406556**	**130,2552222**	**135,226**	**265,4814444**
DEV.ST.C -T_0	*7,811885714*	*9,875524256*	*0,304671413*	*0,385297983*	*34,76511186*	*30,3076067*	*51,01384166*
GS7.T_1.sq.C2-10x.01	20,2362	27,356	-1,53632	2,53556	43,805	135,899	179,704
GS7.T_1.sq.C2-10x.02	29,3347	37,2122	-1,14889	1,05024	62,854	144,109	206,963
GS7.T_1.sq.C2-10x.03	31,3896	38,7527	0,439737	-0,434985	113,006	81,045	194,051
GS7.T_1.sq.C2-10x.20	17,1135	21,5563	-0,448028	0,310251	56,523	135,358	191,881
GS7.T_1.sq.C2-10x.21	22,316	26,868	0,0875447	-0,536258	75,947	66,915	142,862
GS7.T_1.sq.C2-10x.22	16,7662	13,7258	-0,616744	-0,0642118	34,9963	59,6069	94,6031
GS7.T_1.sq.C2-10x.23	12,4237	15,6512	-1,04607	1,56572	32,369	89,611	121,98
GS7.T_1.sq.C2-10x.24	23,1105	28,0813	-0,810922	-0,0860452	49,552	94,794	144,346
GS7.T_1.sq.C2-10x.25	20,1429	25,3419	-0,607469	0,214355	56,252	103,396	159,647
AVERAGE-T_1	**21,42592222**	**26,0606**	**-0,631906811**	**0,506069556**	**58,36714444**	**101,1926556**	**159,5596778**
DEV.ST.C -T_1	*6,019398517*	*8,464402792*	*0,611297993*	*1,019135995*	*24,58232379*	*31,03185209*	*37,12992912*
GS7.T_1.sq.C4-10x.06	18,4659	22,9462	-0,391708	-0,1483	52,892	91,078	143,97
GS7.T_1.sq.C4-10x.07	18,0774	22,874	0,0409114	-0,30881	74,712	64,026	138,738
GS7.T_1.sq.C4-10x.08	18,4229	21,9369	-0,26719	-0,372753	62,394	80,33	142,724
GS7.T_1.sq.C4-10x.09	21,9969	26,879	-0,412111	-0,183322	56,829	94,587	151,417
GS7.T_1.sq.C4-10x.10	22,6376	27,6271	0,667333	-0,427274	80,63	67,599	148,23
GS7.T_1.sq.C4-10x.11	18,2779	22,6065	0,730736	0,206897	78,479	71,55	150,029
GS7.T_1.sq.C4-10x.12	26,5695	32,7972	-0,283639	-0,202719	95,365	92,876	188,241
GS7.T_1.sq.C4-10x.13	19,6433	23,4818	0,147667	-0,679779	62,869	54,722	117,591
GS7.T_1.sq.C4-10x.14	18,973	23,6269	0,0820991	-0,206777	65,135	67,583	132,718
AVERAGE-T_1	**20,34048889**	**24,97506667**	**0,034899833**	**-0,258093**	**69,92277778**	**76,039**	**145,962**
DEV.ST.C -T_1	*2,866709127*	*3,522477065*	*0,429196664*	*0,240239708*	*13,45804763*	*14,2903481*	*18,99312784*
GS7.T_2.sq.C2-10x.02	15,6991	19,1561	-0,248482	-0,262186	141,068	112,567	253,635
GS7.T_2.sq.C2-10x.03	14,8723	18,8847	-0,755325	0,553075	54,13	88,314	142,444
GS7.T_2.sq.C2-10x.04	30,1254	37,7218	0,310891	0,210508	132,397	105,645	238,042

GS7.T$_2$.sq.C2-10x.06	18,0686	23,4941	-0,931429	1,13901	52,147	87,734	139,88
GS7.T$_2$.sq.C2-10x.15	15,6613	20,5566	-0,7753	1,41109	98,091	83,887	181,977
GS7.T$_2$.sq.C2-10x.16	15,3128	19,0747	-0,160715	0,239021	67,541	72,15	139,69
GS7.T$_2$.sq.C2-10x.17	10,3467	13,0885	-0,82246	0,592413	109,014	52,187	161,201
GS7.T$_2$.sq.C2-10x.18	19,3172	24,5232	-0,668742	0,31027	50,115	99,355	149,47
GS7.T$_2$.sq.C2-10x.19	27,182	31,9482	-0,0231632	-0,944139	73,16	73,271	146,431
AVERAGE-T$_2$	**18,50948889**	**23,16087778**	**-0,452747244**	**0,361006889**	**86,407**	**86,12333333**	**172,53**
DEV.ST.C -T$_2$	*6,295615251*	*7,503834801*	*0,433411467*	*0,700917452*	*35,02600442*	*18,64116973*	*43,80355596*
GS7.T$_2$.sq.C4-10x.07	24,3756	28,9726	-0,649099	-0,182458	50,514	109,377	159,89
GS7.T$_2$.sq.C4-10x.08	24,0487	29,4193	-0,10908	-0,392515	77,561	81,997	159,558
GS7.T$_2$.sq.C4-10x.09	17,3176	21,3609	-0,596561	0,0500591	126,902	86,768	213,67
GS7.T$_2$.sq.C4-10x.10	14,0782	17,5904	-0,311383	-0,110996	45,997	63,282	109,279
GS7.T$_2$.sq.C4-10x.11	27,0501	32,9396	-0,50048	-0,248479	145,849	112,712	258,562
GS7.T$_2$.sq.C4-10x.12	19,5034	24,7144	-0,309943	-0,10413	65,38	88,05	153,43
GS7.T$_2$.sq.C4-10x.14	18,4508	22,861	-0,554516	-0,05228	52,024	91,391	143,415
GS7.T$_2$.sq.C4-10x.15	17,9407	22,367	-0,565033	0,133273	44,651	98,971	143,623
GS7.T$_2$.sq.C4-10x.17	18,8574	23,235	-0,100956	-0,522258	81,526	72,421	153,947
AVERAGE-T$_2$	**20,18027778**	**24,82891111**	**-0,410783444**	**-0,158864878**	**76,71155556**	**89,441**	**166,1526667**
DEV.ST.C -T$_2$	*4,114078342*	*4,755728021*	*0,209425496*	*0,206420598*	*36,60331608*	*16,09376263*	*43,94618634*
GS7.T$_3$.sq.C2-10x.01	20,0408	24,1679	0,125805	-0,50315	70,292	72,343	142,635
GS7.T$_3$.sq.C2-10x.02	18,7355	23,2856	0,766487	0,940384	100,472	61,779	162,251
GS7.T$_3$.sq.C2-10x.04	14,9292	17,9148	-0,0060718	-0,627445	43,4433	49,1724	92,6157
GS7.T$_3$.sq.C2-10x.06	9,2545	12,4331	-0,694316	2,03021	33,961	80,602	114,563
GS7.T$_3$.sq.C2-10x.07	8,897	12,498	-1,21741	2,81556	30,7341	53,5164	84,2505
GS7.T$_3$.sq.C2-10x.24	8,586	10,9742	-0,0723902	0,166404	32,3962	49,129	81,5252
GS7.T$_3$.sq.C2-10x.25	8,7255	10,622	-0,499268	-0,190921	26,3809	54,5718	80,9527
GS7.T$_3$.sq.C2-10x.26	8,08962	9,94899	-0,614027	0,156845	22,9568	46,1417	69,0985

GS7.T₃.sq.C2-10x.28	12,2307	15,1667	-0,0091745	-0,425939	44,813	42,6689	87,4818
AVERAGE-T3	**12,16542444**	**15,22347667**	**-0,246707278**	**0,484660889**	**45,04992222**	**56,65824444**	**101,7081556**
DEV.ST.C -T₃	*4,653543946*	*5,41423541*	*0,575691951*	*1,211218389*	*25,09000959*	*12,64312271*	*31,61694874*
GS7.T₃.sq.C4-10x.18	11,8013	14,4141	-0,194154	-0,450896	38,6402	49,7251	88,3653
GS7.T₃.sq.C4-10x.04	13,7052	17,2781	-0,770357	0,317286	36,4573	62,1122	98,5695
GS7.T₃.sq.C4-10x.05	28,0031	33,993	-0,126052	-0,6791	102,992	84,758	187,751
GS7.T₃.sq.C4-10x.06	26,0155	31,1193	-0,015719	-0,881585	62,791	78,093	140,884
GS7.T₃.sq.C4-10x.07	13,1582	16,4917	-0,487845	-0,077525	39,57	78,538	118,108
GS7.T₃.sq.C4-10x.08	18,0312	22,3575	-0,240752	0,0860921	60,413	96,079	156,492
GS7.T₃.sq.C4-10x.09	23,4286	28,5687	-0,647948	-0,195265	52,6	102,099	154,699
GS7.T₃.sq.C4-10x.11	16,6949	20,3163	-0,722119	-0,208541	62,202	73,331	135,533
GS7.T₃.sq.C4-10x.13	12,4169	15,5687	-0,635704	0,003662	34,0871	63,2134	97,3005
AVERAGE-T₃	**18,13943333**	**22,23415556**	**-0,426738889**	**-0,231763544**	**54,41695556**	**76,43874444**	**130,8558111**
DEV.ST.C -T₃	*6,192661524*	*7,281448179*	*0,284976637*	*0,379797746*	*21,60645365*	*16,67325061*	*33,01804438*
GS7.T₄.sq.C2-10x.19	10,838	13,9275	-0,552988	0,596253	38,414	70,924	109,338
GS7.T₄.sq.C2-10x.20	11,0452	13,6297	-0,18234	-0,211898	45,654	51,1472	96,8012
GS7.T₄.sq.C2-10x.23	18,1973	22,1714	-0,645467	-0,383976	47,885	69,404	117,289
GS7.T₄.sq.C2-10x.29	12,9338	16,4827	-0,0317961	0,0995626	54,157	56,356	110,514
GS7.T₄.sq.C2-10x.28bis	8,6294	11,3033	-0,640885	1,0365	30,3542	65,5295	95,8838
GS7.T₄.sq.C2-10x.27	12,0517	15,0946	-0,583626	0,072971	33,6307	56,642	90,2726
GS7.T₄.sq.C2-10x.26	12,1307	15,2236	-0,411354	0,027773	37,0568	61,1796	98,2364
GS7.T₄.sq.C2-10x.08	10,3381	14,408	-1,36202	3,95549	38,534	73,101	111,635
GS7.T₄.sq.C2-10x.09	13,4507	16,1999	-0,271967	-0,479947	38,537	79,103	117,64
AVERAGE-T₄	**12,17943333**	**15,3823**	**-0,520271456**	**0,523636511**	**40,46918889**	**64,8207**	**105,29**
DEV.ST.C -T₄	*2,680899376*	*2,976044712*	*0,382454293*	*1,37143586*	*7,430150852*	*9,151989264*	*10,10102659*
GS7.T₄.sq.C4-10x.07	18,098	22,2578	-0,234233	-0,381259	52,703	66,19	118,893
GS7.T₄.sq.C4-10x.08	24,1782	28,4688	-0,0789185	-0,939535	67,595	72,898	140,492

GS7.T₄.sq.C4-10x.09	19,1889	23,4829	0,155819	-0,22053	81,42	84,409	165,829
GS7.T₄.sq.C4-10x.10	21,3151	25,9999	0,327318	-0,568001	80,615	61,979	142,595
GS7.T₄.sq.C4-10x.11	17,0931	20,751	0,632735	-0,170204	79,767	47,705	127,472
GS7.T₄.sq.C4-10x.12	17,5351	22,3497	-0,84854	0,398776	41,775	77,887	119,662
GS7.T₄.sq.C4-10x.13	19,9487	23,8302	0,149961	-0,769841	56,733	60,296	117,03
GS7.T₄.sq.C4-10x.14	15,0302	18,5188	0,105798	-0,398802	45,02	63,447	108,467
GS7.T₄.sq.C4-10x.17	20,7238	23,9629	-0,0892337	-0,952179	130,901	71,116	202,017
AVERAGE-T₄	**19,23456667**	**23,29133333**	**0,013411756**	**-0,444619444**	**70,72544444**	**67,32522222**	**138,0507778**
DEV.ST.C -T₄	*2,691202486*	*2,874582658*	*0,41123425*	*0,428150054*	*27,25875739*	*10,77095037*	*29,63120796*

M23: Passive tool used to process acorns

SAMPLE	Mean roughness (Sa)	RMS roughness (Sq)	Skew (Ssk)	Excess kurtosis	Max.height of peaks (Sp)	Max. height of valleys (Sv)	Max. height of the surface (Sz)
M23.T₀.ml.3-10x.02	16,6099	20,6332	-0,588002	0,222202	43,551	82,822	126,373
M23.T₀.ml.3-10x.03	17,3836	21,5	-0,786594	0,398333	42,212	80,418	122,63
M23.T₀.ml.3-10x.05	15,5505	19,6811	-0,707959	0,90196	41,472	107,114	148,586
M23.T₀.ml.3-10x.08	12,4061	16,0058	-0,912544	1,30073	75,17	94,864	170,034
M23.T₀.ml.3-10x.09	21,2867	29,151	-0,834558	2,26458	79,873	131,578	211,451
M23.T₀.ml.3-10x.10	17,325	22,1515	0,00285146	0,0421636	53,202	95,196	148,398
M23.T₀.ml.3-10x.13	15,9932	20,3156	-0,714857	0,221185	65,196	76,495	141,691
M23.T₀.ml.3-10x.14	20,9135	25,8651	-0,522672	-0,275796	76,191	91,821	168,012
M23.T₀.ml.3-10x.16	16,9365	20,8461	-0,628469	-0,103299	63,399	83,362	146,761
AVERAGE-T₀	**17,15611111**	**21,79437778**	**-0,632533727**	**0,552450956**	**60,02955556**	**93,74111111**	**153,7706667**
DEV.ST.C -T₀	*2,694891949*	*3,763522094*	*0,267676052*	*0,808734507*	*15,42011429*	*17,0272403*	*26,84563695*
M23.T₀,₁.ml.2-10x.01	14,7187	18,243	-0,322851	-0,0886316	57,241	62,965	120,205

M23.T$_{0,1}$.ml.2-10x.02	12,2497	15,2932	-0,305382	0,131337	39,929	71,47	111,399
M23.T$_{0,1}$.ml.2-10x.03	12,6647	15,5522	-0,16896	-0,383506	65,709	65,264	130,973
M23.T$_{0,1}$.ml.2-10x.04	14,6968	20,1609	-1,26649	3,33362	60,717	108,503	169,22
M23.T$_{0,1}$.ml.2-10x.05	14,6074	18,0989	-0,566169	-0,258447	44,402	59,613	104,015
M23.T$_{0,1}$.ml.2-10x.06	25,672	31,1588	-0,732773	-0,106248	51,054	105,233	156,288
M23.T$_{0,1}$.ml.2-10x.07	18,3803	22,027	-0,530215	-0,597221	41,056	68,575	109,631
M23.T$_{0,1}$.ml.2-10x.08	18,625	23,5616	-0,859387	0,620137	45,596	93,789	139,386
M23.T$_{0,1}$.ml.2-10x.09	20,5003	25,9352	-0,630388	1,50212	56,252	174,597	230,849
AVERAGE-T$_{0,1}$	**16,90165556**	**21,11453333**	**-0,598068333**	**0,461462267**	**51,32844444**	**90,001**	**141,3295556**
DEV.ST.C -T$_{0,1}$	*4,323023586*	*5,172324057*	*0,332684226*	*1,247215304*	*9,155103674*	*36,76604485*	*40,10245943*
M23.T$_1$.ml.2-10x.01	11,6062	14,2347	-0,515642	-0,0798598	43,225	68,36	111,585
M23.T$_1$.ml.2-10x.02	12,3553	15,2421	-0,581024	0,340024	110,441	121,301	231,742
M23.T$_1$.ml.2-10x.03	14,4057	16,8099	-0,268684	-0,834511	72,501	61,013	133,515
M23.T$_1$.ml.2-10x.05	11,7574	14,2174	-0,0977516	-0,708504	31,0394	53,1275	84,1669
M23.T$_1$.ml.2-10x.06	11,6657	13,9384	0,1512	-0,559463	70,021	44,03	114,052
M23.T$_1$.ml.2-10x.09	12,5087	14,9967	-0,210021	-0,650496	45,583	54,746	100,329
M23.T$_1$.ml.2-10x.11	12,2681	15,51	-0,76514	0,601695	35,766	69,827	105,593
M23.T$_1$.ml.2-10x.13	16,8528	20,3785	-0,190778	-0,572056	56,143	73,89	130,033
M23.T$_1$.ml.2-10x.14	11,2224	14,0108	-0,470084	-0,133571	47,007	60,977	107,984
AVERAGE-T$_1$	**12,73803333**	**15,48205556**	**-0,327547178**	**-0,288526867**	**56,85848889**	**67,47461111**	**124,3333222**
DEV.ST.C -T$_1$	*1,796596239*	*2,053502605*	*0,280495619*	*0,501799351*	*24,52324462*	*22,20988884*	*42,90933447*
M23.T$_2$.ml.2-10x.01	11,5178	15,2207	-1,33315	2,52726	68,997	82,931	151,927
M23.T$_2$.ml.2-10x.02	14,8283	19,2734	-1,27557	1,6502	43,813	86,232	130,045
M23.T$_2$.ml.2-10x.04	11,4952	14,4955	-0,496951	0,0303396	34,508	65,0681	99,5761
M23.T$_2$.ml.2-10x.08	11,7978	14,7853	-0,420868	0,120074	44,27	59,26	103,53
M23.T$_2$.ml.2-10x.09	13,3655	16,4182	-0,345175	0,33914	58,774	103,089	161,863
M23.T$_2$.ml.2-10x.11	16,236	20,2061	-0,672112	-0,0423148	66,521	87,233	153,754

M23.T₂.ml.2-10x.14	14,4311	17,7812	-0,279996	-0,133222	56,854	71,382	128,236
M23.T₂.ml.2-10x.19	14,449	17,175	-0,155427	-0,843121	41,0147	58,3646	99,3792
M23.T₂.ml.2-10x.20	13,6314	16,7761	-0,0996932	-0,462458	65,735	78,698	144,433
AVERAGE-T₂	**13,52801111**	**16,9035**	**-0,564326911**	**0,353988644**	**53,38741111**	**76,91752222**	**130,3048111**
DEV.ST.C -T₂	*1,654227328*	*1,960116713*	*0,453548305*	*1,064016257*	*12,71789404*	*14,76692533*	*24,58351485*
M23.T₃.ml.2-10x.03	17,0101	20,4492	-0,411054	-0,432601	38,75	79,834	118,584
M23.T₃.ml.2-10x.04	13,1352	16,6167	-0,421996	0,355465	53,281	91,247	144,528
M23.T₃.ml.2-10x.05	16,7427	22,5417	-0,705574	1,79691	67,208	117,408	184,616
M23.T₃.ml.2-10x.06	13,2705	16,5176	-0,764096	0,645045	35,9602	64,0293	99,9895
M23.T₃.ml.2-10x.07	10,5349	14,0453	-1,01682	2,13224	36,437	83,121	119,558
M23.T₃.ml.2-10.08	8,4138	10,3489	-0,560592	0,0179501	25,985	90,863	116,848
M23.T₃.ml.2-10x.09	13,0673	16,4104	0,151791	0,115051	65,636	51,307	116,944
M23.T₃.ml.2-10x.11	18,7585	22,1787	-0,378434	-0,71852	78,996	90,233	169,229
M23.T₃.ml.2-10x.12	12,5219	15,3199	-0,0659826	-0,396036	36,464	59,7617	96,2257
AVERAGE-T₃	**13,71721111**	**17,15871111**	**-0,463639733**	**0,390611567**	**48,74635556**	**80,86711111**	**129,6135778**
DEV.ST.C -T₃	*3,279748622*	*3,964168046*	*0,355819471*	*0,988584397*	*18,18503881*	*20,12310267*	*30,32257594*

M25: Passive tool used to process roots

SAMPLE	Mean roughness (Sa)	RMS roughness (Sq)	Skew (Ssk)	Excess kurtosis	Max.height of peaks (Sp)	Max. height of valleys (Sv)	Max. height of the surface (Sz)
M25.T_0.ml.2-10x.09	14,8322	18,4025	-0,493168	-0,136015	37,14	122,061	159,2
M25.T_0.ml.2-10x.10	18,3846	22,3523	-0,161045	-0,557836	55,909	94,131	150,04
M25.T_0.ml.2-10x.11	11,2967	14,2794	-0,627619	0,227787	62,891	53,499	116,39
M25.T_0.ml.2-10x.12	15,8681	19,4426	-0,407093	-0,198565	42,535	68,319	110,854
M25.T_0.ml.2-10x.14	11,2432	14,1945	-0,813347	1,02446	43,911	68,023	111,935
M25.T_0.ml.2-10x.5	11,4126	15,3422	-0,913632	2,03819	62,225	78,182	140,407
M25.T_0.ml.2-10x.16	9,1594	11,4949	-0,538973	0,0981621	24,6146	74,7388	99,3534
M25.T_0.ml.2-10x.17	17,0095	21,2445	-0,376024	0,581606	87,285	100,42	187,705
M25.T_0.ml.2-10x.18	10,6464	13,5245	-0,604386	0,621053	36,082	79,733	115,814
AVERAGE-T_0	13,31696667	16,69748889	-0,548365222	0,410982456	50,28806667	82,12297778	132,4109333
DEV.ST.C -T_0	3,250880809	3,777873104	0,227998325	0,777671346	18,8291004	20,48926518	28,85026691
M25.T_1.ml.2-10x.06	17,4749	23,0873	-1,11977	1,51474	51,077	98,432	149,508
M25.T_1.ml.2-10x.07	14,0671	17,0551	-0,0406165	-0,380639	45,407	63,036	108,443
M25.T_1.ml.2-10x.08	14,5684	18,4524	-0,833885	0,464172	36,924	79,087	116,011
M25.T_1.ml.2-10x.09	11,9201	14,8726	-0,526267	0,106972	63,771	109,39	173,161
M25.T_1.ml.2-10x.10	12,9682	16,3052	-0,665974	0,625988	39,467	77,102	116,569
M25.T_1.ml.2-10x.11	15,9623	19,5735	-0,382171	-0,377599	60,278	84,887	145,165
M25.T_1.ml.2-10x.12	38,5734	47,4086	-0,920597	0,137644	84,2	160,801	245,001
M25.T_1.ml.2-10x.13	10,722	13,4298	-0,466985	0,125554	63,142	72,776	135,918
M25.T_1.ml.2-10x.14	14,4514	17,716	-0,232225	-0,379164	38,882	68,437	107,319
AVERAGE-T_1	16,74531111	20,87783333	-0,576498944	0,204185333	53,68311111	90,43866667	144,1216667
DEV.ST.C -T_1	8,430704027	10,32837608	0,34383403	0,612771788	15,58578474	30,12142438	43,72368723
M25.T_2.ml.2-10x.03	13,1693	16,0326	-0,559279	-0,278733	29,339	68,1889	97,5279

M25.T₂.ml.2-10x.04	15,5869	19,4967	-0,700891	0,0122559	41,353	72,292	113,645
M25.T₂.ml.2-10x.05	11,7957	14,6973	-0,459604	0,155513	81,228	73,309	154,537
M25.T₂.ml.2-10x.06	10,3267	12,7238	-0,484765	0,037755	66,535	76,649	143,185
M25.T₂.ml.2-10x.08	16,1389	19,8383	-0,348347	-0,341791	58,759	67,739	126,498
M25.T₂.ml.2-10x.09	19,1719	27,0104	-2,301	9,02921	57,489	164,635	222,124
M25.T₂.ml.2-10x.10	13,4883	16,8414	-0,848875	0,506558	34,226	75,652	109,878
M25.T₂.ml.2-10x.11	13,1382	17,1319	-0,526008	0,487073	44,172	77,972	122,143
M25.T₂.ml.2-10x.12	14,9398	18,5303	-0,377565	-0,0589022	43,128	77,203	120,331
AVERAGE-T₂	**14,19507778**	**18,03363333**	**-0,734037111**	**1,060993189**	**50,69211111**	**83,73776667**	**134,4298778**
DEV.ST.C -T₂	*2,608378098*	*4,058794946*	*0,607942735*	*3,002350288*	*16,61604956*	*30,56434274*	*37,04799221*
M25.T₃.ml.1-10x.08	10,6727	13,5779	-0,601543	0,561963	27,7893	67,0808	94,8702
M25.T₃.ml.1-10x.09	13,2865	16,3385	-0,54687	0,12159	58,469	76,472	134,94
M25.T₃.ml.1-10x.10	10,7233	13,4921	-0,731345	0,490923	29,716	75,021	104,736
M25.T₃.ml.1-10x.11	22,1974	28,9923	-1,3858	5,01877	55,247	198,55	253,797
M25.T₃.ml.1-10x.12	11,2863	15,0233	-1,43933	5,13964	65,257	120,48	185,737
M25.T₃.ml.1-10x.14	16,333	16,333	-0,597037	0,0495564	36,849	65,409	102,258
M25.T₃.ml.1-10x.15	14,1709	17,8136	-0,858715	0,351533	39,105	98,066	137,171
M25.T₃.ml.1-10x.6	11,0286	14,2974	-0,810505	1,185	44,602	76,488	121,09
M25.T₃.ml.1-10x.17	10,3596	12,8159	-0,641541	0,0391789	25,502	79,931	105,433
AVERAGE-T₃	**13,33981111**	**16,52044444**	**-0,845854**	**1,439794922**	**42,50403333**	**95,27753333**	**137,7813556**
DEV.ST.C -T₃	*3,881196441*	*4,950052108*	*0,337456611*	*2,093151036*	*14,37020119*	*42,34953538*	*51,58501292*

GS10: Passive tool used to process ochre

The unused side of the stone for this tool was also analysed and the results are reported in the table in grey.

SAMPLE	Mean roughness (Sa)	RMS roughness (Sq)	Skew (Ssk)	Excess kurtosis	Max.height of peaks (Sp)	Max. height of valleys (Sv)	Max. height of the surface (Sz)
GS10-T_0-ml.5-.10x.01	15,5822	20,0578	0,0679911	0,310871	69,22	81,073	150,293
GS10-T_0-ml.5-.10x.05	37,0047	44,8386	0,600793	-0,194133	130,829	120,392	251,221
GS10-T_0-ml.5-.10x.06	30,681	38,449	0,478633	0,5324	145,518	115,964	261,482
GS10-T_0-ml.5-.10x.08	27,1403	34,7682	-0,590867	0,271011	75,991	129,336	205,327
GS10-T_0-ml.5-.10x.10	26,6751	35,9812	-0,482489	0,763051	116,856	125,493	242,349
GS10-T_0-ml.5-.10x.13	23,8492	31,0022	-0,340076	2,49906	118,613	168,815	287,428
GS10-T_0-ml.5-.10x.15	33,2456	42,4517	-0,603859	0,24975	101,376	137,155	238,531
GS10-T_0-ml.5-.10x.16	35,2138	43,8295	-0,342729	-0,457072	95,211	133,318	228,529
GS10-T_0-ml.5-.10x.14	26,0856	32,18	-0,160513	-0,608936	78,057	89,26	167,317
AVERAGE-T_0	**28,38638889**	**35,95091111**	**-0,152568433**	**0,374000222**	**103,519**	**122,3117778**	**225,8307778**
DEV.ST.C. -T_0	*6,558145836*	*7,764213555*	*0,445900051*	*0,915285493*	*26,3903331*	*25,98197539*	*44,3022876*
GS10.back.T_0.10x.02	21,4312	25,9776	-0,41954	-0,0934096	66,887	104,684	171,571
GS10.back.T_0.10x.10	21,8808	27,6688	-0,621812	0,514934	96,478	108,533	205,011
GS10.back.T_0.10x.05	32,0538	39,9087	-0,0569915	-0,239236	101,993	142,878	244,871
GS10.back.T_0.10x.09	38,9797	50,4414	0,373387	0,363599	156,773	155,56	312,333
GS10.back.T_0.10x.11	29,9526	38,6416	0,343882	0,278553	140,965	108,629	249,595
GS10.back.T_0.10x.12	24,8975	32,9895	-0,448261	1,19866	93,92	159,071	252,99
GS10.back.T_0.10x.13	37,3128	44,6698	-0,209739	-0,43641	99,72	152,318	252,038
GS10.back.T_0.10x.14	44,5279	55,6155	-0,60653	-0,343573	127,519	147,516	275,035
GS10.back.T_0.10x.06	30,1443	38,1395	-0,163407	0,014938	126,553	122,81	249,363
AVERAGE-T_0-back	**31,24228889**	**39,33915556**	**-0,201001278**	**0,139783933**	**112,312**	**133,5554444**	**245,8674444**

DEV.ST.C. -T$_{0}$-back	*7,912844078*	*9,835469103*	*0,370722255*	*0,513634275*	*27,72473158*	*22,26420873*	*39,64457737*
GS10-T$_{3}$-ml.3bis-.10x.01	18,2525	22,8512	0,733024	0,564482	95,083	71,721	166,804
GS10-T$_{3}$-ml.3bis-.10x.02	16,1026	20,9991	1,00102	1,32158	111,116	67,586	178,703
GS10-T$_{3}$-ml.3bis-.10x.09	15,5395	19,5482	-0,160848	0,613519	59,991	112,4	172,391
GS10-T$_{3}$-ml.3bis-.10x.04	30,9584	36,9454	-0,0237773	-0,781983	99,25	109,759	209,009
GS10-T$_{3}$-ml.3bis-.10x.12	27,7208	34,22	-0,241092	-0,237032	96,866	120,734	217,6
GS10-T$_{3}$-ml.3bis-.10x.14	20,7827	27,6979	-0,730074	1,14479	86,67	105,312	191,982
GS10-T$_{3}$-ml.3bis-.10x.15	16,8196	21,5482	0,124009	0,105302	66,044	73,034	139,078
GS10-T$_{3}$-ml.3bis-.10x.03	26,138	32,8083	-0,15231	-0,239542	84,043	114,014	198,057
GS10-T$_{3}$-ml.3bis-.10x.19	17,4997	21,2129	-0,21315	-0,531893	52,926	67,358	120,284
AVERAGE-T$_{3}$	**21,09042222**	**26,42568889**	**0,037422411**	**0,217691444**	**83,55433333**	**93,54644444**	**177,1008889**
DEV.ST.C. -T$_{3}$	*5,720464889*	*6,654506089*	*0,527771449*	*0,736946222*	*19,76737677*	*22,83556853*	*31,86609933*
GS10_T$_{5}$.back_ml.4_10x.02	20,373	25,6191	-0,0753447	0,118113	73,03	106,031	179,061
GS10_T$_{5}$.back_ml.4_10x.03	35,1214	42,236	-0,37078	-0,557443	96,405	140,309	236,714
GS10_T$_{5}$.back_ml.4_10x.04	22,5912	26,8048	0,447264	-0,62263	80,592	73,374	153,966
GS10_T$_{5}$.back_ml.4_10x.05	18,8234	23,6568	-0,205065	-0,151642	64,761	74,731	139,492
GS10_T$_{5}$.back_ml.4_10x.06	22,3619	29,28	-0,609303	0,973273	113,172	111,295	224,468
GS10_T$_{5}$.back_ml.4_10x.07	35,4771	45,0128	0,250068	0,108418	147,852	128,954	276,805
GS10_T$_{5}$.back_ml.4_10x.08	21,0969	26,6604	-0,169364	0,28739	90,82	118,202	209,022
GS10_T$_{5}$.back_ml.4_10x.01	30,7486	37,9532	0,372522	-0,22543	117,871	99,69	217,561
GS10_T$_{5}$.back_ml.4_10x.10	31,9802	44,4829	-1,52545	4,28843	86,319	250,351	336,67
AVERAGE-T$_{5}$-back	**26,50818889**	**33,52288889**	**-0,209494744**	**0,468719889**	**96,758**	**122,5485556**	**219,3065556**
DEV.ST.C. -T$_{5}$-back	*6,718127046*	*8,787235271*	*0,603996854*	*1,510013665*	*25,78346787*	*52,83874254*	*61,01043364*

Appendix C: Brînzeni I GSTs Area Roughness Measurements

Confocal profilometer areal measurements were processed using the open-source software Gwyddion to calculate the seven ISO 25178-2 surface texture areal parameters for the 10 selected GSTs from Brînzeni I. The results are presented in the main text in Chapter 7 as box charts, and the detailed data are provided below. It is important to note that in this section the decimal separator is indicated by the comma. For each stone, up to three 0,5 cm² squares were analysed, and 9 sub-regions of 850 µm² for each square were examined. The average value for each parameter was calculated (and reported in blue in the tables) based on the data from all 9 analysed areas, along with their corresponding standard deviation (in light blue).

Acronym	Parameter	Unit of Measurement
Sa	Arithmetical mean height of the surface	µm
Sq	Root means square height of the surface	µm
Ssk	Skewness of height distribution	unitless
Sku	Kurtosis of height distribution	unitless
Sp	Maximum height of peaks	µm
Sv	Maximum height of valleys	µm
Sz	Maximum height of the surface	µm

BZ#2965-BZ#833

SAMPLE	Mean roughness (Sa)	RMS roughness (Sq)	Skew (Ssk)	Excess kurtosis	Max.height of peaks (Sp)	Max. height of valleys (Sv)	Max. height of the surface (Sz)
BZ#2965-ml.3-10x.01	6,13552	7,89765	-0,859119	1,30393	20,8603	47,2506	68,1109
BZ#2965.ml.3-10x.03	5,29338	6,86044	-0,396959	1,76179	77,135	56,975	134,111
BZ#2965.ml.3-10x.04	10,2572	14,4772	-1,61411	4,94007	30,741	76,783	107,524
BZ#2965.ml.3-10x.05	8,591	10,6036	-0,370938	-0,136383	27,8424	60,0588	87,9012
BZ#2965.ml.3-10x.06	7,249	8,99875	-0,371256	0,103072	20,3197	78,1686	98,4882
BZ#2965.ml.3-10x.07	8,00913	9,69822	-0,141017	0,617601	100,307	84,694	185,001
BZ#2965.ml.3-10x.08	10,3333	13,4455	-0,115326	0,44371	46,804	56,878	103,682
BZ#2965.ml.3-10x.09	5,68478	7,67823	-0,235872	1,77204	39,727	58,1709	97,898
BZ#2965.ml.3-10x.10	6,95984	8,94168	-0,602439	0,71217	24,4032	44,6603	69,0635
AVERAGE	**7,612572222**	**9,844585556**	**-0,523004**	**1,279777778**	**43,12662222**	**62,62657778**	**105,7533111**
DEV.ST.C	*1,848849558*	*2,596745141*	*0,469892885*	*1,529820014*	*27,84952498*	*14,05156007*	*35,86094561*
BZ#833-ml.5-10x.01	7,34429	9,21819	-0,582775	1,07665	22,798	80,025	102,823
BZ#833-ml.5-10x.03	7,45048	9,21751	-0,462096	0,321815	25,073	49,4866	74,5596
BZ#833-ml.5-10x.04	6,95493	9,41032	-0,694723	1,52979	23,7182	40,5179	64,2361
BZ#833-ml.5-10x.05	5,34129	7,02345	-0,47127	0,888144	27,2409	44,2908	71,5317
BZ#833-ml.5-10x.06	9,6107	11,9521	-0,475634	-0,111034	28,2388	52,9838	81,2226
BZ#833-ml.5-10x.08	6,75878	8,58733	-0,617766	1,25192	75,503	52,977	128,48
BZ#833-ml.5-10x.09	5,97129	7,63443	-0,823658	2,05106	66,851	74,828	141,679
BZ#833-ml.5-10x.10	6,27505	8,77632	-0,0958253	8,58476	52,755	92,209	144,964
BZ#833-ml.5-10x.11	7,10798	9,27791	-0,119484	2,90071	65,46	73,67	139,13
AVERAGE	**6,979421111**	**9,01084**	**-0,482581256**	**2,054868333**	**43,07087778**	**62,33201111**	**105,4028889**
DEV.ST.C	*1,20106227*	*1,371414024*	*0,242813408*	*2,604998672*	*21,77271752*	*18,13707068*	*33,42102901*

BZ#5160

SAMPLE	Mean roughness (Sa)	RMS roughness (Sq)	Skew (Ssk)	Excess kurtosis	Max.height of peaks (Sp)	Max. height of valleys (Sv)	Max. height of the surface (Sz)
BZ#5160.ml.3-10x.01	27,1411	33,8327	-0,535738	-0,121319	104,844	112,594	217,438
BZ#5160.ml.3-10x.02	27,0786	33,4023	-0,209603	-0,602779	108,575	89,241	197,816
BZ#5160.ml.3-10x.03	18,2313	22,3738	0,147448	-0,463912	68,998	119,062	188,06
BZ#5160.ml.3-10x.04	16,1047	20,9639	-0,566291	0,783817	50,736	85,016	135,752
BZ#5160.ml.3-10x.05	10,9992	14,6181	-1,25133	1,97335	33,332	67,074	100,405
BZ#5160.ml.3-10x.08	20,7206	24,599	-0,254311	-0,728127	53,734	95,741	149,475
BZ#5160.ml.3-10x.10	15,057	18,6922	0,31927	-0,230704	55,744	84,59	140,333
BZ#5160.ml.3-10x.09	14,9536	18,2872	-0,192811	-0,0236269	51,013	77,074	128,087
BZ#5160.ml.3-10x.06	13,8239	17,8946	-0,682732	0,647441	42,257	78,392	120,649
AVERAGE	**18,23444444**	**22,74042222**	**-0,358455333**	**0,137126678**	**63,24811111**	**89,86488889**	**153,1127778**
DEV.ST.C	*5,711021683*	*6,792757366*	*0,468067336*	*0,86136899*	*26,47283363*	*16,84486761*	*39,20087634*
BZ#5160.ml.4-10x.01	16,0935	20,6396	-0,214464	0,266964	77,868	68,009	145,877
BZ#5160.ml.4-10x.02	12,61	16,2866	0,171744	1,17913	72,854	94,07	166,924
BZ#5160.ml.4-10x.03	39,1059	46,2412	-0,104791	-0,906323	108,739	121,217	229,956
BZ#5160.ml.4-10x.04	19,3627	25,3268	0,172331	0,712589	96,635	86,781	183,416
BZ#5160.ml.4-10x.05	25,35	33,7306	-0,429536	1,32162	118,843	165,802	284,645
BZ#5160.ml.4-10x.06	21,3655	26,8302	-0,547287	-0,122857	76,343	81,144	157,487
BZ#5160.ml.4-10x.08	16,7261	20,3628	-0,3431	-0,502025	63,06	78,626	141,686
BZ#5160.ml.4-10x.09	19,3538	23,7006	0,139898	0,057883	105,079	69,516	174,595
BZ#5160.ml.4-10x.10	25,5774	31,1947	-0,0895735	-0,402436	121,829	113,152	234,981
AVERAGE	**21,72721111**	**27,1459**	**-0,138308722**	**0,178282778**	**93,47222222**	**97,59077778**	**191,063**
DEV.ST.C	*7,755607334*	*8,985594045*	*0,267708545*	*0,765168821*	*21,54209403*	*31,37634866*	*48,37176391*

BZ#6742

SAMPLE	Mean roughness (Sa)	RMS roughness (Sq)	Skew (Ssk)	Excess kurtosis	Max.height of peaks (Sp)	Max. height of valleys (Sv)	Max. height of the surface (Sz)
BZ#6742-ml.1e-10x.01	19,685	24,847	-0,571097	0,349777	48,637	99,687	148,324
BZ#6742-ml.1e-10x.02	27,6708	34,381	-0,311524	0,00637549	91,577	102,084	193,661
BZ#6742-ml.1e-10x.03	22,438	27,2703	0,0142133	-0,26106	70,481	105,29	175,771
BZ#6742-ml.1e-10x.04	21,997	27,3165	-0,0243795	-0,0731759	80,44	89,04	169,48
BZ#6742-ml.1e-10x.05	20,6691	25,2602	-0,255169	-0,213877	60,936	99,446	160,382
BZ#6742-ml.1e-10x.06	15,3568	19,5413	0,350367	-0,113855	58,565	56,758	115,324
BZ#6742-ml.1e-10x.07	20,1996	25,4377	-0,403167	-0,0192614	59,281	80,681	139,963
BZ#6742-ml.1e-10x.09	32,851	42,1176	-0,980087	0,80539	73,868	164,751	238,619
BZ#6742-ml.1e-10x.10	19,5267	23,8899	-0,284717	-0,46081	83,267	77,265	160,532
AVERAGE	22,266	27,78461111	-0,273951133	0,002167021	69,67244444	97,22244444	166,8951111
DEV.ST.C	5,124432917	6,643245778	0,377590806	0,37348454	13,91487972	29,6565483	34,92654108
BZ#6742-ml.1a-10x.01	14,2029	17,6143	-0,598454	0,237502	95,029	132,012	227,041
BZ#6742-ml.1a-10x.02	19,5807	23,9565	-0,604384	-0,338383	44,377	79,406	123,782
BZ#6742-ml.1a-10x.04	17,0514	20,9605	-0,233776	-0,262605	57,483	89,055	146,538
BZ#6742-ml.1a-10x.05	23,8444	30,2323	-0,549035	-0,130548	63,346	104,409	167,755
BZ#6742-ml.1a-10x.06	16,1168	20,1043	-0,521366	0,201429	45,434	78,767	124,201
BZ#6742-ml.1a-10x.08	14,704	18,077	-0,351818	-0,220871	42,446	67,414	109,86
BZ#6742-ml.1a-10x.09	19,9315	26,8958	-0,819156	2,45115	78,309	137,036	215,345
BZ#6742-ml.1a-10x.10	22,9551	30,1745	-1,22043	2,73925	52,178	153,043	205,221
BZ#6742-ml.1a-10x.11	25,7	31,1239	-0,569166	-0,111014	63,429	105,735	169,163
AVERAGE	19,34297778	24,34878889	-0,607509444	0,507323333	60,22566667	105,2085556	165,434
DEV.ST.C	4,149170051	5,423130596	0,282383298	1,201760707	17,38049958	29,73792798	42,9671472
BZ#6742-ml.2-10x.06	31,4538	37,6496	0,250453	-0,813951	111,532	95,041	206,572

BZ#6742.ml.2-10x.07	30,9674	37,8381	-0,255606	-0,511575	117,372	109,67	227,042
BZ#6742.ml.2-10x.05	35,6828	45,372	0,992533	0,810068	163,524	109,964	273,488
BZ#6742.ml.2-10x.09	25,7504	32,4468	0,006826	0,0427468	106,776	134,814	241,59
BZ#6742.ml.2-10x.10	31,4501	37,8144	0,204597	-0,621256	102,476	101,086	203,562
BZ#6742.ml.2-10x.12	30,5949	40,9358	-0,247855	0,90788	121,196	157,633	278,829
BZ#6742.ml.2-10x.14	28,3949	35,1423	-0,618003	0,24382	90,217	136,649	226,866
BZ#6742.ml.2-10x.01	40,4122	48,6493	0,341525	-0,679342	119,879	125,584	245,463
BZ#6742.ml.2-10x.03	30,2807	39,6464	0,415929	0,542397	124,956	119,363	244,319
AVERAGE	**31,66524444**	**39,49941111**	**0,121155444**	**-0,008801356**	**117,5475556**	**121,0893333**	**238,6367778**
DEV.ST.C	*4,212646214*	*4,975406323*	*0,468505297*	*0,67146471*	*20,35258111*	*19,75447658*	*26,09839312*

BZ#375

SAMPLE	Mean roughness (Sa)	RMS roughness (Sq)	Skew (Ssk)	Excess kurtosis	Max.height of peaks (Sp)	Max. height of valleys (Sv)	Max. height of the surface (Sz)
BZ#375.ml.1-10x.01	32,4418	39,8997	0,016614	-0,695587	96,49	142,651	239,141
BZ#375.ml.1-10x.02	26,1734	32,3696	-0,176917	0,105818	83,941	139,304	223,245
BZ#375.ml.1-10x.03	16,8543	21,618	-0,844706	1,29157	74,963	124,421	199,384
BZ#375.ml.1-10x.04	18,8959	23,4651	-0,64539	-0,183787	101,286	85,629	186,915
BZ#375.ml.1-10x.05	15,2178	19,2485	-0,201548	-0,0721492	50,371	65,227	115,598
BZ#375.ml.1-10x.07	23,5519	29,5167	-0,655774	0,286472	112,657	116,448	229,105
BZ#375.ml.1-10x.08	26,3737	32,8417	-0,296279	0,0668254	99,659	140,204	239,864
BZ#375.ml.1-10x.09	23,0907	33,8999	-1,11421	2,85795	96,574	141,066	237,641
BZ#375.ml.1-10x.12	20,0088	25,5888	-1,08482	0,986437	87,711	94,239	181,95
AVERAGE	22,51203333	28,71644444	-0,555892222	0,515949911	89,29466667	116,5765556	205,8714444
DEV.ST.C	5,39551785	6,71123841	0,411890064	1,062650234	18,21191182	28,5250957	40,67595167
BZ#375.ml.5-10x.02	31,8116	43,2376	-1,02376	1,72057	109,607	179,765	289,373
BZ#375.ml.5-10x.03	30,2574	38,8754	-0,995163	0,836343	67,574	158,049	225,623
BZ#375.ml.5-10x.04	39,8945	49,7575	-0,431061	0,206031	141,509	175,438	316,947
BZ#375.ml.5-10x.05	28,2858	37,0114	-1,08357	1,26792	77,819	168,136	245,955
BZ#375.ml.5-10x.06	18,333	24,4447	-1,19215	1,88552	54,764	122,186	176,95
BZ#375.ml.5-10x.07	23,9981	32,8981	-1,24835	2,67967	77,19	163,086	240,276
BZ#375.ml.5-10x.08	30,6669	41,1651	-0,837092	1,34913	176,421	162,102	338,523
BZ#375.ml.5-10x.10	31,6745	42,3601	-1,16601	2,28623	88,672	199,473	288,145
BZ#375.ml.5-10x.11	25,4199	31,6597	-0,232935	-0,0975513	100,777	122,429	223,207
AVERAGE	28,92685556	37,9344	-0,912232333	1,348206967	99,37033333	161,1848889	260,5554444
DEV.ST.C	6,022776817	7,469767907	0,354087099	0,918100962	38,55329719	25,24849123	51,33232839

BZ#3488

SAMPLE	Mean roughness (Sa)	RMS roughness (Sq)	Skew (Ssk)	Excess kurtosis	Max.height of peaks (Sp)	Max. height of valleys (Sv)	Max. height of the surface (Sz)
BZ#3688.ml.1-10x.01	24,2339	30,1388	-0,550452	0,273329	83,053	116,576	199,629
BZ#3688.ml.1-10x.02	16,8873	20,6191	-0,00484763	-0,410442	95,585	82,485	178,07
BZ#3688.ml.1-10x.03	17,5002	22,0698	-0,248244	0,410463	70,056	81,544	151,6
BZ#3688.ml.1-10x.05	13,2764	16,5504	-0,104873	-0,266378	50,4909	48,7857	99,2766
BZ#3688.ml.1-10x.06	23,223	29,3243	-0,321398	-0,108336	84,697	102,984	187,681
BZ#3688.ml.1-10x.07	14,5188	19,3625	-1,19723	1,81656	41,768	83,471	125,239
BZ#3688.ml.1-10x.08	16,3306	19,7751	-0,329375	-0,521024	56,808	62,784	119,592
BZ#3688.ml.1-10x.09	12,3296	15,4339	-0,0795689	0,0101202	51,324	62,183	113,507
BZ#3688.ml.1-10x.11	16,2076	20,0863	0,159232	-0,336733	68,092	62,822	130,915
AVERAGE	17,16748889	21,48446667	-0,297417392	0,096395467	66,87487778	78,18163333	145,0566222
DEV.ST.C	4,092304477	5,096394124	0,396289141	0,715503684	18,22496087	21,6222376	35,81208004

BZ#2964

SAMPLE	Mean roughness (Sa)	RMS roughness (Sq)	Skew (Ssk)	Excess kurtosis	Max.height of peaks (Sp)	Max. height of valleys (Sv)	Max. height of the surface (Sz)
BZ#2964.ml.1-10x.01	20,8022	26,4365	-0,0258998	-0,146816	87,67	88,481	176,151
BZ#2964.ml.1-10x.02	23,8172	29,7197	-0,440065	0,028424	95,156	127,814	222,971
BZ#2964.ml.1-10x.03	29,6714	37,7508	-0,129097	-0,0480563	101,34	129,223	230,563
BZ#2964.ml.1-10x.05	22,3533	28,3163	-0,69342	0,441891	62,754	121,155	183,909
BZ#2964.ml.1-10x.06	21,956	28,9118	-0,322053	0,449798	#96,254	109,164	205,418
BZ#2964.ml.1-10x.08	23,5779	29,2764	-0,204134	-0,00440317	74,564	110,733	185,298
BZ#2964.ml.1-10x.09	21,3574	25,475	-0,0397693	-0,757253	63,429	82,601	146,03
BZ#2964.ml.1-10x.11	22,7115	28,6943	-0,394041	-0,0272927	77,256	104,178	181,434
BZ#2964.ml.1-10x.12	13,2727	16,9992	-0,54602	0,636708	44,871	101,926	146,796
AVERAGE	22,16884444	27,95333333	-0,3104999	0,063666648	78,14377778	108,3638889	186,5077778
DEV.ST.C	*4,228359614*	*5,372340051*	*0,230355762*	*0,413123869*	*18,77584929*	*16,20686012*	*29,54810643*

BZ#6707

SAMPLE	Mean roughness (Sa)	RMS roughness (Sq)	Skew (Ssk)	Excess kurtosis	Max.height of peaks (Sp)	Max. height of valleys (Sv)	Max. height of the surface (Sz)
BZ#6707.ml.1-10x.01	17,5111	20,9071	-0,423848	-0,505479	104,795	99,441	204,236
BZ#6707.ml.1-10x.02	16,6478	22,5559	-1,34529	2,67984	52,543	108,452	160,995
BZ#6707.ml.1-10x.03	19,4893	24,4482	-0,560544	0,571295	57,839	110,272	168,111
BZ#6707.ml.1-10x.04	17,72	21,9329	-0,488274	-0,322091	55,966	83,353	139,319
BZ#6707.ml.1-10x.05	19,2908	23,4937	-0,0592473	-0,564008	62,032	89,421	151,454
BZ#6707.ml.1-10x.06	13,2683	16,0814	-0,463941	-0,290008	48,648	68,783	117,432
BZ#6707.ml.1-10x.07	26,001	32,5429	0,171491	-0,431791	99,751	114,222	213,973
BZ#6707.ml.1-10x.08	22,9407	27,5001	0,0747508	-0,729355	76,341	88,377	164,718
BZ#6707.ml.1-10x.10	13,9507	17,2108	-0,0543671	-0,161052	60,926	56,446	117,371
AVERAGE	18,53552222	22,96366667	-0,349918844	0,027483444	68,76011111	90,97411111	159,7343333
DEV.ST.C	4,041369254	5,009303876	0,460541628	1,061068069	20,53506366	19,49971796	33,70518363
BZ#6707.ml.4-10x.01	19,2951	24,1269	-0,877648	0,555001	56,966	91,665	148,631
BZ#6707.ml.4-10x.02	14,8005	17,8121	-0,554207	-0,345396	42,791	69,641	112,433
BZ#6707.ml.4-10x.04	9,3926	12,8378	-0,360061	1,38609	48,791	65,427	114,218
BZ#6707.ml.4-10x.05	11,1798	13,7069	-0,293051	-0,257034	34,9559	51,0547	86,0106
BZ#6707.ml.4-10x.06	15,6584	19,2106	-0,135319	-0,16291	88,507	75,232	163,739
BZ#6707.ml.4-10x.08	14,5826	17,6275	-0,244492	-0,508323	40,6762	58,0534	98,7296
BZ#6707.ml.4-10x.09	16,703	20,1966	-0,113474	-0,586765	44,875	74,83	119,705
BZ#6707.ml.4-10x.10	10,2408	13,6328	0,176999	1,18765	58,082	52,258	110,34
BZ#6707.ml.4-10x.11	12,0314	15,0608	-0,69787	0,0581717	28,6338	55,4424	84,0762
AVERAGE	13,76491111	17,13466667	-0,344347	0,147387189	49,36421111	65,95594444	115,3202667
DEV.ST.C	3,274256383	3,70902115	0,323085828	0,729918762	17,473067	13,33357893	26,50013542

BZ#N.No.

SAMPLE	Mean roughness (Sa)	RMS roughness (Sq)	Skew (Ssk)	Excess kurtosis	Max.height of peaks (Sp)	Max. height of valleys (Sv)	Max. height of the surface (Sz)
BZ#N.No.ml.2-10x.01	7,69756	9,66558	-0,619984	0,598769	23,5517	48,89	72,4417
BZ#N.No.ml.2-10x.02	8,4343	10,2148	-0,635229	-0,0905975	29,0021	48,3256	77,3277
BZ#N.No.ml.2-10x.03	14,9319	20,167	-1,51419	2,25013	30,407	90,083	120,489
BZ#N.No.ml.2-10x.05	19,9889	24,7345	0,3009	-0,222074	87,264	66,55	153,814
BZ#N.No.ml.2-10x.08	11,0327	14,2066	-0,631307	0,591644	33,399	69,02	102,419
BZ#N.No.ml.2-10x.11	11,9997	15,749	-0,852705	0,926642	35,872	67,485	103,357
BZ#N.No.ml.2-10x.16	9,5356	13,1254	-1,12653	2,27333	31,5452	64,1111	95,6563
BZ#N.No.ml.2-10x.19	14,3347	17,4513	-0,0279379	-0,616664	48,335	72,147	120,482
BZ#N.No.ml.2-10x.21	11,5157	14,7073	-0,969969	0,655682	32,214	68,523	100,737
AVERAGE	**12,16345111**	**15,55794222**	**-0,675216878**	**0,707429056**	**39,06555556**	**66,12607778**	**105,1915222**
DEV.ST.C	*3,809488617*	*4,754077382*	*0,548212127*	*1,010071901*	*19,27350608*	*12,47162555*	*24,50182623*